Universidad Politécnica de Valencia
Escuela Técnica Superior de Ingenieros de Caminos, Canales y Puertos
Departamento de Ingeniería Hidráulica y Medio Ambiente

INVERSE STOCHASTIC MODELLING OF GROUNDWATER FLOW AND MASS TRANSPORT

PhD. Dissertation presented by Harrie-Jan Hendricks-Franssen
Directed by J. Jaime Gómez-Hernández
Valencia, Spain
December 2000

Summary

This dissertation presents a research on the stochastic inverse modelling of groundwater flow and mass transport. The sequential self-calibrating method, an approach that allows to generate multiple equally likely solutions to the inverse groundwater flow problem, has been extended to handle transient groundwater flow, 3-D groundwater flow, groundwater flow in fractured media and the coupled inverse modelling of both groundwater flow and mass transport. Furthermore, the impact of measurement errors has been studied. The algorithm has been implemented in the software INVERTO. The extended approach has been tested in numerous synthetic studies and real-world case studies. The real-world case studies are all related with the underground storage of nuclear waste.

A literature study shows that many of the existing statistically based inverse modelling methods rely on a linearization of the groundwater flow equation. The disadvantage of the linearization is that it is not valid in case the transmissivity shows a strong spatial variability. Furthermore, nearly all methods aim at estimating a single-best solution to the inverse problem, in spite of the fact that it is known that many solutions to the inverse problem exist. The coupled inverse problem of groundwater flow and mass transport is less documented in literature, but the number of methods that does not linearize the flow and transport equation is very limited and the aim is to generate a single-best solution. The sequential-self calibrating method does not linearize the groundwater flow and mass transport equations and generates multiple equally likely solutions to the inverse problem.

The self-calibrating method was extended to handle transient groundwater flow and the joint conditioning of transmissivity and storativity fields. The adjoint state method is used to calculate in an efficient way the gradient of the objective function. The transmissivity and storativity field can be conditioned jointly to the piezometric head data. In case transmissivity and storativity are cross-correlated, co-kriging is used to calculate the perturbations of the transmissivity and storativity field. The extension to transient groundwater flow and the joint conditioning of transmissivity and storativity was tested in two practical studies and one synthetic study. In all cases 100 equally likely solutions for different scenarios were generated. All the realisations could be conditioned closely to the available experimental information. The transient head data just yielded limited modifications in the transmissivity field in the WIPP-case study (New Mexico, U.S.A.), while the transmissivities of a single fracture in the Aspö-case study (Sweden) changed noticeably. The impact of the transient head data is related with the extent of the zone of the aquifer that is influenced by the transient events. In the Aspö-case study it was found that modifications in the transmissivity variogram parameters and the estimated transmissivity measurement error just had a limited influence on the final

results. The impact of considering uncertainty in the boundary conditions was somewhat larger. In both case studies consistent estimates were obtained of a single storativity value. In a synthetic study transmissivity and storativity fields were jointly conditioned to steady-state and transient head data. In all scenarios the steady- state head data had much more importance than the transient head data, also in case of many pumping tests. The transient head data made it possible to improve the characterisation of the spatial variable storativity field and reduce the uncertainty on the characterisation of the storativity field.

The impact of the amount and quality of conditioning data was investigated in two synthetic studies. One was a 3-D synthetic study in which 35 scenarios with different amounts of error-free conditioning data were studied. In this study it was found that the hydraulic conductivity field and the hydraulic head field were characterised better in case more conditioning data were used. A considerable improvement was achieved for the head field and a (much) more limited improvement for the conductivity field. The steady-state head data improved the characterisation of the 3-D head field and also reduced the uncertainty. The value of the conductivity data was found to be more limited although the conductivity data were the most relevant to improve the characterisation of the conductivity field and to reduce the uncertainty associated with the characterisation of the conductivity field. The prediction of particle arrival locations improved, but the prediction of the arrival times did not improve. In the 3-D study also scenarios were studied with a conceptual model mistake or randomly corrupted measurement data. Results were found to be robust for a variogram mistake, but mistakes in the boundary conditions had a more negative impact on the characterisation of the head and conductivity field. The head measurement errors had a marginal impact on the characterisation of the head and conductivity field. However, in the other synthetic study (a 2-D study) in which various scenarios with corrupted measurement data were studied, a larger impact of head measurement errors was found. It was concluded that the relative magnitude of the measurement error with respect to the head differences along the simulation domain is an indication for the negative impact of the measurement errors. It was also found that a correct estimation of the head measurement error by the modeller was important for reducing the negative impact of the corrupted head data on the characterisation of the transmissivity and head field. In case erroneous head data are reproduced too close artefacts on the ensemble average transmissivity maps appear. For transmissivity measurement data a similar conclusion was obtained; in case the transmissivity measurement errors were ignored, the results were worse. Furthermore, unrealistic low estimates of the ensemble variances were obtained in case the magnitude of the measurement error was underestimated. The synthetic study also suggests that transmissivity measurement errors and head measurement errors reinforce themselves.

A next extension of the self-calibrating approach was to 3-D groundwater flow in fractured media. For the modelling of groundwater flow in fractured media

it is considered that flow can take place both in the major fractures and in the background (that may have minor fractures). Nevertheless, not a classical stochastic continuum approach has been applied. It is considered that the major fractures and the background belong to different statistical populations, which implies that the averages, variances and spatial covariances of the material properties differ between the fractures and the background. This implies that each of the statistical populations (zones) is generated separately and just conditioned to data taken in the zone that belongs to the same statistical population. In the inverse modelling each of the different zones is perturbed separately. The approach was tested in two CPU-intensive 3-D case studies. In the Sellafield (United Kingdom) study the information on the fractures was limited and therefore the fractures were generated stochastically. Neverteless, the position of the fractures was to a certain extent imposed by the conditioning data and the geological model. In the Sellafield study three statistical populations were considered: two fracture families and the background. In the Aspö (Sweden) study precise information on the major fracture planes was available and each of the major fracture planes was incorporated deterministically. Each of the major fracture planes and the background formed the different statistical populations, that were generated and perturbed independently. The applied approach was able to reproduce the experimental steady-state and transient head data reasonably well. The conditioning to head data yielded a reduced conductivity contrast between the background and the fractures in the Sellafield study. It was found that also the minor fractures in the background had a significant role in transmitting the pressure drawdowns. In the Aspö study the deterministic model with the major fracture positions was found to be plausible. In the Aspö study the prior estimates of the variances were too low and the spatial variability of the conductivities in the fracture planes increased. The statistical distribution of the fracture plane log conductivities evolved from Gaussian to more skewed.

Finally, the approach was extended to the coupled inverse modelling of groundwater flow and mass transport. The extension of the inverse modelling approach to transport required a numerical scheme to solve the mass transport equation, an expression for the objective function that also included the mismatch to the concentration data and a method to calculate the gradient of the objective function. The derivatives of the objective function with respect to the perturbation of log conductivity are more difficult to evaluate in case also concentration data are present. In the adopted approach only the derivatives of the convective contributions to the transport are considered. The dispersive contributions to the transport are not considered in the gradient calculation. This approach is considered to be good as long as convection dominates over dispersion. Nevertheless, the evaluation of the derivatives requires the solution of a groundwater flow sensitivity equation for each master block at each simulation time step. The method also allows to condition spatial variable porosities, spatial variable retardation coefficients and mass release information together with the flow parameters. The calibration of dispersion coefficients is

not considered as the identification of the dispersion coefficients in strongly or moderately heterogeneous conductivity fields is unstable, the calculations are very cumbersome and the heterogeneous conductivities already account for the macro-dispersion. The performance of the implemented method was tested in a synthetic study. In the synthetic study the boundary conditions, initial conditions, mass release information, dispersivities and porosities were perfectly known. Just the heterogeneous transmissivity field was unknown. Eight scenarios were studied and showed that the best results were obtained in case transmissivity, steady-state head and concentration data were used together in the conditioning procedure. The concentration data contributed to improve the characterisation of the transmissivity, head and, especially, the concentration field, and reduce the uncertainty associated with the characterisation. The improvement was very significant for the part upstream of the row of concentration monitoring locations.

Resumen

Esta tesis presenta una investigación sobre la modelizacion inversa estocástica de flujo subterráneo y transporte de masa. El método secuencial autocalibrante es un método que permite la generación de soluciones equiprobables múltiples para el problema inverso de flujo. Este método ha sido extendido para tratar flujo subterráneo transitorio, flujo en 3-D, flujo en medios fracturados y la modelización inversa acoplada de flujo subterráneo y transporte de masa. Además, se ha estudiado el impacto de errores de medida. El algoritmo se ha implementado en el software INVERTO. El método extendido ha sido probado en numerosos estudios sintéticos y estudios prácticos. Todos los estudios prácticos están relacionados con el almacenamiento en profundidad de residuos nucleares.

Una revisión de la bibliografía indica que muchos de los métodos de modelizacíon inversa estocástica existentes están basados en una linearización de la ecuación de flujo. La desventaja de la linearización es que no es válida cuando la transmisividad muestra una fuerte variabilidad espacial. Además, casi todos los métodos intentan estimar una solución única del problema inverso, a pesar del hecho de que existen múltiples soluciones para ese problema. El problema inverso acoplado de flujo subterráneo y transporte de masa ha sido menos documentado en la literatura, pero el número de métodos que no lineariza las ecuaciones de flujo y transporte es muy limitado y el objetivo es generar una única solución óptima. El método secuencial autocalibrante no lineariza las ecuaciones de flujo y transporte de masa, y genera múltiples soluciones equiprobables para el problema inverso.

El método autocalibrante ha sido extendido para tratar flujo transitorio y la calibración conjunta de campos de transmisividad y coeficientes de almacenamiento. El método de estado adjunto ha sido usado para calcular de una manera efectiva el gradiente de la función objetiva. Los campos de transmisividad y coeficientes de almacenamiento pueden ser condicionados conjuntamente a datos de piezometría. En el caso de que la transmisividad y el coeficiente de almacenamiento están cross-correlacionados, se usa el co-krigeado para calcular las perturbaciones de los campos de transmisividad y el coeficiente de almacenamiento. La extensión al flujo transitorio y el condicionamiento conjunto de transmisividad y el coeficiente de almacenamiento fueron probados en dos estudios prácticos y un estudio sintético. Para todos los casos se generaron 100 soluciones equiprobables para distintos escenarios. En todas las realizaciones los datos experimentales han sido reproducidos satisfactoriamente. Los datos de piezometría transitorio sólo sufrieron pequeñas modificaciones en el campo de la transmisividad en el estudio práctico de WIPP (nuevo Méjico, EE.UU), mientras que las transmisividades de una sólo fractura, en el estudio práctico de Aspö (Suecia)

cambiaron mucho. El impacto de los datos transitorios se relaciona con la parte de la zona del acuífero que es afectada por los eventos transitorios. En el estudio práctico de Aspö se detectó que las modificaciones en los parámetros del variograma de transmisividad y el error de medida de transmisividad sólo tenían una influencia limitada sobre los resultados finales. El impacto de la incertidumbre en las condiciones de contorno fue algo más importante. En los dos estudios prácticos se obtuvieron estimaciones consistentes de un coeficiente de almacenamiento único. En el estudio sintético campos de transmisividad y coeficientes de almacenamiento fueron condicionados conjuntamente a datos estacionarios y transitorios. En todos los escenarios los datos estacionarios tenían mucha más importancia que los datos transitorios, también en el caso de muchos ensayos de bombeo. Los datos transitorios hicieron posible que la caracterización del campo de coeficientes de almacenamiento fueron mejor y redujeron la incertidumbre de la caracterización del campo de coeficientes de almacenamiento.

El impacto de la cantidad y calidad de los datos condicionantes fue investigado en dos estudios sintéticos. Un estudio era en 3-D, en el cuál se estudiaron 35 escenarios con distintos cantidades de datos condicionantes (sin error de medida). En este estudio se concluyó que el campo de conductividades y el campo de alturas piezométricas fueron caracterizados mejor en el caso de que se condicionaba a más datos. El mejoramiento para el campo de alturas era considerable y el mejoramiento para el campo de conductividades era (mucho) más modesto. Los datos de alturas en régimen estacionario mejoraron la caracterización del campo de alturas en 3-D y también redujeron la incertidumbre. El valor de los datos de conductividad era más limitado aunque los datos de conductividad eran los más importantes para mejorar el campo de conductividades y reducir la incertidumbre asociada con la caracterización del campo de conductividades. La predicción de las posiciones de llegada mejoró, pero la predicción de los tiempos de llegada no mejoró. En el estudio en 3-D se estudió también escenarios con un error en el modelo conceptual o errores en los datos de medida. Los resultados eran robustos con respeto a un error en el variograma, pero errores en las condiciones de contorno tenían un impacto más negativo sobre la caracterización del campo de alturas piezométricas y conductividades. Los errores en los medidas de altura tenían un impacto marginal sobre la caracterización del campo de alturas y transmisividades. Sin embargo, en el otro estudio sintético (en 2-D), en el cuál se estudió varios escenarios con datos corruptos, el impacto de los errores de medida de alturas era mayor. Se concluyó que la magnitud relativa del error de medida con respeto a las diferencias de altura sobre la zona de estudio era un indicador para el impacto negativo de los errores de medida. También se concluyó que la estimación correcta del error de la medida por el modelador era importante para reducir el impacto negativo sobre la caracterización de los campos de altura y transmisividades de los errores de medida. En los mapas de transmisividad aparecían artefactos si se reproduje las medidas erróneas de altura. Para las medidas de transmisividad se llegó a una conclusión similar; en

el caso en el que no se toman en cuenta errores de medida de transmisividad los resultados eran peores. Además, las estimaciones de la varianza eran irrealmente bajos en el caso de que la estimación de la varianza de los errores de medida era demasiado bajo. El estudio sintético sugiere que los errores de medida de transmisividad y los errores de medida de alturas se refuerzan.

Otra extensión del método autocalibrante era el flujo en medios fracturados en 3-D. Se considera que el flujo subterráneo en medios fracturados ocurre tanto en las fracturas mayores como en la matriz (que puede tener fracturas más pequeñas). Sin embargo, no se aplicó el método de continuum estocástico clásico. Se considera que las fracturas mayores y la matriz pertenecen a distintas conjuntos estadísticos, lo que significa que los promedios, las varianzas y las covarianzas espaciales de las propiedades del material pueden cambiar entre las distintas fracturas y la matriz. Eso significa que cada uno de los conjuntos estadísticos (zonas) se genera independientemente y sólo condicionado a los datos tomados en la zona que pertenece al mismo conjunto estadístico. En la modelización inversa cada uno de las zonas se perturba independientemente. El método fue probado en dos estudios prácticos en 3-D. En el estudio de Sellafield (Reino Unido) la información sobre las fracturas era limitada y por eso las fracturas fueron generadas estocasticamente. Sin embargo, era posible imponer las posiciones de las fracturas hasta cierto modo por los datos condicionantes y el modelo geológico. En el estudio de Sellafield se consideraron tres poblaciones estadísticas: dos familias de fracturas y la matriz. En el estudio de Äspö (Suecia) se disponía de información precisa sobre los planos de fractura mayores y cada uno de los planos de fracturas mayores fue incorporado en el modelo deterministicamente. Cada uno de los planos de fracturas mayores y la matriz formaban las poblaciones estadísticas distintas, que fueron generados y perturbados independientemente. El método aplicado era capaz de reproducir los datos experimentales de altura (régimen estacionario y régimen transitorio) deforma razonable. En el estudio de Sellafield, el condicionamiento a datos de altura provocó un contraste de conductividad menor entre las fracturas y la matriz. Se concluyó que las fracturas menores en la matriz tenían un papel importante en transmitir el descenso de la presión. En el estudio de Äspö se concluyó que el modelo determinista con las posiciones de las fracturas principales era razonable. En el estudio de Äspö las estimaciones *a priori* de las varianzas eran demasiado bajas y la variabilidad espacial de la conductividad en los planos de fractura aumentó. La distribución estadística de las log conductividades en los planos de fractura cambió de Gaussiano a algo sesgado.

Finalmente, el método fue extendido a la modelización inversa acoplada de flujo subterráneo y transporte de masa. La extensión del método de la modelización inversa a transporte requería un esquema númerico para resolver la ecuación de masa, una formulación para la función objetiva que también incluye la diferencia entre los datos de concentración medidos y simulados, y un método para calcular el gradiente de la función objetiva. Las derivadas de la

función objetiva con respecto a la perturbación de la conductividad son más difíciles para evaluar cuando hay medidas de concentración. En el método usado sólo las derivadas de las contribuciones convectivas al transporte se han considerada. Las contribuciones dispersivas al transporte no han sido consideradas en el calculo de gradiente. Este método es bueno en el caso de que el flujo convectivo domine sobre flujo dispersivo. Sin embargo, la evaluación de las derivadas requiere la solución de una ecuación de sensibilidad de flujo para cada punto maestro y cada paso en el tiempo. El método también permite estimar el campo de porosidades variable en el espacio, los coeficientes de retardo variables en el espacio y la información de fuentes y sumideros de masa conjuntamente con los parámetros de flujo. No se consideró la calibración de los coeficientes de dispersión porque la identificación de los coeficientes de dispersión en campos de conductividad moderadamente o fuertemente heterogéneo es inestable, los cálculos son muy incómodos y las conductividades heterogéneas ya tienen en cuenta la macrodispersión. El método implementado fue probado en un estudio sintético. En el estudio sintético las condiciones de contorno, condiciones iniciales, información de fuentes y sumideros, dispersividades y porosidades se conocían a la perfección. Sólo se desconocía el campo variable de transmisividades. Se estudiaban ocho escenarios y se obtuvieron los mejores resultados para el caso en el que tanto los datos de piezometría, conductividad y concentración fueron usados en el condicionamiento. Los datos de concentración mejoraron la caracterización del campo de transmisividades, la piezometría y, especialmente, las concentraciones, y redujeron la incertidumbre asociada con la caracterización. El mejoramiento fue muy significativo para la parte de aguas arriba.

Resum

Aquesta tesi presenta una recerca sobre el modelat estocàstic invers del fluix d'aigües subterrànies i del transport de massa. El mètode seqüencial autocalibrant, un mètode que permet la generació de solucions equiprobables múltiples per al problema invers de fluix, ha sigut ampliat per a tractar el fluix subterrani transitori, el fluix en 3-D, el fluix en medis fracturats i el modelat invers acoblat de fluix subterrani i transport de massa. A més, s'ha estudiat l'impacte d'errors del mesurament. L'algorisme ha sigut implementat en el programari INVERTO. El mètode ampliat ha sigut provat en nombrosos estudis sintètics i estudis pràctics. Tots els estudis pràctics estan relacionats amb l'emmagatzematge en profunditat de residus nuclears.

Un estudi de documentació indica que molts dels mètodes de modelat invers estocàstic existents estan basats en una linearització de l'equació de fluix. El desavantatge de la linearització és que no és vàlida en el cas que la transmissivitat mostre una forta variabilitat espacial. A més, quasi tots els mètodes intenten considerar una solució única del problema invers, a pesar que hi ha múltiples solucions per a aquest problema. El problema invers acoblat de fluix subterrani i transport de massa s'ha acreditat menys en documentació, però el nombre de mètodes que no linearitzen les equacions de fluix i transport és molt limitat i l'objectiu és generar una única solució òptima. El mètode seqüencial autocalibrant no linearitza les equacions de fluix i transport de massa i genera múltiples solucions equiprobables per al problema invers.

El mètode autocalibrant s'ha ampliat per a tractar el fluix transitori i el calibratge conjunt de camps de transmissivitat i coeficients d'emmagatzematge. El mètode d'estat adjunt s'ha usat per a calcular d'una manera efectiva el gradient de la funció objectiva. Els camps de transmissivitat i els coeficients d'emmagatzematge poden ser condicionats conjuntament a dades de piezometria. En el cas que la transmissivitat i el coeficient d'emmagatzematge estiguen transcorrelacionats, s'usa el mètode de co-krige per a calcular les pertorbacions dels camps de transmissivitat i el coeficient d'emmagatzematge. L'extensió al fluix transitori i el condicionament conjunt de transmissivitat i el coeficient d'emmagatzematge es van provar en dos estudis pràctics i en un de sintètic. En tots els casos, es generaren 100 solucions equiprobables per a distints marcs hipotètics. En totes les realitzacions les dades experimentals s'han reproduït satisfactòriament. Les dades de piezometria transitòria només van resultar en modificacions xicotetes en el camp de la transmissivitat en l'estudi pràctic de WIPP (Nou Mèxic, EUA), mentre les transmissivitats d'una sola fractura en l'estudi pràctic d'Aspö (Suècia) van canviar molt. L'impacte de les dades transitòries es relaciona amb la part de la zona de l'aqüífer afectada pels esdeveniments transitoris. En l'estudi pràctic d'Aspö es va detectar que les modificacions en els paràmetres del variograma de transmissivitat i l'error de mesura de transmissivitat només tenien una influència limitada sobre els resultats finals. L'impacte de la incertesa en les condicions de contorn va ser una miqueta més important. En els dos estudis pràctics es van obtenir estimacions

consistents d'un coeficient d'emmagatzematge únic. En l'estudi sintètic els camps de transmissivitat i els coeficients d'emmagatzematge van ser condicionats conjuntament a dades estacionàries i transitòries. En tots els marcs hipotètics les dades estacionàries tenien molta més importància que les dades transitòries, també en el cas de molts assaigs de bombament. Les dades transitòries van fer possible que la caracterització del camp de coeficients d'emmagatzematge fóra millor i van reduir la incertesa de la caracterització del camp de coeficients d'emmagatzematge.

L'impacte de la quantitat i qualitat de les dades condicionants s'investigaren en dos estudis sintètics. Un estudi era en 3-D, en què s'estudiaren 35 marcs hipotètics amb diferents quantitats de dades condicionants (sense error de mesura). En aquest estudi es va concloure que el camp de conductivitats i el camp d'altures piezomètriques es caracteritzaven millor en el cas que s'usaren més dades. Una millora considerable es va aconseguir per al camp d'altures i una molt més modesta per al camp de conductivitats. Les dades d'altures en règim estacionari van millorar la caracterització del camp d'altures en 3-D i també en van reduir la incertesa. El valor de les dades de conductivitat era més limitat, encara que les dades de conductivitat eren les més pertinents per a millorar el camp de conductivitat i reduir la incertesa associada a la caracterització del camp de conductivitat. La predicció de les situacions d'arribada va millorar, però la predicció dels temps d'arribada no va millorar. En l'estudi en 3-D es van estudiar també marcs hipotètics amb un error en el model conceptual o errors en les dades de mesurament. Els resultats eren ferms respecte a un error en el variograma, però els errors en les condicions de contorn tenien un impacte més negatiu sobre la caracterització del camp d'altures piezomètriques i conductivitats. Els errors en els mesuraments d'altura tenien un impacte marginal sobre la caracterització del camp d'altures i transmissivitats. No obstant això, en l'altre estudi sintètic (en 2-D), en què es van estudiar diversos marcs hipotètics amb dades poc fiables, es va trobar que l'impacte dels errors de mesurament d'altures era major. Es va concloure que la magnitud relativa de l'error de mesurament respecte a les diferències d'altura sobre la zona d'estudi és un indicador per a l'impacte negatiu dels errors de mesurament. També es va concloure que l'estimació correcta de l'error de la mesura pel modelador era important per a reduir l'impacte negatiu de les dades sobre la caracterització dels camps d'altura i transmissivitats dels errors de mesurament. En el cas que es reproduïsquen mesures erònies d'altura massa exactes apareixen en els mapes de transmissivitat. Per als mesuraments de transmissivitat es va arribar a una conclusió semblant; en el cas que els errors de mesurament de transmissivitat no es tingueren en compte els resultats eren pitjors. A més, s'obtingueren estimacions de la variància irrealment baixes en el cas que l'estimació de la magnitud dels errors de mesurament fóra infravalorat. L'estudi sintètic també suggereix que els errors de mesurament de transmissivitat i els errors de mesurament d'altures es reforcen.

Una altra extensió del mètode autocalibrant era el fluix en medis fracturats en 3-D. Es considera que el fluix subterrani en medis fracturats ocorre tant en les fractures majors com en la matriu (que pot tenir fractures més xicotetes). No obstant això, no es va aplicar el mètode de continuum estocàstic clàssic. Es considera que les fractures majors i la matriu pertanyen a conjunts estadístics diferents, que significa que les mitjanes, les variàncies i les covariàncies espacials de les propietats de la

material poden canviar entre les distintes fractures i la matriu. Això significa que cadascun dels conjunts estadístics (zones) es genera independentment i només condicionat a les dades preses en la zona a què pertany al mateix conjunt estadístic. En el modelat invers cadascuna de les zones diferents es pertorba independentment. El mètode es va provar en dos estudis pràctics en 3-D. En l'estudi de Sellafield (Regne Unit) la informació sobre les fractures estava limitada i per això les fractures es van generar estocàsticament. No obstant això, era possible imposar les posicions de les fractures fins a certa manera per les dades condicionants i el model geològic. En l'estudi de Sellafield es consideraren tres conjunts estadístics: dues famílies de fractures i la matriu. En l'estudi d'Aspö (Suècia) es disposava d'informació precisa sobre els plans de fractura i cadascun dels plans de fractures majors es va incorporar en el model determinísticament. Cadascun dels plans de fractures majors i la matriu formaven els conjunts estadístics diferents, que van ser generats i pertorbats independentment. El mètode aplicat era capaç de reproduir les dades experimentals d'altura (règim estacionari i règim transitori) bé. En l'estudi de Sellafield, el condicionament a dades d'altura va provocar un contrast de conductivitat menor entre les fractures i la matriu. Es va concloure que les fractures menors en la matriu tenien un paper important a transmetre el descens de la pressió. En l'estudi d'Aspö es va concloure que el model determinístic amb les posicions de les fractures principals era raonable. En l'estudi d'Aspö les estimacions *a priori* de les variàncies abans eren massa baixes i la variabilitat espacial de la conductivitat en els plans de fractura van augmentar. La distribució estadística dels logarismes de conductivitats en els plans de fractura va canviar de Gaussiano a un poc més esbiaixat.

Finalment, el mètode es va ampliar al modelat invers acoblat de fluix subterrani i transport de massa. L'extensió del mètode del modelat invers a transport requeria un esquema numèric per a resoldre l'equació de massa, una formulació per a la funció objectiva que també inclou la diferència entre les dades de concentració mesurades i simulades i un mètode per a calcular el gradient de la funció objectiva. Les derivades de la funció objectiva respecte a la pertorbació de la conductivitat són més difícils per a avaluar en el cas que hi haja mesures de concentració. En el mètode usat només s'han considerat les derivades de les contribucions convectives al transport. Les contribucions dispersives al transport no s'han considerat en el càlcul de gradient. Aquest mètode és adequat en el cas que el fluix convectiu domine sobre el fluix dispersiu. No obstant això, l'avaluació de les derivades requereix la solució d'una equació de sensibilitat de fluix per a cada punt mestre i cada pas en el temps. El mètode també permet estimar el camp de porositats variable en l'espai, els coeficients de retardament variables en l'espai i la informació de fonts i descàrrega de massa, conjuntament amb els paràmetres de fluix. El calibratge dels coeficients de dispersió no es va considerar perquè la identificació dels coeficients de dispersió en camps de conductivitat moderadament o fortament heterogeni és inestable, els càlculs són molt incòmodes i les conductivitats heterogènies ja tenen en compte la macrodispersió. El mètode implementat va ser aplicat en un estudi sintètic, on les condicions de contorn, condicions inicials, informació de fonts i descàrrega, dispersivitats i porositats es coneixien perfectament. Només es desconeixia el camp variable de transmissivitats. S'estudiaven vuit marcs hipotètics i els millors resultats s'obtingueren per al cas que tant les dades de piezometria, conductivitat i concentració s'usaven en el

condicionament. Les dades de concentració van millorar la caracterització del camp de transmissivitats, piezometria i, especialment, concentracions, i van reduir la incertesa associada amb la caracterització. El millorament va ser molt significatiu per a la part d'aigua amunt.

Agradecimientos

Esta tesis es el resultado de cinco años de trabajo. Sin embargo, este trabajo no lo he hecho sólo y muchas personas han hecho posible que se realizase y que fuera agradable. En primer lugar quiero agradecer a mi director de la tesis, Jaime Gómez-Hernández, por darme la oportunidad de hacer este trabajo de investigación. Fue en Octubre 1994 cuando le escribí un correo electrónico con la pregunta si podía realizar el doctorado en su grupo de investigación en Valencia. Al final he hecho cinco años de investigación en lo que quería hacer: modelos físicos con un enfoque muy estocástico. También quiero agradecer a Jaime por su supervisión profesional del trabajo de la investigación y darme todas las oportunidades que necesitaba. También quiero agradecer a José Capilla y Andrés Sahuquillo, co-autores de algunos artículos que publicamos. A Andrés quiero agradecerle en especial su contribución en el desarrollo de las ecuaciones del estado adjunto continuas en el tiempo.

La Empresa Nacional de Residuos Radioactivos S.A. (ENRESA) financió a través de la Universidad Politécnica de Valencia los cinco años de investigación.

Mis compañeros de trabajo me ayudaron con los problemas del día a día y por ello quiero darles las gracias a Eduardo Cassiraga, David Martinez, Xian-Huan Wen, Min Zhang, Carolina Guardiola, Rafa Aliaga y Javier Rodrigo. El resto de los compañeros del departamento me ayudó también en pasar el tiempo bien y recordaré las comidas en "Derecho" y las visitas al bar. También quiero agradecer a las secretarias del departamento, Mari e Isabel.

En los fines de semana fueron las visitas al campo, la montaña y el mar de la Comunidad Valenciana y alrededores de las cuáles disfruté mucho y que me hicieron olvidar preocupaciones del trabajo.

Estos cinco años he estado lejos de mi familia y la mayor parte de mis amigos. Incluso he estado a veces lejos de Amaia, a pesar de estar físicamente cerca. Les agradezco su apoyo.

Curriculum vitae

Harrie-Jan Hendricks Franssen was born on the 13th of August 1970 in Groesbeek, the Netherlands. He went to primary school in Groesbeek and to secondary school in Nijmegen. He terminated secondary school in 1988 and started that year the study of soil science at the Agricultural University of Wageningen (The Netherlands). In 1994 he finished his study *cum laude* and the main subjects were soil contamination, mathematical statistics and environmental sociology. At the end of his study he stayed seven months in Sevilla (Spain) for a practical training period of regional soil science and land evaluation. In addition he worked for an engineers office in Deventer (The Netherlands) and fulfilled his social service at the department of research methods of the Winand Staring Centre (Wageningen). From January 1996 to January 2001 he did a PhD research at the department of hydraulic and environmental engineering of the Technical University of Valencia (Spain). In this period the research was done that is detailed in this dissertation. From February 2001 onwards he will work as postdoc at the Insitute of Hydromechanics and Water Resources Management of ETH (Zürich, Switzerland).

List of publications in international journals

Hendricks Franssen HJWM, van Eijnsbergen AC, Stein A (1997). Use of Spatial Prediction Techniques and Fuzzy Classification for Mapping Soil Pollutants. *Geoderma, 77,* 243-262.

Hendricks Franssen HJWM, Gómez-Hernández JJ, Sahuquillo A, Capilla JE (1999). Joint simulation of transmissivity and storativity fields conditional to hydraulic head data. *Advances in Water Resources Research,* 23, 1-13.

Gómez-Hernández JJ, Hendricks Franssen HJWM, Cassiraga EF (2000). Stochastic analysis of flow response in a three-dimensional fractured block. Accepted for publication in the *International Journal of Rock Mechanics.*

Hendricks Franssen HJWM, Gómez-Hernández JJ (2001). 3D Inverse modelling of groundwater at a fractured site using a stochastic continuum model with multiple statistical populations. Submitted to *Stochastic Environmental Research and Risk Assessment.*

Hendricks Franssen HJWM, Gómez-Hernández JJ (2001). Impact of measurement errors in the sequential self-calibrated approach. Submitted to *Groundwater.*

Hendricks Franssen HJWM, Gómez-Hernández JJ, Sahuquillo A (2001). The worth of concentration data in the coupled inverse modelling of groundwater flow and mass transport. In preparation. To be submitted to *Water Resources Research.*

List of international congress publications

Hendricks Franssen HJWM, Gómez-Hernández JJ (1997). Impact of Random Function Model Choice on Groundwater Mass Transport Modelling. In: Soares, A, Gómez-Hernández, JJ, Froidevaux, R (Eds.) *GeoENV I - Geostatistics for Environmental Applications*, p. 101-110. Kluwer Academic Publishers.

Hendricks Franssen HJWM, Gómez-Hernández JJ, Sahuquillo A, CapillaJE (1997). Stochastic inverse modelling of transient groundwater flow. In: Pawlowsky-Glahn, V (Ed.) *IAMG'97. Proceedings of The Third Annual Conference of the International Association for Mathematical Geology*, p. 778–783. CIMNE.

Hendricks Franssen HJWM, Cassiraga EF, Gómez-Hernández JJ, Sahuquillo A, Capilla JE (1998). Inverse modelling of groundwater flow in a 3-D fractured medium. In: Gómez-Hernández, JJ, Soares, A, Froidevaux, R. (Eds.) *GeoENV II - Geostatistics for Environmental Applications*, p. 283–294. Kluwer Academic Publishers.

Hendricks Franssen HJWM, Gómez-Hernández JJ, Sahuquillo A, Capilla JE (1999). Joint simulation of transmissivity and storativity fields conditional to hydraulic head data. In: Journel, AG (Ed.). *Report 12*. Stanford Centre for Reservoir Forecasting.

Gómez-Hernández JJ, Hendricks Franssen HJWM, Sahuquillo A, Capilla JE (2000). Calibration of 3-D transient groundwater flow models for fractured rock. In: Stauffer, F, Kinzelbach, W, Kovar, K, Hoehn, E (Eds.) *ModelCARE'99 – Calibration and reliability in groundwater modelling: Coping with uncertainty*, p. 185-194. IAHS Press.

Sahuquillo A, Hendricks Franssen HJWM, Gómez-Hernández JJ, Capilla JE (2000). Computational aspects of the coupled inversion of groundwater flow and mass transport. In: Stauffer, F, Kinzelbach, W, Kovar, K, Hoehn, E (Eds.) *ModelCARE'99 – Calibration and reliability in groundwater modelling: Coping with uncertainty*, p. 222-228. IAHS Press.

Hendricks Franssen HJWM, Gómez-Hernández JJ (2000). The impact of head measurement errors in sequential self-calibration. CD-Rom of Geostats 2000.

Hendricks Franssen HJWM, Gómez-Hernández JJ, Sahuquillo A, Capilla JE (2000). Multiple solutions to a 3-D inverse groundwater flow problem in fractured rock. Abstracts of EGS2000.

Hendricks Franssen HJWM, Gómez-Hernández JJ (2000). Multiple simulations of a 3-D fractured medium conditioned to various types of data. In: Heuvelink, GBM, Lemmens, MJPM (Eds.) Accuracy 2000. Proceedings of the 4th International Symposium on Spatial Accuracy Assessment in Natural Resources and Environmental Sciences, p. 293-300. Delft University Press.

Hendricks Franssen HJWM, Gómez-Hernández JJ, Sahuquillo A (2001). Multiple equally likely solutions to a coupled inverse problem. Accepted for the Third IMA Conference on Modelling Permeable Rocks.

Hendricks Franssen HJWM, Gómez-Hernández JJ, Sahuquillo A (2001). The worth of concentration data for aquifer characterisation. Accepted for EGS2001.

Table of Contents

List of Tables

List of figures

1 Introduction

This chapter is the introduction of this dissertation dedicated to the "stochastic inverse modelling of groundwater flow and mass transport". Section 1.1 describes briefly the practical situation we face and, in general, practical situations for which this research is relevant. In addition, it is explained why a stochastic approach is applied in groundwater hydrology and mass transport (section 1.2). The reasons behind an inverse modelling approach, and more specifically, a stochastic inverse modelling approach, are also detailed (section 1.3). Finally, an outline of the thesis is given in section 1.4.

1.1 The problem

The problem that is dealt with in this dissertation is the underground storage of nuclear waste. Candidate sites for the construction of an underground repository of nuclear waste are profound slightly permeable geological formations like crystalline rock, salt or clay. Conceptually it does not make a difference if the repository would contain other kinds of high-toxic waste, or would be a septic tank or even a surface landfill. The problem we face is the accidental release of contaminants from the repository. Such an accidental release is normally caused by a technical failure. In case such a failure occurs the important question is whether the contaminants will harm nature, animal life or human life. In order to respond the question it is necessary to estimate the time it takes for the contaminants to travel from the release point by the groundwater to the biosphere, and the concentration or activity of the contaminant with which it reaches the biosphere.

These estimations are not straightforward. Normally, just a limited amount of information on the subsurface is available. Experimental information on hydraulic conductivities, hydraulic heads or adsorption properties from the subsurface is in general very expensive, especially in case of deep underground waste disposals in low permeable rock formations. An additional complication factor is that the "unknown" properties frequently show a strong spatial variation. These spatial variations are in part related with geological variations in the subsurface. The fact that a limited amount of information is available on the aquifer properties that show a complex spatially variable pattern makes it necessary to:

- Obtain reliability measures on the estimates of, for example, the travel times of the particles. A stochastic approach is able to quantify the uncertainty on the estimates (see section 1.2).
- Use the available information as efficiently as possible. This is made possible by inverse modelling, which is capable to include experimental information non-linearly related with the state variables (see section 1.3)

The practical studies in this dissertation are all related with nuclear waste disposals. As stated before, the approach would be similar for other contaminant releases. In some studies the research area was a candidate location for the storage of nuclear waste (e.g. the WIPP-site in New Mexico, U.S.A. (see sections 2.3 and 3.4)). In other cases the research area was related with an underground test laboratory, which means that diverse geological, hydraulic and tracer tests were carried out in order to learn to what extend it was possible to estimate the test outcomes by numerical models (e.g. the Aspö-site near Oskarshamn in Sweden (see sections 3.5 and 5.4) and the site near Sellafield in the United Kingdom (see section 5.3)).

Although the focus is on the accidental release of contaminant from a waste disposal, the approach developed in this dissertation is applicable in a groundwater flow or mass transport study where we want to make estimations with a limited amount of data. Examples could be:

- Decrease of groundwater levels. In case historical observations on hydraulic head are available, together with for example rainfall or recharge data, the hydraulic head data could be incorporated in the model by conditioning the aquifer properties to the observations. The calibrated model of the aquifer properties would allow us to make predictions on the variation of the groundwater levels for future rainfall and groundwater extraction scenarios. In this context, a study was carried out in the province of Alicante (Spain) where groundwater levels decreased due to an enhanced groundwater extraction (related with tourism) that is not presented in this dissertation.
- Drinking water protection zones. Recently some studies were published that considered the stochastic characterisation of drinking water protection zones (e.g. Vassalo *et al.*, 1998; Guadagnini and Franzetti, 1999; van Leeuwen *et al.*, 1999). Available experimental information on hydraulic conductivity and hydraulic head could be used to get an improved characterisation of the aquifer properties around drinking water wells.
- Aquifer remediation. In this case the aquifer is already contaminated and the aim is to de-contaminate the aquifer and estimate the decrease of the contaminated area and the concentrations during, for example, pump-and-threat remediation techniques. Also in this case the conditioning of the aquifer properties to head and concentration data helps to improve the aquifer characterisation and as such the prediction of the effects of the remediation.

1.2 Modelling uncertainty: a stochastic approach

The prediction of contaminant transport from a repository to the biosphere is especially complicated due to the spatially variable aquifer properties. More over, just a limited amount of information is available on these spatially variable properties. A stochastic approach is applied in order to build a

stochastic model of the spatially variable attributes and to build a probability density function of the output variables of interest.

The main, although not exclusive, focus in this dissertation is on the spatial variability of hydraulic conductivity. Also other aquifer properties like the storativity coefficient vary in space, but the spatial variability of hydraulic conductivity is thought to be the most consequential one (Smith and Schwartz, 1981ab). The stochastic subsurface hydrology and mass transport literature focus nearly exclusively on the spatial variability of hydraulic conductivity.

The alternative for a stochastic approach would be a deterministic one. However, the disadvantage of such an approach is that not enough information is available to determine the hydraulic conductivity for each point of the aquifer. One could use a uniform hydraulic conductivity obtained by averaging the sample values, or divide the aquifer in a limited number of zones with a constant hydraulic conductivity. However, this approach results in biased estimates of groundwater flow velocities. A smooth representation of hydraulic conductivity will not capture the highest and lowest groundwater flow velocities. Even the use of a kriged hydraulic conductivity field as the input to the groundwater flow equation will miss the paths with the highest and lowest groundwater flow velocities.

To capture the fast particle travel paths, related with high hydraulic conductivities and high groundwater flow velocities, it is necessary that the input hydraulic conductivity field to the groundwater flow equation has the spatial variability observed in the field. However, due to the fact that the exact position of zones with high and low hydraulic conductivity is uncertain, a statistical model should be built with the probability density functions of all the local hydraulic conductivities. A spatial random function model is adopted to model the spatial variability of one or more spatially variable attributes. Multiple equally likely realisations can be generated from the random function model adopted. Each of the realisations has a "natural" spatial variability, but due to the fact that they have been built from a limited amount of data the locations with high and low hydraulic conductivity differ between the realisations. In Chapter 2 details are presented on the random function model, its parametrization and the generation of multiple realisations from it.

The stochastic approach, in which multiple equally likely realisations of hydraulic conductivity (and possibly other parameters) are used as input to the groundwater flow equation, results also in multiple equally likely outputs of the groundwater flow and mass transport equation. As a result the uncertainty in the predictions of groundwater flow and mass transport can be evaluated after solving the groundwater flow and mass transport equation for a sufficiently large number of realisations. In case we want to predict the transport of a contaminant from a repository to the biosphere, the probability

density function of the travel times of the radionuclides from the repository to the biosphere can be obtained.

The uncertainty is not just related with the spatial variability of input parameters to the groundwater flow and mass transport equations. Also the following sources of uncertainty, relevant for the prediction of groundwater flow and mass transport exist:

- Measurement errors. The available measurement data may be incorrect due to equipment failure or human failure. It is important to estimate the magnitude of possible measurement errors. Measurement errors are usually included in the parametrization of the adopted random function model. In section 4.2 special attention is paid to this type of uncertainty.
- Conceptualization errors. This means that physical or chemical processes that occur in reality are not included in the model. It may also refer to an incorrect delimitation of the study area (the aquifer) or the use of wrong boundary conditions. Examples are neglecting diffusion of contaminants in the rock matrix or neglecting density-driven groundwater flow in case of considerable differences in the groundwater density in the study domain. In this dissertation errors in the boundary conditions have been considered.
- Numerical errors. The solution of the groundwater flow and mass transport equation is an approximation. Care should be taken that a sufficient accurate solution of the state equations is obtained and that the set tolerance for iterative methods is sufficiently low. Normally the modeller is able to control the numerical errors.

The groundwater flow and mass transport equation can be solved numerically or analytically (see e.g. De Marsily, 1986; Kinzelbach, 1986 and Zheng and Bennett, 1995). However, for an analytical solution restrictive assumptions like homogeneous aquifer properties have to be made. Semi-analytical solutions (e.g. Bakr *et al.*, 1978; Gutjahr *et al.*, 1978; Dagan, 1982ab; Gelhar and Axness, 1983; Gelhar, 1986) can handle the spatial variability of hydraulic conductivity, but also these solutions can only be applied under relative restrictive assumptions like a small hydraulic conductivity variance, simple aquifer geometries and boundary conditions. In this dissertation numerical methods are used to solve the groundwater flow and mass transport equation so that solutions are obtained for strongly heterogeneous aquifers, irregular aquifers, complex boundary conditions, fractured media and the like.

1.3 Reducing the uncertainty: inverse modelling

Multiple equally likely realisations of hydraulic conductivity and other parameters are easily conditioned to hydraulic conductivity data and those parameters or state variables linearly linked with the attributes being modelled. However, conditioning spatial images of hydraulic conductivity to hydraulic head data or concentration data is less straightforward. Hydraulic conductivity

and hydraulic head are non-linearly related by the groundwater flow equation and hydraulic conductivity and contaminant concentration are non-linearly related through the coupled groundwater flow and mass transport equations. Determining input parameters to the groundwater flow and mass transport equation that reproduce the hydraulic head and contaminant concentration data is commonly known as the inverse problem.

The main idea is that hydraulic head data contain, indirectly, important information on the aquifer properties so that it is important to incorporate this information in the characterisation process. Furthermore, concentration data also contain important information on the aquifer properties. The aim is therefore to condition the hydraulic conductivity and other parameters to head and concentration measurements so that the input parameters to the groundwater flow and mass transport equation reproduce the measured head and concentration data. It is expected that the calibrated input data that reproduce the head and concentration data are closer to the real parameter values than the input data that could not reproduce the head and concentration data.

However, the traditional inverse problem is known to be ill-posed. The ill-posedness refers to (Carrera and Neuman, 1986b):

- The non-solvability of the problem. In this case no solution can be found because the observations are not within the range of the model.
- The non-uniqueness of the solution. This occurs if the model is not a one-to-one mapping between the observation domain and the parameter domain.
- The instability of the problem. This is the case if the inverse solution exists but is not continuous on the observation domain.

In general, it is impossible to find a unique solution because there is little experimental information and the aim may be the estimation of many parameters, like for example the hydraulic conductivities, on a fine grid that covers the aquifer. Not a unique solution exists to this problem and many possible solutions can be found that reproduce the experimental information. There are two main traditional approaches to reduce the non-uniqueness and the instability: zonation and interpolation. In the zonation approach the aquifer is divided in a limited number of zones for which the aquifer parameters are estimated (e.g. Carrera and Neuman, 1986abc). In the interpolation approach a limited number of geostatistical parameters is estimated and with help of the estimated parameters and the measurement data a smoothly varying estimate of one or more of the aquifer parameters is obtained (e.g. Kitanidis and Vomvoris, 1983). However, in the approach followed in this dissertation there is no identifiability problem because many equally likely solutions are obtained, and not just one single solution. Each of the equally likely solutions is conditioned to information on the state variables. Furthermore, the drawbacks of the zonation approach and the interpolation approach are avoided. In both cases a smoothed representation of the transmissivity field is obtained, that will not be able to reproduce the highest and lowest groundwater velocities in the

study area. However, in case each of the equally likely solutions is conditioned to information on the state variables, as is the approach followed in this dissertation, there is no identifiability problem because many equally likely solutions are obtained, and not just one single solution.

The sequential self-calibrating method (SCM) (Sahuquillo *et al.*, 1992; Gómez-Hernández *et al.*, 1997; Capilla *et al.*, 1997) was developed to obtain realistic estimates of state variables of the aquifer together with an uncertainty model. In this purpose, estimates of the aquifer parameters had to reflect the spatial variability as observed in the field. The method strives to integrate as much information as possible by conditioning the realisations to the maximum amount of data possible.

This dissertation presents an extension of the SCM to:

- Transient groundwater flow and the generation of spatially variable storativities.
- 3-D groundwater flow and groundwater flow in fractured media.
- The coupled inverse modelling of groundwater flow and mass transport, with conditioning to both piezometric head and concentration data.

1.4 Outline of the dissertation

This dissertation is about the stochastic inverse modelling of groundwater flow. The aim is to build multiple equally likely models of the aquifer parameters that are conditioned to hydraulic head and concentration data. This approach allows to quantify the uncertainty in the predictions, which is one of the main objectives of the approach. In the research related with this dissertation the following topics were tackled:

- Conditioning to transient head data. Transient head data carry information on the aquifer properties. This information may be used to improve the characterisation of the spatially variable hydraulic conductivities. Transient head data also allow to condition the storativity coefficients. The SCM (Sahuquillo *et al.*, 1992; Gómez-Hernández *et al.*, 1997; Capilla *et al.*, 1997) was extended to handle transient groundwater flow and the joint conditioning of transmissivity and storativity fields.
- Impact of the amount and quality of the conditioning data. It is considered that experimental data are essential in the prediction of groundwater flow and mass transport. The aim of the inverse modelling procedure is to use the experimental information as efficiently as possible. In this dissertation we analyse the impact of the amount and quality of the conditioning data, the trade-off between hydraulic head data and hydraulic conductivity data, the impact of measurement errors in hydraulic conductivity and/or hydraulic head data, and the impact of the modeller decision on the data quality.

- The inverse modelling of 3-D groundwater flow. Frequently the simplification of a study area to a 2-D domain can not be justified, especially in case of contaminant transport modelling. Therefore the inverse modelling procedure was extended to 3-D.
- The inverse modelling of groundwater flow in 3-D fractured media. It was investigated whether the algorithm was able to generate multiple equally likely 3-D hydraulic conductivity images conditioned to steady-state and transient-state hydraulic head data for very CPU-intensive cases. Fractured media were studied in which the fractures were represented by a porous medium equivalent and in which the different fractures were treated as different statistical populations.
- The coupled inversion of groundwater flow and mass transport. Concentration data also carry important information on the aquifer properties; conditioning to these data is therefore not only considered important for improving the characterisation of the contamination plume, but also for improving the characterisation of the aquifer. Furthermore, concentration data also allow to estimate transport parameters. The SCM was further extended to the coupled inverse modelling of groundwater flow and mass transport.

The contributions of this dissertation are the following:

- A literature research on the methods for the inverse modelling of groundwater flow.
- The mathematical extension of the SCM to the incorporation of transient head data and the joint conditioning of transmissivity and storativity realisations. Furthermore, the optimisation approach was formulated and improved. The extended SCM was implemented in the software INVERTO, written in C.
- Application of the SCM for the inverse modelling of steady and transient groundwater flow in a synthetic study and two practical studies. Especial attention was paid in these studies on the data worth and the sensitivity of the obtained results.
- Analysis of the impact of the amount and quality of the conditioning data (hydraulic head and hydraulic conductivity) on the reproduction of hydraulic conductivity, hydraulic head and mass transport were studied using two extensive synthetic studies. Also the impact of some conceptual errors was studied.
- The mathematical extension of the SCM to 3-D groundwater flow and multiple statistical populations. Multiple statistical populations are introduced to handle zones in the simulation domain with clearly different geostatistical properties. The extensions were again implemented in the software INVERTO.
- The inverse modelling of 3-D groundwater flow in fractured media using a stochastic continuum approach. In a case study the fractures were implemented stochastically, while in another case study they were implemented deterministically.

- A literature research on the methods for the inverse modelling of both groundwater flow and mass transport.
- A mathematical formulation of the coupled stochastic inverse modelling of groundwater flow and mass transport. This mathematical formulation was also implemented in the software INVERTO.
- The relative worth of each of the pieces of information was studied. A synthetic study was carried out in which multiple realisations were conditioned to transmissivity data, hydraulic head data and concentration data.

Chapter 2 presents the geostatistical simulation approach and the numerical solution methods of the (forward) groundwater flow and mass transport equations. Also, a study is presented analysing the impact of different geostatistical models on the groundwater flow and mass transport predictions.

Chapter 3 contains a literature review of methods for the inverse modelling of groundwater flow. In addition, the extension of the SCM to transient groundwater flow and the joint conditioning of transmissivity and storativity is presented. Three studies in which this methodology was used (one synthetic study and two case studies) are presented in detail.

Chapter 4 handles two comprehensive synthetic studies on the impact of the amount and quality of the conditioning data on the characterisation of the head and conductivity field and the predictions of mass transport.

Chapter 5 presents a short summary on the existing approaches to model groundwater flow and mass transport in fractured media. In addition, the adopted approach for the (inverse) modelling of groundwater flow in fractured media is introduced. The chapter centres in two case studies in which the inverse modelling of groundwater flow in fractured media is studied. The two studies differ in the way the fractures are handled.

Chapter 6 presents a literature review on the most relevant existing methods for the inverse modelling of both groundwater flow and mass transport. In addition, the mathematical formulation of the coupled inverse modelling of groundwater flow and mass transport is detailed. Also computer implementation aspects are discussed. Finally, a synthetic study on the coupled inverse modelling is presented. In this study multiple realisations conditioned to transmissivity, hydraulic head and concentration data are generated. The simulated transmissivity, hydraulic head and concentration fields are compared with the reference fields for different scenarios, the scenarios differing in the amount and kind of conditioning data.

2 A stochastic numerical approach

In order to reduce the uncertainty on groundwater flow and mass transport predictions it is crucial to reduce the uncertainty on the spatial variable hydraulic conductivities (K). It is assumed that spatial variable conductivities are in general one of the main sources of uncertainty on groundwater flow predictions. Geostatistical methods can be used to incorporate information which reduces the uncertainty on the spatial variable hydraulic conductivity field.

Section 2.1 repeats basic geostatistical theory and the methods of geostatistical interpolation and simulation that are used in relation with the sequential self-calibrating method or in other studies presented in this dissertation. In this section it is explained how hydraulic conductivity measurements and soft information on hydraulic conductivities can be used in the simulation of spatial variable hydraulic conductivities realisations. In section 2.2 the numerical methods are presented which are used to solve the groundwater flow and mass transport equations. These methods have been implemented in the computer code INVERTO. At this stage we do not consider yet the presence of observations on the state variables hydraulic head or concentration. However, geostatistical simulation may have been used to condition input parameters of the groundwater flow and mass transport equations (hydraulic conductivities and storativities) to measurement data. In section 2.3 a study is presented in which numerical methods to solve the groundwater flow and mass transport equation are combined with geostatistical methods to integrate measurement data. The purpose of the study is to compare the impact of using different geostatistical methods to integrate these data.

2.1 The geostatistical approach and simulations of spatial variable attributes

This section gives a short summary on basic concepts of geostatistics and geostatistical simulation. It is shown how geostatistical simulation can be used to incorporate measurement data of aquifer parameters like hydraulic conductivity and storativity. In section 2.1.1 the random function model is presented. In section 2.1.2 and 2.1.3 some geostatistical methods are detailed which are used in studies related to this dissertation. Finally, section 2.1.4 explains the Monte Carlo approach, which forms an essential part of the methodology adopted in the sequential self-calibrating approach.

2.1.1 The Random Function Model

Throughout this dissertation a random function model is adopted for the variables like hydraulic conductivity, hydraulic head and concentration. A

random function is a set of random variables $Z(\mathbf{u})$, Z being a variable like temperature, moisture content or hydraulic conductivity and $\mathbf{u}$ a location in a domain Ω. The random variables are usually dependent. The spatial law of the random function $Z(\mathbf{u})$ is constituted by all N-variate (N being the number of random variables at different locations) cumulative distribution functions; for any positive integer N and for any choice of the locations. The N random variables relate to the same attribute at N different locations.

In practice the analysis is limited to cumulative distribution functions involving no more than two locations at a time. The one- and two-point cumulative distribution functions of the random function are location dependent. In order to determine these cumulative distribution functions and their moments repetitive measurements should be available: multiple values for the same attribute at the same location. In practice this is never possible because we will have just one value for that attribute at that specific location. The problem we are faced with is due to the adopted random function model in which each value at each location is seen as a random variable; the accidental outcome of some unknown statistical process.

The above described problem is circumvented by a decision on stationarity. The stationarity decision implies that different measurement data within the domain Ω can be pooled to estimate the mentioned one- and two-point cumulative distribution functions. It implies that the attribute is stationary in the studied domain. However, stationarity is a property of the random function model and at the same time a decision of the modeller, but not a characteristic of the studied variable. Stationarity never can be proven or rejected by means of the data: there are no repetitive samples from the studied variable at the different locations in the domain Ω.

The random function $Z(\mathbf{u})$ is stationary in Ω if the N-variate cumulative distribution function is the same for any set of N random variables. The decision on stationarity is usually limited to the one-point and two-point cumulative distribution functions, and the first two moments of the random function. A random function model is said to be stationary of order two if the expected value of an attribute exists and is constant in the domain Ω and if the two-point covariance as a function of separation distance between two points exists and only depends on that separation distance.

The adoption of a multivariate random function model is similar to a univariate random function model. Some decision on joint second-order stationarity has to be adopted.

2.1.2 Geostatistical interpolation and simulation

In this section it is explained how the parameters of the adopted random function model can be inferred from the measurement data. After inferring the

parameters from the adopted random function model unbiased estimates with minimum variance of the attribute can be obtained at any location in the studied domain. The result is a more smoothed representation of the spatial variations of the attribute value than in reality. Geostatistical interpolation, kriging, is used to obtain the unbiased estimates with minimum variance. The kriging methods are in general not so interesting for subsurface hydrology because the use of kriged fields as input parameters to the groundwater flow equation yields biased estimates of groundwater flow velocities. More interesting are geostatistical simulation methods. These methods yield multiple equally likely realisations of the attribute at any location in the domain and an unbiased estimate of the groundwater velocities may be obtained.

2.1.2.1 Inferring parameters of the Random Function Model

As explained in secton 2.1.1, a stationarity assumption has to be made in order to estimate one-point and two-point statistics of the random function model. In practice, different measurement data within the study domain are pooled together in order to estimate the statistics. The mean is estimated by calculating the arithmetical average in case no preferential sampling was done. However, it is very common in subsurface hydrology that a preferential sampling scheme is used. This may be due to physical constraints or because a zone of the study domain is of special interest. In case of a preferential sampling scheme the cell declustering technique (Deutsch and Journel, 1992) can be used to estimate the mean. Unfortunately, few attention is paid in subsurface hydrology to the impact of the sample design (number of samples, configuration) on the accuracy of the predictions.

The covariance function is calculated by plotting the separation distance of all pairs of measurement data versus the covariance for those pairs of measurement data. The result is a data set with for each of the comparison pairs a covariance and the separation distance. However, in practice, the variogram is normally used to model the spatial correlation. The definition of the variogram does not require the existence of a constant mean and finite variance for the random function. In this case a sufficient condition is that the random function increments $Z(\mathbf{u})$ - $Z(\mathbf{u}+\mathbf{h})$ ($\mathbf{h}$ being the separation distance) are stationary of order two (Goovaerts, 1997). This condition is also called the intrinsic hypothesis (Journel and Huijbregts, 1978, p. 33). The variogram is also estimated by grouping pairs of measurement data in distance classes. The pairs in one distance class have a similar, but not necessarily equal, separation distance. The variogram is estimated by:

$$\gamma^*(\mathbf{h}) = \frac{1}{2N(\mathbf{h})} \sum_{i=1}^{N(\mathbf{h})} \left[z(\mathbf{u}_i) - z(\mathbf{u}_i + \mathbf{h})\right]^2$$

where $\gamma(\mathbf{h})$ is the semi-variance for a vector $\mathbf{h}$ apart, $N(\mathbf{h})$ is the number of pairs of data locations a vector $\mathbf{h}$ apart, $z(\mathbf{u}_i)$ is the value for attribute z at location $\mathbf{u}_i$

and $z(\mathbf{u}_i+\mathbf{h})$ is the value for attribute z at a vector $\mathbf{h}$ apart from location $\mathbf{u}_i$. Normally the variogram is estimated by allowing a tolerance of $\Delta\mathbf{h}$ around the separation distance $\mathbf{h}$, in order to get enough comparison pairs in each class. After estimating the experimental semivariances for different distance classes a model variogram has to be obtained because semivariances for any possible separation vector $\mathbf{h}$ will be needed. Not any function can be used as a variogram model: the positive definite condition should hold. Some models are commonly used because they are known to be positive definite. These models are also used in the studies presented in this dissertation and are the ones that can be selected in the software that implements the sequential self-calibrating method (INVERTO).

The spherical model:

$$\gamma(h)=\begin{cases} c_0+c\left[1.5\dfrac{h}{a}-0.5\left(\dfrac{h}{a}\right)^3\right] & h\leq a \\ c_0+c & h>a \end{cases} \tag{2.1}$$

Exponential model:

$$\gamma(h)=c_0+c\left[1-\exp\left(\frac{-3h}{a}\right)\right] \tag{2.2}$$

Gaussian model:

$$\gamma(h)=c_0+c\left[1-\exp\left(\frac{-3h^2}{a^2}\right)\right] \tag{2.3}$$

Power model:

$$\gamma(h)=h^{\omega} \qquad 0<\omega<2 \tag{2.4}$$

In the expressions above c_0 is the nugget effect, c the sill minus the nugget and a the range (in case of the spherical model) or the practical range (the exponential and the Gaussian model). The nugget effect is a discontinuity at the origin of the variogram and makes that the semivariance suddenly jumps from zero for distance zero to the nugget value for a separation distance slightly larger than zero metres. The nugget effect is attributed to measurement errors and small scale variability. The range or the practical range is the distance until which spatial autocorrelation exists between data. The sill is the asymptotic maximum

semivariance value. For practical purposes, one can state that the semi-variance is very close to the sill value for distances beyond the range value.

The models are expressed here in their isotropic form, which means that the semivariance as function of the separation distance is independent of the direction. The models can be applied in 1-D, 2-D and 3-D. The positive definition condition holds for any linear combination of the models specified. A variogram model can therefore also be a combination of two or more of the specified models, each model having different values for its parameters.

Equations 2.1 until 2.4 are for isotropic variogram models. However, in subsurface hydrology we frequently have to deal with anisotropy, the change of the pattern of spatial variability with orientation. We can distinguish between geometric and zonal anisotropy. In case of geometric anisotropy the directional variograms have only different range values, but the same shapes and sill values. We could visualise this anisotropy by an ellipse. A coordinate transformation helps to model this anisotropy: the coordinate axes are rotated counter clockwise until the x-axis coincides with the main direction of spatial continuity. The next step is to rescale the ellipse to a circle with radius equal to the minor range. Zonal anistropy means that the sill value is a function of the direction. If both range values and sill values are a function of direction the modelling of the variogram consists of the following steps:

1. A first contribution to the variogram is an isotropic structure with a sill equal to the sill in the direction of less variance.
2. The second contribution only depends on the direction of the largest variance. The sill for the second contribution corresponds to the difference in sill between the direction with most variance and the perpendicular direction with less variance. Furthermore, the range for the second contribution is equal to the range in the direction of the largest variance. The second contribution is found in two steps. First, the coordinate axes are rotated counter clockwise until the x-axis identifies the direction of maximum continuity and lower variance. The rotation angle is equal to ϕ. Second, the axes are rescaled so that the second contribution does not contribute to the direction of the lowest sill. The range in the direction of the lowest sill is set to infinity. The total operation can be summarised, both for geometric and zonal anistropy, as follows:

$$\begin{Bmatrix} h'_\xi \\ h'_\eta \end{Bmatrix} = \begin{bmatrix} 1 & 0 \\ 0 & a_\xi / a_\eta \end{bmatrix} \begin{bmatrix} \cos\phi & sin\phi \\ -sin\phi & \cos\phi \end{bmatrix} \begin{Bmatrix} h_x \\ h_y \end{Bmatrix}$$

where the left hand side vector corresponds to the new coordinate values, h_x and h_y correspond to the vector of original coordinates and the two matrices take care of the transformation of the original coordinates to the new coordinate values, so that they define an isotropic model in the new coordinates. The angle ϕ is equal to the counter clockwise rotation of the x-axis to the direction of major continuity and the parameters a_ξ and a_η are the

minimum and maximum range respectively. In case of zonal anistropy a_ξ/a_η is equal to zero.

For 3-D anisotropy we may need a maximum of three angles to describe the transition from one coordinate system to the final coordinate system. However, in this dissertation a maximum of two angles is used to model 3-D anisotropy and therefore the discussion on anisotropy in 3-D is limited here to two angles. The first angle corresponds to the angle ϕ of the 2-D system. Next, the intermediate axes are rotated an angle θ counter clockwise around the former x-axis. The new coordinate system can be adjusted to the 3-D anisotropy by rescaling two of the three axes of the new coordinate system. The total operation can be summarised as follows:

$$\begin{Bmatrix} h_{\xi'} \\ h_{\eta'} \\ h_{\zeta'} \end{Bmatrix} = \begin{bmatrix} 1/a_{\xi'} & 0 & 0 \\ 0 & 1/a_{\eta'} & 0 \\ 0 & 0 & 1/a_{\zeta'} \end{bmatrix} \begin{bmatrix} \cos\phi & sin\phi & 0 \\ -sin\phi\cos\theta & \cos\phi\cos\theta & sin\theta \\ sin\phi sin\theta & -sin\theta\cos\phi & \cos\theta \end{bmatrix} \begin{Bmatrix} h_x \\ h_y \\ h_z \end{Bmatrix}$$

where a_ξ, a_η and a_ζ are the ranges along the new coordinate axes ξ, η and ζ and θ is the second rotation angle.

2.1.2.2 Geostatistical interpolation

After obtaining the parameters of the random function we can use the random function model to obtain estimates of the attribute of interest at locations where we did not have measurements (section 2.1.2.3 explains the simulation of multiple equally likely realisations, which is more interesting for applications in groundwater hydrology). The variogram model is used to obtain the model covariances. Model covariances can be obtained for any pair of locations; covariances between measurement points can be obtained and covariances between a measurement point and a location where we want to estimate the value of the attribute. The most common form of kriging is simple kriging (SK). An unbiased estimate with minimum variance for the value of an attribute at a certain location is obtained in the following way:

$$Z^*_{SK}(\mathbf{u}) = \sum_{i=1}^{n(\mathbf{u})} \lambda_i^{SK}(\mathbf{u})[Z_i(\mathbf{u}) - m] + m$$

where $n(\mathbf{u})$ is the number of data involved in the kriging estimate (for SK equal to the number of measurement data), $\lambda_i^{SK}(\mathbf{u})$ are the assigned kriging weights to each of the observation data, $Z_i(\mathbf{u})$ the data value at the i-th observation location and m the stationary constant mean. The kriging weights for each of the measurement data are obtained by solving the simple kriging system:

$$\begin{bmatrix} C(\mathbf{u}_1-\mathbf{u}_1) & \cdots & C(\mathbf{u}_1-\mathbf{u}_{n(\mathbf{u})}) \\ \vdots & \ddots & \vdots \\ C(\mathbf{u}_{n(\mathbf{u})}-\mathbf{u}_1) & \cdots & C(\mathbf{u}_{n(\mathbf{u})}-\mathbf{u}_{n(\mathbf{u})}) \end{bmatrix} \begin{Bmatrix} \lambda_1^{SK}(\mathbf{u}) \\ \vdots \\ \lambda_{n(\mathbf{u})}^{SK}(\mathbf{u}) \end{Bmatrix} = \begin{Bmatrix} C(\mathbf{u}_1-\mathbf{u}) \\ \vdots \\ C(\mathbf{u}_{n(\mathbf{u})}-\mathbf{u}) \end{Bmatrix}$$

where C are the model spatial autocovariances and the left hand side matrix contains the autocovariances between observation points and the right hand side vector the autocovariances between observation points and grid cells at which an estimation of the value for the unknown attribute Z is required. The variance of the simple kriging estimate is:

$$\sigma_{SK}^2(\mathbf{u}) = C(0) - \sum_{i=1}^{n(\mathbf{u})} \lambda_i^{SK}(\mathbf{u}) C(\mathbf{u}_i - \mathbf{u})$$

where $C(0)$ is the spatial autocovariance for separation distance zero.

Ordinary kriging allows to account for local variations in the mean by limiting the domain of stationarity to the local neighbourhood centred on the location where an estimation of the attribute value is required. Ordinary kriging is therefore more robust to non-stationarity. In chapter 3 we will see the use of ordinary kriging in the self-calibrating method. The ordinary kriging estimate is:

$$Z_{OK}^*(\mathbf{u}) = \sum_{i=1}^{n(\mathbf{u})} \lambda_i^{OK}(\mathbf{u}) Z_i(\mathbf{u})$$

The unknown local mean does not appear in the expression because it is filtered out by forcing the kriging weights to sum to one:

$$\sum_{i=1}^{n(\mathbf{u})} \lambda_i^{OK}(\mathbf{u}) = 1$$

The kriging weights are obtained then as follows:

$$\begin{bmatrix} C(\mathbf{u}_1-\mathbf{u}_1) & \cdots & C(\mathbf{u}_1-\mathbf{u}_{n(\mathbf{u})}) & 1 \\ \vdots & \ddots & \vdots & 1 \\ C(\mathbf{u}_{n(\mathbf{u})}-\mathbf{u}_1) & \cdots & C(\mathbf{u}_{n(\mathbf{u})}-\mathbf{u}_{n(\mathbf{u})}) & 1 \\ 1 & 1 & 1 & 0 \end{bmatrix} \begin{Bmatrix} \lambda_1^{OK}(\mathbf{u}) \\ \vdots \\ \lambda_{n(\mathbf{u})}^{OK}(\mathbf{u}) \\ \mu_{OK}(\mathbf{u}) \end{Bmatrix} = \begin{Bmatrix} C(\mathbf{u}_1-\mathbf{u}) \\ \vdots \\ C(\mathbf{u}_{n(\mathbf{u})}-\mathbf{u}) \\ 1 \end{Bmatrix}$$

where $\mu(\mathbf{u})$ is the Lagrange multiplier. The Lagrange multiplier has to be introduced in order to ensure that the kriging weights sum to one under the condition that an unbiased estimate with minimum variance is obtained.

The ordinary kriging variance is:

$$\sigma_{OK}^2(\mathbf{u}) = C(0) - \sum_{i=1}^{n(\mathbf{u})} \lambda_i^{OK}(\mathbf{u}) C(\mathbf{u}_i - \mathbf{u}) - \mu_{OK}(\mathbf{u})$$

In some cases it may be inappropiate to consider the mean even constant in a local neighbourhood. In such a case the local mean in a neighbourhood is modelled as a function of the coordinates. The application of kriging with a trend model is rare in subsurface hydrology applications. Normally there is no physical evidence for a varying trend. An exception is the interpolation of hydraulic head values. However, normally groundwater flow models are used to predict the hydraulic head at unvisited locations. In section 2.3 an application of geostatistical interpolation (and simulation) with a trend model is given. The kriging with trend estimator is given by:

$$Z_{KT}^*(\mathbf{u}) = \sum_{i=1}^{n(\mathbf{u})} \lambda_i^{KT}(\mathbf{u}) Z_i(\mathbf{u})$$

with the following constraints:

$$\sum_{i=1}^{n(\mathbf{u})} \lambda_i^{KT}(\mathbf{u}) f_k(\mathbf{u}_i) = f_k(\mathbf{u})$$

where f_k are unknown trend functions. $f_k(\mathbf{u}_i)$ is the function value at a measurement location and $f_k(\mathbf{u})$ is the function value at a location (grid cell) where an estimation is required. The kriging weights are obtained by solving the following kriging system (just linear trend functions are allowed in the example given bellow):

$$\begin{bmatrix} C_R(\mathbf{u}_1 - \mathbf{u}_1) & \cdots & C_R(\mathbf{u}_1 - \mathbf{u}_{n(\mathbf{u})}) & 1 & x_1 & y_1 \\ \vdots & \ddots & \vdots & 1 & \vdots & \vdots \\ C_R(\mathbf{u}_{n(\mathbf{u})} - \mathbf{u}_1) & \cdots & C_R(\mathbf{u}_{n(\mathbf{u})} - \mathbf{u}_{n(\mathbf{u})}) & 1 & x_{n(\mathbf{u})} & y_{n(\mathbf{u})} \\ 1 & 1 & 1 & 0 & 0 & 0 \\ x_1 & \cdots & x_{n(\mathbf{u})} & 0 & 0 & 0 \\ y_1 & \cdots & y_{n(\mathbf{u})} & 0 & 0 & 0 \end{bmatrix} \begin{Bmatrix} \lambda_1^{KT}(\mathbf{u}) \\ \vdots \\ \lambda_{n(\mathbf{u})}^{KT}(\mathbf{u}) \\ \mu_0^{KT}(\mathbf{u}) \\ \mu_1^{KT}(\mathbf{u}) \\ \mu_2^{KT}(\mathbf{u}) \end{Bmatrix} = \begin{Bmatrix} C_R(\mathbf{u}_1 - \mathbf{u}) \\ \vdots \\ C_R(\mathbf{u}_{n(\mathbf{u})} - \mathbf{u}) \\ 1 \\ x \\ y \end{Bmatrix}$$

where x and y are the x- and y-coordinate values at the measurement locations or the location where an estimate is required. In the expression multiple Lagrange parameters appear. The extension to interpolations in 3-D domains and higher order trend functions is straightforward. The variance of the kriging estimator with trend is:

$$\sigma_{KT}^2(\mathbf{u}) = C_R(0) - \sum_{i=1}^{n(\mathbf{u})} \lambda_i^{KT}(\mathbf{u}) C_R(\mathbf{u}_i - \mathbf{u})$$

where (**u**) again refers to locations where an estimation is required and $\mathbf{u}_i$ to one of the n measurement locations.

The spatial autocovariances cannot be obtained easily in case of the presence of a trend. The aim is to obtain a variogram from the data, which are corrected for the spatial variable mean. However, both the variogram and the spatial variable mean are unknown so that an iterative procedure is required to estimate the mean. Mathematical techniques have been developed to estimate the variogram (e.g. De Marsily, 1986), but an alternative is to estimate the variogram in the direction in which no trend seems to appear.

In case we want to estimate the value of an attribute Z and we have measurement data not only of the attribute, but also of an other attribute which shows a strong correlation with the attribute Z, kriging techniques should be used which are able to incorporate the secondary information. Many different approaches are commented in literature (see e.g. Goovaerts (1997) for an overview), but for this dissertation only ordinary cokriging is relevant:

$$Z^*_{CK}(\mathbf{u}) = \sum_{i}^{n_i(\mathbf{u})} \lambda_i^{CK}(\mathbf{u}) Z_i(\mathbf{u}) + \sum_{j}^{n_j(\mathbf{u})} \mu_j^{CK}(\mathbf{u}) Y_j(\mathbf{u})$$

where $n_i(\mathbf{u})$ is the number of data for the principal variable Z involved in the kriging estimate and $n_j(\mathbf{u})$ is the number of data for the secondary variable Y involved in the kriging estimate. $Y_j(\mathbf{u})$ is the value for the secondary variable Y at the j-th measurement location and $\mu_j(\mathbf{u})$ is the cokriging weight for that measurement location. There are two constraints:

$$\sum_{i=1}^{n_i(\mathbf{u})} \lambda_i^{CK}(\mathbf{u}) = 1$$

$$\sum_{j=1}^{n_j(\mathbf{u})} \mu_j^{CK}(\mathbf{u}) = 0$$

The cokriging weights can be obtained from the following expression:

$$\begin{bmatrix} \mathbf{K}_{ii} & \mathbf{K}_{ij} & 1_i & 0_i \\ \mathbf{K}_{ji} & \mathbf{K}_{jj} & 0_j & 1_j \\ 1_i^T & 0_j^T & 0 & 0 \\ 0_i^T & 1_j^T & 0 & 0 \end{bmatrix} \begin{Bmatrix} \lambda_i^{CK}(\mathbf{u}) \\ \lambda_j^{CK}(\mathbf{u}) \\ \mu_i^{CK}(\mathbf{u}) \\ \mu_j^{CK}(\mathbf{u}) \end{Bmatrix} = \begin{Bmatrix} [C_{ii}(\mathbf{u}_i - \mathbf{u})]^T \\ [C_{ji}(\mathbf{u}_j - \mathbf{u})]^T \\ 1 \\ 0 \end{Bmatrix}$$

where $\mathbf{K}_{ii}$, $\mathbf{K}_{ji}$, $\mathbf{K}_{ij}$ and $\mathbf{K}_{jj}$ are the matrices with the auto and cross covariances for the first and second variable; $C_{ii}(\mathbf{u}_i\text{-}\mathbf{u})$ and $C_{ji}(\mathbf{u}_j\text{-}\mathbf{u})$ are autocovariances and

cross-covariances between the data and the location where the estimate is required; 1_i, 1_j, 0_i and 0_j are unit and null vectors and the superscript T means "transposed".

The crosscovariances between the variables Y and Z should be estimated from the experimental data. Two Lagrange multipliers (μ_i and μ_j) appear in the solution of the cokriging system. They are related with the two given constraints. The cokriging variance is given by:

$$\sigma_{CK}^2(\mathbf{u}) = C_{ii}(0) - \mu_i^{CK}(\mathbf{u}) - \sum_{i=1}^{n_i(\mathbf{u})} \lambda_i^{CK}(\mathbf{u}) C_{ii}(\mathbf{u}_i - \mathbf{u}) - \sum_{j=1}^{n_j(\mathbf{u})} \lambda_j^{CK}(\mathbf{u}) C_{ji}(\mathbf{u}_j - \mathbf{u})$$

Finally, a kriging technique which also should be included in this short summary is indicator kriging (Journel, 1983). This technique has been used in the incorporation of soft information on the positions of fractures in the groundwater flow modelling at the Sellafield site (see section 5.3). Indicator kriging is a powerful parameter free interpolation technique. The measurement data are transformed into indictor data by the following transform:

$$i(\mathbf{u}; z_k) = \begin{cases} 1 & Z(\mathbf{u}) \le z_k \\ 0 & Z(\mathbf{u}) > z_k \end{cases}$$

where i is the indicator transform and z_k the treshold value. It is common in an indicator kriging study to do the indicator transform for different treshold values. These may be values of especial interest like an established critical contamination level by law. The ordinary indicator kriging estimate is:

$$I(\mathbf{u}; z_k) = \sum_{j=1}^{n(\mathbf{u})} \lambda_j^{IK}(\mathbf{u}; z_k) I_j(\mathbf{u}; z_k)$$

where I is the indicator data and z_k the treshold. The following constraint is applied:

$$\sum_{j=1}^{n(\mathbf{u})} \lambda_j^{IK}(\mathbf{u}; z_k) = 1$$

The indicator kriging weights are obtained by solving the following indicator kriging system:

$$\begin{bmatrix} C_I(\mathbf{u}_1 - \mathbf{u}_1; z_k) & \cdots & C_I(\mathbf{u}_1 - \mathbf{u}_{n(\mathbf{u})}; z_k) & 1 \\ \vdots & \ddots & \vdots & 1 \\ C_I(\mathbf{u}_{n(\mathbf{u})} - \mathbf{u}_1; z_k) & \cdots & C_I(\mathbf{u}_{n(\mathbf{u})} - \mathbf{u}_{n(\mathbf{u})}; z_k) & 1 \\ 1 & 1 & 1 & 0 \end{bmatrix} \begin{Bmatrix} \lambda_1^{IK}(\mathbf{u}; z_k) \\ \vdots \\ \lambda_{n(\mathbf{u})}^{IK}(\mathbf{u}; z_k) \\ \mu^{IK}(\mathbf{u}; z_k) \end{Bmatrix} = \begin{Bmatrix} C_I(\mathbf{u}_1 - \mathbf{u}; z_k) \\ \vdots \\ C_I(\mathbf{u}_{n(\mathbf{u})} - \mathbf{u}; z_k) \\ 1 \end{Bmatrix}$$

where the subscript I indicates that the spatial autocovariances are for the indicator transformed data. An indicator variogram is calculated in a similar way as a normal variogram; the main difference is that the indicator transform of the data is used. The indicator kriging system is normally solved several times for the same data set: the solution is calculated for different treshold values of interest.

All the presented kriging estimators have simulation equivalents. These simulation equivalents are more interesting for subsurface hydrological applications than the interpolation algorithms. The input of a kriged map of hydraulic conductivity to a groundwater flow model (the spatial variability of hydraulic conductivity is thought to be the most consequential one for the prediction of groundwater flow) yields biased estimates of groundwater flow velocities. The kriged map misses the highest and lowest hydraulic conductivity values that in reality exist. The kriging interpolator smoothes the spatial variable hydraulic conductivity field and although the kriging interpolator has convex properties the extreme kriged values are close to the highest and lowest measured value. However, it is clear that the highest and lowest measured values are normally not the highest and lowest values of all the area that is subject to study. Given that extreme hydraulic conductivities are "missed" on the kriging map, also the highest groundwater velocities won't be found with the kriged map as input to the groundwater flow simulator. This, on its turn has important consequences: the high flow paths play a crucial role in for example the escape of radioactive particles from a repository or the transport of contaminants from a pollution source.

2.1.2.3 Geostatistical simulation

Geostatistical simulation allows to generate multiple spatial realisations of an attribute. These realisations have a spatial variability comparable to what is observed in the field (the model variogram of the realisation is similar to the variogram modelled from the experimental data or the variogram adopted by the modeller).

Sequential Gaussian simulation allows to generate multiple realisations of an attribute with a multiGaussian random function model. The method consists of a series of steps:

1. The experimental data on the attribute Z have to be normal score transformed. The normality of the two-point distribution of the resulting normal-score variable is then checked. If the biGaussian assumption is not invalidated sequential Gaussian simulation could be used to simulate multiple realisations.
2. The normal score transformed data are used in the sequential simulation. A random path defines the order in which the different grid cells are visited. At each grid cell the kriging estimate and variance are obtained by solving a simple kriging system. The normal score transformed measurement data are

used in the kriging together with the values simulated at previously visited grid cells (the data set). A variogram of the normal score transformed data should be used.

3. The kriging estimate and variance define a conditional cumulative distribution function (ccdf) of the attribute at a grid cell. A value is drawn from the ccdf and added to the data set. The simulation continues for a new grid cell and continues until all grid cells are visited.
4. The simulated values for the normal score transform of the attribute are back-transformed to simulated values for the original variable.
5. Step 1 until 4 are repeated for as many realisations as necessary.

The sequential MultiGaussian simulation algorithm was also extended to simulate multiple variables jointly (Gómez-Hernández and Journel, 1993). In that case all variables are normally transformed. The simulation starts with the most important or better spatial auto-correlated variable. At each node a value is simulated for the variable in a similar way as described before. However, as a next step colocated simple cokriging is used to determine the mean and variance (and thus the ccdf) of the second variable. The normal score transformed data from the second variable, the previously simulated values for the second variable and also the previously simulated colocated value of the first variable are used in the conditioning. A simulated value is drawn from the ccdf for the second variable and added to the data set. The procedure can continue in a similar way for more variables and ends also with the back-transform of the normal-score values for all the variables.

Sequential Gaussian simulation does not allow for any significant spatial correlation of extreme values. This is due to the maximum entropy property (Goovaerts, 1997, p. 272) of the Gaussian random function model. If we calculate indicator variograms for a series of treshold values for an attribute simulated with a MultiGaussian random function model we see that the indicator variograms tend to pure nugget effect models (no spatial autocorrelation) for extreme treshold values. More over, it can be demonstrated theoretically that the little spatial autocorrelation of the extreme values is inherent to the MultiGaussian random function model.

Gómez-Hernández and Wen (1998) showed that this property of the MultiGaussian random function model may be very consequential. The spatial continuity of very low and very high conductivity values has an important impact on the groundwater flow and the transport of contaminants. The presence of a long path of high conductivity values close to a nuclear waste repository has an important impact on the travel times of radionuclides from the repository to the biosphere. If the path with high conductivities is not present in the input hydraulic conductivity field to the simulations, the risk associated with the accidental release of radionuclides from the repository will be severely underestimated. Gómez-Hernández and Wen (1998) propose to check alternative models (both with and without continuity in the extreme

values) in the simulations. They also state that from the experimental data no definitive conclusion on multigaussianity can be given. The biGaussian properties of the data set can be tested, but biGaussian properties by no means mean multiGaussian properties. However, if the data set does not seem to have biGaussian properties no multiGaussian simulation should be applied.

Sequential indicator simulation (Gómez-Hernández and Srivastava, 1990) is an approach that could be applied in case it is expected that the MultiGaussian approach is not valid. Sequential indicator simulation is more cumbersome than MultiGaussian simulation because indicator variograms for a series of treshold values have to be estimated. The approach consists of the following steps:

1. Indicator transforms of the values for attribute Z should be made. The indicator transforms should be made for K different treshold values. It is common to choose the treshold values in correspondence with the 1st decile of the experimental Z data, the 2nd decile and so on.
2. The indicator transformed data for K treshold values are used in the sequential simulation. A random path defines the order in which the different grid cells are visited. At each grid cell the indicator kriging estimates are obtained by solving an indicator kriging system for each treshold value. The indicator transformed measurement data and the values simulated at previously visited grid cells (the data set) are used as conditioning information in the kriging. For each treshold value a different indicator variogram is used.
3. The indicator kriging estimates for the K treshold values are used to build a complete ccdf. However, the following problems may occur:
   - The indicator kriging estimate has a value below zero or above one. This problem may occur because the kriging estimator has non-convex properties.
   - The indicator kriging estimates are not a non-decreasing function of the treshold values. This is possible because the indicator kriging system is separately solved for each of the treshold values. An extreme case could be that for two succeeding treshold values the indicator transformed data set is the same. In case different indicator variograms are adopted for the two treshold values, at some grid cells the kriged value for the higher treshold value may be lower than the kriged value for the lower treshold value. These problems can be in big part avoided by not defining classes without any datum and not adopting indicator variogram models that change suddenly between two treshold values.

   Also a posteriori methods can be used to correct the simulated ccdf´s at each grid cell. In order to build a complete ccdf at each grid cell some interpolation between the K treshold values has to be made. Furthermore, an extrapolation beyond the smallest treshold and the largest treshold are necessary. Different interpolation/extrapolation models can be used, but it is common to interpolate linearly between the treshold values, while a power or hyperbolic model is used to extrapolate beyond the tresholds.

4. A value is drawn from the ccdf and added to the data set. The simulation continues for a new grid cell and continues until all grid cells are visited.
5. Step 1 until 4 are repeated for as many realisations as necessary.

The sequential indicator simulation can be extended to simulate multiple variables in a similar way as for the MultiGaussian sequential simulation. Sequential indicator cosimulation is also used to include soft information in the simulation of the principal variable. An example of the use of soft information in the sequential indicator simulation is found in section 5.3. Geological information is used in that study in the simulation of hydraulic conductivity fields.

2.1.2.4 Monte Carlo approach

The common approach in this dissertation is to use multiple equally likely realisations of hydraulic conductivity in a Monte Carlo study of groundwater flow and mass transport. Also other input parameters of the groundwater flow and mass transport equation (storativity coefficients, boundary conditions, retardation coefficients) may be stochastically characterised. The Monte Carlo method consists of calculating the solution of the groundwater flow and possibly also the mass transport problem for each of the realisations. The output parameters (hydraulic head and mass concentration as a function in space and time) can be analysed statistically. The construction of a multivariate probability distribution function as input to the groundwater flow and mass transport equation results also in a multivariate probability distribution function of the output parameters. In section 2.1.2.3 the generation of multiple equally likely realisations was discussed. This procedure is used to generate hydraulic conductivity realisations conditioned to hard and soft conductivity data. The next step is to solve the groundwater flow and mass transport equations for each of these realisations. Section 2.2 presents the numerical methods for solving groundwater flow and mass transport. Figure 2.1 illustrates the Monte Carlo approach.

The advantages of the Monte Carlo approach as compared with semi-analytical approaches are the following:

- Analytical methods involve some kind of linear approximation. However, this linear approximation is only approximately valid for hydraulic conductivity variances below one. The Monte Carlo approach is not limited by some hydraulic conductivity variance, although for very large variances in CPU-intensive cases (> 10,000 grid cells) it is more difficult to find the numerical solution of the groundwater flow equation that is close enough to the unknown, real solution. In other words, the iterative groundwater flow solver may not be able to find a good enough solution in those specific cases.
- Analytical methods involve in general simplifying approximations of the aquifer boundaries and these methods are not able to handle complicated

aquifer configurations. Monte Carlo methods can handle much more easily these complicated aquifer configurations.

- The Monte Carlo method makes it possible to estimate the complete probability distribution of a variable at each grid cell of the numerical models. The analytical methods generally just yield the first two moments of the output variables.
- The Monte Carlo method is able to handle various input variables with multivariate probability density functions. This is more problematic in an analytical approach.
- A mixture of multiple population systems can be handled (see for instance section 5.3) by the Monte Carlo method. This is more complicated for the analytical method.
- Analytical methods are restricted to a MultiGaussian spatial distribution of the hydraulic conductivities. Monte Carlo methods also can handle non MultiGaussian spatial distributions.
- The above mentioned restrictions of the analytical methods are even more apparent for the inverse modelling of groundwater flow.

Of course analytical methods also have advantages over numerical methods and the Monte Carlo approach such as less CPU-time and the possibility to calculate an exact solution in any desired point in space and time. However, it is evident that for the goals of the research presented in this dissertation (see Chapter 1) the Monte Carlo method was the best approach.

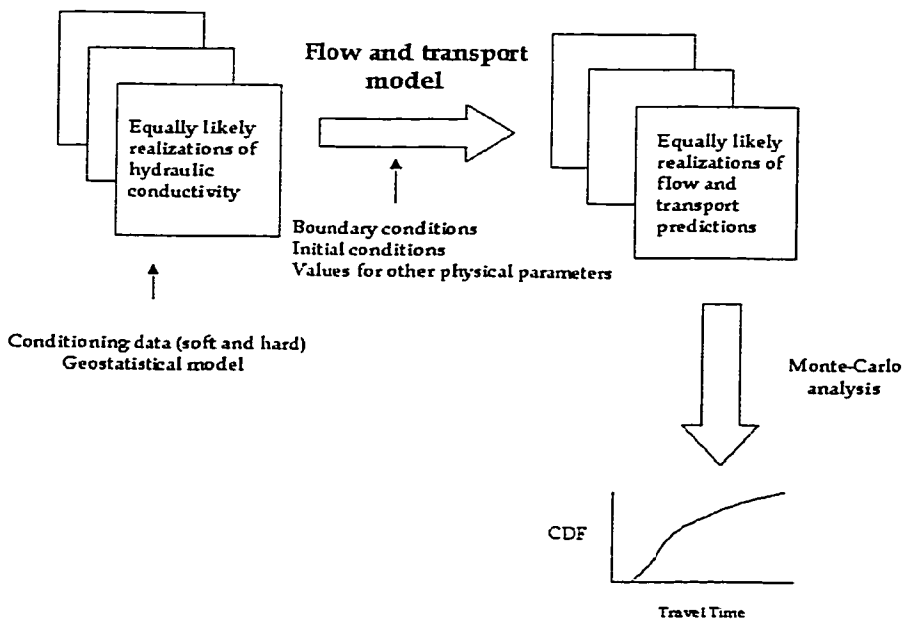

Figure 2.1 Schematic illustration of the Monte-Carlo method.

2.2 Groundwater flow and mass transport equations

Realisations of spatial variable hydraulic conductivity (and probably also storativity), generated by geostatistical simulation methods (see section 2.1.2.3) that incorporate hard and soft information are used as input to groundwater flow simulations and mass transport simulations. If the realisations are used in a Monte Carlo approach it is possible to obtain an ensemble of equally likely solutions of the groundwater flow problem and, if required, the contaminant mass transport problem. In section 2.2.1 the numerical solution of the groundwater flow problem is detailed. In section 2.2.2 two different approaches that are used to solve a contaminant mass transport problem are presented. The numerical methods used to solve the groundwater flow problem and the mass transport problem are implemented in the code for the inverse modelling of groundwater flow and mass transport named INVERTO. In Chapter 3 and Chapter 6 the details of the algorithm for the inverse modelling of groundwater flow and mass transport are presented; in this section just the forward formulations of the state equations are handled.

2.2.1 Solving the groundwater flow equation

The 3-D constant density transient groundwater flow equation for heterogeneous media is given by (e.g. De Marsily, 1986):

$$\frac{\partial}{\partial x}(K(x,y,z)\frac{\partial h}{\partial x})+\frac{\partial}{\partial y}(K(x,y,z)\frac{\partial h}{\partial y})+\frac{\partial}{\partial z}(K(x,y,z)\frac{\partial h}{\partial z})+ \\ q(x,y,z,t)=S_s(x,y,z)\frac{\partial h}{\partial t} \tag{2.5}$$

in which x, y and z are the spatial co-ordinates [L], K is hydraulic conductivity [L/T], h is hydraulic head also function of space and time [L], q are sinks and sources [T^{-1}], S_s is specific storage [L^{-1}] and t is time [T]. This equation may be simplified in some specific cases. The most frequent applied simplifications in practice are:

- Time dependent variations in groundwater flow are neglected and steady-state groundwater flow is modelled; $\partial h/\partial t=0$ and the right hand side of the equation cancels. In case also recharge and discharge can be neglected ($q(x,y,z,t)=0$) the equation reduces further to the Laplace type steady-state groundwater flow equation.
- In case the vertical dimension of the aquifer is limited compared to the horizontal extension, the vertical component of the groundwater flow may be neglected setting $\partial h/\partial z=0$, in which case a term disappears from equation 2.5. In that case we model the 2-D horizontal groundwater flow so that instead of the hydraulic conductivity the spatial variable transmissivity $T(x,y)$ is used, q is expressed in [L/T] and $S(x,y)$ is the spatial variable dimensionless storativity coefficient integrated over depth. T and S are given in the 2-D case by the following equations:

$$T(x,y) = K(x,y,z)b(x,y)$$

$$S(x,y) = S_s(x,y,z)b(x,y)$$

in which $b(x,y)$ is the spatially variable aquifer depth. Throughout this dissertation storativity coefficient is used as the terminology for both S and S_s.

- It is frequent that the storativity coefficient is considered to be constant in space if there is no evidence for a strong spatial variability. On the contrary, in the different studies that have been carried out for this dissertation hydraulic conductivity always is considered spatially variable. Spatial variability in hydraulic conductivity is considered to be the most consequential one with respect to uncertainties in the prediction of groundwater flow (Smith and Schwartz, 1981ab).

The transient groundwater flow equation for heterogeneous media is solved by numerical methods. Semi-analytical methods are suitable to approximate the solution of the groundwater flow equation for heterogeneous media with a natural log conductivity inferior to one. However, here the interest is to solve the groundwater flow equation not only for aquifers with small hydraulic conductivity variance, but also for aquifers with a (very) large hydraulic conductivity variance. Finite differences or finite elements are the most common methods to solve the groundwater flow equation (see e.g. Kinzelbach, 1986; Wang and Anderson, 1982; Zheng and Bennett, 1995). An important advantage of finite elements is that the elements can be adjusted to the aquifer boundaries and refined around pumping and injection locations. In spite of these advantages a finite difference approximation is implemented for the following reasons:

- Finite elements methods are more CPU intensive. In case of forward simulations this would only be a minor problem, but in case of inverse modelling in which the groundwater flow equation has to be solved numerous times and for numerous different conductivity fields this is a serious limitation.
- The treatment of input and output data and the graphical display would be more complicated and would probably need the development of specialised software. The problem of variable support is also difficult to handle.

The finite difference approach consists of three main steps:

1. The spatial-temporal domain is discretized. A grid divides the flow region and the time interval is divided into time steps.
2. The partial derivatives of the groundwater flow equation are approximated by finite differences, which results in a linear system of equations.
3. This linear system of equations is solved and the nodal head values are obtained.

A fully implicit solution to the transient groundwater flow equation is calculated. An implicit solution is unconditionally stable; therefore the instability problems of the explicit solution are avoided.

The aquifer we consider has a regular parallel-piped shape, with nx cells in the x-direction, ny cells in the y-direction and nz cells in the z-direction. The total number of grid cells is equal to N (nx x ny x nz). A cell is indicated by the indices (i,j,k), i being the counter on x, j the counter on y and k the counter on z. The flow is solved for nt time steps and t is the time step counter.

The finite difference approximation replaces the partial derivatives by its numerical approximations. For example, the partial derivative $\partial h/\partial x$ for cell (i,j,k) is approximated by:

$$\frac{\partial}{\partial x}\left(K(x,y,z)\frac{\partial h}{\partial x}\right) \approx \frac{1}{\Delta x_{ijk}}\left(K_{ijk,i-1jk}\frac{h_{i-1jk}-h_{ijk}}{\Delta x_{ijk,i-1jk}}\right)+\frac{1}{\Delta x_{ijk}}\left(K_{ijk,i+1jk}\frac{h_{i+1jk}-h_{ijk}}{\Delta x_{ijk,i+1jk}}\right)$$

in which $K_{ijk,i-1jk}$ en $K_{ijk,i+1jk}$ are interblock hydraulic conductivities between cells $(i-1,j,k)$ and (i,j,k) and the cells (i,j,k) and $(i+1,j,k)$, Δx_{ijk} is the grid cell width along the x-direction and $\Delta x_{ijk,i-1jk}$ is the distance along the x-direction between the grid cell centres of (i,j,k) and $(i-1,j,k)$. The interblock hydraulic conductivities are estimated by the geometric or the harmonic average. The geometric average between the neighbouring cells (i,j,k) and $(i-1,j,k)$ is given by:

$$K_{ijk,i-1jk} = \sqrt{K_{ijk}K_{i-1jk}}$$

The harmonic average is given by:

$$K_{ijk,i-1jk} = \frac{2K_{ijk}K_{i-1jk}}{K_{ijk}+K_{i-1jk}}$$

The partial derivative with respect to time is estimated by:

$$\frac{\partial h}{\partial t} \approx \frac{h_{ijk}^{t+1}-h_{ijk}^{t}}{\Delta t}$$

Where the hyperscript is used to refer to the time step. Replacing all partial derivatives by finite differences approximations and considering parallelepiped grid cells results in the following equation for an active grid cell (i,j,k) whose neighbour grid cells are also active:

$$
\begin{aligned}
&K_{ijk,i-1jk}\Delta y_{ijk}\Delta z_{ijk}\frac{h_{i-1jk}^{t+1}-h_{ijk}^{t+1}}{\Delta x_{ijk,i-1jk}}+K_{ijk,i+1jk}\Delta y_{ijk}\Delta z_{ijk}\frac{h_{i+1jk}^{t+1}-h_{ijk}^{t+1}}{\Delta x_{ijk,i+1jk}}+\\
&K_{ijk,ij-1k}\Delta x_{ijk}\Delta z_{ijk}\frac{h_{ij-1k}^{t+1}-h_{ijk}^{t+1}}{\Delta y_{ijk,ij-1k}}+K_{ijk,ij+1k}\Delta x_{ijk}\Delta z_{ijk}\frac{h_{ij+1k}^{t+1}-h_{ijk}^{t+1}}{\Delta y_{ijk,ij+1k}}+\\
&K_{ijk,ijk-1}\Delta x_{ijk}\Delta y_{ijk}\frac{h_{ijk-1}^{t+1}-h_{ijk}^{t+1}}{\Delta z_{ijk,ijk-1}}+K_{ijk,ijk+1}\Delta x_{ijk}\Delta y_{ijk}\frac{h_{ijk+1}^{t+1}-h_{ijk}^{t+1}}{\Delta z_{ijk,ijk+1}}+q_{ijk}^{t+1}=\\
&S_{ijk}\Delta x_{ijk}\Delta y_{ijk}\Delta z_{ijk}\frac{h_{ijk}^{t+1}-h_{ijk}^{t}}{\Delta t}
\end{aligned}
\tag{2.6}
$$

where Δx, Δy and Δz are the grid cell sizes or the distances between the centres of two adjacent grid cells in the x-, y- and z-direction respectively. In the equation the convention is used that a positive q [L^3T^{-1}] corresponds to recharge and a negative q to discharge. The unity of storativity is per metre [L^{-1}]. Rearranging gives:

$$
\begin{aligned}
&K_{ijk,i-1jk}\Delta y_{ijk}\Delta z_{ijk}\frac{h_{i-1jk}^{t+1}}{\Delta x_{ijk,i-1jk}}+K_{ijk,i+1jk}\Delta y_{ijk}\Delta z_{ijk}\frac{h_{i+1jk}^{t+1}}{\Delta x_{ijk,i+1jk}}+K_{ijk,ij-1k}\Delta x_{ijk}\Delta z_{ijk}\frac{h_{ij-1k}^{t+1}}{\Delta y_{ijk,ij-1k}}+\\
&K_{ijk,ij+1k}\Delta x_{ijk}\Delta z_{ijk}\frac{h_{ij+1k}^{t+1}}{\Delta y_{ijk,ij+1k}}+K_{ijk,ijk-1}\Delta x_{ijk}\Delta y_{ijk}\frac{h_{ijk-1}^{t+1}}{\Delta z_{ijk,ijk-1}}+K_{ijk,ijk+1}\Delta x_{ijk}\Delta y_{ijk}\frac{h_{ijk+1}^{t+1}}{\Delta z_{ijk,ijk+1}}-\\
&(\frac{\Delta y_{ijk}\Delta z_{ijk}K_{ijk,i-1jk}}{\Delta x_{ijk,i-1jk}}+\frac{\Delta y_{ijk}\Delta z_{ijk}K_{ijk,i+1jk}}{\Delta x_{ijk,i+1jk}}+\frac{\Delta x_{ijk}\Delta z_{ijk}K_{ijk,ij-1k}}{\Delta y_{ijk,ij-1k}}+\frac{\Delta x_{ijk}\Delta z_{ijk}K_{ijk,ij+1k}}{\Delta y_{ijk,ij+1k}}+\\
&\frac{\Delta x_{ijk}\Delta y_{ijk}K_{ijk,ijk-1}}{\Delta z_{ijk,ijk-1}}+\frac{\Delta x_{ijk}\Delta y_{ijk}K_{ijk,ijk+1}}{\Delta z_{ijk,ijk+1}}-\frac{S_{ijk}\Delta x_{ijk}\Delta y_{ijk}\Delta z_{ijk}}{\Delta t})h_{ijk}^{t+1}+q_{ijk}^{t+1}=\\
&-\frac{S_{ijk}\Delta x_{ijk}\Delta y_{ijk}\Delta z_{ijk}}{\Delta t}h_{ijk}^{t}
\end{aligned}
$$

The system of equations can be expressed in the following way:

$$
\left([A]-\frac{[D]}{\Delta t}\right)\{h^{t+1}\}+\{q\}=-\frac{[D]}{\Delta t}\{h^{t}\} \tag{2.7}
$$

where A is the N x N conductance matrix, h the N x 1 vector with nodal heads at time step t or t+1, q the N x 1 vector with recharges and discharges, D the N x N storage matrix and Δt the time step.

The matrix A contains the elements A_{lm} (l=1, ..., N; m=1, ..., N). Each row l of the matrix A refers to one of the active cells and only has a maximum seven non-zero values. The elements that can be non-zero are those for which m refers to a grid cell located north (N), south (S), west (W), east (E), up (U) or down (D) to the active cell ($m \in \{N, S, W, E, U, D\}$), and for the diagonal element. The

following expressions are found for the elements of A in case both l and m refer to active grid cells:

$$A_{lm} = K_{lm} \frac{\Delta x_l \Delta z_l}{\Delta y_{lm}} \qquad m \in \{N, S\}$$

$$A_{lm} = K_{lm} \frac{\Delta y_l \Delta z_l}{\Delta x_{lm}} \qquad m \in \{W, E\}$$

$$A_{lm} = K_{lm} \frac{\Delta x_l \Delta y_l}{\Delta z_{lm}} \qquad m \in \{U, D\}$$

$$A_{ll} = -\sum_{m \in \{N,S\}} \frac{\Delta x_l \Delta z_l K_{lm}}{\Delta y_{lm}} - \sum_{m \in \{W,E\}} \frac{\Delta y_l \Delta z_l K_{lm}}{\Delta x_{lm}} - \sum_{m \in \{U,D\}} \frac{\Delta x_l \Delta y_l K_{lm}}{\Delta z_{lm}}$$

where we have changed the indexing as follows:

$$K_{lm} = K_{ijk,i-1jk} \qquad m \in \{W\}$$

$$K_{lm} = K_{ijk,i+1jk} \qquad m \in \{E\}$$

$$K_{lm} = K_{ijk,ij-1k} \qquad m \in \{S\}$$

$$K_{lm} = K_{ijk,ij+1k} \qquad m \in \{N\}$$

$$K_{lm} = K_{ijk,ijk-1} \qquad m \in \{D\}$$

$$K_{lm} = K_{ijk,ijk+1} \qquad m \in \{U\}$$

$$\Delta x_l = \Delta x_{ijk}$$

$$\Delta y_l = \Delta y_{ijk}$$

$$\Delta z_l = \Delta z_{ijk}$$

$$\Delta x_{lm} = \Delta x_{ijk,i-1jk} \qquad m \in \{W\}$$

$$\Delta x_{lm} = \Delta x_{ijk,i+1jk} \qquad m \in \{E\}$$

$$\Delta y_{lm} = \Delta y_{ijk,ij-1k} \qquad m \in \{S\}$$

$$\Delta y_{lm} = \Delta y_{ijk,ij+1k} \qquad m \in \{N\}$$

$$\Delta z_{lm} = \Delta z_{ijk,ijk-1} \qquad m \in \{D\}$$

$$\Delta z_{lm} = \Delta z_{ijk,ijk+1} \qquad m \in \{U\}$$

Each element q_l of vector $\{q\}$ contains the sum of recharge and discharge at grid cell l. For matrix D only the diagonal elements corresponding to active cells are non-zero:

$$D_{ll} = S_l \Delta x_l \Delta y_l \Delta z_l$$

Equation 2.7 for time step t+1 can be expressed more compact:

$$[\xi]\{h^{t+1}\} = \{\beta\} \tag{2.8}$$

For grid cell l the following equation is obtained:

$$\xi_W h_W^{t+1} + \xi_E h_E^{t+1} + \xi_N h_N^{t+1} + \xi_S h_S^{t+1} + \\ \xi_U h_U^{t+1} + \xi_D h_D^{t+1} + \xi_l h_l^{t+1} = \beta_l$$

in which the coefficients ξ are elements of the NxN matrix $[\xi]$. The following subscripts have been used: l is the reference grid cell, W stands for the grid cell west of it, E for the grid cell east of it, N north of it, S south of it, U for the grid cell above it and D for the grid cell below it. The coefficients ξ replace the interblock conductivities, cell widths, storativity coefficient and time step of equation 2.6. The β_i accounts for sinks and sources, the head solution at time t, the storativity coefficient and the timestep and is an element of the Nx1 vector β. The expressions for the coefficients are (grid cell and neighbour grid cells are active):

$$\xi_m = A_{lm} \qquad m \in \{N, S, E, W, U, D\}$$

$$\xi_l = A_{ll} - \frac{D_l}{\Delta t}$$

$$\beta_l = -\frac{D_{ll}}{\Delta t} h_l^t - q_l^{t+1}$$

The time dependent solution of the system state is obtained by consecutively solving system (2.8) for each time step starting with h^0 equal to the initial conditions.

The elements of [A] and {q} and [D] are slightly modified when the active cell or one of the neighbouring cells are of prescribed head. In case that grid cell l is a prescribed head value then the only non-zero values at row l of equation 2.7 are:

$$A_{ll} = 1$$

$$q_l = h_l^{\Gamma}$$

where h_l^{Γ} is the prescribed head value at grid cell l.

The elements of matrix A at row l when neighbouring cell m is of prescribed head also change. Below there is an example for a grid cell with no recharge or discharge and to the east of which there is a prescribed head value of h_m^{Γ}.

$$A_{lm} = 0$$

$$q_l = -K_{lm} \frac{\Delta y_l \Delta z_l}{\Delta x_{lm}} h_m^{\Gamma}$$

Besides prescribed head boundary conditions also prescribed flux boundary conditions (including impermeable boundaries) can be considered. Prescribed head values, prescribed flux values and impermeable grid cells are not only placed on boundaries, but may also be placed at no-boundary grid cells. Both internal and boundary prescribed head or flux values may be variable in time.

After building the linear system of equations an efficient and accurate method has to be used to find the head solution. In section 3.3 details are given on the methods used to solve the linear system of equations.

2.2.2. Solving the mass transport equation

The 3-D mass transport equation is given by (e.g. De Marsily, 1986):

$$\frac{\partial}{\partial x}\left(\frac{D_{xx}}{R}\frac{\partial c}{\partial x}+\frac{D_{xy}}{R}\frac{\partial c}{\partial y}+\frac{D_{xz}}{R}\frac{\partial c}{\partial z}\right)+\frac{\partial}{\partial y}\left(\frac{D_{yx}}{R}\frac{\partial c}{\partial x}+\frac{D_{yy}}{R}\frac{\partial c}{\partial y}+\frac{D_{yz}}{R}\frac{\partial c}{\partial z}\right)+ \tag{2.9}$$
$$\frac{\partial}{\partial z}\left(\frac{D_{zx}}{R}\frac{\partial c}{\partial x}+\frac{D_{zy}}{R}\frac{\partial c}{\partial y}+\frac{D_{zz}}{R}\frac{\partial c}{\partial z}\right)-\frac{\partial}{\partial x}\left(c\frac{v_x}{R}\right)-\frac{\partial}{\partial y}\left(c\frac{v_y}{R}\right)-\frac{\partial}{\partial z}\left(c\frac{v_z}{R}\right)-\lambda_D c+\frac{q_s}{\phi}c_s=\frac{\partial c}{\partial t}$$

in which x, y and z are the spatial co-ordinates [L], D_{xx}, D_{xy}, D_{xz}, D_{yx}, D_{yy}, D_{yz}, D_{zx}, D_{zy} and D_{zz} are the elements of the dispersivity tensor D [L^2/T], c is the mass concentration [M/L^3], R is the retardation coefficient [-], v is the seepage groundwater flow velocity [L/T], λ_D is the decay constant [T^{-1}], q_s is the flow rate of a fluid source or sink per unit aquifer volume [T^{-1}], ϕ is the aquifer porosity [-], c_s is equal to the contaminant concentration if it is a sink, if it is a source it is the concentration of the fluid source [M/L^3] and t is time [T]. The groundwater velocity, and therefore also the elements of the dispersivity tensor vary in space and, in case of transient groundwater flow, also in time. The retardation coefficient and the porosity may also vary in space. It is assumed that only linear equilibrium adsorption occurs. In case of non-linear adsorption, the retardation coefficient would be a function of concentration and the equation would be expressed differently. In case of non-equilibrium adsorption, reaction kinetics would have to be introduced in the equation. Pore groundwater velocity is given by:

$$\begin{Bmatrix} v_x \\ v_y \\ v_z \end{Bmatrix} = -\frac{1}{\phi}\begin{bmatrix} K_{xx} & K_{yx} & K_{zx} \\ K_{xy} & K_{yy} & K_{zy} \\ K_{xz} & K_{yz} & K_{zz} \end{bmatrix}\begin{Bmatrix} \partial h/\partial x \\ \partial h/\partial y \\ \partial h/\partial z \end{Bmatrix}$$

The groundwater flow velocities are easily obtained from the solution of the groundwater flow equation. The dispersion tensor D consists of the following elements:

$$D=\begin{bmatrix} D_{xx} & D_{yx} & D_{zx} \\ D_{xy} & D_{yy} & D_{zy} \\ D_{xz} & D_{yz} & D_{zz} \end{bmatrix}$$

$$D_{xx}=\alpha_L\frac{v_x^2}{v}+\alpha_T\frac{v_y^2}{v}+\alpha_T\frac{v_z^2}{v}$$

$$D_{xy}=D_{yx}=(\alpha_L-\alpha_T)\frac{v_x v_y}{v}$$

$$D_{xz} = D_{zx} = (\alpha_L - \alpha_T)\frac{v_x v_z}{v}$$

$$D_{yz} = D_{zy} = (\alpha_L - \alpha_T)\frac{v_y v_z}{v}$$

$$D_{yy} = \alpha_T \frac{v_x^2}{v} + \alpha_L \frac{v_y^2}{v} + \alpha_T \frac{v_z^2}{v}$$

$$D_{zz} = \alpha_T \frac{v_x^2}{v} + \alpha_T \frac{v_y^2}{v} + \alpha_L \frac{v_z^2}{v}$$

where α_L is longitudinal dispersivity [L], α_T transversal dispersivity [L] and v is the modulus of the groundwater pore velocity [L/T].

In the different studies carried out for this dissertation the groundwater flow equation has been solved in two very different ways: an Eulerian and a Lagrangian solution method are used. The Eulerian solution method is also the basis for the inverse modelling of coupled groundwater flow and mass transport (see Chapter 6). Therefore the focus is on this method. In addition the Lagrangian solution method for the groundwater flow equation is presented. This method was used to track particles through the simulation domain in some studies presented in this dissertation (see sections 2.3, 4.1 and 5.3).

2.2.2.1 Eulerian approach

Like for solving the groundwater flow equation a finite differences approach has been adopted to solve the mass transport equation. A finite differences approach has clear disadvantages for solving the mass transport equation as compared to the finite elements approach. The finite differences approach is less suitable to adapt the numerical model to the aquifer boundaries and to refine the grid around pumping wells and contaminant sources. Both the finite differences and the finite elements approach are sensitive to numerical instabilities and oscillations in the solutions (Zheng and Bennett, 1995). The finite differences approach has been adopted because it is less CPU intensive than the finite elements approach. Another reason to adopt the finite differences approach is for consistency with the solution of the flow equation. Especially in the context of the inverse modelling of both groundwater flow and mass transport (see Chapter 6) it is important to reduce the needed CPU time as much as possible. The finite differences approach consists of the same main three steps as given in section 2.2.1. We consider again the regular parallelpiped shaped aquifer. The components of the mass transport equation associated with advective transport are obtained as follows:

$$\frac{\partial}{\partial x}\left(c\frac{v_x}{R}\right)=\left[\frac{1}{\Delta x_{ijk}}\left((1-\alpha)c_{i+1jk}+\alpha c_{ijk}\right)\left(-K_{ijk,i+1jk}\frac{h_{i+1jk}-h_{ijk}}{\Delta x_{ijk,i+1jk}\phi R_{ijk,i+1jk}}\right)\right]-$$
$$\left[\frac{1}{\Delta x_{ijk}}\left(\alpha c_{i-1jk}+(1-\alpha)c_{ijk}\right)\left(-K_{ijk,i-1jk}\frac{h_{ijk}-h_{i-1jk}}{\Delta x_{ijk,i-1jk}\phi R_{ijk,i-1jk}}\right)\right]$$

where α is a weighting term and $R_{ijk,i+1jk}$ is the retardation coefficient calculated at the interface of the grid cells ijk and $i+1jk$. The retardation coefficient at the cell interface is the arithmetical average of the retardation coefficients for the grid cells ijk and $i+1jk$. In case of central weighting α is equal to 0.5. If upstream weighting is applied α is either 0 or 1: 1 if the velocity at the grid cell interface is positive, 0 if the velocity is negative. Upstream weighting avoids the artificial oscillations associated with the central weighting scheme. The disadvantage of upstream weighting is that it is only accurate to the first-order and introduces a second-order truncation error. This truncation error introduces numerical dispersion. The effect of numerical dispersion on the solution of the mass transport equation is the same as "real" dispersion. From the equation it can be seen that the pore groundwater velocities are calculated from the solution of the groundwater flow equation and evaluated at the grid cell interfaces. The terms associated with convective transport in the vertical direction and along the north/south direction can be obtained in a similar way.

The components associated with dispersive transport are calculated in the following way:

$$\frac{\partial}{\partial x}\left(\frac{D_{xx}}{R}\frac{\partial c}{\partial x}+\frac{D_{xy}}{R}\frac{\partial c}{\partial y}+\frac{D_{xz}}{R}\frac{\partial c}{\partial z}\right)=$$
$$\frac{1}{\Delta x_{ijk}}\left(\frac{D_{xx_{ijk,i+1jk}}}{R_{ijk,i+1jk}}\frac{c_{i+1jk}-c_{ijk}}{\Delta x_{ijk,i+1jk}}\right)+\frac{1}{\Delta x_{ijk}}\left(\frac{-D_{xx_{ijk,i-1jk}}}{R_{ijk,i-1jk}}\frac{c_{ijk}-c_{i-1jk}}{\Delta x_{ijk,i-1jk}}\right)+$$
$$\frac{1}{(\Delta x_{ijk})}\left(\frac{D_{xy_{ijk,i+1jk}}}{R_{ijk,i+1jk}}\frac{c_{i+1j+1k}+c_{ij+1k}-c_{i+1j-1k}-c_{ij-1k}}{\Delta y_{ijk,ij-1k}+\Delta y_{ijk,ij+1k}}\right)-$$
$$\frac{1}{(\Delta x_{ijk})}\left(\frac{D_{xy_{ijk,i-1jk}}}{R_{ijk,i-1jk}}\frac{c_{ij+1k}+c_{i-1j+1k}-c_{ij-1k}-c_{i-1j-1k}}{\Delta y_{ijk,ij+1k}+\Delta y_{ijk,ij-1k}}\right)+$$
$$\frac{1}{(\Delta x_{ijk})}\left(\frac{D_{xz_{ijk,i+1jk}}}{R_{ijk,i+1jk}}\frac{c_{i+1jk+1}+c_{ijk+1}-c_{i+1jk-1}-c_{ijk-1}}{\Delta z_{ijk,ijk-1}+\Delta z_{ijk,ijk+1}}\right)+$$
$$\frac{1}{(\Delta x_{ijk})}\left(\frac{D_{xz_{ijk,i-1jk}}}{R_{ijk,i-1jk}}\frac{c_{ijk+1}+c_{i-1jk+1}-c_{ijk-1}-c_{i-1jk-1}}{\Delta z_{ijk,ijk-1}+\Delta z_{ijk,ijk+1}}\right)$$

From the expressions above it can be seen that not only grid cells adjacent to the central grid cell appear in the expressions, but also grid cells diagonal to it. The

contribution of the diagonal grid cells is related with the non-zero values for the off-diagonal elements of the dispersion tensor. For 3-D transport this means that 27 grid cells are involved in estimating the concentration at one grid cell. In case transport takes place parallel to one of the main axes the off-diagonal elements of the dispersion tensor cancel to zero and just 7 grid cells are involved in replacing the derivatives for one grid cell. The dispersion terms D_{xx}, D_{xy} and D_{xz} are evaluated at the interfaces between the two neighbouring grid cells in the x-direction. The equations below detail the procedure for the terms introduced above and for the simple case of cubic grid cells.

$$D_{xx_{ijk,i+1jk}} = \left(\alpha_L v^2_{x_{ijk,i+1jk}} + \alpha_T v^2_{y_{ijk,i+1jk}} + \alpha_T v^2_{z_{ijk,i+1jk}}\right) / v_{ijk,i+1jk}$$

$$D_{xx_{ijk,i-1jk}} = \left(\alpha_L v^2_{x_{ijk,i-1jk}} + \alpha_T v^2_{y_{ijk,i-1jk}} + \alpha_T v^2_{z_{ijk,i-1jk}}\right) / v_{ijk,i-1jk}$$

$$D_{xy_{ijk,i+1jk}} = \left((\alpha_L - \alpha_T) v_{x_{ijk,i+1jk}} v_{y_{ijk,i+1jk}}\right) / v_{ijk,i+1jk}$$

$$D_{xy_{ijk,i-1jk}} = \left((\alpha_L - \alpha_T) v_{x_{ijk,i-1jk}} v_{y_{ijk,i-1jk}}\right) / v_{ijk,i-1jk}$$

$$D_{xz_{ijk,i+1jk}} = \left((\alpha_L - \alpha_T) v_{x_{ijk,i+1jk}} v_{z_{ijk,i+1jk}}\right) / v_{ijk,i+1jk}$$

$$D_{xz_{ijk,i-1jk}} = \left((\alpha_L - \alpha_T) v_{x_{ijk,i-1jk}} v_{z_{ijk,i-1jk}}\right) / v_{ijk,i-1jk}$$

with:

$$v_{ijk,i-1jk} = \sqrt{v^2_{x_{ijk,i-1jk}} + v^2_{y_{ijk,i-1jk}} + v^2_{z_{ijk,i-1jk}}}$$

$$v_{ijk,i+1jk} = \sqrt{v^2_{x_{ijk,i+1jk}} + v^2_{y_{ijk,i+1jk}} + v^2_{z_{ijk,i+1jk}}}$$

In the terms above seepage groundwater velocities appear which can not be evaluated at the cell interfaces in the same way as seen before. The velocity components in the x-direction can be evaluated easily for two neighbouring cells in the x-direction. The seepage groundwater velocities in the y- and z-direction, for the two neighbouring cells along the x-axis are obtained by interpolating groundwater seepage velocities that are evaluated at surrounding cell interfaces. For cubic grid cells the following expressions are obtained:

$$v_{x_{ijk,i-1jk}} = -K_{ijk,i-1jk} \frac{h_{ijk} - h_{i-1jk}}{\Delta x_{ijk,i-1jk}}$$

$$v_{x_{ijk,i+1jk}} = -K_{ijk,i+1jk} \frac{h_{i+1jk} - h_{ijk}}{\Delta x_{ijk,i+1jk}}$$

$$v_{y_{ijk,i-1jk}} = \frac{1}{4}\left(v_{y_{i-1jk,i-1j+1k}} + v_{y_{i-1jk,i-1j-1k}} + v_{y_{ijk,ij+1k}} + v_{y_{ijk,ij-1k}}\right)$$

$$v_{y_{ijk,i+1jk}} = \frac{1}{4}\left(v_{y_{i+1jk,i+1j+1k}} + v_{y_{i+1jk,i+1j-1k}} + v_{y_{ijk,ij+1k}} + v_{y_{ijk,ij-1k}}\right)$$

$$v_{z_{ijk,i+1jk}} = \frac{1}{4}\left(v_{z_{i+1jk,i+1jk+1}} + v_{z_{i+1jk,i+1jk-1}} + v_{z_{ijk,ijk+1}} + v_{z_{ijk,ijk-1}}\right)$$

$$v_{z_{ijk,i-1jk}} = \frac{1}{4}\left(v_{z_{i-1jk,i-1jk+1}} + v_{z_{i-1jk,i-1jk-1}} + v_{z_{ijk,ijk+1}} + v_{z_{ijk,ijk-1}}\right)$$

The boundary grid cells do not have four surrounding grid cell interfaces, but just two. Therefore just these two velocities are averaged to interpolate the velocity. For the same reason for the corner grid cells just one velocity (the nearest by velocity) is used.

The derivative of concentration with respect to time is estimated by finite differences:

$$\frac{\partial c}{\partial t} \approx \frac{c_{ijk}^{t+1} - c_{ijk}^{t}}{\Delta t}$$

A fully implicit solution to the mass transport equation is calculated. An implicit solution is unconditionally stable; the instability problems of the explicit solution are avoided. However, there are other reasons why the time step size has to be constrained.

One numerical problem is the artificial oscillation. This problem occurs for advection dominated problems. It is possible to reduce the mesh size such that this oscillation does not occur. However, in case of advective transport only the reduction of the grid cell sizes cannot solve the oscillation problems. More over, also in case of both advective and dispersive transport the needed grid cell sizes may be so small that the solution of the mass transport equation becomes

unacceptable CPU intensive. The degree to which the transport is dominated by advection is measured by the grid Peclet number (*Pe*). The Peclet number indicates whether oscillation problems may occur. In case the number is below 2 no problems are expected. The Peclet number is defined as:

$$Pe = \frac{v\Delta x}{D} = \frac{\Delta x}{\alpha_L}$$

Upstream weighting avoids the problem of artificial oscillation, but aggravates the problem of numerical dispersion. The problems with numerical dispersion are avoided by using sufficiently small time steps, so that the Courant number is less than one. The Courant number is given by the following expression:

$$C_r = \frac{v\Delta t}{\Delta x}$$

where Δt is the time step [T] and Δx [L] is the grid cell size.

Replacing all the derivatives of the mass transport equation results in the following equation for an active grid cell whose neighbour grid cell is also active (For simplicity sakeness off-diagonal dispersion terms are omitted; groundwater flow is supposed to be parallel to one of the three main axes of the simulation domain and perpendicular to the other two axes. The grid cells are supposed to be cubic):

$$\left(\frac{D_{xx_{ijk,i-1jk}}}{\Delta x_{ijk}^2 R_{ijk,i-1jk}} - \frac{\alpha v_{x_{ijk,i-1jk}}}{\Delta x_{ijk} R_{ijk,i-1jk}}\right) c_{i-1jk}^{t+1} + \left(\frac{D_{xx_{ijk,i+1jk}}}{\Delta x_{ijk}^2 R_{ijk,i+1jk}} - \frac{-(1-\alpha) v_{x_{ijk,i+1jk}}}{\Delta x_{ijk} R_{ijk,i+1jk}}\right) c_{i+1jk}^{t+1} +$$
$$\left(\frac{D_{yy_{ijk,ij-1k}}}{\Delta y_{ijk}^2 R_{ijk,ij-1k}} - \frac{\alpha v_{y_{ijk,ij-1k}}}{\Delta y_{ijk} R_{ijk,ij-1k}}\right) c_{ij-1k}^{t+1} + \left(\frac{D_{yy_{ijk,ij+1k}}}{\Delta y_{ijk}^2 R_{ijk,ij+1k}} - \frac{-(1-\alpha) v_{y_{ijk,ij+1k}}}{\Delta y_{ijk} R_{ijk,ij+1k}}\right) c_{ij+1k}^{t+1} +$$
$$\left(\frac{D_{zz_{ijk,ijk-1}}}{\Delta z_{ijk}^2 R_{ijk,ijk-1}} - \frac{\alpha v_{z_{ijk,ijk-1}}}{\Delta z_{ijk} R_{ijk,ijk-1}}\right) c_{ijk-1}^{t+1} + \left(\frac{D_{zz_{ijk,ijk+1}}}{\Delta z_{ijk}^2 R_{ijk,ijk+1}} - \frac{-(1-\alpha) v_{z_{ijk,ijk+1}}}{\Delta z_{ijk} R_{ijk,ijk+1}}\right) c_{ijk+1}^{t+1} -$$
$$\left(\begin{array}{l} \frac{-\alpha v_{x_{ijk,i+1jk}}}{\Delta x_{ijk} R_{ijk,i+1jk}} + \frac{-(1-\alpha) v_{x_{ijk,i-1jk}}}{\Delta x_{ijk} R_{ijk,i-1jk}} + \frac{-\alpha v_{y_{ijk,ij+1k}}}{\Delta y_{ijk} R_{ijk,ij+1k}} + \\ + \frac{-(1-\alpha) v_{y_{ijk,ij-1k}}}{\Delta y_{ijk} R_{ijk,ij-1k}} + \frac{-\alpha v_{z_{ijk,ijk+1}}}{\Delta z_{ijk} R_{ijk,ijk+1}} + \frac{-(1-\alpha) v_{z_{ijk,ijk-1}}}{\Delta z_{ijk} R_{ijk,ijk-1}} \end{array}\right) c_{ijk}^{t+1} -$$
$$\left(\begin{array}{l} \frac{D_{xx_{ijk,i-1jk}}}{\Delta x_{ijk}^2 R_{ijk,i-1jk}} + \frac{D_{xx_{ijk,i+1jk}}}{\Delta x_{ijk}^2 R_{ijk,i+1jk}} + \frac{D_{yy_{ijk,ij-1k}}}{\Delta y_{ijk}^2 R_{ijk,ij-1k}} + \\ + \frac{D_{yy_{ijk,ij+1k}}}{\Delta y_{ijk}^2 R_{ijk,ij+1k}} + \frac{D_{zz_{ijk,ijk-1}}}{\Delta z_{ijk}^2 R_{ijk,ijk-1}} + \frac{D_{zz_{ijk,ijk+1}}}{\Delta z_{ijk}^2 R_{ijk,ijk+1}} + \frac{1}{\Delta t} + \lambda_D - \frac{q_s^{out}}{\phi} \end{array}\right) c_{ijk}^{t+1} + \frac{q_s^{in} c_s}{\phi} =$$
$$\frac{-c_{ijk}^{t}}{\Delta t}$$

In the expression a distinction is made between mass extraction (q^{out}), with a concentration equal to the local concentration, and mass injection (q^{in}) with the contaminant concentration of the water being injected.

A more compact expression of the finite differences formulation of the mass transport equation is:

$$\left(\left(\left[\frac{E}{R}\right]\right)-\left[\frac{1}{\Delta t}\right]-[\lambda_D]+\left[\frac{q_s^{out}}{\phi}\right]\right)\{C^{t+1}\}+\{F\}=-\frac{1}{\Delta t}\{C^t\} \qquad (2.10)$$

where E/R is the matrix containing the terms E_{lm}/R_{lm}; E_{lm} are the convection and dispersion terms and R_{lm} the interblock retardation coefficients, $[1/\Delta t]$ is a diagonal matrix with one divided by the time step on the diagonal terms, $[\lambda_D]$ is a matrix with the decay constants on the diagonal, $[q^{out}/\phi]$ is a matrix with the mass extractions divided by the porosity on the diagonal terms, C the vector with the concentration values at time step t or time step t+1 and F the vector with mass injection and boundary conditions.

The matrix E/R contains the elements $[E/R]_{lm}$ (l=1, ..., N; m=1, ..., N). Each row l of the matrix E/R refers to one of the active cells and only has a maximum seven non-zero values (the off-diagonal dispersion terms are omitted). The elements that can be non-zero are those for which m refers to a grid cell located north (N), south (S), west (W), east (E), up (U) or down (D) to the active cell l ($m \in \{N, S, W, E, U, D\}$), and for the diagonal elements. The following expressions are found for the elements of E/R in case both l and m refer to active grid cells:

$$\left(\frac{E}{R}\right)_{lm}=\frac{D_{xx_{lm}}}{\Delta x_l^2 R_{lm}}-\frac{\alpha v_{x_{lm}}}{\Delta x_l R_{lm}} \qquad m\in\{W\}$$

$$\left(\frac{E}{R}\right)_{lm}=\frac{D_{xx_{lm}}}{\Delta x_l^2 R_{lm}}+\frac{(1-\alpha)\alpha v_{x_{lm}}}{\Delta x_l R_{lm}} \qquad m\in\{E\}$$

$$\left(\frac{E}{R}\right)_{lm}=\frac{D_{yy_{lm}}}{\Delta x_l^2 R_{lm}}-\frac{\alpha v_{y_{lm}}}{\Delta x_l R_{lm}} \qquad m\in\{S\}$$

$$\left(\frac{E}{R}\right)_{lm}=\frac{D_{yy_{lm}}}{\Delta x_l^2 R_{lm}}+\frac{(1-\alpha)\alpha v_{y_{lm}}}{\Delta x_l R_{lm}} \qquad m\in\{N\}$$

$$\left(\frac{E}{R}\right)_{lm} = \frac{D_{zz_{lm}}}{\Delta x_l^2 R_{lm}} - \frac{\alpha v_{z_{lm}}}{\Delta x_l R_{lm}} \qquad m \in \{D\}$$

$$\left(\frac{E}{R}\right)_{lm} = \frac{D_{zz_{lm}}}{\Delta x_l^2 R_{lm}} - \frac{(1-\alpha) v_{z_{lm}}}{\Delta x_l R_{lm}} \qquad m \in \{U\}$$

$$\begin{aligned}\left(\frac{E}{R}\right)_{ll} = &\sum_{m\in\{E\}}\left(\frac{\alpha v_{x_{lm}}}{\Delta x_l R_{lm}} - \frac{D_{xx_{lm}}}{\Delta x_l^2 R_{lm}}\right) + \sum_{m\in\{W\}}\left(\frac{(1-\alpha) v_{x_{lm}}}{\Delta x_l R_{lm}} - \frac{D_{xx_{lm}}}{\Delta x_l^2 R_{lm}}\right) + \\ &\sum_{m\in\{N\}}\left(\frac{\alpha v_{y_{lm}}}{\Delta y_l R_{lm}} - \frac{D_{yy_{llm}}}{\Delta y_l^2 R_{lm}}\right) + \sum_{m\in\{S\}}\left(\frac{(1-\alpha) v_{y_{lm}}}{\Delta y_l R_{lm}} - \frac{D_{yy_{lm}}}{\Delta y_l^2 R_{lm}}\right) + \\ &\sum_{m\in\{U\}}\left(\frac{\alpha v_{z_{lm}}}{\Delta z_l R_{lm}} - \frac{D_{zz_{lm}}}{\Delta z_l^2 R_{lm}}\right) + \sum_{m\in\{D\}}\left(\frac{(1-\alpha) v_{z_{lm}}}{\Delta z_l R_{lm}} - \frac{D_{zz_{lm}}}{\Delta z_l^2 R_{lm}}\right)\end{aligned}$$

where we have changed the notation according to:

$$v_{x_{lm}} = v_{x_{ijk,i-1,jk}} \qquad m \in \{W\}$$

$$v_{x_{lm}} = v_{x_{ijk,i+1,jk}} \qquad m \in \{E\}$$

$$v_{y_{lm}} = v_{y_{ijk,ij-1k}} \qquad m \in \{S\}$$

$$v_{y_{lm}} = v_{y_{ijk,i+1,jk}} \qquad m \in \{N\}$$

$$v_{z_{lm}} = v_{z_{ijk,ijk-1}} \qquad m \in \{D\}$$

$$v_{z_{lm}} = v_{z_{ijk,ijk+1}} \qquad m \in \{U\}$$

$$D_{xx_{lm}} = D_{xx_{ijk,i-1,jk}} \qquad m \in \{W\}$$

$$D_{xx_{lm}} = D_{xx_{ijk,i+1jk}} \qquad m \in \{E\}$$

$$D_{yy_{lm}} = D_{yy_{ijk,ij-1k}} \qquad m \in \{S\}$$

$$D_{yy_{lm}} = D_{yy_{ijk,ij+1k}} \qquad m \in \{N\}$$

$$D_{zz_{lm}} = D_{zz_{ijk,ijk-1}} \qquad m \in \{D\}$$

$$D_{zz_{lm}} = D_{zz_{ijk,ijk+1}} \qquad m \in \{U\}$$

$$R_{lm} = R_{ijk,i-1jk} \qquad m \in \{W\}$$

$$R_{lm} = R_{ijk,i+1jk} \qquad m \in \{E\}$$

$$R_{lm} = R_{ijk,ij-1k} \qquad m \in \{S\}$$

$$R_{lm} = R_{ijk,ij+1k} \qquad m \in \{N\}$$

$$R_{lm} = R_{ijk,ijk-1} \qquad m \in \{D\}$$

$$R_{lm} = R_{ijk,ijk+1} \qquad m \in \{U\}$$

The elements of the matrix λ_D are zero, except for the diagonal elements, which are equal to the decay coefficient at the corresponding cell.

The same holds for the matrix $[q_s^{out}/\phi]$ which is also diagonal and with values equal to the mass extraction divided by the porosity.

Finally, the elements of the vector F are given by:

$$F_l = \left(\frac{q_s^{in} c_s}{\phi} \right)_l$$

Equation 2.10 for time step t+1 can be expressed more compact:

$$[\eta]\{C^{t+1}\} = \{\zeta^t\} \tag{2.11}$$

For grid cell l the following equation is obtained:

$$\eta_W C_W^{t+1} + \eta_E C_E^{t+1} + \eta_N C_N^{t+1} + \eta_S C_S^{t+1} +$$
$$\eta_U C_U^{t+1} + \eta_D C_D^{t+1} + \eta_l C_l^{t+1} = \zeta_l^t$$

in which the coefficients η are elements of the NxN matrix $[\eta]$ that replace the convective and dispersive terms, the constant retardation factor, the time step between the transport solution at time t and the transport solution at time t+1, the decay coefficient and the mass sinks. The following subscripts have been used: l is the reference grid cell, W stands for the grid cell west of it, E for the grid cell east of it, N north of it, S south of it, U for the grid cell above it and D for the grid cell below it. The ζ_l^t accounts for the transport solution at time t, the time step, the mass sources and the boundary conditions and is an element of the vector ζ. The expressions for the coefficients are (grid cell and neighbour grid cells are active):

$$\eta_m = \left(\frac{E}{R} \right)_{lm} \qquad m \in \{N, S, W, E, U, D\}$$

$$\eta_l = \left(\frac{E}{R} - \frac{1}{\Delta t} - \lambda_D + \frac{q_s^{out}}{\phi} \right)_{ll}$$

$$\zeta_l^t = \frac{-C_l^t}{\Delta t} - F_l$$

The time dependent solution of the system state is obtained by consecutively solving system (2.10) for each time step starting with C^0 equal to the initial conditions.

The elements of $[E/R]$, $[1/\Delta t]$, $[\lambda_D]$, $[q_s^{out}/\phi]$ and $\{F\}$ are slightly modified when the active cell or one of the neighbouring cells are of prescribed concentration.

In case that grid cell l is a prescribed concentration value then the only non-zero values for elements of matrix E/R at row l are:

$$\left(\frac{E}{R}\right)_{ll} = 1$$

$$F_l = c_l^{\Gamma}$$

where C_l^{Γ} is prescribed concentration at grid cell l.

The elements of matrix E/R at row l, when neighbouring grid cell m is of prescribed concentration also change. Below there is an example for a grid cell l with no mass injection and to the east of which there is a prescribed concentration value of c_m^{Γ}.

$$\left(\frac{E}{R}\right)_{lm} = 0$$

$$F_l = \left(\frac{D_{xx_{lm}}}{\Delta x_l^2 R_{lm}} - \frac{\alpha v_{x_{lm}}}{\Delta x_l R_{lm}}\right) c_m^{\Gamma}$$

After building the linear system of equations an efficient and accurate method has to be used to find the concentration solution. The linear system is solved by the same method as the resulting linear system from the groundwater flow equation. In section 3.3 details are given on the methods used to solve the linear system of equations.

2.2.2.2 Lagrangian approach

The advantage of the Lagrangian methods is their numerical stability; oscillation problems and numerical dispersion are avoided. Nevertheless, the Lagrangian methods provide less information and it is not straightforward to obtain the spatiotemporal concentration distribution. Lagrangian methods are usually used to estimate the transport of particles from some location to a control plane. In this dissertation the Eulerian method is used for the stochastic inverse modelling of contaminant transport. However, the Lagrangian method is used in some other studies. Therefore here some details on the method are given. The particle tracking procedure is implemented in the program 3DTRANSP.

In the particle tracking method particles are moved step by step through the simulation domain. From the groundwater flow solution the seepage

groundwater flow velocities at all the cell interfaces are obtained by the following equation:

$$v_{ijk,i-1jk} = -\frac{K_{ijk,i-1jk}}{\phi}\frac{h_{ijk} - h_{i-1jk}}{\Delta x_{ijk,i-1jk}}$$

However, by this means we only obtain the seepage groundwater flow velocities at the cell interfaces and not at any other point of the aquifer. Some interpolation method should be adopted to estimate the components of the groundwater velocity vector at the rest of the aquifer.

The groundwater flow velocities at any point in the aquifer are obtained by trilinear interpolation of the groundwater flow velocities calculated at the cell interfaces. For 3-D transport problems the eight nearest evaluated components of the groundwater flow velocity vector at cell interfaces are used to estimate the groundwater flow velocity at the desired location. The eight components are associated with the centres of the eight cell interfaces and they form the corners of an imaginary grid cell in the interpolation procedure. After defining:

$$\alpha_x = \frac{x - x_1}{\Delta x}$$

$$\alpha_y = \frac{y - y_1}{\Delta y}$$

$$\alpha_z = \frac{z - z_1}{\Delta z}$$

where x_1,y_1 and z_1 are the minimum coordinate values on x, y and z for the imaginary grid cell in which the particle is contained; x, y and z are the coordinate values for the point at which we want to estimate the velocity components and Δx, Δy and Δz are the grid cell widths along the three coordinate axes. The velocity compounds found by trilinear interpolation are:

$$\begin{aligned}
&v_x(x,y,z) = \\
&(1-\alpha_x)(1-\alpha_y)(1-\alpha_z)v_x(x_1,y_1,z_1) + \alpha_x(1-\alpha_y)(1-\alpha_z)v_x(x_1+\Delta x,y_1,z_1) + \\
&\alpha_x\alpha_y(1-\alpha_z)v_x(x_1+\Delta x,y_1+\Delta y,z_1) + (1-\alpha_x)\alpha_y(1-\alpha_z)v_x(x_1,y_1+\Delta y,z_1) + \\
&(1-\alpha_x)(1-\alpha_y)\alpha_z v_x(x_1,y_1,z_1+\Delta z) + \alpha_x(1-\alpha_y)\alpha_z v_x(x_1+\Delta x,y_1,z_1+\Delta z) + \\
&\alpha_x\alpha_y\alpha_z v_x(x_1+\Delta x,y_1+\Delta y,z_1+\Delta z) + (1-\alpha_x)\alpha_y\alpha_z v_x(x_1,y_1+\Delta y,z_1+\Delta z)
\end{aligned}$$

$$
\begin{aligned}
&v_y(x,y,z) = \\
&(1-\alpha_x)(1-\alpha_y)(1-\alpha_z)v_y(x_1,y_1,z_1)+\alpha_x(1-\alpha_y)(1-\alpha_z)v_y(x_1+\Delta x,y_1,z_1)+ \\
&\alpha_x\alpha_y(1-\alpha_z)v_y(x_1+\Delta x,y_1+\Delta y,z_1)+(1-\alpha_x)\alpha_y(1-\alpha_z)v_y(x_1,y_1+\Delta y,z_1)+ \\
&(1-\alpha_x)(1-\alpha_y)\alpha_z v_y(x_1,y_1,z_1+\Delta z)+\alpha_x(1-\alpha_y)\alpha_z v_y(x_1+\Delta x,y_1,z_1+\Delta z)+ \\
&\alpha_x\alpha_y\alpha_z v_y(x_1+\Delta x,y_1+\Delta y,z_1+\Delta z)+(1-\alpha_x)\alpha_x\alpha_z v_y(x_1,y_1+\Delta y,z_1+\Delta z)
\end{aligned}
$$

$$
\begin{aligned}
&v_z(x,y,z) = \\
&(1-\alpha_x)(1-\alpha_y)(1-\alpha_z)v_z(x_1,y_1,z_1)+\alpha_x(1-\alpha_y)(1-\alpha_z)v_z(x_1+\Delta x,y_1,z_1)+ \\
&\alpha_x\alpha_y(1-\alpha_z)v_z(x_1+\Delta x,y_1+\Delta y,z_1)+(1-\alpha_x)\alpha_y(1-\alpha_z)v_z(x_1,y_1+\Delta y,z_1)+ \\
&(1-\alpha_x)(1-\alpha_y)\alpha_z v_z(x_1,y_1,z_1+\Delta z)+\alpha_x(1-\alpha_y)\alpha_z v_z(x_1+\Delta x,y_1,z_1+\Delta z)+ \\
&\alpha_x\alpha_y\alpha_z v_z(x_1+\Delta x,y_1+\Delta y,z_1+\Delta z)+(1-\alpha_x)\alpha_x\alpha_z v_z(x_1,y_1+\Delta y,z_1+\Delta z)
\end{aligned}
$$

For the interpolation of each of the three velocity components the eight nearest groundwater flow velocities (calculated at the cell interfaces) from the groundwater flow model are used. The position of the cell interfaces and therefore the localisation of the imaginary grid cell is different for the three velocity components. The obtained groundwater flow velocities vary continuously in space. The disadvantage is that the interpolation scheme is not mass conservative. An alternative interpolation scheme would have been simple linear interpolation, where just the two nearest groundwater flow velocities are used to calculate each of the groundwater flow velocities. The groundwater flow velocities vary then in a piecewise fashion along the simulation domain (Zheng and Bennett, 1995).

When the groundwater flow velocities at all points of the aquifer can be obtained the particles can be tracked throughout the simulation domain. If one particle is released at some point in the aquifer, the displacement vector can be obtained directly from the groundwater velocity field. The particle is moved step by step. For each new step the local groundwater flow velocity vector is used to move the particle. Therefore the steps should be small, especially in case of a strong heterogeneity in groundwater flow velocities. The equation of the pathline is given by:

$$
\begin{aligned}
\frac{dx(t)}{dt} &= \frac{v_x}{R} \\
\frac{dy(t)}{dt} &= \frac{v_y}{R} \\
\frac{dz(t)}{dt} &= \frac{v_z}{R}
\end{aligned}
$$

where dx, dy and dz are the displacements in the x-, y- and z-direction respectively and dt is the time step for one displacement. The new particle locations can be found then by:

$$\begin{Bmatrix} x_{new} \\ y_{new} \\ z_{new} \end{Bmatrix} = \begin{Bmatrix} x_{old} \\ y_{old} \\ z_{old} \end{Bmatrix} + \begin{Bmatrix} \dfrac{v_x(x_{old}, y_{old}, z_{old})}{R(x_{old}, y_{old}, z_{old})} dt_1 \\ \dfrac{v_y(x_{old}, y_{old}, z_{old})}{R(x_{old}, y_{old}, z_{old})} dt_1 \\ \dfrac{v_z(x_{old}, y_{old}, z_{old})}{R(x_{old}, y_{old}, z_{old})} dt_1 \end{Bmatrix}$$

where x_{old}, y_{old}, z_{old} are the initial coordinates of the particle, x_{new}, y_{new}, z_{new} are the new coordinates of the particle and dt is the time step needed to move the particle from one position to the other. A higher accuracy of the predictions can be obtained by not using the velocities at the starting location to track the particle, but using information on velocities along the complete particle travel path. The family of Runga-Kutta methods are normally used to integrate information on velocities along the travel path (Kinzelbach, 1986; Zheng and Bennett, 1995). However, by using a smaller time step the simpler procedure can have the same accuracy as for example the fourth order Runga-Kutta method. The particle can be tracked until the boundaries of the simulation domain, a control plane or a discharge location.

The particle tracking method that is used in this dissertation reduces the needed CPU-time because the constant displacement (CD) scheme instead of the traditional constant time step (CT) scheme is implemented (Wen and Kung, 1995, 1996; Wen and Gómez-Hernández, 1996). In strongly heterogeneous aquifers the constant time step has to be very small in order to give accurate solutions; the particles can not pass "too fast" the parts of the aquifer with the highest groundwater flow velocities. The constant time step is therefore limited according the highest groundwater flow velocities. However, the same time step is used for the parts of the aquifer with low groundwater flow velocities, which is inefficient. The constant displacement method uses a constant displacement and the needed time to make the displacement is calculated.

2.3 Impact of random function model choice on groundwater flow and mass transport predictions

This section shows an application in which a numerical groundwater flow and mass transport model were used to predict the groundwater flow and mass transport at the WIPP site, a candidate storage location for nuclear waste in New Mexico, U.S.A. Four different multivariate probability density functions were adopted for the modelling of the spatially variable transmissivities. The impact of the random function model adopted on the simulation results is investigated.

2.3.1 Introduction

Geostatistical methods are used for modelling the spatial variability of hydraulic properties (see also section 2.1). In this study, only transmissivity (T) is considered to be variable in space. Hydraulic conductivity and transmissivity are regarded as the most consequential parameters for flow and transport (Smith and Schwartz, 1981a, 1981b). For illustration purposes we have used the WIPP (Waste Isolation Pilot Plant) data set. It consists of transmissivity data from a confined aquifer in a dolomite rock formation in New Mexico (USA) overlying a potential repository for transuranic waste. The data set displays an apparent E-W trend and an apparent bimodality on its histogram. The trend can be accounted for by using a RF model which explicitly incorporates it, such as the RF model used for universal kriging (Journel and Huijbregts, 1978), or else, the trend can be implicitly incorporated in the model through conditioning and a zonal anisotropic variogram. The bimodality of the sample is dealt with by the following two approaches:

- A single-mode Gaussian histogram with same mean and variance as the sample data is adopted and all other deviations from the multiGaussian model are supposed to be due to sampling fluctuations.
- A normal-score transform of the data is taken, the realisations are generated in the Gaussian space and the resulting realisations are back transformed as such ensuring an almost perfect reproduction of the sample histogram in all realisations.

This study analyses the results obtained after processing the realisations through a complex non-linear transfer function (groundwater flow and mass transport equations) with the aim of evaluating the impact of RF model choice. Other studies have compared the performances of similar geostatistical models for linear estimation, namely the interpolation of an environmental variable. Journel and Rossi (1989) show that interpolation of a variable using both ordinary kriging and universal kriging yields nearly exactly the same results. However, they use for both ordinary kriging and universal kriging the same variogram model, while in practice the variogram models should differ for the two cases. On the contrary, in some specific case studies it is found that

universal kriging gives better results than ordinary kriging (e.g. Webster and Burgess, 1980).
Four different sets of 200 realisations of log$T$ have been generated. The four sets are coded as follows depending on the RF model choice:

- OK-NSCORE. No trend, variate is normal score of data.
- OK-UNTRAN. No trend, variate is log$T$.
- UK-NSCORE. Linear trend, variate is normal score of data.
- UK-UNTRAN. Linear trend, variate is log$T$.

In addition, the four different sets of log$T$ realisations are compared in two mass transport situations (with and without intra-cell dispersion).

2.3.2 Theory

Flow and mass transport in a confined aquifer is considered. Flow is assumed to be at steady-state, saturated and to take place in 2-D. The full density is assumed constant. Transmissivity is spatially variable. Equation 2.5 simplifies then to:

$$\frac{\partial}{\partial x}\left(T(x,y)\frac{\partial h}{\partial x}\right)+\frac{\partial}{\partial y}\left(T(x,y)\frac{\partial h}{\partial y}\right)=0 \qquad (2.12)$$

Mass is transported in the aquifer by convection and dispersion. Linear adsorption has not been taken into account since this process as long as it is considered spatially homogeneous will not influence the relative differences between the breakthrough curves in the different sets of simulated fields apart from a multiplicative factor. The mass transport equation 2.9 simplifies then to:

$$\frac{\partial}{\partial x}\left(D_{xx}\frac{\partial c}{\partial x}+D_{xy}\frac{\partial c}{\partial y}\right)+\frac{\partial}{\partial y}\left(D_{yy}\frac{\partial c}{\partial y}+D_{yx}\frac{\partial c}{\partial x}\right)-\left[\frac{\partial}{\partial x}(v_x c)+\frac{\partial}{\partial y}(v_y c)\right]=\frac{\partial c}{\partial t} \qquad (2.13)$$

Transmissivity fields for the four different RF models are generated by sequential simulation. In section 2.1.2.3 of this dissertation more information on the generation of MultiGaussian fields is found. Details on the generation of multiGaussian fields by sequential simulation can be found in Gómez-Hernández and Journel (1993) and Gómez-Hernández and Cassiraga (1994). The generation of realisations for the RF models with trend differs only slightly from the simulation of multiGaussian fields as described by Gómez-Hernández and Journel (1993). The local conditional probability distribution functions (cpdfs) are assumed to be Gaussian with mean and variance identified to the universal kriging estimate and the universal kriging variance.

Because of the clustered sampling (see also Figure 2.2) it is difficult to test whether the logtransform of the data follows a Gaussian histogram or not. For this reason, normal-score transformed data and log-transformed data have been used. The differences between the four sets of simulated fields are as follows:

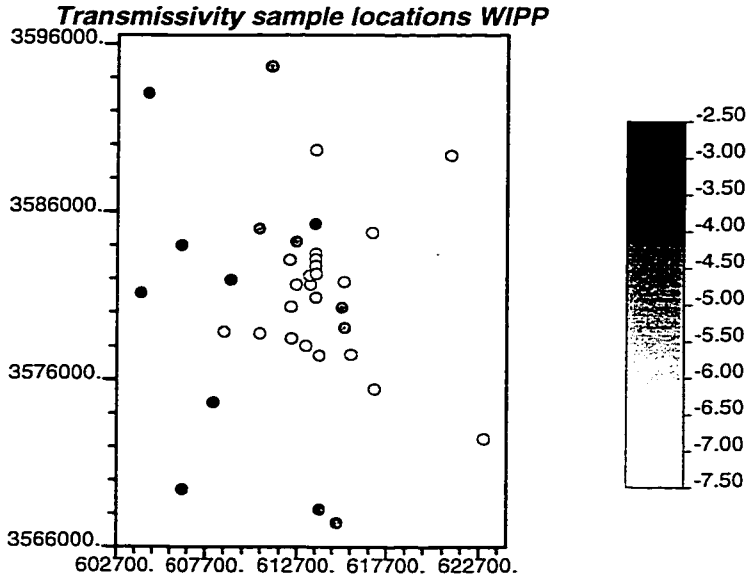

Figure 2.2 Transmissivity sample locations at the WIPP-site.

- OK-NSCORE. A variogram of the normal scores is computed. The cpdfs are obtained by solving the ordinary kriging equations, conditional to normal score data. The final realisation is back transformed to the original space.
- OK-UNTRAN. A variogram of the log transformed data is computed. The cpdfs are calculated by solving the ordinary kriging equations, conditional to the logtransformed data. The final realisation is exponentiated to produce T realisations.
- UK-NSCORE. A variogram of the normal score residuals is determined (this is the variogram of the normal score transformed log$T$ data, after the linear spatial trend has been filtered out, more details on this later). The cpdfs are calculated by solving the universal kriging equations, conditional to the normal score transformed data. A normal score back transform yields the T realisation.
- UK-UNTRAN. A variogram of the residuals of the logtransformed data is computed. The cpdfs are calculated by solving the universal kriging equations, conditional to the residuals of the log$T$ data. Exponentiation results in the T field.

2.3.3 Software

In this study the software used is different from the software used in the other practical studies and synthetic studies presented in this dissertation. Therefore some information on the software used in this study is given. The transmissivity fields are generated with the SGSIM program from GSLIB (Deutsch and Journel, 1992). For the simulation of fields from RF's with trend a modified version of the algorithm is used. This modified version of the program has been tested and it was found that over a large amount of realisations the

ensemble local mean and the ensemble local variance are approximately equal to the UK-estimate and UK-variance, respectively. This test is done because there is no proof that the applied algorithm would yield realisations from the RF model embedded into UK. Four sets of 200 fields have been generated. For each field equation 2.12 was solved using standard five-point block-centred finite differences as implemented in the program FLOW (Wen, 1995). Along the four edges of the field, prescribed head boundaries have been used. The prescribed head values are the same as those used by LaVenue *et al* (1990) in their modelling of the WIPP site. Equation 2.13 was solved by means of the program TRANSP (Wen and Kung, 1995). This program solves the mass transport equation by a Lagrangian approach: particle tracking for dispersion-free transport and random walk for transport with dispersion. Particles are released at a certain location in the field at the beginning of the simulation (instantaneous injection) and breakthrough curves at a given control plane are determined. To better account for the heterogeneity of the transmissivity field without the requirement of too-large a discretization in time, a constant displacement step instead of a constant time step has been used (Wen and Kung, 1996; Wen and Gómez-Hernández, 1996).

2.3.4 Results

2.3.4.1 The data set

From the original WIPP data set, as reported by LaVenue *et al* (1990), 36 measurements have been retained. They correspond to the data falling within the simulation domain, with the exception of the datum corresponding to well P-18 that has been removed because the value seems to be unreliably low for a dolomite rock (Freeze and Cherry, 1979). The simulation domain corresponds to an area of about 20 km in the x-direction and 30 km in the y-direction, discretized into 43 by 61 square cells of 500 by 500 metres. The drillings are not equally spaced over the region, but preferentially located in the centre part of the region overlying the panels that will host the waste when the site is operational. The experimental histogram of all 36 data (plus the anomalous low datum) is displayed in Figure 2.3. The histogram displays an apparent bimodality with two populations segregated at a cut-off of about -5.5 log(m^2/s).

2.3.4.2 Variograms

The experimental variogram of $\log T$ for the x-direction does not tend to stabilise at any distance (indicative of a possible trend in this direction). In the y-direction, however, a sill value is reached after some distance. This behaviour is noticed both for the log-transformed values and for the normal-score transformed values.

For the two RF models in which the trend is accounted for implicitly through the variogram, a spherical model with both geometric and zonal anisotropy is fitted to the experimental variograms. The model variograms for the log-

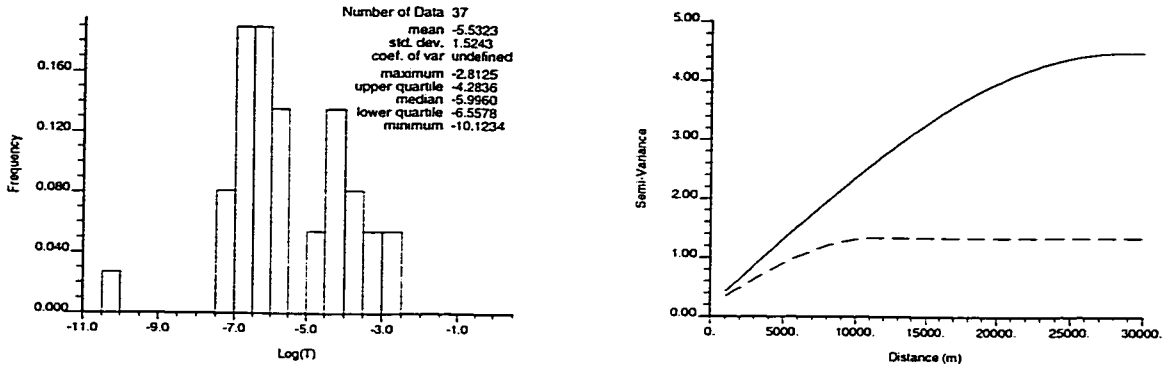

Figure 2.3 Histogram of log transmissivity data (left). Model variograms for log transmissivity in the North-South (dash) and East-West (solid) directions (right).

transformed data are shown in Figure 2.3 (similar models are fitted to the normal-score data). For the RF models in which a linear trend is considered, the variogram of the residuals is taken to be isotropic and equal to the variogram of the data in the N-S direction, since this is the direction in which the trend is not apparent.

2.3.4.3 Generation of the transmissivity fields

Four sets of 200 log$T$ realisations each, are generated by sequential simulation. Figure 2.4 shows the first field generated in each method. The impact of the random function model choice is already apparent. The RF models that use the normal-score transform of the data produce realisations with a much more abrupt variation than the models that use the logtransform of the data. Due to the exact reproduction of the sample histogram the apparent bimodality seen on the sample histogram (see Figure 2.3) is also found on the generated realisations. Both models are able to reproduce the E-W trend: the NSCORE models with a quasi-step function, the UNTRAN models with a more gradual variation. The differences between the OK and the UK simulations are not very large. This finding confirms that conditioning will impose the trend in the realisations even if the RF model does not incorporate it explicitly. The main difference between the OK and the UK-simulations is the slightly larger continuity in the N-S direction displayed by the OK-simulations. The reason for this enhanced N-S continuity lays on the zonal anisotropy used to model the variogram with different sills in the N-S and E-W directions.

2.3.4.4 Flow and transport simulation

The four models are compared in two different transport situations. A release of particles in the geometric centre of the field (the geometric centre corresponds with the location of the WIPP waste panels) is considered and calculations are made by particle tracking (no dispersion) and by random walk (with

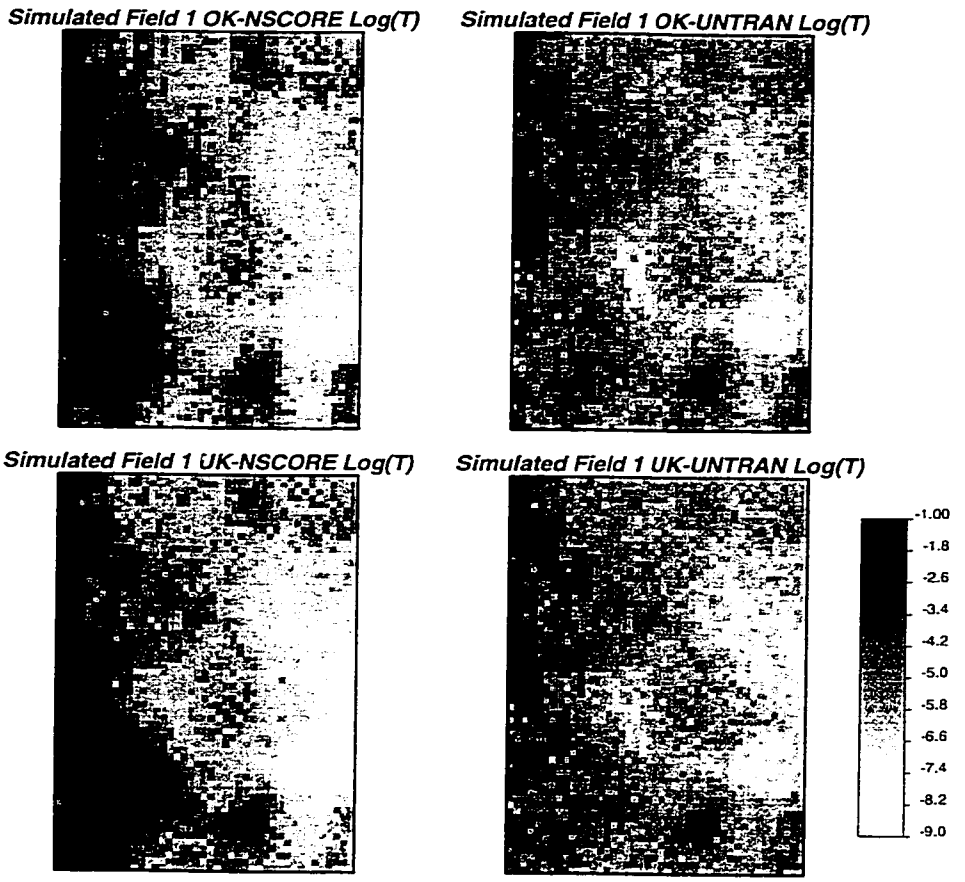

Figure 2.4 The first simulated log transmissivity field of each set.

dispersion). This resembles the potential release from the nuclear waste repository at WIPP and corresponds to the risk evaluation for a scenario of failure. The four RF models are compared in terms of the results of the transport simulations. Cumulative statistics of the arrival locations and arrival times of the released particles at a selected control plane are computed and compared for the different cases. Figure 2.5 illustrates the simulation experiment.

The groundwater flow equation has been solved for the 800 (4 x 200) log$T$ fields. The prescribed head boundaries impose an average flow oriented on the northnortheast-southsouthwest direction (from the upper boundary to the lower boundary). Flow velocities in the x-direction are much lower than flow velocities in the y-direction. The highest flow velocities in both the x-direction and the y-direction are found near the left boundary, which is due to the high log$T$ values in this part of the area. A highly permeable zone near the left boundary produces a channelling effect for the particles travelling near it. This high zone tends to be wider near the lower boundary. Flow velocities are the smallest near the right boundary, especially in the right-lower corner.

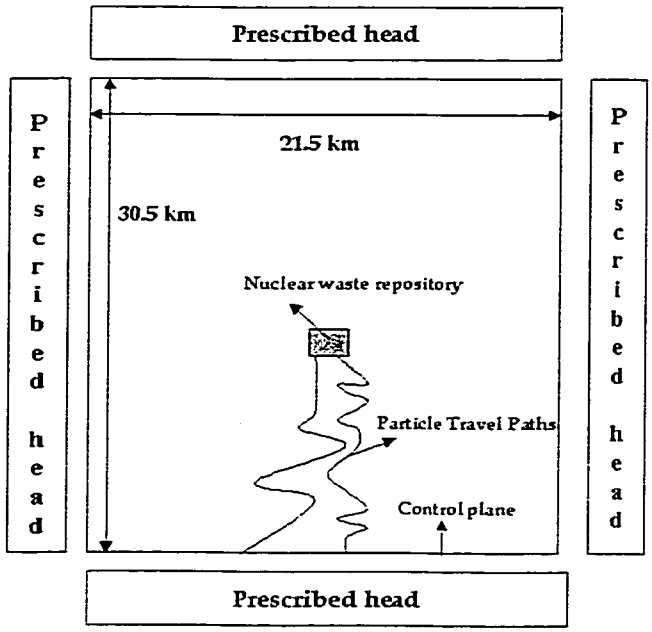

Figure 2.5 Schematic overview of the simulated flow and transport situation at the WIPP-site.

For the mass transport simulations, 2000 particles are released in each of the 800 log$T$ fields from the geometric centre of the field. Cumulative breakthrough curves at the lower boundary are obtained. Two cases are analysed, one considering advective transport only, and another considering both advective and dispersive transport. For the latter case, the longitudinal and transversal dispersivities are set to 10 m and 1 m respectively (cell size is 500 by 500 m).

Table 2.1 summarises some basic statistics about the arrival locations of the particles to the control plane for the four RF models. In general, it can be seen that considering dispersion has little influence on the arrival locations of the particles. The value for the transversal dispersivity considered is too small to make a difference. For the UK-sets and the OK-sets the results show that accounting for the trend explicitly in the model (UK-sets) shifts the arrival locations to the right by an amount which is only of the order of a discretization cell. The differences in average arrival location of the particles from the NSCORE and UNTRAN sets are also on the order of the width of the discretization cell (~500 m) although slightly larger than the differences between the OK- and UK- sets.

(in meters)	mean	Std.dev.	max.	upper quartile	Median	Lower quartile	min.
OK-NSCORE	8885	1012	11016	9411	9012	8587	5231
UK-NSCORE	9302	673	11017	9693	9252	9027	6462
OK-UNTRAN	8284	1057	10528	9000	8446	7769	3879
UK-UNTRAN	8567	915	10513	9064	8775	8105	3554
OK-NSCORE **	8879	1018	11527	9436	9020	8585	4958
UK-NSCORE **	9301	677	11150	9701	9248	9033	5896
OK-UNTRAN **	8282	1062	10700	9000	8452	7760	3514
UK-UNTRAN **	8563	916	10600	9057	8767	8097	3343

**simulations including dispersion

Table 2.1. Statistics of particle arrival locations to the lower boundary, given in m from the lower left corner.

More important differences can be noticed while comparing the spread of the arrived particles at the lower left boundary. This spread is an indication about the uncertainty in the transport simulations. The standard deviation of the particle arrival locations for the models explicitly accounting for the trend is lower than for the models without the trend. This effect is bigger for the models using the log-transform than the models using the normal-score transform. Furthermore, for the model without the trend, it seems to make little difference which transform is used. The reduced spread of the particle arrival locations can be explained by a reduced uncertainty in the RF model that explicitly incorporates the trend. In spite of the fact that the log conductivity realisations for the models that use the log-transform and the normal-score transform have a clearly different aspect, the differences in the arrival locations are small. The conductivity differences between the two RF models are smaller for the part of the aquifer between the particle release locations and the particle arrival locations. The differences between the models that use the log-transform and the models that use the normal-score transform are for example bigger in the Western part of the aquifer.

The cumulative breakthrough curves for the different cases are given in Figure 2.6. The breakthrough curves for the OK-sets and UK-sets are very similar when intra-cell dispersion is considered and very close to having a lognormal distribution. Differences in log$T$ values between the fields from the OK-sets and the fields from the UK-sets tend to have less impact on the breakthrough curves in case of intra-cell dispersion: transversal dispersion causes mass exchange between faster and slower flowlines, which results in more "averaged" travel times of the particles. This effect is similar when comparing the obtained breakthrough curves for the cases with intra-cell dispersion and the breakthrough curves obtained for the cases without intra-cell dispersion; intra-cell dispersion reduces the tails of the breakthrough curve due to the

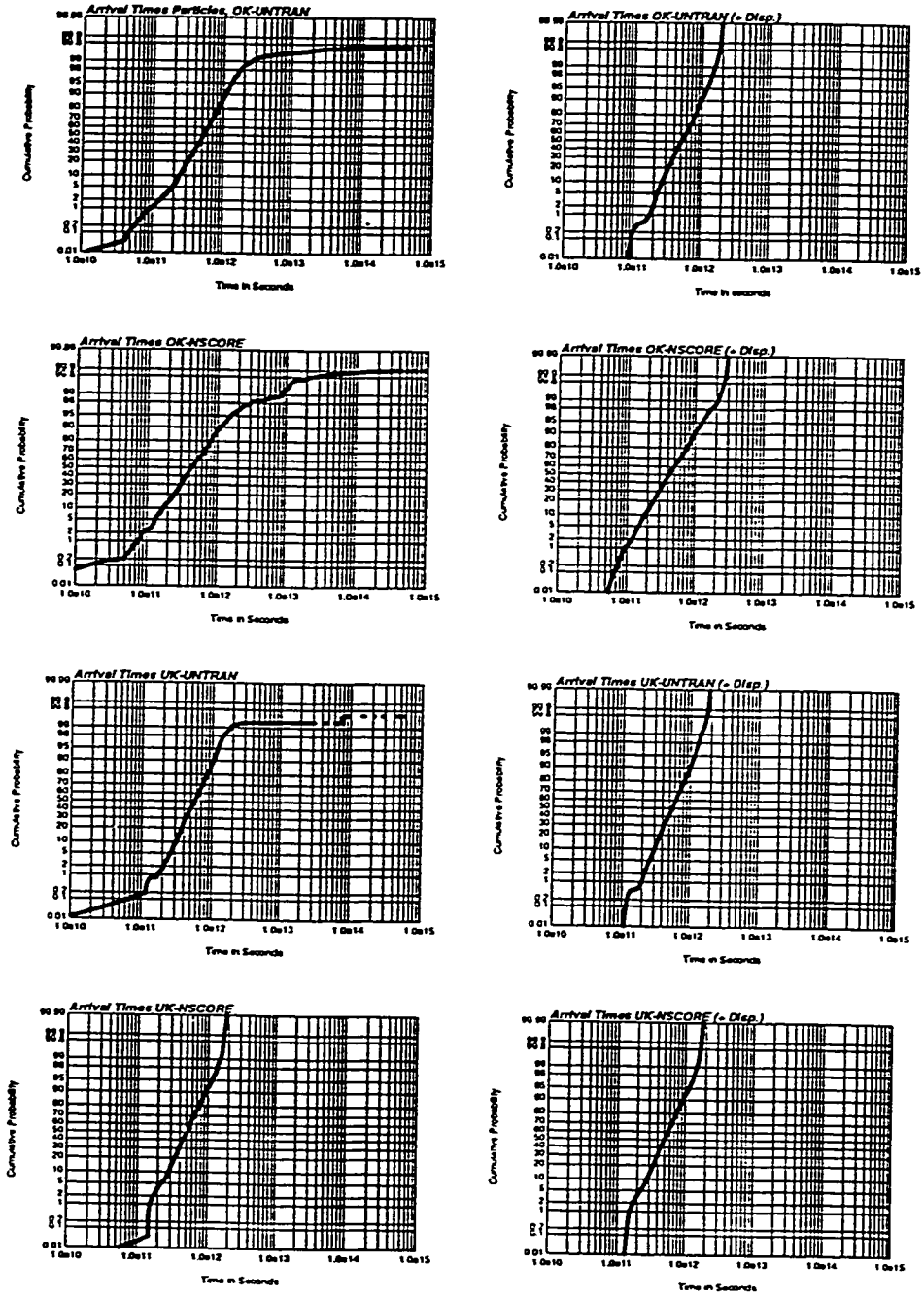

Figure 2.6 Breakthrough curves for the four different sets, both for non-dispersive mass transport and dispersive mass transport. The curves are obtained from 200 realizations.

transversal mass exchange between fast and slow travel paths. The effect of including intra-cell dispersivity is considerable. The resulting breakthrough curves from the NSCORE sets and the UNTRAN sets are comparable, but differ more than the breakthrough curves for the UK- and OK-sets. The breakthrough curves from the NSCORE sets are in general more abrupt. In terms of concentration this would mean that for the UNTRAN sets the first breakthrough occurs earlier, but that for the NSCORE sets a higher peak value would be obtained.

2.3.4.5 Conclusions

1. The differences in the transport simulations between the UK- and the OK-sets are in general small, particularly taking into account the distance travelled by the particles relative to the size of the simulation domain. One of the differences between the two sets is the smaller standard deviation in arrival locations for the UK- realisations than for the OK- ones in the transport situations considered. If we consider that the standard deviation is a measure of the uncertainty, the UK- RF results in less uncertain simulations for this transport situation, partly due to the explicit incorporation of the trend in the RF model.

2. Of the three effects analysed (trend, normal-score transform, and intra-cell dispersion), it seems that, for this particular data set, results are robust to the way the trend is modelled and also to the use of normal-scores. There are significant differences between results in which intra-cell dispersion is represented and those in which it is not. The breakthrough curves are more affected by the inclusion of intra-cell dispersion than by the choice of the random function model. If one takes into account that there are many more sources of uncertainty (e.g. uncertainty with respect to the prescribed head boundaries, probably nonsteady flow regime), which are not considered in this case study, one may conclude that the extra modelling effort and the difficult estimation of the variogram of the residuals are not worth the effort to account explicitly for the trend in the RF model. With respect to the use of the normal score transform in the simulation it can be stated that in spite of the clearly visible differences between the simulated fields, the impact has not been very big in these transport simulations. The most important impact was found on the breakthrough curves, especially in their tails. However, the visible differences in simulated fields suggest that, for other transport situations, the normal score transform may have a larger impact. The decision on the use of the normal score transform is relevant in groundwater modelling where the normal distribution to model the sample data frequency distribution is most often adopted independently of how well the sample data follow a Gaussian distribution. The decision on whether to use or not a normal distribution for log transmissivity (or for hydraulic conductivity) is difficult to support, particularly when data are few and highly clustered. In the case of the WIPP-study, for instance, the small sample could have resulted in the apparent bimodality. An alternative

would have been to smooth the sample histogram before doing the normal-score transform in order to alleviate the sharp biomodality. In these occasions, short of indirect information that may support one or other RF model, we suggest considering the two models and use as uncertainty estimate the total uncertainty spanned by both models.

3 Inverse modelling of groundwater flow

As explained in Chapter 1, general interest exists in the characterisation of the spatial variability of the transmissivity field, because it is thought that uncertainty about the heterogeneous transmissivity field is the most consequential one with regard to the uncertainty on groundwater flow predictions (Smith and Schwartz, 1981). The geostatistical methods presented in Chapter 2 are capable of incorporating different sources of information, which reduce the uncertainty on the heterogeneous transmissivity field. Examples of data which are integrated by geostatistical methods and reduce the uncertainty are hydraulic conductivity measurements or seismic information (see also Chapter 2). In addition, there exists interest in using hydraulic head measurements to constrain the unknown transmissivity field. Hydraulic head measurements are cheaper to obtain and in general more abundant than transmissivity measurements. Due to the fact that transmissivity depends on hydraulic head non-linearly through the groundwater flow state equation, the use of hydraulic heads for transmissivity characterisation is not a trivial procedure. Trial-and-error procedures have been used in the past to obtain the spatial distribution of transmissivities that best reproduces the observed transmissivities and the observed hydraulic heads. Some decades ago, automated procedures were developed in order to solve this problem. The problem is commonly known as the groundwater flow inverse problem. It refers to the estimation of parameters in the groundwater flow equation, such as transmissivity, using measurements on state variables, such as hydraulic head. In this chapter the self-calibrating method, a stochastic inversion method, is presented. The self-calibrating method solves the groundwater flow inverse problem using a Monte Carlo approach. Therefore, we refer to it as a method for the stochastic inverse modelling of groundwater flow. Section 3.1 gives a literature research on inverse modelling of groundwater flow. The research is not exhaustive, but presents in some detail eight of the most relevant methods. Section 3.2 introduces in detail the self-calibrating method (SCM) and its extension to handle transient groundwater flow and the joint calibration of transmissivities and storativities. Section 3.3 details the numerical implementation of the self-calibrating algorithm for the inverse modelling of groundwater flow. Section 3.4 presents the application of the SCM in the inverse modelling of transient groundwater flow and the calibration of a single storativity at the WIPP site. Section 3.5 describes another application of the SCM for the inverse modelling of different steady-state flow regimes at a Swedish site. Also a sensitivity study is included. Section 3.6 is a slightly modified version of an article published in the journal Advances in Water Resources Research (Hendricks Franssen *et al.*, 1999) presenting a synthetic study carried out on the joint simulation of transmissivity and storativity fields conditional to steady-state and transient-state head data in different flow regimes and with different (synthetic) measurement campaigns.

3.1 Literature research inverse modelling of groundwater flow

The inverse methods reviewed are grouped as explained next. Section 3.1.1 and 3.1.2 contain methods which rely on a linearization of the groundwater flow equation in order to linearly relate hydraulic head to transmissivity and possibly to recharge. The variables are treated in a stochastic framework using a random function model. This random function is described with a few parameters, the values of which are estimated by maximum likelihood. Then, estimates of the input parameters and output variables at any point in the domain are obtained using linear estimation theory. The linearized cokriging method from Kitanidis and others (Kitanidis and Vomvoris, 1983; Hoeksema and Kitanidis, 1984) and the semi-analytical linearized method by Dagan and Rubin (Dagan, 1985; Rubin and Dagan, 1987a; Rubin and Dagan, 1987b; Dagan and Rubin, 1988) are discussed.

Next, some methods are discussed which circumvent the limitations of the linearization of the groundwater flow equation. These methods take into account the non-linear dependence of transmissivity on hydraulic heads by solving the groundwater flow equation numerically and starting an iterative optimisation process afterwards, in which the groundwater flow equation is solved numerous times. Section 3.1.3 discusses the zonation procedure by Carrera and Neuman (Carrera and Neuman, 1986a; Carrera and Neuman, 1986b; Carrera and Neuman, 1986c). Section 3.1.4 presents the self-calibrating method, the first method which uses a stochastic simulation approach to solve the groundwater flow inverse problem without linearizing the groundwater flow equation (Sahuquillo *et al.*, 1992; Gómez-Hernández *et al.*, 1997; Capilla *et al.*, 1997 and Capilla *et al.*, 1998). An introduction to the self-calibrating method is given here in order to situate the development of this method in a historical context. In section 3.2 details on the method will be presented. Sections 3.1.5 and 3.1.6 present two other methods that use a Monte Carlo approach in combination with a numerical solution of the groundwater flow equation in solving the groundwater flow inverse problem. The two methods differ in the employed non-linear optimisation technique. They are the Pilot Point Method by de Marsily, LaVenue and others (LaVenue *et al.*, 1995; RamaRao *et al.*, 1995) and the Markov Chain Monte Carlo Method by Oliver and others (Oliver *et al.*, 1996; Oliver *et al.*, 1997).

We also discuss two other methods which take into account the non-linear relationship between transmissivities and hydraulic head using an iterative approach to get a better description of the random function model, more precisely its covariance. These methods start with the linearization of the groundwater flow equation, but continue after the first step by linearizing the flow equation around the updated estimates, re-estimating the covariance matrices and using the hydraulic head residuals (the differences between simulated and measured heads) as the updated piezometric conditioning information. The iterative procedure continues until the hydraulic head data are

reproduced sufficiently close. Apart from the iterative nature, the methods described in this chapter have the same philosophy as the methods discussed in sections 3.1.1 and 3.1.2, namely, once the random function model is defined, the input parameters and the output variables are obtained using linear estimation. They are the Fast Fourier Transform Method by Gutjahr and others (Gutjahr *et al.*, 1994; Hughson and Gutjahr, 1998) and the iterative cokriging-like technique by Yeh and others (Yeh *et al.*, 1995; Yeh at el., 1996; Hanna and Yeh, 1998).

3.1.1 Linearized cokriging method

Methodology

Introduction

The linearized cokriging approach, developed by Kitanidis and others (Kitanidis and Vomvoris, 1983; Hoeksema and Kitanidis, 1984), is the first one to use geostatistics in the inverse modelling of groundwater flow. The two seminal papers that present the theoretical basis of the method are discussed next. In the first paper (Kitanidis and Vomvoris, 1983) the approach is applied for 1-D steady groundwater flow, and, in the second paper (Hoeksema and Kitanidis, 1984) an extension is made to 2-D steady groundwater flow. The inversion can be extended to the case in which sinks and sources are present. Boundary conditions may also be subject to calibration.

In the 70's an increasing amount of papers was devoted to the statistical treatment of the groundwater flow inverse problem. The linearized cokriging approach treats the inverse problem geostatistically; the random transmissivity field and the random hydraulic head field are related by a linearization of the steady groundwater flow equation. Then, cokriging is used to estimate hydrogeologic parameters (transmissivities and possibly boundary conditions and/or leakage rates) on a grid covering the aquifer.

The steps in the calibration process

As in any geostatistical approach, the spatial variability of the parameters is mathematically described using a random function model. Kitanidis and Vomvoris (1983) state that the main advantage of their application of the geostatistical approach to inverse modeling is that it avoids the problem of large dimensionality by drastically reducing the number of independent parameters to be estimated as explained next.

1. *Identification of the structure of the parameter field - structure selection.*

A geostatistical model is adopted for the random fields of transmissivity, hydraulic head and eventually recharge. Once a geostatistical model is adopted the only degree of freedom is the functional representation of the variogram (whether it is exponential, spherical, or otherwise), whether the model is

stationarity or non-stationarity and if the model is non-stationary, which is the drift. These decisions leave as only parameters to be determined those defining the variograms and those defining the constant mean (stationary model) or the drift function (non-stationary model). Kitanidis and Vomvoris (1983) state that the parameter identification should be repeated for a number of random function models and possibly for a number of conceptual models on the system behaviour (for instance with and without recharge) until the most appropriate model is found. Attention is usually restricted to models which have been chosen on the basis of their performance in past applications. The aim of the structure selection step is to choose a model in agreement with the data and as simple as possible (the parsimony principle). Kitanidis and Vomvoris state that model selection criteria like Akaike´s criterion could serve as a guide, because the model selection has a multiobjective nature, although we have our doubts on this respect due to the strict underlying assumptions that are need to come up with the information criterion. All available prior information should be taken into account in the selection of the most appropriate model for the structure of the hydrogeologic parameter field.

2. *Identification of the structure of the parameter field - maximum likelihood estimation of structural parameters.*

For the model selected the parameters defining the joint random function model for transmissivity, hydraulic head and recharge are estimated simultaneously by maximum likelihood. The likelihood function is written in terms of the vector of mean values (for transmissivity, hydraulic head and possibly recharge, at each node in the domain) and the (cross) covariance matrices among these parameters. In turn, means and cross-covariances are given as a function of a few structural parameters, such as, constant means or drift coefficients (if a drift is assumed for the mean) or the correlation ranges for the covariances. It is assumed that the joint probability function of the measurements of all observable quantities (both parameters and state variables) is multi-Gaussian. The joint normality assumption is consistent with first-order analysis, for which the hydraulic head is a linear function of multi-Gaussian log transmissivity. The hydraulic head mean values, the hydraulic head covariance and the log transmissivity-hydraulic head cross-covariance which appear in the likelihood expression are obtained from the transmissivity mean value and the transmissivity covariance by a first-order linearization of the groundwater flow equation. This first-order linearization is considered to be valid up to variances of $\log_{10}$ transmissivity of 1.0. The linearized groundwater flow equation is solved by analytical (1-D) or numerical (2-D) methods. The structural parameters defining mean and covariance functions are estimated by maximum likelihood so that the probability that the given measurements would occur is maximised. Gauss-Newton optimisation is used to estimate, in an iterative fashion, the structural parameters.

3. Identification of the structure of the parameter field - model validation and diagnostic checking.

The validity of the assumed geostatistical structure is tested by the following procedure. The error covariance matrix for the estimated geostatistical parameters is determined. In addition, the significance of the parameter estimates and the consistency between model and data can be tested statistically. On the basis of these statistical tests the hypothesised structure is accepted or modified (Kitanidis and Vomvoris, 1983). It is unfortunate that all these tests have to rely on the prior hypothesis of joint multi-Gaussianity of the different parameters; hypothesis that cannot be verified and is stronger than the consistency that it is being tested.

4. Estimates of hydrogeological parameters by kriging.

Once the physical model and the geostatistical structure have been decided upon and its structural parameters have been determined by maximum likelihood, point estimates of the hydrogeologic parameters can be obtained by cokriging. The estimation of log transmissivity at a certain location is a weighted sum of point measurements of log transmissivity and hydraulic head. The weights are obtained by solving a linear system of equations (cokriging system) so that the log transmissivity estimate is unbiased and the estimation error variance is minimum. In the estimation procedure the covariance matrices of transmissivity and hydraulic head and the cross covariance matrix of transmissivity-hydraulic head are used. These covariance matrices had been obtained using the first order approximation of the groundwater flow equation, as described in step 2.

Application

Hoeksema and Kitanidis (1984) present an application of the linearized cokriging approach to a real case study. They apply the linearized cokriging approach to the Jordan aquifer of Iowa, USA. The model is for 2-D steady-state flow in a leaky confined aquifer and with prescribed head boundary conditions. A total of 31 steady-state head and 56 log transmissivity measurements are available. The case study illustrates the iterative approach in the model selection: the conceptual models considered are groundwater flow without leakage, groundwater flow with leakage and groundwater flow with leakage, discarding two head measurements. This last model yields results that pass the multi-Gaussian model validation and diagnostic checking tests. The conclusion was that there is leakage and that two head measurements are unreliable.

Some important characteristics of the method

The geostatistical approach for inverse modelling explicitly handles the uncertainty associated with spatially variable phenomena. In addition, the linearized cokriging approach circumvents the ill-posedness of the inverse

problem by using just a few parameters in the inversion procedure, which are the parameters describing the geostatistical structure of the log transmissivity random function. Once these parameters are known, the transmissivity and the heads can be determined on any grid by the use of the standard cokriging equations.

It should be noted that the linearized cokriging approach has a limited field of application. The (cross) covariance matrices and the estimated means for hydraulic head are obtained by a first-order linearization of the groundwater flow equation. This linearization is valid for $\log_{10}$ transmissivity variances below 1.0, and in practice $\log_{10}$ transmissivity variances above 1.0 are common. The use of the transmissivity field obtained by this approach as input to a groundwater flow solver (which does not linearize the groundwater flow equation) will yield a deviation between the measured and simulated heads. This deviation will grow with the magnitude of the log transmissivity variance.

As most of the methods revised in this section, it was originally aimed at determining a unique single best solution to the inverse groundwater flow problem. As a by-product, the maximum likelihood approach provides a lower bound of the error covariance matrix that could be used for the generation of multiple solutions to the inverse groundwater flow problem; simulations of the errors can be made to be added to the "optimal" transmissivity field producing simulations of the transmissivity field around the optimum. However, since the covariance matrix is just an approximation of the real covariance matrix, and, in any case, the covariance only captures the linear relationship between two variables, the solution of the flow equation using the transmissivity fields generated in this way will be only approximations of the measured heads.

The linearized cokriging approach as presented by Kitanidis and co-workers seems not to be very flexible for extensions to transient groundwater flow, and for the simultaneous estimation of different parameters, such as transmissivity, storativity or recharge. Sun and Yeh (1992) extended the linearized cokriging approach to transient groundwater flow, making use of adjoint state equations.

An advantage of the linearized cokriging method is that the CPU time usage is small compared to other methods.

More comments on the linearized cokriging approach can be found in section 3.1.3, in the discussion of the characteristics of the zonation procedure.

3.1.2 The linearized semi-analytical approach

Methodology

Introduction

The work by Dagan and Rubin (Dagan, 1985; Rubin and Dagan, 1987a; Rubin and Dagan, 1987b; Dagan and Rubin, 1988) is closely linked to the work of Kitanidis and others. The approach which is used to calibrate the transmissivity field to hydraulic head data does not differ much from the linearized cokriging approach. A main difference is that, in the linearized semi-analytical approach, a Bayesian updating procedure is used instead of cokriging. Four papers illustrate the development of the linearized semi-analytical approach. The first paper (Dagan, 1985) presents the methodology in a general framework. In the second paper (Rubin and Dagan, 1987a), the method is extended for the estimation of a constant, but random, effective recharge after relaxing some of the assumptions. The third paper (Rubin and Dagan, 1987b) illustrates the approach using a case study. The fourth paper is an extension to incorporate transient head measurements and to the estimation of the storativity (Dagan and Rubin, 1988). Dagan and Rubin were the first to solve the inverse problem for time-dependent flow in an analytical framework, but Carrera and Neuman (1986a, 1986b) defined a numerically-based procedure to solve this problem some years before (see section 3.1.3).

The steps in the calibration process

The steps to be taken in the linearized semi-analytical approach are similar to the ones which have to be taken in the linearized cokriging approach. However, the authors pay less attention to the first and last step regarding the structure selection and focus on the second step, the maximum likelihood procedure.

1. *Maximum likelihood estimation of structural parameters.*

The starting point is steady-state or transient-state flow with the presence of recharge in a 2-D domain at which some transmissivity measurements and hydraulic head measurements have been taken. The aim is to estimate a vector of structural parameters which describe the random transmissivity field jointly with the random head field. Generally these parameters are the average log transmissivity, the log transmissivity variance and the integral scale of transmissivity. In order to estimate the parameters a number of assumptions are made (Rubin and Dagan, 1987a):

(i) The variance of $\log_{10}$ transmissivity is smaller than one so that the groundwater flow equation can be linearized by a first-order small perturbation analysis.

(ii) Log transmissivity is normally distributed with constant mean and isotropic exponential covariance.

(iii) The average head shows a quadratic trend in space.

In case of transient groundwater flow the following additional assumptions are made (Dagan and Rubin, 1988):

(iv) Storativity is constant in the spatial domain and recharge is constant in space, but variable in time.

(v) The transient groundwater flow equation is split in two parts. One part corresponds to the flow field after the effects of the pumping wells are filtered out, and the other part is related exclusively to the pumping wells. The part which is related exclusively to the pumping wells is expressed by a generalisation of the Theis elementary solutions for each well in an unbounded domain and for time depending pumping rate. The measured transmissivity or, if a transmissivity measurement at the well is not available, the effective transmissivity value is used in the generalisation of the Theis elementary solution.

(vi) The remaining part of the solution, with the effect of the pumping wells filtered out, is related to the recharge and to the boundary conditions. It is assumed that the expected head value has a slowly varying quadratic trend in time. In addition, a quasi steady-state representation is adopted, describing the transient groundwater flow as a series of (different) steady states in time. The average head component is related directly to the recharge and indirectly to the boundary conditions, while some others terms in which time derivatives appear are neglected.

(vii) The residual head (the head minus the expected head after filtering out the effects of the pumping wells) is assumed to satisfy a Poisson equation and the time derivative is neglected for the same reasons as mentioned before.

(viii) The effect of the presence of boundaries is taken into account in an indirect, approximate way. First, the justification for adopting the presentation of the head as a gradually, in space and time, varying function, results partly from the boundary conditions. Second, the covariances of the transmissivity and hydraulic head values at two different points are taken equal to those pertaining to an unbounded domain. This holds if the points are sufficiently far from the boundaries. In particular, it is considered that, in a band of one integral scale from the boundary, this assumption does not hold. In the work of Dagan (1985) an even more restrictive assumption was made: the flow domain was assumed infinite.

The linearization of the groundwater flow equation and the assumption that log transmissivity is normally distributed with constant mean and exponential covariance make it possible to derive, by a small perturbation approach (Green's function techniques), the head covariance and the cross covariance between transmissivity and head. Dagan (1985, section 3) made these derivations for a uniform head gradient and Rubin and Dagan (1987a, section 2) made derivations for the more general case of a quadratic trend in head values,

so that also recharge can be identified. Finally, Dagan and Rubin (1988, section 5) derived the covariances for the case of time-dependent (quasi-steady) groundwater flow.

Once the head covariance and the head-log transmissivity cross-covariance are derived, the likelihood function can be written in terms of the structural parameters that will be subject to identification using a maximum likelihood approach.

2. *Some spatial invariant parameters can be estimated.*

The constant storativity, the effective recharge can be incorporated in the likelihood expression and estimated, together with their variances, during the maximum likelihood procedure. The effective recharge would be a function of time in case of transient groundwater flow. If recharge and storativity are the only quantities of interest the calculations can be concluded at this point.

3. *Estimates of hydrogeological parameters by Bayesian updating.*

After the structural parameters are determined, the values for the hydrogeological parameters and their estimation variances are estimated by a Bayesian updating procedure. It is assumed that log transmissivity, hydraulic head and recharge are multivariate normal distributed. The updated expected transmissivity value (also referred to as the conditional expected transmissivity) is the sum of the unconditional transmissivity plus a weighted linear combination of transmissivity residuals and a weighted linear combination of head residuals. The weights are solutions, in this special case, of a cokriging system. It is considered that these weights are also random variables, because the estimation of the vector of structural parameters (see step 1) is associated with uncertainty. A linearization technique is used to expand the weights as a sum of the estimated weights plus a weighted linear combination of the errors of estimation of structural parameters. As a result, in the expression of the conditional transmissivity covariance an extra error term appears associated with the uncertainty in the estimation of the structural parameters.

The application of the linearized semi-analytical approach in two case studies

We will discuss two applications of the linearized semi-analytical approach. One is taken from Rubin and Dagan (1987b) and is about the inverse modelling of steady-state groundwater flow with the presence of constant recharge. The other study deals with transient groundwater flow with the presence of time-variable recharge (Dagan and Rubin, 1988).

Rubin and Dagan (1987b) deal with the inverse modelling of groundwater flow at the Avra Valley aquifer in Arizona (USA). A total of 106 transmissivity values and 98 water heads are available. The aquifer is divided into two regions, north and south, because the transmissivity in the northern part is

significantly higher on average than that of the southern part. The spatially variable log transmissivity and the effective recharge are determined separately, and simultaneously, for the two subregions of the aquifer. The maximum likelihood procedure results in the estimation of the vector of structural parameters and its associated estimation error covariance matrix. It is found that incorporating head measurements reduces the uncertainty associated with the estimation of the vector of structural parameters. The maximum likelihood procedure is also carried out for only transmissivity data or only hydraulic head data. It is found that the use of both transmissivity and hydraulic head data results in the lowest estimation variances. The method also indicates that some recharge may exist, although of a small magnitude.

Dagan and Rubin (1988) deal with the inverse modelling of transient groundwater flow on a section of Israel's coastal aquifer. The aquifer is of 120 km length and 12-20 km width and the case study focuses on a subarea of 7 by 7 km, about 9 km east of the coastline. The region is an area with intensive pumping in summer time and artificial recharge through wells in winter time. The modelling was carried out for the period of October 1970 until April 1971. In total 5 transmissivity measurements were available and 40 hydraulic head measurements were taken each month. There is a total of 29 pumping wells in the region. The drawdown induced by pumping at the wells has been computed using the monthly pumping and injection records. These drawdowns are subtracted from the observed head. By means of the maximum likelihood method the structural parameters are estimated. It is found that values for the structural parameters are strongly correlated over time. The estimation of the structural parameters and the estimation of transmissivity and storativity show (1) that the first-order approximation of the flow equation was valid for this aquifer, (2) that the quasi-steady approach was valid (the estimates for the structural parameters show little changes between months), (3) that the maximum likelihood estimations of the structural parameters have a relatively small variance, and (4) that the maximum likelihood estimates for consecutive months display a variation of the order of the spread indicated by the variance of estimation. In addition, it is found that the storativity is a parameter of low spatial variability. The recharge was estimated by different methods. The estimates of recharge are close to estimates made by multiseasonal and regional water balances and estimates based on texture analysis. It was found that the head measurements improve the characterisation of the transmissivity field dramatically; with only five transmissivity measurements it was hardly possible to characterise the transmissivity field while with the help of the hydraulic head data a more detailed identification was possible.

Graham and Tankersley (1994) derive closed-form expressions for the unconditional head covariance, the cross-covariance between head and log-transmissivity and the cross-covariance between head and recharge. These covariances are derived from a linearization of the groundwater flow equation using spectral transform techniques and assuming an infinite aquifer. (In

addition, it is assumed that the recharge has a zero mean and that is uncorrelated with transmissivity.) Once the covariances are known, the method proceeds as described earlier by applying co-kriging to the data. The difference with the method of Rubin and Dagan is the treatment of recharge. Whereas Rubin and Dagan estimate a spatial average of the recharge, Graham and Tankersley produce a smooth spatially variable estimate of recharge.

Graham and Neff (1994) apply the method presented by Graham and Tankersley (1994) to the Upper Floridan Aquifer in North-eastern Florida. A subarea of the aquifer in which the assumption of a constant mean hydraulic head gradient could be made was selected. The following parameters: mean log transmissivity, log transmissivity variance, log transmissivity correlation scale, mean recharge, recharge variance, recharge correlation scale, mean head gradient and head variance, are estimated from the data. The results of the estimation procedure show that the estimation head variance is clearly lower in the case in which both head and transmissivity data are used than in the unconditional case. However, the transmissivity data have little contribution to this reduction. The estimation log transmissivity variance is also clearly reduced by the use of head data. In this particular case, this is mostly due to the large amount of head data available compared to the few transmissivity measurements. It was also concluded that considering recharge in the estimation process had a large impact in the resulting estimated log transmissivity field. On the other hand, the resulting estimate map of recharge is successful in identifying an area of spring recharge and to capture the major features of the known areal recharge patterns.

Some important characteristics of the method.

The same comments which were made in the discussion of the linearized cokriging approach also hold for the linearized semi-analytical approach and are repeated below. The differences between the methods are minor.

In principle, the linearized semi-analytical approach poses the inverse modelling of groundwater flow in a more general framework than the linearized cokriging approach. The Bayesian updating approach is a more general framework than the cokriging approach to obtain the conditional moments from the unconditional moments for, say, transmissivity. The Bayesian updating is not limited to Gaussian processes and produces the complete characterisation of the variable of interest, not just the expected value and the covariance. However, in a reply, Kitanidis (1986) states that for other than multi-normal distributed variables the integration of the equations involved in the Bayesian updating equations can only be achieved numerically with a prohibitive computational cost. In addition, Kitanidis argues that the data seldom include sufficient information to determine the finer details of the joint probability density function of the properties of interest. Finally, he states that even if the complete probability density function of transmissivity is

known no general and computationally efficient method is known to derive the probability density function of the piezometric head. Another difference between the linearized cokriging procedure and the linearized semi-analytical approach is that, in the linearized semi-analytical procedure, an analytical solution to the linearize equation is used, while Kitanidis and others in their later works use a numerical procedure to solve the linearized groundwater flow equation and to obtain the covariance matrices (Hoeksema and Kitanidis, 1984). Analytical solutions can only be obtained for simple geometries, boundary conditions and input distributions. On the contrary, numerical solutions can account for complex geometries, boundary conditions and inputs.

It should be noted that the linearized semi-analytical approach has a limited field of application, like the semi-analytical cokriging approach. The (cross) covariance matrices and the estimated means are obtained by a first-order linearization of the groundwater flow equation. This linearization is valid for $\log_{10}$ transmissivity variances below 1.0. However, in practice $\log_{10}$ transmissivity variances above 1.0 are common. In addition, the effect of the boundaries is neglected. Rubin and Dagan (1987a) use more restrictive assumptions with respect to the boundary conditions than Kitanidis and others in order to solve the linearized groundwater flow equation. In particular, Rubin and Dagan state that the assumptions made to solve the equation are violated for the zone which is within one integral scale of the boundary. Finally, and most importantly, the use of the transmissivity field obtained as input to a groundwater flow solver will yield a deviation between the measured and the simulated heads. This deviation will grow as the log transmissivity variance increases.

The method determines a unique single best solution of the inverse groundwater flow problem. The disadvantage of a single best solution of the inverse groundwater flow problem is that it is always smooth and it can never represent reality. However, given that the entire statistical structure of the variables of interest is also determined, it is possible to use their covariance matrix to simulate multiple solutions to the inverse groundwater flow problem. The big disadvantage is that, in any case, the solution to the groundwater flow equation in the generated fields will not honour the measured heads due to the approximation.

The linearized semi-analytical approach seems not to be very flexible for extensions to complex domains, three-dimensional flow, simultaneous estimation of a number of possibly spatially variable parameters or the combined inverse modelling of groundwater flow and mass transport. The extension Dagan and Rubin (1988) made to transient groundwater flow is a quasi steady-state approach. However, others extended the method successfully to more complex situations. Sun and Yeh extended the linearized approach to transient groundwater flow, making use of adjoint state equations (Sun and Yeh, 1992). They found that considering transient groundwater flow yielded

much better results than the quasi steady-state approach of Dagan and Rubin (1988). Grenier *et al* (1996) extended the method of Dagan and Rubin to cases of non uniform groundwater flow and non stationarity of the mean log transmissivity by a scale separation approach. In the scale separation approach the hypothesis of locally uniform flow is made and conditioning is limited to neighbouring data points for a spatial covariance model derived from scale-separation considerations. However, the methodology is not suited for the high non-uniformities encountered near wells.

An advantage of the linearized cokriging method is that it is not CPU intensive and that it is conceptually simple.

3.1.3 The zonation procedure

Methodology

Introduction

The theoretical basis of the zonation procedure, a method for the inverse modelling of groundwater flow developed by Carrera and Neuman, has been published in a series of three papers (Carrera and Neuman, 1986a, Carrera and Neuman, 1986b, Carrera and Neuman, 1986c). Later the method was extended for the inverse modelling of coupled groundwater flow and mass transport (e.g. Medina, 1993, Medina and Carrera, 1996).

In the method developed by Carrera and Neuman for solving the inverse groundwater flow problem, the exact formulation of the steady or transient groundwater flow equation is used, without linearizing it. The inverse problem solution is obtained by an iterative fashion, in which the groundwater flow equation is solved numerous times. The most important characteristic of the method is that aquifer parameters are estimated for a limited number of zones which partition the aquifer. Different parameters can be estimated for each zone such as, values and directions of principal hydraulic conductivities in anisotropic media, specific storage, boundary conditions, or recharge rates.

The steps in the calibration process

The method of Carrera and Neuman can be summarised by the following six steps (Carrera and Neuman, 1986b):

1. *Choose an initial set of parameters.*
The following model parameter values have to be initialised and may be subject to calibration: values and directions of the principal components of hydraulic conductivities, specific storage, boundary conditions and recharge rates. The covariance matrix of all model parameters has to be provided, too. Argumenting that prior errors in model parameters can occur due to different causes and calling upon the central limit theorem, the authors conclude that the

errors must be Gaussian with zero mean. The parameter covariance matrix C_p is block diagonal, its diagonal components being the covariance matrices C_i for the different parameters; it is assumed that prior estimates of the various types of parameters are mutually uncorrelated. The covariance matrix of an individual parameter C_i is the product of a known or unknown positive scalar and a known symmetric positive-definite matrix V_i.

The covariance matrix of the prior head errors C_h has to be given, too. Carrera and Neuman use again the central limit theorem to state that prior head errors are Gaussian with zero mean; the reason being that there are a large number of contributing factors to the head errors (Carrera and Neuman, 1986a). The covariance matrix of the prior head errors C_h is the product of a positive, possibly unknown, scalar and a symmetric positive definite matrix V_h, which may be unknown up to one or more parameters. The authors state that errors at different well locations are normally weakly correlated and that this correlation is not likely to change with time. It means that the head errors show weak spatial auto-correlation. This auto-correlation structure is considered invariant in time. The head errors may show temporal correlation, due to systematic components of the prior head errors.

The prior errors in the model parameters and the prior head errors are considered independent.

2. *Solve the groundwater flow equation.*

The groundwater flow equation (steady or transient) is solved by the finite elements method. The input parameter values necessary to solve the groundwater flow equation are, for the first iteration, the prior estimates, for the subsequent iterations the updated values.

3. *Compute the gradient.*

During the calibration, all the unknown parameters will be estimated; the likelihood that, given the observations, the estimated parameter values are true, is optimised. A likelihood function is formulated that results in an objective function to be minimised that penalises the deviation between the predicted heads and the measured ones (weighted by the matrix V_h) and the deviation between the updated parameter values and their prior estimates (weighted by the matrices V_i).

The objective function value can be calculated after the groundwater flow equation is solved. Then, the gradient of the objective function with respect to the model parameters is determined. This requires, for each parameter, the sensitivity of the model fit with respect to the perturbation of that particular parameter. Carrera and Neuman apply the adjoint state method to calculate the gradient in an efficient way (Carrera and Neuman, 1986b, see also Carrera *et al.*, 1990). The adjoint state method makes it possible to calculate the gradient of the objective function without having to calculate the sensitivity matrix (the Jacobian matrix), which may result in important savings in CPU time in case the number of measurement spatial locations is less than the number of model parameters. (The adjoint state equations, like the groundwater flow equations, are solved by finite elements.)

4. Compute the updating direction.
Non linear optimisation algorithms are used to calculate the updating direction. Carrera and Neuman alternate three different optimisation algorithms during the calibration process, namely Fletcher-Reeves Conjugate Gradients, Broyden and Fletcher-Powell-Davidon. It was found that alternating different optimisation algorithms yields a faster convergence (Carrera and Neuman, 1986b) than using any of these algorithms independently. Fletcher-Reeves Conjugate Gradients does not use an estimation of second order derivatives of the objective function with respect to the model parameters. The other two algorithms make use of the second order derivatives and apply different methods to estimate the Hessian matrix.
Once the updating direction is know, the objective function is minimised in the direction of the updating direction by Newton's method.
5. Update the parameter estimates.
The one-dimensional minimisation by Newton's method in the updating direction provides the step size that multiplied by the gradient in the updating direction yields a vector that added to the previous iteration estimates results in the updated parameter estimates.
6. Check for Convergence.
Several criteria are used to decide whether to stop the calibration process or not. If none of the criteria is met a new iteration is carried out (return to step 2), otherwise the procedure stops. The stopping criteria are:

(i) the gradient norm is less than a prescribed minimum.
(ii) the ratio of the norm of the gradient at the end of the iteration to the gradient norm at the beginning of the iteration is smaller than a prescribed value.
(iii) the objective function value decreases below a user defined value.
(iv) the relative change in objective function value falls below a prescribed value.

Carrera and Neuman rely most on criterion (ii), although the initial norm of the gradient is dependent on the initial parameter estimates. With respect to criterion (iv) they state that there are cases that the relative change in objective function becomes very small and, in spite of this, parameter values change significantly later (Carrera and Neuman, 1986b).

Model selection criteria

Steps 1 until 6 summarise the calibration process once a given zonation is selected and a given covariance model is adopted. This model selection is a key step in the potential success of the calibration process and for this reason, Carrera and Neuman suggest the analysis of alternative models and the application of a model selection criteria to decide which model is most adequate. They take advantage of the model structure identification work carried out in the context of Box-Jenkins time series analysis and consider the Akaike Information Criterion, the Akaike Maximum Entropy Principle, the Hannan Criterion and the Kashyap Criterion. The four criteria are based on the

principle of parsimony in that, everything being equal, the model with the smallest number of parameters is chosen. In general, the criteria balance the model fit (e.g. the differences in observed and simulated heads) and the number of parameters to achieve this fit. The application of the model selection criteria results, in general, in a zonation of the aquifer in a small number of zones, for each of which the parameter values are estimated. The zonation is such that if the number of zones would be augmented the model selection criterion would give a less favourable result because the increase of the number of parameters is not compensated by a sufficient improvement in the model fit.

Numerical experiments

Two examples of application of the zonation procedure for the inverse modelling of groundwater flow are given by Carrera and Neuman (1986c). A synthetic example, and a real case study. We will give some results from the synthetic study. The paper demonstrates, however, that the method can also handle successfully real world situations.

In the synthetic example a 2-D groundwater flow problem in a square aquifer is considered. A mix of different boundary conditions are used: no flow boundaries at the top and right, a prescribed head boundary at the bottom and a prescribed flow boundary at the left. The aquifer is divided in nine constant transmissivity zones. Two wells are pumped from the beginning of the simulation period. The steady-state flow problem prior to pumping and the transient flow problem during 1000 days are solved by a finite elements code. In total 18 head measurements are taken from the "true" head field. These head measurements are corrupted by white Gaussian noise. Nine sets of head measurements are considered: three sets from three different scenarios; the scenarios differ in the degree in the amount of noise added to the head measurements. The noise has zero mean and variable standard deviations of 0.01 m, 0.10 m and 1.0 m. The following conclusions can be drawn (Carrera and Neuman, 1986c):

- In the case that transmissivities are estimated from steady-state data, without prior information on transmissivity, the solutions are somewhat unstable. The results are better for head data which are less corrupted by noise than for head data which are corrupted by noise with a standard deviation of 1.0 m.
- Including prior information on transmissivities improves the estimates of transmissivity. The final estimates lie, in general, between the prior estimates and the estimates without prior information.
- The error covariance matrix is a good representation of the actual errors. It is also illustrated how this matrix could be used to analyse the relative worth of data. Including transient data together with steady-state data reduces all the eigenvalues of the error covariance matrix by about half order of magnitude in both cases indicating a reduction of the uncertainty on the estimates.

- Carrera and Neuman illustrate how the error covariance matrix can be used for monitoring network design both in space and time. The determinant, the condition number and the individual eigenvalues of the matrix are useful criteria to compare monitoring networks.
- In another experiment, ten different conceptual models are considered, each with a different transmissivity zonation pattern. The aforementioned model selection criteria are used to choose the best parameter zonation pattern among a number of given alternatives. Carrera and Neuman find that the Kashyap criterion is the most appropriate among the four criteria tested, because it recognises that if the head data are corrupted severely with white noise there is little justification for an elaborate model with a lot of parameters.
- The method has also been applied successfully to estimate simultaneously different kind of parameters, like transmissivities, areal recharge, flow across the left boundary and head at the bottom boundary.

Some important characteristics of the method

The work of Carrera and Neuman addressed various new issues. It was novel not to linearize the groundwater flow equation for the solution of the inverse problem and successively improve the estimates of the aquifer parameters by an iterative approach. Furthermore, they used new approaches in the context of groundwater flow inverse modelling, like the adjoint state approach for the calculation of the gradient (a more detailed discussion can be found in Carrera *et al.*, 1990) and the alternating of different optimisation algorithms in determining the updating direction from the calculated gradient.

The inverse groundwater flow problem is solved by taking into account the non-linear relationship between hydraulic heads and transmissivities. The method can therefore also be applied to transmissivity fields which have a $\log_{10}$ variance above one; the method is not limited to transmissivity fields with a small variance as the methods presented in section 3.1.1 and 3.1.2.

In order to circumvent the ill-posedness of inverse problems and to achieve a meaningful solution the authors propose the estimation of model parameters on a limited number of zones which divide the aquifer. A disadvantage of this is that the spatial representation of the aquifer parameters is too smooth. Moreover, it is somewhat artificial to assign constant parameter values to large zones. Notice that for example in the linearized cokriging approach (see section 3.1.1), in which also a single best smooth solution is determined, the calibrated transmissivities vary gradually instead of step-wise throughout space. In the linearized cokriging approach and the iterative cokriging-like technique a series of structural parameters which describe the cross correlated random fields of hydraulic head and transmissivity are calibrated. Carrera and Neuman calibrate the spatially variable values of transmissivity directly, so that, in order to get a well-defined parameter estimation problem, the number of zones at which parameter values are estimated has to be limited. Carrera and Neuman state

that the number of zones in which to divide the aquifer may be determined by model selection criteria. Furthermore, the authors stress the importance of including prior information about the parameters in the estimation criterion to reduce the degree of ill-posedness of the problem.

In a comparison made by Carrera and Glorioso (1991) of the linearized cokriging approach (see section 3.1.1) and the zonation procedure it is suggested that the methods are basically the same, except at the stage in which the groundwater flow equation is linearized and because the zonation procedure continues the calibration by an iterative approach. According to Carrera and Glorioso (1991) the linearized cokriging approach yields the same results as the zonation procedure after the first iteration. Subsequent iterations result in an improved calibration of the aquifer parameters. In a reply, Kitanidis states that the linearized cokriging approach does yield the same results as the first iteration of the zonation procedure. According to him, the linearized cokriging approach yields unbiased estimates with minimum variance and a reliable estimation of the error covariance matrix. The zonation procedure, on the contrary, yields biased estimates of the aquifer parameters and a not accurate estimation of the error covariance matrix, especially in case of a fine discretization of the aquifer. Kitanidis states that this bias is due to the parameter estimation employed procedure in which the covariance parameter estimation is detached from the estimation of the spatial variable (Kitanidis, 1996).

The zonation method determines a unique single best solution to the inverse groundwater flow problem. See the sections 3.1.1 and 3.1.2 for the disadvantages associated with a single best solution to the inverse problem. However, as all methods that provide an estimation error covariance, their single best estimate together with the estimation error covariance can be used to generate realisations with expected value equal to the estimate and covariance equal to the error covariance.

The method is flexible to handle complex groundwater flow situations with mixed boundary conditions and non rectangular domains due to its numerical nature. The method allows to estimate a series of aquifer parameters and has already been extended to the combined inverse modelling of groundwater flow and mass transport (Medina, 1993; Medina and Carrera, 1996).

3.1.4 The self-calibrating method

Methodology

Introduction

The self-calibrating method (SCM) was first outlined by Sahuquillo *et al* (1992). An extended description together with applications was presented in a series of three papers by Gómez-Hernández *et al.* (1997) and Capilla *et al.* (1997, 1998).

This discussion focuses in the latter three papers. Further extensions of the method to transient groundwater flow, 3D groundwater flow, flow in fractured media and coupled inverse modelling of flow and transport are presented in this dissertation (Chapters 3, 5 and 6).

The SCM can be considered as the first inverse stochastic simulation method aiming to the direct generation of realisations of transmissivity fields conditional to both transmissivity and piezometric head measurements. Besides, conditioning to piezometric head is achieved through the solution of the groundwater flow equation, not through any linearization. The difference with respect to the zonation procedure of Carrera and Neuman is in the parameterisation of the transmissivity spatial distribution of each realisation. In the SCM, the spatially variable transmissivity values are parameterised as the sum of a seed transmissivity field obtained by standard geostatistical techniques plus a perturbation of the entire field which is expressed as a linear function of the perturbations at a selected number of locations referred to as master blocks.

The steps in the calibration process

1. *Generate a seed field.*
A seed transmissivity field is generated which honours the transmissivity data and displays the spatial variability observed in the field and modelled by a variogram. At this stage, prior estimates of other parameters, like boundary conditions and interior recharge or leakage rates, are made. These prior estimates can be subject of updating during the calibration process if deemed necessary.
2. *Solve the groundwater flow equation.*
The 2-D steady groundwater flow equation is solved by the finite differences method using the parameter values of the current iteration for the transmissivity field, boundary conditions and recharge rates.
3. *Evaluate the penalty function.*
In the self-calibrating method an objective function similar to the one used by Carrera and Neuman is employed. The objective function is the sum of squared differences between measured and simulated heads, weighted by a head error matrix, plus a sum of squared deviations between the updated parameter values and the prior estimated parameter values, weighted by the covariance matrix of the corresponding parameter. Weights are assigned to the two terms of the objective function. It is common to repeat the calibration procedure (steps 1 to 6) for different weights. The objective function value can be calculated after the groundwater flow equation is solved.
4. *Compute the updating direction.*
In addition, a first-order approximation of the solution of the groundwater flow equation in the updated transmissivity field (and eventually updated boundary conditions and updated estimates of recharge rates) is obtained by a first order Taylor series expansion around the head solution in the transmissivity field from the previous iteration. Notice that the linearization is made after solving

the full groundwater flow equation and calculating the objective function value and its only purpose is to define an updating direction. The transmissivity update is expressed as a linear function of the updated values at a selected number of master blocks spread over the aquifer in a regular way; therefore, the number of parameters to optimise is equal to the number of master blocks. The procedure is based on the computation of the sensitivity coefficients required to compute the gradient of the objective function.

5. Update the parameter estimates.

The perturbations at the master blocks, which are the subject of the optimisation, are determined by the product of the updating direction and the step size. These perturbations are then interpolated to all the grid cells by ordinary kriging. The updated transmissivity field is the sum of the transmissivity field at the end of the previous iteration plus the perturbation field. In a similar way updated boundary conditions (sum of the boundary conditions at the end of the previous iteration and calculated perturbations) and updated leakage or recharge rates (a sum of rates at the end of the previous iteration and calculated perturbations) can be obtained.

6. Check for Convergence.

A number of criteria is used to decide whether to stop the calibration process or not. If none of the criteria is met, the procedure continues back to step 2, using the updated parameter estimates as the seeds for the next iteration. The stopping criteria are:

(i) the objective function value decreases below a user defined value.

(ii) the relative change in objective function value falls below a prescribed value.

(iii) the number of iterations reaches a user defined maximum number of iterations.

Numerical Experiments

In Capilla *et al.* (1997) a number of controlled numerical experiments are presented. In all cases, a 2-D rectangular domain (60 x 60 grid cells) under steady-state flow without sources or sinks is considered. Heads are prescribed along all four boundaries. The reference $\log_{10}$ transmissivity field has zero mean, unit variance and isotropic correlation distance of one third of the domain size. Uncertainty in boundary conditions is not considered. The reference heterogeneous transmissivity field is sampled at a few locations for transmissivity and head values which are used as conditioning data for the generation of transmissivity fields. In the base case, the reference log transmissivity field and the reference steady-state head field are sampled at 30 locations and a total of 100 master blocks are laid out on a regular grid. With respect to this base case some variations are studied, such as sensitivities to the log transmissivity variance, the number of conditioning data, or the number of master blocks. For each scenario 10 transmissivity realisations are generated conditional to transmissivity and head measurements. The main findings are:

- The transmissivity fields are conditional to the steady-state head data, since the head data are reproduced by the solution of the groundwater flow equation in the resulting fields. It is found that conditioning to head data, in addition to transmissivity data, improves the overall reproduction of the reference head field and at the same time reduces its uncertainty, with respect to the case in which only transmissivity data are used for conditioning. Similarly, conditioning to head data also improves the transmissivity estimates. Satisfactory results are also obtained for a reference field with $\log_{10}$ transmissivity variance as high as 2.0. It is found that, there is a threshold on the number of head data beyond which it is not worth to collect any additional head data.
- When the variogram of the seed field departs from the model variogram used for its generation (due to ergodic fluctuations) the updating procedure corrects the seed field so that the final update field has a variogram which is closer to the model one.
- From a sensitivity analysis on the number of master blocks it is concluded that at least 3 master blocks per range in each direction are needed in order for the algorithm to work.

Wen *et al.* (1996) present another synthetic study which demonstrates the worth of piezometric head data versus transmissivity data. A synthetic 2-D reference field of 30 km by 30 km which has been discretized into 60 by 60 square cells of 500 m is used. The reference $\log_{10}$ transmissivity field had a mean of -0.6, a variance of 0.75, and an isotropic spherical variogram with a range of 8000 m. The steady-state groundwater flow equation is solved by finite difference using prescribed boundary conditions, resulting in the reference head field. Then, the advective travel paths and travel times of four particles are computed. To determine the relative impact that measurements of transmissivity and head would have in the advective travel predictions, 64 different sampling configurations were considered with different combinations of head and log transmissivity data sampled from the reference fields. For each of the 64 sampling configurations, 250 conditional realisations of transmissivity were generated. The main conclusions are, the best predictions are obtained with the largest number of data of both type, transmissivity data have a larger impact than head data in the prediction of travel times, whereas the opposite is true for the prediction of travel paths. It was also found that when no or little data are available, head measurement are more valuable than transmissivity measurements; however, there is a threshold number of head measurement beyond which additional measurements are virtually irrelevant.

Application of the methodology to the WIPP-site

Capilla *et al.* (1998) apply the SCM to the inverse modelling of groundwater flow at the WIPP (Waste Isolation Pilot Plant) site. See section 2.3 for details on the WIPP site. Here we just add that due to some secondary processes like halite dissolution, subsidence, and calcium sulphate hydration, fluid density is

spatially variable. Groundwater flow due to the spatial variability of fluid density has been taken into account.

Capilla *et al.* (1998) assume confined 2-D steady-state flow in the Culebra formation without sinks and sources. Along all boundaries, prescribed head values are set which were obtained from preliminary reports by SANDIA National Laboratories. The conditioning data are 33 steady-state head measurements, 37 transmissivity measurements, and 31 water density measurements. Groundwater flow and advective transport is analyzed. Particles are released from the hypothetical repository and arrival times, and arrival locations, to the southern boundary of the model area are computed.

A total of 300 log transmissivity seed fields are generated, conditional to the transmissivity measurements and displaying the spatial variability observed in the field and modelled by a spherical variogram. The variogram is modelled as the sum of three nested structures, which take into account a strong zonal anisotropy. For each of the fields the groundwater flow equation is solved by finite differences using 43 by 61 square blocks of 500 m by 500 m. The 300 transmissivity fields are then calibrated to steady-state heads. The most important results are:

- The SCM can be applied to a real case with strong spatial heterogeneity.
- Conditioning the transmissivity fields to steady-state heads results in a reduction of the ensemble variance of both transmissivity and hydraulic head. Also uncertainty about the travel paths and arrival times of the released particles reduces noticeably.
- When the boundary conditions are calibrated together with the transmissivities, the reproduction of the measured heads improves. The side effect is a reduction of the travel times due to the systematic reduction of the overall gradient across the formation.

Some important characteristics of the method

Like the zonation procedure, discussed in section 3.1.3, the Pilot Point Method (Section 3.1.5) and the Markov Chain Monte Carlo Method (Section 3.1.6), the SCM is not limited to transmissivity fields with small variances because no first-order approximation is made to establish the dependence between piezometric head and transmissivity. The full groundwater flow equation is iteratively solved numerous times in order to match the measured heads. As such, if the final updated parameters are used as input to the groundwater flow equation the measured heads are reproduced. On the contrary, for the methods presented in section 3.1.1 and 3.1.2 this is not the case.

The SCM aims to the generation of an ensemble of conditionally simulated transmissivity fields (and eventually an ensemble of boundary conditions and recharge) calibrated (conditioned) to steady-state head measurements. This has

a clear advantage compared with a single best solution of the inverse groundwater flow problem, particularly for later analysis of mass transport. Using the ensemble of transmissivity fields generated, it is possible to compute not only the probability density functions of the input parameters, but also the probability density functions of output variables such as travel times or solute concentrations at given control locations.

The method is, due to its numerical nature, flexible to handle complex groundwater flow situations with mixed boundary conditions and non rectangular domains. The method has been extended to the inverse modeling of transient groundwater flow and calibration of storativities (section 3.2), three dimensional groundwater flow in fractured media (see Chapter 5) and the joint inverse modelling of groundwater flow and mass transport (see Chapter 6). Further extensions are possible with the only limitation being the computer resources because the method is very CPU intensive.

3.1.5 The pilot point method

Methodology

Introduction

Originally the Pilot Point method was formulated as a standard inverse groundwater flow problem yielding a single "best" map of conductivities (de Marsily *et al.*, 1984). However, we will discuss the newest version of the Pilot Point method (RamaRao *et al.*, 1995; LaVenue *et al.*, 1995) which pursues the generation of multiple realisations like the self-calibrating method (see sections 3.1.4 and 3.2).

The aim of the method is to generate a large ensemble of equally likely transmissivity fields, each of which is in agreement with all the measured data and, in this respect, can be considered a plausible model of the true aquifer transmissivity field. The methodology can handle both steady and transient groundwater flow, in 1-D, 2-D or 3-D, with the possibility of spatially variable fluid density. In the discussion of the method we will focus on the 2-D problem (the authors do not present 1-D or 3-D examples).

The steps in the calibration process

The method, which is implemented in the GRASP-INV code, consists of the following steps (these steps are repeated for each simulated transmissivity field (RamaRao *et al.*, 1995):

1. *Simulation of a transmissivity field.*
The turning bands simulation method is used to generate a transmissivity field which is conditional to the transmissivity measurements.

2. *Solution of the groundwater flow equation.*
The steady or transient groundwater flow equation is solved for the transmissivity field with given boundary conditions by finite differences. A fully implicit scheme is used to solve the transient groundwater flow equation. It is possible to handle cases with spatially variable fluid density.
3. *The objective function.*
The model fit criterion is a weighted sum of the squared deviations between the computed and measured pressures at each location and time where they are available. During the calibration process the fit between computed and measured pressures improves. In case of transient groundwater flow first the inverse problem for steady groundwater flow is solved (so that the solution of the flow equation is close to the measured steady pressure values) and afterwards the transient flow problem. The steady-state calibration should not be degraded during the course of transient calibration and therefore different weights can be given to the steady part of the objective function and the transient part.
4. *Calculation of sensitivity coefficients for the objective function.*
In case the model fit between computed and measured pressures is not good enough, the sensitivity coefficients of the objective function with respect to a change of the transmissivity in each grid block are calculated. The objective is to determine the grid blocks with the highest sensitivities. These sensitivity coefficients are obtained through adjoint sensitivity analysis. Because of the considerable amount of CPU time needed to compute them, the authors developed an ad hoc method that does not require their exact computation at each grid block.
5. *Pilot Point Location.*
A main characteristic of the method is the use of pilot points. A pilot point is defined by its spatial location and by the transmissivity value assigned to it. The pilot points are placed at locations where their potential for reducing the objective function is the highest, that is, the locations where the absolute value of the sensitivity coefficients is the largest. The authors found from computer experiments that using one or three pilot points in the optimisation yields very similar results, because normally the grid cells with the highest absolute values for the sensitivity coefficients are located next to each other.
6. *Optimisation and updating.*
The authors distinguish between two optimisation levels. At the inner optimisation level, the transmissivity values at the pilot point locations are determined through an iterative non-linear optimisation procedure, that alternates Fletcher Reeves algorithm, the Broyden algorithm and the Davidon-Fletcher-Powell algorithm. Once the optimal transmissivities at the pilot point locations are determined, the transmissivity field is updated using kriging and a new iteration of the outer optimisation level starts. (Back to step 4 to recompute the sensitivity coefficients and determine new locations for the pilot points.)

7. Convergence criteria.

At the inner iteration level, during which the transmissivities at the pilot point locations are calculated, a total of five convergence criteria are used to decide whether to stop the optimisation process:

(i) the objective function value drops below a prescribed minimum.

(ii) the number of iterations equals a prescribed maximum number of inner iterations.

(iii) the ratio of the norm of the gradient to the initial norm decreases below a prescribed value.

(iv) the gradient norm is less than a prescribed minimum

(v) the relative change in objective function falls below a prescribed value.

At the outer iteration level two convergence criteria are used, which determine whether the calibration process as a whole is finished. These convergence criteria are:

(i) the objective function value drops below a prescribed minimum.

(ii) the number of iterations equals a prescribed maximum number of outer iterations.

Some important characteristics of the method

Many of the comments given about the self-calibrating method also hold for the Pilot Point Method; the method can handle cases with a variance of the $\log_{10}$ transmissivity field above 1.0 and generates an ensemble of equally likely solutions to the groundwater flow inverse problem. See section 3.1.4 for more detailed comments about these advantages.

The main differences between the Pilot Point Method and the self-calibrating method stand from their different initial aims. The Pilot Point Method was originally devised for estimation purposes, in this respect the concept of pilot point was very appropriate: the single point that should be modified in a kriging map that would produce the best approximation to the measured piezometric heads. This concept can be applied and has been extended into a simulation context. However, in a simulation context, the idea of modifying sequentially an initially heterogeneous field is suboptimal. In this respect, the self-calibrating method, which was devised for stochastic simulation, does not focus on optimal location of pilot points but on a simple way to parameterise a perturbation to an initial seed field that can be easily optimised and that will ensure that the final updated field does not depart dramatically from the original seed field. The master blocks in the self-calibrating method and the pilot points in the Pilot Point Method have the same purpose, parameterise a perturbation of a transmissivity field. In the self-calibrating method, the master block perturbations cover the whole formation and are computed all at once, whereas, in the Pilot Point Method, the pilot point values are computed sequentially and are located at the locations with higher sensitivity coefficients. The authors of the self-calibrating method state that at least 3 master blocks per correlation range are necessary (Capilla *et al.*, 1997). On the contrary, the

authors of the Pilot Point Method state that the use of just one pilot point in each inner iteration is optimal (RamaRao *et al.*, 1995).

The method is, due to its numerical approach, flexible to handle complex groundwater flow situations with mixed boundary conditions and non rectangular domains. The method can already handle variable density groundwater flow, estimation of different aquifer parameters and three-dimensional groundwater flow. Further extensions are possible with main limitation the CPU time because the method is very CPU intensive.

Application of the methodology to the WIPP-site

The methodology has been applied for the inverse modelling of groundwater flow at the WIPP-site (LaVenue *et al.*, 1995). Before we already presented a brief site description (see section 2.3).

The authors assume a 2-D flow system, because of the existence of low permeability beds above and below the Culebra formation. The north-western boundary of the modelling domain is partly a no flow boundary and along the other boundaries prescribed heads are imposed. The prescribed head values are obtained by kriging the observed heads. The variogram and the measured transmissivities are used to generate conditional simulations of transmissivity. The calibration of the transmissivity field is constrained to the kriged transmissivity plus or minus three times the kriging standard deviation.

In total 70 transmissivity fields are calibrated to steady-state heads and transient-state heads. The transient-state heads come from three different pumping tests, all performed in 1988. An analysis of the resulting transmissivity fields after calibrating to steady-state heads shows that the root mean squared error (RMSE) between calculated and observed steady-state heads is between 1.5 and 2.5 m for most of the fields. It is found that if the initial mismatch between simulated and measured heads is larger, more pilot points have to be placed to calibrate the transmissivity field.

The calibrated transmissivity fields have been used in the simulation of non reactive mass transport. Particles are released from a point in the Culebra formation which coincides with the centroid of the waste panels and are transported to the southern WIPP site boundary. For each transmissivity field the travel time to this boundary and the travel path are determined. Travel times were also computed for a set of unconditional transmissivity field and for a set of transmissivity fields conditional only to the transmissivity values. It is found that the more conditioning data are used, the less is the uncertainty in travel time estimates and travel paths. Comparing the impact of using additional data, it is evident how the uncertainty in the advective transport predictions is progressively reduced as additional types of data are used,

starting with transmissivity data, then steady-state head data, and finally, transient-state head data.

The uncertainty on the boundary conditions has not been subject of investigation in this study. However, the authors expect that considering uncertainty in the boundary conditions would not change the end results, because the large drawdowns that have been produced in the Culebra are much more significant during the calibration process than the uncertainty in the boundary conditions.

3.1.6 The Markov Chain Monte Carlo method

Methodology

Introduction

The Markov Chain Monte Carlo Method (MCMC) (Oliver at al., 1996; Oliver *et al.*, 1997) has the same objectives as the methods we have discussed in sections 3.1.4 and 3.1.5; that is, to generate an ensemble of equally likely transmissivity/conductivity fields conditional to hydraulic head data, transmissivity/conductivity data and possibly other prior information. In earlier work, Oliver and others (Oliver, 1994; Chu *et al.*, 1995; Oliver, 1996) attempted the generation of equally likely transmissivity fields by adding a spatially distributed error to the smooth single best solution of the inverse groundwater flow problem. However, the two papers we discuss here start with simulations of transmissivity/conductivity (not solutions to the inverse problem) and each of them is then conditioned to hydraulic head data. MCMC determines the ensemble of realisations by an optimisation approach different from the non linear optimisation algorithms used in the self-calibrating method and the Pilot Point Method. MCMC can handle 1-D, 2-D and 3-D steady and transient groundwater flow.

The steps in the calibration process

The authors do not describe, in a systematic way, the steps taken in the MCMC for the generation of the conditional transmissivity fields. From the information in the two papers by Oliver *et al.* (1996, 1997), they can be summarised as follows:

1. *Simulation of a transmissivity field.*
A transmissivity field, conditional to transmissivity measurements, is generated by a Markov chain method. The conditional simulation of a transmissivity field is approached as a minimisation problem, with the weighted sum of the misfit of the variogram of the simulated field with respect to the objective variogram as the objective function. As a result, the simulated transmissivity field will reproduce the hard transmissivity data and the model variogram. This simulation technique is based on the same grounds as the simulated annealing

techniques described by Deutsch and Journel (1992). Oliver *et al* (1997) propose a computationally efficient algorithm for the generation of the fields.

2. *Solution of the groundwater flow equation.*

The full steady or transient groundwater flow equation is solved by finite differences for the transmissivity field with given boundary conditions.

3. *The objective function.*

The objective function to be minimised is given by the sum of the weighted squared deviations between measured and simulated heads.

4. *Calculation of sensitivity coefficients.*

The sensitivities of the model responses for changes in the transmissivities in the domain are calculated. The calculation of the sensitivity coefficients is based on a linearization of the groundwater flow equation by a Taylor series expansion.

5. *A transition is made.*

The Markov chain method is used again to propose a transition of the transmissivity field. The information of the sensitivities is used to propose transitions with a high probability of acceptance. If the new transmissivity field results in a reduction of the objective function value, the transition is accepted, if not, the transition is accepted or rejected according to a given probability law. Oliver *et al* (1997) consider two kind of transitions: global ones, in which new values of the transmissivity are drawn at all locations, and local ones, in which just the permeability at a single location is altered. Global transitions yield a series of independent realisations of the transmissivity field, while local transitions result in a series of inter-correlated realisations. It is easier and computationally more efficient to generate and evaluate local transitions, however, it is not easy to determine how many local transitions are necessary to obtain independent realisations. Oliver *et al* (1997) apply suggestions from the literature to determine the number of local transitions to generate independent realisations.

6. *Convergence criteria.* Oliver *et al* (1996, 1997) do not specify explicitly their criteria to stop the perturbation of the transmissivity field. They refer to "a sufficiently close reproduction of the heads" and a "very small convergence rate".

Numerical experiments

Oliver *et al* (1997) consider 2-D transient groundwater flow in an area of 457 m by 457 m discretized into 225 square grid blocks. The four edges are no flow boundaries. A pumping well is located in the centre of the domain. Two $\log_{10}$ transmissivity fields are generated, each with a mean of 3.4 but with variances of 0.25 and 1.0. The 2-D spatial continuity is described by an isotropic spherical variogram with a range of 183 m. The groundwater flow equation is solved for the two fields and piezometric head samples are obtained at five locations. At each measurement location ten samples in time are taken since the start of the pumping. Equally likely transmissivity fields (solutions of the groundwater flow inverse problem) are generated according to three methods. In the first method, local transitions are made without using sensitivity information from

the groundwater flow model to propose these transitions. In the second and third methods, the sensitivity coefficients are used to improve the acceptance probability of the transitions. The second method uses local transitions and the third one uses global transitions. The three methods are evaluated by the number of independent realisations of transmissivity conditional to hydraulic head data obtained in a certain amount of time.

For the reference transmissivity field with the lowest variance it is found that the third method yields the best results in the sense that the largest number of independent realisations (namely 200) is generated in a certain amount of time. The second method yields less favourable results, 1200 local transitions are needed to generate independent realisations (only 31 independent realisations are generated). The first method yielded no conditional realisations: not considering the sensitivity information coming from the groundwater flow equation prevented the method from generating realisations reproducing the measured hydraulic heads.

For the case of the reference $\log_{10}$ transmissivity field with a variance of 1.0 the results are quite different. Again the first method yielded no conditional realisations, but, this time, the second method yielded more independent realisations than the third one (14 versus 8). For both methods, the number of independent realisations was smaller as compared with the case of a variance of 0.25. It seems that for slightly non-linear problems, global transitions are the best to obtain the largest number of independent realisations of the transmissivity field. However, for highly non-linear problems, local transitions are the most efficient to obtain the largest number of independent realisations, because it is difficult to determine a global perturbation yielding a transmissivity field that matches the hydraulic head data. A series of local transitions, on the contrary, is more likely to produce a field matching the hydraulic head data.

Some important characteristics of the method

MCMC, like the self-calibrating method, and the Pilot Point Method, is not limited to a small variance of transmissivity, and it is flexible enough to handle complex geometries and boundary conditions. See sections 3.1.4 and 3.1.5 for more details. Below we will focus on the differences between MCMC and the self-calibrating method and the Pilot Point Method.

In the MCMC the initial transmissivity field is generated with a variogram very close to the model variogram. The other methods generate an initial transmissivity field which, due to ergodic fluctuations, does not necessarily reproduce the variogram if the domain size is not much larger than the correlation length. As such, we expect that the ensemble of initial transmissivity fields shows less dispersion for MCMC than for self-calibrating or Pilot Point Method. In addition, during the calibration of the transmissivity fields to the

hydraulic head data, MCMC ensures that the variogram of transmissivities is not altered. The self-calibrating method and the pilot point method do not constrain the transmissivity variogram during the calibration of the fields to the head data, and, in this respect, they can be utilised as variogram identification algorithms.

The optimisation method used in MCMC is very different from the method used in the other two methods. While the other two methods use standard non linear optimisation algorithms, MCMC uses simulated annealing. The use of sensitivity coefficients to determine the transitions from one transmissivity field to the next increases the acceptance probability of any given transitions. Oliver *et al* (1996) state that although the proposed transitions are based on the posterior linearization of the groundwater flow equation, the "true" distribution of transmissivity fields (conditioned to hydraulic head data) is sampled as long as the "correct" acceptance criterion for transitions is used.

The numerical examples presented by Oliver *et al.* (1997) indicate that MCMC is extremely CPU intensive, much more than the Pilot Point Method and the self-calibrating method. The proposals of Oliver *et al* (1997) result in an important reduction of costs for the application of the simulated annealing method as optimisation tool in the inverse modelling of groundwater flow; however, the method is still not efficient enough as compared to the more "classical" non linear optimisation algorithms.

3.1.7 The Fast Fourier Transform Method

Methodology

Introduction

The Fast Fourier Transform Method was originally a method to solve the inverse groundwater flow problem by relating the random head field and the random transmissivity field by linearizing the groundwater flow equation in the Fourier space. The (cross) covariances are found by a spectral representation. As such, the method is very similar to the ones presented in the sections 3.1.1 and 3.1.2, since it is based on a linearization of the flow equation. Later this method has been extended to account for the non-linear relationship between transmissivity and hydraulic head in the computation of the head covariance and the head-transmissivity cross-covariance using an iterative approach. Moreover, the method does not calibrate a single best smoothed transmissivity field, but a simulated transmissivity field which resembles the spatial variability as observed in the field. Therefore the method is also referred to as an iterative co-conditional simulation approach. We focus in the presentation of the method by Gutjahr *et al.* (1994). However, in this paper, Gutjahr and co-workers devote few comments to the iterative aspect of the approach. Later Yeh and others (Yeh *et al.*, 1995; Yeh *et al.*, 1996) discuss the iterative approach and present its mathematical basis. Section 3.1.8 will present

the discussions by Yeh and co-workers. The Fast Fourier Transform Method was not the first method to take into account the non-linear relationship between transmissivity and hydraulic head neither the first method aiming to produce multiple realisations of co-conditional transmissivity fields. We discuss the Fast Fourier Transform now because it is a direct modification of the methods presented in the sections 3.1.1 and 3.1.2, in order to overcome a principal problem of those methods, the limitation to transmissivity fields with a small variance, stressed by the methods that have been presented in sections 3.1.3 until 3.1.6.

The steps in the calibration process

1. *Estimate covariances.* The authors consider 2-D steady-state groundwater flow in an unbounded domain. The objective is to simulate a transmissivity field conditional to both transmissivity and hydraulic head data. It is assumed that transmissivity and hydraulic head are second-order stationary random fields. The groundwater flow equation is linearized by a small-perturbation analysis. Then the spectral representation algorithm is applied to get a relationship between the spectral components of transmissivity and head, from which it is extremely easy to derive the spectral density of hydraulic head and the cross-spectral density of hydraulic head and transmissivity. Finally, the auto and cross-covariances are obtained by using the two-dimensional inverse Fourier transform (Gutjahr and Wilson, 1989). Thus, the (cross) covariances are obtained through a linearization approach, like in the linearized cokriging method and the linearized semi-analytical method.
2. *Co-conditional simulation.* The Fast Fourier Transform algorithm is applied to generate unconditioned transmissivity and head fields with the (cross) covariance functions determined in step 1 (Gutjahr *et al.*, 1994). Conditioning is understood as reproduction of the transmissivity data and as reproduction of the linear relationship between head and log-transmissivity established before. In order to apply this step it has to be assumed that transmissivity and hydraulic head are jointly multivariate normal distributed. The conditional realisations of transmissivity and hydraulic head are found by the sum of the unconditional transmissivity and hydraulic head fields plus a weighted linear combination of differences between measured and simulated data (both transmissivity and heads). The weights are determined by solving a cokriging system. Until now, the procedure to determine transmissivity statistics conditioned to transmissivity and hydraulic head data is very similar to the methods presented in sections 3.1.1 and 3.1.2. The main and very important difference with the methods in sections 3.1.1 and 3.1.2 is that the authors focus on simulated fields instead of estimated fields.
3. *Solve the groundwater flow equation.* The resulting transmissivity field is used, together with boundary conditions, to solve the groundwater flow equation for hydraulic head. The simulated heads will differ from the measured heads, especially if the log transmissivity variance is large. The new head

field satisfies the continuity equation. The head field based on the linearized relation between transmissivity and head does not satisfy this relation.

4. *Apply again cokriging.* The way the pseudo-conditional transmissivity field generated in step 2 and the deviation between the generated heads and the measured heads are used is not clear from the 1994 paper. However, Hughson and Gutjahr (1998) give some additional details on the calibration. The groundwater flow equation is linearized again around the new parameters and the (cross) covariances are re-evaluated; the differences between simulated and observed heads are used together with the transmissivities to cokrige a transmissivity perturbation field, which added to the old simulated transmissivity field yields an updated transmissivity field. Then return to step 2.
5. *Stopping criterion.* The calibration process is stopped if the head field is sufficiently close to the measured head data.

Numerical experiments

Gutjahr and others test the methodology with numerical experiments.

The experiment is carried out in a square 2-D aquifer of side equal to 6.3 log-transmissivity integral scale. A synthetic transmissivity field and the steady-head solution of the groundwater flow equation is used as reference. Several transmissivity fields with a mean $\log_{10}$ transmissivity of -3 and different variances are considered. Prescribed head boundaries are imposed on the left and right boundaries of the system so that a uniform head gradient parallel to the x-axis is created. The upper and lower boundary of the system are impermeable. In total 30 transmissivity and 30 head samples are taken from the reference fields which are then used in the conditioning procedure. Different scenarios are studied and for each scenario 100 conditioned fields are generated. In order to compare the conditioned fields, particles were tracked (no diffusion) from the centre of the field to the boundary, and travel paths and travel time distributions were computed. Four cases with varying number of conditioning data are studied: (i) no conditioning, (ii) 30 transmissivity values only, (iii) 30 head values only and (iv) 30 head and 30 transmissivity values. Three different cases with respect to the $\log_{10}$ transmissivity variance are studied: (i) a variance of 0.25, (ii) a variance of 1.0 and (iii) a variance of 2.0.

For the case of a $\log_{10}$ transmissivity field with variance 1.0 it is found that more conditioning data (head and transmissivity) result in less variance in the arrival times of the particles. However, using 30 head values and no transmissivity values the variance in the travel times was hardly reduced. It is concluded that transmissivity data are most influential for variance reduction of arrival times estimates. With respect to the arrival locations of the particles it is found that using 30 head conditioning data (and no transmissivity values) yields a notable reduction in the variance of the arrival location, while using 30 conditioning transmissivity data (and no head values) hardly reduces this variance. It seems

that hydraulic head data reduce mainly the uncertainty in the travel paths. For the $\log_{10}$ transmissivity variance of 2.0 the iterative approach reduces the uncertainty in the travel times and travel paths (compared are the results without using an iterative approach and the results after the 4th iteration). Furthermore, the simulated head values after the 4th iteration are very close to the measured head values. The conditional distributions obtained for the case of a $\log_{10}$ transmissivity variance of 2.0 by the iterative approach are compared with the "true" distributions. The "true" distributions are obtained by brute force after generating a very large number of transmissivity fields conditioned only to transmissivity measurement and selecting those fields in which the solution of the groundwater flow equation reproduces closely the measured heads. For each of these transmissivity fields the groundwater flow in the domain has been solved and the fields for which the measured head values are closely reproduced are maintained. These fields are used to calculate at several locations the distributions of hydraulic head and transmissivity and compare them with the distributions of head and transmissivity for the iteratively conditioned fields. It is found that after the 4th iteration the conditional distributions approach very well the true ones in most cases.

Hughson and Gutjahr (1998) carry out a similar synthetic computer experiment using also transient head data. They find that while steady state head data attribute significantly to characterise the hydraulic head and transmissivity field, transient head data just yield a minor additional improvement of the characterisation of the transmissivity and hydraulic head field. The estimation of the travel times of the particles (released in the aquifer and transported to a control plane) does not improve. However, transient head data are found to have a positive impact on the characterisation of the travel paths of particles.

Some important characteristics of the method

The comments below refer to the advantages the Fast Fourier Transform Method has as compared with the linearized methods from section 3.1.1 and 3.1.2.

The Fast Fourier Transform Method (FFTM) is an attempt to circumvent the problem of the first-order linearization of the groundwater flow equation. The linearization based on a first-order approximation is only valid if the unconditional variance of $\log_{10}$ transmissivity is less than 1.0. Gutjahr and others (1994) start with a procedure very similar to the linearized cokriging method, but update later iteratively the transmissivity field with the aim to match the measured heads. The iterative approach results finally in a transmissivity field in which the solution of the groundwater flow equation reproduces the measured heads. The iterative approach allows to handle cases with a variance of $\log_{10}$ transmissivity above 1.0.

Gutjahr and others (1994) and Hughson and Gutjahr (1998) give little information about the iterative approach so that it is difficult to determine to what extent the proposed methodology avoids the problems associated with the linearization of the groundwater flow equation. For example, the authors do not make clear whether they update the hydraulic head covariance matrix, the hydraulic head- transmissivity cross-covariance matrix or the transmissivity covariance matrix at each iteration. Iteratively updated or not, in all cases these (cross) covariance matrices are estimated by a first-order approximation of the groundwater flow equation.

Gutjahr and others use a simulation approach for solving the inverse groundwater flow problem. Although they do not state it explicitly, their aim is to determine a sufficient number of equally likely transmissivity simulations conditioned to transmissivity and head measurements. This has a clear advantage compared with a single best solution of the inverse groundwater flow problem. By means of a solution in the form of an ensemble of transmissivity fields the probability density functions of different input variables of the flow and transport equations are obtained and in addition it is possible to obtain the probability density functions of output variables like particle travel times or arrival positions.

The Fast Fourier Transform Method seems moderately flexible for extensions to more complex domains, three-dimensional flow, simultaneous estimation of a number of possibly spatial variable parameters or the combined inverse modelling of groundwater flow and mass transport. A problem is that, like in the presented linearized methods in 3.1.1 and 3.1.2, the (cross) covariance matrices have to be determined by a linearization of the groundwater flow equation. However, the method is more flexible than the linearized methods because if these covariance matrices can be computed the method can handle more complex situations using the iterative approach. Recently an extension to handle transient groundwater flow has been made (Hughson, 1997; Hughson and Gutjahr, 1998).

3.1.8 The iterative co-kriging like technique

Methodology

Introduction

The second method we discuss which incorporates the non-linear relationship between transmissivity and hydraulic head fields is the iterative cokriging-like technique (ICT) by Yeh and others. We discuss the method as presented in two recently published papers (Yeh *et al.*, 1995; Yeh *et al.*, 1996), although later the method has been changed in the sense that a simulation approach is adopted (Hanna and Yeh, 1998). The method starts like the linearized cokriging approach. In addition, the linear estimator is improved in an iterative manner. The two papers differ in the method in which the iterative update is made. We

discuss both of the methods, with emphasis in the method presented in the later paper. This method is very similar to the iterative method of section 3.1.7 (the Fast Fourier Transform Method), but with a better discussion of the iterative approach used.

The steps in the calibration process

The first step in ICT is a straight application of the linearized cokriging method with no iterations. However, ICT continues with an iterative process which improves the characterisation of the transmissivity field. The two articles formulate two different iterative updating processes.

1. *"Classical" cokriging.* As in sections 3.1.1 and 3.1.2. A very short summary is given here. A calibrated transmissivity field is obtained by a cokriged estimate of transmissivities and heads. The necessary (cross) covariance matrices are obtained from a linearization of the groundwater flow equation by a first order approximation. This is the philosophy not only of the linearized cokriging approach (see section 3.1.1), but also of the Fast Fourier Transform Method (see section 3.1.7). The way the (cross) covariances are obtained varies. The perturbation-spectral analysis used in the Fast Fourier Transform Method to obtain the (cross) covariance matrices is applied by Yeh at al., 1995. A numerical method is used by Yeh at al., 1996.

2. *Solve the groundwater flow equation.* The resulting (smooth) transmissivity field is used in a finite elements steady-state groundwater flow solver. (The field used here is obtained by cokriging, as opposed to the Fast Fourier Method which starts from a simulated field.). Notice that now the groundwater flow equation is solved and not a linearized version of it. The two articles use two different approaches to solve the groundwater flow equation:

   (i) The observed head values at the sample locations are placed as internal constant-head boundary conditions. Therefore, the simulated head values are equal to the measured head values. The measured head values in this case have no influence on the calibration of the transmissivity field since they are always reproduced exactly. (Yeh *et al.*, 1995).

   (ii) The flow equation is solved without setting constant-head boundary conditions at the grid cells corresponding to the head sample locations (Yeh *et al.*, 1996).

3. *Apply cokriging again.* The two approaches mentioned in step 2 are followed by the application of cokriging, but the procedure differs.

   (i) Cokriging is used again, but this time the transmissivity estimate is not only function of the measured transmissivity and head data, but also of all the head data resulting from the solution of the flow equation. It results in a new cokriged transmissivity field, which is again used as input to the groundwater flow equation (Yeh *et al.*, 1995).

   (ii) The updated transmissivity at a certain location is the transmissivity value from the previous iteration plus a weighted linear combination

of the head residuals (a head residual is the difference between the cokriging head estimate and the measured head value at a head measurement location). The weights are determined by solving again a cokriging system. For solving the cokriging system updated estimates of the conditional transmissivity covariance matrix, the conditional hydraulic head covariance matrix and the conditional head-transmissivity cross covariance matrix are needed. The conditional transmissivity covariance matrix is easy to update. The other two covariances are updated by approximating the residual heads by a first-order Taylor series. The sensitivity matrix which appears in the resulting expression is estimated by an adjoint state sensitivity method subject to boundary conditions. The covariance matrices are updated at each iteration (Yeh *et al.*, 1996).

4. *Stopping criterion.* The two different iterative approaches, as described in step 2 and step 3 use also different stopping criteria.

- If the absolute change in the head value between two succeeding iterations decreases below a specified tolerance at all grid cells, the calibration process is terminated.
- If the absolute difference in the variance of the estimated transmissivity field between two successive iterations is smaller than a prescribed tolerance the iteration stops.

Numerical experiments

In Yeh *et al.* (1996) a synthetic study is presented to test the iterative cokriging-like technique. The results obtained from the iterative approach are compared with the results from the non-iterative approach. Synthetic heterogeneous transmissivity fields are generated by a multiGaussian random field generator with an exponential anisotropic variogram. These transmissivity fields are considered as reference fields. The 2-D steady-state groundwater flow equation with a constant-rate pumping well, no flux conditions at the upper and lower boundaries and prescribed heads at the left and right boundaries is solved for these fields.

First a deterministic inverse problem is solved. Yeh *et al.* (1996) use the term deterministic in the sense that the inverse problem has a unique solution; the head values at all the grid nodes of the flow solver are known and all the transmissivity values near the left boundary (one value for each streamline) are known. The solution of the deterministic inverse problem taking head and transmissivity values from a reference transmissivity field with a low variance ($\log_{10}$ transmissivity variance = 0.38) resembles for both the iterative and non-iterative approach very well the "real" transmissivity field. However, even in this case the non-iterative approach gives a too smooth transmissivity field, whereas the iterative approach results in a transmissivity field with a spatial variability closer to the "true" field. The solution of the deterministic inverse problem for a reference transmissivity field with high variance ($\log_{10}$

transmissivity variance = 3.01) results in a very smooth calibrated transmissivity field for the non-iterative approach and a calibrated transmissivity field for the iterative case which is again closer to the "real" transmissivity field. It is shown that due to the linear approximation of the groundwater flow equation in the non-iterative approach the updated transmissivity field is of bad quality, in spite of the fact that the heads at all the grid cells are known.

Also a stochastic inverse problem is solved, which means that the hydraulic head values are known on a limited number of locations. In total 30 error-free head measurements and 5 error-free transmissivity measurements are taken from the "true" fields. It is found that the iteratively updated transmissivity field reveals better the structures of the "true" transmissivity field than the transmissivity field obtained by the non-iterative (classical co-kriging) approach. Comparing the updated transmissivity field by the non-iterative approach to the updated transmissivity field by the iterative approach, the latter is closer to the "real" field than the former and it is less smooth. However, the iteratively updated transmissivity field is still smoother than the "true" field due to the fact that the updating is achieved by starting from a smooth kriged field and adding smooth (kriged) perturbation surfaces.

It should be commented that in the synthetic experiments conducted (not only for this method but in almost all cases) the reference log-transmissivity fields are multiGaussian. Therefore, the methods are bound to work, since a key decision in the development of the algorithms is that the log-transmissivity fields are multiGaussian. However, in practice, frequently the spatial distribution of transmissivities may be non-multiGaussian and it is very common that not enough data are available to conclude whether the spatial auto-correlation pattern of transmissivities is multiGaussian or not (Gómez-Hernández and Wen, 1998).

Some important characteristics of the method

In this discussion we focus on the second version of the method (Yeh *et al.*, 1996). The use of the measured heads as boundary conditions in the solution of the groundwater flow equation does not seem very appropriate.

The iterative cokriging-like technique is an attempt to circumvent the problem of the first-order linearization of the groundwater flow equation. The linearization based on a first-order approximation is only valid if the unconditional variance of transmissivity is less than 1.0. Yeh and others use as a starting point the cokriging approach and apart from the efforts made to take into account the non-linear relation between transmissivity and hydraulic head by an additional iterative approach nothing new is added as compared to the linearized cokriging approach. The newest variant of the method (Yeh *et al.*, 1996) has the same philosophy as the linear methods of section 3.1.1 and 3.1.2 in

the sense that the resulting iterative estimator of transmissivity is unbiased with minimal variance. Notice that other methods, developed earlier, like the zonation procedure of Carrera and Neuman (see section 3.1.3), the self-calibrating method (see section 3.1.4) and the Pilot Point Method (see section 3.1.5) already took into account the non-linear relation between transmissivity and hydraulic head.

The final estimated transmissivity fields are conditional to the transmissivity measurements and close to the hydraulic head measurements, although the reproduction of the hydraulic head measurements is not explicitly stated in the calibration process. In spite of this, the transmissivity field will in general honour the measured hydraulic heads reasonably, also for transmissivity variances above 1.0. The updating of the transmissivities is based on a first-order approximation of the hydraulic head covariance matrix and the hydraulic head-transmissivity cross-covariance matrix. In addition, the transmissivity covariance matrix at later iterations is also influenced by the linearizations, because in the updating equation of the transmissivity covariance matrix the hydraulic head covariance matrix and the cross covariance matrix appear. The fact that the (cross) covariance matrices are updated using a first-order approximation means that the quality of the updated transmissivity fields is worse if the transmissivity variance is higher; especially the estimation of the auto-correlation pattern of the transmissivity field is expected to become biased.

The main difference between the method presented by Yeh *et al.* (1996) and the Fast Fourier Transform Method (see section 3.1.7) is that Yeh and co-workers produce single best estimates of the inverse groundwater flow equation as opposed to Gutjahr and co-workers who produce equally likely realisations. The methodology to achieve their goal is virtually the same, but the Fast Fourier Transform Method should be deemed as superior since the transmissivity fields generated with this method resemble the spatial variability of transmissivity as observed in the field and modelled by a covariance function. However, later Hanna and Yeh (1998) presented their method in a simulation context, so that their approach is very similar to the one of Hughson and Gutjahr (1998).

Like the Fast Fourier Transform Method, the iterative cokriging-like method seems moderately flexible for extensions to more complex groundwater flow and possibly mass transport problems, for the same reasons as given in section 3.1.7.

3.2 The self-calibrating method

In section 3.1.4 a summary on the self-calibrating method (SCM) has been given and the philosophy of the method has been introduced. In this section the details of the method are discussed and some modifications and extensions of the method are presented:

- The more CPU efficient adjoint state approach is adopted for calculating the gradient of the objective function.
- The method is extended to the inverse modelling of transient groundwater flow and the joint conditioning of transmissivity and storativity fields.
- Some other extensions of the method, like using a discretization into rectangular or prismatic (but regular) grid cells, the possible presence of multiple statistical populations, and 3-D groundwater flow are presented in more detail in latter sections, although some reference is also given in this section.

The sequential self-calibrating method is implemented in the software INVERTO. Appendix I gives detailed instructions on the format of the different input files to INVERTO.

Figure 3.1 summarises the different steps to be taken in the SCM. The first step consists of generating multiple equally likely realisations of input parameters to the groundwater flow equation like hydraulic conductivity and, for transient groundwater flow, also storativity. The multiple equally likely realisations are drawn from an adopted random function model (see section 2.1) for these variables. The realisations of hydraulic conductivity and storativity are conditioned to hard and soft information by sequential MultiGaussian simulation (Gómez-Hernández and Journel, 1993) or sequential indicator simulation (Gómez-Hernández and Srivastava, 1990). The second step in the sequential self-calibrating method consists of the numerical solution of the groundwater flow equation. The steady-state or transient-state groundwater flow equation is solved for the generated couples of spatially variable hydraulic conductivity and storativity fields. Details on the numerical solution of the groundwater flow equation were given in section 2.2.1 and are therefore not repeated here. In this section, the rest of the steps to be taken in the sequential-self-calibrating method are presented. In section 3.2.1 the penalty function is discussed. In section 3.2.2 the parametrisation of the perturbation field is explained. Section 3.2.3 details the gradient calculation. Section 3.2.4 describes how the updating direction is calculated from the gradient. Section 3.2.5 explains the optimisation of the stepsize from the updating direction. Finally, section 3.2.6 presents the convergence criteria.

3.2.1 Penalty function

After solving the 2-D or 3-D steady or transient groundwater flow equation the simulated hydraulic heads are compared with the measured ones. If the

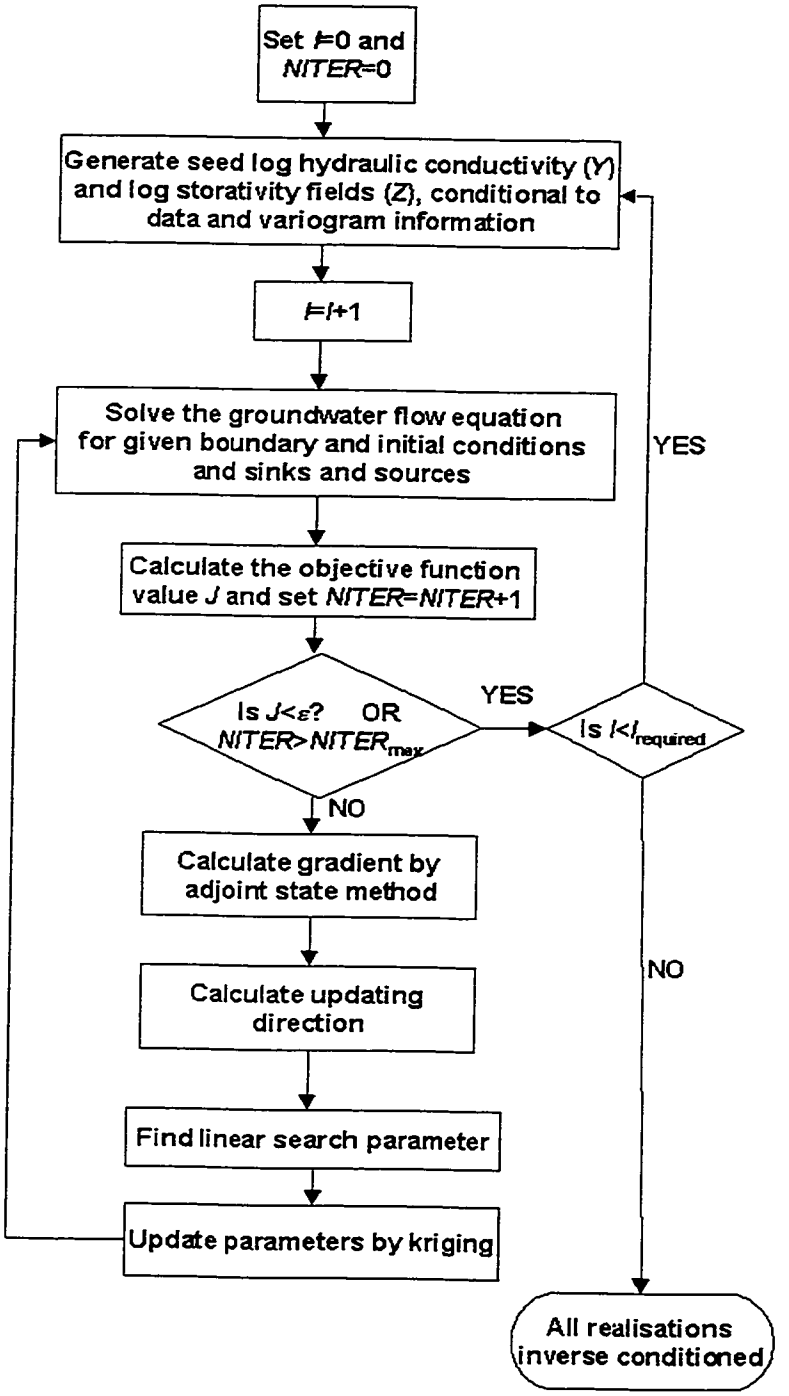

Figure 3.1 Schedule of the steps taken in the self-calibrating method.

simulated values are close to the measured values there may be no need for an additional calibration process; the transmissivity field Y ($Y = \log_{10}T$) and the storativity field Z ($Z = \log_{10}S$) are conditional to not only transmissivity data, but also hydraulic head data. However, if the simulated values are not close to the measured ones (see later), an additional calibration process starts. An objective function measures the deviation between measured and simulated hydraulic heads.

$$J = \sum_{t=1}^{N_t}\sum_{i=1}^{N_h} \xi_{it}(h_{i,t}^{SIM} - h_{i,t}^{MEAS})^2 + \psi_1 \sum_{i}^{N_T}(Y_i^{SIM} - Y_i^{MEAS})^2 + \psi_2 \sum_{i}^{N_S}(Z_i^{SIM} - Z_i^{MEAS})^2 \qquad (3.1)$$

where the first term corresponds to the head discrepancies at the different time steps (if only steady-state flow is simulated this corresponds to the first and only time step), the second term to the discrepancies between initial estimates of transmissivities and updated transmissivity values and the third term to the discrepancies between initial estimates of storativities and updated storativity values. N_h is the number of head measurement locations, N_t the number of time steps with head measurements, N_T the number of transmissivity measurements, N_S the number of storativity measurements, $h_{i,t}$ the heads, Y_i the decimal log transform of transmissivity, Z_i the decimal log transform of storativity and the superscripts *SIM* and *MEAS* refer to "simulated" and "measured" respectively. The weights ξ_{it} are chosen inverse-proportional to the estimated measurement errors. The values of the trade-off coefficients ψ_1 and ψ_2 can be chosen in accordance with the estimated variances of transmissivity and storativity; in any case they should be determined to balance the contribution of each term to the total value of the objective function. However, it is common to set the trade-off coefficients equal to zero (Therefore there is no penalty to the departure of the final fields from the initial estimate). The measured and simulated values are compared at the times and places that measurement data are available. However, the simulated values do not correspond exactly with the locations of the measurement data, and have to be interpolated on the measurement locations. Spatial interpolation is performed according:

$$\{h_{i,t}^{SIM}\} = [B]^T \{h_{ijk}^{SIM}\} \qquad (3.2)$$

where $h_{i,t}^{SIM}$ is a vector of length $N_h{*}N_t$ which contains the simulated hydraulic heads at the measurement locations and times, obtained by interpolating from the simulated hydraulic head solutions; h_{ijk}^{SIM} is a vector with the hydraulic head solution at the N nodes and N_t time steps; B is an interpolation matrix of dimensions $(N{*}N_t) \times (N_h{*}N_t)$ which transforms the vector with simulated heads at the N nodes in the vector with heads at the N_h measurement points. The interpolation matrix contains weights for the interpolation of the nodal heads to the measurement locations. In practice, non zero weights are assigned only to the nodes surrounding the measurement locations. The weights are calculated

inverse proportional to the distance between the node and the measurement location although other interpolation techniques could be used.

It is common to measure the mismatch between simulated and measured heads by the sum of squared deviations. In particular, Carrera and Neuman (1986a) show that under certain assumptions, this corresponds to maximising the likelihood that the estimated parameter values are true, given the observations. If J is smaller than a predefined tolerance value the simulated transmissivity field Y and the storativity field Z are considered to be conditional to the hydraulic head data. If J is not small enough, an optimisation process starts in order to perturb the transmissivity field and possibly the storativity field. Besides the transmissivity and the storativity field, also uncertainty on the boundary conditions may be considered and prescribed head values along the boundaries may be perturbed in order to improve the match to the experimental head data.

3.2.2 The parametrisation of the perturbation field

The calculation of a perturbation field ΔY, a perturbation field ΔZ and a perturbation Δh^{Γ} of the prescribed head boundaries is parameterised as function of the individual perturbations at a number of selected locations, referred to as master blocks. The master blocks include also the prior locations with conductivity measurements. The values away from the master blocks are obtained by ordinary (co-)kriging interpolation of the master block perturbations. The following equations are used:

$$\Delta Y_{ij} = \sum_{k=1}^{N_{p,Y}} \lambda_{ij}^{k} \Delta Y_k + \sum_{k=1}^{N_{p,Z}} \mu_{ij}^{k} \Delta Z_k \tag{3.3}$$

$$\Delta Z_{ij} = \sum_{k=1}^{N_{p,Y}} \nu_{ij}^{k} \Delta Y_k + \sum_{k=1}^{N_{p,Z}} \omega_{ij}^{k} \Delta Z_k \tag{3.4}$$

$$\Delta h_{ij}^{\Gamma} = \sum_{k=1}^{N_p^{\Gamma}} \alpha_{ij}^{k} \Delta h_k^{\Gamma}$$

where $N_{p,Y}$ is the number of master locations for perturbing log transmissivity, $N_{p,Z}$ is the number of master locations for perturbing log storativity, N_p^{Γ} is the number of master locations at boundaries with prescribed head values, ΔY_k, ΔZ_k and Δh_k^{Γ} are the perturbations of, respectively, transmissivity, storativity and prescribed heads at the master locations, the coefficients λ_{ij}^k, μ_{ij}^k, ν_{ij}^k, ω_{ij}^k are the co-kriging weights for the interpolation of the perturbation at location ij from the master location perturbations and the coefficients α_{ij}^k are the ordinary kriging weights for the interpolation of the perturbation at location ij from the master location perturbations at the prescribed head boundaries. The weights

μ_{ij}^k and ν_{ij}^k are equal to zero in case no cross-correlation is considered between transmissivity and storativity. The perturbations at the master blocks with prior measurement data are fixed to zero in case the data is believed to be error-free. The weights referred to in the equations are obtained by solving a (co) kriging system:

$$\begin{bmatrix} C_{\Delta Y_1 \Delta Y_1} & \cdots & C_{\Delta Y_{N_{p,Y}} \Delta Y_1} & C_{\Delta Y_1 \Delta Z_1} & \cdots & C_{\Delta Y_{N_{p,Y}} \Delta Z_1} & 1 & 0 \\ \vdots & C_{\Delta Y_k \Delta Y_k} & \vdots & \vdots & C_{\Delta Y_k \Delta Z_k} & \vdots & 1 & 0 \\ C_{\Delta Y_1 \Delta Y_{N_{p,Y}}} & \cdots & C_{\Delta Y_{N_{p,Y}} \Delta Y_{N_{p,Y}}} & C_{\Delta Y_1 \Delta Z_{N_{p,Z}}} & \cdots & C_{\Delta Y_{N_{p,Y}} \Delta Z_{N_{p,Z}}} & 1 & 0 \\ C_{\Delta Z_1 \Delta Y_1} & \cdots & C_{\Delta Z_{N_{p,Z}} \Delta Y_1} & C_{\Delta Z_1 \Delta Z_1} & \cdots & C_{\Delta Z_{N_{p,Z}} \Delta Z_1} & 0 & 1 \\ \vdots & C_{\Delta Z_k \Delta Y_k} & \vdots & \vdots & C_{\Delta Z_k \Delta Z_k} & \vdots & 0 & 1 \\ C_{\Delta Z_1 \Delta Y_{N_{p,Y}}} & \cdots & C_{\Delta Z_{N_{p,Z}} \Delta Y_{N_{p,Y}}} & C_{\Delta Z_1 \Delta Z_{N_{p,Z}}} & \cdots & C_{\Delta Z_{N_{p,Z}} \Delta Z_{N_{p,Z}}} & 0 & 1 \\ 1 & 1 & 1 & 0 & 0 & 0 & 0 & 0 \\ 0 & 0 & 0 & 1 & 1 & 1 & 0 & 0 \end{bmatrix} \begin{Bmatrix} \lambda_{ij}^1 \\ \lambda_{ij}^k \\ \lambda_{ij}^{N_{p,Y}} \\ \mu_{ij}^1 \\ \mu_{ij}^k \\ \mu_{ij}^{N_{p,Z}} \\ m_1 \\ m_2 \end{Bmatrix} = \begin{Bmatrix} C_{\Delta Y_1 \Delta Y_{ij}} \\ \vdots \\ C_{\Delta Y_{N_{p,Y}} \Delta Y_{ij}} \\ C_{\Delta Z_1 \Delta Y_{ij}} \\ \vdots \\ C_{\Delta Z_{N_{p,Z}} \Delta Y_{ij}} \\ 1 \\ 0 \end{Bmatrix}$$

$$\begin{bmatrix} C_{\Delta Y_1 \Delta Y_1} & \cdots & C_{\Delta Y_{N_{p,Y}} \Delta Y_1} & C_{\Delta Y_1 \Delta Z_1} & \cdots & C_{\Delta Y_{N_{p,Y}} \Delta Z_1} & 1 & 0 \\ \vdots & C_{\Delta Y_k \Delta Y_k} & \vdots & \vdots & C_{\Delta Y_k \Delta Z_k} & \vdots & 1 & 0 \\ C_{\Delta Y_1 \Delta Y_{N_{p,Y}}} & \cdots & C_{\Delta Y_{N_{p,Y}} \Delta Y_{N_{p,Y}}} & C_{\Delta Y_1 \Delta Z_{N_{p,Z}}} & \cdots & C_{\Delta Y_{N_{p,Y}} \Delta Z_{N_{p,Z}}} & 1 & 0 \\ C_{\Delta Z_1 \Delta Y_1} & \cdots & C_{\Delta Z_{N_{p,Z}} \Delta Y_1} & C_{\Delta Z_1 \Delta Z_1} & \cdots & C_{\Delta Z_{N_{p,Z}} \Delta Z_1} & 0 & 1 \\ \vdots & C_{\Delta Z_k \Delta Y_k} & \vdots & \vdots & C_{\Delta Z_k \Delta Z_k} & \vdots & 0 & 1 \\ C_{\Delta Z_1 \Delta Y_{N_{p,Y}}} & \cdots & C_{\Delta Z_{N_{p,Z}} \Delta Y_{N_{p,Y}}} & C_{\Delta Z_1 \Delta Z_{N_{p,Z}}} & \cdots & C_{\Delta Z_{N_{p,Z}} \Delta Z_{N_{p,Z}}} & 0 & 1 \\ 1 & 1 & 1 & 0 & 0 & 0 & 0 & 0 \\ 0 & 0 & 0 & 1 & 1 & 1 & 0 & 0 \end{bmatrix} \begin{Bmatrix} \nu_{ij}^1 \\ \nu_{ij}^k \\ \nu_{ij}^{N_{p,Y}} \\ \omega_{ij}^1 \\ \omega_{ij}^k \\ \omega_{ij}^{N_{p,Z}} \\ m_1 \\ m_2 \end{Bmatrix} = \begin{Bmatrix} C_{\Delta Y_1 \Delta Z_{ij}} \\ \vdots \\ C_{\Delta Y_{N_{p,Y}} \Delta Z_{ij}} \\ C_{\Delta Z_1 \Delta Z_{ij}} \\ \vdots \\ C_{\Delta Z_{N_{p,Z}} \Delta Z_{ij}} \\ 1 \\ 0 \end{Bmatrix}$$

$$\begin{bmatrix} C_{\Delta h_1^\Gamma \Delta h_1^\Gamma} & \cdots & C_{\Delta h_{N_p^\Gamma}^\Gamma \Delta h_1^\Gamma} & 1 \\ \vdots & C_{\Delta h_k^\Gamma \Delta h_k^\Gamma} & \vdots & 1 \\ C_{\Delta h_1^\Gamma \Delta h_{N_p^\Gamma}^\Gamma} & \cdots & C_{\Delta h_{N_p^\Gamma}^\Gamma \Delta h_{N_p^\Gamma}^\Gamma} & 1 \\ 1 & 1 & 1 & 0 \end{bmatrix} \begin{Bmatrix} \alpha_{ij}^1 \\ \alpha_{ij}^k \\ \alpha_{ij}^{N_p^\Gamma} \\ m \end{Bmatrix} = \begin{Bmatrix} C_{\Delta h_1^\Gamma \Delta h_{ij}^\Gamma} \\ \vdots \\ C_{\Delta h_{N_p^\Gamma}^\Gamma \Delta h_{ij}^\Gamma} \\ 1 \end{Bmatrix}$$

The three kriging systems show how the different weights are calculated. C refers to the modelled spatial covariances in 1-D, 2-D or 3-D. With respect to the co-kriging systems for interpolating transmissivity and storativity perturbations: the left-hand side matrix gives the modelled spatial covariances between the master block locations. The upper left block of this matrix handles the covariances of the primary variable (Y), the lower left and upper right block present the cross covariances between the primary and the secondary variable (Z) and the lower right block gives the covariances of the secondary variable. The right hand side vector contains the modelled spatial (cross) covariances between a grid cell and the different master blocks. The left-hand side of

kriging system for interpolating the prescribed head perturbations contains the modelled covariances between the master blocks located at the prescribed head boundaries and the right hand side the modelled spatial covariances between the grid cell and the master block locations. The covariance model for prescribed head perturbations is usually estimated on the basis of expert knowledge. The parameters m, m_1 and m_2 are Lagrange multipliers.

By solving these kriging systems, the weights λ_{ij}^k, μ_{ij}^k, υ_{ij}^k, ω_{ij}^k and α_{ij}^k are obtained for the interpolation of perturbations at master blocks to a grid cell. For each grid cell a kriging system has to be solved.

The master blocks form an essential part of the methodology because they reduce the dimensionality of the optimisation problem. However, the problem remains on how many master blocks have to be used and which their configuration should be. Details are given in the section 3.3.

3.2.3 Calculation of the gradient

In the section 3.2.2 it was shown how perturbations, calculated at a number of master blocks, are interpolated to the rest of the grid cells. However, it has not been discussed yet how the perturbations are calculated at those master blocks. The aim is to calculate the perturbations that produce the largest reduction in the objective function value (recall that we want to reduce the objective function value in order to reduce the mismatch between measured and simulated heads). Therefore, the gradient vector containing the partial derivatives of the objective function with respect to perturbations at the master block locations must be calculated. Below it is explained step by step how the gradient vector is calculated.

The hydraulic head values h are the N x N_t state variables, N being the number of discretization grid cells and N_t the number of times at which the groundwater flow equation is solved. A vector p of length M contains all the parameters which are calibrated. The length M of the vector is therefore equal to $N_{p,Y}+ N_{p,Z}+ N_p^{\Gamma}$. Heads and parameters are related through N x N_t state equations (Carrera *et al.*, 1990):

$$\{\Psi(\{h\},\{p\})\}=0$$

One possible way to formulate the transient groundwater flow equation in matricial form is (equation 2.7 in section 2.2.1):

$$\left([A]-\frac{[D]}{\Delta t}\right)\{h^{t+1}\}+\{q\}=-\frac{[D]}{\Delta t}\{h^{t}\}$$

where $[A]$ was the N x N conductance matrix, h the N x 1 vector with nodal heads at time step t or t+1, q the N x 1 vector with recharges and discharges, D the N x N storage matrix and Δt the time step. Therefore, ψ for two succeeding time steps is given by:

$$\{\Psi_t\}=\left([A]-\frac{[D]}{\Delta t^t}\right)\{h^t\}+\{q\}+\frac{[D]}{\Delta t^t}\{h^{t-1}\}=0$$

$$\{\Psi_{t+1}\}=\left([A]-\frac{[D]}{\Delta t^{t+1}}\right)\{h^{t+1}\}+\{q\}+\frac{[D]}{\Delta t^{t+1}}\{h^t\}=0$$

where Δt^t is the time step between t-1 and t, Δt^{t+1} the time step between t and t+1 and h^t is an N-dimensional vector of hydraulic heads for the time step t.

The Lagrangian of the objective function (which we want to minimise) subject to the above formulated constraints is:

$$\Im = J + \{\lambda\}^T\{\Psi\}$$

where λ is a N x N_t dimensional vector of Lagrange multipliers (also called adjoint states). For each time that the adjoint state equation is solved an N dimensional vector of Lagrange multipliers is estimated. The obtained Lagrange multipliers for the state $\{\psi_t\}$ are $\{\lambda^t\}$, the ones for the state $\{\psi_{t+1}\}$ are $\{\lambda^{t+1}\}$ etcetera. The derivatives of the Lagrangian with respect to the perturbations parameters are given by:

$$\frac{d\Im}{d\{p\}}=\frac{dJ}{d\{p\}}=\frac{\partial J}{\partial\{p\}}+\frac{\partial J}{\partial\{h\}}\frac{\partial\{h\}}{\partial\{p\}}+\{\lambda\}^T\left(\frac{\partial\{\Psi\}}{\partial\{p\}}+\frac{\partial\{\Psi\}}{\partial\{h\}}\frac{\partial\{h\}}{\partial\{p\}}\right)$$

The derivative of the Lagrangian with respect to the perturbation parameters is similar to the derivative of the objective function with respect to the perturbation parameters.

This can also be written as:

$$\frac{dJ}{d\{p\}}=\frac{\partial J}{\partial\{p\}}+\left(\frac{\partial J}{\partial\{h\}}+\{\lambda\}^T\frac{\partial\{\Psi\}}{\partial\{h\}}\right)\frac{\partial\{h\}}{\partial\{p\}}+\{\lambda\}^T\frac{\partial\{\Psi\}}{\partial\{p\}} \qquad (3.5)$$

The adjoint state is chosen as the solution of the following equation:

$$\frac{\partial J}{\partial \{h\}} + \{\lambda\}^T \frac{\partial \{\Psi\}}{\partial \{h\}} = 0 \tag{3.6}$$

Equation 3.5 can be simplified then:

$$\frac{dJ}{d\{p\}} = \frac{\partial J}{\partial \{p\}} + \{\lambda\}^T \frac{\partial \{\Psi\}}{\partial \{p\}} \tag{3.7}$$

The vector of adjoint states is obtained by solving equation 3.6 and the result can be used to calculate the gradient of the objective function.

First we will explain how the adjoint states are obtained. The two derivatives in equation 3.6 are given by:

$$\frac{\partial J}{\partial \{h^t\}} = 2\sum_{i=1}^{N_h} \xi_{it} (h_i^{t,SIM} - h_i^{t,MEAS}) \tag{3.8}$$

The derivatives of the states with respect to the vector of hydraulic heads at time step t are only non-zero for the time steps t and t+1:

$$\frac{\partial \{\Psi_t\}}{\partial \{h^t\}} = \left([A] - \frac{[D]}{\Delta t^t} \right) \tag{3.9}$$

$$\frac{\partial \{\Psi_{t+1}\}}{\partial \{h^t\}} = \frac{[D]}{\Delta t^{t+1}} \tag{3.10}$$

Combining the equations 3.8 until 3.10 above with equation 3.6 gives the following expression:

$$2\sum_{i=1}^{N_h} \xi_{it} (h_i^{t,SIM} - h_i^{t,MEAS}) + \{\lambda^t\}^T \left([A] - \frac{[D]}{\Delta t^t} \right) + \{\lambda^{t+1}\}^T \left(\frac{[D]}{\Delta t^{t+1}} \right) = 0$$

Rearranging gives:

$$\{\lambda^t\}^T \left([A] - \frac{[D]}{\Delta t^t} \right) = -2\sum_{i=1}^{N_h} \xi_{it} (h_i^{t,SIM} - h_i^{t,MEAS}) - \{\lambda^{t+1}\}^T \left(\frac{[D]}{\Delta t^{t+1}} \right) \tag{3.11}$$

Notice that this equation is very similar to the equation 2.7 for solving the groundwater flow equation. However, a difference is observed with respect to

the vector of unknowns (the heads in case of the groundwater flow equation and the adjoint states for the adjoint state equation). While the solution for time step t enters on the right-hand side of equation 2.7 and the solution for time step t+1 on the left-hand side of that equation, for the solution of equation 3.11 it is the opposite. Therefore equation 3.11 has to be solved backwards in time, starting from $\{\lambda^{Nt+1}\}=0$. The similarity of the equation with the groundwater flow equation makes it possible to save important amounts of CPU time. The equation is solved in a way similar to the groundwater flow equation.

The adjoint state equations can also be formulated continuous in time. In some cases, this formulation may have important advantages. Appendix II presents an adjoint state formulation for the case that the temporal domain is not discretized.

The expressions of the derivatives of equation 3.7 are:

$$\frac{\partial J}{\partial\{p\}} = 2\psi_1 \sum_{i=1}^{N_T} (Y_i^{SIM} - Y_i^{MEAS}) + 2\psi_2 \sum_{i=1}^{N_S} (Z_i^{SIM} - Z_i^{MEAS})$$

$$\frac{\partial\{\Psi_t\}}{\partial\{p\}} = \frac{\partial[A]}{\partial\{p\}}\{h^t\} - \frac{\partial[D]}{\partial\{p\}\Delta t^t}\{h^t\} + \frac{\partial\{q\}}{\partial\{p\}} + \frac{\partial[D]}{\partial\{p\}\Delta t^t}\{h^{t-1}\} \qquad (3.12)$$

The derivatives which appear in the equation above are given below. The derivatives have to be given with respect to perturbations of transmissivity, storativity and prescribed head conditions.

First the derivatives of the conductance matrix are handled. These derivatives are zero, except the derivatives with respect to perturbations of the transmissivity field. Furthermore, the derivatives with respect to perturbations of the transmissivity field depend on the way the interblock transmissivity is calculated. In case the geometric mean is preferred (see section 2.2.1) the following expression for an element of the conductance matrix was found for example:

$$A_{lm} = K_{lm} \frac{\Delta y_l \Delta z_l}{\Delta x_{lm}} \qquad m \in \{W, E\} \wedge m \notin (\Gamma^h)$$

The used notation is explained in section 2.2.1 below equation 2.7. Γ^h refers to the contour at which heads are prescribed.

The expressions for the other elements of the conductance matrix are similar. The following expressions are obtained:

$$\frac{\partial A_{lm}}{\partial \Delta Y_k} = 0 \qquad m \notin \{N, S, E, W, U, D\} \vee m \in (\Gamma^h) \qquad (3.13)$$

$$\frac{\partial A_{lm}}{\partial \Delta Y_k} = A_{lm} \frac{\lambda_l^k + \lambda_m^k}{2} \qquad m \in \{N,S,E,W,U,D\} \wedge m \notin (\Gamma^h) \tag{3.14}$$

$$\frac{\partial A_{ll}}{\partial \Delta Y_k} = -\sum_{m \in N,S,E,W,U,D} A_{lm} \frac{\lambda_l^k + \lambda_m^k}{2} \tag{3.15}$$

In the expressions above the index k refers to a master block. N (North), S (South), E (East), W (West), U (Up) and D (Down) refer to the position of the neighbour cell with respect to the cell indexed with l. The previous expressions are only for the cases in which either only transmissivity is perturbed or if both transmissivity and storativity are perturbed, they are not cross-correlated.

In case the harmonic mean is preferred the expressions above change. Below one example is given, the expressions for the other elements of the conductance matrix are similar, just the grid cell dimensions may change:

$$\frac{\partial A_{lm}}{\partial \Delta Y_k} = \frac{1}{2} \frac{K_{lm}^2}{\Delta x_{lm}} \Delta y_l \Delta z_l \left(\frac{\lambda_l^k}{K_l} + \frac{\lambda_m^k}{K_m} \right) \qquad m \in \{W,E\} \wedge m \notin (\Gamma^h) \tag{3.16}$$

$$\begin{aligned} \frac{\partial A_{ll}}{\partial \Delta Y_k} = & -\sum_{m \in E,W} \frac{1}{2} \frac{K_{lm}^2}{\Delta x_{lm}} \Delta y_l \Delta z_l \left(\frac{\lambda_l^k}{K_l} + \frac{\lambda_m^k}{K_m} \right) - \sum_{m \in N,S} \frac{1}{2} \frac{K_{lm}^2}{\Delta y_{lm}} \Delta x_l \Delta z_l \left(\frac{\lambda_l^k}{K_l} + \frac{\lambda_m^k}{K_m} \right) \\ & - \sum_{m \in U,D} \frac{1}{2} \frac{K_{lm}^2}{\Delta z_{lm}} \Delta x_l \Delta y_l \left(\frac{\lambda_l^k}{K_l} + \frac{\lambda_m^k}{K_m} \right) \end{aligned} \tag{3.17}$$

The derivatives of the vector of sinks and sources with respect to the perturbations follow next. The expressions below are for the case that the geometric interblock mean is preferred. In case the harmonic mean is used to calculate the interblock conductivities, the grid cell dimensions would appear in the expressions like in the equations 3.16 and 3.17.

$$\frac{\partial q_l}{\partial \Delta Y_k} = \sum_{\substack{m \in N,S,E,W,U,D \\ m \in \Gamma^h}} \left(A_{lm} \frac{\lambda_l^k + \lambda_m^k}{2} \right) h_m^\Gamma \tag{3.18}$$

$$\frac{\partial q_l}{\partial \Delta h_k^\Gamma} = \sum_{\substack{m \in N,S,E,W,U,D \\ m \in \Gamma^h}} A_{lm} \alpha_m^k \tag{3.19}$$

Finally, the derivatives of the storativity matrix with respect to the perturbations are given. These derivatives are only non-zero in case of modifications of the log transformed storativity coefficient. Again it is assumed that the storativity and transmissivity fields are not cross-correlated. The elements of the matrix D account for prismatic grid cells.

$$\frac{\partial D_{ll}}{\partial \Delta Z_k} = \omega_l^k D_{ll}$$

In case the storativity coefficient is assumed constant throughout the aquifer this derivative takes the following expression:

$$\frac{\partial [D]}{\partial Z} = [D]$$

The expressions for the derivatives are used in equation 3.12 and together with the solution of equation 3.11, the solution of equation 3.7 can be found. Doing so, a vector g of length $N_{p,Y}$+ $N_{p,Z}$+ N_p^{Γ} containing the partial derivatives of the objective function with respect to parameter perturbations is found. The vector g is composed as shown below:

$$g^T = \{g_1 \quad g_2 \quad \cdots \quad g_{N_{p,Y}+N_{p,Z}+N_p^{\Gamma}}\} = \left\{ \frac{\partial J}{\partial \Delta Y_1} \quad \frac{\partial J}{\partial \Delta Y_2} \quad \cdots \quad \frac{\partial J}{\partial \Delta Y_{N_{p,Y}}} \quad \frac{\partial J}{\partial \Delta Z_1} \quad \frac{\partial J}{\partial \Delta Z_2} \quad \cdots \quad \frac{\partial J}{\partial \Delta Z_{N_{p,Z}}} \quad \frac{\partial J}{\partial \Delta h_1^{\Gamma}} \quad \frac{\partial J}{\partial \Delta h_2^{\Gamma}} \quad \cdots \quad \frac{\partial J}{\partial \Delta h_{N_p^{\Gamma}}^{\Gamma}} \right\}$$

3.2.4 Calculating the updating direction from the gradient

The gradient found is not equal to the updating direction; non-linear optimisation algorithms are used to calculate the updating direction from the gradient. Searching along the gradient is not the most efficient way to find – in a number of iterations – the minimum of the objective function. A more efficient way is to search along an updating direction calculated from the gradient. Carrera and Neuman (1986c) found that alternating different non linear optimisation algorithms results in a faster convergence. This approach is also adopted in the self-calibrating method. Four different non linear optimisation algorithms are alternated in the optimisation.

The steepest descent algorithm sets the updating direction in the direction of the gradient. This algorithm is used for so-called pacer iterations; after using all the other non-linear optimisation algorithms during a number of iterations, the updating direction is set back in the direction of the gradient in order to stabilise the convergence (Scales, 1985). If the step size in the updating direction is sufficiently small the biggest reduction in the objective function value is obtained by searching in the gradient direction. The updating direction d is given by (the subscript refers in this case to the iteration number):

$$\{d\}_k = -\{g\}_k$$

It is advantageous to use information on second order derivatives in the convergence process. This could be done by modified Newton methods. However, second derivatives are not available analytically and the approximation of the Hessian matrix (the matrix containing the partial second order derivatives of the objective function with respect to the perturbation parameters) by finite differences requires a considerable number of gradient evaluations. Conjugate gradient methods are used as an alternative to modified Newton methods; the number of iterations required will be bigger, but the total amount of time spent evaluating the objective function and its gradient will be reduced. The Hestenes-Stiefel conjugate gradients algorithm and the Fletcher-Reeves conjugate gradients algorithm are implemented (Scales, 1985). Both calculate the updating direction using information on the calculated gradient and in the last two iterations. The updating direction according Hestenes-Stiefel conjugate gradients is given by:

$$\{d\}_k = -\{g\}_k + \left(\frac{\{\Delta g\}_{k-1}^T \{g\}_k}{\{\Delta g\}_{k-1}^T \{d\}_{k-1}} \right) \{d\}_{k-1}$$

where the subscript k-1 refers to the previous iteration and Δg_{k-1} is the difference in gradient between the current iteration and the previous iteration.

The updating direction according Fletcher-Reeves conjugate gradients is:

$$\{d\}_k = -\{g\}_k + \left(\frac{\{g\}_k^T \{g\}_k}{\{g\}_{k-1}^T \{g\}_{k-1}} \right) \{d\}_{k-1}$$

On non-quadratic functions it can happen that the updating direction becomes almost orthogonal to the gradient and hence little progress can be made. The Fletcher-Reeves method has not a build-in tendency to correct for this, but the Hestenes-Stiefel variant of conjugate gradients has a built-in tendency to reset the updating direction automatically to the steepest descent direction (Scales, 1985).

A fourth algorithm which has been implemented is the Davidon-Fletcher-Powell Quasi-Newton method. This method estimates the Hessian matrix with second derivatives from subsequent calculations of the gradient. The estimate of the Hessian matrix improves during the optimisation process. The advantage of using estimates of second order derivatives is that it improves the convergence and robustness as compared to the conjugate gradients method. However, the disadvantage is that the method requires much more storage so that it is not suitable for very large problems.

$$\{d\}_k = -\left([H]_{k-1} + \frac{\{\Delta x\}_{k-1}\{\Delta x\}_{k-1}^T}{\{\Delta x\}_{k-1}^T\{\Delta g\}_{k-1}} - \frac{[H]_{k-1}\{\Delta g\}_{k-1}\{\Delta g\}_{k-1}^T[H]_{k-1}}{\{\Delta g\}_{k-1}^T[H]_{k-1}\{\Delta g\}_{k-1}} \right)\{g\}_k$$

In which H is the Hessian matrix and Δx is the difference in the vector of parameter values between the current iteration and the previous iteration.

The four algorithms are alternated in calculating the updating direction. The criteria which are used in changing the algorithms are in correspondence with the findings from Carrera and Neuman (1986c). Details are given in section 3.3.

3.2.5 Determining the step size

The step size in the updating direction is determined by a linear search method. The parameter updating is given by:

$$\{\Delta x\}_k = \alpha_k \{d\}_k$$

The scalar α_k is determined by linear search. The procedure is explained in section 3.3.

The updating of the transmissivity and storativity field is limited to values which are not too far from the expected transmissivity and storativity values in order to stabilise the calibration process. The values of transmissivity and storativity are limited to an interval of the cokriging estimate plus or minus three times the cokriging standard deviation (see section 2.1.2.2 for the explanation of the cokriging estimation and the cokriging variance). Also the updating of the prescribed head values at the boundaries is limited to some maximum and minimum values. However, in this case the user defines directly the maximum allowed change of the prescribed boundary heads. The value is ideally based on expert knowledge.

The following equation gives the maximum and minimum parameter values. μ refers to the (co)kriging estimate and σ to the (co)kriging standard deviation.

$$
\begin{Bmatrix} Y_1^{min} \\ Y_2^{min} \\ \vdots \\ Y_{N_{p,Y}}^{min} \\ Z_1^{min} \\ Z_2^{min} \\ \vdots \\ Z_{N_{p,Z}}^{min} \\ h_1^{\Gamma,min} \\ h_2^{\Gamma,min} \\ \vdots \\ h_{N_p^\Gamma}^{\Gamma,min} \end{Bmatrix} \leq \begin{Bmatrix} Y_1 \\ Y_2 \\ \vdots \\ Y_{N_{p,Y}} \\ Z_1 \\ Z_2 \\ \vdots \\ Z_{N_{p,Z}} \\ h_1^\Gamma \\ h_2^\Gamma \\ \vdots \\ h_{N_p^\Gamma}^\Gamma \end{Bmatrix} \leq \begin{Bmatrix} Y_1^{max} \\ Y_2^{max} \\ \vdots \\ Y_{N_{p,Y}}^{max} \\ Z_1^{max} \\ Z_2^{max} \\ \vdots \\ Z_{N_{p,Z}}^{max} \\ h_1^{\Gamma,max} \\ h_2^{\Gamma,max} \\ \vdots \\ h_{N_p^\Gamma}^{\Gamma,max} \end{Bmatrix} \longrightarrow \begin{Bmatrix} \mu(Y_1) - 3\sigma(Y_1) \\ \mu(Y_2) - 3\sigma(Y_2) \\ \vdots \\ \mu(Y_{N_{p,Y}}) - 3\sigma(Y_{N_{p,Y}}) \\ \mu(Z_1) - 3\sigma(Z_1) \\ \mu(Z_2) - 3\sigma(Z_2) \\ \vdots \\ \mu(Z_{N_{p,Z}}) - 3\sigma(Z_{N_{p,Z}}) \\ h_1^\Gamma - (\Delta h)^{expert} \\ h_2^\Gamma - (\Delta h)^{expert} \\ \vdots \\ h_{N_p^\Gamma}^\Gamma - (\Delta h)^{expert} \end{Bmatrix} \leq \begin{Bmatrix} Y_1 \\ Y_2 \\ \vdots \\ Y_{N_{p,Y}} \\ Z_1 \\ Z_2 \\ \vdots \\ Z_{N_{p,Z}} \\ h_1^\Gamma \\ h_2^\Gamma \\ \vdots \\ h_{N_p^\Gamma}^\Gamma \end{Bmatrix} \leq \begin{Bmatrix} \mu(Y_1) + 3\sigma(Y_1) \\ \mu(Y_2) + 3\sigma(Y_2) \\ \vdots \\ \mu(Y_{N_{p,Y}}) + 3\sigma(Y_{N_{p,Y}}) \\ \mu(Z_1) + 3\sigma(Z_1) \\ \mu(Z_2) + 3\sigma(Z_2) \\ \vdots \\ \mu(Z_{N_{p,Z}}) + 3\sigma(Z_{N_{p,Z}}) \\ h_1^\Gamma + (\Delta h)^{expert} \\ h_2^\Gamma + (\Delta h)^{expert} \\ \vdots \\ h_{N_p^\Gamma}^\Gamma + (\Delta h)^{expert} \end{Bmatrix}
$$

3.2.6 Convergence criteria

When the new parameter values are found, the objective function value J is calculated again. Probably a new iteration is started in order to reduce J further. The calibration is terminated in any of the following cases:

- J decreases below a user defined value. It means that the hydraulic heads are reproduced closely enough. The quality of the hydraulic head data should be taken into account (see section 4.2).

- During a (large) number of iterations, the reduction of J is below a user-defined (very low) value. A reason may be, that the hydraulic head values cannot be reproduced, another explanation may be that the solution got stucked in a local minimum, from which it apparently cannot escape. However, it is frequently observed, also by other authors (Carrera and Neuman, 1986c) that although J does not reduce during a large number of iterations, suddenly J may again reduce significantly.

- The user defined maximum number of iterations is exceeded.

3.3 Numerical aspects of the self-calibration

The methodology presented in section 3.2 was implemented in the computer program INVERTO. In this section some of the numerical procedures and issues on the computer implementation are highlighted. Some numerical methods are explained in other sections. The numerical method to solve the groundwater flow equation is explained in section 2.2.1. The same finite difference method is also applied to solve the adjoint state system (equation 3.11). These numerical methods are therefore not discussed in this section. The section discusses numerical procedures and computer implementation issues related with the geostatistical simulation, the solution of the groundwater flow equation and the non-linear optimisation.

Multiple zones for multiple statistical populations

The aquifer may be divided in multiple zones with different statistical properties. The zonification of the aquifer should not be confused with the zonation approach of Carrera and Neuman (section 3.1.3). They divide the aquifer in zones with constant values for the different parameters. In the SCM the aquifer can be divided into zones with a different random function model for hydraulic conductivity and possibly other parameters. Only in case of a clear geological evidence the aquifer is divided in multiple zones. It should be reminded that the approach is robust for non-stationarities because of the conditioning to measurement data and the use of the ordinary kriging algorithm for the interpolation of the perturbations. Chapter 5 shows how the concept of multiple statistical populations is used for the inverse modelling of groundwater flow in fractured media.

In case the aquifer is divided in multiple zones the two most important modifications in the SCM are:

- The hydraulic conductivity realisations are generated such that the hydraulic conductivities simulated for zone 1 are just conditioned to the hydraulic conductivity data of zone 1, the hydraulic conductivities for zone 2 are just conditioned to the hydraulic conductivity data of zone 2, etctera. For each zone a different mean hydraulic conductivity value and variogram have to be specified.
- The perturbation at a master block only affects the grid cells located in the same zone as the master block. The perturbation at a grid cell is therefore not influenced by the master blocks located in a zone different from the zone of the grid cell.

Variogram definition

The 3-D variograms for hydraulic conductivity and storativity coefficient are specified for each zone of the aquifer. In case the aquifer is not divided into multiple zones just one variogram for hydraulic conductivity and the storativity

coefficient are specified. A variogram may consist of up to two contributing structures plus one nugget effect. A spherical model, exponential model and Gaussian model can be specified. For details on the variogram definition see section 2.1.2.

Transient flow: initial heads and time discretisation

In case 2-D or 3-D transient groundwater flow is simulated initial heads have to be specified. The software INVERTO allows for two options: a user-supplied definition of the initial head values and the solution of the steady-state flow equation as starting point for the transient flow. In case transient groundwater flow departs from a steady-state flow regime, the best strategy is to condition the transmissivity realisations first to steady-state head data. The transmissivity realisations already conditioned to steady-state head data are the starting point for the conditioning to transient head data. Other research groups (Pilot Point Method, zonation approach) also found that a sequential conditioning to first steady-state heads and later transient heads yields the best results.

A maximum flexibility is implemented for the time step Δt: the user can specify the magnitudes of each of the time steps in a separate file, or can choose to define the time steps for all the simulation period by just using three parameters:

$$(\Delta t_n) = (\Delta t_0)^{DTCOEF * n}$$

Where Δt_n is the n-th time step, Δt_0 the start time step, *DTCOEF* the multiplication factor and n the counter on the simulation time step.

Solving the linear system of equations

The numerical solution of the groundwater flow equation and the mass transport equation can be written in the form of a linear system of equations as given by equations 2.8 and 2.11. It is of crucial importance to solve this linear system of equations using a minimum of CPU-time, because in the inverse modelling procedure the flow and possibly the transport equation have to be solved numerous times. The left-hand side matrix ξ of size N x N of equation 2.8 and the matrix η of equation 2.11 are not stored completely, because this would only allow solutions for problems with some hundreds of grid cells. It is common to store only the bandwidth of the matrices ξ and η which may have non-zero values, so that the storage requirements for these matrices are reduced to N x bandwidth. The bandwidth of ξ is, for example, equal to (2 x nx x ny) +1 in case $nz>nx$ and $nz>ny$. Making use of the fact that the matrix ξ is symmetric storage requirements can be reduced to the bandwidth (nx x ny) +1. However, for very large 2-D problems and most 3-D problems this is not a satisfying solution because the storage requirements for ξ still may exceed the system capacities. Therefore the matrices ξ and η are stored in the so-called SLAP

(Sparse Linear Algebra Package) format; only the values different from zero of the ξ and η matrices are stored. It reduces further the storage requirements, because each line of the matrices ξ and η has as a maximum just seven respectively 27 values different from zero. In the case of the ξ matrix for example the seven non-zero values are related to the six interblock conductivities and the diagonal element. However, not only the non-zero values have to be stored, but also the matrix entries. The reduction in storage requirements is very significant and makes it possible to handle very large flow problems. The SLAP format to store the non-zero entries of the ξ matrix is used together with an iterative solution of the linear system of equations. The BiConjugate Gradient Squared Method with Incomplete LU Decomposition Preconditioning is used to solve the linear system of equations iteratively. The user has to supply a tolerance value, a maximum number of allowed iterations and a guess solution, which is used as the starting point in the iterative procedure to find the solution. If the calculated error decreases below the tolerance value the solution of the linear system stops and the last found solution is stored. The same happens if the maximum number of iterations is reached. Some tests need to be done in order to determine the tolerance value that gives a satisfying solution to the groundwater flow equation or mass transport equation and minimises the CPU time at the same time. If reducing the tolerance value does not result in noticeable changes in the calculated heads or concentrations, the tolerance value may be considered sufficiently low. The maximum number of iterations should be big enough, although in practice we found that it is not necesary to increase this number above 500.

Some other efforts are made to guarantee that a sufficient precise solution of the groundwater flow equation is found, that the amount of consumed CPU time is reduced and that in case of convergence problems a solution of the groundwater flow equation is found which is as precise as possible. The following implementations are made:

- Supplying the best possible guess solutions. For example, during the linear search, the groundwater flow equation is solved for different try values that correspond to an increasing perturbation of the transmissivity field (and possibly other parameters). The supplied guess solution during the linear search is the solution of the groundwater flow equation for an already tested "try" value that is the most close to the actually tested "try" value.
- In case of no convergence, other attempts are made to solve the linear system of equations by changing the guess vector or the number of iterations. The final solution replaces the guess vector, in case this solution is not much worse than the original guess solution. Another strategy consists of reducing the number of iterations (if it is found that the error starts to increase after a number of iterations) and using the last solution for the reduced number of iterations as the new guess solution.
- In case that after a number of trials not a satisfying solution is found the tolerance is increased step-by-step, until the linear system of equations can be solved satisfactorily for that tolerance. In those cases that the linear

system of equations is solved with a modified tolerance value, a message is printed to a file, indicating the problems.

Especially for large 3-D problems, with the presence of fractures, convergence problems may appear. This is due to the fact that locally two neighbouring grid cells may have hydraulic conductivities which differ more than a factor 10^6 in magnitude. The consequence is that the conductance matrix ξ is nearly singular, and in combination with a large number of equations, this complicates finding the unique solution of the groundwater flow or the mass transport equations.

Interpolating the simulation results to the exact measurement locations

In section 3.2 it was mentioned that the exact measurement locations may not coincide with the grid cell centres. In order to compare simulated and measured data it is necessary to interpolate the values simulated at the grid cell centres to the measurement locations. In expression 3.2 an interpolation matrix B appears. However, no further attention has been paid in section 3.2 to measurement locations that do not coincide with the grid cell centres. The equations 3.8 and 3.11 would include the interpolation matrix B for the case that the measurement locations are not all located on the grid cell centres.

INVERTO uses a simple inverse squared distance weighting to estimate the simulated head value at a measurement location. An alternative to interpolation by inverse squared distance weighting would be kriging, but it is considered that for this interpolation it is not necessary to use the much more cumbersome and CPU-intensive kriging algorithm. The procedure consists of the following steps:

1. The grid cells that surround the measurement location are selected. In case the grid cells are squared or cubic and the size of the grid cell is l, the grid cells are selected whose grid cell centres are less than $2.3l$ from the measurement location.
2. The simulated head values for the selected grid cells are used to estimate the simulated head value at the measurement location. The estimation is a linear combination of the simulated head values:

$$h_{i,t}^{SIM} = \sum_{i=1}^{n} \lambda_i h_{ijk}^{SIM}$$

where λ_i is the weight for the i-th grid cell. The weights are proportional to the inverse squared distance. The weights sum to one:

$$\lambda_i = \frac{\frac{1}{(d_i^2)}}{\sum_{i=1}^{n} \frac{1}{d_i^2}}$$

where d_i is the distance between the i-th grid cell and the measurement location.

The same interpolation procedure is used in the solution of the adjoint state system, where the interpolation has to be used to obtain the solution of equation 3.11.

Locating the master blocks

The number of master blocks should be as small as possible in order to reduce the number of independent parameters describing the perturbation fields. However, this number should be large enough so that there are enough degrees of freedom for the optimisation process to determine the perturbation fields that result in a match to the piezometric heads (Capilla *et al.*, 1997).

As a rule of thumb two master blocks per correlation range are considered. Capilla *et al.* (1997) found that three master blocks per correlation range was optimal. However, in the synthetic experiment carried out by Capilla *et al.* the master blocks are fixed through the optimisation procedure. If the master blocks are allowed to change as the iterations proceed the number of master blocks per correlation range can be reduced. The master blocks are laid out on a regular grid with a random starting point. It was found that this procedure yields a faster convergence than laying them out completely at random. The density of the master blocks in the x-, y- and z-direction need not be the same. Anisotropy should be accounted for in the location of the master blocks by allocating more master blocks in the direction with less spatial continuity.

The positions of the master blocks change during the optimisation. This also enhances the convergence and avoids artefacts in the final updated transmissivity and/or storativity fields. If the master blocks have fixed positions the largest perturbations are always at the master blocks, while this does not have to correspond necessarily with reality. Moreover, the positions of the master blocks are initialised with a different random seed for each realisation in order to avoid artefacts on the ensemble average transmissivity and storativity fields.

Transmissivity and storativity measurement locations are always included in the set of master blocks. In case of error-free transmissivity and storativity measurements, the perturbations at data locations are forced to be null, otherwise the perturbations at these locations are allowed to vary within an interval proportional to the magnitude of the error measurement variance.

The computer program INVERTO allows the master blocks to be "inactive" in part of the aquifer. Although master blocks are spread over the aquifer, the perturbation at some of the master blocks can be fixed to zero. This can be of use in case the aquifer is divided in a large number of grid cells and the head

responses to a pumping test, that affected just a small part of the aquifer, have to be calibrated. In that case it is convenient to allow only perturbations in the part of the aquifer which might be affected by the pumping test. Doing so, the amount of required CPU time is reduced.

Perturbation of boundary conditions

In case the prescribed heads along the boundary are also subject to calibration the perturbations are optimised at a limited number of master blocks. The perturbations are interpolated to the rest of the prescribed grid cells. In principle any interpolation technique could be used for the interpolation; here ordinary kriging has been used for the interpolation. Therefore, a variogram has to be defined. It may not be an easy task to define the variogram. However, it should be realised that the kriging weights assigned to the perturbations at the master blocks determine the perturbations at the boundary grid cells. For a given range value and variogram model the relative magnitude of the nugget (nugget/sill) determines the values for the kriging coefficients. Therefore, it is not necessary to know the absolute values for the nugget effect and the sill. In case the nugget is zero (which is the normal case for the interpolation of perturbations of boundary heads) the sill value has not to be known. Furthermore, the variogram model and the range value for the conductivities can be adopted for the boundary heads. The spatial correlation structure for the head residuals (the head values corrected for the large-scale trend) is supposed to be close to the spatial correlation pattern of the conductivities.

The master blocks are located randomly on the boundaries. Like the master blocks for the conductivities, their positions change during the optimisation. Moreover, for each of the realisations a different seed is used to initialise the master block positions.

Another important parameter in the calibration of the boundary heads is the maximum head change allowed on the boundaries. This parameter limits the maximum total perturbation at any of the boundary grid cells. The user should specify the maximum allowed perturbation on the boundaries by expert knowledge.

Reducing the CPU-time needed to calculate the gradient

The most CPU intensive part of the inverse modelling is the calculation of the gradient. It is therefore important to reduce as much as possible the CPU-time needed to calculate the gradient. The solution of equation 3.12 requires the calculation of the partial derivatives of all the matrix and vector elements with respect to the perturbations at each of the master blocks. Furthermore, these derivatives have to be calculated for each of the time steps at which the groundwater flow equation is solved.

An example may illustrate the required calculations. We have to solve a transient inverse problem with 10,000 grid cells, 25 time steps and 250 master blocks for conductivity and 75 master blocks for the boundary heads. It means that a gradient vector of 325 elements has to be calculated. The part of the gradient corresponding to the conductivity perturbations (250 elements) requires calculating the derivatives of all the elements of the conductance matrix ($10000*10000=10^8$ elements) with respect to all the master blocks (equations 3.13 till 3.17); $2.5 * 10^{10}$ calculations in total. These calculations have to be repeated for 25 time steps: $6.25 * 10^{11}$ calculations are required. Furthermore, it requires calculating the derivatives of all the elements of the vector q with respect to those perturbations (equation 3.18) (again at all time steps): $6.25 * 10^7$ calculations. Finally, for the part of the gradient corresponding to the perturbations of the prescribed heads at the boundaries the derivatives of all the elements of the vector q with respect to the perturbations (equation 3.19) (again at all time steps) have to be calculated: $1.875 * 10^7$ calculations.

The CPU-time needed is reduced by just calculating the partial derivatives of the non-zero elements of the conductance matrix with respect to the conductivity perturbations. In case of 2-D flow on the grid of 10,000 (100 x 100) grid cells just 48,416 calculations have to be made. The total amount of calculations is reduced to $3.026 * 10^8$ for the derivatives of the A matrix and $2.425 * 10^6$ for the derivatives of the q vector. The amount of calculations needed to derive the derivatives of the q vector with respect to perturbations of the prescribed boundary heads is reduced to $7.275 * 10^5$.

Another CPU-time reduction is achieved by only evaluating the derivatives of the conductance matrix with respect to conductivity perturbations that are known to be non-zero. It means that not only the calculation of those derivatives is avoided with the value of the elements of the conductivity matrix equal to zero, but also the derivatives where the kriging coefficients are zero. Remember that for the interpolation of the perturbation value at a grid cell the perturbations at a limited number (user-defined) of master blocks is used. The master blocks selected are those which are statistically more close. A matrix is built which contains for each of the grid cells the weights for the master blocks which participate in the interpolation. Together with the weights also an index is stored for each of the master blocks, which is used to identify the master block. The result is that for each of the master blocks, only the partial derivatives for which it is known that the kriging coefficients are different from zero have to be evaluated. In case twelve master blocks are used to interpolate the perturbation at a grid cell the amount of required calculations reduces to $1.45248 * 10^7$ for the derivatives of the A matrix and $1.164 * 10^5$ for the derivatives of the q vector. The amount of calculations needed to derive the derivatives of the q vector with respect to perturbations of the prescribed boundary heads is reduced to $1.164 * 10^5$. However, the CPU-time reduction is not as strong as the reduction in the amount of calculations suggests, because a

selection of the master blocks which yield non-zero kriging weights, on the basis of the stored indices, is required.

It was thought that the CPU-time needed could be reduced even further as the interblock conductivities between two grid cells are calculated for each time step. However, this interblock conductivity value will be the same for each time step so that the repeating calculations of the interblock conductivities are unnecessary. See also figure 3.2 that summarises the steps to be taken to calculate the gradient. Therefore it was thought to avoid these unnecessary evaluations by calculating the interblock conductivity just once, and solving the derivatives for one time step after the other. In other words, the cycling over the time steps was moved from an outer loop to an inner loop. Surprisingly, the needed CPU-time increases; this might be due to some necessary evaluations that have to be made after changing the time step. Therefore, this intent to reduce further the needed CPU-time was proven not to be successful.

Rotating the optimisation algorithms and optimising the step size in the updating direction

Figures 3.3 until 3.5 show three flow diagrams with the outline of the procedure to update the parameters. Figure 3.3 shows the main steps. The formulas given in section 3.2 are used. The only aspect that should be highlighted is the rotating of the non-linear optimisation algorithm used to calculate the updating direction from the gradient.

- If little progress is made in reducing the objective function value, the optimisation algorithm is changed. Carrera and Neuman found that changing the optimisation algorithm when the objective function value reduction was small frequently yielded a new reduction of the objective function value. Therefore, if the objective function reduction is less than 1% a change is made to another algorithm.

- The same algorithm is used during a maximum of eight iterations.

- The sequence of the algorithms used is: Fletcher-Reeves Conjugate Gradients, Hestenes-Stiefel Conjugate Gradients, Quasi Newton and Steepest Descent.

Figures 3.4 and 3.5 give some details on the calculation of the optimal step size in the updating direction. It can be seen that the procedure consists of three main loops. In the first loop an approximately optimal scalar parameter is determined, and in the subsequent two loops the estimation is refined. In the first loop the search is stopped if increasing the scalar parameter results in an objective function value clearly above the initial objective function value. The search is also stopped if a clear increase in objective function value is found during two subsequent searches. It is assumed that the one-dimensional

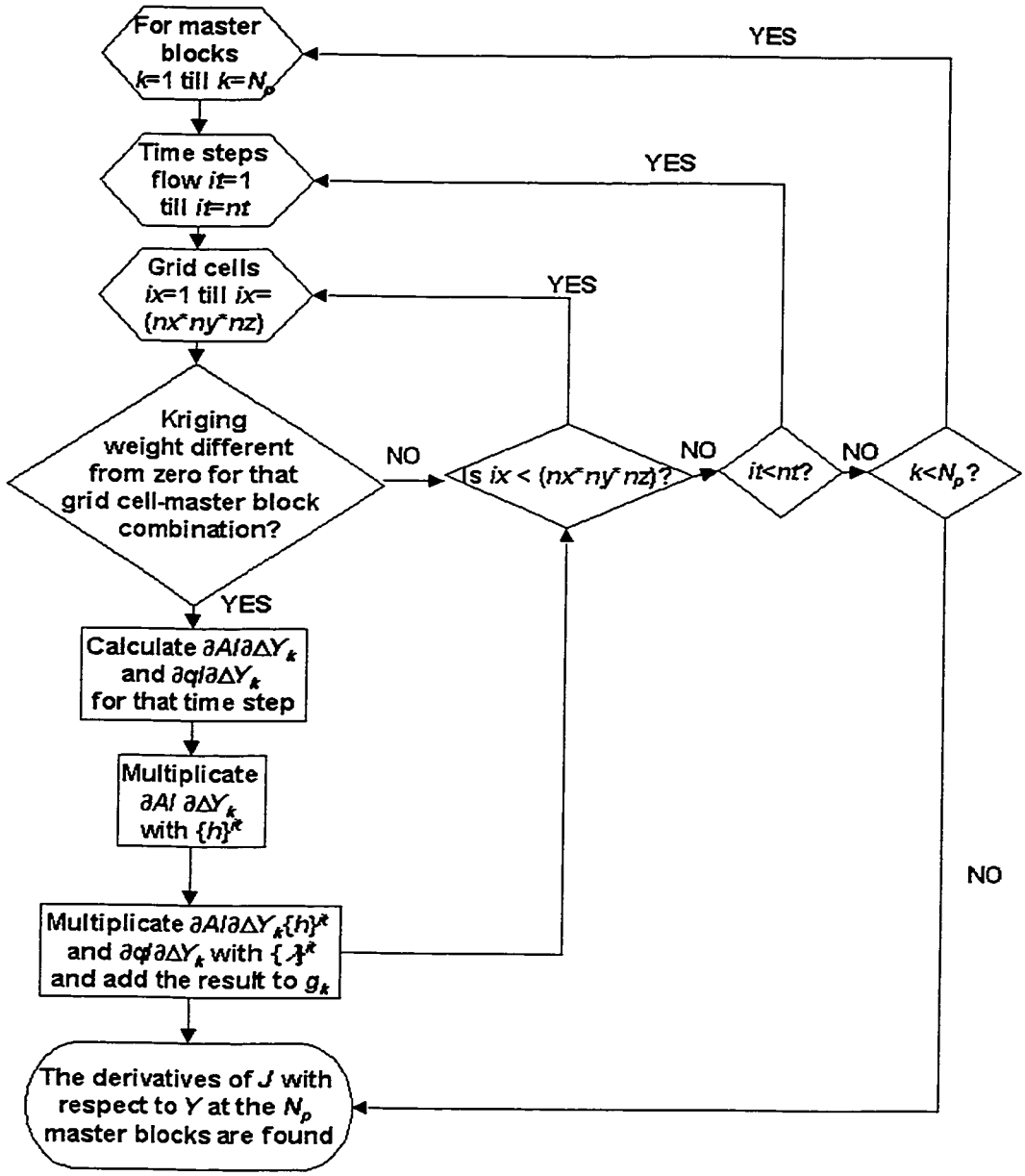

Fig 3.2 The procedure to calculate the gradient.

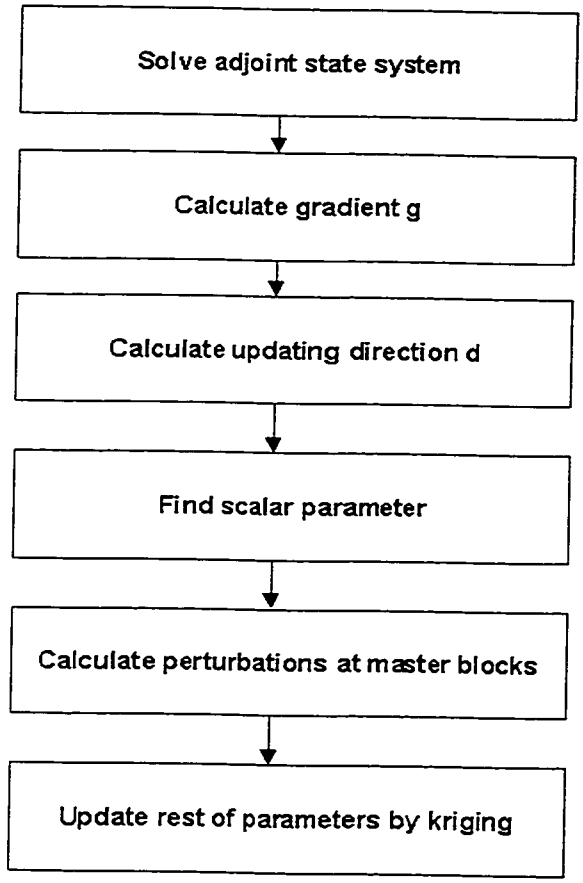

Figure 3.3 Global procedure to update the parameters.

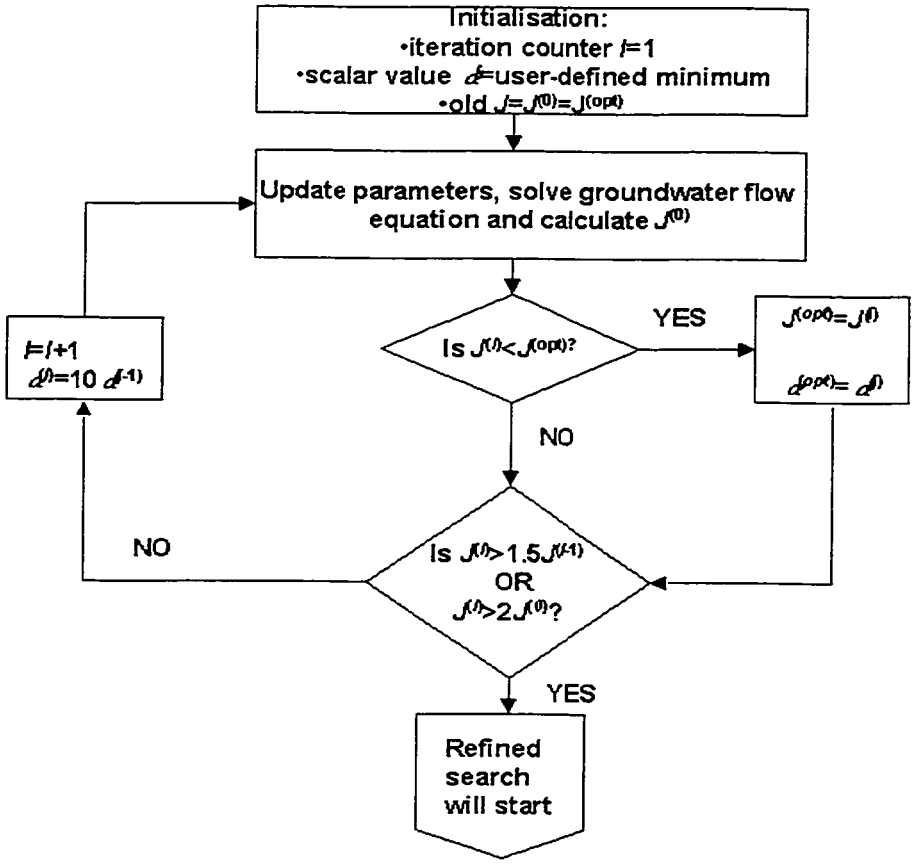

Figure 3.4 Linear search to calculate the relaxation factor used to obtain the updating direction.

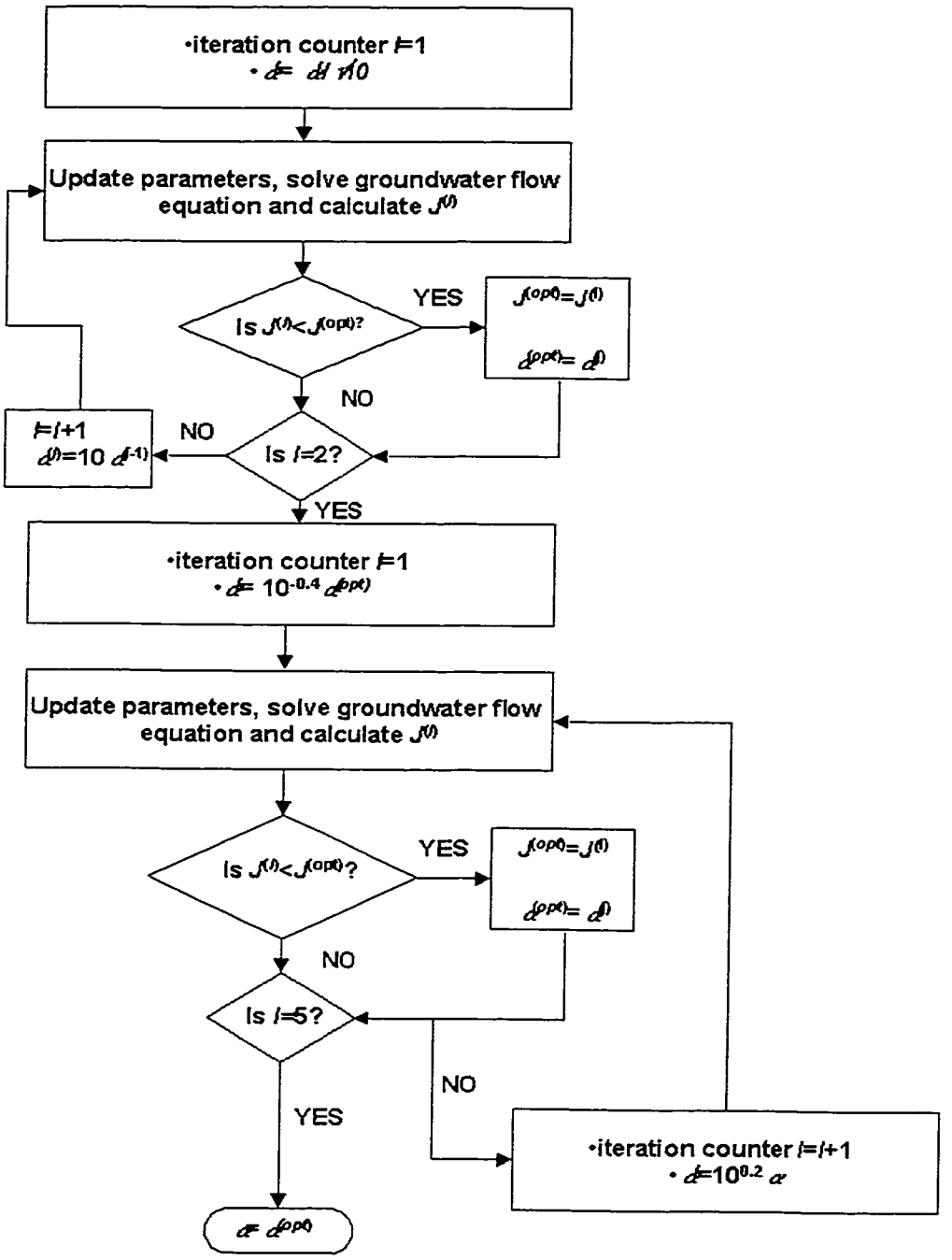

Figure 3.5 Refined procedure to calculate the optimal relaxation factor.

trajectory which is searched has a nearly quadratic curvature, so that a clear increase in objective function value along the trajectory indicates that continuing along that trajectory will only give worse results. See Figures 3.4 and 3.5 for more details.

Interpolating the perturbation

If we would apply simple kriging to interpolate the perturbations, a considerable amount of CPU time and storage capacity would be consumed in many practical studies, because in a "normal" study more than hundred master blocks are located. Therefore, to calculate the perturbation at a grid cell, only a limited number of master blocks is used. The master blocks used are these with the highest spatial correlation with respect to the grid cell. Ordinary kriging is used to interpolate the perturbations. Earlier in this section it was already explained that this simplification reduces the needed CPU time to calculate the gradient.

The interpolation of the perturbations is carried out considering only the grid cells and master blocks which are located in the same zone.

3.4 Inverse modelling of transient groundwater flow at the WIPP site

In this section an application of the SCM is described. The program INVERTO has been used to carry out the inverse modelling. Sections 3.2 and 3.3 give the details on the SCM and the numerical methods implemented in the program. The interested reader finds further details in the INVERTO manual, which is attached as an Appendix to this thesis. More information on the WIPP site is also found in section 2.3.

3.4.1 Data used in the inverse modelling procedure

The algorithm has been applied for the inverse modelling of groundwater flow at the WIPP-site, New Mexico, USA. The data are obtained from a confined aquifer in a dolomite rock formation, about 600 meter below the earth surface, overlying a potential repository for transuranic waste. The simulation domain corresponds to an area of about 20 km in the x-direction and 30 km in the y-direction, discretized into 43 by 61 square cells of 500 by 500 metres. The data are obtained from Lavenue *et al.* (1990) and consist of: 36 transmissivity measurements (one datum, corresponding to well P-18, has been removed because the value seems to be unreliably low for dolomite rock), 34 undisturbed equivalent freshwater heads and prescribed head boundaries. The drillings are not equally spaced over the region, but preferentially located in the center part of the region overlying the panels that will host the waste if the site is licensed. These data have been used for the inverse simulation of steady groundwater flow; spatial variation in fluid density has not been taken into account. The inverse modelling of steady-state groundwater flow has also been carried out taking into account uncertainty on the prescribed heads along the boundaries.

The inverse simulation of transient flow has been carried out for the pumping test at the well WIPP-13 from the 12th of January 1987 until the 17th of February 1987 with a pumping rate varying from 1.89 l/s to 1.99 l/s. It was the highest pumping rate applied at a well at the WIPP-site, so that this pumping test was considered to be the one that could yield drawdowns in the most extended area, as such yielding interesting information for the inverse calibration with transient data. Initial steady-state head data and transient head data from 15 measurement points during the 35 days have been used (Beauheim, 1987a). Another pumping test which has been used for inverse simulation of transient flow is the one performed at the well H-3 during the period of the 15th of October 1985 until the 16th of December 1985 with a constant pumping rate of $3.08 * 10^{-1}$ l/s. Also in this case steady-state heads for the first time step (without pumping) and transient heads from 15 measurement points during the 62 days have been used (Beauheim, 1987b). Initial estimates of the storativity in the neighbourhood of the pumped wells were 10^{-5} (H-3) and 10^{-4} (WIPP-13).

3.4.2 Results from the inverse modelling at the WIPP site

In total 100 fields, conditional to the 36 hard transmissivity measurements, have been generated by sequential simulation, taking into account a linear trend in the west-east direction (See also section 2.3). As variogram of the residuals with respect to the trend, the variogram of the transmissivity in the north-south direction, in which no trend seems to appear, has been used. The variogram and other descriptive statistics can be found in section 2.3. Inverse simulation for steady-state flow has been carried out, making use of 100 master grid cells, which are changed during the optimisation and located on a regular grid with random starting point. The non-linear optimisation algorithms change at least once each five iterations. However, in case the objective function value reduction is less than 1% between two succeeding iterations the algorithm is also alternated. In case the prescribed heads in the boundaries are calibrated 40 master blocks are located along the boundaries. The maximum allowed head change on the boundaries is plus or minus 2.0 metres.

The 100 inverse calibrated fields have been averaged and the ensemble variance has been calculated. It results in the maps shown in Figure 3.6, which are displayed together with the universal kriging maps, which are only conditional to transmissivity and not to steady-state heads. The use of steady-state heads results in important modifications to the transmissivity field. The average field for steady-state data is less smooth, two areas in the East appear with transmissivity below -8.0 $\log(m^2/s)$, in the Southwest an extended area with transmissivity above -2.0 $\log(m^2/s)$ arises and the iso-transmissivity line of e.g -4.0 $\log(m^2/s)$ changes its position considerably. The ensemble variance map shows less modifications. On the Northern boundary the additional conditioning to head data even yields a variance increase and both on the Northern and the Eastern boundary the most elevated variances (above 2.0 $(\log(m^2/s))^2$) are found. It can be appreciated that the map with ensemble variances becomes less smooth due to the conditioning to head data, while prior to the inverse conditioning the map has a very smooth aspect.

Also 100 transmissivity fields conditioned to steady-state heads are generated for the case that uncertainty on the boundary conditions is considered. Figure 3.7 shows the average perturbations of the prescribed heads along the four boundaries. The average perturbation has a smooth aspect and remains below 2.0 metres. The perturbations yield an enhanced head gradient in the north-south direction in the western and central parts of the aquifer. In the eastern part of the aquifer, on the contrary, the north-south head gradient decreases. The effect on the flow velocities is similar as for the changes in the transmissivity field that were found considering uncertainty on the transmissivities only: an increase of flow velocities in the western part of the aquifer and a decrease of flow velocities in the eastern part. In case uncertainty on the boundary conditions is considered the uncertainty is divided between uncertainty on the transmissivity field and uncertainty on the boundary

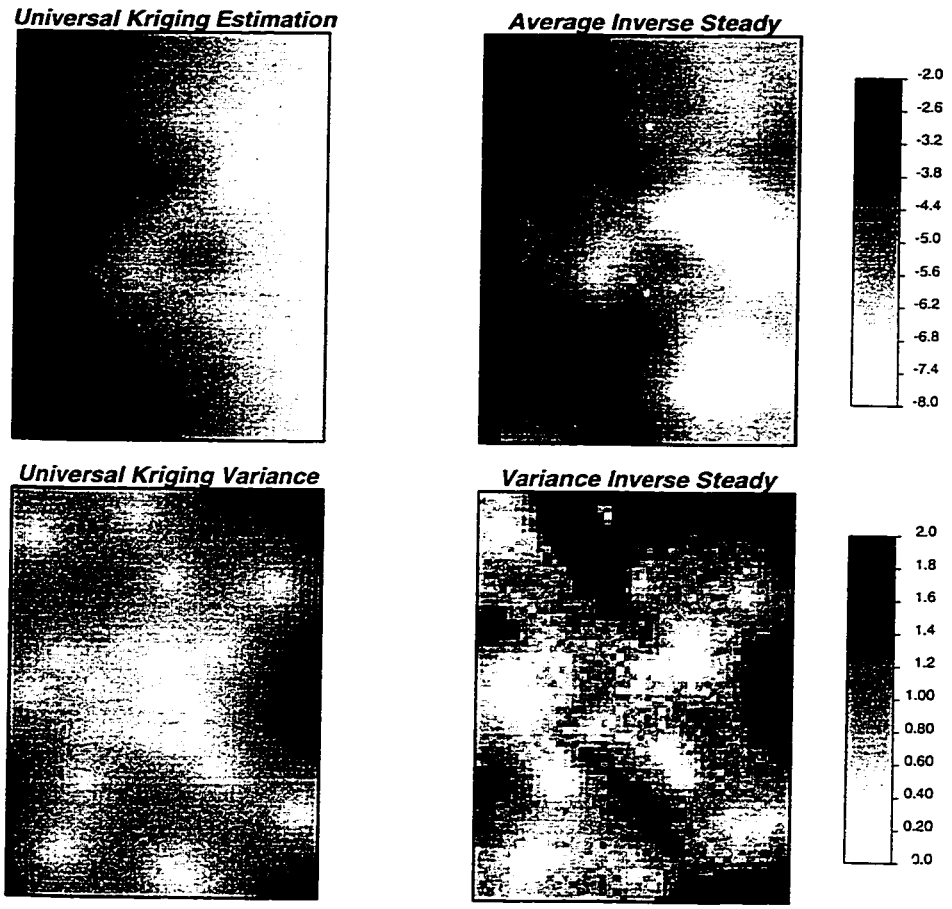

Figure 3.6 Universal Kriging Map and Universal Kriging Variance Map for the WIPP-domain (left) and Average Obtained Transmissivity Field and Variance of Obtained Transmissivity Field for inverse modelling with steady-state heads (right). Units: logT.

conditions. The result is that the average transmissivity perturbation for the 100 realisations is smaller than for the 100 inverse calibrated transmissivity fields that do not take into account uncertainty on the boundary conditions. The two average inverse calibrated transmissivity fields display the same patterns, but the average transmissivity field for the case that the boundary conditions are calibrated is somewhat smoother. See Figure 3.8. The average ensemble variance for the transmissivity field that takes into account uncertainty on the boundary conditions is lower along most of the simulation domain, because part of the uncertainty that otherwise is attributed to the transmissivity field is attributed now to the boundary conditions. The main uncertainty reduction, as compared with the average transmissivity field that does not take into account uncertainty on the boundary conditions, is found in some zones near the boundaries.

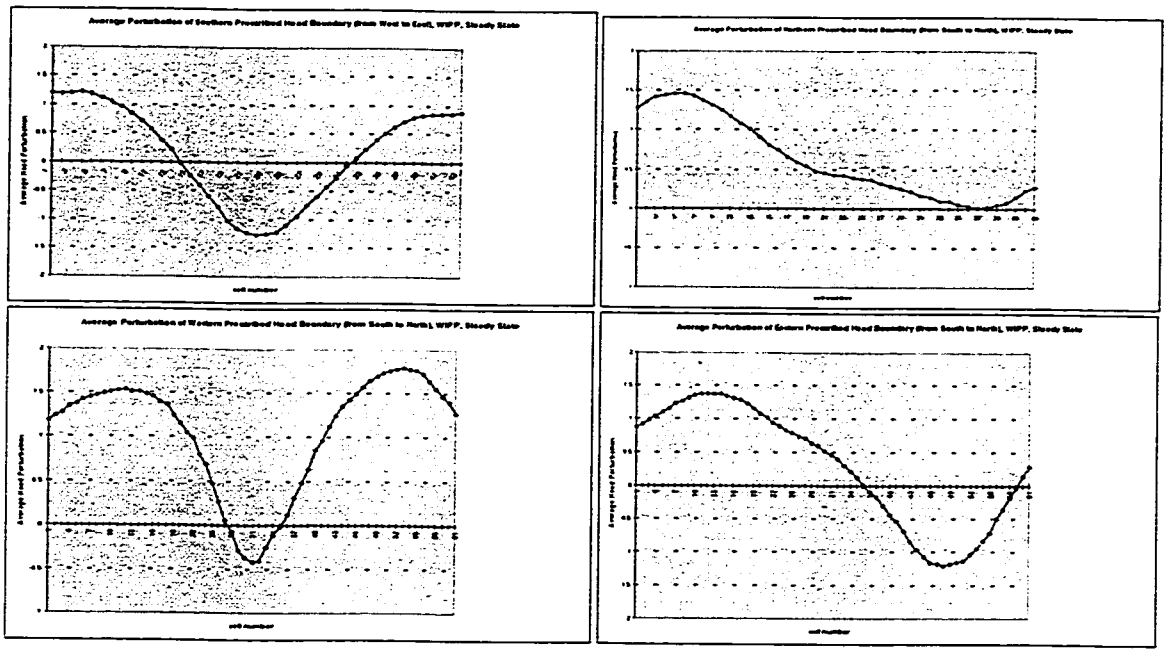

Figure 3.7 Ensemble averaged prescribed head perturbations (m) along the four boundaries. From the left to the right and from above to below the perturbations along the Southern boundary (from West to East), the Northern boundary (from West to East), the Western boundary (from South to North) and the Eastern boundary (from South to North) are given. The realisations are conditioned to steady-state head data.

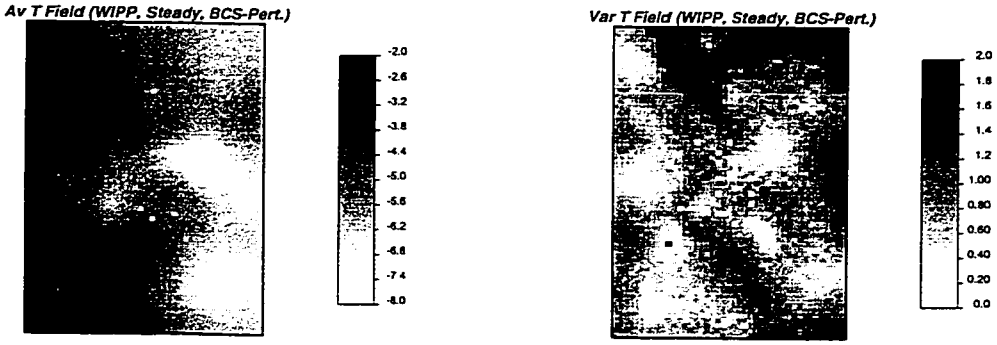

Figure 3.8 Average Inverse Calibrated Transmissivity Field (left) and Variance of Transmissivity Field (right) for inverse modelling with steady-state heads and taking into account uncertainty on the prescribed boundary heads. Units: logT.

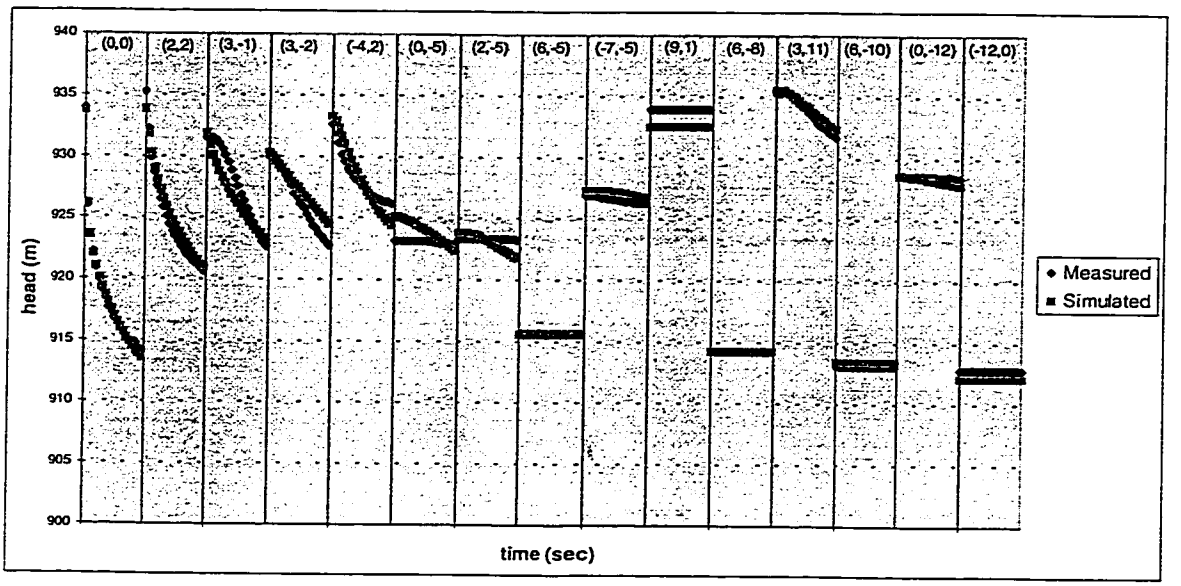

Figure 3.9 Comparison between measured heads during the pumping at WIPP-13 and simulated heads for realisation 2, after inverse calibration. Each vertical slice represents one of the measurement points. At the top of the vertical slice the distance in grid cells with respect to the pumping location is located. For example: (2,2) means that the grid cell is located two cells East of the pumping location and two cells North of the pumping location. The grid cell size is 500 m.

The inverse modelling of transient flow has been carried out making use of 200 master grid cells, equally spread over the simulation domain. The simulated and measured heads are compared at 20 (WIPP-13) or 21 (H-3) time steps, equally spread over the pumping periods. Inverse modelling of transient flow, making use of the pumping test at WIPP-13, has been successful; the final simulated heads fit the measured heads good, see Figure 3.9 for the fit displayed for field 2. Ensemble statistics over 100 fields show that the obtained average transmissivity field is modified in the area around the pumping well WIPP-13; see Figure 3.10. The cells around the well have a higher transmissivity value, but for only six cells the change is more than 0.5 log(m^2/s). Northwest of the zone around the well, transmissivities decrease. Another interesting phenomenon is a zone which stretches from south of the well to the northwest (up to the border) with slightly increased transmissivities (maximum change +0.25 log(m^2/s)). In general, changes with respect to the average transmissivity field for inverse modelling of steady flow are:

- not very large due to the fact that the initial mismatch of the transient data was not very large and
- not very spread because the area influenced by the pumping test is little as compared to the extensions of the complete study area. A pumping test that would influence most of the study area is likely to result in changed transmissivities throughout the field.

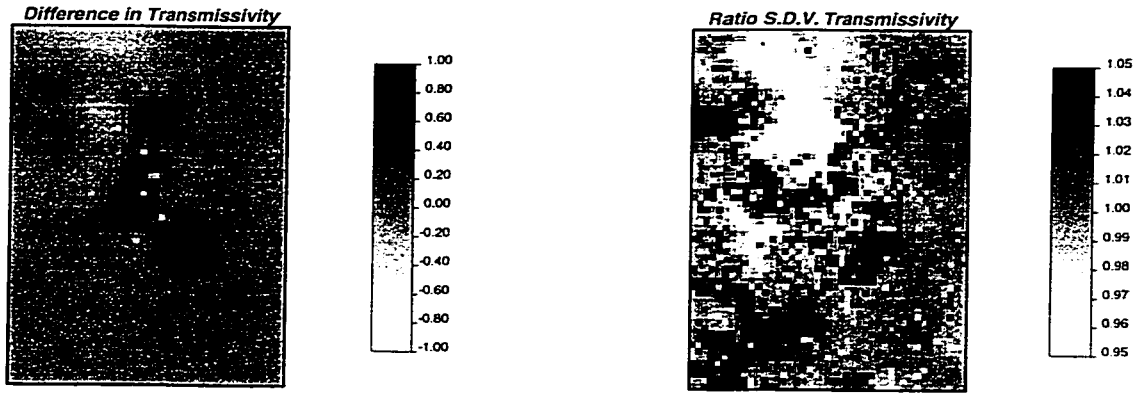

Figure 3.10 Comparison between the transmissivity field obtained after inverse modeling with transient heads from pumping test at WIPP-13 and inverse modeling with steady-state heads. Left: difference in ensemble average field (transient - steady), expressed in logT. Right: ratio in standard deviation of transmissivity (transient / steady).

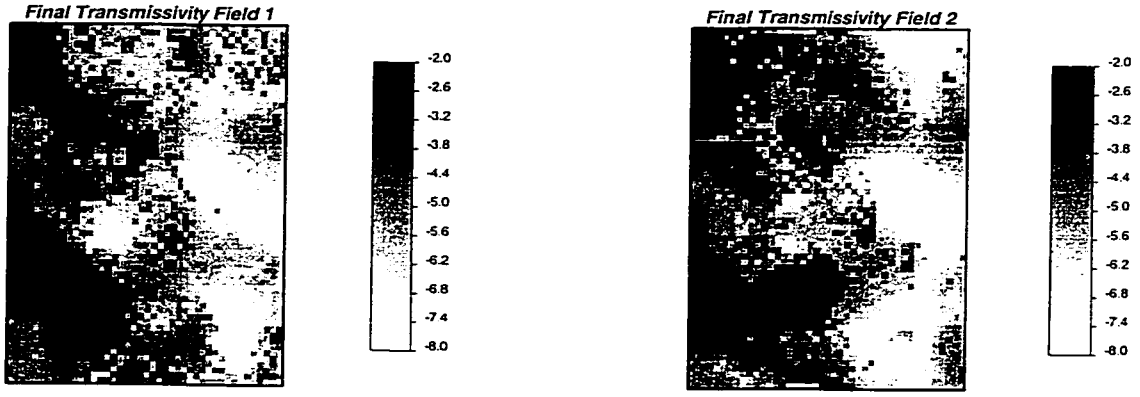

Figure 3.11 Two Simulated Transmissivity Fields, conditional to transmissivity measurements, steady-state heads and transient heads (pumping WIPP-13). Units: logT.

The variance map shows that in an area stretching from the pumping well to the northwest until the border, the standard deviation in transmissivity over the 100 fields has decreased more than 5%, as compared with the equivalent value from inverse conditioned fields using only steady-state heads. Inverse modelling of transient flow by means of the observed head drawdowns due to pumping at H-3 resulted in even less extended modifications in the average transmissivity field and more over, only at two grid cells the change was bigger than 0.50 log(m^2/s). Two simulations of transmissivity, conditional to transmissivity measurements, steady-state heads and head measurements during pumping at WIPP-13 are displayed in Figure 3.11.

	WIPP-13	*H-3*
Initial Storativity (S)	$1.00 * 10^{-4}$	$1.00 * 10^{-5}$
Average Updated S	$9.37 * 10^{-6}$	$1.13 * 10^{-5}$
Std. Dev. Updated S	$3.23 * 10^{-6}$	$2.33 * 10^{-6}$
Maximum Updated S	$2.40 * 10^{-5}$	$1.70 * 10^{-5}$
Minimum Updated S	$1.10 * 10^{-6}$	$6.00 * 10^{-6}$

Table 3.1 Some statistics from the calibrated storativities over the 100 fields, around the wells WIPP-13 and H-3.

From the calibration of the storativity around the pumping wells WIPP-13 (data from pumping test WIPP-13 are used) and H-3 (test at H-3) can be concluded (see Table 3.1) that the variance over the 100 realisations is low and that the values are very consistent. For the test at WIPP-13 in all 100 cases the updated storativity is lower than the initial estimate and the average updated storativity is even more than a factor 10 lower than the initial estimated storativity; we conclude that the initial estimate of the storativity around WIPP-13 has been too high. The values found around WIPP-13 and H-3 are close to the ones given by Beauheim (1987a and 1987b). Transient head information allowed to correct the initially too high estimate of the storativity around WIPP-13.

3.4.3 Conclusions

This case study was carried out after the extension of the sequential self-calibrating method to the inverse modelling of transient groundwater flow. In this study the conditioning to transient heads, besides steady-state heads and transmissivity measurements, resulted only in an improved characterisation of the transmissivity field around the pumping wells. The calibration of storativities around the pumping wells resulted in an important updating of storativity of more than a factor 10 around pumping well WIPP-13. In general, the variance in calibrated storativities over 100 fields is low and the results obtained are consistent.

3.5 Inverse modelling of a single fracture at the Aspö site

In this section, a second application of the SCM for the inverse modelling of time dependent groundwater flow is described. This study was carried out within the TRUE-1 project, a project for the modelling of groundwater flow and mass transport in a single fracture at the Aspö site. Again the reader is referred to the sections 3.2 and 3.3 for details on the SCM and the numerical methods implemented in the program. The interested reader may find further details in the INVERTO manual, which is attached as an Appendix to this dissertation.

3.5.1 Site information and input parameters

The method has been applied to an area of 20 x 20 m in a single fracture with spatially variable transmissivities. The fracture is located in a crystalline rock formation at the Aspö site, an underground rock laboratory in Sweden. The Aspö site is located on the island of Aspö close to the South Swedish coast. The main objective of the TRUE-1 project was to predict the transport of reactive and non-reactive tracers within a single fracture. The overall aim of the TRUE-1 project was to test to what extend the numerical models are able to predict the migration of radioactive particles given a reasonable amount of experimental information. An understanding of the hydrogeological properties is crucial to make accurate predictions of the travel paths and the travel times of radionuclides from some injection point to some monitoring point. The objective of this particular study was to use steady-state and transient hydraulic head data to improve the characterisation of the transmissivities along the fracture plane. In order to study the stability of the solution found a sensitivity study is carried out.

A pumping test has been carried out with a pumping rate of 0.20 litres per minute. In total, five transmissivity data, five steady-state piezometric head data prior to the start of the test and the head evolution at five locations during the pumping are available. Figure 3.12 shows the measurement locations. It is not possible to obtain a confident estimation of the $\log_{10}$ transmissivity variogram with only five data. Therefore the variogram is estimated with the help of geological knowledge. A spherical variogram model is adopted with a sill equal to the transmissivity data variance and a range equal to 3.0 metres. The standard deviation of the measurement error is estimated by 0.5 $\log_{10}$ (m^2/s).

The groundwater flow equation is solved numerically; the domain is divided into squared grid cells of 0.4 metres; the total number of grid cells is 2,500. For the transient simulations the temporal domain is discretised in 10 steps; the size of the first step is 2.0 seconds and the magnitude of the subsequent time steps grows with a factor of 1.8. As boundary conditions, prescribed heads are used, their values are derived from an extrapolation of the five steady-state values

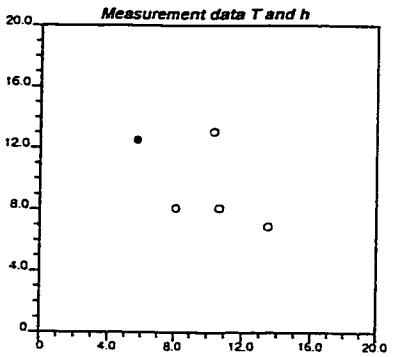

Figure 3.12. Map showing the five locations where transmissivity and piezometric head were measured (before and during pumping). The black dot indicates the location where the pumping test was carried out.

prior to pumping. The initial estimate of the spatially constant storativity is 3.5 * 10^{-7}.

3.5.2 Results after conditioning to transmissivities and heads

A total of 100 $\log_{10}$ transmissivity realisations are generated and calibrated by SCM to piezometric head data. A total of 207 master blocks are used to minimise the objective function. Most of the master blocks (196) are located on a regular grid with random starting point. The other 11 master blocks are located randomly as they can not be incorporated in the regular grid (14 x 14) of master blocks. As for the study presented in section 3.4 a non-linear optimisation algorithm changes at least once each five iterations. In case that the reduction of the objective function is less than 1% between two successive iterations the algorithm is also alternated. Figure 3.13 shows the calibration of a single realisation. Figure 3.14 shows the ensemble mean and variance over the 100 $\log_{10}$ transmissivity realisations prior to the inverse calibration. These realisations are therefore only conditioned to five transmissivity data. The ensemble transmissivity field is very homogeneous because very few conditioning data are available. Figure 3.14 also shows the ensemble mean field and variance computed over the 100 $\log_{10}$ transmissivity realisations, after conditioning to piezometric head data (before and during the pumping) and to $\log_{10}$ transmissivity data. In the ensemble mean transmissivity field a slightly conductive zone in the centre and a zone with relatively high conductivities in the Northeast appear. The transmissivity in the rest of the fracture has increased in general slightly. The piezometric head data, from the pumping test, allowed a more detailed characterisation of the transmissivities in the fracture plane.

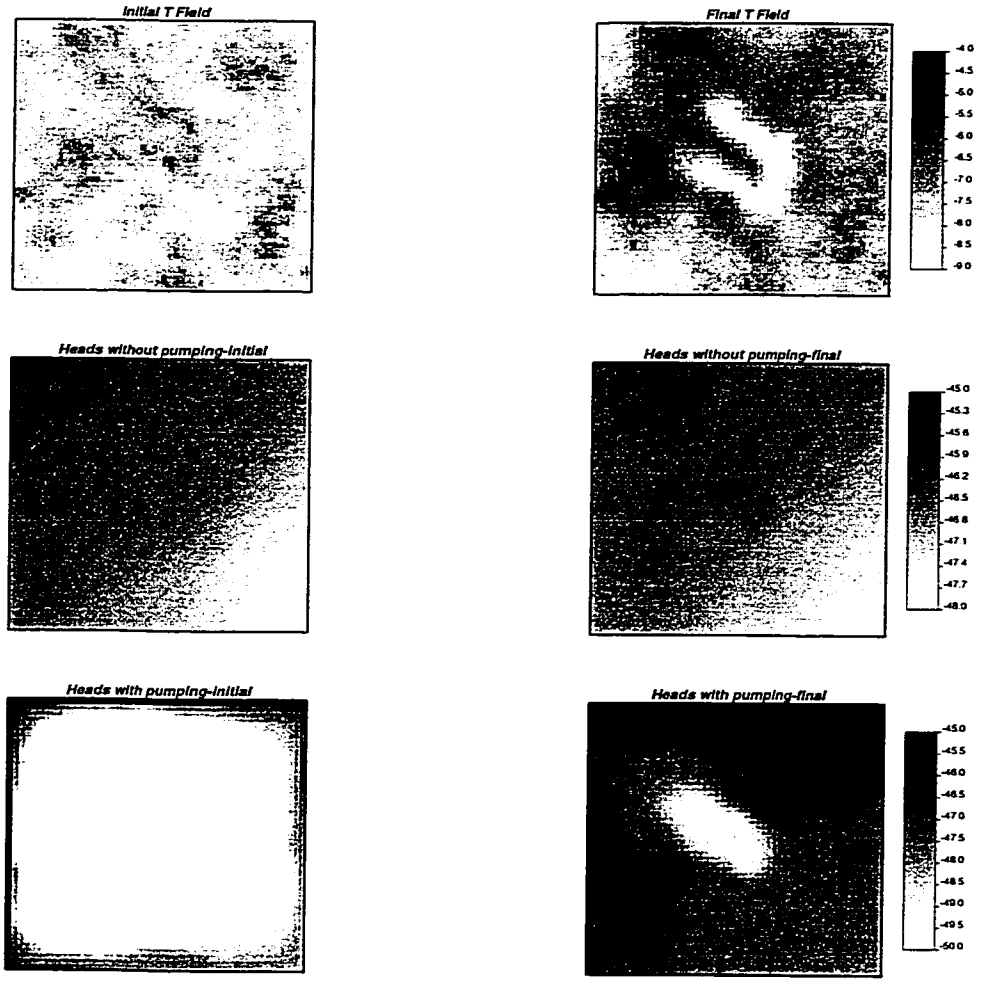

Figure 3.13. The calibration of a single realisation. The figures on the left show the $\log_{10}$ transmissivity and the simulated heads in the transmissivity field without calibration. The figures on the right show the $\log_{10}$ transmissivity and the heads simulated after calibration.

3.5.3 Sensitivity analysis of inverse modelling results

It is clear that significant uncertainty on the values of some of the parameters exists. The effect of the uncertainty of some of the parameters has been analysed through a sensitivity analysis. Next, the results of inverse modelling are presented for the following cases:

- Absence of log transmissivity measurement errors (case 1).
- A log transmissivity range of 1.5 m instead of 3.0 m (case 2).
- Calibration of the prescribed head values together with the calibration of the transmissivity field (case 3). In this case 56 master blocks are located on the prescribed head boundary grid cells. The maximum head change allowed along the boundary is 3.0 metres.

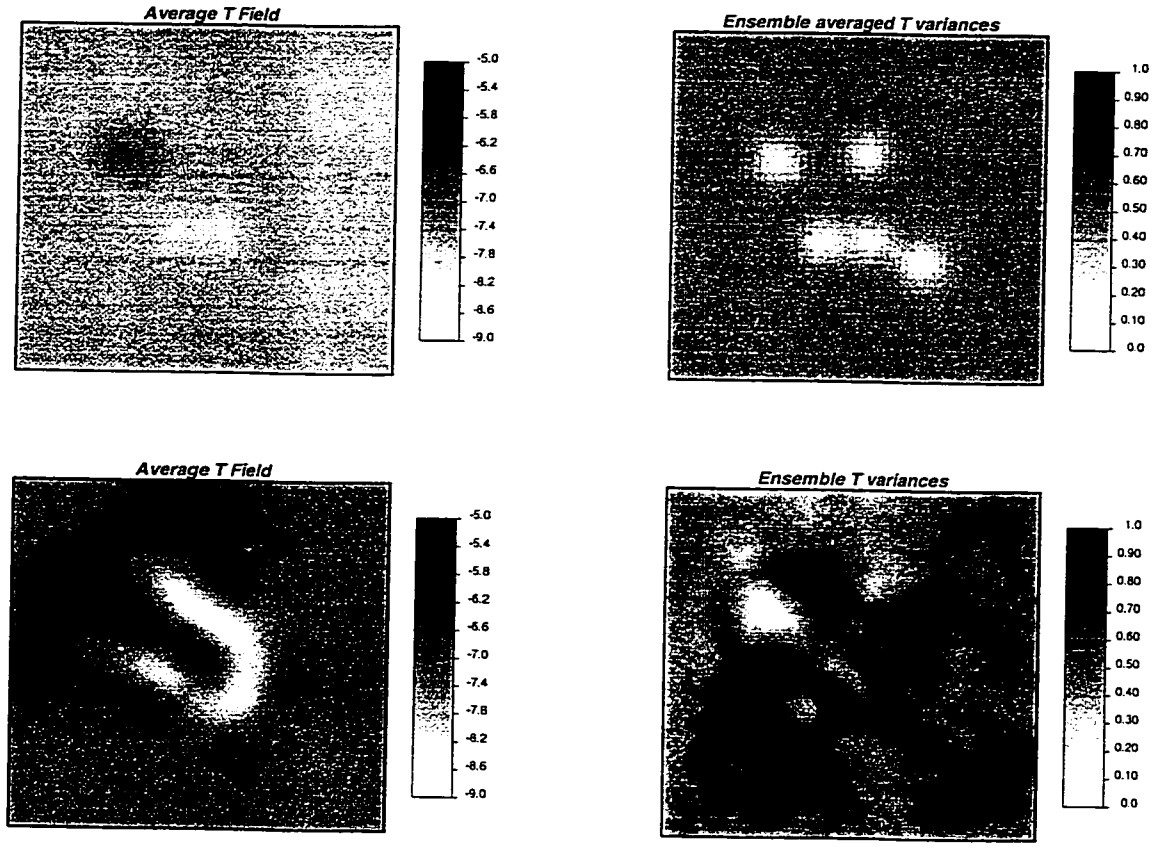

Figure 3.14. The $\log_{10}$ transmissivity ensemble mean and variance. In the upper figures the fields only conditioned to $\log_{10}$ transmissivity data are shown. The figures below show the fields conditioned to piezometric head besides the $\log_{10}$ transmissivity data.

Figure 3.15 shows the ensemble average field and variance of the 100 $\log_{10}$ transmissivity fields for the different cases. The average $\log_{10}$ transmissivity does not change much for the cases 1 and 2. The slightly conductive zone which appears in the centre is less pronounced and the transmissivities in the rest of the field are larger than in the base case. When the boundary conditions are calibrated (case 3) the average $\log_{10}$ transmissivity field changes less (as compared with the modification of the average log transmissivity field in the base case), because part of the conditioning of the transmissivity fields to the hydraulic head data is achieved by calibrating the prescribed head boundary values. Figure 3.16 shows the ensemble average head perturbations along the boundaries. Although the average perturbations are in general small (less than 1.0 metres and clearly below the maximum change allowed of 3.0 metres) they have a clear impact on the characterisation of the transmissivity field. Also in case 3 a slightly conductive zone appears, but the $\log_{10}$ transmissivity in the rest of the field goes up little in comparison with the average field just conditioned

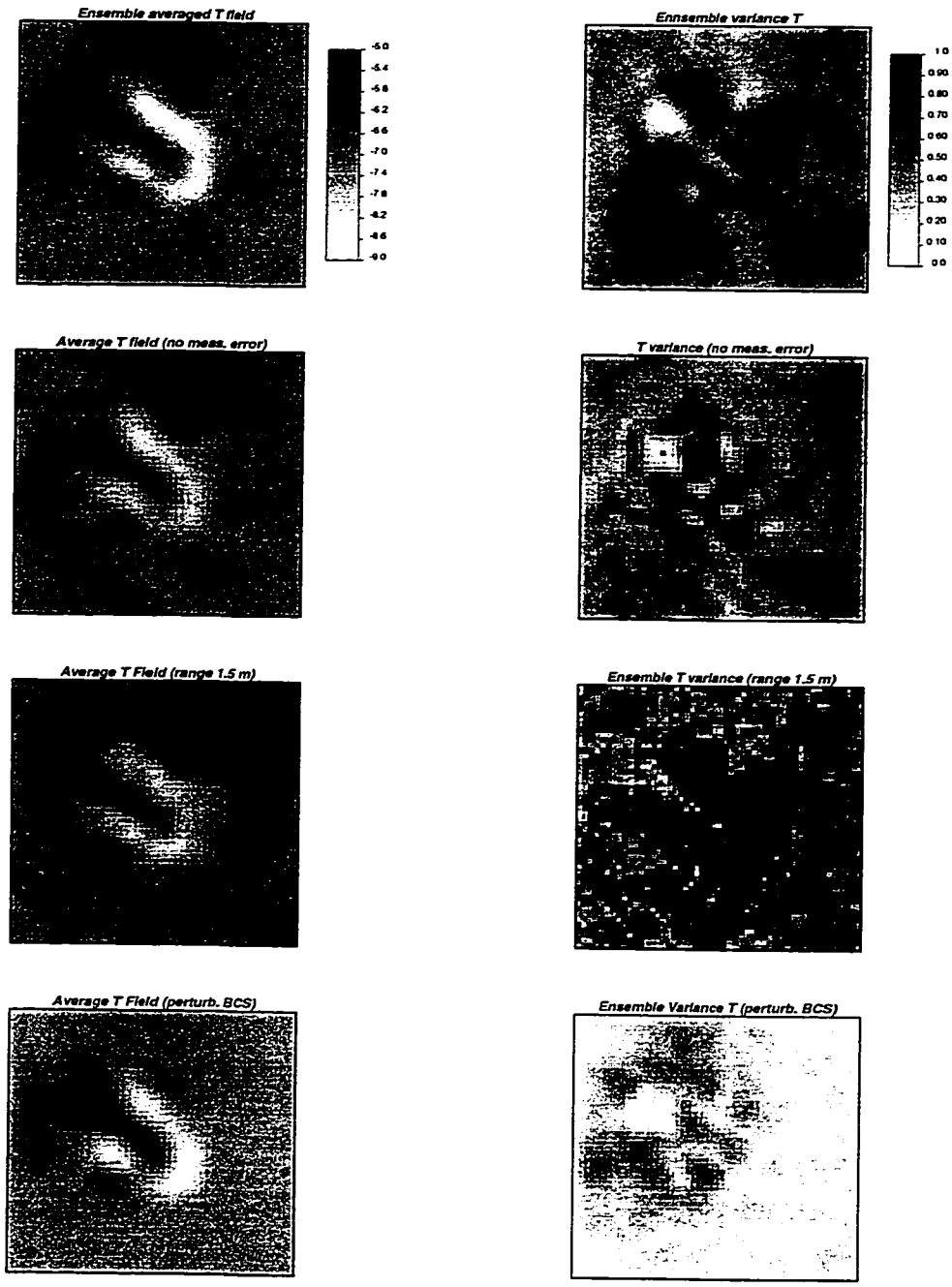

Figure 3.15. The ensemble mean $\log_{10}$ transmissivity field and its variance. Above the maps for the standard situation are shown. The second row corresponds to the fields for case 1, the third row corresponds to case 2 and the fourth row to case 3.

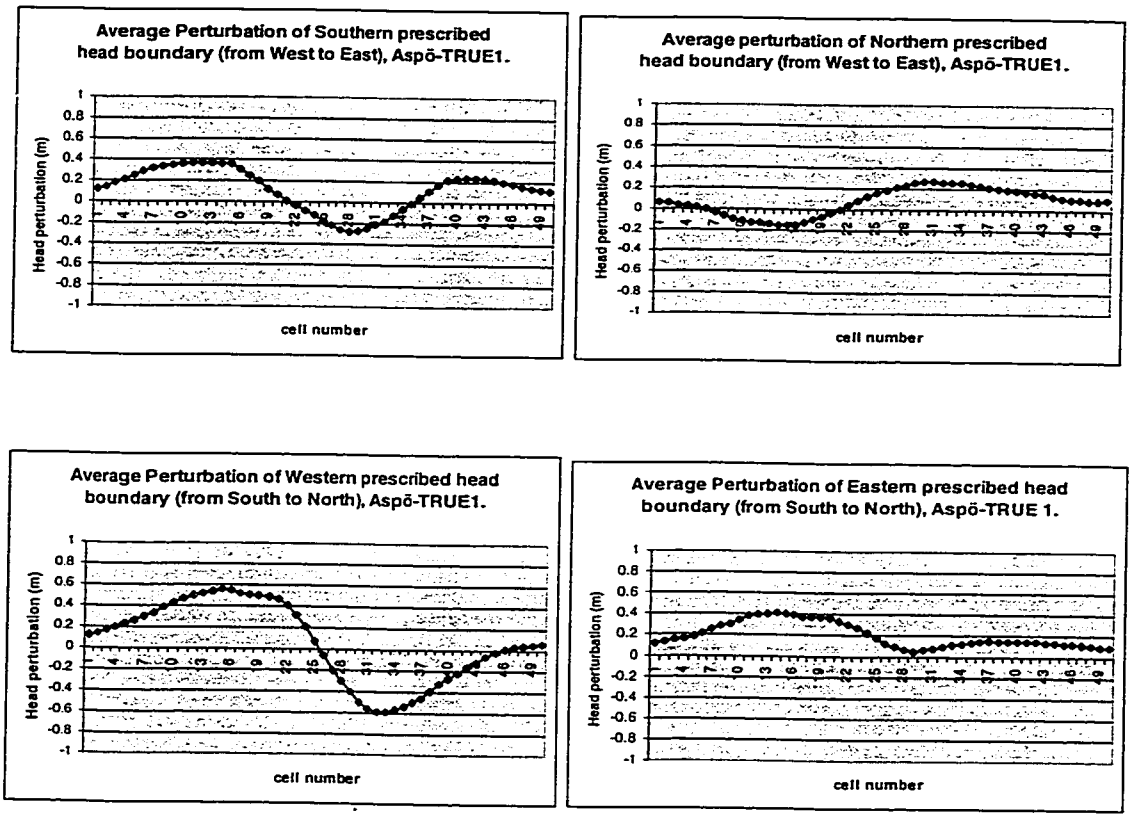

Figure 3.16. The ensemble averaged perturbations of prescribed head values along the boundaries.

to $\log_{10}$ transmissivity data, and this increase is much smaller than in the base case (Figure 3.14). The ensemble variances of $\log_{10}$ transmissivity in case 2 show that the variances are larger in nearly all the field, as compared with the base case. In case of a small range value more data are needed to characterise the transmissivity field. The calibration of the boundary conditions (case 3) yields a very important reduction of the $\log_{10}$ transmissivity variances. The uncertainty is divided between the piezometric head values at the boundaries and the uncertainty on the transmissivity values in the field (the fracture plane).

The average piezometric head fields are similar for the different cases except in case 3 during the pumping. The change of the piezometric head values on the boundary changes the hydraulic head field significantly. The fields with the hydraulic head variances change more, especially in case 2.

3.5.4 Conclusions

The incorporation of piezometric head data has an important effect on the calibration of the transmissivity fields. If the values of some of the parameters are modified the structure of the mean transmissivity field does not change much, in general terms. The ensemble transmissivity variances are more

sensitive to modifications in the parameter values. The main impact on the characterisation of the transmissivity fields is found for the case that the uncertainty on the values of the prescribed heads on the boundaries is considered.

3.6 Joint simulation of transmissivity and storativity fields conditional to steady-state and transient-state hydraulic head data

In sections 3.4 and 3.5 two real world case studies were presented in which hydraulic head data from different flow regimes were used in the inverse conditioning procedure. However, real world cases have the disadvantage that the predicted aquifer properties can not be verified. The outcomes of other experiments may be predicted using the calibrated aquifer properties, but this still is not a thoroughly check on the results of the inverse modelling. Synthetic experiments serve to control the outcomes of the prediction with the known real values. More over, tests can be carried out to check the impact of changing the value of one or more of the input parameters on the final results.

3.6.1 Introduction

The motivation of this synthetic study was the extension of the SCM to the joint generation of transmissivity and storativity fields conditional to transmissivity, storativity, steady-state heads and transient head measurements. None of the other inverse conditional simulation methods (RamaRao *et al*, 1995; Gutjahr *et al*, 1994; Hanna and Yeh, 1998) have considered the joint generation of transmissivity and storativity. And, although the extensions of any of those methods to handle transient head data may appear as straightforward, only the pilot point method (RamaRao *et al.*, 1995) has been demonstrated with transient data. The new implementation of the SCM method was applied to a synthetic case built on real data from the Waste Isolation Pilot Plan in New Mexico (see also sections 2.3 and 3.4). This site is characterised by a strong spatial variability. The objective of the synthetic study was not to draw any conclusion about the WIPP site (the data sets involving storativity values were taken from a synthetic storativity field generated on the basis of real measurements). The main objectives were: (1) to prove the capability of SCM to generate jointly conditional realisations of transmissivity and storativity. (2) to analyse the impact that considering the spatial variability of storativity may have into the characterisation of the formation.

Section 3.2 details the mathematical formulation of the joint simulation of logtransmissivity and logstorativity fields conditioned to steady-state and transient hydraulic head data.

3.6.2 A synthetic study based on real data

We have tested the performance of the method using a synthetic aquifer resembling the Culebra formation at the Waste Isolation Pilot Plant in New Mexico (USA). The reference fields are built conditional to the log decimal conductivity data (Y), the log decimal storativity data (Z) and hydraulic head data (h) given in the reports by LaVenue *et al.* (1990) and Cauffman *et al.* (1990).

A total of seven different scenarios has been analysed. For each scenario 100 equally likely Y-Z field couples are generated conditional to Y, Z and h data. In this synthetic study we have not considered errors in the measurements or in the covariance estimate. However, these errors could be easily accounted for. The reason for assuming error-free data is because we were interested into analysing the impact of the spatial variability of both transmissivity and storativity, and did not want the results to be also affected by error measurements. For all seven scenarios the same reference Z field has been used. The seven scenarios differ with respect to the reference Y field, the sampling density of the reference Z field, the sampling density of the reference h field and the amount, location and pumping rates of the pumping wells.

3.6.2.1 Spatial domain

The study is carried out in a rectangular domain of 21.5 km × 30.5 km discretized into 43 × 61 square cells of 500 m × 500 m in size. This domain corresponds to the WIPP model area. The boundary conditions are prescribed heads along the perimeter of the modelling site, the values used are the same reported by LaVenue *et al.* (1990) in their model, implying an average gradient of 32 m across the formation forcing flow from north to south.

3.6.2.2 Reference transmissivity fields

Two different reference Y=log$T$ fields have been generated. Field 1 is generated by sequential simulation conditioned to 36 Y measurements. Field 2 is generated by self-calibration conditioned to 36 Y measurements and 34 steady-state head measurements. For the generation of field 1, and the seed field necessary by the self-calibration of field 2, a modified version of the sequential simulation program GCOSIM3D (Gómez-Hernandez and Journel, 1993) has been used. This modification accounts for a linear trend in the logtransmissivity field (Hendricks Franssen and Gómez-Hernandez, 1997). The variogram of the logtransmissivity residuals is spherical with nugget 0.195 $(\log(m^2/s))^2$, sill of 1.33 $(\log(m^2/s))^2$ and an isotropic range of 11.3 km. The two reference fields Y_1 and Y_2 are shown in Figure 3.17.

The reference fields are sampled at the same 36 locations at which logtransmissivity is reported by LaVenue *et al.* (1990) (See Figure 3.18).

3.6.2.3 Reference storativity field

Thirteen S data from the WIPP area have been used to estimate a variogram of Z=log$S$. An isotropic spherical variogram with nugget 0.02 $(\log(m/m))^2$, sill of 1.78 $(\log(m/m))^2$ and range of 11.8 km has been adopted for Z. The Z variogram and the Z data have been used as input to the sequential simulation program GCOSIM3D for the generation of a conditional simulation of Z, which

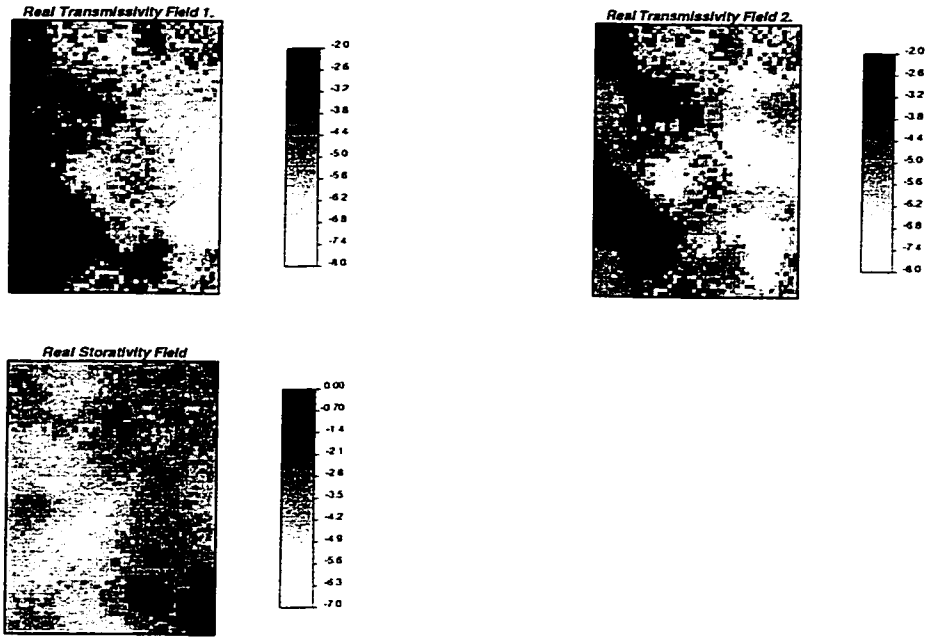

Figure 3.17. Reference fields. Logtransmissivity reference field Y_1 is generated by sequential simulation just conditional to 36 logtransmissivity measurements from the WIPP site; logtransmissivity reference field Y_2 is generated by self-calibration conditional to 36 logtransmissivity measurements and 34 steady-state head data from the WIPP site; logstorativity reference field is generated by sequential simulation conditional to 13 measurements from the WIPP site.

is used as the reference Z field for all seven scenarios. (The realisation is conditional to the 13 S values measured at WIPP.) The reference Z field is shown in Figure 3.17.

There is no apparent statistical cross-correlation between measured logtransmissivity and measured logstorativity at the locations in which both parameters were available. Therefore, the logstorativity and logtransmissivity fields are generated independently of each other.

Three samples are taken from the reference storativity field. Sample 1 contains 13 values at the WIPP measurement locations. Sample 2 contains 30 samples regularly spaced over the site. Sample 3 contains 9 samples, also regularly spaced. (See Figure 3.18.)

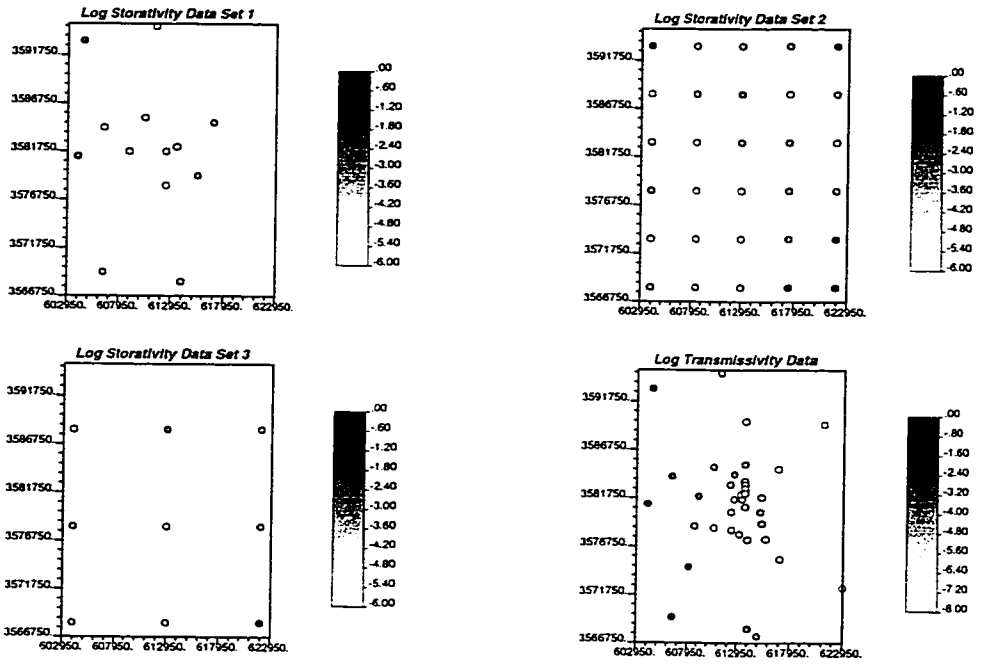

Figure 3.18. Location of the logtransmissivity and logstorativity sample data sets.

3.6.2.4 Reference hydraulic heads

Three pumping test scenarios have been considered differing on the number of wells and rates being pumped. In all cases, the reference transmissivity and storativity fields are used to determine the reference hydraulic heads that are later sampled to produce hydraulic head measurement data sets. The initial heads for the transient simulations correspond to the steady-state heads prior to pumping.

Pumping test scenario 1. It mimics one of the long term pumping tests performed at the WIPP site. A single well pumps at a constant rate of 1.93 l/s during 35 days. Hydraulic head is monitored at 34 locations (the same ones monitored at the WIPP site). (See Figure 3.19.) At each location, head is reported at 21 time steps, the step size follows a geometric progression of ratio 1.2. This pumping test, although realistic, only acts over a limited area of the modelling domain.

Pumping test scenario 2. In order to affect the entire formation with a transient event, 24 wells, regularly distributed, are pumped at a rate of 1.93 l/s during 35 days. Hydraulic head is monitored at 35 locations randomly chosen within the site. (See Figure 3.19.) The sampling frequency is the same as above.

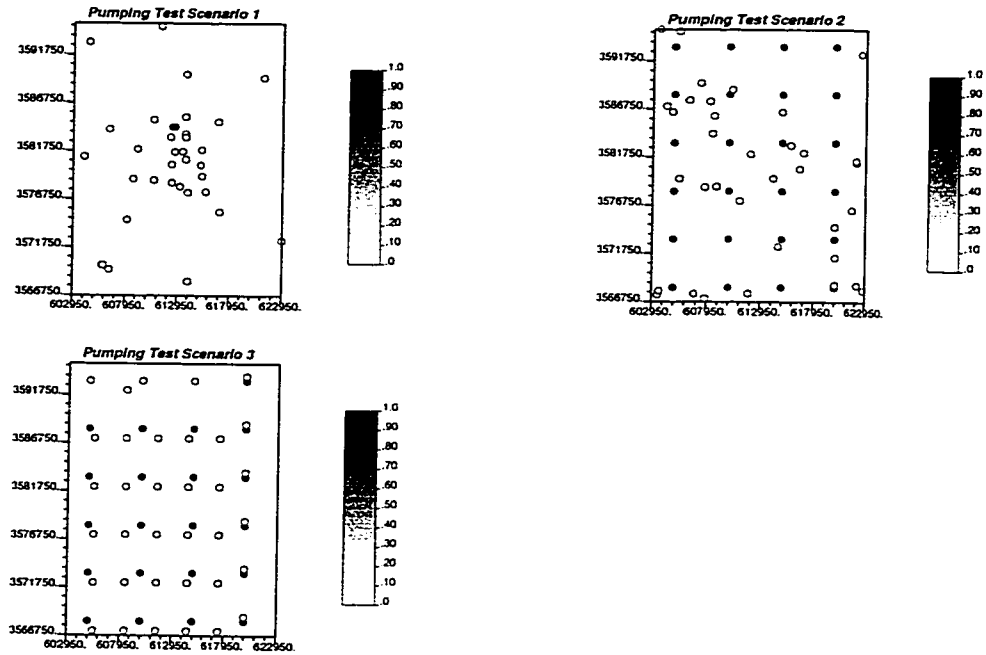

Figure 3.19. Location of pumping wells (black dots) and head monitoring locations (white dots).

Pumping test scenario 3. In order to analyse the effect of varying pumping rates, and correspondingly, a large heterogeneity on head drawdowns, 24 wells, regularly distributed, are pumped at rates varying between 0.00193 l/s and 193 l/s. Hydraulic head is monitored at 35 locations distributed regularly so that each pumping well has a monitoring location nearby. (See Figure 3.19.) The sampling frequency is the same as above.

3.6.2.5 Seven scenarios analysed

A number of scenarios has been studied to analyse how the different type of data influences the characterisation of the spatial heterogeneity of the logtransmissivity and logstorativity reference fields, as well as the reproduction of the hydraulic head reference fields. Seven combinations of the sample data sets described above have been chosen to define the seven scenarios studied. These scenarios are summarised in Table 3.2.

For each scenario, the challenge is the joint generation of couples of logtransmissivity and logstorativity fields conditional to the given sample data sets. The definition of the scenarios aims to analyse the influence of:

Scenario	*Reference Transmissivity Field*	*Pumping Test Scenario*	*Storativity Data Set*
1	2	1	1
2	2	1	2
3	1	2	1
4	1	2	2
5	1	2	3
6	1	3	1
7	1	3	2

Table 3.2. The seven scenarios. Reference transmissivity field: 1= conditioned to transmissivity measurements from WIPP, 2= conditioned to transmissivity and steady-state head measurements from WIPP. Pumping test scenario: 1= single well pumping test with 34 head monitoring locations corresponding to WIPP sampling locations, 2= multiple well pumping test with 35 randomly selected head monitoring locations, 3= multiple well pumping test with pumping rates varying from well to well and 35 head monitoring locations evenly distributed over the aquifer. Storativity data set: 1= 13 sampling locations corresponding to the WIPP sampling locations, 2= 30 sampling locations on a regular grid, 3= 9 sampling locations on a regular grid.

1. The number of pumping wells. (Comparison between scenarios 1 and 3, and between scenarios 2 and 4.)
2. The spatial heterogeneity of head drawdowns. (Comparison between scenarios 3 and 6, and between scenarios 4 and 7.)
3. The position of the head monitoring points. (Comparison between scenarios 3 and 6, and between scenarios 4 and 7.)
4. The number of storativity samples. (Comparison between scenarios 1 and 2, between scenarios 3, 4 and 5, and between scenarios 6 and 7.)

For illustration purposes, Figure 3.20 shows a realisation from scenarios 1 and 4.

3.6.3 Results from synthetic study

For each scenario, the self-calibrating method is used to generate 100 Y-Z field couples. No statistical correlation was considered between the two parameters, resulting in a simpler updating of the seed fields than if such a correlation had been considered: the weights μ_{ij}^k and υ_{ij}^k in (eq. 3.3 and 3.4) are zero. However, there is an implicit correlation, through the transient groundwater flow equation, since each couple is conditional to the same set of transient head data.

The sequential self-calibration generates Y-Z field couples conditional to the measured, Y, Z and h data. Conditioning to the Y and Z data is automatic in the

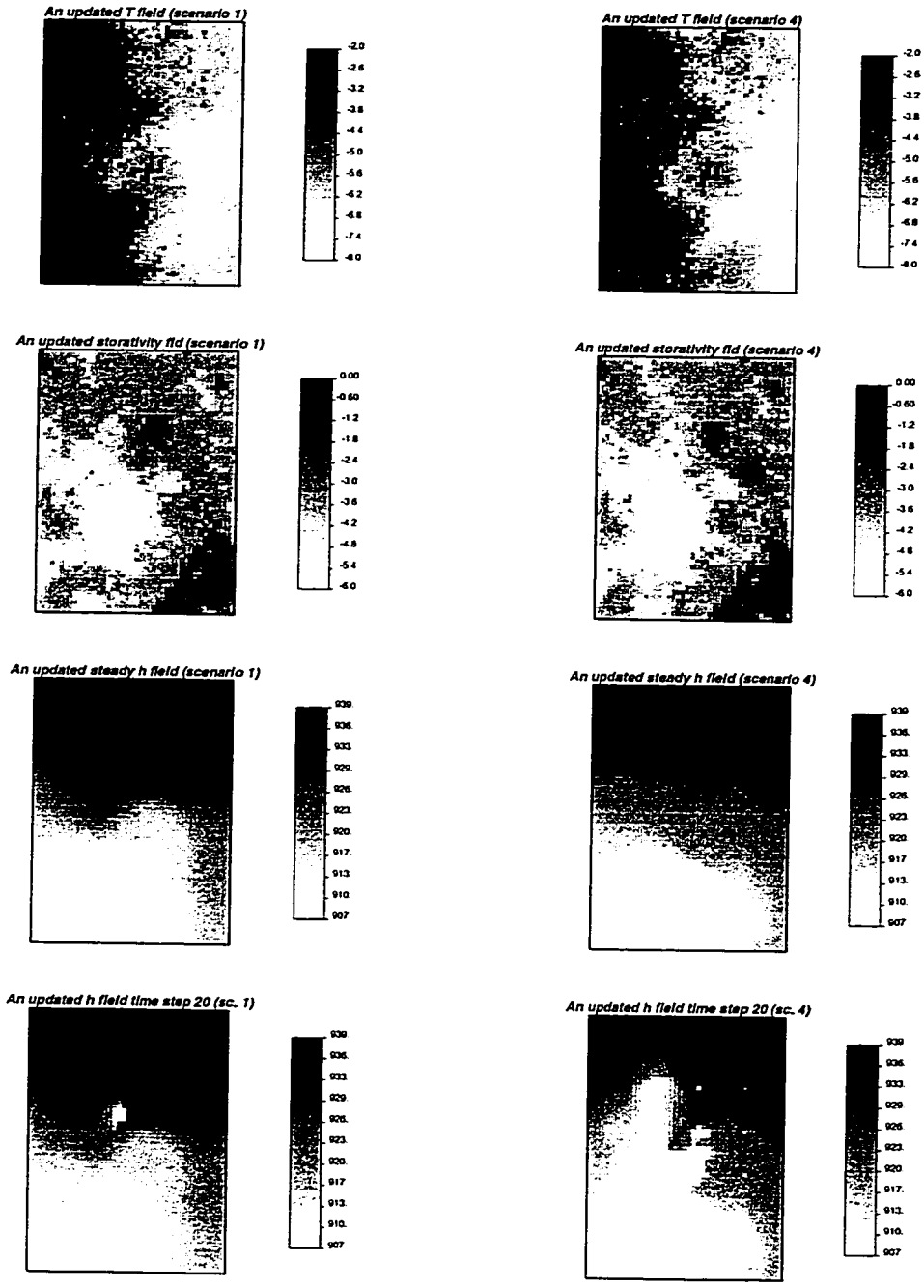

Figure 3.20. A realisation from scenarios 1 (left) and 4 (right). The logtransmissivity and logstorativity field couples conditional to Y, Z and h data are shown together with the steady-state head solution and the head field at the end of the pumping period (the latter two fields are the solution of the flow equation in the Y-Z couple and are also conditional to the h measurements).

seed field generation step, and posterior updating; however, conditioning to the h data (in the sense that the solution of the transient flow equation using the updated Y-Z couple reproduces, within a preset tolerance limit, the measured heads) is carried out through an optimisation algorithm that does, in principle, not ensure exact reproduction of the measured heads. In this respect, in scenarios 1 through 5, the final values of the objective function (not reported) are close to zero, indicative of a good conditioning in all realisations. However, for scenarios 6 and 7, which correspond to the pumping scenario that produces very heterogeneous drawdowns (as large as a hundred meters in some wells) to achieve conditioning to the measured transient heads was difficult and CPU time consuming: some realisations required more than one hundred iterations in the non-linear optimisation step, as opposed to less than ten iterations on average for the rest of the scenarios.

The next issue addressed is how conditioning to the input data sets helps in improving the characterisation of the logtransmissivity, logstorativity and hydraulic head fields over the entire model area. For this purpose, the comparison between the generated fields and the reference ones is made through the use of the average absolute error (AAE), and the average ensemble variance (AEV):

$$AAE(X) = \frac{1}{NNODES} \sum_{i=1}^{NNODES} \left| \overline{X}_{SIM,i} - X_{REF,i} \right|$$

$$AEV(X) = \frac{1}{NNODES} \sum_{i=1}^{NNODES} \sigma_{X_i}^2$$

where $NNODES$ is the number of discretization grid cells, and i is a grid cell index, X represents either logtransmissivity (Y), logstorativity (Z), or head (h) for a given time step, the overbar indicates ensemble average, that is, the average, at a given grid cell, through the 100 realisations, the subscript SIM refers to the realisations, and the subscript REF to the reference values; finally, $\sigma_{X_i}^2$ is the ensemble variance of X at a given node. The smaller these averages are, the better characterised, the Y, Z and h fields are. (Notice that if the above averages were computed over the conditioning points only, they would be zero in the Y and Z fields, and close to it for the h field.)

To evaluate the impact of the successive conditioning to steady-state and to transient heads, the AAE is computed in the fields only conditioned to logtransmissivity or logstorativity data, then after conditioning to steady-state head data, and finally after conditioning to transient head data.

Figure 3.21 shows the ensemble average Y and Z seed fields for the different scenarios. These ensembles averages are conditioned only to the Y or Z data, respectively, and therefore, do not carry any information about the flow behaviour of the formation.

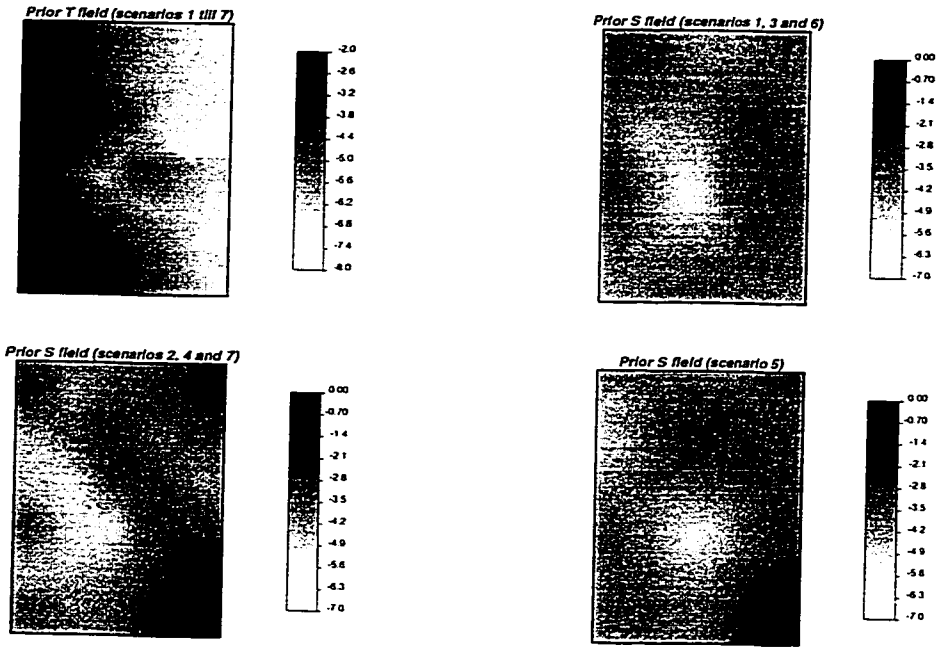

Figure 3.21. Ensemble average of the seed fields. Since the seed fields do not incorporate any hydraulic head information, these ensemble averages correspond to the kriging estimates.

Figures 3.22 and 3.23 show the ensemble average Y field for all seven scenarios alongside their respective reference fields. Recall that the difference between the two Y reference fields is that scenarios 1 and 2 use a logtransmissivity conditional to the 36 logtransmissivity data and the 34 steady-state head data provided in the report by LaVenue *et al.* (1990) whereas scenarios 3 through 7 use a logtransmissivity field that is only conditional to the same 36 logtransmissivity data. These ensemble averages should be compared to those in Figure 3.21 to appreciate how conditioning to the head data helps in a better delineation of the main patterns of spatial variability existing in the reference fields. It is difficult to distinguish large differences between the ensemble averages in Figure 3.22, or among those in Figure 3.23, which indicates that the aspects differentiating the scenarios are not very important for the characterisation of the logtransmissivity field, in this specific case. This is corroborated when analysing the $AAE(Y)$ in Table 3.3. This table shows the $AAE(Y)$ computed in the seed fields of Figure 3.21, in the ensemble average of the updated fields after conditioning to steady-state heads (not displayed in any figure) and in the ensemble averages of the updated fields after conditioning to steady and transient-state heads shown in Figures 3.22 and 3.23. The $AAE(Y)$ displays a noticeable decrease after conditioning to steady-state head data and a

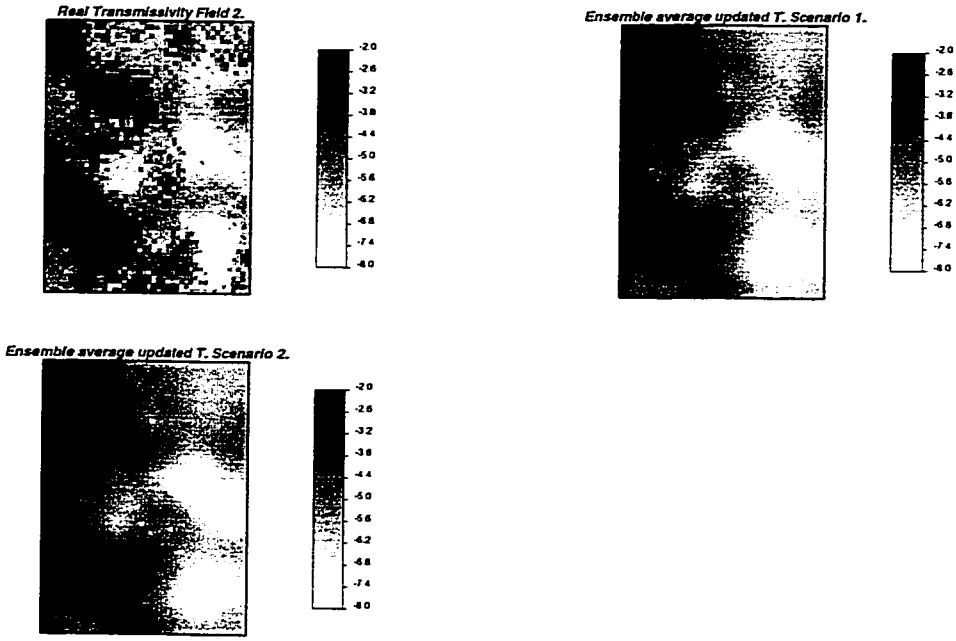

Figure 3.22. Ensemble average of the logtransmissivity fields conditional to Y, Z and h data for scenarios 1 and 2. The reference field Y_2 is also shown.

much smaller decrease after conditioning to transient heads. It appears that conditioning to between 30 and 40 logtransmissivity and steady-state head data is enough for a good characterisation of the logtransmissivity spatial variability.

Table 3.3 also shows the $AEV(Y)$ that can be interpreted as an average measure of local uncertainty. All scenarios that use Y_1 as the reference logtransmissivity field display a reduction on $AEV(Y)$ from the seed fields to the updated fields after self-calibration to the transient head data. This indicates a reduction in the uncertainty on the prediction of the reference field by the ensemble of conditional realisations. However, scenarios 1 and 2 that use Y_2 as the reference field display a small increase on $AEV(Y)$ from the seed fields to the updated fields self-calibrated to the transient head data. This behaviour is most likely due to the mismatch between the variogram used for the generation of the seed fields (the same for all scenarios and for the generation of Y_1) and the variogram of Y_2. The calibration to the steady-state head data, carried out for the generation of Y_2, modified the seed field producing a reference field with a larger intrinsic variability, and therefore a variogram with a larger sill than the one used for the generation of the seed field, as it can be noticed in Figure 3.17.

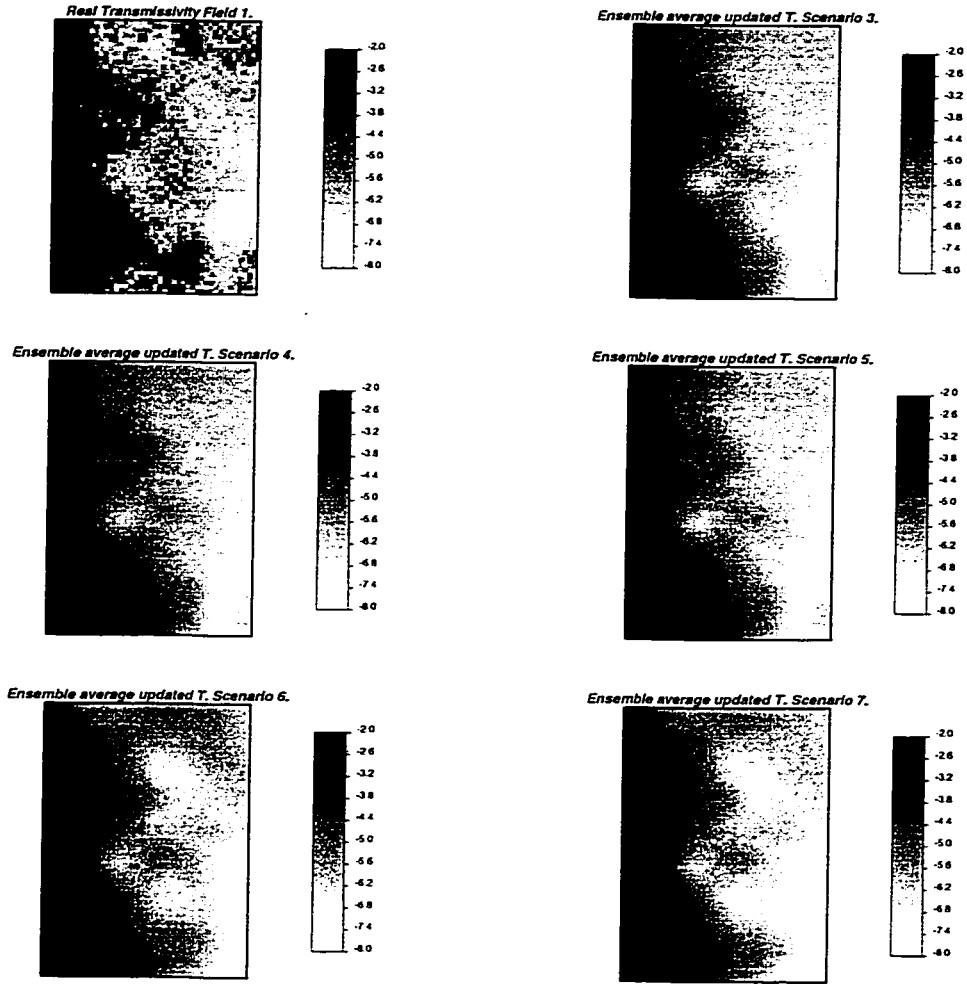

Figure 3.23. Ensemble average of the logtransmissivity fields conditional to Y, Z and h data for scenarios 3 to 7. The reference field Y_1 is also shown.

Figure 3.24 shows the ensemble average Z field for all seven scenarios alongside the reference field. These fields should be compared to those in Figure 3.21 to notice the impact that conditioning to transient heads has in a better characterisation of the logstorativity field. In six out of the seven scenarios, conditioning to transient head reduces the value of $AAE(Z)$ by a factor between 4% and 11% (see Table 3.3). The reduction is more important in those scenarios with multiple pumping tests since they affect a larger part of the aquifer. An illustrative case is scenario 2 with a single pumping test, whereas the reduction of the $AAE(Z)$ is 4% when computed over all the formation, it is as large as 45% if the computation is limited to the 1.5 km × 1.5 km affected by the test.

The sampling pattern and frequency of Z data play important roles in the reduction of the $AAE(Z)$. The reduction is larger for the scenarios with 30

Scenario	Cond. Stage	AAE(Y) log(m²/s)	AEV(Y) log(m²/s)²	AAE(Z) log(m/m)	AEV(Z) log(m/m)²
1	Y, Z	0.892	1.05	0.856	1.19
	steady *h*	0.745	0.85		
	transient *h*	0.741	1.06	0.826	0.79
2	Y, Z	0.892	1.05	0.563	0.55
	steady *h*	0.745	0.85		
	transient *h*	0.744	1.04	0.541	0.44
3	Y, Z	0.652	0.90	0.856	1.19
	steady *h*	0.586	0.60		
	transient *h*	0.574	0.65	0.808	0.84
4	Y, Z	0.652	0.90	0.563	0.55
	steady *h*	0.586	0.60		
	transient *h*	0.583	0.59	0.525	0.45
5	Y, Z	0.652	0.90	0.752	2.68
	steady *h*	0.586	0.60		
	transient *h*	0.593	0.67	0.759	1.05
6	Y, Z	0.652	0.90	0.856	1.19
	steady *h*	0.588	0.59		
	transient *h*	0.578	0.88	0.762	0.96
7	Y, Z	0.652	0.90	0.563	0.55
	steady *h*	0.588	0.59		
	transient *h*	0.580	0.78	0.527	0.57

Table 3.3. Logtransmissivity and logstorativity characterisation measures. *AAE* is the average absolute error and *AEV* is the average ensemble variance, both are computed cell by cell through the ensemble of 100 realisations. To appreciate the impact that conditioning to heads has in the characterisation process, both *AAE* and *AEV* are given for the seed fields (just conditioned to *Y* and *Z* data), for the updated fields conditioned to steady-state head data and for the final updated fields conditional also to transient heads.

logstorativity data than for those with only 13 data, but it is also larger for the scenarios of 9 regularly spaced data than for the 13 irregularly sampled values.

A more important effect of the conditioning to transient head than the reduction of *AAE*(Z) is the reduction of the *AEV*(Z). The *AEV*(Z), interpreted as a measure of the degree of local uncertainty in the estimates of logstorativity, is

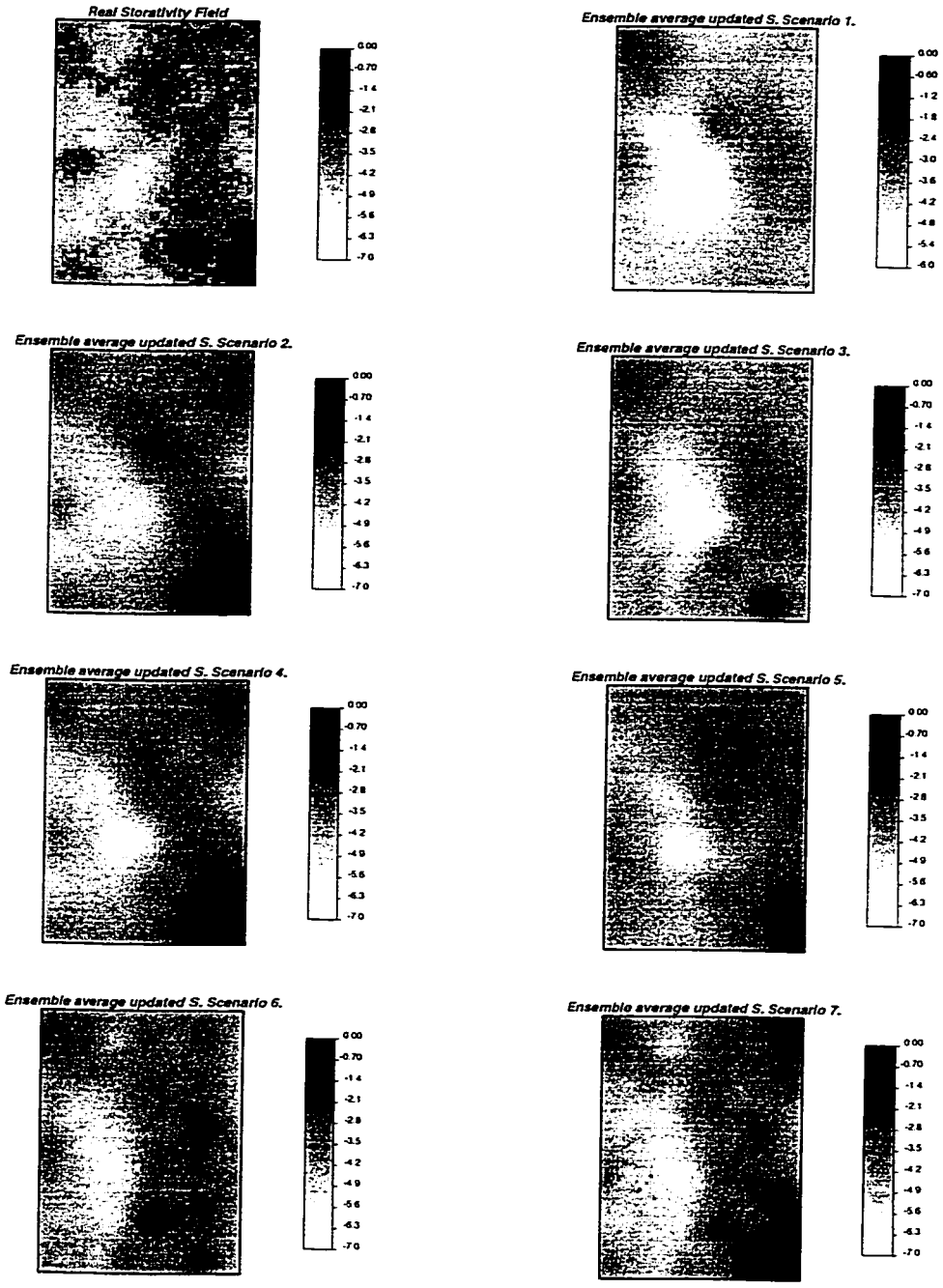

Figure 3.24. Ensemble average of the logstorativity fields conditional to Y, Z and h data for the seven scenarios. The reference logstorativity field is also shown.

substantially reduced in most scenarios, indicating that the ensemble of conditional realizations fluctuate more closely about its mean value than the ensemble of realizations not conditioned to head data. The lesser logstorativity data there are, the larger the reduction of the ensemble variance is. The largest reduction occurs for scenario 5 (61%) with only 9 Z data. The smaller reduction occurs when the drawdown heterogeneity is large (scenarios 6 and 7).

The ensemble averages of both logtransmissivity and logstorativity realisations do not change much among the different scenarios. It appears as if using multiple pumping wells does not help in improving the characterisation of the main patterns of spatial variability of Y and Z. For this particular case study, the main reason explaining this uniformity is that all realisations and all scenarios with the same logtransmissivity reference field are conditional to the same steady-state heads. This conditioning seems to be enough for the characterisation of the main patterns of Y spatial variability. Additional conditioning to transient head data only produces local updates of the Y and Z fields which are enough to match the transient head data but hardly noticeable in the average fields. (It must be stressed here that this behaviour is specific to this data set. The example in section 3.5 indicated that the steady-state head data without pumping were less consequential for the characterisation of the transmissivity field).

To determine the degree of reproduction of the reference fields by the realisations, the discrepancy between realisations and reference is measured by the $AAE(h)$ at times 0 (steady-state), 17 days and 35 days (end of the pumping period). These values are also computed in the seed fields, and in the fields conditional only to steady-state heads, with the objective to analyse how conditioning to different types of head data helps in reproducing the heads everywhere within the simulation domain. See Table 3.4.

In all cases, as expected, the $AAE(h)$ is always reduced after conditioning to head data. It is interesting to notice that conditioning to steady-state head data helps improving the overall prediction of the steady-state reference field but has little impact in the overall prediction of the transient-state reference fields. Further conditioning to transient data drastically reduces the departure between measured and predicted transient head values. This effect is particularly noticeable for scenarios 6 and 7 in which the head drawdowns are very heterogeneous and the predictions in the seed fields or the steady-state conditioning data depart more than 300 m on average at the end of the pumping period.

3.6.4 Summary and conclusions

This synthetic study gave an example of the inverse modelling of groundwater flow with the conditioning to transient head data and to the joint generation of logtransmissivity and logstorativity fields. The main differences as compared

Scenario	*Time (days)*	*AAE Initial (m)*	*AAE Updated Steady (m)*	*AAE Updated Transient (m)*
1	0	2.22	0.60	0.61
	17	3.60	1.61	0.69
	35	4.52	2.12	0.76
2	0	1.98	0.60	0.61
	17	2.14	0.73	0.68
	35	2.26	0.83	0.75
3	0	1.04	0.55	0.59
	17	3.81	3.61	3.39
	35	5.56	5.40	5.20
4	0	1.03	0.54	0.62
	17	2.58	2.30	2.15
	35	3.35	3.10	2.90
5	0	1.03	0.55	0.68
	17	3.94	3.58	2.90
	35	5.29	4.98	3.75
6	0	1.03	0.55	0.58
	17	183.0	202.9	11.9
	35	321.2	360.0	22.8
7	0	1.03	0.55	0.57
	17	104.5	103.1	7.46
	35	193.9	193.0	13.0

Table 3.4. Hydraulic head characterisation measures. The average absolute error computed cell by cell through the ensemble of 100 realisations is determined for the seven scenarios: at steady-state prior to pumping (time 0), at 17 days after pumping started and at the end of the pumping period (35 days). To appreciate the effect of conditioning to the head data, the *AAE* is computed in the seed fields just conditioned to *Y* and *Z* data (*AAE* initial), for the updated fields conditioned to steady-state head data (*AAE* updated steady) and for the final updated fields conditional also to transient heads (*AAE* updated transient).

with the conditioning of logtransmissivity fields only are that the seed fields of logtransmissivity and logstorativity are generated using co-simulation and that they are updated using co-kriging.

The self-calibrating algorithm has been tested in different situations regarding the number and type of conditioning data, and in all cases, was capable of generating conditional realisations of logtransmissivity and logstorativity.

In this study we have not considered data measurement errors or uncertainty on the boundary conditions or the variogram in order to focus on the worth of the different sources of data. However, SCM is able to handle these sources of uncertainty. Chapter 4 presents an extensive study on the impact of measurements and/or conceptualisation errors.

There is a clear trade-off between the different types of data with regard to the characterisation of the different parameters and variables involved. This synthetic study does not present a systematic analysis of these trade-offs, although points to the potential that the self-calibrating algorithm has for the design of the monitoring strategy that will result in the best characterisation of the variables of interest.

3.7 Some final comments with respect to the results of the studies

Results from three different studies were presented in the sections 3.4 through 3.6.

The method performed satisfactorily in all cases. In the case of transient flow it was found that the use of transient data may introduce important modifications in the final calibrated transmissivity field; this was the case of the inverse modelling of groundwater flow in a single fracture (section 3.5). Steady-state head data without pumping hardly modified the transmissivity realisations in that case. However, in the two other studies, transient data only yielded local modifications of the transmissivity field. The latter results could be considered as the expected results in case the number of locations with transient head measurements is equal to or smaller than the number of locations with steady-state head measurements.

It was found that the calibration of a single storativity value yielded very consistent results. The variance between the different fields was relatively small and a final value was only weakly dependent on the initial value (tests have been made for initial storativity values 10 times higher or lower than the "real" estimated initial storativity).

The performance of the non-linear optimisation algorithms has been studied too. It was found that Hestenes-Stiefel Conjugate Gradients (HS-CJG) yields the most important reductions in objective function value, followed, by far, by both the Quasi-Newton (QN) and the Fletches-Reeves Conjugate Gradients (FR-CJG). It has been suggested (Scales, 1985) that on non-quadratic functions FR-CJG may introduce an updating direction nearly orthogonal to the gradient so that little progress is made. In these cases, HS-CJG resets the updating direction automatically to the direction of the gradient. Moreover, QN was the algorithm with the largest number of consecutive iterations with a reduction of less than 1% of the objective function. It has been found that using only three algorithms (without QN) did not slow down the process of convergence; probably, the rather simple approximation of the Hessian by the QN-method is not accurate enough.

If the locations of the master grid cells remain the same over all simulated fields, artefacts appear in the ensemble average transmissivity field and the variance of the transmissivity field. Changing the locations of the master grid cells from realisation to realisation yields smooth ensemble fields. In addition, it was found that initialising the master grid cells on a regular grid with random starting point was better than locating them totally at random.

4 Impact of data amount and quality in sequential self-calibration

The success of the conditioning to hydraulic head and conductivity data depends, among others, on the amount and quality of the measurement data. It is expected that the measurement data have less value if they are corrupted with measurement error. It is also expected that the correct estimation of the average error of the measurement data may have an impact on the modelling results. In this chapter, two synthetic studies are presented in which the impact of the amount and quality of the measurement data on the simulation results is evaluated.

In Section 4.1 the impact of the amount of measurement data on the characterisation of a 3D aquifer and the prediction of groundwater flow is studied. For different scenarios a large number of inverse conditioned realisations is generated, and the ensemble averaged fields are compared to the reference fields in order to draw conclusions about the influence of the amount of conditioning data. A similar study in 2-D was carried out by Wen *et al.* (1996).

In Section 4.2 two synthetic studies are presented which analyse the impact of measurement errors (hydraulic conductivity and/or hydraulic head) in the stochastic inverse modelling of groundwater flow. All the scenarios studied can be divided in two different approaches: (1) The modeller assumes the data to be error free while the data have some error. In this case, the attempt is to reproduce erroneous data, thus a negative impact is expected on the results obtained. (2) The modeller makes a correct estimation of the magnitude of the measurement errors, and in this case it is expected that it is only the worse quality of the measurement data that influences the obtained results negatively.

4.1 Impact of the amount of conditioning data: a 3-D study

The impact of the amount of conditioning data is investigated in a 3-D synthetic study. A synthetic study is used in order to have a controlled experiment to test the impact of the amount of measurement data; in a real-world case study the reality is unknown and just in rare cases many experimental data are available. The specific aim of this study was to compare the value of the hydraulic head data with the value of the hydraulic conductivity data for the characterisation of the conductivity field, hydraulic head field and mass transport. Calculations are carried out for various sample data sets. A similar study was carried out by Wen *et al.* (1996) in a 2-D domain. The main differences between their study and this one are the different boundary conditions (mostly impermeable boundaries instead of prescribed head boundaries) and the fact that groundwater flow in a 3-D domain is simulated. The conclusions are compared with the conclusions

from Wen *et al.* (1996). Furthermore, the impact of the amount of conductivity and head data on the aquifer characterisation can also be compared with the (negative) impact of measurement errors. The same synthetic study was extended for the case of corrupted measurement data (see section 4.2). The hydraulic head and hydraulic conductivity data are obtained from sampling the reference fields. The amount of hydraulic conductivity and hydraulic head samples varies between the different sample data sets. In total 100 equally likely realisations are conditioned to the experimental data, for each of the sample data sets. The conditioning is carried out by INVERTO. Only steady-state flow is considered and there are no sinks and sources. The ensemble averaged conductivity and head fields are compared with the reference conductivity and head fields. Furthermore, in each of the conditioned realisations one particle is released from a centre location and transported to the bottom of the model. A particle tracking method is used to model the transport of the particle. The ensemble averaged particle arrival location is compared with the reference particle arrival location. Also two scenarios are studied with erroneous boundary conditions. Finally, one scenario is studied with an incorrect model variogram.

4.1.1 Reference fields

A MultiGaussian hydraulic conductivity reference field is generated with an ensemble mean of -7.0 ($\log_{10}$ (m/s)), a spherical variogram with nugget zero, sill 2.0 ($\log_{10}$ (m/s))^2 and range 300 m in the horizontal plane and 150 m in the vertical direction. The reference hydraulic conductivity values are generated for a grid with 30 x 30 x 15 cubic cells (13,500 cells in total) of 50 m in the size. The total domain has extensions of 1500 x 1500 x 750 metres. The groundwater flow equation is solved for impermeable boundaries, except the surface and the bottom boundaries at which prescribed head values are imposed. At the top of the model a prescribed head value of 28 m and at the bottom a prescribed head of 0 m is set. These boundary conditions force a flow from the top of the model downwards. The transport of particles in the domain is also simulated; one particle is released a few grid cells above the centre of the block. Figure 4.1 shows the reference hydraulic conductivity and hydraulic head fields.

4.1.2. Sample data sets

In total 35 different data sets are sampled from the 3-D reference fields; the data sets differ in the amount of conductivity and head data. The amount of head data goes up until a maximum of 300, while the maximum of conductivity data is 64. The reference data are obtained from random or regular sampling of the 3-D grid.

4.1.3 Conditioning

INVERTO was used to condition 100 realisations to the conductivity and head data. The error-free conductivity data were reproduced exactly, while the error-

Figure 4.1. Reference hydraulic conductivity and hydraulic head field. Shown are (from left to right and from above to below): 3-D reference Y, Y at z=3, Y at z=7 and Y at z=11, 3-D reference h, h at z=3, h at z=7 and h at z=11.

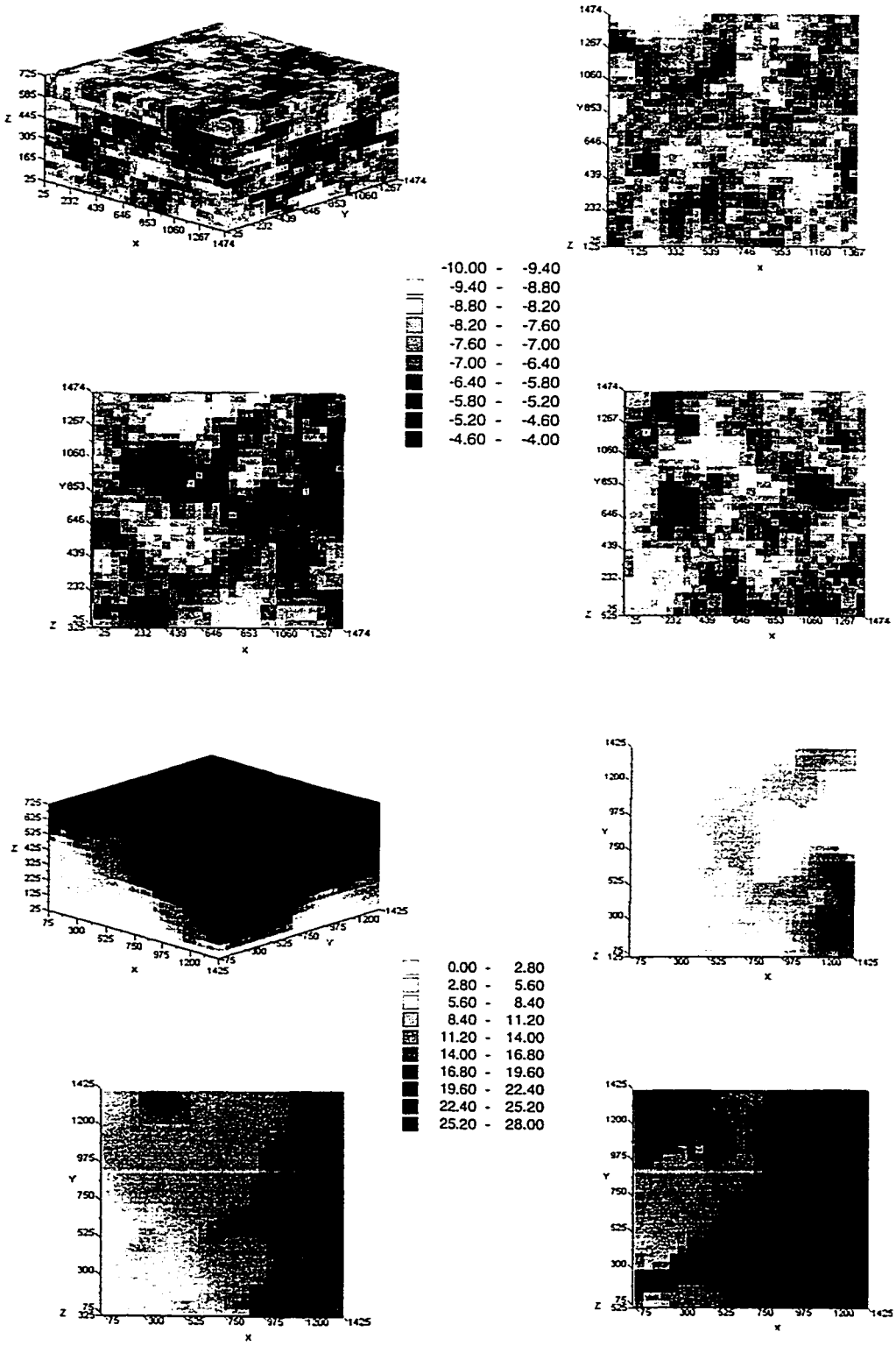

free hydraulic head data were reproduced as close as possible. In each of the realisations 216 master blocks were located. The master blocks are located on a regular grid with random starting point. The conductivity perturbation at a grid cell is obtained from the interpolation of the conductivity perturbations at the 12 closest master blocks. The positions of the master blocks changed during the conditioning as explained in section 3.3. During a maximum of five iterations the same non-linear optimisation algorithm is used, but the algorithm changes faster in case the objective function reduction is less than 1% in an iteration. Figure 4.2 shows for two of the sample data sets a realisation of the hydraulic conductivity-hydraulic head couple, conditional to the experimental data. The ensemble averaged hydraulic head and hydraulic conductivity fields over the 100 realisations are calculated and compared with the reference fields:

$$AAE(X) = \frac{1}{NNODES} \sum_{i=1}^{NNODES} \left| \overline{X}_{SIM,i} - X_{REF,i} \right|$$

$$AESD(X) = \frac{1}{NNODES} \sum_{i=1}^{NNODES} \sigma_{X_i}$$

where *AAE* is the average absolute error, *AESD* the average ensemble standard deviation, *NNODES* the number of discretization grid cells, and i is a grid cell index, X represents either decimal log conductivity or steady-state hydraulic head (h), the overbar indicates ensemble average (the average at a grid cell through the 100 realisations), the subscript *SIM* refers to the realisations, and subscript *REF* to the reference (real) values; finally, σ_{X_i} is the ensemble standard deviation of X at a given node. The smaller *AAE* and *AESD* are, the better characterised the transmissivity and hydraulic head fields are.

In each of the 100 realisations generated for each sample data set a particle is released close to the centre of the block, which is transported to the bottom boundary of the simulation domain. The average arrival location is compared with the real arrival location according to the following equation:

$$AAE(X) = \sqrt{\left(\left(\frac{1}{NSIM} \sum_{j=1}^{NSIM} x_{SIM,j}\right) - x_{REF}\right)^2 + \left(\left(\frac{1}{NSIM} \sum_{j=1}^{NSIM} y_{SIM,j}\right) - y_{REF}\right)^2}$$

where X represents arrival location, *NSIM* the number of realisations, x the x-coordinate of the arrival location, y the y-coordinate of the arrival location and j the simulation number. The spread around the mean arrival location is measured by the average ensemble standard deviation in the particle arrival location:

Figure 4.2a. One realisation of hydraulic conductivity and hydraulic head for K=0 and H=0. The figures are in the same order as in Figure 1.

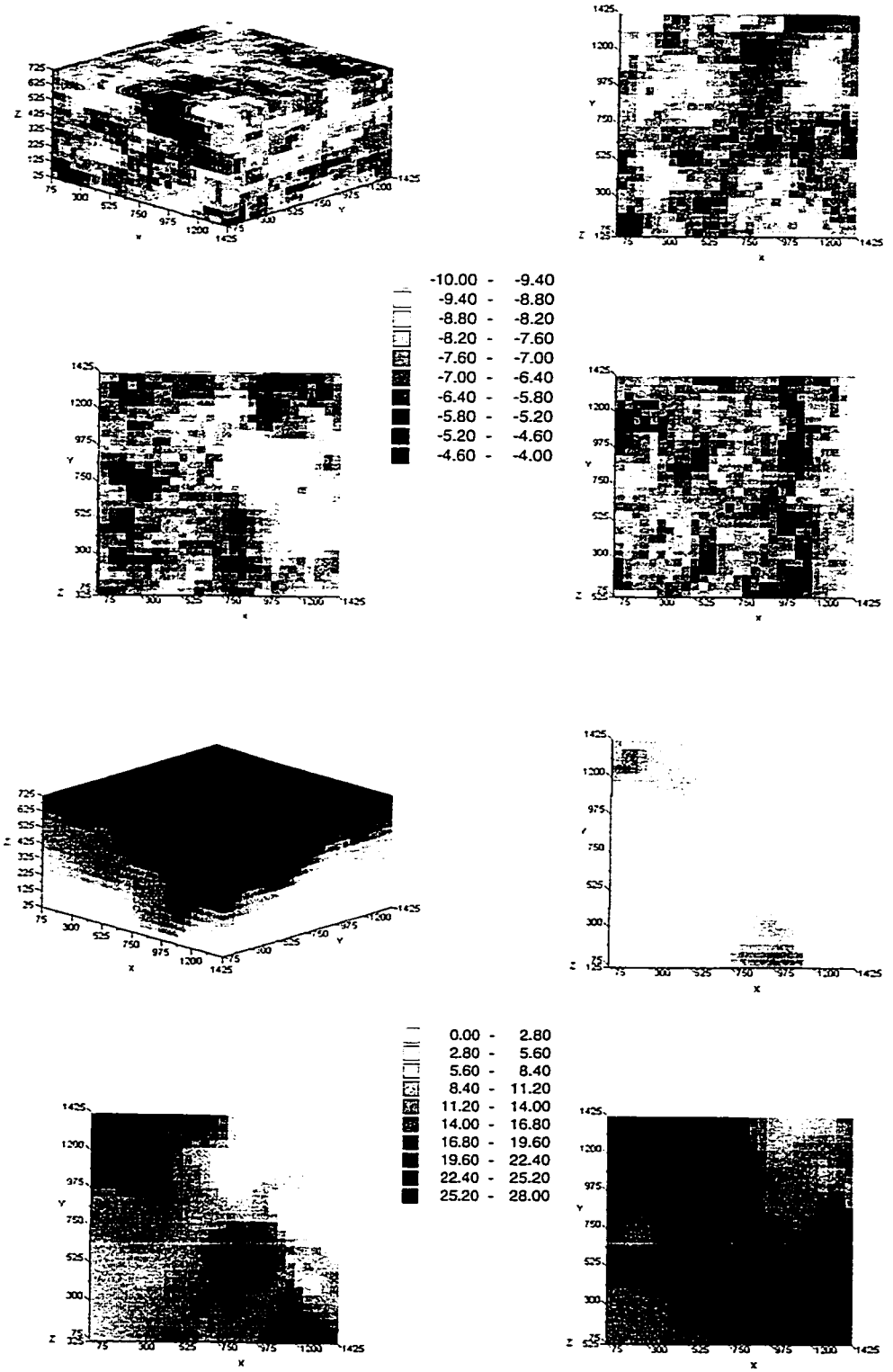

Figure 4.2b. One realisation of hydraulic conductivity and hydraulic head for K=32 and H=150. The figures are in the same order as in Figure 1.

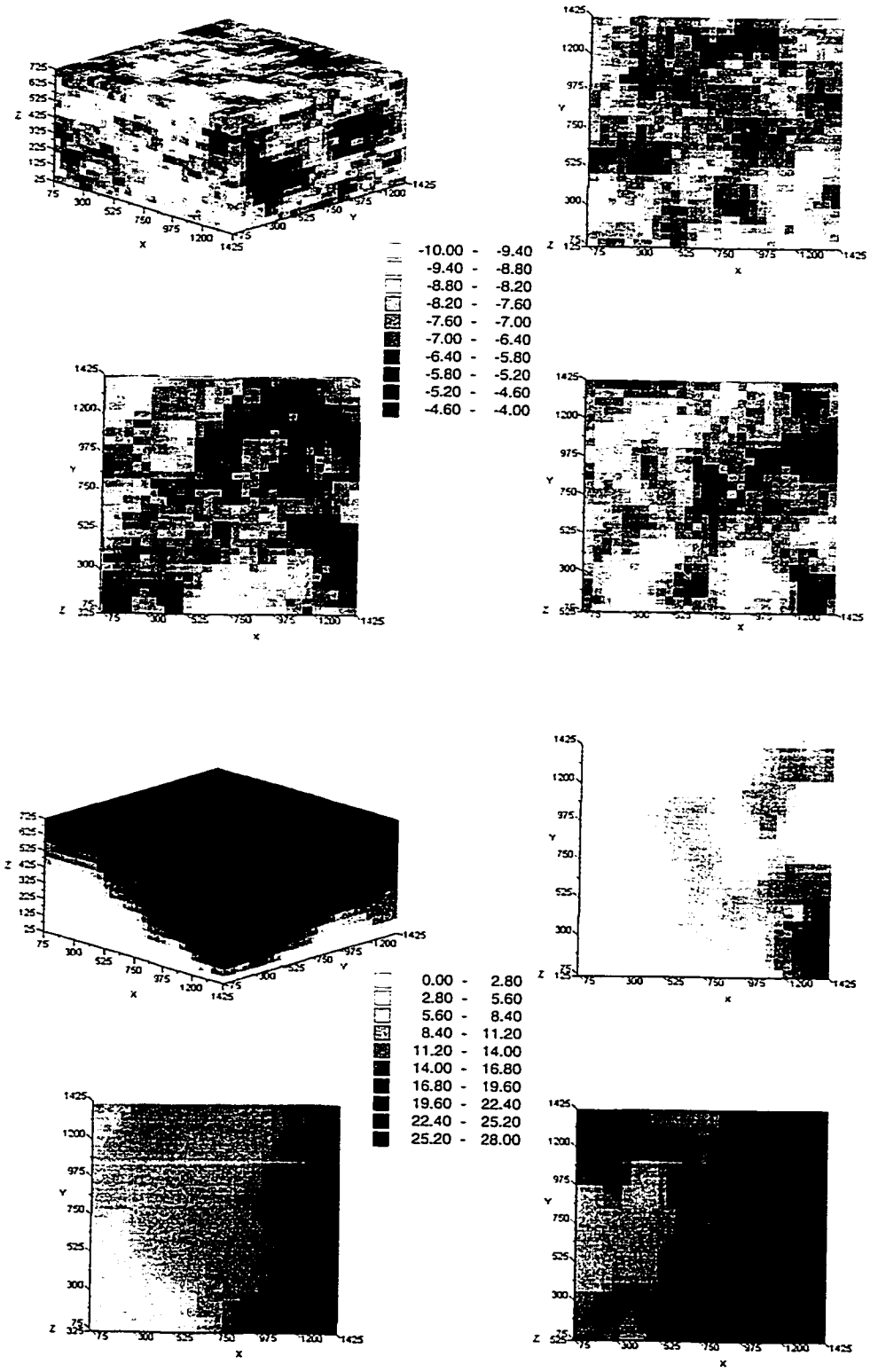

$$AESD(X) = \sqrt{\frac{1}{NSIM}\sum_{j=1}^{NSIM}\left(x_{SIM,j} - \left(\frac{1}{NSIM}\sum_{j=1}^{NSIM} x_{SIM,j}\right)\right)^2 + \frac{1}{NSIM}\sum_{j=1}^{NSIM}\left(y_{SIM,j} - \left(\frac{1}{NSIM}\sum_{j=1}^{NSIM} y_{SIM,j}\right)\right)^2}$$

4.1.4 Results

The *AAE* and *AESD* for hydraulic conductivity, hydraulic head and particle arrival locations are given in Tables 4.1 until 4.3.

The main conclusion with respect to the characterisation of the hydraulic conductivity field is that the *AAE* reduction is limited; for the maximum amount of conditioning data (64 hydraulic conductivity data and 300 hydraulic head data; K=64, H=300) the *AAE* reduction is still just 13%. It can also be concluded that the hydraulic conductivity data contribute more to reduce the *AAE* for hydraulic conductivity than hydraulic head data. It is surprising that 32 head data do not yield any *AAE* reduction; at least 64 head measurement data are needed to reduce the *AAE*. This probably can be explained by the

AAE (m/s)	K=0	K=8	K=16	K=32	K=64
H=0	1.00	0.99	0.97	0.95	0.93
H=8	1.00	0.99	0.98	0.96	0.93
H=16	1.01	0.99	0.98	0.96	0.93
H=32	1.02	1.00	0.99	0.97	0.93
H=64	0.99	0.98	0.96	0.95	0.92
H=150	0.94	0.93	0.91	0.91	0.88
H=300	0.93	0.91	0.91	0.90	0.87

AESD (m/s)	K=0	K=8	K=16	K=32	K=64
H=0	1.00	0.99	0.98	0.96	0.93
H=8	1.09	1.03	0.98	0.96	0.94
H=16	1.10	0.99	0.99	0.98	0.94
H=32	1.10	1.02	1.03	0.98	0.94
H=64	1.06	0.97	0.98	0.96	0.93
H=150	1.05	0.99	0.96	0.92	0.92
H=300	1.03	0.96	0.97	0.92	0.90

Table 4.1. Logconductivity characterisation measures. *AAE* is the average absolute error and *AESD* is the average ensemble standard deviation, both are computed cell by cell through the ensemble of 100 realisations. The *AAE* and *AESD* are given for all the sample data sets. The amount of hydraulic head conditioning data is plotted on the vertical axis. The amount of hydraulic conductivity data is plotted on the horizontal axis. The results are standardised by setting *AAE* and *AESD* to 1.0 for the scenario with no data (K=0 and H=0).

Figure 4.3a. Average logconductivities (above) and *AESD* (below) for logconductivity for K=8 and H=8. The same layers are shown are as in Figure 1.

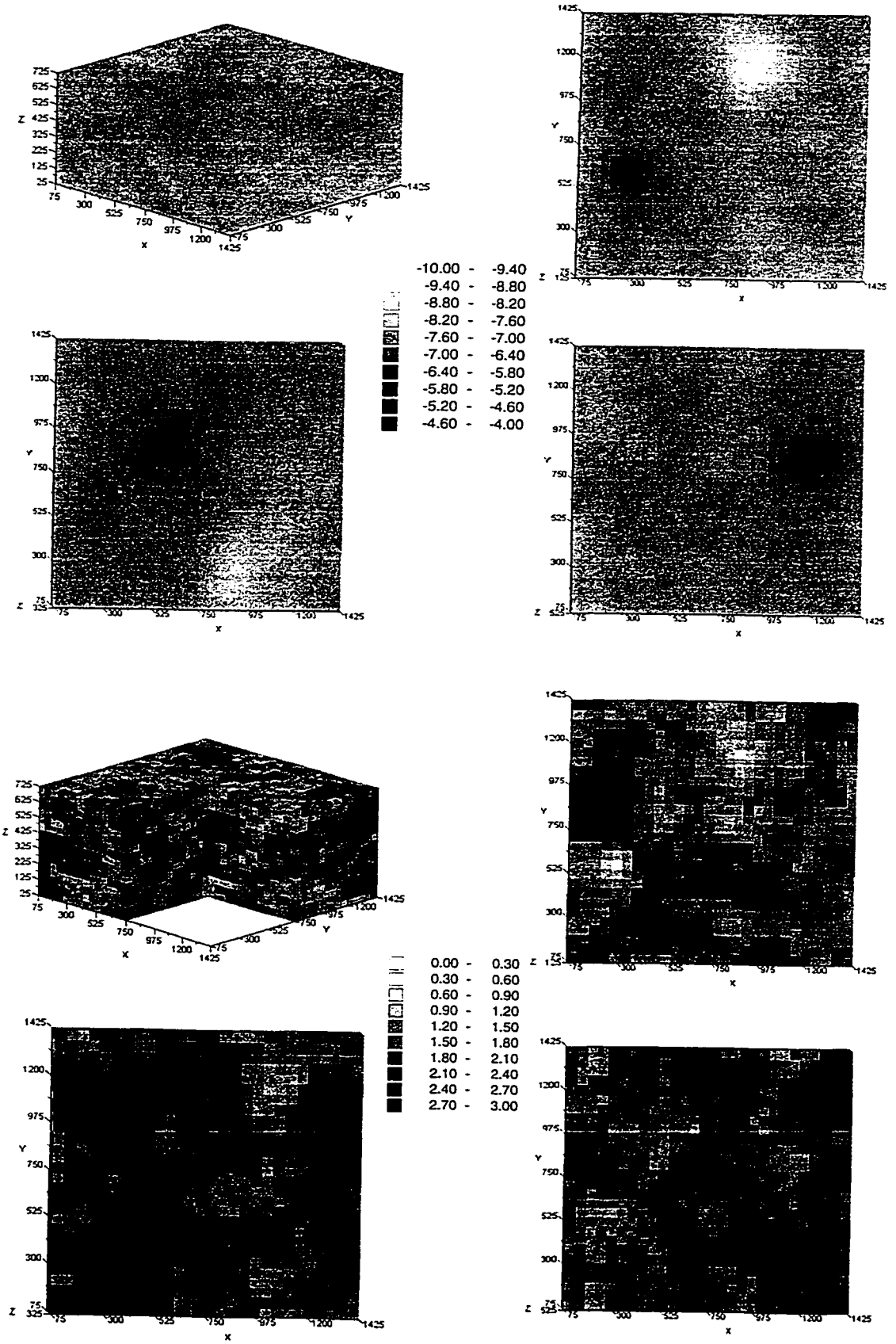

Figure 4.3b. Average $\log_{10} K$ (above) and *AESD* (below) for logconductivity for K=32 and H=64. The same layers are shown are as in Figure 1.

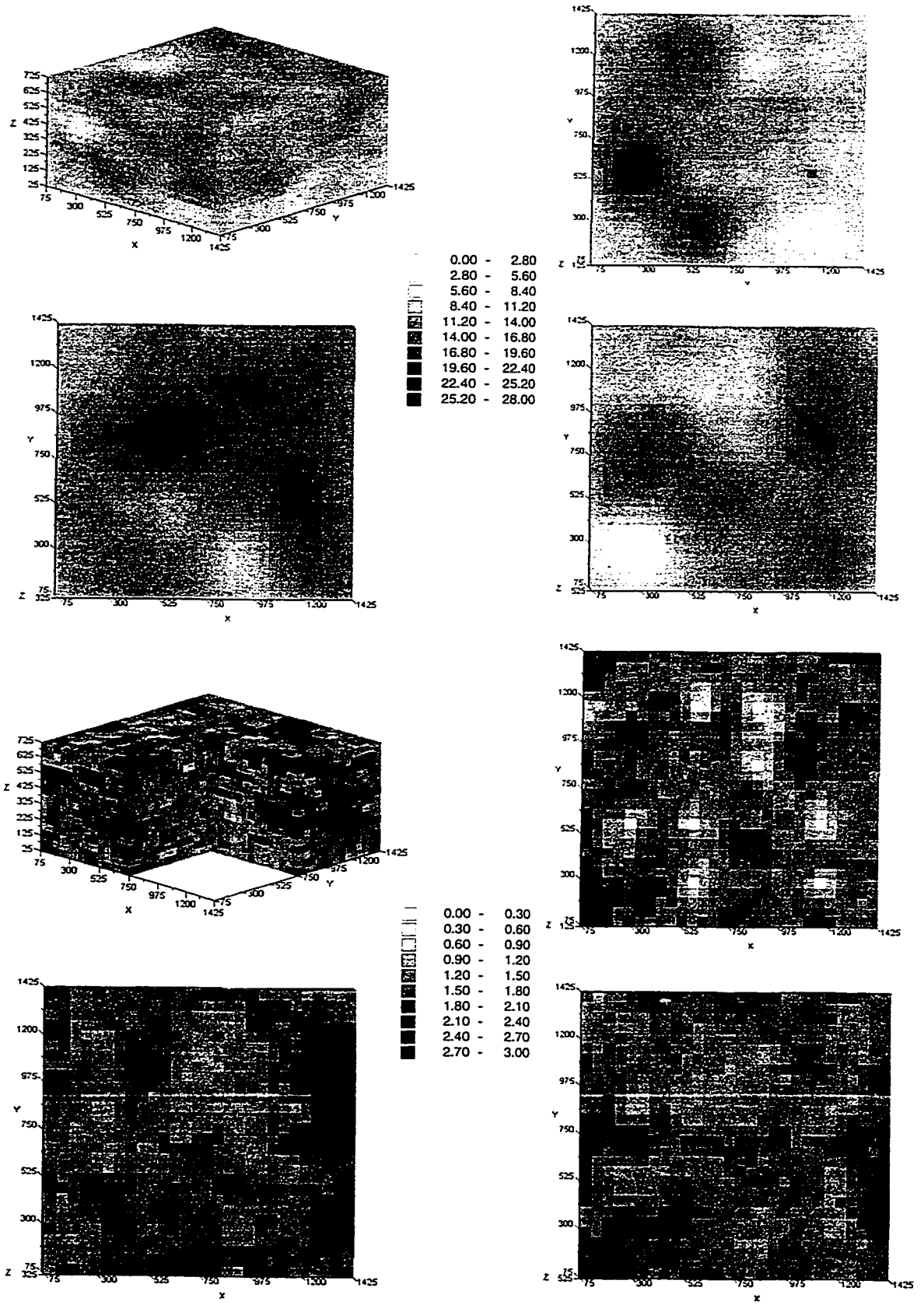

Figure 4.3c. Average $\log_{10} K$ (above) and *AESD* (below) for logconductivity for K=64 and H=300. The same layers are shown are as in Figure 1.

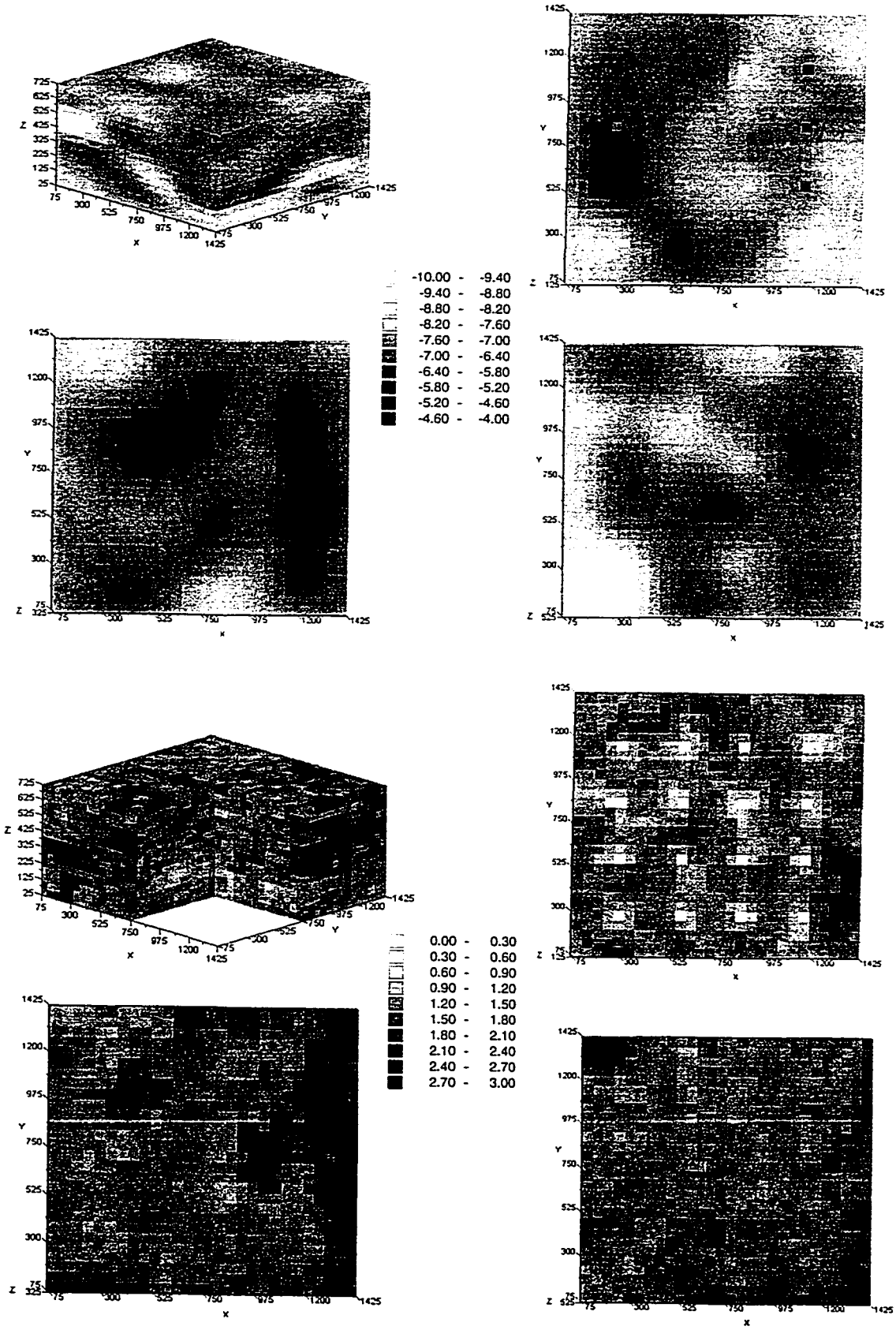

AAE (m)	K=0	K=8	K=16	K=32	K=64
H=0	1.00	0.89	0.85	0.92	0.92
H=8	0.74	0.70	0.73	0.70	0.70
H=16	0.60	0.57	0.58	0.56	0.58
H=32	0.55	0.53	0.53	0.51	0.52
H=64	0.40	0.40	0.40	0.40	0.40
H=150	0.33	0.32	0.32	0.31	0.32
H=300	0.26	0.26	0.26	0.26	0.25

AESD (m)	K=0	K=8	K=16	K=32	K=64
H=0	1.00	1.00	0.97	0.95	0.88
H=8	0.81	0.78	0.75	0.75	0.72
H=16	0.72	0.68	0.67	0.67	0.63
H=32	0.64	0.60	0.57	0.58	0.54
H=64	0.53	0.48	0.47	0.46	0.43
H=150	0.44	0.39	0.38	0.37	0.36
H=300	0.36	0.34	0.37	0.33	0.31

Table 4.2. Hydraulic head characterisation measure. *AAE* is the average absolute error and *AESD* is the average ensemble standard deviation, both are computed cell by cell through the ensemble of 100 realisations. The *AAE* and *AESD* are given for all the sample data sets. The amount of hydraulic head conditioning data is plotted on the vertical axis. The amount of hydraulic conductivity data is plotted on the horizontal axis. The results are standardised by setting *AAE* and *AESD* to 1.0 for the scenario with no data (K=0 and H=0).

difference between the variogram for the reference conductivity field and the model variogram. The *AESD* reduction is also not as strong as possibly would be expected: for K=64 and H=300 10%. Head data hardly help to reduce the *AESD*(*K*) and the first 32 head data result even in an increase for the *AESD*. This *AESD* increase possibly also can be explained by the mismatch between the variogram for the reference field and the model variogram. Figure 4.3 shows some average ensemble hydraulic conductivity fields and images of the average ensemble variances for different amounts of sample data. The figures illustrate that the impact of the amount of measurement data on the characterisation of the *K* field (compare with the reference *K* field, Figure 4.1) is not so clear. Nevertheless, the characterisation of the conductivities of layer 7 improves. The figures also illustrate that the ensemble variances are lower in case more measurement data are available.

The inverse modelling has a much more pronounced effect on the characterisation of the hydraulic head field. While the *AAE*(*K*) reduction is relatively small, the *AAE*(*h*) reduction is very significant. For the case of K=64 and H=300 the reduction is 75%. The hydraulic conductivity data hardly

AAE (m)	K=0	K=8	K=16	K=32	K=64
H=0	1.00	0.90	0.84	0.86	0.94
H=8	0.68	0.54	0.59	0.63	0.60
H=16	0.65	0.44	0.56	0.56	0.57
H=32	0.56	0.45	0.48	0.48	0.46
H=64	0.32	0.30	0.33	0.34	0.31
H=150	0.39	0.32	0.29	0.34	0.35
H=300	0.35	0.35	0.38	0.34	0.24

AESD (m)	K=0	K=8	K=16	K=32	K=64
H=0	1.00	1.02	1.04	0.91	1.04
H=8	1.01	1.03	0.99	0.94	0.98
H=16	0.94	0.91	0.89	0.95	0.79
H=32	0.93	0.97	0.89	0.97	0.80
H=64	1.02	0.92	0.90	0.96	0.76
H=150	0.85	0.79	0.70	0.70	0.69
H=300	0.78	0.79	0.90	0.70	0.64

Table 4.3. Transport characterisation measure. *AAE* is the average absolute error in the arrival location and *AESD* the average ensemble standard deviation in the particle arrival location. The *AAE* and *AESD* are given for all the sample data sets. The amount of hydraulic head conditioning data is plotted on the vertical axis. The amount of hydraulic conductivity data is plotted on the horizontal axis. The results are standardised by setting *AAE* and *AESD* to 1.0 for the scenario with no data (K=0 and H=0).

contribute in reducing the *AAE*(h) and the hydraulic head data nearly exclusively contribute to the *AAE*(h) reduction. Especially for the cases with a considerable amount of hydraulic head data (H $\geq$ 64) the *AAE*(h) hardly differs between the cases with the minimum of conductivity data (K=0) and the maximum of conductivity data (K=64). From the results it can also be observed that the first head data yield the most important *AAE*(h) reduction. The uncertainty in the ensemble of head solutions, as expressed by the *AESD*(h), also reduces very significantly in case more measurement data are available. For the maximum amount of measurement data (K=64 and H=300) the *AESD*(h) is 70% lower than for the case that not any conditioning data is used. Also for this characterisation measure it is found that the first head data yield the most important improvements. The head data have a more important impact on the *AESD*(h) reduction than the conductivity data, although the influence of the conductivity data is more significant than it was for the *AAE*(h). Figure 4.4 shows some average ensemble hydraulic head fields and average ensemble variances for different amounts of sample data. The figures show clearly how the characterisation of the head field improves in case more measurement data are available.

Figure 4.4a. Average head (above) and *AESD* (below) for hydraulic head for K=8 and H=8. The same layers are shown are as in Figure 1.

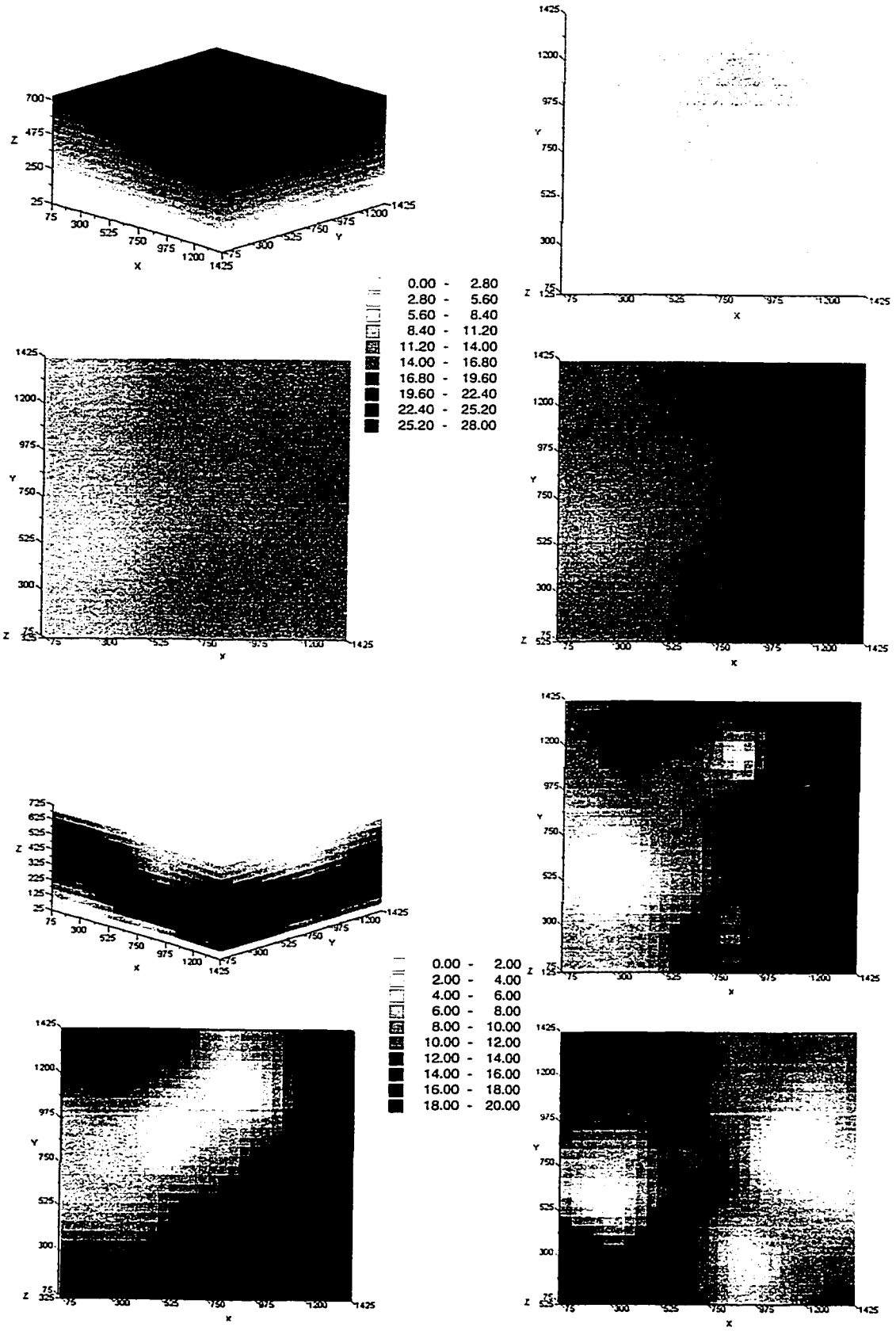

Figure 4.4b. Average head and *AESD* (below) for hydraulic head for K=32 and H=64. The same layers are shown are as in Figure 1.

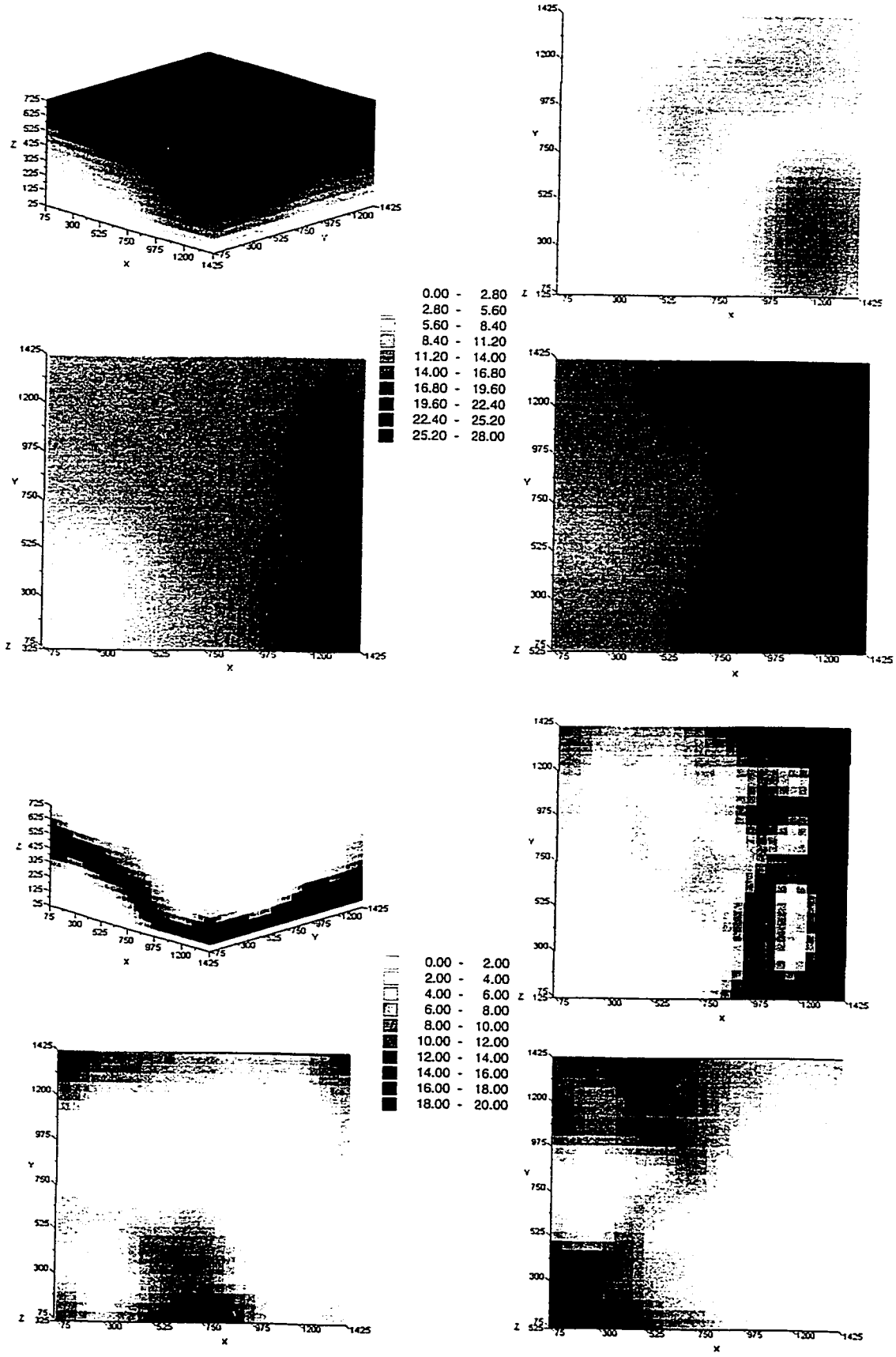

Figure 4.4c. Average head (above) and *AESD* (below) for hydraulic head for K=64 and H=300. The same layers are shown are as in Figure 1.

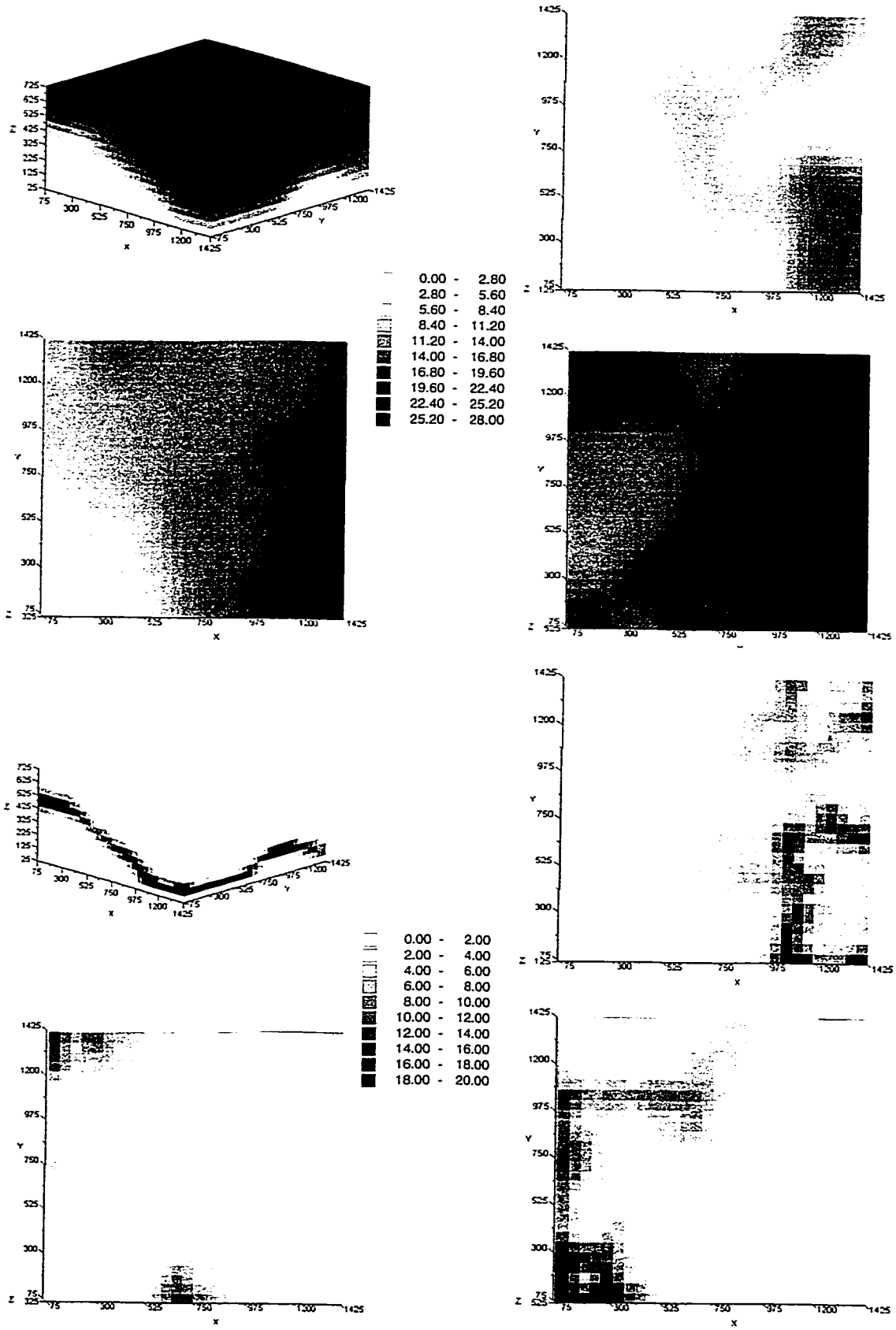

Figure 4.5 shows histograms on the average particle arrival locations for different sample data sets. The average particle arrival location is closer to the real particle arrival location in case more conditioning data are used. Especially the hydraulic head data contribute to the improved estimation of the particle arrival location. The impact of the hydraulic conductivity is much smaller. For instance, 16 hydraulic conductivity data yield an *AAE* reduction of 16% (compared with a situation of no data.) while 16 hydraulic head data yield an *AAE* reduction of 35%. For the 35 sample data sets, the *AAE* reduction for the estimation of the particle arrival location is close to the *AAE*(h) reduction. This may also illustrate that the estimation of the particle arrival location is more affected by the characterisation of the hydraulic head field than by the characterisation of the hydraulic conductivity field. In other studies (Wen *et al.*, 1996; Hughson, 1997; Hughson and Gutjahr, 1998) it was also found that the estimation of the particle travel paths and the particle arrival locations improved mainly thanks to the piezometric head data, and to a much lesser extent thanks to the hydraulic conductivity data. The uncertainty reduction is 76% in the case of the largest amount of measurement data (K=64, H=300). On the contrary to what is observed for the *AAE*(K) and the *AAE*(h) the *AAE* for the particle arrival location does not decrease so smoothly as function of the amount of head and conductivity data. For example, the *AAE* for K=64, H=150 is larger than the *AAE* for K=0 and H=64. These irregularities may be caused by the fact that just one particle is released and that it is transported through just a small part of the study domain. In case more particles (from different locations) would be released and an *AAE* would be calculated over all the transport experiments a smoother *AAE* decrease is expected. The *AESD* for the particle arrival position is not reduced as strong as the *AAE*. The maximum *AESD* reduction is 36% and achieved for the maximum amount of measurement data (K=64, H=300). Like for the characterisation of the hydraulic conductivity and the hydraulic head field, the *AESD* reduction is less than the *AAE* reduction. For the characterisation of the K and h fields the difference between the *AAE* and *AESD* reduction was small, but for the particle arrival location the difference is bigger. Due to the fact that in this case again an irregular reduction in the characterisation measure as function of the amount of measurement data is found, it is not possible to draw conclusions from this observation.

4.1.5 Results for conceptual errors

The conditioning is also carried out for erroneous boundary conditions and an incorrect variogram. These scenarios are not discussed in section 4.2 because they are considered conceptual model errors instead of measurement errors. The boundary conditions (even the prescribed heads along Dirchlet boundaries) are not measured, although they may be indirectly obtained from measurement data. The variogram mistake could be studied in the context of the measurement data. It would be necessary to estimate the variogram from the sample data set, condition 100 realisations and repeat this exercise a number of times for the same amount of conductivity data, but different sample

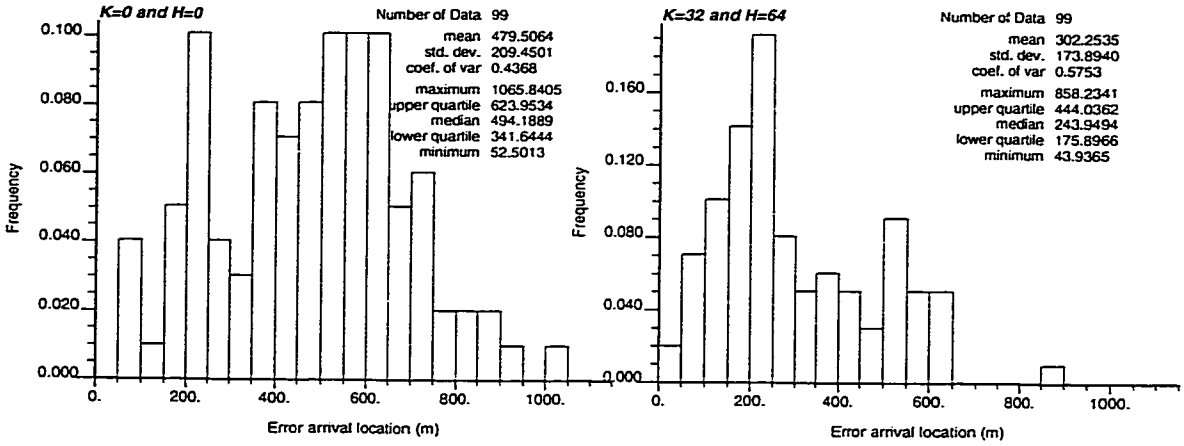

Figure 4.5 Histogram of the distances (in metres) between the simulated arrival locations and the reference arrival location. The ensemble statistics do not coincide with Table 4.3 because in Table 4.3 the difference between the ensemble averaged arrival location and the reference location is calculated and here the absolute differences for the individual realisations. (left) Histogram for the scenario with K=0 and H=0. (right) Histogram for the scenario with K=32 and H=64.

configurations. Here the aim was simpler; study the impact of a wrong variogram. We do not mind whether the variogram mis-specification is due to sample fluctuations or a wrong expert estimate.

Two errors in the boundary conditions are studied. The first is the specification of prescribed head boundaries along all the sides of the cube (scenario Flow.1). In reality just on the top and the bottom of the domain prescribed head values are imposed. The prescribed heads on the other four boundaries decrease linearly from 28 m on the top surface until 0 m on the bottom in the scenario Flow.1. The second error on the boundary conditions that is studied is an error in the prescribed head values on the top surface of the model; in reality the head is 28 m while in this scenario the head is 30 m (scenario Flow.2). In both scenarios the conditioning is carried out allowing the head values along the boundaries to change. In the first case the change of the prescribed head values along the boundaries could result in a non-linearly varying head value along the four sides of the model. This could be more in correspondence with the real flow system in spite of the fact that a fundamental mistake is made in the physical behaviour of the system. In the second case the prescribed head values on the top surface of the model could decrease from the specified value of 30 m to the real value of 28 m. Both in the scenarios Flow.1 and Flow.2 100 master blocks are located on the boundaries. The maximum allowed head change is 3.0 metres. In both scenarios 32 hydraulic conductivity and 64 hydraulic head data are used in the conditioning.

	AAE(*Y*) (m/s)	*AESD*(*Y*) (m/s)	*AAE*(*h*) (m)	*AESD*(*h*) (m)
K=32,H=64	0.95	0.96	0.40	0.46
Flow.1	0.96	0.97	0.52	0.48
Flow.2	0.94	0.96	0.46	0.51
Vario.1	0.92	0.75	0.39	0.38

AAE (m)	*AAE*(X) (m)	*AESD*(X) (m)
K=32,H=64	0.34	0.96
Flow.1	0.34	0.86
Flow.2	0.33	0.95
Vario.1	0.19	0.80

Table 4.4. Logconductivity, hydraulic head and particle transport characterisation measures. *AAE* is the average absolute error and *AESD* is the average ensemble standard deviation. The results are standardised by setting *AAE* and *AESD* to 1.0 for the scenario with no data (K=0 and H=0).

Table 4.4 summarises the results of this simulation exercise. The characterisation of the hydraulic conductivity is hardly influenced by the errors on the boundary conditions. The characterisation of the piezometric heads is more affected by the errors. For scenario Flow.1 the *AAE*(*h*) is the same as for K=32, H=32. In other words, the use of prescribed heads along the four sides of the cube instead of impermeable boundaries has the same effect as reducing the amount of head data by half. Nevertheless, the calibration of those prescribed heads along the four sides of the cube modifies the head values near the boundaries; the heads near the boundaries are closer to the reference head values after the calibration than before the calibration. The *AESD*(*h*) increases less than the *AAE*(*h*). For the scenario Flow.2 the *AAE*(*h*) increase is half as big as for the scenario Flow.1. The fact that the *AAE*(*h*) increase is less seems logical, because just 900 grid cells (the top plane of 30 x 30 cells) instead of 1800 grid cells (four planes of 30 x 15 cells) are affected by an error. The ensemble averaged average head difference between the top plane and the bottom plane reduces from 30.0 m until 29.3 m during the conditioning. In reality the difference is 28.0 metres. The *AESD*(*h*) increase is bigger for the scenario Flow.2 than for the scenario Flow.1. Nevertheless, the *AESD*(*h*) is still below the *AESD*(*h*) for the error-free scenario with K=32 and H=32. As the errors in the boundary conditions have no effect on the characterisation of the hydraulic conductivity field, but result in a worse characterisation of the hydraulic head field it would be expected that also the transport characterisation is worse. However, the average absolute error in the particle arrival location and its average ensemble standard deviation are not significantly modified. For the scenario Flow.1 an improvement is achieved, while for scenario Flow.2 the outcomes of the characterisation measures are similar. It is believed that the sample fluctuation error explains the observed behaviour. If many different transport experiments would be carried out for the same scenario a bigger error

on the estimation of the arrival location and a more elevated average ensemble standard deviation would be expected.

In the scenario Vario.1 the used range is double as compared with the range value of the model variogram. This is the only difference with the standard simulations and again 32 hydraulic conductivity data and 64 hydraulic head data are used as conditioning data. The too long range has not a negative impact on the characterisation of the hydraulic head and hydraulic conductivity field. On the contrary, the characterisation of the hydraulic head and the hydraulic conductivity field improve slightly as compared with the scenario with the same amount of conditioning data and the correct variogram. This is not in correspondence to what would be expected and also explained by sample fluctuation. On the other hand, it may also indicate robustness of the characterisation of the conductivity and head field on errors in the variogram. The average ensemble standard deviation decreases even significantly. This decrease can be explained by the fact that the ensemble of seed hydraulic conductivity fields has a lower standard deviation due to the enhanced spatial continuity. Also the updated hydraulic conductivity fields maintain this characteristic, because the same variogram is used to interpolate the perturbations. The lower ensemble standard deviations for the hydraulic conductivity affect to some extent, through the groundwater flow equation, also the ensemble standard deviation of the hydraulic heads.

Finally, the variograms of the seed conductivity fields and the updated conductivity fields are compared with the variogram for the reference field. The averaged ensemble semi-variances are calculated for three directions (x, y and z) and for 17 distance classes. All these averaged ensemble semi-variances are compared with their equivalents for the reference field. For each distance class the mean squared error (between the semi-variances for the reference field and the semi-variances for the realisations) is calculated and for the three directions (x, y, z) the average of the different mean squared errors is calculated. For the x-direction the initial mean squared error, averaged over 17 distance classes is 0.328. After calibration it is 0.314. For the y-direction the initial averaged mean squared error is 0.278 and the final mean squared error is 0.220. For the z-direction the initial averaged mean squared error is 0.249 and the final mean squared error is 0.270. The general conclusion is that the characterisation of the conductivity variogram is slightly better after calibration, through the influence of the head conditioning data. The mean squared errors of the semi-variances decrease (during the inverse modelling) for the x- and y-direction for the lags of less than 500 metres and for the z-direction for lags of less than 200 metres. This shows that indeed the semi-variances for distances below the range value are closer to the semi-variances of the reference field.

4.1.6 Discussion

From the results of the synthetic study it can be concluded that both hydraulic conductivity and hydraulic head data help in reducing the uncertainty on

groundwater flow and mass transport. However, the uncertainty on the hydraulic head field and the prediction of particle transport paths is reduced much stronger than the uncertainty on hydraulic conductivity. Can this conclusion be generalised?

In section 3.6 it is shown that the *AAE* of transmissivity is between 10% and 16% lower after the additional conditioning to 34 steady-state head data (compared with a scenario of zero conditioning data and using in both cases 36 transmissivity data). The *AAE* of steady-state hydraulic head reduces between 34% and 73%; a much more significant reduction. Therefore, also in the study presented in section 3.6 it was found that the inverse conditioning to steady-state heads has a stronger impact on the characterisation of the head field than on the characterisation of the conductivity field. However, in the study presented in section 3.6 the *AAE* reduction of transmissivity due to the conditioning to steady-state head data was stronger than in the synthetic study presented in this section. The difference may be due to specific circumstances related to the synthetic study. A factor of importance may be that all the boundary grid cells are prescribed heads in the study of section 3.6, while in the study of section 4.1 most of the boundary grid cells are impermeable. Wen *et al.* (1996) carried out a similar study in a 2-D domain. They found that in case of a sufficient number of transmissivity data (15 or 20 in that study) the additional *AAE*(*Y*) reduction by conditioning to steady-state head data was limited. The inverse conditioning on hydraulic head data had a much stronger impact on the characterisation of the head field than on the characterisation of the transmissivity field. Nevertheless, the *AAE*(*Y*) reduction found by them in case of conditioning to steady-state head data was stronger than in the synthetic study presented in this section. Wen *et al.* (1996) also used prescribed head values along all boundaries. Hughson and Gutjahr (1998) also found that conditioning to steady-state head data (in a stochastic inverse framework) had a stronger impact on the characterisation of the head field than on the transmissivity field. The additional conditioning to 16 steady-state head data (after a previous conditioning to 16 transmissivity data) resulted in an *AAE*(*h*) reduction of 79% and an *AAE*(*Y*) reduction of 31%.

For the study presented in section 3.6 the amount of conditioning transmissivity data was constant, so that the trade-off between the transmissivity data and the head data could not be investigated in that study. Therefore, it can not be checked whether, like in this synthetic study, the hydraulic conductivity data have less impact on the characterisation in general. The 2-D synthetic study by Wen *et al.* (1996) also investigated the trade-off between hydraulic head data and transmissivity data. The results they obtain are comparable with the results obtained in this synthetic study in the sense that the hydraulic head data contribute more to the characterisation of the fields than the transmissivity data. However, the transmissivity data were found to have more importance than in this synthetic study.

Gutjahr *et al.* (1994), Wen *et al.* (1996), Hughson (1997) and Hughson and Gutjahr (1998) investigated also the impact of the amount of conditioning data on the characterisation of transport. Wen *et al.* (1996) found somewhat different results as compared with this synthetic study. The estimation of particle arrival locations is both improved by transmissivity data and hydraulic head data, probably associated with the more significant $AAE(Y)$ reduction in that study. Wen *et al.* (1996) do not obtain an improved estimation of the travel times by the inverse conditioning. Hughson and Gutjahr (1998) and Hughson (1997) report that head conditioning data especially help to improve the estimation of the particle travel paths and the particle arrival locations. The head data help less in the estimation of the particle arrival times. Gutjahr *et al.* (1994) found that head data improve the estimation of the particle travel paths, while transmissivity data hardly help to improve the estimation of the travel paths. Also in that study it was found that head data just result in a marginal improvement of the estimated particle travel times. In general, consistent results are obtained in different synthetic studies on the stochastic inverse modelling of groundwater flow. Head data mainly help in improving the characterisation of travel paths and particle arrival locations. Head data have little impact on the estimation of particle travel times. Transmissivity data, on the contrary, hardly improve the estimation of travel paths, but have more value for estimating the particle travel times. For this 3-D synthetic study the conclusions are similar, with the only difference that the relative importance of head data (as compared with conductivity data) is even a bit bigger.

In the design of a sampling scheme in a groundwater flow study these findings could be used. However, not only the data worth but also the costs of each measurement should be taken into account. A combination of a prior estimation of the uncertainty reduction and a prior estimation of the costs of a measurement campaign (including personnel costs etcetera) could be used to estimate the optimal number of each type of measurements. A prior estimation of the uncertainty reduction for different sample schemes could be obtained by means of a synthetic study that is thought to resemble the studied aquifer. An optimisation routine can determine the optimal measurement strategy or simply select the best measurement strategy from a limited number of alternatives. In more advanced studies not only the amount of hydraulic conductivity and hydraulic head data but also their spatial configuration should be taken into account. However, the synthetic study should be limited in the number of scenarios because the needed CPU-time may exceed the computer capacities.

Multiple synthetic studies will give us more insight in the complex relationships between amount and configuration of the measurement data, variogram parameters, boundary conditions, recharge or leakage and the uncertainty in the prediction of groundwater flow and mass transport. The application of a sophisticated strategy in the data selection, based on an optimisation of the expected uncertainty reduction per cost unit, will also give

new information and experience on network design and the relationships between the data and the uncertainty in the predictions.

4.1.7 Conclusions

The conditioning of multiple realisations on steady-state head measurements (inverse modelling) yields an improved characterisation of both the hydraulic conductivity and hydraulic head field. The average absolute error decreases as function of the amount of measurement data. The steady-state head data have much more impact on the characterisation of the head field than on the characterisation of the hydraulic conductivity field.

The conditioning on steady-state head data also yields a reduction in the average ensemble variance of the hydraulic head and hydraulic conductivity field. Also in this case the impact on the uncertainty reduction of the hydraulic head field is much stronger than the impact on the hydraulic conductivity field.

The conditioning to hydraulic conductivity data helps mainly to reduce the average absolute error and the average ensemble standard deviation of the hydraulic conductivity field. The impact of the hydraulic conductivity data is in general less than the impact of the hydraulic head data, but this may depend on the case.

Conditioning to steady-state head data and hydraulic conductivity data reduces the average absolute error in the prediction of the particle arrival locations. The prediction of the particle arrival times is not improved. It is found that hydraulic head data have an important influence on the prediction of the particle travel paths while hydraulic conductivity data are more important for the prediction of travel times.

The calculations for a scenario with a wrong variogram model (double range) show the robustness of the simulation outcomes for errors in the variogram parameters. However, more study is needed to investigate this robustness; the outcomes may be strongly affected by sample fluctuations and different results may be obtained for other parameter configurations. The study also shows that head data could help to improve the characterisation of the conductivity variogram.

The characterisation of the hydraulic head field is more affected by a mis-specification of the boundary conditions. We will see in section 4.2 that even an (unbiased) average head measurement error of 1.0 metre or an (unbiased) average hydraulic conductivity measurement error of 0.5 $\log_{10}$ units have less impact on the characterisation of the hydraulic head field than the errors in the boundary conditions presented in this section. Nevertheless, the results were found to be relatively robust for the studied errors in the boundary conditions.

4.2 Impact of the quality of conditioning data

The aim of the sequential self-calibrating method (SCM) for the stochastic inverse modelling of groundwater flow and/or contaminant transport is to generate an ensemble of equally likely realisations of hydraulic conductivity (and possibly other parameters) and their corresponding hydraulic heads. All the realisations should be consistent with a prior model of spatial variability, generally given by a variogram function, and reproduce measurement data like hydraulic conductivities, hydraulic heads and possibly other data. It is expected that the more experimental data are used for the conditioning of realisations, the closer the ensemble mean of the realisations to the real values should be. The quality of the final characterisation of the conductivities and head (and possibly other parameters) depends largely on the amount and quality of the measurement data. In this context, it is important to know the quality of the measurement data (maybe through an estimate of the measurement error standard deviation) and to take into account the measurement errors in the stochastic inverse modelling procedure.

A good way to analyse the impact of the measurement errors in inverse modelling is by means of synthetic studies. However, little attention has been paid to the impact of erroneous measurement data. We are not aware of any paper on inverse modelling which focused primarily on the impact of measurement errors, and particularly, that analysed the potential bias introduced by considering erroneous data as error-free. In some synthetic studies an inverse parameter estimation is carried out with corrupted head and transmissivity data (Kitanidis and Vomvoris, 1983; Carrera and Neuman, 1986c). However, these papers just shown how a single best estimate of the groundwater flow parameters and its estimation variance are affected by these measurement errors, but no comparative studies are presented. Anderman and Hill (1999) use corrupted concentration data for conditioning in a Monte Carlo based approach, and they conclude that accounting for measurement errors yields less accurate results. Sun *et al.* (1998) identify diverse parameters in a synthetic study imitating a remediation design problem, with and without measurement errors. The authors conclude that the measurement errors have only a secondary effect on the results, while model structure errors (such as incorrect zonation of the aquifer) are much more consequential. Finsterle and Najita (1998) propose alternatives to the standard least-squares formulation of the inverse problem. They argue that the least-squares formulation is more susceptible to outliers introduced by measurement errors. They test the performance of different estimators in a synthetic study with non-Gaussian random errors and systematic modelling errors.

In the above referenced studies, the error analysis is limited to comparing one or two scenarios with and without measurement errors, but no analysis of the modeler decision with respect to the measurement errors is done. In practice, the modeler always has to assess the uncertainty on the measurement data, and

the correctness of his or her decision may have an important impact. Therefore, we focus here on the impact of the measurement errors, and especially, on the differences between recognizing and modeling this error, and neglecting the error, thus incorrectly considering the data as error free. This section also analyzes cases with two different sources of error. The errors are in all cases uncorrelated Gaussian noise with zero mean. Considering the errors as Gaussian is typically justified by the central limit theorem; multiple random measurement errors tend to converge to a normal distribution. However, we think that the issue of systematic, correlated and/or not normal distributed errors is important, and could be an interesting theme for future research.

Two extensive synthetic studies are presented in which the impact of measurement errors is analyzed. The reference fields are moderately to strongly heterogeneous hydraulic conductivity fields. The paper focuses on the way the measurement errors are treated, distinguishing between two main scenarios: (1) the modeler assumes the data are error free when they are not, (2) the modeler recognizes that the data have measurement errors, makes an estimation of their magnitude, and accounts for them in the simulation. Apart from this, the main differences between the scenarios are the magnitude of the measurement errors and the measurement error sources (hydraulic head and/or hydraulic conductivity). A sufficiently large number of equally likely conductivity fields is generated and the outcomes are analyzed in terms of both the ensemble means (and its departure from the reference fields) and the ensemble standard deviations.

4.2.1 Modelling measurement errors by sequential self-calibration

As compared to the procedure outlined in section 3.2 some specifications have to be made to indicate how measurement errors are handled in the sequential self-calibrating method.

In the first step to be taken in the sequential self-calibrating approach, the generation of the permeability field, conductivity measurement errors are taken into account, by properly modifying the right-hand side of the kriging system used to determine the local conditional cumulative distribution functions during the sequential visit of all nodes in the sequential simulation algorithm.

Conductivity measurement errors also affect the interpolation of the perturbations. At each grid cell a maximum and minimum allowed Y value are set, equal to the kriged Y value plus or minus three times the kriging standard deviation (see section 3.2). It is through the kriging standard deviation, which is affected by the error measurements, that these are considered in the optimization process. (Notice also, that at data locations, the kriging standard deviation is equal to the error standard deviation; therefore allowing the final conditional field to depart from the seed field at data locations.)

The head measurement errors can be taken into account by setting the tolerance value proportional to the measurement error. Remember that if the objective function value is smaller than a user-predefined tolerance value, the field is considered to be conditional to the piezometric head values, otherwise the algorithm proceeds. The tolerance value should be set considering the magnitude of the head measurement errors. To be more precise, the tolerance value is proportional to the variance of the head measurement error. Also, the weights used to compute the objective function can be used to discriminate between measurements with different measurement errors. In case of large measurement errors, the measured heads do not need to be reproduced perfectly. On the contrary, if the measurement errors are not taken into account to set the tolerance limit, it is expected that the closer reproduction of the erroneous head measurements will yield worse results.

4.2.2 Synthetic studies

The impact of measurement errors in either or both hydraulic conductivity and hydraulic head on the characterization of the ensemble of Y and h fields is studied in two different synthetic studies. The first study is two-dimensional. The main part of the second synthetic experiment was already presented in section 4.1. Here we present the results related to the corrupted measurements. In both studies, the hydraulic head field is at steady-state.

4.2.2.1 2-D synthetic study

The reference Y field is multiGaussian with a mean of –7.0 and an isotropic variogram with zero nugget, sill of 1.5 $(\log_{10} m^2/s)^2$ and range of 150 m. It is generated over a grid of 50 by 50 square cells, covering an area of 500 by 500 m. The solution of the groundwater flow equation in the reference Y field, with no-flow boundaries at the east and west boundaries and prescribed uniform heads in the north and south boundaries imposing a 0.01 m/m gradient that makes water flow from south to north, provides the reference h field. Both reference fields are sampled randomly for 35 collocated Y-h sample pairs. Figure 4.6 shows the reference Y and h fields. These samples are error-free data. When erroneous data are needed, a random Gaussian noise of zero mean and given standard deviation is added to the sample data.

The different scenarios studied in this synthetic study are summarised in Table 4.5. The inverse modelling in scenario 1 is carried out using error-free data, and the results are measured to assess the impact of error measurements in the remaining scenarios. The different scenarios combine measurement errors on hydraulic conductivities and hydraulic heads, the magnitude of the errors is also varied, and whether they are properly accounted for or not. The following is an explanation of the rationale behind each scenario. Scenarios 2 and 5 study the impact of errors only in head measurements. The difference between the

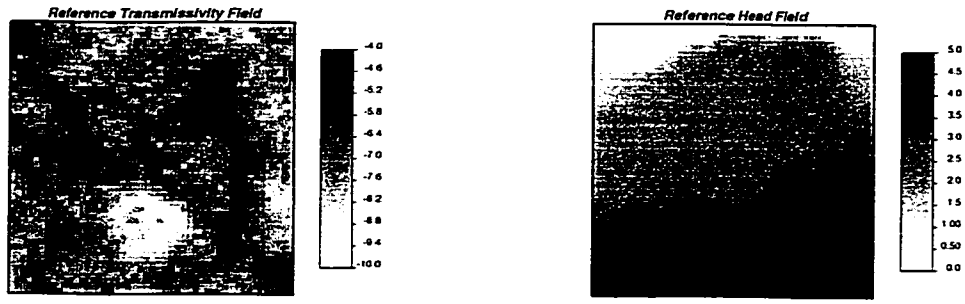

Figure 4.6. Reference log transmissivity and hydraulic head field for the 2-D synthetic study.

Scenario	Meas. Std. Dev. h	Modelled error h?	Meas. Std. Dev. Y	Modelled error Y
1	0		0	
2.1	0.25	Correct	0	
2.2	0.25	Wrong (bit)	0	
2.3	0.25	Wrong	0	
3.1	0		0.5	Correct
3.2	0		0.5	Wrong
4.1	0.25	Correct	0.5	Correct
4.2	0.25	Wrong	0.5	Correct
4.3	0.25	Wrong	0.5	Wrong
5.1	1.00	Correct	0	
5.2	1.00	Wrong	0	
5.3	1.00	Correct	0	
6.1	1.00	Correct	0.5	Correct
6.2	1.00	Wrong	0.5	Correct
6.3	1.00	Wrong	0.5	Wrong

Table 4.5. The scenarios studied in the first (2-D) synthetic study. The table makes reference to "wrong" or "correct" modelling of the measurement errors. In case of hydraulic head measurement errors tolerance values of 2.35 and 35 are used for error standard deviations of 0.25 and 1.0 respectively. In case the head errors are not modelled correctly the tolerance values are 0.35 and 2.35 for error standard deviations of 0.25 and 1.0 respectively. See the text for the procedure in the "wrong" and "correct" modelling of transmissivity measurement errors.

scenarios is the magnitude of the standard deviation of the Gaussian distribution from which the errors are drawn: 0.25 m for scenario 2, and 1.00 m for scenario 5. Scenario 3 studies the impact of errors only in logtransmissivity. Scenarios 4 and 6 study the impact of errors in both logtransmissivity and hydraulic head measurement. In the scenarios 5 and 6 it was necessary to allow for changes on the prescribed heads along the boundaries, in case the erroneous head measurements had to be reproduced close. For all scenarios a number of subscenarios is studied analyzing the impact of properly accounting for the measurement errors. The head measurement errors are properly accounted for when their error standard deviation is used to set the tolerance and to build the objective function that determines the stop of the iterations in the non-linear optimization process of the self-calibrating algorithm. The head measurement errors are not properly accounted for when the iterations in the non-linear optimization continue until the objective function (perfect reproduction of erroneous measurements) is zero or the maximum number of iterations is reached. The logtransmissivity measurement errors are properly accounted for when their variance is filtered out from the variogram and then they are considered to build the envelope of variability within which the resulting updated field must lie—perturbations at data locations are allowed by a magnitude proportional to the logtransmissivity measurement error. The logtransmissivity measurement errors are not properly accounted for when they are interpreted as short scale variability and their variance is not filtered out of the variogram—the perturbations at data locations are thus forced to be null.

For each scenario 100 seed logtransmissivity fields are generated conditional to the 35 sample logtransmissivity data and head data (with or without errors, properly accounting or not for the measurement errors, depending of the scenario). Next, the solution of the groundwater flow equation is obtained for each field. Then, the ensemble of conditional logtransmissivity and hydraulic head fields is evaluated by the average absolute error (*AAE*), and the average ensemble standard deviation (*AESD*). The smaller *AAE* and *AESD* are, the better characterised the transmissivity and hydraulic head fields are.

Table 4.6 summarises the *AAE* and *AESD* for all the scenarios. The upper part of the table gives the information to study the impact of hydraulic head measurement errors and the way they are modelled. From this information two main conclusions can be drawn:

(1) An increase in the hydraulic head measurement errors results in a worse characterisation of the average ensemble head and transmissivity field. The ensemble standard deviations increase.
(2) The increase of the *AAE* is more pronounced in case the hydraulic head measurement errors are neglected by the modeller.

	AAE(h) (m)	*AESD*(h) (m)	*AAE*(Y) ($\log_{10}(m^2/s)$)	*AESD*(Y) ($\log_{10}(m^2/s)$)
Impact h measurement errors				
1	0.121	0.257	0.622	1.03
2.1	116 %	119 %	100 %	100 %
2.2	115 %	112 %	103 %	101 %
2.3	116 %	108 %	105 %	100 %
5.3	267 %	175 %	113 %	98 %
5.2	365 %	159 %	120 %	98 %
Impact Y measurement errors				
1	0.121	0.257	0.622	1.03
3.1	93 %	86 %	103 %	104 %
3.2	94 %	72 %	105 %	78 %
Impact h and Y measurement errors				
1	0.121	0.257	0.622	1.03
4.1	111 %	125 %	105 %	108 %
4.2	112 %	119 %	109 %	108 %
4.3	116 %	77 %	114 %	85 %
6.1	231 %	147 %	109 %	100 %
6.2	314 %	168 %	121 %	109 %
6.3	321 %	142 %	130 %	89 %

Table 4.6. The performance measures for the different scenarios in the first (2-D) synthetic study. The performance measures are expressed in a percentage as compared with scenario 1 (=100%), for which the absolute values are given.

From Table 4.6 it can be seen that even for the case with the smallest hydraulic head measurement error the average ensemble fields are less close to the reference fields in case the errors are not taken into account in the modelling. Although the *AAE* for hydraulic head does not differ between the scenarios 2.1, 2.2 and 2.3, the *AAE* for transmissivity is the lowest for scenario 2.1, higher for scenario 2.2 and the highest for scenario 2.3.

The incorrect modelling procedure has a much more pronounced effect in case of bigger measurement errors: the *AAE* for especially hydraulic head, but also transmissivity are clearly higher and thus worse for scenario 5.2 as compared with scenario 5.3. However, the *AESD* for head is lower in scenario 5.2 as in 5.3. The lower *AESD* for head shows that the ensemble standard deviation is lower

in case the erroneous data are reproduced closely and may indicate that not modelling the head measurement errors yields unrealistic low estimates of the ensemble standard deviations.

Figure 4.7 shows the calculated ensemble average head and transmissivity field for the scenarios 1, 2.1, 2.3, 5.2 and 5.3 and the ensemble standard deviations of head and transmissivity for the scenarios 1, 5.2 and 5.3. Figure 4.8 shows the transmissivities and heads for some of the realisations. It can be noticed, on one hand, that the average head and transmissivity maps differ more from the reference maps in case the head measurement error is bigger and in case the errors are not correctly modelled. The zones of the maps which show the most important deterioration going from scenario 1 (no measurement errors) until scenario 5.2 (the biggest errors, incorrectly modelled) correspond with the zones around the measurement observation points with the biggest measurement errors. In the corresponding transmissivity maps artefacts appear around these zones which are created by the inverse modelling procedure in order to reproduce the erroneous head data. The too close reproduction of erroneous head data results in the generation of multiple islands on the ensemble averaged maps. The artefacts are also visible on the individual realisations, the most clearly for scenario 5.2.

Table 4.6 also summarises the impact of transmissivity measurement errors on the *AAE* and *AESD*. Some main conclusions can be drawn:

(1) The transmissivity measurement error standard deviation of 0.5 $\log_{10}$ unit has not such a negative impact on the characterisation of the head and transmissivity field as a head measurement error standard deviation of only 25 cm.
(2) The incorrect modelling (neglecting) of the measurement errors yields also in this case the worse results. It is mainly the *AAE* for transmissivity which increases.
(3) Surprisingly, the *AESD* decreases significantly for the cases that the transmissivity measurement errors are not modelled.

It is found that the no modelling of transmissivity measurement errors, in which the calibration of the transmissivity field is more restricted yields worse results than in the case the error is taking into account. Again is found that a good estimation of the error standard deviation by the modeller is important for the best estimation of the head and transmissivity field. However, a stronger and also more surprising result is that the ensemble standard deviation decreases in case the errors are not modelled (compare the scenarios 3.1 and 3.2). We think that this could be explained by a combination of two effects. First, the perturbation of the transmissivity field is more limited than in the case the measurement errors are recognised by the modeller (see the explanation on SCM). Second, not allowing to change the transmissivity at the 35 measurement points and remaining the transmissivities there fixed to the corrupted data may reduce the freedom to reproduce with the incorrect transmissivity realisations

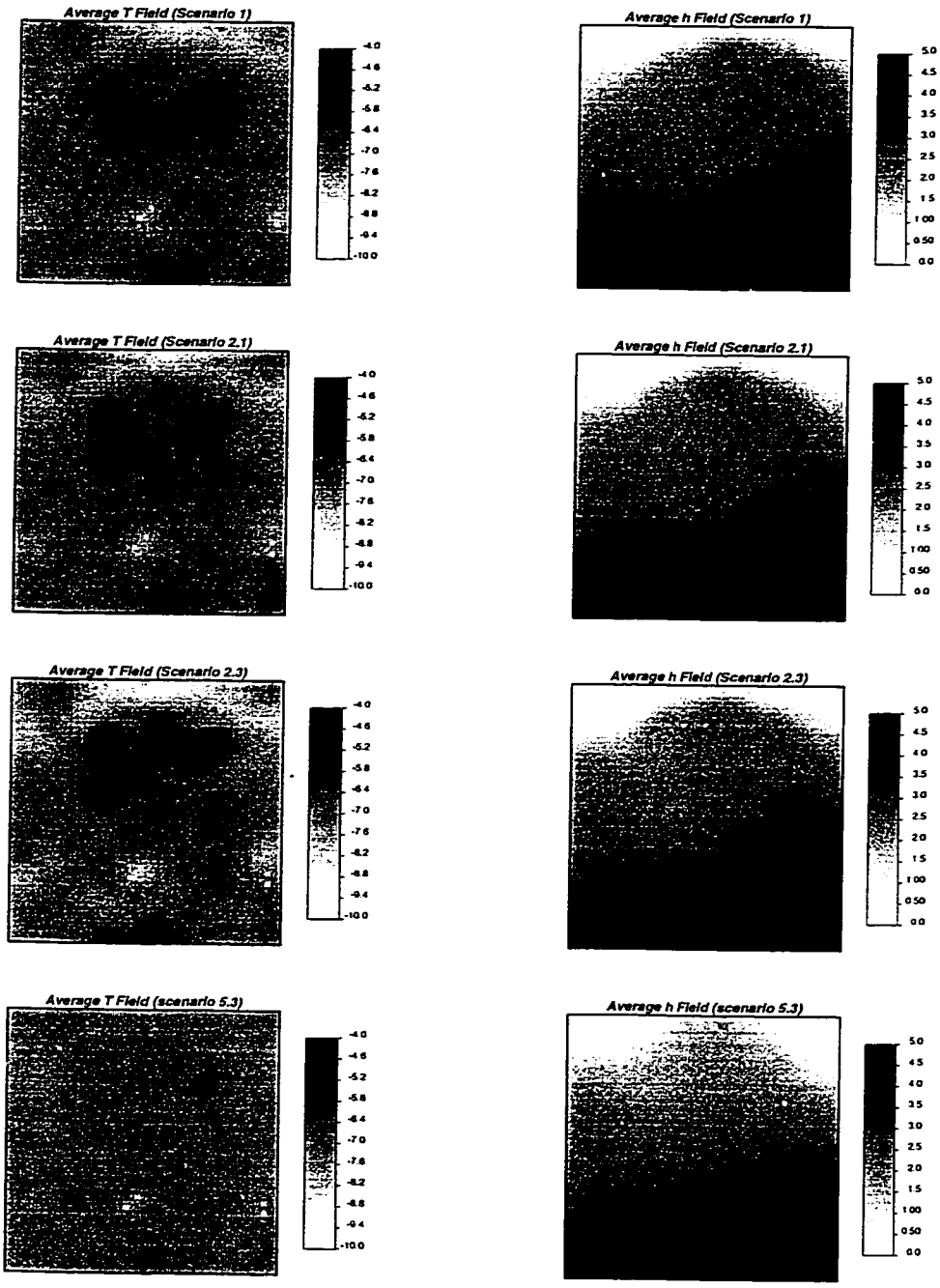

Figure 4.7 Ensemble average head and log transmissivity fields for some of the studied scenarios and ensemble standard deviations of log transmissivity and head for the scenarios 1, 5.3 and 5.2.

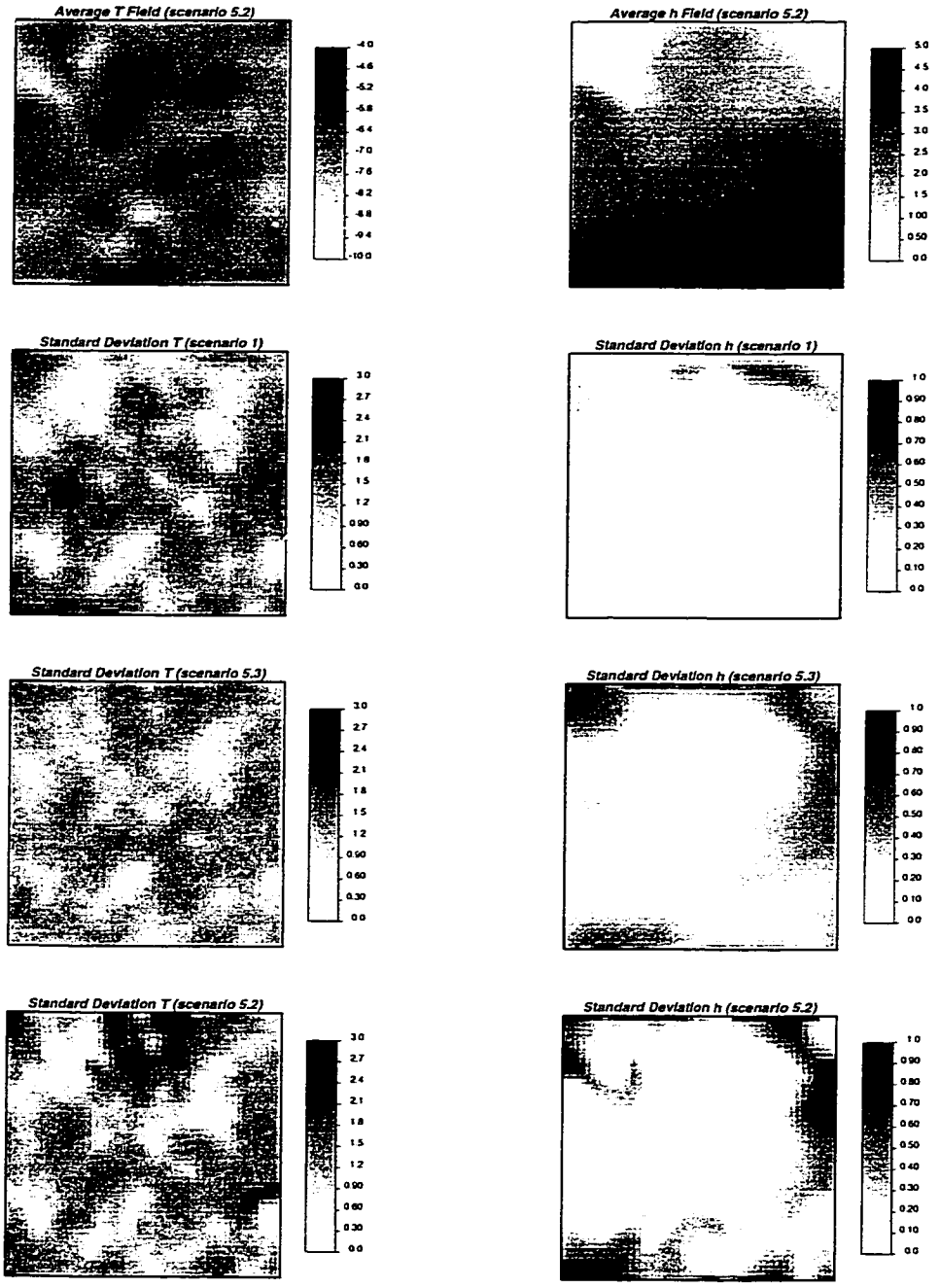

Figure 4.7 (continued). Ensemble average head and log transmissivity fields for some of the studied scenarios and ensemble standard deviations of log transmissivity and head for the scenarios 1, 5.3 and 5.2.

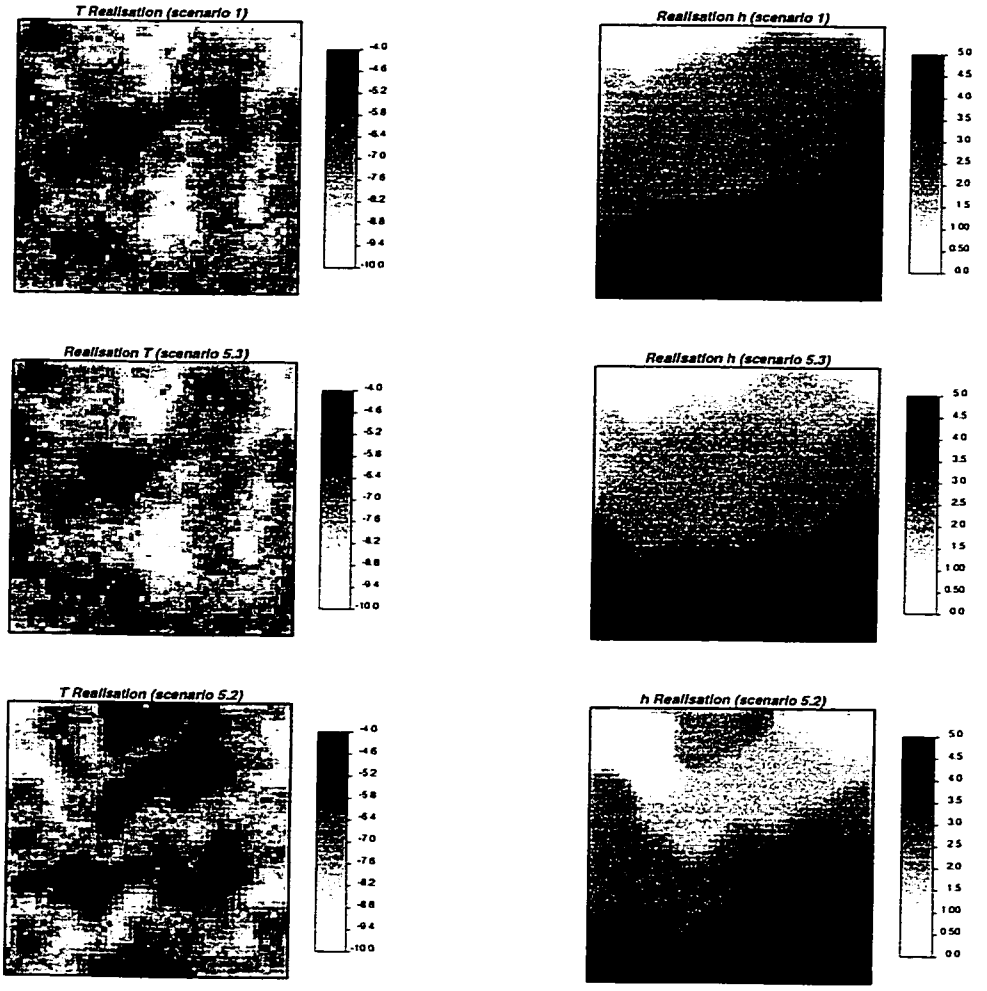

Figure 4.8 For each of the scenarios 1, 5.3 and 5.2 one realisation of head and log transmissivity is displayed. The realisations are conditioned to transmissivity and (probably erroneous) hydraulic head data. Notice the artefacts on the transmissivity field closely conditioned to erroneous head data (scenario 5.2).

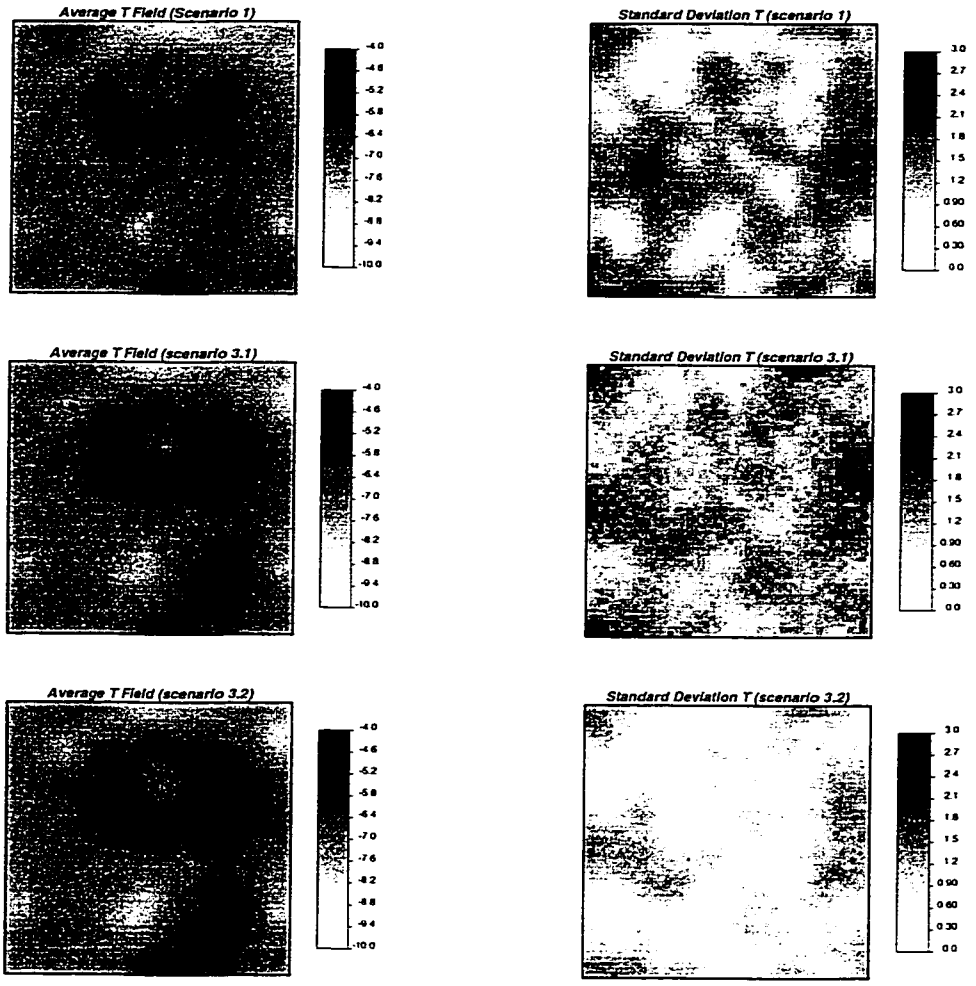

Figure 4.9 Ensemble average log transmissivity fields and ensemble standard deviations of log transmissivity for the scenarios 1, 3.1 and 3.2. Notice that the main difference between the scenarios 3.1 and 3.2 is in the ensemble standard deviations. The ensemble standard deviations are unreasonable low for scenario 3.2, in which the error of the transmissivity data is not modelled.

the head data so that the dispersion in the found solutions decreases. The *AESD* decrease is observed in all scenarios where transmissivity measurement errors are involved. It indicates that not modelling transmissivity measurement errors results in unrealistic low standard deviation estimates. If the transmissivity measurement errors are modelled, on the contrary, a slight increase of the *AESD* is observed (as compared to the scenario with no measurement error), which is according the expectations. The impact of the transmissivity measurement errors is relatively small and does not appear very clear on the

maps. Figure 4.9 gives the ensemble average and ensemble standard deviation transmissivity maps for the scenarios 1, 3.1 and 3.2.

In the scenarios 4 and 6 a combination of transmissivity and hydraulic head measurement errors is modelled. Again is found that not modelling the errors (scenarios 4.3 and 6.3) yields the worse results. The results indicate that the incorrect modelling of the head measurement errors affects both the characterisation of heads and transmissivities, while the no modelling of the transmissivity errors mainly influences the characterisation of the transmissivities negatively. The question can be posed whether the two sources of measurement errors show an interaction, which makes their impact different than the sum of the two. Scenarios 4.1, 4.2 and 4.3 show that for the identification of heads no interaction is found. The *AAE* increase of head for the different scenarios corresponds quite close with the sum of the *AAE* increases from the scenarios 2 (head measurement errors only) and scenario 3 (transmissivity measurement errors only). On the contrary, for transmissivity it is found that the impact of a combination of the two error sources results in a stronger *AAE* increase than would be expected on the basis of the simulations for the scenarios 2 and 3. The interaction of the two sources of measurement errors is stronger in case one or two of the measurement error sources are not modelled correctly. For scenario 6 the *AAE* increase of head is stronger than expected in case of scenario 6.1, but less than expected for the scenarios 6.2 and 6.3. Finally, the *AAE* increase of transmissivity is for the scenarios 6.1 and 6.3 again stronger than expected while for the scenario 6.2 the increase is close to what would be expected from the simulation outcomes of the scenarios 2 and 3. In summary, while for the head characterisation no clear interaction is found between head and transmissivity measurement errors, these errors tend to show a synergy in case of the characterisation of transmissivity.

4.2.2.2 3-D synthetic study with corrupted data

The 3-D synthetic study was already presented in section 4.1. In this section results are presented for this synthetic study in case corrupted data are used in the conditioning process. The aim is to verify the conclusions from the 2-D synthetic study. The head differences along the domain are considered to be more typical for a regional study. In section 4.1 more information on the synthetic study is given.

Eight scenarios are studied with corrupted hydraulic head measurements. Table 4.7 summarises some scenarios studied where 64 head data are corrupted with a normal distributed error with zero mean and standard deviation of 1 metre. Also 32 error-free conductivity data are used in the conditioning. The difference between the scenarios is the degree to which the erroneous head measurements are reproduced. In scenario 7.1 the modeller takes into account the measurement error and does not try to reproduce the experimental head data too close. However, in the scenario 7.2 and especially 7.3 the modeller aims

Scenario	*Meas. Std. Dev. h*	*Modelled error h?*	*Meas. Std. Dev. Y*	*Modelled error Y*
Default	0		0	
7.1	1.0	Correct	0	
7.2	1.0	Wrong (bit)	0	
7.3	1.0	Wrong	0	
8.1	0		0.5	Correct
8.2	0		0.5	Wrong
8.3	0		2.0	Correct
8.4	0		2.0	Wrong

Table 4.7 The scenarios studied in the 3-D synthetic study. In the default scenario 32 error free hydraulic conductivity and 64 hydraulic head samples are taken. In the rest of the scenarios the same amount of samples is taken, but the head or conductivity samples are corrupted. The table makes reference to "wrong" or "correct" modeling of the measurement errors. In case of the hydraulic head measurement error the tolerance value is 80 in case of a correct modeling procedure and 40 for scenario 7.2 and 20 for scenario 7.3. See the text for the procedure in the "wrong" and "correct" modeling of the hydraulic conductivity measurement errors.

Scenario	*AAE(h) (m)*	*AESD(h) (m)*	*AAE(Y) (log_{10}(m/s))*	*AESD(Y) (log_{10}(m/s))*
Default	1.15	1.59	0.94	1.20
Impact h measurement errors				
7.1	108 %	104 %	100 %	99 %
7.2	107 %	100 %	100 %	99 %
7.3	107 %	100 %	100 %	102 %
Impact Y measurement errors				
8.1	100 %	101 %	101 %	105 %
8.2	100 %	98 %	100 %	98 %
8.3	103 %	130 %	105 %	181 %
8.4	106 %	104 %	115 %	102 %

Table 4.8 The performance measures for the different scenarios in the 3-D synthetic study. The performance measures are expressed in a percentage as compared with the default scenario (=100%), for which the absolute values are given.

at reproducing the erroneous head data too close. The results are compared with the default scenario where the same amount of error free measurement data is used in the conditioning process. Table 4.8 gives the performance measures of the simulations. From Table 4.8 it can be concluded that the measurement errors, first of all, have little impact and second, that the impact of the modelling (scenarios 7.2 and 7.3 versus 7.1) influences even less. The head measurement errors only result in an increase of the *AAE* of head, while the other measures do not change significantly. This increase is not very significant if we compare it with the impact of the amount of error free head samples on the *AAE* of hydraulic head. If we compare the results for scenario 7.2 with the results for scenario 7.1 we find even some small improvements (lower *AESD* for hydraulic head) and the supposed too close reproduction of the head data does not affect negatively the characterisation of the head and conductivity fields. For scenario 7.3, with an ever more close reproduction of the erroneous head data, the only change is an increase of the *AESD* for hydraulic conductivity. It may be a first indication of a worse identification of the reference fields due to the too close reproduction of erroneous data, but it is in any case not very convincing. The fact that a same head measurement error of 1.0 metre has such a different effect in this 3-D synthetic study than in the 2-D synthetic study we attribute to the following reasons:

(1) In the 3-D study the head difference is 28 m along 750 m vertical direction. In the 2-D study the difference was 5 m along 500 m horizontal direction. In the last case the impact of a measurement error of 1 m is much bigger than in the first case. It seems logical that the head error has to be compared with the scale of the study and the head differences along the domain in order to predict the impact of the head measurement errors.

(2) The reproduction of the heads does not increase as much as would be expected from the set tolerance value. In case of the too low tolerance values (scenarios 7.2 and 7.3) the number of cases increases that the conditioning of a realisation is terminated due to incremental convergence or a maximum number of iterations. This can be seen for example if we calculate:

$$AAE(X) = \frac{1}{MEASPTS} \sum_{i=1}^{MEASPTS} \left| \overline{X}_{SIM\,i} - X_{MEAS\,i} \right|$$

In this case the difference is calculated between the average head at a location over the 100 realisations and the measurement datum at that location, *MEASPTS* being the number of measurement points. *AAE*(*X*) is 0.58 m for scenario 7.1, 0.37 m for scenario 7.2 and 0.35 m for scenario 7.3. Hardly a difference is found between scenario 7.2 and 7.3 in the reproduction of experimental head data and also the decrease in *AAE*(*X*) between scenarios 7.1 and 7.2 is less than would be expected. The calibration in case of scenarios 7.2 and, especially, 7.3 terminates frequently due to incremental convergence. It is found that in case of the corrupted data the algorithm has more problems in reproducing the experimental data, although the experimental head data are still reproduced reasonably well.

However, the worse reproduction of the corrupted head data makes that the maps are not influenced so negatively by the corrupted head data as could be expected.

In summary, the main reason for the much more negative impact of the same head measurement errors in the 2-D synthetic study than in this synthetic study are the smaller head differences along the simulation domain and the smaller head gradients. However, also a numerical effect (the termination of the calibration due to incremental convergence) made that the negative impact of the head measurement errors in this synthetic study was somewhat less than it could have been.

Also four scenarios were studied with corrupted hydraulic conductivity measurements. See Table 4.7 for the studied scenarios. In all cases 32 hydraulic conductivity measurements are corrupted with a normal distributed noise with zero mean and standard deviation of 0.5 or 2.0 $\log_{10}$ (m/s). The 64 head measurements are error-free. For the case of an error standard deviation of 0.5 $\log_{10}$ (m/s) the effects are minimal. In case a correct modelling procedure is applied only the *AESD* for hydraulic conductivity clearly increases. The error of 2.0 $\log_{10}$ (m/s) has a more pronounced effect and in case of a correct modelling procedure the *AESD* of hydraulic head and especially hydraulic conductivity increase very significantly. The *AAE* of head and conductivity just increase marginally, in spite of the apparent big measurement error. An incorrect modelling procedure hardly results in an *AESD* increase, so that the *AESD* then are much lower than the *AESD* obtained in the correct modelling procedure. We see again, like in the 2-D synthetic study, that an unrealistic low standard deviation is obtained in case the hydraulic conductivity measurement errors are not modelled. The *AAE* are bigger in case of the incorrect modelling procedure as compared with the correct modelling procedure, which confirms the results from the 2-D study. Nevertheless, the differences are not very big in spite of the big measurement errors and the main consequence of the no modelling of hydraulic conductivity measurements errors are unrealistic low estimates of the ensemble standard deviations.

4.2.3 Discussion

It has been shown that it is important to make a correct estimate of the hydraulic conductivity/transmissivity measurement error variance and the hydraulic head measurement variance. In case a correct estimate is made the simulation outcomes are more favourable than in the same case in which the measurement errors are not modelled. Therefore the estimation of the measurement error variances is an important step in the SCM. Expert knowledge on the estimation of the measurement errors can be obtained from practitioners for instance. The hydraulic head measurement error variance may depend to a great deal on the measurement conditions. Measuring piezometric head in an unconfined shallow aquifer has a very minimal error, while

measuring piezometric head in a deep rock formation may be associated with a bigger measurement error. Hydraulic conductivity measurements or hydraulic conductivities obtained from hydraulic tests are in general more suspectable to errors. We think that the field specialists are the persons who overview the best the different sources of errors in the measurements from which an estimation of the magnitude of the error can be made. The more data incorporated in the stochastic inverse modelling and the better the estimate of the quality of the data, the better the identification of aquifer parameters like transmissivity/conductivity and storativity.

A way to study the impact of head measurement errors in a case study would be to make a little synthetic study with similar head differences along the domain as in reality and conductivities and conductivity standard deviations which are thought to be realistic. Multiple simulations could be generated for different scenarios, the difference between the scenarios being the magnitude of the measurement error.

However, also without such a detailed pre-study an insight on the estimation of the possible impact of the measurement errors could be obtained. This insight could be obtained by a combination of the estimation of the measurement error variances and the head gradients along the domain. For example, in case the transport of particles under natural flow conditions in a low permeable rock formation has to be predicted, on a scale of some tens of metres and just small head differences, the impact of measurement errors may be important. On the contrary, in case the groundwater flow in a shallow aquifer to a pumping well has to be predicted, with an important head gradient induced by the pumping the impact of head measurement errors is expected to be of little importance.

4.2.4 Conclusions

In the 2-D synthetic study presented in this article it is found that both hydraulic head and transmissivity measurement errors result in a worse identification of the reference fields as compared with a situation with the same amount of error-free samples. In both cases the characterisation of the hydraulic head and transmissivity reference fields is better in case the modeller estimates correctly the measurement error variance and takes into account the measurement errors in the modelling as outlined in the article. The worse characterisation of the transmissivity and head fields for the case that the modeller tries to reproduce the erroneous head data is visible on the transmissivity maps in the form of artefacts. In case the transmissivity measurement errors are not modelled the ensemble standard deviation of transmissivity becomes unrealistic low. The synthetic study does not clearly reveal the existence of an interaction between hydraulic head measurement errors and transmissivity measurement errors. In the simulated scenarios with both head and transmissivity measurement errors the impact of the different

sources of error on the transmissivity field characterisation was bigger than the sum of the individual impacts.

The 3-D synthetic study shows that the impact of the measurement errors is related to the head differences along the domain. In the 3-D study the ratio between the head measurement errors and the head differences along the domain is less than in the 2–D study and the head measurement errors hardly affect the characterisation of the head and transmissivity fields. The simulations also show that the hydraulic conductivity measurement errors and the way they are modelled have an impact on the identification of the head and conductivity fields. However, the impact on the estimation of the ensemble averaged fields is relatively little. The estimation of the ensemble standard deviations is much more affected by the modelling procedure. In case the conductivity measurement errors are not modelled the conductivity ensemble standard deviations are unrealistic low.

In general it can be concluded that the negative impact of hydraulic conductivity and hydraulic head measurement errors depends on the scale of the study and the head variation along the domain. A correct estimate of the measurement errors yields a better characterisation of the aquifer parameters than not taking into account the measurement errors. Reproducing erroneous head data closely gives artefacts on the head and conductivity maps, while neglecting the error of hydraulic conductivity data yields unrealistic low conductivity ensemble standard deviations.

5 Inverse modelling of groundwater flow in 3-D fractured media

The inverse modelling of groundwater flow in 3-D fractured media is very complicated; the question is how to represent the fractured medium. In this chapter it is shown how a porous medium representation of the fractured medium can give satisfactory results. Chapter 5.1 gives a brief summary on different approaches for the modelling of groundwater flow in a fractured medium. Section 5.2 describes the strategy that uses the SCM to handle fractured media. Section 5.3 presents a case study for which the SCM was applied. In this case study, the fractures were incorporated stochastically in the modelling procedure. Finally, section 5.4 presents another extensive practical study. In this study the fractures are incorporated deterministically in the model.

5.1 Approaches to model groundwater flow in fractured media

A fractured formation consists of fractures and a rock matrix. When groundwater flow (and mass transport) in fractured rock is studied representations of both the fractures and the rock matrix have to be made. Below three approaches to build a conceptual model are detailed. The summary on the three approaches is taken from Wen and Cvetkovic (1995). More details on the modelling of groundwater flow and mass transport in fractured media can be found in their work. In this section just a brief description of each of the three approaches is given.

5.1.1 Discrete fracture network models

Discrete fracture network models attempt to represent the actual geometry of all fractures in a given fractured medium. In order to describe the positions of all the fractures, the orientation, shape, size and aperture of each of the individual fractures are needed. It is supposed that with the geometrical information on the fracture positions and the hydraulic properties of individual fractures, fluid flow in the fractured rock can be predicted. The rock matrix may be either impervious (no void space) or it may have additional void of a different character than the fractures. In case the rock matrix is impervious only groundwater flow in the fractures is considered. In case the rock matrix is pervious both groundwater flow in the rock matrix and in the fractures is modelled. In case the matrix is pervious either a porous medium representation of the matrix can be adopted or fracturing on a smaller scale can be considered. However, in general the rock matrix is considered impervious in discrete fracture network models.

The data needed to describe the geometry of the fracture network are obtained from outcrops, underground excavation or borehole investigations. The experimental data consist normally of the fracture locations, the fracture orientations, the fracture-tracer lengths, the percentage of fractures that terminate against other fractures as a function of orientation and the transmissivities of individual fractures estimated from hydraulic tests. The collected data are used to estimate parameters of 2-D or 3-D fracture geometry. It is obvious that the experimental information is associated with uncertainty. Furthermore, it is probable that for larger scale problems not all fractures are included. Therefore, it is common to build discrete fracture networks stochastically. In that case the fracture geometric properties are represented in terms of distribution functions and the distribution parameters are inferred from field measurements. Different kind of statistical distributions, with or without spatial correlation in the fracture plane positions, are used. The parameters inferred can also be used to generate multiple equally likely realisations of the fracture network. The realisations can be conditioned on the positions of fracture planes and their hydraulic properties. For each of the realisations the groundwater flow equation can be solved and a stochastic characterisation of the flow response is obtained. The focus in the stochastic generation of fracture networks has shifted from 2-D models to 3-D models. Different conceptual models have been proposed for assigning the fracture geometry (size, shape, orientation and location), for example the Baecher model, the Dershowitz model, the Levy-Lee model and the Nearest Neighbour model. Wen and Cvetkovic (1995) offer some details on these models and also give a short summary on other models. In all models the fracture shape and size distribution are defined a priori. Most of the models assume a constant aperture for the fractures.

For the solution of the groundwater flow equation in the fractured site some issues should be addressed. The hydraulic parameters for each of the fractures have to be defined. A flow network has to be built from the fracture network, and the hydraulic mixing at fracture intersections has to be defined.

The main problems of discrete fracture network models are:

- It is not easy to obtain reliable 3-D geometry data. Especially the fracture sizes are difficult to determine.
- The existence of preference flow paths on fracture planes can, in general, not be adequately modelled by the discrete fracture network models.
- In order to build reliable fracture networks many of the parameters have to be considered stochastically. A large number of realisations is needed in order to build a statistically sound analysis of the flow response.
- For large-scale sites normally a large number of fractures has to be generated and for all of them various parameters have to be defined. Normally this is not feasible.
- The relation between fracture geometry and hydraulic and transport properties is still an open issue.

- The discrete fracture network models are not very flexible for the conditioning to experimental data. As such, they are less flexible in the inverse modelling of groundwater flow.

5.1.2 Equivalent continuum models

Equivalent continuum models do not treat fractures explicitly, unless they are very large. In an equivalent continuum model heterogeneity is modelled using a limited number of regions, each of them with uniform properties. It is thought that if the volume is large enough a representative hydraulic unit of the model is obtained. This is the so-called Representative Elementary Volume (REV). However, for fractured rocks the REV is not practical as it is usually too large and no measurement is available on its scale. An alternative to the traditional REV concept-based deterministic continuum model is the stochastic continuum approach. In the stochastic continuum approach the hydraulic conductivities (and possibly other parameters) are considered at the measurement scale as space random functions defined over a continuum. A random function model is adopted for the spatial distributed values of the hydraulic conductivity.

The main data source for stochastic continuum models are hydraulic conductivity values obtained from single-hole packer tests. From the experimental data, statistics (e.g. mean, variance, spatial autocorrelation) can be derived needed to estimate the conditional probability density functions at unsampled locations. In many cases, it is difficult to estimate a full 3-D hydraulic conductivity variogram due to the scarcity of data and the spatial configuration of the measurement data. Fractured zones can be incorporated in the stochastic continuum models.

On the contrary to the discrete fracture network models, it is straightforward to relate hydraulic conductivities and hydraulic properties. The continuum theories and stochastic theories of flow and transport can be directly applied to model the groundwater flow for the fractured site. The groundwater flow equation is solved as for a porous medium. Therefore both analytical and numerical methods can be applied. However, the hydraulic conductivity variance is in general large for fractured media so that it is more common to use numerical methods to solve the groundwater flow in the fractured medium. Furthermore, various existing methods for the inverse modelling of groundwater flow or both groundwater flow and mass transport can be applied to condition the hydraulic conductivity realisations on hydraulic head and/or concentration data. Finally, the approach is also flexible to condition on soft information on hydraulic conductivities, for example by means of indicator based geostatistical simulation algorithms.

The main problems of stochastic continuum models are:

- The fractures are not correctly represented. This makes the stochastic continuum models difficult to use in the modelling of contaminant transport.
- For small-scale problems it may be inappropiate as a few fractures control the groundwater flow. The direct incorporation of the fracture plane position would therefore be desirable in a small-scale problem.
- The different data have a different support which can not be known from the tests.

5.1.3 Hybrid models

Hybrid models combine discrete fracture network models and stochastic continuum models. The continuum properties of the grid blocks are estimated and, at the same time, geometrical information on the fracture positions (either stochastically or deterministically) is used. Different kinds of hybrid models are reported in the literature.

One example of a method is closely linked with the stochastic continuum model and consists of modelling the fracture zones deterministically and the rest of the zone with a stochastic continuum approach. The hydraulic properties of the fracture zones could also be modelled randomly, if required. This approach could also be considered a stochastic continuum method with a non-stationary hydraulic conductivity (mixture of multiple populations).

Another approach consists of incorporating the fractures deterministically as in the discrete approach and modelling the background fracturing by a continuum model.

In general, the hybrid method is promising as it can combine the advantages of discrete fracture network models and stochastic continuum models. However, still additional research is needed to develop further the methodology with respect to:

- The connections between the discrete fracture network and the stochastic continuum model.
- To couple more effectively the description of large scale fractures and a stochastic continuum representation.
- A general framework to incorporate both hard and soft information that have a different support and to link the local and the regional scales in the model.

5.2 Fractured media in the sequential-self calibrating approach

In section 5.1 different approaches for the simulation of groundwater flow in fractured media were presented. The stochastic continuum approach was one of the approaches. This approach is used in the inverse modelling of groundwater flow with INVERTO. However, in case information on the fracture positions is incorporated the approach could also be considered a hybrid approach. In this section details are given on the use of the sequential-self calibrating approach and INVERTO for the inverse modelling of groundwater flow in fractured media. This section discusses some themes that were already introduced briefly before.

Generation of seed fields

For each of the grid cells a hydraulic conductivity value is generated. A distinction is made between fractures and background. The fracture positions may be determined deterministically, on the basis of experimental information, or may be generated stochastically. In the last case the position of the fractures differs between the seed fields. Nevertheless, the positions of the fractures may also in that case be constrained by the conditioning information.

Both in the cases of deterministically imposed fractures and stochastically generated fractures the hydraulic conductivities for the fractures and background are generated separately. The hydraulic conductivities for the background are conditioned to background hydraulic conductivity data. The hydraulic conductivities in each of the fracture planes are conditioned to hydraulic conductivity data from the fracture plane. This can be achieved by treating each of the fracture planes as separate zones (deterministic case) or by grouping the fractures into families with the same orientation, using a variogram with a long range in the fracture plane and a very short range in the direction perpendicular to it (stochastic case).

It is believed that one of the main advantages to include the background in the groundwater flow model is that some fractured zones are not detected by the measurement data. The stochastic continuum approach is therefore in the context of inverse modelling extra valuable because it allows for generating zones in the background with enhanced conductivity, indicating the possible existence of other fractures.

Solving the groundwater flow equation

In section 3.3 some problems related to the solution of the linear system of equations were highlighted. These problems frequently occur for the solution of groundwater flow in fractured media due to the local (very) large hydraulic conductivity contrasts. Section 3.3 gives some methods applied to circumvent (in part) these problems.

Inverse conditioning to hydraulic head data

The hydraulic conductivity seeds are conditioned to the hydraulic head data. Perturbations calculated for master blocks located in the background only affect background grid cells. Perturbations calculated for master blocks located in a fracture plane affect only that fracture plane. In case that the fracture planes are deterministically defined each fracture plane is a different zone and therefore not affected by perturbations in other zones (fracture planes). In case the fracture planes were stochastically generated it is also ensured that the perturbation calculated at a master block just affects the conductivities at the grid cells that belong to the same zone as the master block. This is achieved by the interpolation of the perturbations with a variogram that has a very small range in the direction perpendicular to the fracture plane orientation.

In the study presented in section 5.3 some tests were made to study the possible change, during the inverse conditioning of the zonification: a grid cell was allowed to change from background to fracture or from fracture to background. When a sharp conductivity decrease was detected (during the inverse modelling) for part of a fracture, the fracture plane was changed to background. On the contrary, an important conductivity increase for the background made it possible that the background became fracture. However, it was found that this strategy hardly yielded differences as compared with fractures and background that are fixed during the conditioning of the realisation:

- Probably the transition from background to fracture is non-operative because the objective function is relatively insensitive to swapping some fractures and background. Second, since the perturbations are interpolated with the variogram for the background, it is not possible to account for the possible orientation of the fracture.
- Another problem may be that, in general, many possible solutions to the groundwater flow inverse problem exist. Even when using hydraulic conductivity seed realisations that do not have the fractures on the right position, solutions can be found that reproduce the hydraulic head data.

Multiple zones/multiple statistical populations

Notice that, in summary, the concept of multiple zones representing multiple statistical populations is important in the inverse modelling of groundwater flow in fractured media. The fractures and the background form different statistical populations, each one having a different mean, variance and variogram for hydraulic conductivity. Furthermore, different fractures or different groups of fractures represent different statistical populations. As they are different statistical populations, in the geostatistical simulation they are also generated independently, each one having its own statistics and own conditioning data. Finally, also in the inverse conditioning procedure they are treated separately. In each of the zones corresponding to different statistical

populations an amount of master blocks is located. The perturbations optimised at the master blocks just affect their zone.

5.3 Inverse modelling of groundwater flow at the 3-D fractured site of Sellafield: stochastic generation of fractures

The following study illustrates the use of the SCM for the inverse modelling of groundwater flow in fractured media. SCM was applied to calibrate a 3-D groundwater flow model for the fractured site of Sellafield (United Kingdom). An important difference between this practical study and the study that will be presented in section 5.4 is that the positions of the fractures are generated stochastically, while in the study of section 5.4 the positions of the fractures are imposed deterministically. In this case a geological model was available with information on the fracture positions. However, not enough information with sufficient precision was available to impose the fracture positions deterministically.

5.3.1 Introduction

Near the city of Sellafield (United Kingdom) a program has been carried out with the objective to construct a nuclear waste repository in the geological formation Borrowdale, formed by slightly permeable fractured volcanic rocks. In the formation a pumping test was carried out (the RCF3 pumping test) that was the main inverse conditioning information.

The analysis of the RCF3 pumping test was undertaken by the Technical University of Valencia (UPV) on behalf of the Spanish Nuclear Waste Management Agency (ENRESA) using a stochastic continuum approach. Besides ENRESA, also the nuclear waste management organisations from France (ANDRA and IPSN), Sweden (SKB), United Kingdom (Nirex and EA) and Japan (SKI and PNC) participated in the project. The model uses a continuum representation of the fractured volcanic tuff at Sellafield, whereby the study area is discretized in cubic cells of size 20 m and the cells are classified as either containing a major fracture or containing just background fracturing. Scalar conductivities are assigned to each block depending on its classification and following spatial patterns according to a random function model. The random function model is used to impose a number of constraints to the conductivity fields, such as average values, variances or spatial correlations that should be observed in the spatially heterogeneous field. Also, the random function we use is always conditional, that is, the measured conductivity data are reproduced in the conductivity fields. However, all these constraints imposed by the random function model on the heterogeneous field are not enough to uniquely identify the conductivity values at every cell. On the contrary, they serve to specify an ensemble of alternative conductivity fields, referred to as conditional realisations, all of them meeting the constraints, and anyone being a plausible representation of reality. The analysis of all conditional realisations yields an uncertainty model on conductivities at unsampled locations. The analysis of the pressure responses of all conditional realisations yields, in turn, a model of uncertainty on pressure predictions.

The information available to build the random function model of the study area was provided in two stages. In the first stage, the data consisted, mainly, on structural information about the fracture geometry and transmissivity measurements at specific borehole intervals. No pressure data was given and the objective of this phase of the study was to predict the pressure evolution in response to the RCF3 pumping test. In the second stage, the pressure data was released and it was requested to re-evaluate the model built in the previous phase and to predict again the effect of the RCF3 pumping test. A new random function model had to be built. There is a third phase of the study for which no additional data on flow or pressure was released consisting in the prediction of the effects of sinking a shaft along the trace of the RCF3 well.

In the first phase, standard geostatistical techniques can be used to draw realisations from a random function model based only on conductivity data (Deutsch and Journel (1998) and Goovaerts (1997)). In the second phase, the need to produce conductivity realisations conditioned to pressure data, in the sense that the solution of the state equations reproduces the measured pressures, goes beyond the realm of random function modelling into inverse modelling. For this phase, INVERTO was applied. The Sellafield RCF3 pumping test exercise was, in fact, the testing ground for the extension of INVERTO to 3-D groundwater flow in fractured media.

The three phases of the study will be referred to, hereafter, as the blind prediction phase, the calibration phase and the shaft sinking phase. The section 5.3 continues with a presentation of the stochastic formulation of the groundwater flow at the site along some details on the generation of the conductivity realisations for the first two phases. A presentation of the models used in these two phases, with results and discussion, follows. Next, the shaft sinking phase, which does not receive as much attention, given the lack of experimental data with which to compare the predictions, and finally, some conclusions.

5.3.2 Blind prediction phase

During the blind prediction phase, only data on hydraulic conductivity are available. There exist both hard and soft data on K but no piezometric head data. The structural model with the geologists's interpretation of the geometry of the main fractures can be considered as soft data since it will help to identify in space likely locations of high conductivities. The conductivities derived from the many tests carried out in the site are considered as hard data. A combination of indicator sequential simulation (Gómez-Hernández and Srivastava, 1990) and Gaussian sequential simulation (Gómez-Hernández and Journel, 1993) is used to generate each one of the conditional realisations of conductivity fields used in the prediction phase.

The model domain is discretized into cubic cells, then the generation of each realisation consists of the following steps:

- The structural model is used to classify those cells that are intersected by one of the interpreted major fractures as highly likely to be indeed intersected by a fracture. This is not a deterministic classification, given that the structural model is interpretative in nature. There is some likelihood that fractures do not exactly follow the structural model, hence its soft nature and the allowance to classify a block crossed by one of the fractures in the structural model not to be fractured. A sensitivity analysis, described later, was carried out to decide on the best likelihood that should be given to the structural model.
- The structural information collected in the wells is considered as hard and is used to classify some of the cells as intersected or not by a major fracture. This classification is deterministic.
- Sequential indicator simulation is used to generate a binary realization of the model block, which results in a block in which each cells is labelled as intersected or not by a major fracture. Sequential indicator simulation was introduced in section 2.1.2.3 and is best suited for the generation of conditional binary realisations and can account for both hard and soft data. It is remembered that the technique requires, besides the conditioning data, as input, the indicator variogram of the binary variable.
- Once the binary field has been generated, conductivity values are assigned to the grid cells. Sequential Gaussian simulation is used in the process. The cells intersected by major fractures are generated independently of the rest, and in all cases conditional to the measured conductivity values. Sequential Gaussian simulation assigns conductivities to a set of cells drawing the values from a Gaussian distribution, ensuring that a certain correlation length is preserved, and respecting the measurements. The correlation length is imposed through a variogram, which, in this case, measures the average square difference between two cells a certain distant apart.

The program ISIM3D (Gómez-Hernández and Srivastava, 1990) has been used for the indicator simulation of the binary variables and the program GCOSIM3D (Gómez-Hernández and Journel, 1993) for the Gaussian generation of the conductivities within each of the two components of the binary simulation.

5.3.3 Calibration phase

During the calibration phase, the measured piezometric heads registered during the pumping test are incorporated into the characterisation of the conductivity spatial distribution. The objective of this phase is to use the realisations generated during the blind prediction phase, referred hereafter as seed realisations, and update them so as to reproduce the new information on piezometric head evolution. The updating phase is carried out using INVERTO.

Specifically in this case, the intrablock conductivity is determined by the geometric average of adjacent cells.

At the end of both the prediction and the calibration phases, there is an ensemble of hydraulic conductivity fields and the corresponding ensemble of piezometric head solution (in time and space) of the numerical approximation of the flow equation. The statistical analysis of these ensembles of realisations produces models of uncertainty for both conductivities and piezometric heads that serve to assess the degree of confidence on the predictions made using these models.

5.3.4 Site model and conductivity realisations

Next, we describe the specific data used to construct the random function models, the details of the numerical solution of the flow equation, and how fractures are treated in the 3-D continuum model.

The primal objective of the model is to predict the piezometric head evolution measured at a number of monitoring intervals in response to a constant piezometric head drawdown test carried out in the RCF3 well.

5.3.4.1 Geometrical model

The model block is a parallelepiped of 1000 m by 1000 m by 600 m, composed of a total of 50 by 50 by 30 cubic cells of 20 m by 20 m by 20 metres. The geometrical model is decided upon after considering the relative position of the monitoring intervals with regard to the pumping test source zone, the available computer resources and the need to have a grid as fine as possible. The grid should be as fine as possible in order to capture the impact of major fractures in the flow behaviour of the modelled area. The block is centred in the RCF3 well and extends vertically between elevations -400 m and -1000 m. The constant head drawdown test is carried out in a packed-off interval stretching between -640 m and -680 m.

From the NIREX reports (Nirex, 1995abc) it is apparent that the major fractures should be classified as pertaining to, at least, two main families. Therefore, any cell of the model can belong to any of three populations: intersected by a major fracture in fracture family 1, intersected by a major fracture in fracture family 2, or not intersected by any major fracture. This scenario presents some additional complications for the generation of the conductivity fields with regard to the procedure discussed in the previous section, since the geometry of the block cannot be characterised by a binary variable. The ternary characteristics of the conductivity model require two stochastic simulations for the generation of the geometry by indicator conditional simulation (one for each fracture family) using the code ISIM3D. Three stochastic simulations are required for the assignment of conductivities to every cell by Gaussian sequential simulation

(one for each fracture family and one for the blocks not intersected by any major fracture) using the code GCOSIM3D.

Fracture family 1 is the most abundant, has azimuth NW-SE and dips 40 degrees. Fractures F1, F2, F3, F200/F210, F209 and F211 belong to this family. Fracture family 2 is less abundant, has azimuth NEE-SWW and dips 70 degrees. Fractures F201, F203 and F205/F206 belong to this family. All the available data from the NIREX reports (Nirex, 1995abc) were reviewed and all data on fracture geometry and conductivity were retained and classified as conditioning data for either the indicator simulation, i.e., the simulation of the geometry, or for the Gaussian simulation, i.e., the simulation of the conductivities. Each datum was tagged as corresponding to a fracture from fracture family 1, a fracture from fracture family 2, or otherwise, and was used to condition the generation of the corresponding member.

In addition to the hard data values obtained from the NIREX reports, there was a structural model in which the main fractures were defined by three-dimensional triangular meshes. This structural model had been built by reconciling the data observed in the different boreholes. Since the correlation of a given fracture across boreholes was not always evident, several structural models were built during the life of the project. The one provided was the most recent one—admittedly the most accurate—but, in all cases, not devoid of uncertainty. For this latter reason, the information from the structural model was used as soft information for the conditioning of the indicator simulation by assigning to it a certain likelihood that the numerical cells intersected by a fracture will indeed be classified as fractured cells. The likelihood associated with the structural model was varied and a final value was chosen by analysing the flow responses of realisations with different likelihoods.

Figure 5.1 presents two seed realisations of the conductivities, in them it can be seen the impact that accounting for the structural model has in the final rendition of the model geometry. The figure shows a block diagram with a cutout along the RCF3 well trace. The geometry of the conductivity of the image on the left was generated without accounting for the structural model, that is, a zero likelihood was attached to it; the image on the right was generated assigning a likelihood of 75% to the structural model. In this latter case, during the indicator simulation approach, the likelihood is used to enforce that 75% of the cells crossed by the fractures in the structural model are actually included in the final realisation. The main differences in the two images in Figure 5.1 are apparent: on the left, fracture planes tend to cluster along fracture planes determined by the hard conditioning data, whereas, on the right, the fractured cells spread more over the block. In both realisations, the proportions of cells intersected by each fracture family remains constant, and the orientation of the fracture families is clearly seen. After generating a few realisations with different likelihoods, ranging from 60% up to 100%, and analysing their flow

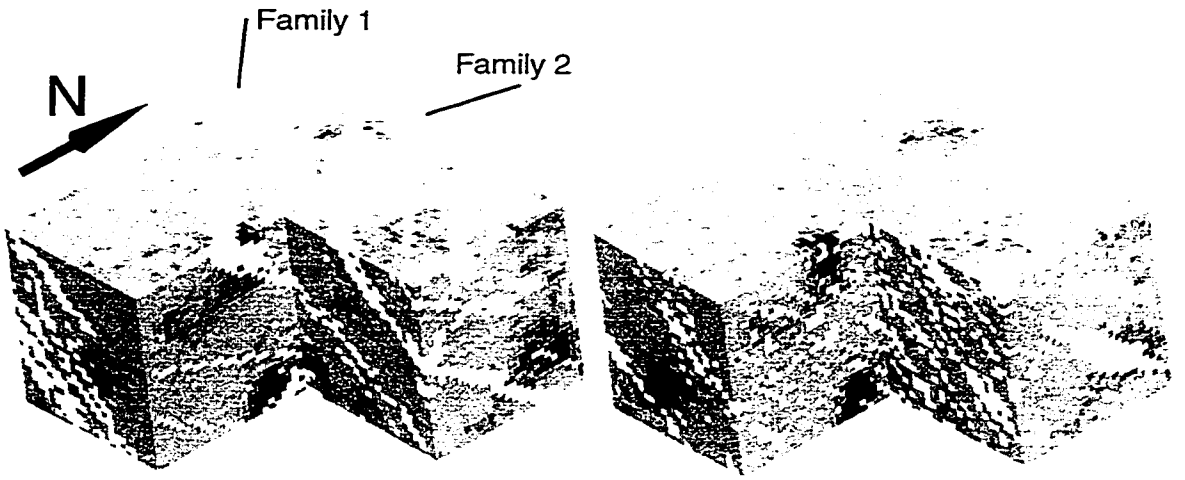

Figure 5.1. Two seed realisations with a cut-out exposing the position of the RCF3 well. Each realisation was generated using a different likelihood for the structural model. Left, likelihood of zero (the structural model is not used to condition the geometry), right, likelihood of 75%, three quarters of the cells interpreted as containing a main fracture in the structural model are retained in the final numerical model.

response, it was decided to retain the realisations generated with a likelihood on the structural model of 75%.

Additional parameter values necessary for the generation of the geometry files are the proportions of cells in the entire numerical block that are intersected by fractures from family 1 and by fractures from family 2. These two values were set to 19% for family 1 and to 7% for family 2. These values correspond to the proportions of cells intersected by the two fracture families in the structural model. In addition to the proportions, indicator variograms are needed, since these indicator variograms could never been derived from the few available data, their parameters were postulated in order to ensure that, in each generation, fracture-like structures were generated. It means that cells intersected by any given fracture should tend to align in planes according to the orientation of each fracture family. This is achieved by utilising an indicator variogram model with very long ranges in the fracture plane and a range of 60 m in the orthogonal direction (recall that the discretization cell size is 20 m).

For the generation of any given geometry, two indicator simulations were needed. Each indicator simulation identifies the cells which are crossed by members of each fracture family. Each simulation is generated independently of the other. The two simulations are then merged together resulting in a block with cells marked as intersected by fracture family 1 or 2, everything else being background cells. For the generation of the cells intersected by family 1, there were 45 hard data and 3145 soft data. For the generation of the cells intersected by fracture family 2, there were 5 hard data and 192 soft data. In addition, in

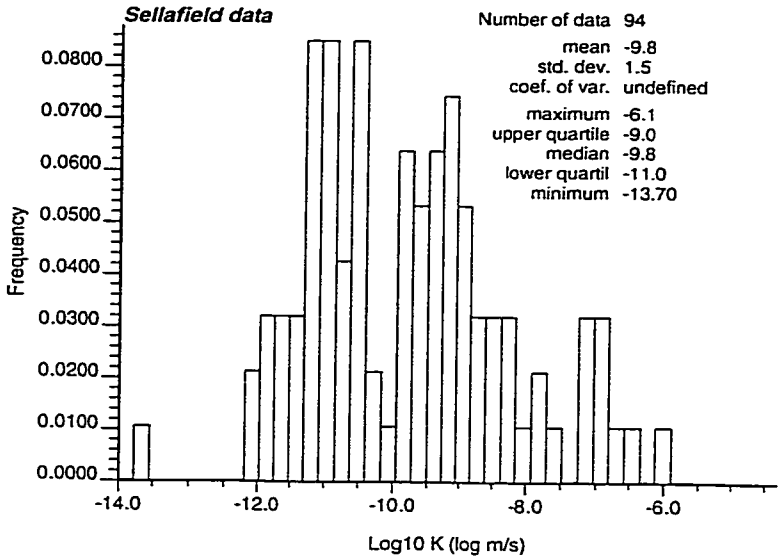

Figure 5.2. Histogram of the 84 hard conductivities available for both fracture families and for the background fracturing, in logarithmic scale.

both generations there were 34 locations known not to be intersected by any fracture family that were also used as hard data.

The geometric description of the model block is the only characteristic that remains unchanged from the blind prediction phase to the calibration phase. It is the only characteristic of the model for which we do not have tools to update during the calibration phase.

Twenty realisations of the geometry were generated. The selection of the number of realisations was based on the computer resources and time constraints to complete the work. Had these constraints not existed, the number of realisations generated should have been larger, allowing a more statistically sound analysis of the ensemble of final results.

5.3.4.2 Seed Conductivity Fields

Each of the realisations of geometry generated in the previous step was then infilled with conductivity values. The histogram of the 94 hard conductivity values obtained from the NIREX reports is shown in Figure 5.2. It was considered that we wanted to have a strong contrast on conductivities between fractured and background cells. It was decided that the conductivities to be assigned to the fractured cells, independently of the family to which they belong, would follow a uniform distribution between 10^{-7} ms^{-1} and 10^{-5} ms^{-1}, and a correlation length of 200 m in the fracture plane. The conductivities assigned to the background cells would have a lognormal distribution with log K mean of -13 $\log_{10}$ ms^{-1}, log K variance of 1 $\log^2_{10}$ ms^{-1}, and an isotropic

correlation with range of 200 metres. The value of -13 for the mean logconductivity of the background cells was based on preliminary calculations of the equivalent block permeability of a block of similar size non intersected by major fractures (Nirex, 1995c). As will be seen during the calibration phase, this large contrast imposed between fractured and background cells is too large and it will reduce after conditioning to the piezometric head decline data.

The right image of Figure 5.1 displays one of the 20 realisations generated.

5.3.4.3 Blind Predictions

Each of the 20 conductivity realisations are input to the groundwater flow equation. Only piezometric head drawdowns are considered for the flow simulations. Initial conditions correspond to a hydrostatic piezometric head within the block, that is, homogeneous piezometric heads in the entire block. The piezometric head values at the boundary cells remain unchanged through the simulation and equal to their hydrostatic piezometric head initial values. Two of the cells next to the geometrical centre of the model, corresponding to the 40 m packer interval between -640 m and -680 m in which the piezometric head drawdown test was carried out, are subject to an instantaneous drawdown of 158 metres. A uniform storativity value of 10^{-7} m^{-1} is used.

The solution of the flow equation in each of the 20 conductivity realisations results in an ensemble of 20 realisations of the piezometric head evolution both in time and space. For each of the piezometric head monitoring locations, the 20 predicted values are used to build a probability distribution function from which the median value, the first quartile and the last quartile were retained for display purposes. Figures 5.3 and 5.4 show the predicted piezometric head drawdowns at the 13 monitoring intervals and the corresponding measured values. A projection of the location of the 13 monitoring locations onto a vertical plane is shown in Figure 5.5 where the relative position of the monitoring locations with respect to the source zone can be seen. For reference purposes, Table 5.1 reports the wells and sections corresponding to each of the monitoring locations.

The observed piezometric head drawdowns are fairly well reproduced by the median of the probability distributions derived from the 20 realisations with maybe the exception of section 2, for which the measured response is much stronger than the one predicted by the stochastic realisations. For section 2, not only the median underestimates the observed value, but, at 1000 hours, it is larger than the predicted upper quartile. For the rest of the sections, the measured drawdown is, in all cases, within the interval bracketed by the lower and upper quartiles. Notice, in Figure 5.5 that monitoring interval number 2 is in the same well and directly above the source zone.

The interval formed between the lower and upper quartiles—the width of which is called the interquartile range—can be seen as a measure of uncertainty

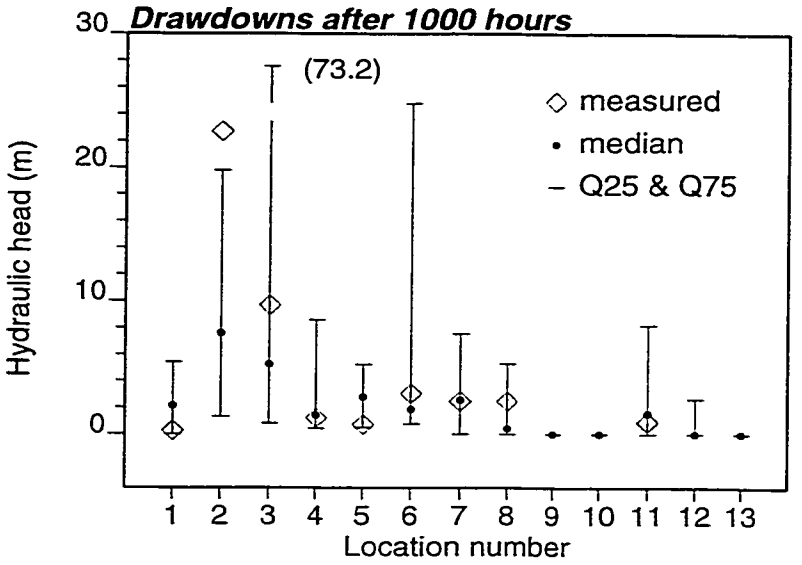

Figure 5.3. The measured piezometric head drawdowns 1000 hours after the beginning of the drawdown test are depicted along the median and both quartiles (Q25 and Q75) of the probability distribution obtained from the 20 stochastic realizations, blind prediction phase. Drawdowns are given at the 13 monitoring locations displayed in Figure 5.5.

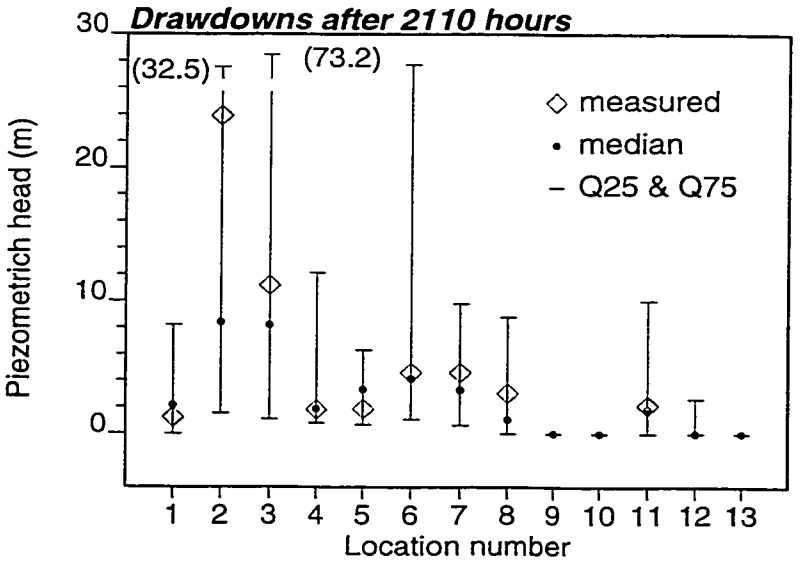

Figure 5.4. Same as Figure 5.3, but now drawdowns are shown at 2110 hours, the end of the drawdown test.

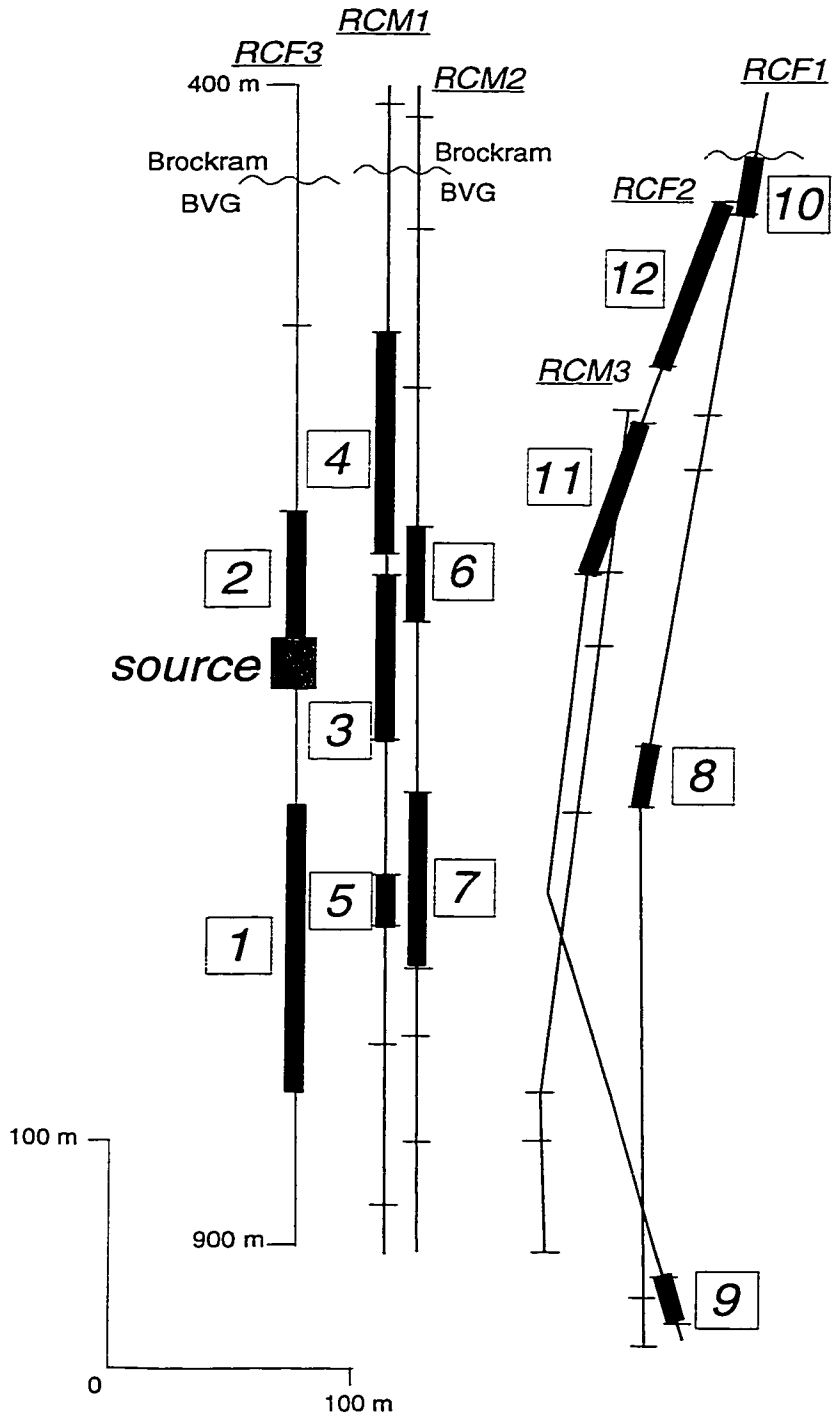

Figure 5.5. Projection onto a vertical plane of the wells on which the source and monitoring locations are located.

1	RCF3-P2	5	RCM1-P9	9	RCF1-P8	13	BH5-P1
2	RCF3-P5	6	RCM2-P8	10	RCF1-P5		
3	RCM1-S7	7	RCM2-S11	11	RCF2-P6		
4	RCM1-S6	8	RCF1-P7	12	RCF2-P4		

Table 5.1. Well reference and section number for each of the 13 locations displayed in Figures 5.1 and 5.2.

on the predictions of the piezometric head drawdowns. Uncertainty that, in this particular case, stems from the unknown spatial variability of the conductivity fields. (Other uncertainties such as those related to the conceptual model, or to the initial or boundary conditions are not contemplated.) The interquartile range is particularly large for sections 2, 3 and 6. As already mentioned, section 2 is in the same well as the source and sections 3 and 6 about the same elevation as the source zone in the two closest wells to the pumping well. This large uncertainty is in part due to the coarse discretization used to model the site which allocate only two or three cells between the source zone and the aforementioned monitoring zones and, therefore, making their response very sensitive to the individual conductivity cells assigned to these connecting cells.

As an alternative measure of the performance of the flow model, the percentage of the monitoring zones that respond to the drawdown test is also reported. Figure 5.6 shows the time evolution of the observed percentage of monitoring intervals with measurable response along as the median, lower and upper quartiles of the probability distributions of percentage of monitoring intervals with response derived from the 20 stochastic realisations. The ensemble of realisations allows to carry out a probabilistic analysis not only of the parameter or state variables but of any transform or function of them. The prediction of the observed percentage by the median of the distribution is very good except for times larger than 1000 hours for which the numbers of zones is underestimated. The uncertainties about this prediction are very large, out of the 20 realisations it appears that there are a few of them that do not show any response even after 2110 hours.

A numerical comparison between the experimental drawdown measurements at the end of the experiment and the median predicted values, along with the experimental response time as compared to the median predicted response times is given in Table 5.2. From this table, it can be appreciated again that the relative error in the prediction of the observed drawdowns by the median values, is acceptable except for section 2. The predicted response time median values show larger discrepancies than the drawdowns, with the largest mismatches occurring for sections 4, 8 and 11. The explanation for these mismatches may be due to the existence of some horizontal connection about the source zone which is not captured by the model of spatial variability. It can

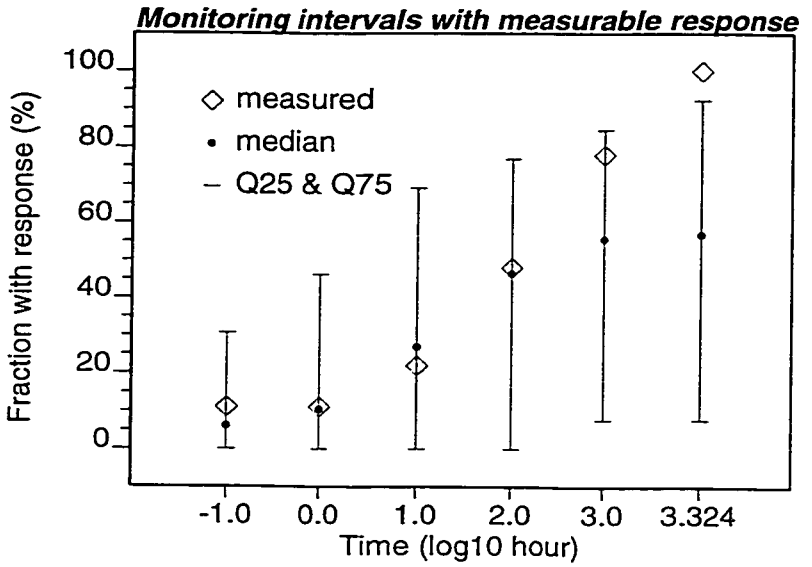

Figure 5.6. Time evolution of the percentage of monitoring zones with measurable response, blind prediction phase.

Location	Median head Draw. (m)	Experim. head draw. (m)	Median response time (h)	Experim. response time (h)
1 RCF3-P2	2.5	1.3	286.0	380.0
2 RCF3-P5	8.4	23.5	2.7	2.1
3 RCM1-S7	8.2	11.6	5.0	0.9
4 RCM1-S6	1.9	1.8	52.0	4.5
5 RCM1-P9	3.4	2.4	16.9	24.0
6 RCM2-P8	4.2	5.5	9.9	3.9
7 RCM2-S11	3.4	4.5	11.8	30.0
8 RCF1-P7	1.4	4.0	632.0	32.0
9 RCF1-P8	no	no	no	no
10 RCF1-P5	no	no	no	no
11 RCF2-P6	1.9	1.6	46.5	240.0
12 RCF2-P4	no	no	no	no
13 BH5-P1	no	no	no	no

Table 5.2. Head drawdowns at the end of the test and response times. Comparison between measurements and median predictions. Blind prediction phase.

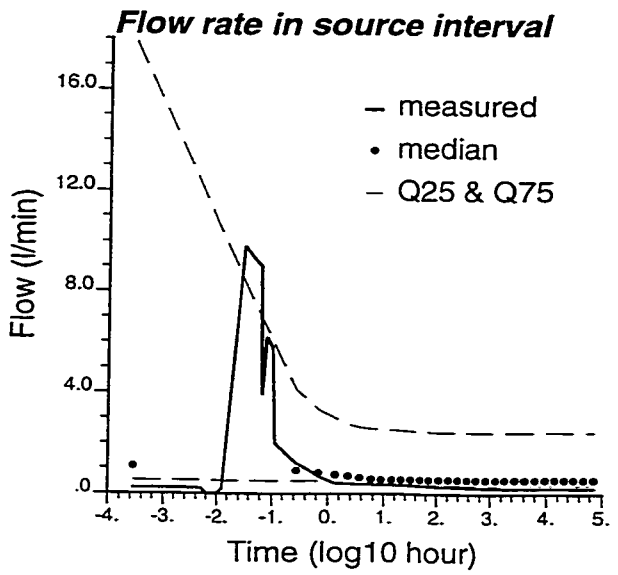

Figure 5.7. Time evolution of the flow rate into the source interval, blind prediction phase.

be seen that the predicted median response is basically proportional to the distance from the source to the monitoring zones whereas the observed values display some deviations with respect to this behaviour.

Another important measure of the performance of the model is the prediction of the flow rate into the source interval. Proper reproduction of flows in the formation are of paramount importance for the correct assessment of the safety of a site considered as a potential host to a nuclear waste repository. Figure 5.7 shows the measured flow into the formation along with the median, lower and upper quartiles of the probability distributions of flows derived from the 20 realisations. Notice the logarithmic scale in the time axis used to highlight the sudden inflow which occurred into the source interval in the first few minutes of the test. The predicted median flow shows a small decline in the first 10 hours after which it remains practically constant and slightly above the measured values. Except for the first 10 hours, the median prediction can be considered good. It is interesting to observe the wide envelope about the median provided by the two quartiles. This envelope is wide enough to enclose the measured flows, indicating that some of the realisations were able to produce large flows at the beginning of the flow simulation but it also indicates that some of the realisations have relatively large "steady-state" values.

The large contrast between the mean conductivity values for the fractured and non-fractured cells together with the strong anisotropy imposed by the continuity of the fractured cells is evident in the depression ellipsoid provoked by the drawdown test. Figure 5.8 shows four horizontal cross-sections of the median piezometric head drawdowns. Although no quantitative scale is given,

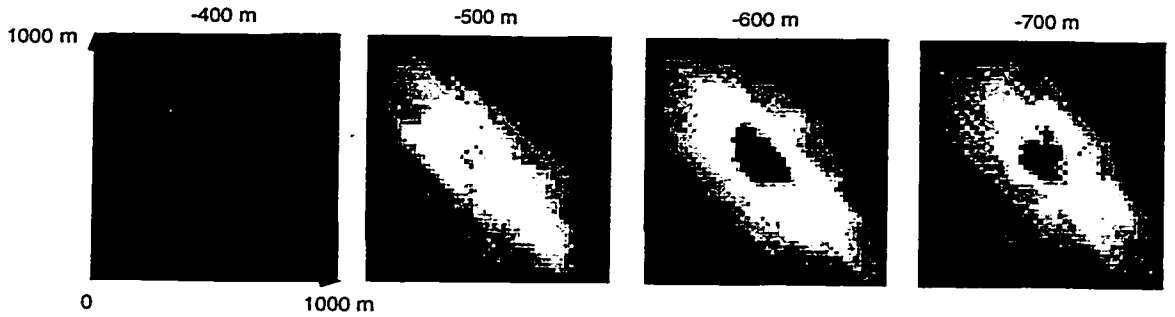

Figure 5.8. Blind prediction phase. Horizontal cross-section through a block containing the median piezometric head drawdowns at the end of the test (2110 hours). On top the section elevations. Largest displayed drawdown is 50 m at -600 m. The test was carried out in the interval (-640 m, -680 m).

the interest of the figure lies on the display of the anisotropic depression zone that develops in the model block.

5.3.4.4 Calibrated conductivities field

All the measured values reported in the previous figures were not available at the time the predictions were made. There were provided later for calibration purposes. Using the time evolution of piezometric head drawdowns to calibrate the 20 seed conductivity fields by way of the self-calibrating algorithm, 20 calibrated conductivity fields are generated. Each one of these calibrated fields maintains the same geometry as the seed fields, that is, they have the same distribution of cells intersected by major fractures and background cells. At the same time, each of the calibrated fields matches the same measured conductivity data used to generate the conditional seed fields and approaches as close as the self-calibrating algorithm allows the measured drawdowns.

The same performance measures used to evaluate the blind predictions are used during the calibration phase. In addition to the 13 monitoring locations from the previous phase, 18 more monitoring locations are used. These additional monitoring locations provided verification data for the calibrated model. They are located in wells RCF2, RCF3, RCM1, RCM2 and RCM3 as indicated in Table 5.3.

In total 211 master blocks are distributed over the matrix, 210 master blocks over fracture family one and 100 master blocks over fracture family two. It should be stressed that in the optimisation of the Y perturbations at the master blocks it is taken into account that perturbations of Y at a master block in a certain zone only affect the Y of that zone and not of the other zones. The perturbations ΔY which are optimised at the master blocks belonging to the rock matrix are interpolated to all the grid cells belonging to the rock matrix. The perturbations ΔY which are optimised at the master blocks belonging to the

14	RCF3-P6	19	RCM1-S10	24	RCM3-S4	29	RCM3-S7
15	RCF3-P1	20	RCM2-S9	25	RCM3-P5	30	RCF2-P5
16	RCM1-S5	21	RCM2-S10	26	RCM3-P6	31	RCM1-P8
17	RCM1-S8	22	RCM2-P9	27	RCM3-P6		
18	RCM1-S9	23	RCM2-S12	28	RCM3-P7		

Table 5.3. Well reference and section number for each of the 18 monitoring locations used during the calibration phase in addition to those in Table 5.1.

fracture family one are interpolated to all the grid cells belonging to the fracture family one. Finally, the perturbations ΔY which are optimised at the master blocks belonging to the fracture family two are interpolated to all the grid cells belonging to the fracture family two.

Figures 5.9 and 5.10 show the measured piezometric heads at all 31 locations at times 1000 hours and 2110 hours along with the predicted median and quartiles values derived from the corresponding frequency distribution functions built with the 20 calibrated realisations. The first 13 monitoring locations in the figures are used as conditioning data for the generation of the stochastic realisations. Had conditioning been achieved exactly, the predicted interquartile interval should be null and coincident with the measured value. This is so for most of the 13 conditioning sections, with the notable exceptions of sections 2 and 3, the same ones for which the median blind prediction was the farthest from the measurements or for which the largest interquartile ranges were predicted. It is clear, that for sections 2 and 3, there is some feature that the model is missing that prevents the self-calibrating algorithm from achieving perfect conditioning. However, it is also noticeable that even for those conditioning sections with the poorest reproduction of the measured drawdowns, the interquartile range is much narrower than it was during the blind prediction phase. Of the additional 18 verification sections, the ones with a relatively large interquartile range and for which the median prediction does not get close enough to the measured values are sections 17, 21, and 31; all of them located in the closest wells to RCF3. This reinforces our conjecture that there may be some local feature around the source location that has not been captured by the proposed model.

The percentage of monitoring zones that responds to the drawdown test was also computed and is shown in Figure 5.11. The effect of conditioning is noticeable, the interquartile range at any given time has decreases substantially with respect to the blind prediction phase. Also the percentage response for the later times 1000 h and 2110 h is now bracketed within the interquartile range of the predicted percentages. The only deviation with respect to the measurements and with respect to the blind predictions is the overprediction of monitoring zones responding to the drawdown test at 100 h.

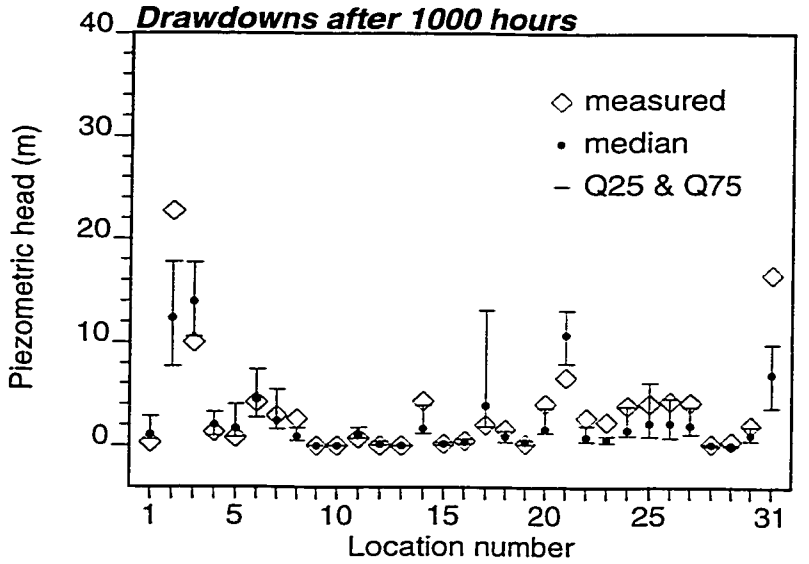

Figure 5.9. The measured piezometric head drawdowns 1000 hours after the beginning of the drawdown test are depicted along the median and both quartiles (Q25 and Q75) of the probability distribution obtained from the 20 stochastic realisations, calibration phase. Drawdowns are given at 13 calibration locations and additional 18 monitoring locations.

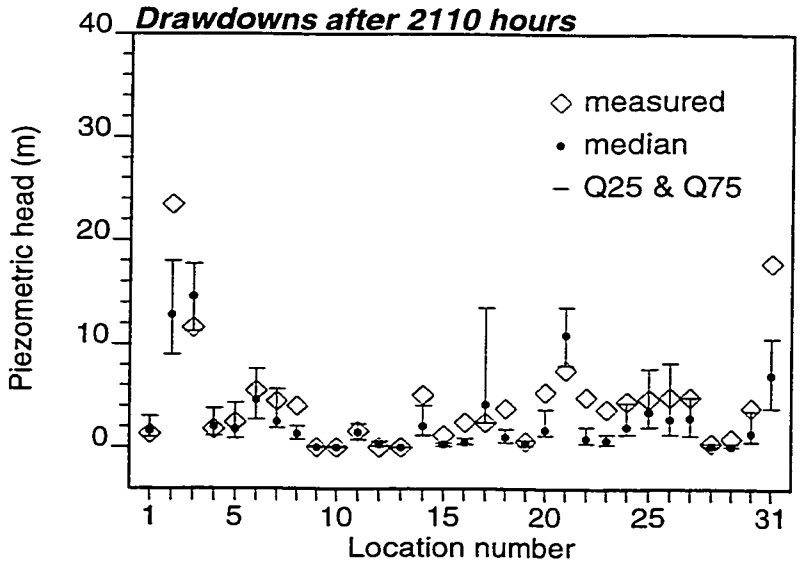

Figure 5.10. Same as Figure 5.9 but now drawdowns are shown at 2110 hours, the end of the drawdown test.

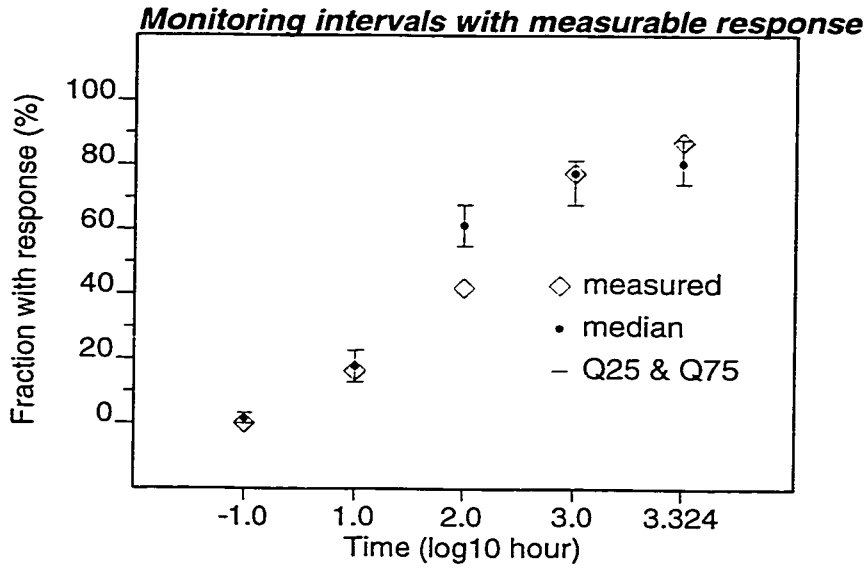

Figure 5.11. Time evolution of the percentage of monitoring zones with measurable response, calibration phase.

Similarly to the prediction phase, Table 5.4 shows a numerical comparison between measured drawdowns and experimental response times with their corresponding median predictions from the set of calibrated realisations. Recall that the 13 first monitoring zones correspond to the conditioning zones. For these 13 sections, the prediction of the drawdowns is very good, and the prediction of the response times improves slightly from their values from the blind prediction phase, except for section 1 that shows a poorer prediction. For the remaining 18 zones, the predictions are only fair. However, even if the median predictions are only fair, one should not forget that within a stochastic framework these predictions do not have a real meaning unless they are accompanied by a measure of the uncertainty attached to them. The interquartile range is used as the uncertainty measure for the drawdowns; see Figures 5.9 and 5.10.

The reduction on the overall variability of the predicted flows into the source location with respect to the blind prediction phase is also substantial. Figure 5.12 shows the median predicted flows and the two quartiles. As opposed to the results in Figure 5.6, there is virtually no envelope of predictions which implies that the high flows observed during the first few minutes of the tests are not captured by any of the 20 calibrated realisations. In order to appreciate the degree of uncertainty on flow predictions and how well the ``steady-state" flow of the later part of the test is reproduced, a blow-up of Figure 5.12 is given in Figure 5.13. The interquartile range around the median prediction is almost zero and the predicted flow based on the calibrated realisations is a good approximation of the measured values. If, in addition, we consider the volume of water that was collected at the source zone, the calibrated realisations will

Location	*Median head Draw. (m)*	*Experim. head draw. (m)*	*Median response time (h)*	*Experim. response time (h)*
1 RCF3-P2	1.6	1.3	52.0	380.0
2 RCF3-P5	12.8	23.5	0.7	2.1
3 RCM1-S7	14.6	11.6	0.7	0.9
4 RCM1-S6	2.0	1.8	22.0	4.5
5 RCM1-P9	1.8	2.4	34.0	24.0
6 RCM2-P8	4.6	5.5	6.0	3.9
7 RCM2-S11	2.5	4.5	34.0	30.0
8 RCF1-P7	1.3	4.0	65.0	32.0
9 RCF1-P8	0.0	0.0	no	no
10 RCF1-P5	0.0	0.0	no	no
11 RCF2-P6	1.5	1.6	52.0	240.0
12 RCF2-P4	0.3	0.0	no	no
13 BH5-P1	0.0	0.0	no	no
14 RCF3-P6	2.1	5.1	14.0	19.0
15 RCF3-P1	0.3	1.2	no	380.0
16 RCM1-S5	0.5	2.4	149.0	167.0
17 RCM1-S8	4.2	2.4	12.0	19.0
18 RCM1-S9	1.0	3.8	79.0	180.0
19 RCM1-S10	0.4	0.6	404.0	360.0
20 RCM2-S9	1.7	5.4	22.0	5.7
21 RCM2-S10	10.9	7.5	2.5	1.8
22 RCM2-P9	0.9	4.9	52.0	28.0
23 RCM2-S12	0.7	3.7	99.0	55.0
24 RCM3-S4	2.0	4.5	65.0	14.0
25 RCM3-P5	3.5	4.7	43.0	18.0
26 RCM3-S5	2.8	4.9	65.0	2.8
27 RCM3-P6	2.9	4.9	43.0	6.5
28 RCM3-P7	0.2	0.4	no	480.0
29 RCM3-S7	0.1	0.9	no	480.0
30 RCF2-P5	1.4	3.9	65.0	2.8
31 RCM1-P8	7.1	17.9	3.0	1.0

Table 5.4. Head drawdowns at the end of the test and response times. Comparison between measurements and median predictions. Calibration phase.

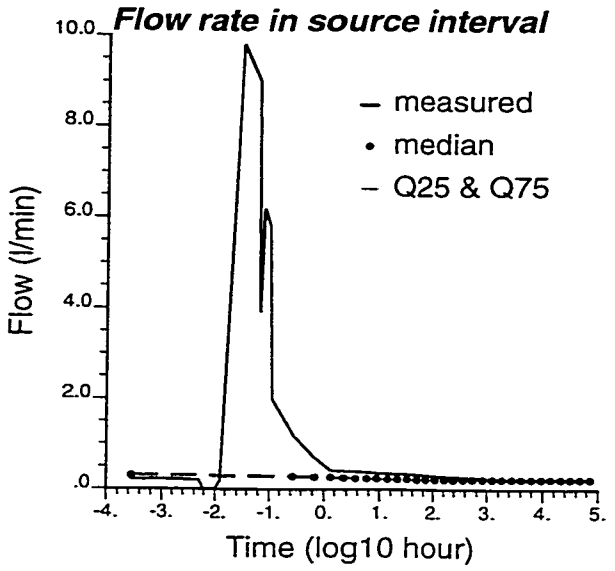

Figure 5.12. Time evolution of the flow rate into the source interval, calibration phase.

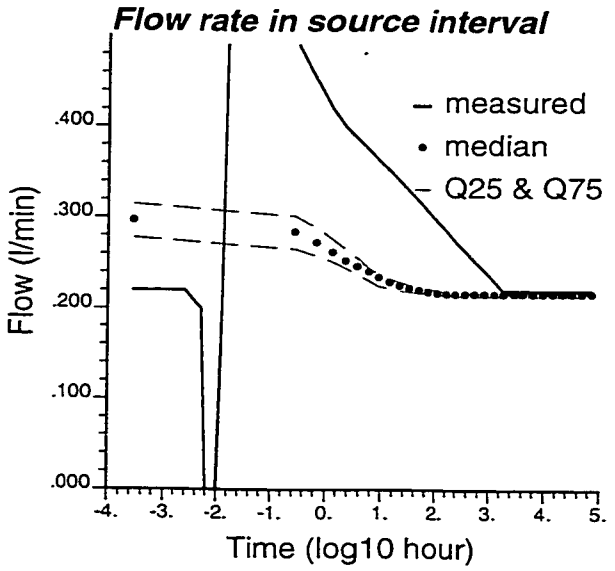

Figure 5.13. Blow-up of Figure 5.12.

match almost perfectly the experimental values given that the very large flows occur during a short period of time.

A very interesting result of this calibration phase is given by the spatial distribution of the ensemble mean piezometric drawdowns. Figure 5.14 shows the same four cross-sections of the model block displayed in Figure 5.8 at the

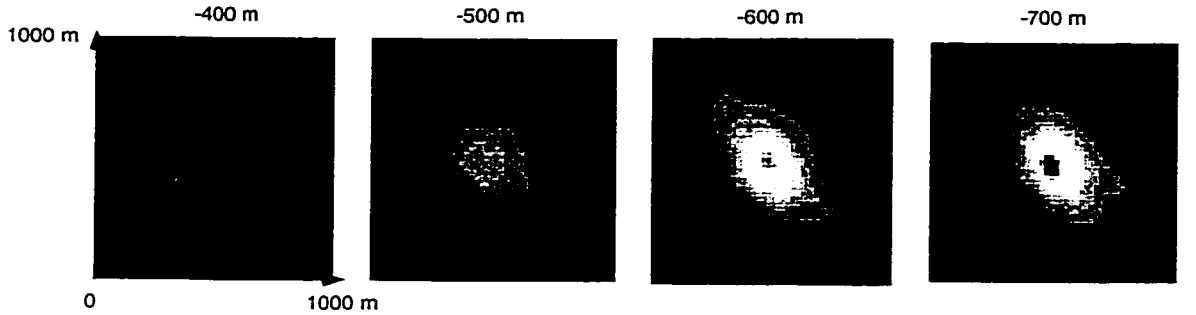

Figure 5.14. Calibration phase. Horizontal cross-section through a block containing the median piezometric head drawdowns at the end of the test (2110 hours). Largest displayed drawdown is 30 m at -600 m. On top the section elevations. The test was carried out in the interval (-640 m, -680 m).

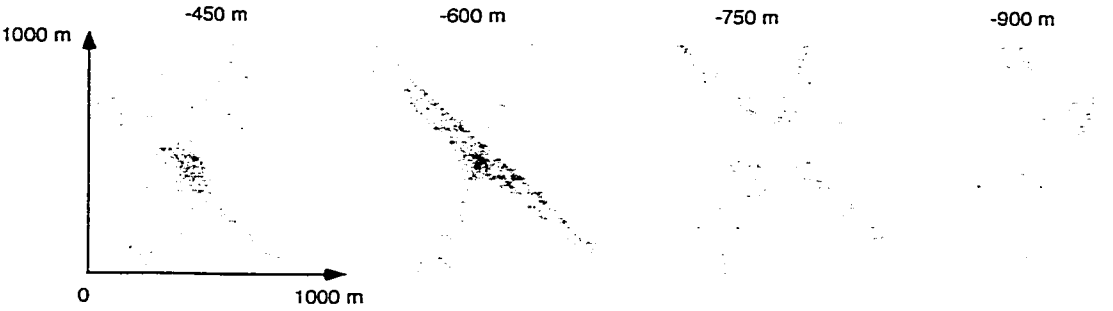

Figure 5.15. Horizontal cross-sections through the median of the perturbations applied to the seed realizations to obtain calibrated realizations. On top the section elevations. Dark shades are negative (minimum -2 log (m/s)), light shades positive (maximum 1 log (m/s)). Fractured blocks decrease their conductivity whereas background blocks increase it, especially around the well.

end of the drawdown test. The strong anisotropy on the spatial distribution of the piezometric heads disappears, resulting in a much more isotropic response; as if the cells representing the background fracturing played a larger role in the propagation of the drawdown imposed at the source. Indeed, the perturbations applied to the cells in the realisations used for the blind prediction phase show two preponderant characteristics. Cells intersected by main fractures decrease their conductivity, whereas background cells increase their values, the latter especially within the volume in which most of the monitoring zones are located (see Figure 5.15).

5.3.4.5 Additional conditioning to transient head data

In section 5.3.4.4 just the final head drawdown data were used in the conditioning. However, also information from intermediate time steps can be included in the inverse modelling. This transient information may improve further the characterisation of hydraulic conductivities and it also allows to estimate the storativity coefficient.

Location	*Median head Draw. (m)*	*Experim. head draw. (m)*	*Median response time (h)*	*Experim. response time (h)*
1 RCF3-P2	1.2	1.3	112.6	380.0
2 RCF3-P5	21.6	23.5	0.2	2.1
3 RCM1-S7	13.6	11.6	0.5	0.9
4 RCM1-S6	3.5	1.8	19.1	4.5
5 RCM1-P9	1.4	2.4	10.7	24.0
6 RCM2-P8	7.3	5.5	1.7	3.9
7 RCM2-S11	1.5	4.5	67.6	30.0
8 RCF1-P7	0.6	4.0	304.4	32.0
9 RCF1-P8	0.0	0.0	no	no
10 RCF1-P5	0.0	0.0	no	no
11 RCF2-P6	1.0	1.6	160.0	240.0
12 RCF2-P4	0.0	0.0	no	no
13 BH5-P1	0.0	0.0	no	no
14 RCF3-P6	4.7	5.1	12.7	19.0
15 RCF3-P1	0.2	1.2	423.3	380.0
16 RCM1-S5	0.5	2.4	80.4	167.0
17 RCM1-S8	3.1	2.4	4.7	19.0
18 RCM1-S9	0.6	3.8	225.0	180.0
19 RCM1-S10	0.4	0.6	240.0	360.0
20 RCM2-S9	3.5	5.4	36.4	5.7
21 RCM2-S10	6.7	7.5	4.1	1.8
22 RCM2-P9	0.6	4.9	63.0	28.0
23 RCM2-S12	0.3	3.7	201.2	55.0
24 RCM3-S4	2.2	4.5	47.3	14.0
25 RCM3-P5	2.3	4.7	50.7	18.0
26 RCM3-S5	2.7	4.9	14.2	2.8
27 RCM3-P6	1.9	4.9	27.5	6.5
28 RCM3-P7	0.1	0.4	534.7	480.0
29 RCM3-S7	0.1	0.9	802.0	480.0
30 RCF2-P5	0.7	3.9	3.5	2.8
31 RCM1-P8	11.6	17.9	2.3	1.0

Table 5.5. Head drawdowns at the end of the test and response times. Comparison between measurements and median predictions. Calibration phase including transient head data.

Realisation	*Calibrated Storativity Coefficient (m^{-1})*
1	$9.20 * 10^{-7}$
2	$8.84 * 10^{-7}$
3	$1.15 * 10^{-6}$
4	$6.25 * 10^{-7}$
5	$6.61 * 10^{-7}$
6	$8.00 * 10^{-7}$
7	$8.36 * 10^{-7}$
8	$5.01 * 10^{-7}$
9	$1.16 * 10^{-6}$
10	$1.52 * 10^{-6}$
11	$2.24 * 10^{-6}$
12	$1.16 * 10^{-6}$

Table 5.6. Estimated storativity coefficients for the twelve realisations.

The groundwater flow during the pumping experiment was modelled dividing the period to be modelled in 25 time steps. The first time step had a magnitude of 200 seconds and subsequent time steps had a magnitude of 1.5 times of the preceding time step. The same amount of master blocks was used in the conditioning as in the conditioning round that just used steady-state head drawdown data.

Just 12 realisations, due to the CPU time restrictions, were conditioned to the transient head data. Table 5.5 shows a numerical comparison between measured drawdowns and experimental response times with their corresponding median predictions from the set of calibrated realisations. Although 12 realisations are in any case too little to make a sound statistical analysis, it is clear from Table 5.6 that the production of the final head drawdowns improves. The important head drawdowns are reproduced much better and this is more than enough to counterbalance the worse reproduction of the small head drawdowns. It seems that the transient head data help in finding the conductivity perturbation that reproduces better the final head drawdowns. It would be expected that the transient head data help more in reproducing the head reproduction at intermediate time steps. However, Table 5.5 shows that the response times are not reproduced better than in the case the transient head data were not included (compare Table 5.5 and Table 5.4). Finally, the transient head data allow to estimate the storativity coefficients. Table 5.6 gives the estimates of the storativity coefficients for the twelve realisations.

5.3.4.6 Transport simulations for a hypothetical flow regime

It has been investigated whether the improved characterisation of the 3-D hydraulic conductivity block also resulted in a reduced uncertainty on the

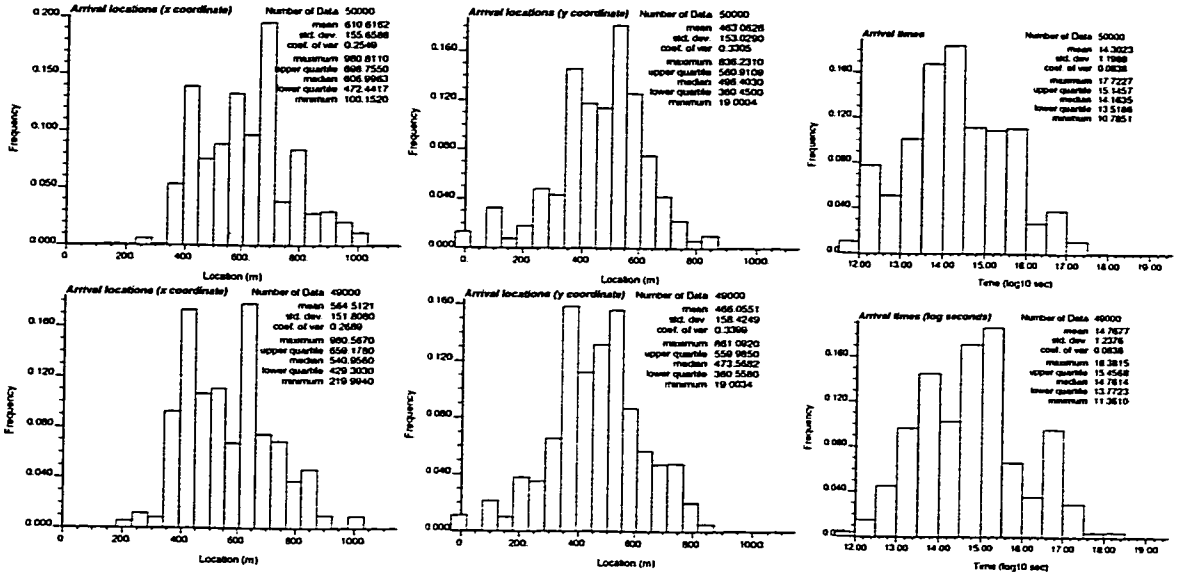

Figure 5.16. Histograms of arrival locations and times of the released particles on the control plane. Above: statistics for hydraulic conductivity blocks not conditional to head drawdown data. Below: statistics for hydraulic conductivity blocks conditional to head drawdown data.

predictions of transport simulations in a hypothetical steady-state flow regime. Therefore advective transport simulations have been carried out for the 50 hydraulic conductivity blocks only conditioned to hard and soft information on hydraulic conductivities and the 50 updated hydraulic conductivity blocks, which are also made conditional to the steady-state head drawdown data. Transport simulations on the Sellafield site have been carried out with a 3-D particle tracking program. For each simulation 1000 particles are released from three grid cells near the centre of the block, which correspond with the potential repository of nuclear waste. The particles are transported downwards by a steady-state flow field with imposed head values along all boundaries; the highest head values at the top, the lowest at the bottom and a linear head gradient along the other sides. The bottom boundary of the block serves as the control plane at which arrival positions and times of the particles are registered. Figure 5.16 shows the histograms of the arrival times and locations of all the particles on the control plane, for the 50 simulations which are not calibrated to head drawdown data and the 50 simulations which are calibrated to head drawdown data. Calibration to the head drawdown data results in longer travel times (mainly due to the less conductive fractures) and the mean arrival location on the x,y-plane is shifted 50 m to the East. However, the uncertainty about the arrival locations and arrival times has not been reduced and remains more or less the same. It is thought that there are two main reasons for this. First, the hydraulic conductivity blocks have been conditioned to hydraulic heads from a different flow regime. If hydraulic head data from the used flow regime would be available, this would help more in reducing the uncertainty about travel paths. Second, the method does not improve the identification of

the fractures in the block. The orientation of the fractures is known from geological data, the conductivities in the fracture zones are calibrated by inverse modelling, but a very exact identification of the locations of the fractures is not possible. Because the fractures determine highly the travel paths of the particles (in most individual realisations it was found that the particles are channelled and transported through the highly conductive fractures) the uncertainty on the arrival positions is not reduced.

5.3.5 Discussion

From the stochastic analysis of the results obtained in the blind prediction phase we can conclude that the ensemble of realisations is consistent with the experimental data, in the sense that the measurements are bracketed by the envelope of predictions derived from the ensemble of realisations. The degree of heterogeneity of the controlling parameters is large and this results in relatively large prediction uncertainty intervals, even though the seed conductivity realisations used in this phase are conditioned to a number of measured conductivity values. Resource constraints prevented us from running more than 20 realisations, we forecast that if more realisations had been generated a larger spread on the predictions will occur.

Although the entire analysis of how to include the structural geology model in the model block has not been presented, it is clear that incorporating the information about main fracture geometry as soft data for the construction of the geometry of the model block is valuable. Other types of soft information, such as extensive well logs or mineralogical analysis, that could provide soft information on the cell conductivities was available in the NIREX reports and their use could improve the characterisation of the site. Again, resource constraints prevented us from attempting to use these data, the main reason being the difficulty to quantify the relationship between the soft data and hydraulic conductivity, even when such a relationship can be easily established in qualitative terms.

The additional conditioning of the seed realisations used in the blind prediction phase to the spatiotemporal measurements of piezometric head reduced substantially the range of predictions for all the variables analysed. The additional data serve to constrain more the realisations making them more alike to each other and therefore making predictions also similar to each other across realisations.

The drawdown data are better reproduced, although not exactly reproduced. The conditioning process, being an optimisation process, cannot ensure exact reproduction of the target data. The generalised decrease of conductivity on the fractured cells and its counterpart increase of conductivity on the background cells observed during the calibration phase is partly a consequence of a too large difference between the mean values of the frequency distributions used to characterise the fractured and background cells. It is also indicative that in the

pressure response of the rock, both main fractures and background fracturing play a major role, not all pressure variations propagate just through the main fractures.

The use of a stochastic continuum to model the spatial variability of conductivity in the model area emphasises the role of heterogeneity in the characterisation of the flow behaviour of the model area. It also shows that there is no need to resort to a hydro-mechanical process coupling to explain the observed responses. All piezometric head observations are consistent with the range of possible outcomes obtained with the heterogeneous realisations, both in the blind prediction and the calibration phases.

Finally, it was found that the use of the calibrated conductivity fields in the simulation of contaminant transport from the potential nuclear waste repository to a control plane did not reduce the uncertainty in the predictions, as compared with conductivity fields just conditioned to hard and soft conductivity data. The hydraulic head data did not help to improve the characterisation of the main fracture plane positions. For the predictions of contaminant transport the identification of the major fracture planes is crucial.

5.3.6 Hydraulic effects of shaft sinking

The calibrated conductivity fields obtained in the previous phase were then used to predict the flow response of the model block to the sinking of a shaft through the centre of the model domain down to an elevation of -680 metres. The same flow model used in the previous phases was applied for these predictions with changes in the boundary conditions and in the source terms. For the boundary and initial conditions we assume that the block is initially at hydrostatic equilibrium, initial values are set to zero at all cells, including the cells on the block faces which constitute the boundary conditions. These boundary conditions allow to simulate drawdowns directly. To model the effect of the shaft sinking, the boundary conditions on the top face are modified and the shaft is considered as a time varying boundary line as it sinks. For the boundary conditions at the top face we solve a two-dimensional steady-state version of the groundwater flow equation with a drawdown of 400 m at the centre cell. The centre cell is the one through which the shaft crosses and 400 m is the depth of the top face of the model block. The 400 m represents also, approximately, the drawdown that will be produced by turning that cell to atmospheric pressure if we consider the saturated overburden of 400 metres. The construction of the shaft, at a rate of 1.25 m every day, is simulated in intervals of 16 days (the time needed to cross a cell of 20 m) by turning the cells through which the shaft traverses into prescribed drawdown cells with values corresponding to atmospheric pressure. The predictions based on the 20 realisations allow building a probability distribution from which the median and the two quartiles are retained. Figure 5.17 shows the drawdowns in wells RCM1 and RCM2 for elevations -640 m and -680 m. In these figures, the beginning of the time axis corresponds to the instant in which the shaft has

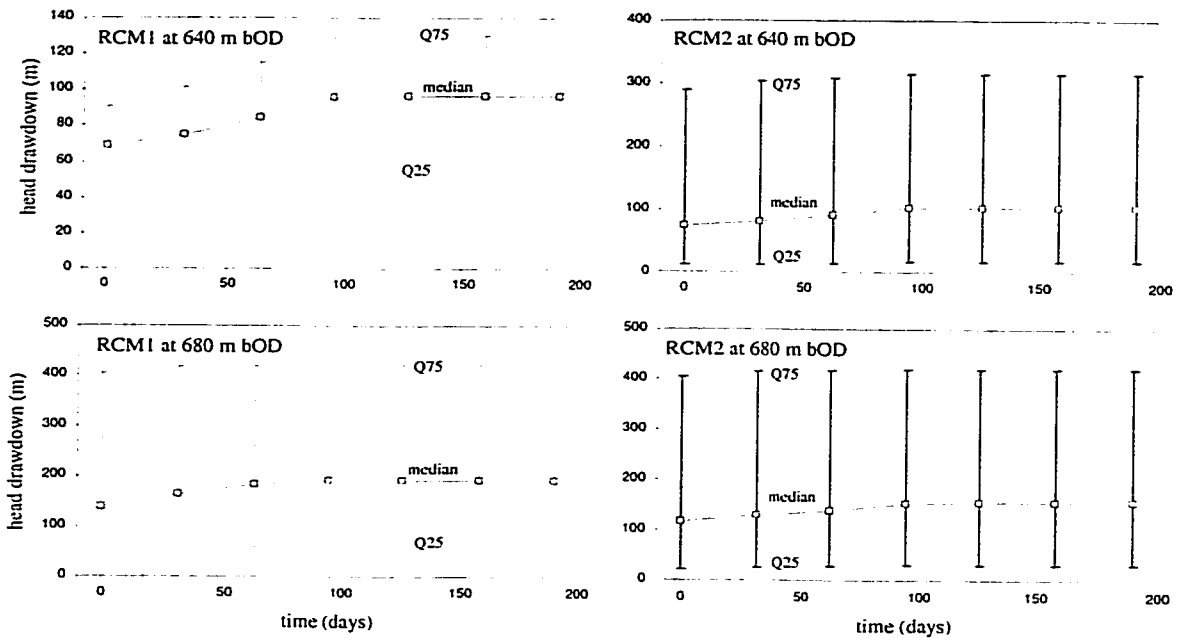

Figure 5.17. Drawdowns at wells RCM1 and RCM2 and elevations -640 m and -680 m. Median predictions and lower and upper quartiles. Zero time corresponds to the instant for which the shaft is at -600 m.

sunk to -600 metres. The median drawdown curves stabilise at about the time in which the shaft reaches its maximum depth of -680 m. The uncertainty intervals given by the interquartile range are very wide even though the realisations had been calibrated to both conductivity and piezometric head measurements. Notice also that the distribution of drawdowns is non-symmetric with respect to the median value.

Figure 5.18 shows the predicted water inflows to two sections of the shaft, at the moments the shaft has reached the bottom of the section and for steady-state conditions. The inflows are small and the spread of values across realisations is not as large as for the drawdown predictions.

The lack of experimental data from the shaft sinking prevents the evaluation of the accuracy of the predictions.

5.3.7 Conclusions

Two sets of conclusions can be reached from this study, one is methodological, related to the application of stochastic continuum models and the self-calibrating approach for the modelling and prediction of the flow behaviour of a block of fractured rock, and the other one is site specific.

On the methodological side, it can be said that a stochastic continuum model has been successfully applied for the simulation of a fractured block with a

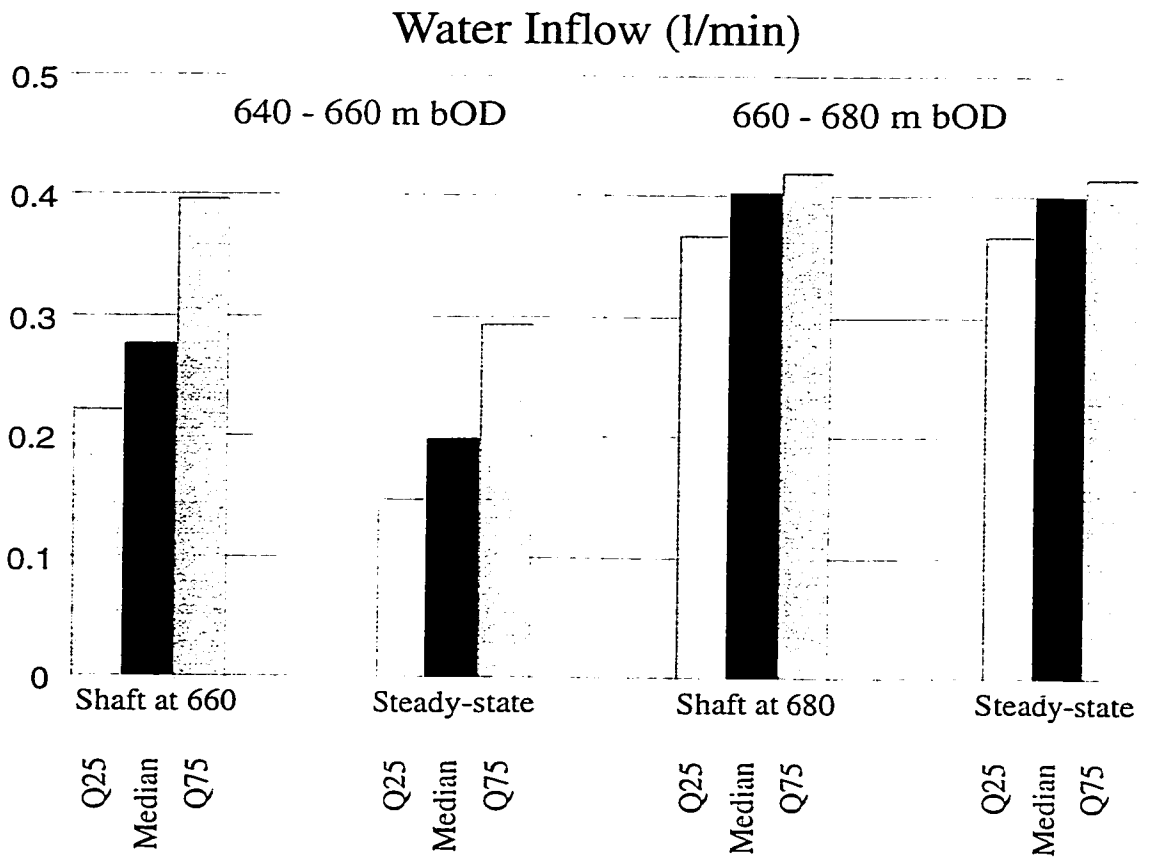

Figure 5.18. Range of inflows into two sections of the shaft at two different instants during the shaft sinking.

number of advantages with respect to discrete fracture models. It is straightforward to use the geometry data and the conductivity data to condition the model, there is no need for special treatment of the interface between fractures and the background matrix, nor is there any need for a special handling of fracture intersections. The series of conductivity realisations generated during the blind prediction phase are consistent with the measurements inasmuch the experimental values are within the range of predicted values. The use of the self-calibrating algorithm to calibrate the previous realisations to the measured piezometric heads allows reducing the uncertainty on the predictions of not only the piezometric heads but also of other response variables. However, when using those realisations for predictions under very different boundary conditions, the prediction uncertainty is still large.

On the site specific side, the evolution of the conductivity fields before and after calibration indicates that possibly the contribution of the background fracturing to the diffusion of pressure variations within the block is stronger that would be anticipated from a large conductivity contrast with respect to the main

fractures. It should be mentioned that a similar conclusion was reached by NIREX (personal communication) using an alternative approach.

5.4 Inverse modelling of groundwater flow at the 3-D fractured site of Aspö (Sweden): deterministic fracture incorporation

In section 5.3 the inverse modelling of groundwater flow at a 3-D fractured site was presented. In that study the information on the fracture plane positions was limited, although sufficient data were available to estimate the orientations of the main fracture families. In this section a study is presented in which detailed information on the positions of the main fracture planes was available. This study is carried out at the Aspö site, which was already introduced very briefly in section 3.5. The study was carried out in the context of the TRUE (Tracer Retention Understanding Experiment) Block Scale Project, in which diverse international research groups participated. The overall aim of the project was the prediction of the transport of contaminants in a network of fractures on the scale of tens of metres. A large amount of experimental data was collected for this purpose and the different research groups tried to predict the transport of contaminants, using the available experimental data as efficient as possible.

Section 5.4.1 introduces the TRUE Block Scale project and its different stages. Section 5.4.2 gives the implementation of the structural model, section 5.4.3 the hydraulic conductivity data and the simulation of hydraulic conductivity seeds and section 5.4.4 the hydraulic head data and the inverse conditioning to the hydraulic head data. Section 5.4.5 gives an analysis of the simulation outcomes, section 5.4.6 a comparison of the simulation outcomes at different stages of the project and section 5.4.7 gives results from transport simulations. Finally, section 5.4.8 includes a discussion on the results of the study and some conclusions.

5.4.1 The TRUE-Block Scale project

The investigations are carried out at the underground rock laboratory at Aspö, located on the island Aspö near the village of Oskarshamn. Oskarshamn is situated on the coast of South Sweden, about 300 km South of Stockholm. The underground rock laboratory at Aspö has been mined in a crystalline rock formation. Experiments related to the underground storage of nuclear waste are carried out at the site. However, the site is not a candidate for the storage of nuclear waste, but a test site which has to make clear to what extent numerical models can predict the effects of nuclear waste storage or the effects of an eventual accidental release of radionuclides.

A spiralling tunnel is the main access to the different niches from which the experiments are performed. The tunnel is acting as an artificial sink. At the intersections of some main fracture planes with the tunnel high water inflow rates occurred and therefore some of these fracture planes had to be grouted in order to reduce the water inflow rates. For the experiment concerning this study a number of boreholes has been drilled from the rock into the formation

at a depth ranging between 300 m and 550 m below ground surface. These boreholes have served to conduct mineralogical analysis, hydraulic tests and tracer tests. Figure 5.19 illustrates the positions of the tunnel and the boreholes.

The geological information obtained from the boreholes, mostly concerning major fracture intersections, served to build a structural model of the fracture plane positions. The structural model evolved with the drilling of each new borehole. However, the latest borehole information hardly modified the fracture plane orientations and no new fracture planes were found. The information on the positions of the main fracture planes is summarised in diverse so-called updates of the structural model; the early 1997 structural

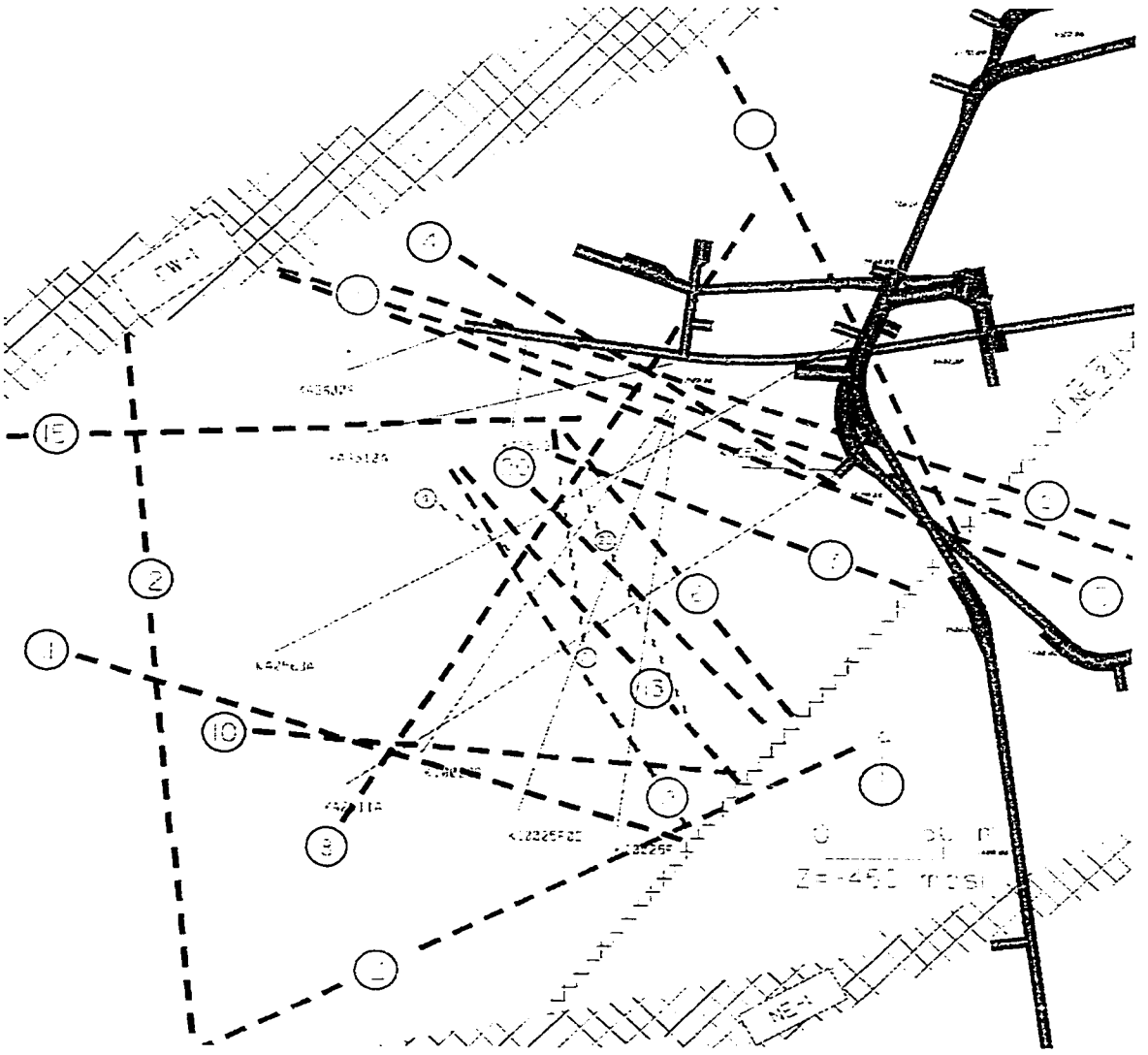

Figure 5.19. The March'99 structural model with the main structures (at 450 m depth), together with the boreholes and part of the tunnel. The figure is taken from Hermansson (2000).

model (Hermansson and Follin, 1997), the October 1997 structural model (Hermansson, 1998a), the September 1998 structural model (Hermansson, 1998b) and the March 1999 structural model (Doe, 1999). In section 5.4.2 details on the implementation of the structural model in our approach are given. Figure 5.19 shows a visualisation of the March 1999 structural model. It can be seen that most fractures are NNW-SSE oriented. Many of the fracture planes are parallel and do not form a suitable fracture network for transport experiments. However, in the central part of the domain (fractures 13, 20, 21 and 22) a fracture network was found suitable for transport experiments. A major aim at the initial stage of the project was finding a suitable network of transport experiments.

The boreholes are divided in various sections that are disconnected. Many experiments were carried out along the borehole with the aim to determine the local hydraulic conductivities or, more especifically, the hydraulic conductivity of fracture planes that intersect the boreholes. The hydraulic conductivities were determined by flow logging on 5 m intervals (Gentzschein, 1997a; Gentzschein, 1997b and Gentzschein, 1998) and by build-up tests (Gentzschein, 1996; Adams, 1998; Gentzschein and Morosini, 1998; Adams *et al.*, 1999 and Gentzschein and Ludvigson, 2000). Furthermore, flow difference measurements could also be used to estimate hydraulic conductivities (Rouhianen and Heikkinen, 1998a, 1998b, 1999a, 1999b). All these tests provided important local information on hydraulic conductivities and storativities.

In the TRUE Block Scale project diverse series of hydraulic experiments, and later also tracer test experiments, were carried out. The first experiments were oriented on the characterisation of the fracture network and the properties (transmissivity, storativity) of the main fractures. During subsequent tests, the network conductivity was better characterised and the aim was to predict the transport of particles in the fracture network. Five main interference test stages were carried out:

- The preliminary tests (Andersson *et al.*, 1998). In total 19 tests were carried out; 13 short-term tests (duration less than four hours, and in 11 of the 13 cases 30 minutes) and 6 other tests of duration 24 or 48 hours. At diverse borehole sections, without a clear preference for a zone, the pressure was dropped and at the other borehole sections the pressure changes were monitored. For one of the interference tests of longer duration, also a tracer test was carried out.
- The PT-tests (Andersson *et al.*, 1999). In total four interference tests were carried out and for one of the four interference tests four tracer tests were made; in four different boreholes tracer was injected.
- Phase A tests (Andersson *et al.*, 2000a). In total five interference tests were carried out and for two of them multiple (non-reactive) tracer tests (three and five) were done. The selected two interference tests were thought to yield high mass recoveries for a larger number of tracer injection locations. The injection locations were selected with the objective to test multiple

travel paths that could be suitable for posterior injection of reactive tracers. The different research groups that participated in the TRUE-Block Scale Project predicted the outcomes of the tracer tests.

- Phase B tests (Andersson *et al.*, 2000b). In total ten tracer tests were carried out for one selected pumping location. Eight different injection locations were tested, two of them for the injection of two different tracers. The selected pumping location was the one that was thought to give the maximum number of travel paths with a high mass recovery. The different preceding interference tests were used to determine the pumping location.
- Phase C tests (Byegard and Winberg, 2000). The same pumping location as in the Phase B tests was also used in the Phase C tests. In total five injection locations were used in the Phase C tests. In each of the injection locations multiple reactive and non-reactive tracers were used. The different research groups had to predict the outcomes from these tracer tests. The five injection locations were selected on the basis of the outcomes of the preceding tracer tests. The aim was to select five transport paths with an expected high mass recovery. One of the transport paths was for a single fracture, the others were for a network of fractures.

More information was collected in the context of the TRUE Block Scale project. However, this information was not used in the modelling study presented in this section. The other collected information consists of borehole images (Carlsten, 1998a, 1998b), mineralogical studies (Tulborg, 1998), seismic information (Cosma *et al.*, 1998) and groundwater chemistry (Andersson and Laaksoharju, 1999; Säfvestad and Andersson, 1999a; Säfvestad and Andersson, 1999b; Andersson and Säfvestad, 2000).

5.4.2 The implementation of the structural model

The groundwater flow model assumes that flow takes place in both the main fracture planes and the background fractures. Therefore the full domain is considered in the model and not only the main fracture planes. The elements not belonging to the main fractures are referred to hereafter as "background". The background cells contain both rock matrix and background fracturing.

The flow model extends over an area of 247 m (1786.7 to 2033.3 m Easting) by 227 m (7046.7 to 7273.3 Northing) by 287 m (-573.3 to -286.7 m depth). The area is divided into 37 by 34 by 43 cubic grid cells of size 20/3 m. It would have been preferable to use a smaller grid cell size, however, in order to reduce the required CPU time it was not possible to reduce the grid cell sizes more. The observed size of the fracture planes is in general less than 1 metre so that cubic grid cells of 6.6667 m are a very coarse representation of the fracture planes. Another consequence of the "coarse" fracture planes is the artificial

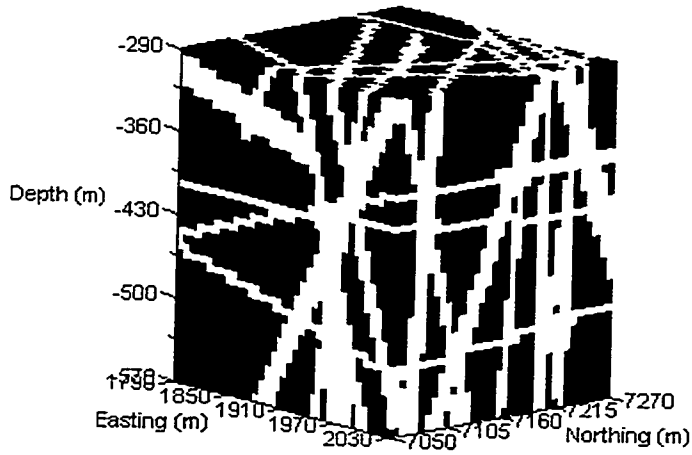

Figure 5.20. Classification of the model grid cells into cells corresponding to fracture planes (white) and cells not corresponding to any fracture plane (black).

enhancement of the connection between the different fracture planes near fracture intersections.

A total of four modelling analyses were performed. The difference between them is based on the amount of information used to build them, which was incorporated to the modelling as it was provided from the experts.

For the two most recent modelling analyses the March 1999 structural model (Doe, 1999) was used for the definition of the fracture planes and the fracture lateral extents (Hermanson, 1998b; Doe, 1999). The program FRACNET was used to calculate which grid cells from the numerical model are intersected by the fracture planes. The grid cells can be divided then between grid cells intersected by one or more fracture planes and grid cells which are not intersected by any fracture plane (the background fracture cells). Figure 5.20 shows a binary classification of the model cells distinguishing between those cells that are intersected by one or more cells and those which are not. The model includes 21 fracture planes. For each grid cell a reference to the fracture planes that intersect it is stored.

5.4.3 Simulation of hydraulic conductivity fields

For the most recent simulation stage hydraulic conductivity data from three different sources were used:

- flow logging on 5 m intervals (Gentzschein, 1997a; Gentzschein, 1997b and Gentzschein, 1998). This resulted in a total of 101 hydraulic conductivity data for the background.
- POSIVA flow log data. The POSIVA flow log data for the boreholes KA2511A, KA2563A, KA3510A, KI0025F02 and KI0025F03 (Rouhianen and Heikkinen, 1998a, 1998b, 1999a, 1999b) are used to estimate transmissivities. The interpreted transmissivities from this information were supplied to me by Bill Dershowitz (see also Dershowitz, 2000). Resulting in a total of 169 extra conductivity data for the background.
- build-up tests (Gentzschein, 1996; Adams, 1998 and Gentzschein and Morosini, 1998), including the compiled data set of estimated transmissivities at the intersections between boreholes and fracture planes (Doe, 1999). Fracture conductivities were determined from transient tests when available, otherwise from steady-state tests. If more than one transient test is available, the geometric mean of the estimates is used. This resulted in a total of 23 transmissivity data for the fracture planes. For each of the fracture planes a database is built; for some of the fracture planes no transmissivity data are available, the maximum number of transmissivity data for any of the fracture planes is four. The conductivities used in the model are the transmissivities obtained from the data divided by the numerical model grid block size (6.6667 m).

Figure 5.21 shows the histogram of the hydraulic conductivity data. The hydraulic conductivity data were used to generate the conditional hydraulic conductivity seeds by sequential Gaussian simulation. Each hydraulic conductivity seed is obtained by merging the independent realisation of each of the 22 populations (21 fracture planes plus background). Each population is generated in the log-space and later backtransformed into the decimal space. To generate each of the populations, besides the conditioning data, it is necessary to provide the overall mean conductivity and a variogram. The mean conductivity of each population is obtained from the data values of that population, except for those fracture planes with no data, in which case a mean equal to the mean of all fractures is used. For the variograms, there is no data in any population to estimate a meaningful variogram, therefore a variogram model is adopted. For all 22 populations, the same variogram for $\log_{10}$-conductivity is used: spherical, with a range of 40 m, a nugget 0.1 $(\log(m/s))^2$ and a sill of 1.0 $(\log(m/s))^2$.

When merging the 22 populations, fracture plane cells always prevail over background cells. However, those cells that are intersected by more than one fracture plane form the fracture intersection zones (FIZs). The conductivity assigned to a grid cell in a FIZ is equal to the geometric mean of the conductivities of each of the fractures intersecting the cell. Figure 5.22 shows a view of a hydraulic conductivity seed.

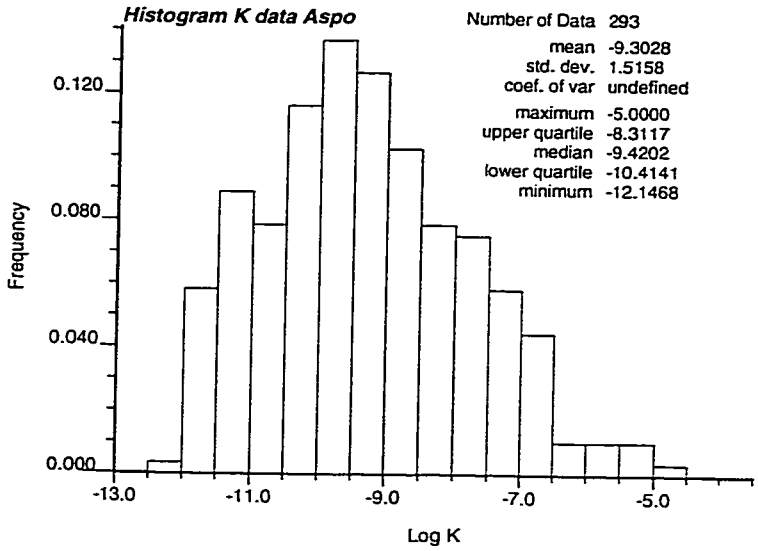

Figure 5.21. Histogram of the hydraulic conductivity data ($\log_{10}$ (m/s)).

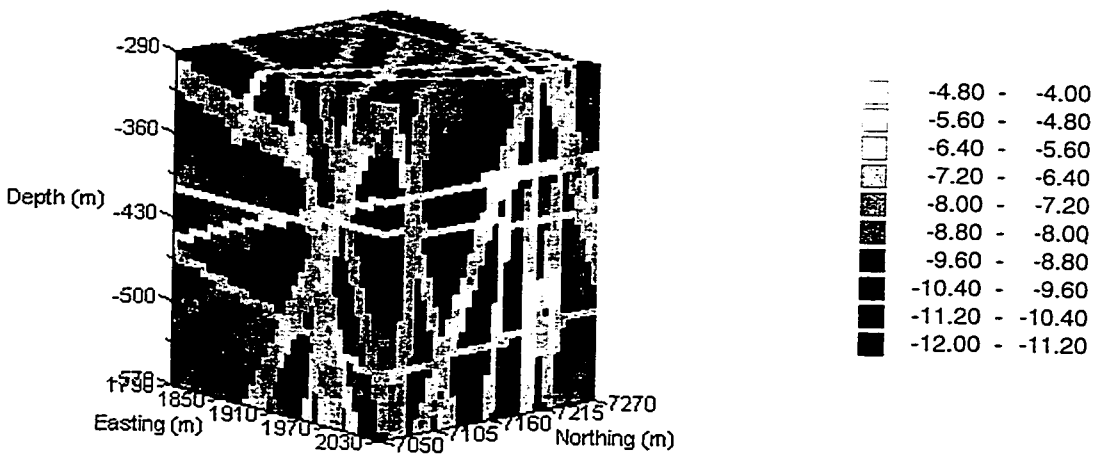

Figure 5.22. Hydraulic conductivity seed realisation ($\log_{10}$ (m/s)). This realisation is conditioned to the information on the fracture plane positions and hydraulic conductivity data.

5.4.4 Conditioning to hydraulic head data

The seed hydraulic conductivity fields are the starting point to obtain conductivity fields conditioned to hydraulic head data. Boundary conditions had to be supplied to the model. Prescribed heads were imposed along all the six sides of the cube. The prescribed heads were obtained from the regional groundwater flow model (Svensson, 1997). Part of the tunnel, at atmospheric pressure, is also included in the model. Since it was known that the hydraulic heads were not completely at steady-state and kept decreasing by the sink effect of the tunnel, and since the self-calibrating approach is capable to calibrate the

boundary conditions too, it was decided to use the heads from the regional groundwater flow model as a starting value for the calibration of the boundary conditions, too.

The conditioning to the transient test information is carried out on a smaller grid in order to reduce the needed CPU time. Advantages are that more realisations could be conditioned to transient test information and also the numerical stability of the groundwater flow solution improves. The smaller grid has 20 by 20 by 22 grid cells (8800 grid cells in total), with the same grid cell sizes as for the steady-state groundwater flow simulation, and extends from 1853.3 to 1986.7 m Easting, 7113.3 to 7246.7 m Northing and 573.3 to 426.7 m depth. For the conditioning to transient data, we consider only drawdowns, not absolute piezometric heads, and since the transient tests to which the realisations are conditioned do not last enough for their effects to reach the boundary cells, zero drawdown initial conditions were used, and zero drawdowns were prescribed at the boundary cells.

5.4.4.1 Conditioning to steady-state head data

A total of 51 steady-state head data, from nine boreholes, were used as conditioning data. One thousand master blocks were used in the conditioning procedure; 100 master blocks are located in the background on a regular grid with a random starting point, and 900 master blocks are located randomly on the different fracture planes with a minimum of 12 master blocks for each fracture plane. For the calibration of the boundary conditions, 100 master blocks were considered, and a maximum deviation of 20 m with respect to the heads from the regional groundwater flow model is allowed. The locations of the master blocks vary between realisations and during the conditioning of a single realisation the master block positions also change between iterations of the conditioning algorithm.

During the inverse conditioning step, the possibility of treating the FIZs as an independent population arouse, and after some tests it was decided to treat them so. The alternative to treat the FIZs as the geometric average of the conductivity values of the intersecting fractures was discarded after considering that at the intersections conductivity could be either enhanced or reduced depending on physical and mechanical factors.

5.4.4.2 Conditioning to transient head data

The seed fields used for the conditioning to transient head data are those obtained after conditioning to steady-state head data. A total of five short-term (about 30 minute duration) tests and a long-term test (72 hour duration) were used in the conditioning procedure. Due to CPU limitations no more tests were included in the inverse modelling. The five short-term tests formed part of 19 preliminary tests. The five short-term tests were selected out of the 19 tests for the conditioning procedure for the following reasons:

- They focused on the fractures that form a fracture network that was used later in the tracer tests for Phase A, B and C.
- The injection locations were located in the zone in which later the tracer tests of Phase A, B and C were carried out.

The PT-tests were not used in the conditioning, but the pumping location in one of the PT-tests, the PT-4 test, was the same as in the A4 test; the flow situations in the PT-4 test and the A4 test are similar.

The Phase A4 test was used in the conditioning procedure. Preference was given to this test, because the pumping location in this test was also used in the Phase B and the Phase C tests, of which the outcomes had to be predicted.

Table 5.7 gives information on the selected tests in the inverse modelling.

At 13 monitoring locations, the transient response to all tests was used as conditioning data; and, at 16 additional locations, the transient response to the long-term test was also available and used for conditioning.

Borehole section	Test conditi-ons*	Flow period (h)	Easting (m)	Northing (m)	Depth (m)
KI0023B:P4	CH, -386 m	0.5	1907	7175	479
KA2563A:R1	CH, -307 m	0.5	1870	7177	503
KI0025F:R5	CH, -410 m	0.5	1947	7179	469
KI0023B:P7	CH, -280 m	0.5	1922	7198	468
KI0023B:P2	CH, -236 m	0.5	1894	7154	488
KI0023B:P6	CQ, 2.3 l/min	289.5	1915	7186	473

*CH= Constant head drawdown, CQ=Constant pumping rate

Table 5.7. The interference tests included in the inverse modelling of transient groundwater flow. The constant pumping rate test is the A4 test.

A decision was taken to calibrate a single homogeneous storativity value for all realisations, instead of considering spatially variable storativities. The main reason was to save CPU time during the calibration of the seed fields, although it would have been possible to calibrate jointly couples of realisations of conductivity and storativity. For the calibration of the single homogeneous storativity the seed value was 10^{-6} m^{-1}.

For the short-term tests of 30 minute duration, the temporal domain was discretised in four time steps, the first time step being the smallest one. For the Phase A4 test the initial time step was 5 minutes and the magnitude of the

subsequent time steps increased with a factor 1.5. This resulted in a total of 15 time steps.

A total of 1000 master blocks was used in the conditioning to the short-term test data, 100 of them located in the background and 900 in the fracture planes. For the conditioning to the long-term test a total of 1500 master blocks was used, 500 of them located in the background and 1000 in the fracture planes. Like for the inverse modelling of steady-state groundwater flow the master blocks located in the background were laid on a regular grid with random starting point. The master blocks located in the fracture planes were distributed randomly with a minimum of 12 master blocks per fracture plane.

5.4.5 Simulation results

In this section the results corresponding to the last simulation round are presented. This section is divided in four subsections. In section 5.4.5.1 some comments on the performance of INVERTO and numerical problems encountered are given. In section 5.4.5.2 the results of the conditioning of multiple realisations to hydraulic conductivity data and steady-state head data are presented. In section 5.4.5.3 the conditioning to transient head information is discussed. Both in section 5.4.5.2 and in section 5.4.5.3 the focus is on the evolution of fracture plane conductivities. Section 5.4.5.4 gives a small summary on the simulation results.

5.4.5.1 Performance of INVERTO and numerical problems

As stressed in the sections 3.3 and 5.2, the large conductivity contrasts between the fracture plane and the background, on average 3.5 orders of magnitude and locally up to 10 orders of magnitude, cause serious problems during the numerical solution of the groundwater flow equation. This is due to the nearly singular left hand side conductance matrix. Nevertheless, sufficient close solutions to the groundwater flow equation were found. This could be checked by using the final results as input to the groundwater flow equation and reducing the allowed error of the numerical solution. In case the hydraulic head solution was very similar to the solution for the larger error, the solution of the linear system of equations was sufficiently close. In the inverse modelling the error criterium is relaxed as compared to the "normal" forward solution of a groundwater flow problem; in a transient groundwater flow inverse problem the groundwater flow equation has to be solved thousands of times and each time a sufficient precise solution has to be found. Although in general it was not a problem to find a sufficiently close solution, in a limited amount of cases the solution found was not sufficiently close. In those cases the realisation was not included in the analysis.

INVERTO was in general able to reproduce the experimental head data sufficiently close. The steady-state head data and the head responses to the five short-term tests could be reproduced closely in all cases. More problems were

encountered to reproduce the head drawdowns to the long-term transient test. A specific numerical problem that in a limited amount of cases hindered the reproduction of the head drawdowns was a simulated head decrease for a pumping test equal to zero metres everywhere in the domain, except for the pumping location. In that case the partial derivatives of the objective function with respect to changes in the hydraulic conductivity at the master blocks are zero or very small. The result may be that the optimisation algorithms are not able to generate the perturbation that extends the head decrease in the simulation domain. Another problem is related to the joint simulation of multiple transient tests. The conditioning of different transient tests may be difficult because normally conductivity perturbations around each of the pumping wells are needed to reproduce the experimental head data. The gradient vector contains all the master blocks, including the master blocks around the different wells. However, the optimal scalar parameter that is used to be multiplied with the updating direction vector may be different for the groups of master blocks that can be associated with the different wells. The gradient vector is just multiplied with one scalar parameter and a common result is that the conditioning initially just improves the head reproduction near one of the pumping wells. In general, the contradictory objectives may prevent a satisfactory reproduction of all the transient tests. Therefore, the different transient tests are incorporated sequentially. INVERTO also allows for setting the perturbations equal to zero except for a window around one or more pumping wells. This makes it possible to reproduce the head drawdown data for one pumping test without having contradictory objectives, and later incorporate the other pumping tests one-by-one.

5.4.5.2 Conditioning to hydraulic conductivity and steady-state head data

A total of 12 conductivity realisations was conditioned to hydraulic conductivity and steady-state head data. Section 5.4.3 explains how the hydraulic conductivity seeds are generated. Section 5.4.4 explained the conditioning to steady-state head data. For each of the seed conductivity realisations, the average hydraulic conductivity in the background, each of the 21 fracture planes, and the fracture intersection zones are calculated. These averages for each of the realisations are, in turn, averaged over the 12 realisations. See Table 5.8. The average background hydraulic conductivity over the 12 realisations is –10.0 $\log_{10}$ (m/s) and the average fracture plane conductivity –6.7 $\log_{10}$ (m/s), a difference of more than three orders of magnitude. The differences in average conductivity among the fracture planes are also considerable and the most conductive fracture plane (fracture plane #5; -4.7 $\log_{10}$ (m/s)) is more than three orders of magnitude more conductive than the less conductive fracture plane (fracture plane #13; -8.1 $\log_{10}$ (m/s)). The differences in average fracture plane conductivities among realisations are small.

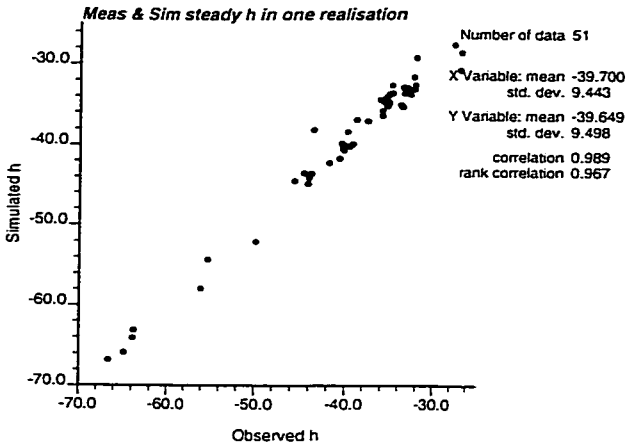

Figure 5.23. Comparison of the simulated and measured steady-state head values, for a realisation.

In the next step, the seeds were conditioned to steady-state head data. Figure 5.23 shows the reproduction of the steady-state head data. Figure 5.24 gives the results from one of the realisations with the updated hydraulic conductivities and the spatial distribution of steady-state heads after conditioning. From the figure it can be seen that the prescribed head boundaries force a flow in the direction towards the tunnel on the North and East sides. The conditioning to steady-state head data induces important local conductivity changes with regard to the seed fields. However, there is not a clear trend in these changes like in the Sellafield study, where an important reduction in the conductivity contrast between background and fractures was observed due to the conditioning to the piezometric head data. The following observations can be made after analysing the results:

- Conditioning to steady-state head data hardly modifies the average conductivity contrast between background and fracture planes. Just a small increase is observed due to a decrease in the background conductivity (average over 12 realisations –10.2 $\log_{10}$ (m/s)). See Table 5.8.
- The contrast on average conductivities among the fracture planes decreases slightly (See again Table 5.8). In particular, fracture plane number 5 with the largest average conductivity in the seed realisations decreases from –4.7 to –5.5 $\log_{10}$ (m/s). On the contrary, fracture plane 13 with the smallest average conductivity in the seed realisations increases from –8.1 to –7.4 $\log_{10}$ (m/s). The largest difference between average conductivities after conditioning is between fracture plane 8 (–5.4 $\log_{10}$ (m/s)) and fracture plane 6 (–8.3 $\log_{10}$ (m/s)). Figure 5.25 illustrates the conductivity changes during the conditioning to steady-state head data.
- The contrast in average fracture plane conductivities among realisations increased during the conditioning to steady-state head data. This indicates that the estimated prior ensemble variances were too low. For most of the fracture planes both increases and decreases in the average

	Conditioned to geology and K data	Conditioned to steady heads	Conditioned to five short-term tests	Conditioned to long duration tests
Background	-10.01	-10.21	-10.13	-10.21
Fr. Plane 1	-6.59	-6.59	-6.61	-6.62
Fr. Plane 2	-6.34	-6.11	-6.06	-6.17
Fr. Plane 3	-6.54	-6.41	-6.18	-6.21
Fr. Plane 4	-7.27	-7.13	-7.10	-7.15
Fr. Plane 5	-4.71	-5.46	-5.38	-5.41
Fr. Plane 6	-7.94	-8.33	-8.22	-8.27
Fr. Plane 7	-5.58	-6.32	-6.12	-6.13
Fr. Plane 8	-5.45	-5.35	-5.52	-5.69
Fr. Plane 10	-7.01	-7.00	-7.04	-7.10
Fr. Plane 12	-7.83	-7.88	-7.85	-7.86
Fr. Plane 13	-8.05	-7.38	-7.29	-7.33
Fr. Plane 15	-7.64	-7.78	-7.80	-7.80
Fr. Plane 16	-5.36	-5.70	-5.78	-5.89
Fr. Plane 17	-5.96	-5.97	-5.96	-6.02
Fr. Plane 18	-7.04	-6.93	-6.96	-6.84
Fr. Plane 19	-6.70	-6.93	-6.95	-6.92
Fr. Plane 20	-6.95	-6.81	-6.65	-6.79
Fr. Plane 21	-8.05	-7.61	-7.48	-7.80
Fr. Plane 22	-7.22	-7.07	-7.01	-7.20
Fr. Plane 23	-7.05	-7.06	-7.07	-7.04
Fr. Plane 24	-6.34	-6.33	-6.33	-6.34
FIZ	-6.58	-6.46	-6.99	-7.57

Table 5.8. Average fracture plane conductivities after different conditioning stages. The averages are calculated over 12 realisations after conditioning to geology and conductivity data and after conditioning to steady-state head data. The averages are calculated over 10 realisations after conditioning to five short-term transient tests and over 8 realisations after conditioning to long duration tests.

fracture plane conductivity are observed throughout the set of generated realisations. Just fracture plane number 5 shows a decrease in average fracture plane conductivity for all the realisations, while a decrease in average fracture plane conductivity for all the realisations is just observed for fracture plane 13.

- Also related with a too low estimate of the prior ensemble variance is the increase in spatial variability of hydraulic conductivity within the realisations. Although the average fracture plane conductivities do not change so much, the variances of the fracture plane conductivities increase. More over, the distributions of the fracture plane conductivities become more skewed for many of the fracture planes in most of the twelve realisations.

Figure 5.24. Results after conditioning to steady-state head data, for one single realisation. From left to right, from above to below and continuing on the next page: 3-D steady-state head solution (m), steady-state head solution for slices at 550 m, 470 m, 390 m and 310 m depth. An updated 3-D hydraulic conductivity image ($\log_{10}$ (m/s)) and slices at 550 m, 470 m, 390 m and 310 m depth.

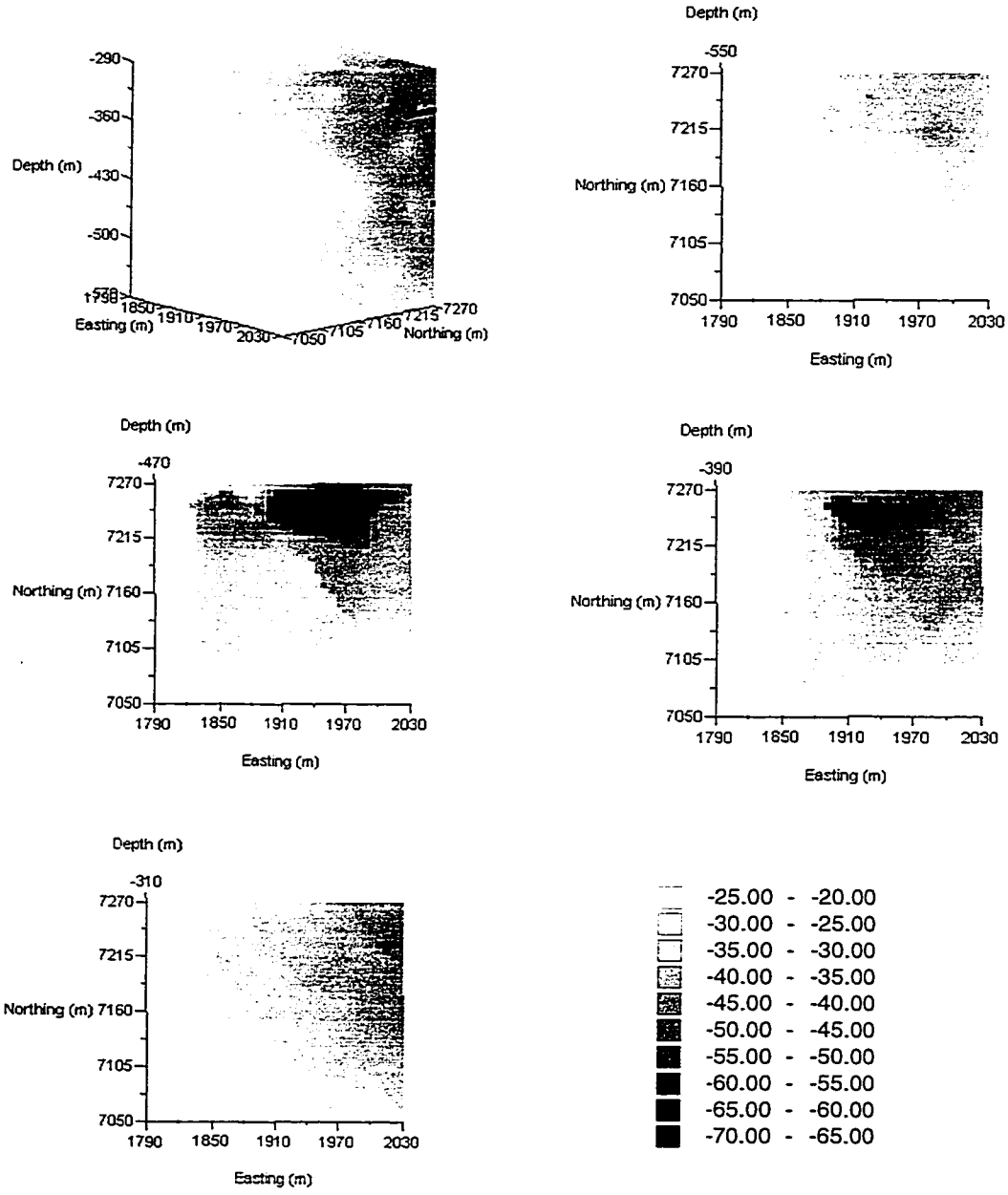

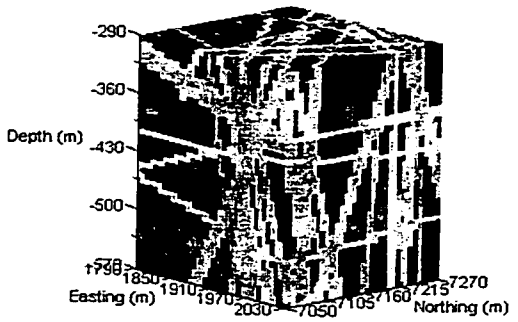
-290
-360
Depth (m)
-430
-500
1790
1850
1910
1970
2030
Easting (m)
7050
7105
7160
7215
7270
Northing (m)

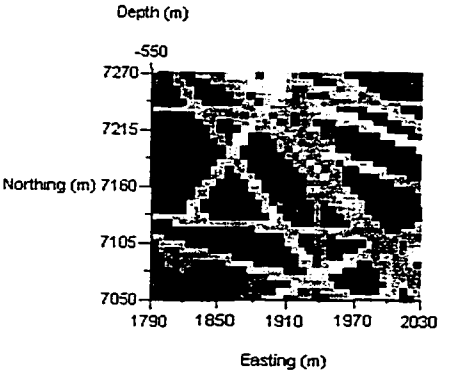
Depth (m)
-550
7270
7215
Northing (m) 7160
7105
7050
1790
1850
1910
1970
2030
Easting (m)

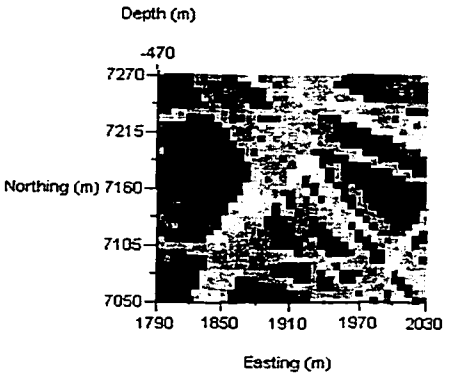
Depth (m)
-470
7270
7215
Northing (m) 7160
7105
7050
1790
1850
1910
1970
2030
Easting (m)

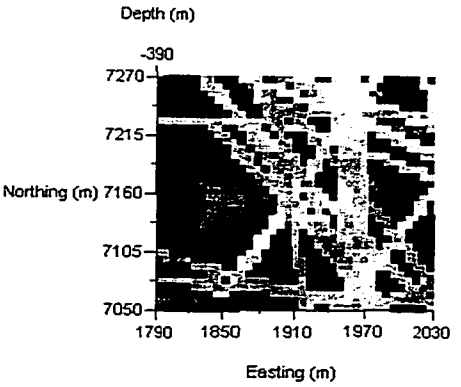
Depth (m)
-390
7270
7215
Northing (m) 7160
7105
7050
1790
1850
1910
1970
2030
Easting (m)

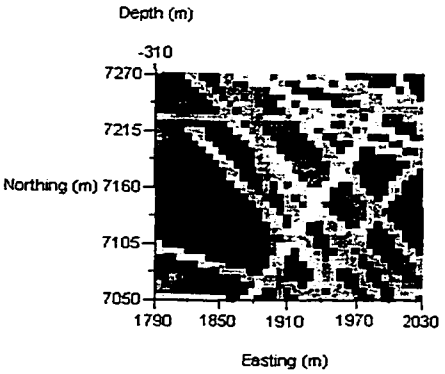
Depth (m)
-310
7270
7215
Northing (m) 7160
7105
7050
1790
1850
1910
1970
2030
Easting (m)

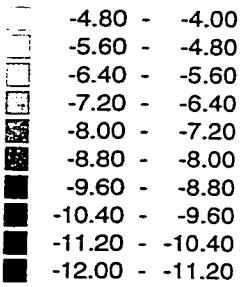
-4.80 - -4.00
-5.60 - -4.80
-6.40 - -5.60
-7.20 - -6.40
-8.00 - -7.20
-8.80 - -8.00
-9.60 - -8.80
-10.40 - -9.60
-11.20 - -10.40
-12.00 - -11.20

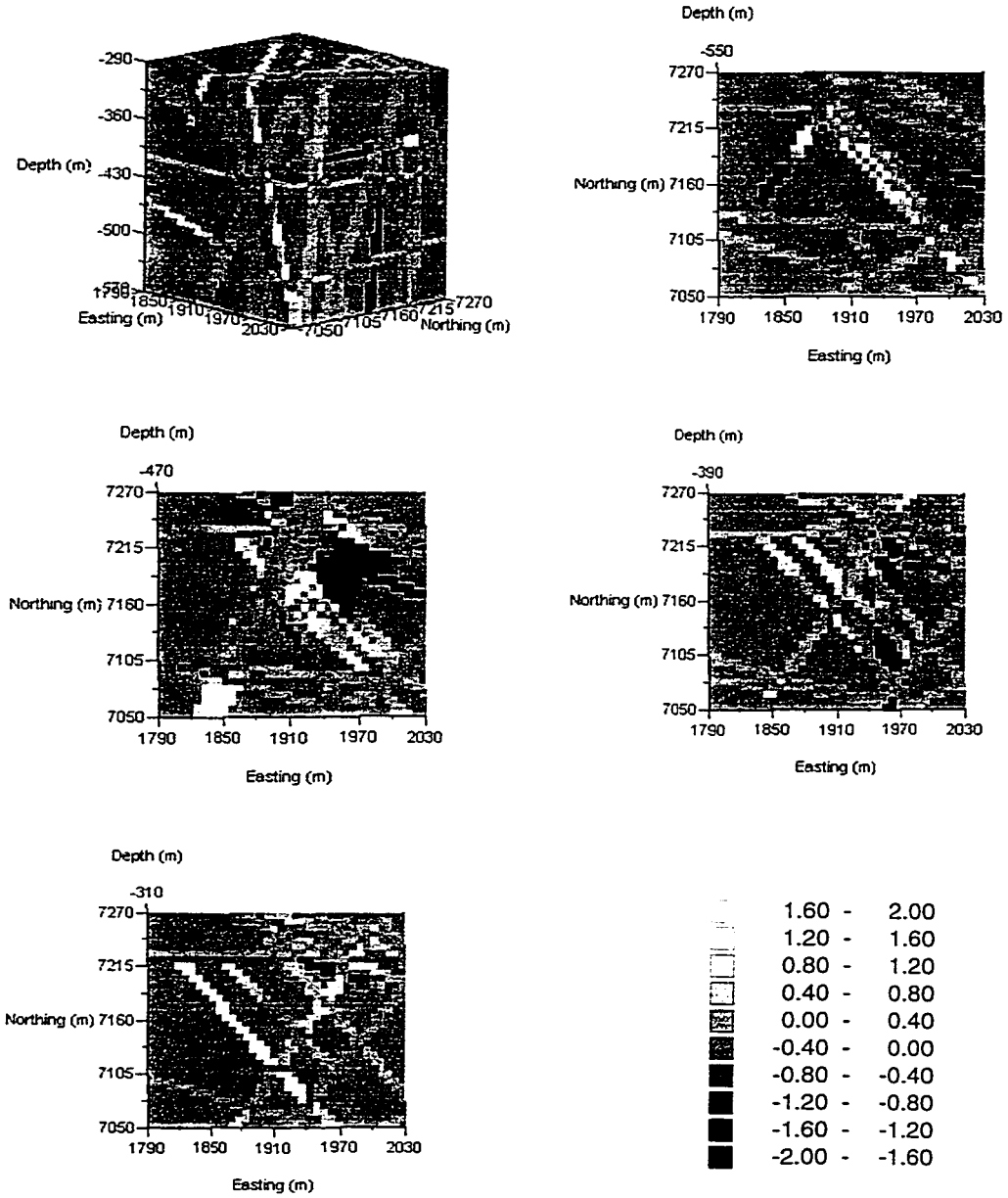

Figure 5.25. Hydraulic conductivity perturbation during conditioning to steady-state head data, for one realisation. From the left to the right and from above to below: 3-D image of hydraulic conductivity perturbation ($\log_{10}(m/s)$), hydraulic conductivity perturbation for slices at 550 m depth, 470 m depth, 390 m depth and 310 m depth.

Together with the hydraulic conductivities also the prescribed heads along the boundaries were allowed to change during the conditioning. The most important head perturbations, with respect to the head values deduced from the regional groundwater flow model of 1996 are made on the Northern boundary of the model, near the tunnels. This may indicate that the influence of the tunnel on the head distribution is stronger than was supposed by the boundary heads prescribed initially. All the simulations showed, in general, a head decrease on the boundaries with a larger decrease in the zones near the tunnels on the Northern and Eastern model boundary. The observed decrease of the boundary heads in the calibration is consistent with the observed decreases of the "steady-state head" values in the years 1996 until 1999.

5.4.5.3 Conditioning to transient head data

Of the 12 realisations conditioned to steady-state head data, only 8 could be conditioned to all the transient information (10 realisations were conditioned to the short-term transient tests, but not to the long term test). For two of the 12 realisations it was not possible to obtain a sufficiently close solution of the groundwater flow equation. For two other realisations the reproduction of the experimental heads was not satisfactory. For all 8 realisations the reproduction of the experimental heads was satisfactory. Figure 5.26 shows, for a single realisation, the head drawdowns in the transient tests. It is clear from the figure that the head decreases extend along the orientation of the fracture planes, in the NNW-SSE direction and in the vertical direction. It was checked that the drawdowns induced by the tests did not reach the boundaries, so that the zero drawdown prescribed boundary conditions are consistent with the tests. For some transient tests in some realisations the assumption could not be justified completely, but in general the assumption is not violated.

In addition to conditioning the conductivity fields, for each realisation a single storativity value was calibrated. Table 5.9 gives the calibrated single storativity values for all the realisations; these values are very similar for all realisations.

Simulation number	Calibrated Storativity (m^{-1})
3	$1.50 * 10^{-8}$
4	$1.90 * 10^{-8}$
5	$2.07 * 10^{-8}$
6	$2.20 * 10^{-8}$
9	$1.80 * 10^{-8}$
10	$2.20 * 10^{-8}$
11	$3.60 * 10^{-8}$
12	$1.30 * 10^{-8}$

Table 5.9. Calibrated single storativity values for the different realisations. Only eight realisations could be generated.

Figure 5.26. Hydraulic head drawdown (m) during the long-term pumping test. This solution corresponds to one realisation conditioned to all the pieces of information. From the left to the right and from above to below: 530 m depth, 510 m depth, 490 m depth, 470 m depth (pumping location) and 450 m depth.

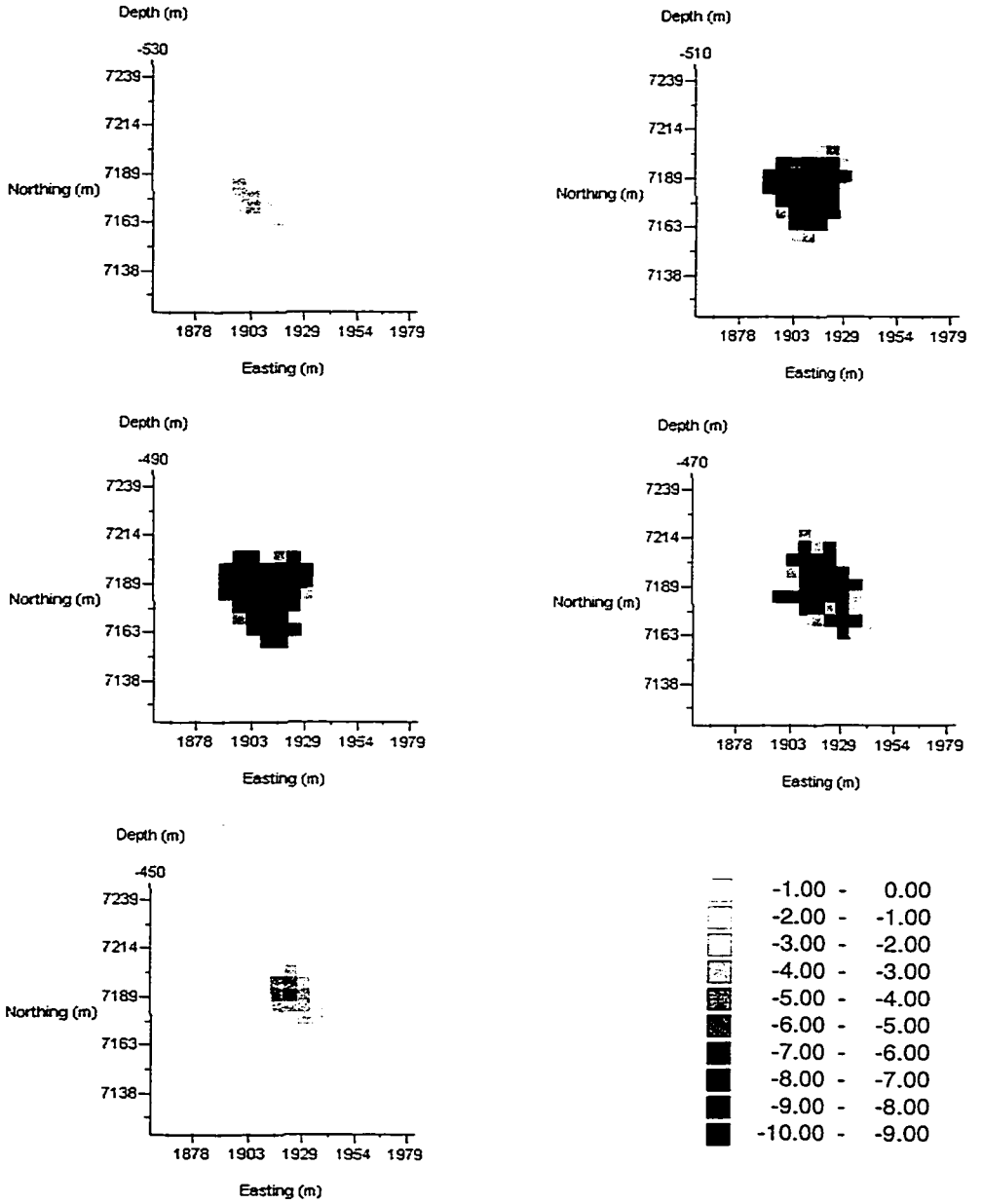

With regard to the changes in conductivity during the process of conditioning to the transient data, these modifications are very localized in each fracture plane and do not represent large changes neither for the background nor for the fracture planes. The average conductivities are hardly affected by the calibration, each fracture changes in average less than 0.3 $\log_{10}$ (m/s) units. See Table 5.8. The fracture planes that are the main target of the transient tests (fracture planes 6, 7, 13, 19, 20, 21 and 22, which are likely candidates for tracer tests in a latter stage of the experiment) decrease their average fracture plane conductivity up to a maximum value of 0.3 $\log_{10}$ (m/s) units. The most important conductivity changes, however, are observed in the FIZs; the average conductivity for the FIZ grid cells decreases 0.6 $\log_{10}$ (m/s) units. This decrease, however, is thought to be a numerical artefact: due to the coarse discretization of the fracture zones, the volume of the model representing fracture intersections is too large, especially for fractures which are subparallel, the fractures are too connected. To compensate this artificial connectivity the hydraulic conductivity of the FIZ grid cells is decreased considerably. This decrease should be interpreted as a mechanism of the algorithm to compensate for the enhanced connectivity and no physical explanation should be sought.

In spite of the fact that the average fracture plane hydraulic conductivities hardly change, the variances of the average fracture plane hydraulic conductivity increase during the conditioning to the transient tests. With the variance of the average fracture plane hydraulic conductivity we refer to the variations in the average conductivity for a certain fracture plane from one realisation to another. This increase is in addition to the increase observed during the conditioning to steady-state head data.

Also an additional increase is found in the conductivity variance within each of the fracture planes. However, this increase is limited to the fracture planes that are affected by the conditioning to the transient head data. Figure 5.27 shows the conductivity perturbation applied to condition to transient head data, for a certain realisation and for one of the fracture planes. It is clear that, locally, important hydraulic conductivity changes are induced. Some parts of the fracture planes become much less conductive (with a conductivity similar to the background material), while other parts of the fracture plane have very high conductivities. Also the spatial correlation of the applied perturbations can be seen clearly in the figure. Figure 5.28 gives a histogram with the hydraulic conductivities for the fracture plane 20 before the inverse conditioning (just conditioned to hydraulic conductivity data) and after the inverse conditioning to the transient head data. The graphs illustrate the variance increase for the fracture plane and also show that the distribution, initially close to Gaussian, becomes more skewed. These tendencies were observed in all realisations, for many of the fracture planes affected by the transient tests and were already observed during the conditioning to steady-state head data and reinforced during the conditioning to transient head data.

Figure 5.27. Hydraulic conductivity perturbation ($\log_{10}$ (m/s) (for one single realisation) due to conditioning to hydraulic head responses from six interference tests. From the left to the right and from above to below: 550 m depth, 510 m depth, 470 m depth, fracture plane 20.

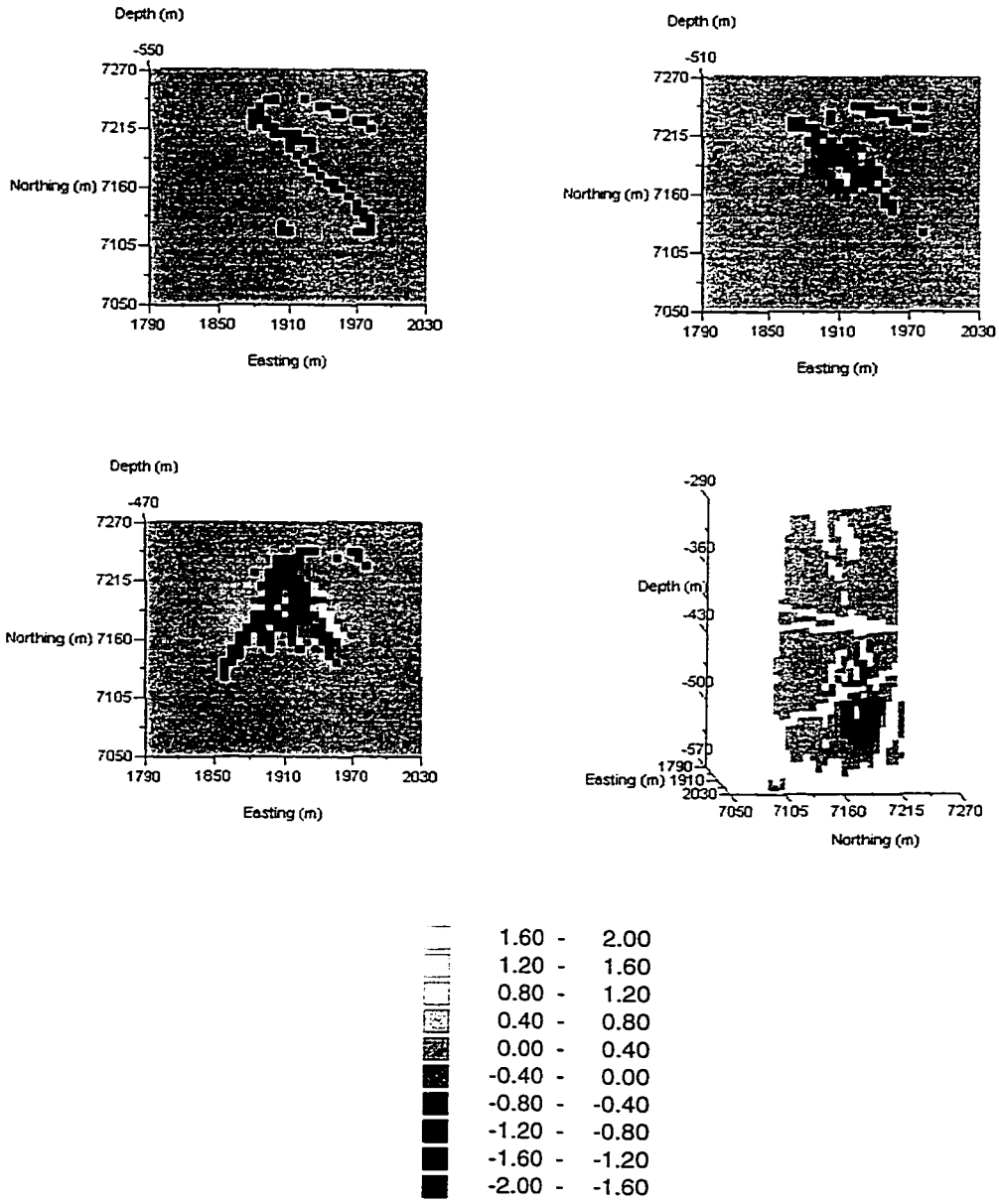

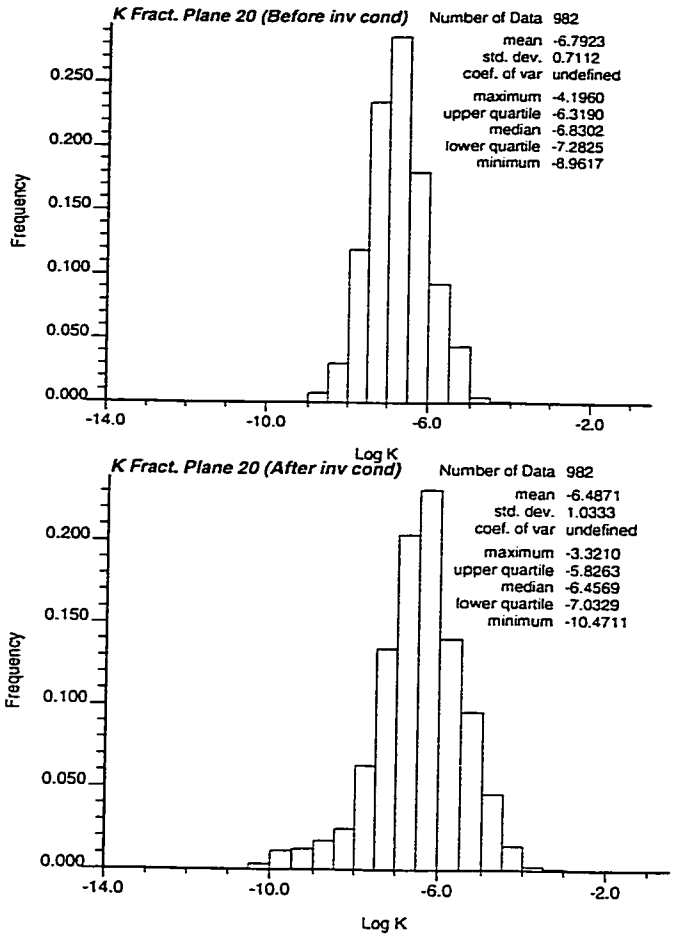

Figure 5.28. Statistical distribution of hydraulic conductivities ($\log_{10}$ (m/s) for one single realisation. (a) before conditioning to any head data, (b) after conditioning to steady and transient head data.

5.4.5.4 Summary on simulation outcomes

In total 8 realisations were conditioned to geology (structural model with fracture plane definitions), conductivity data, steady-state head data and head drawdown data from transient tests. The following can be concluded after the complete conditioning to the experimental information:

- The reproduction of the piezometric heads (steady-state and transient) is good for the eight realisations.
- The geological model with the position of 21 main fracture planes is plausibe. Although locally the conductivity decreased very significantly, the average conductivities for the fracture planes were in all cases above the average background conductivity. The contrast between the average background conductivity and the average fracture plane conductivity hardly changed during the conditioning (it showed a very small increase).

- The contrast in the ensemble average conductivities of the different fracture planes, originally obtained from the analysis of the few data available, decreased slightly. However, for some fracture planes, it was evident that the initial conductivity estimates were too high or too low. More precisely, for three fracture planes their average conductivity (computed over all realisations) changed more than 0.5 $\log_{10}$ m/s after conditioning (the maximum change was 0.69 $\log_{10}$ units).
- A consistent decrease for the conductivities at the FIZ grid cells is observed. This is attributed to a numerical correction for the artificially enhanced fracture network conductivity related to the spatial discretization of the domain used.
- The prior estimates of the fracture plane conductivity variances were too low. In most of the fracture planes, a variance increase is observed. This variance increase is observed throughout all the realisations. Also the ensemble variances of the average fracture plane conductivities increase. Furthermore, the statistical distributions of the log conductivities in many fracture planes become more skewed (initially the distribution of the log conductivities is Gaussian).
- Consistent estimates of the single storativity are found. The average calibrated storativity is $2.07 * 10^{-8}$ m^{-1} and the values range between $1.3 * 10^{-8}$ m^{-1} and $3.6 * 10^{-8}$ m^{-1} over the eight realisations.
- The final calibrated prescribed boundary heads are smaller than their initial guesses, with some pronounced decrease near the tunnel. This decrease appears consistent with the observed reduction in the piezometric head in the entire laboratory since its construction.

5.4.6 Simulation outcomes for other conditioning rounds

The results from the last conditioning round, as presented before, are thought to be the most valuable, as the realisations were the most data charged. However, it is also interesting to compare the results with other simulation rounds, in which less experimental information was used.

The previous to last simulation round (simulation round 3) differs from the last simulation round in the following aspects:

- Fracture plane 13 had a different position in the model.
- POSIVA flow log data were not included. As a result just 101 hydraulic conductivity data for the background were used.
- 45 steady-state head data were used in the conditioning procedure, instead of 51 steady-state head data.
- The transient head responses at only 13 monitoring locations were included as conditioning information.

The average fracture plane conductivities for the seed realisations hardly differ between the previous to last conditioning round and the last conditioning round. See Table 5.10 for the ensemble averaged average fracture plane

	Conditioned to geology and K data	Conditioned to steady heads	Conditioned to five short-term tests
Background	-10.20	-10.43	-10.41
Fr. Plane 1	-6.54	-6.55	-6.56
Fr. Plane 2	-6.31	-6.21	-6.17
Fr. Plane 3	-6.61	-6.61	-6.47
Fr. Plane 4	-7.28	-7.18	-7.17
Fr. Plane 5	-4.67	-5.40	-5.49
Fr. Plane 6	-7.97	-7.65	-7.69
Fr. Plane 7	-5.63	-5.81	-5.69
Fr. Plane 8	-5.43	-5.67	-5.56
Fr. Plane 10	-7.03	-6.99	-6.97
Fr. Plane 12	-7.76	-7.86	-7.87
Fr. Plane 13	-8.15	-8.21	-8.08
Fr. Plane 15	-7.68	-7.85	-7.81
Fr. Plane 16	-5.35	-5.91	-5.90
Fr. Plane 17	-6.00	-6.09	-6.06
Fr. Plane 18	-7.03	-7.35	-7.38
Fr. Plane 19	-6.70	-6.68	-6.56
Fr. Plane 20	-6.97	-6.51	-6.43
Fr. Plane 21	-8.15	-7.89	-7.14
Fr. Plane 22	-7.20	-6.94	-6.95
Fr. Plane 23	-7.04	-7.17	-7.18
Fr. Plane 24	-6.33	-6.35	-6.34
FIZ	-6.65	-7.02	-6.94

Table 5.10. Average fracture plane conductivities ($\log_{10}$ (m/s) after different conditioning stages in the before-last simulation round. Compare the results with the results obtained in the last simulation round (Table 5.8). The averages are calculated over 8 realisations after conditioning to geology and conductivity data and after conditioning to steady-state head data. The averages are calculated over 7 realisations after conditioning to five short-term transient tests.

conductivities. The difference in average fracture plane conductivity (averaged over 8 realisations in case of the before-last conditioning round) between the two simulation rounds is never bigger than 0.1 $\log_{10}$ units. The differences remain small during the conditioning to steady-state head data. The fractures that showed a stronger conductivity increase or decrease in the last simulation round, showed a similar behaviour in the previous to last simulation round. However, for two fracture planes the differences are larger. The ensemble average conductivity of fracture plane 13 was -8.2 $\log_{10}$ (m/s) in the previous to last simulation round while it was -7.4 $\log_{10}$ (m/s) in the last simulation round. It is interesting to notice that the most important difference is found for the only fracture plane that had not the same position in the two simulation rounds with

the largest value for the last round. Also the ensemble averaged average conductivity of fracture plane 6 differs significantly between the two simulation rounds: it was -7.7 $\log_{10}$ (m/s) in the previous to last conditioning round and -8.3 $\log_{10}$ (m/s) in the last conditioning round. The fracture planes 6 and 13 have the same orientation and are located close to each other. The incorrect location of fracture plane 13 in the previous to last simulation round may have caused that fracture plane 6 had a higher conductivity than in the last simulation round; fracture plane 6 "compensated" some of the missing conductivity due to the incorrect location of fracture plane 13. Finally, a significant difference in the ensemble average conductivities is found for the FIZ grid cells. Also the transient tests do not yield significant differences in average fracture plane conductivities between the previous to last and last simulation round, apart from the differences mentioned. This indicates that with respect to the ensemble averaged average fracture plane conductivities the main differences can be attributed to modifications in the geological model, while the amount of head and conductivity data do not have a significant influence.

Another comparison measure is the ensemble variance of the previous to last fracture plane conductivities. Although the previous to last and last simulation rounds yield very similar ensemble average fracture plane conductivities (for almost all fracture planes), the ensemble variance of these fracture plane conductivities could differ. The variances are more elevated in the previous to last simulation round than in the last simulation round. In any case, it should be stressed that these ensemble variances are calculated over only seven realisations for the previous to last simulation round and over ten realisations in the last simulation round. Not enough for a reliable estimate of these statistics. The largest variance in the previous to last simulation round is due to considerable higher uncertainty on the average conductivity of fracture planes 20, and especially, 21 and 22. In this context it is interesting to notice that in the last simulation round the additional piezometric head data were located close to the fracture planes 20, 21 and 22. It could be argued that this extra experimental information reduced especially the uncertainty on these average fracture plane conductivities. In summary, therefore the ensemble variance of the average fracture plane conductivities is larger in the last simulation round than in the before last simulation round.

The earlier two modelling stages differed with respect to the last simulation rounds in the following aspects:

- The October 1997 or the September 1998 structural model were used. These models did not include some essential features (like fracture planes 13, 21 and 22). For these earlier modelling stages the same extensions of the model were used.
- The POSIVA flow log data were not included and neither the hydraulic conductivity data from build-up tests were used.
- The FIZ grid cells were not considered and simply the generated hydraulic conductivity for one of the fracture planes was taken.

- The prescribed head values according to Svensson (1997) were not subject to calibration, because then the experimental steady-state head data used in the modelling were from the same year as the prescribed boundary head values.
- A smaller number of steady-state head data was available; in the 1st conditioning round 21 steady-state head data and in the 2nd conditioning round 29 steady-state head data.
- A smaller number of conditioning transient information was used. In the 1st and 2nd conditioning rounds the head responses at 26 monitoring locations to five short-term tests and one long-term test were incorporated.

In these earlier simulation rounds (the first two rounds) just one single realisation was generated conditional to experimental information so that it is not worth to analyse in detail the differences between those simulation rounds and the last simulation round. However, it is observed that in those simulation rounds the average fracture plane conductivities after calibration were relatively close to the ensemble averaged average fracture plane conductivities at the same conditioning stage in the last simulation round. The fracture planes that are the most conductive (fracture planes 5, 8, 16 and 17) and the less conductive (fracture planes 6, 12 and 15) are the same in these early simulation rounds and the last simulation round. The differences between the early simulation rounds and the last simulation round are bigger than the differences between the before-last and last simulation round, but in terms of average fracture plane conductivities the differences are not big.

5.4.7 Tracer test simulations

The final aim of the TRUE Block Scale project was to predict the outcome of the tracer tests. The UPV team was not involved in the direct prediction of the outcome of the tracer tests; however, we wanted to check by means of a simple and fast method (particle tracking) how far the simulated results were from the measured data.

Particle tracking is done for all tracer tests in which KI0023B:P6 was the sink. The sink was selected in the TRUE Block Scale project after studying in detail the structural model, the hydraulic responses and testing some possible sink locations. Table 5.11 gives a summary on the characteristics and objectives of the tracer tests.

Table 5.12 compares the simulated and measured median travel times for the different tracer tests. The simulated results are displayed for three different porosity values.

- A single porosity value is a spatial constant. The value is calculated so that the differences between the decimal logarithm of the simulated and measuredmedian arrival times are minimised. The same constant value is used throughout all the realisations. The optimum porosity value was $2.34 * 10^{-4}$.

Test	Injection section	Tracer	Structures tested	Recovered mass (%)
A4-1	KI0025F03:P6	Amino-G Acid	22,20,21	>34 (54-64?)
A4-2	KI0025F03:P7	Rhodamine WT	23	0
A4-3	KI0025F03:P5	Uranine	20,21	> 31 (51-61?)
B1a	KI0025F03:P5	Helium, Uranine	20,21	100
B1b	KI0025F03:P6	Amino-G Acid	22,20,21	>46 (51-56?)
B1c	KI0025F02:P5	Rhodamine WT	20,21	>37 (42-47?)
B2a	KI0025F03:P6	Helium, Uranine, Yb-EDTA	22,20,21	>60 (70?)
B2b	KI0025F02:P3	ReO_4	21	>98 (100?)
B2d	KI0025F03:P7	Gd-DTPA	23,20,21	>88 (90?)
B2e	KI0025F03:P3	In-EDTA	21	>49 (55?)
B2g	KI0025F03:P5	Helium, Uranine, Naphtion.	20,21	100
B2h	KI0025F02:P6	Rhodamine WT	22,20,21	42 (45?)

Table 5.11. The tracer tests that are used to compare the model results and the experimental data. For the recovered mass the weighted recovery is given, and in brackets the estimated total recovery.

- The results are also calculated for porosity values that differ according to the flow path. For each tracer test a different porosity value is optimised. This porosity value is the same for all the realisations. In case the same flow path is tested in multiple tracer tests (like KI0025F03:P05 - KI0023B:P6, KI0025F03:P06 - KI0023B:P6 and KI0025F03:P07-KI0023B:P6) the tracer tests are used together to estimate a porosity value for the flow path. Table 5.13 gives the optimised porosity values for each of the flow paths.
- Finally, all the tracer tests are used to optimise a spatially constant porosity value for each of the realisations. In that case the porosity value differs between the realisations. Table 5.14 gives the optimised porosity values for the realisations.

As could be expected, a spatially constant porosity value that does not vary between the realisations gives the worst results. The differences between the

Table 5.12. Comparison between simulated and measured median arrival times (hours) for multiple tracer tests.

Tracer test A4-3. 100% Mass recovery in simulations.

Realisation	Measured	Model (uniform porosity)	Model (flow path dependent porosity)	Model (realisation dependent porosity)
3	77.7	156.4	96.0	75.8
4	77.7	153.1	94.0	36.4
9	77.7	19.5	11.9	42.0
10	77.7	2.1	1.3	6.3
11	77.7	42.0	25.8	42.2
13	77.7	103.2	63.3	51.5

Tracer test B1a. 100% Mass recovery in simulations.

Realisation	Measured	Model (uniform porosity)	Model (flow path dependent porosity)	Model (realisation dependent porosity)
3	32.5	426.5	261.8	206.8
4	32.5	332.2	203.9	78.9
9	32.5	38.5	23.7	83.2
10	32.5	3.7	2.3	10.9
11	32.5	73.3	45.0	73.6
13	32.5	199.8	122.6	99.7

Tracer test B2g. 100% Mass recovery in simulations.

Realisation	Measured	Model (uniform porosity)	Model (flow path dependent porosity)	Model (realisation dependent porosity)
3	13.5	179.1	110.0	86.8
4	13.5	174.4	107.1	41.4
9	13.5	21.8	13.4	47.0
10	13.5	2.3	1.4	6.7
11	13.5	46.2	28.4	46.4
13	13.5	115.8	71.1	57.8

Tracer test A4-1. 50% Mass recovery in simulations.

Realisation	Measured	Model (uniform porosity)	Model (flow path dependent porosity)	Model (realisation dependent porosity)
3	108.8			
4	108.8			
9	108.8			
10	108.8	208.4	94.9	617.9
11	108.8	234.4	106.8	235.5
13	108.8	241.0	109.8	120.2

Tracer test B1b. 0% Mass recovery in simulations.

Realisation	Measured	Model (uniform porosity)	Model (flow path dependent porosity)	Model (realisation dependent porosity)
3	160.1			
4	160.1			
9	160.1			
10	160.1			
11	160.1			
13	160.1			

Tracer test B2a. 50% Mass recovery in simulations.

Realisation	Measured	Model (uniform porosity)	Model (flow path dependent porosity)	Model (realisation dependent porosity)
3	147.0			
4	147.0			
9	147.0			
10	147.0	218.3	99.4	647.1
11	147.0	572.0	260.5	574.6
13	147.0	311.8	142.0	155.5

Tracer test A4-2. 17% Mass recovery in simulations.

Realisation	Measured	Model (uniform porosity)	Model (flow path dependent porosity)	Model (realisation dependent porosity)
3				
4				
9				
10		76.0	21.8	225.2
11				
13				

Tracer test B2d. 50% Mass recovery in simulations.

Realisation	Measured	Model (uniform porosity)	Model (flow path dependent porosity)	Model (realisation dependent porosity)
3	118.9			
4	118.9			
9	118.9			
10	118.9	118.9	34.1	352.4
11	118.9	283.4	81.3	284.7
13	118.9	2116.6	606.9	1055.8

Tracer test B1c. 83% Mass recovery in simulations.

Realisation	Measured	Model (uniform porosity)	Model (flow path dependent porosity)	Model (realisation dependent porosity)
3	153.0	78.1	109.0	37.9
4	153.0	325.6	454.6	77.4
9	153.0			
10	153.0	95.2	132.9	282.2
11	153.0	29.5	41.2	29.7
13	153.0	221.3	308.9	110.4

Tracer test B2b. 100% Mass recovery in simulations.

Realisation	Measured	Model (uniform porosity)	Model (flow path dependent porosity)	Model (realisation dependent porosity)
3	286.4	59.5	105.4	28.9
4	286.4	690.2	1222.1	164.0
9	286.4	65.2	115.4	140.6
10	286.4	68.7	121.6	203.6
11	286.4	635.6	1125.4	638.4
13	286.4	153.1	271.1	76.4

Tracer test B2e. 83% Mass recovery in simulations.

Realisation	Measured	Model (uniform porosity)	Model (flow path dependent porosity)	Model (realisation dependent porosity)
3	561.0	221.4	2104.3	107.3
4	561.0			
9	561.0	110.0	1045.5	237.2
10	561.0	20.5	195.0	60.8
11	561.0	51.3	488.2	51.6
13	561.0	27.9	265.3	13.9

Tracer test B2f. 67% Mass recovery in simulations.

Realisation	Measured	Model (uniform porosity)	Model (flow path dependent porosity)	Model (realisation dependent porosity)
3	122.7	358.2	203.3	173.7
4	122.7			
9	122.7			
10	122.7	299.6	170.0	888.2
11	122.7	35.9	20.4	36.0
13	122.7	566.7	321.5	282.7

Flow path	Porosity
KI0025F03:P5-KI0023B:P6 (tests A4-3, B1a and B2g).	$1.4393 * 10^{-4}$
KI0025F03:P6-KI0023B:P6 (tests A4-1, B1b and B2a).	$1.0677 * 10^{-4}$
KI0025F03:P7-KI0023B:P6 (tests A4-2 and B2d).	$6.7221 * 10^{-5}$
KI0025F02:P5-KI0023B:P6 (test B1c).	$3.2726 * 10^{-4}$
KI0025F02:P3-KI0023B:P6 (test B2b).	$4.1513 * 10^{-4}$
KI0025F03:P3-KI0023B:P6 (test B2e).	$2.2291 * 10^{-3}$
KI0025F03:P2-KI0023B:P6 (test B2h).	$1.3303 * 10^{-5}$

Table 5.13. Optimised porosity values for different flow paths.

Realisation	Porosity
3	$1.137 * 10^{-4}$
4	$5.57 * 10^{-5}$
9	$5.058 * 10^{-4}$
10	$6.950 * 10^{-4}$
11	$2.355 * 10^{-4}$
13	$1.170 * 10^{-4}$

Table 5.14. Optimised porosity values for different realisations.

configuration as in the tracer tests. For tracer test B1a for example a median arrival time of less than 4 hours is found for one realisation, while for another realisation it is 427 hours.

realisations tend to be large, in spite of the fact that all these realisations are conditioned to many data, including a flow situation with the same pumping

The results improve as the porosity values are allowed to change between flow paths and between realisations. Nevertheless, a large uncertainty on the median travel times remains. These results illustrate the need to use the concentration data in a sophisticated way in the inverse modelling. Chapter 6 presents the methodology to incorporate the concentration data.

The uncertainty found is large, and for many of the realisations an important difference between the measured and simulated median travel time is found. Nevertheless, the following should be taken into account:

- It is found that for repeated pumping tests important differences in travel times are observed. These differences are probably due to natural variations in the groundwater flow at the Aspö-site (Peter Andersson, personal communication). However, the transient behaviour of the natural groundwater flow is not included in the model and data are missing to take it into consideration. As a consequence, the model will not be able to obtain different travel times for pumping tests that are the same, except for the time

of the year that they are carried out. Another consequence is that the measured median travel times do not need to be reproduced exactly as the model can not incorporate the processes that produce the variations in the groundwater flow.

- The tracers are subjected to other processes that are not incorporated in the modelling of the tracer transport. These processes (for example matrix diffusion, but also small-scale dispersion) may also influence the median arrival time.

5.4.8 Discussion and conclusions

Besides the findings specific to the TRUE Block Scale experiment discussed in section 5.4.5, a more general discussion and conclusion are given next.

It was possible to generate hydraulic conductivity realisations over domains of more than 54,000 grid cells conditioned to a large amount of experimental information, including not only data on conductivity but also on piezometric heads. However, at the same time it was clear that the required CPU-time is the most important limitation in this study. It would have been desirable to generate more than ten realisations over a finer discretized study domain, in order to have enough realisations to start a minimum statistical analysis of the results and to have a better representation of the large number of fractures included in the domain. However, although computers will be faster and will allow for more realisations and more grid cells, another important limitation in the simulation of groundwater flow in fractured media is the numerical solution of the groundwater flow equation. Given the very large contrast in conductivity between fracture planes and background, better solvers for large nearly singular linear system of equations have to be developed. Most probably this is a more severe limitation than the limitation on CPU-time.

The study illustrates how a stochastic continuum approach is able to solve in a satisfying way groundwater flow at a fractured site. It is thought that the approach used here in which multiple statistical populations are used to explicitly incorporate information on fracture plane positions and properties, is successful (Section 5.3 showed already a successful application of the method in a fractured medium in which the fractures are defined stochastically). At the moment the method is able to calculate conductivity perturbations for each statistical population separately. A very interesting extension of this approach would allow the calibration of the locations of each population, that is, during the calibration process, not only the conductivity values could change but also the classification of a cell as belonging to a given population. In this particular case, a major challenge would be to develop a methodology that includes the possibility that a grid cell changes from fracture plane to background or the other way around during the conditioning process.

The sequential incorporation of information is in general advantageous as compared to the simultaneous incorporation of different sources of information. On one hand, the simultaneous incorporation of all sources of information may yield instabilities; convergence is improved with the sequential addition of information. On the other hand, the sequential incorporation of conductivity data, steady-state head data and transient head data from different tests also allows a better study of the effect that different pieces of information have on the hydraulic conductivity estimates.

Another issue that is important to address is the upscaling and downscaling of hydraulic conductivities. Even if in the future more finely discretized groundwater flow models are used, the problem of scale can not be avoided. For example, it is not feasible that the groundwater flow equation at the Aspö site would be solved for grid cells of 1 m in the size (an adequate cell size to incorporate the fractures) as this would result in many millions of grid cells. Furthermore, it is common that hydraulic conductivity data from different scales are available. Therefore it will be important to consider the upscaling and downscaling of data in INVERTO.

6 Coupled inversion of groundwater flow and mass transport

Information on the transport of contaminants in the groundwater can be used as an indirect source of information on the groundwater flow velocities and thus on aquifer properties like hydraulic conductivity and storativity. If we are able to condition realisations of hydraulic conductivity (and possibly other variables) to mass transport information we should get a better characterisation of the aquifer properties and reduce our uncertainty on the local aquifer properties. This would allow us to improve our predictions on the aquifer behaviour for different (future) groundwater flow and mass transport regimes. As a consequence, predicting of contaminant concentrations at unsampled locations should improve. Earlier we observed, in studies like the ones presented in sections 4.1 and 5.3, or others carried out by Wen *et al.* (1996) and Hughson and Gutjahr (1998) that conditioning to conductivity and hydraulic head data hardly improved the estimates of the particle travel times. We expect that conditioning on mass concentrations will also improve estimates of travel times.

The sequential self-calibrating method has been extended for the conditioning to concentration data in an Eulerian framework. The focus will be on non-reactive transport, but the algorithm is derived for linear reactive transport in chemically heterogeneous media. The joint inverse modelling of conductivities accounting for groundwater flow and mass transport is considered. One of the main problems that had to be tackled was the CPU-intensity of the calculations and its reduction. Some simplifications are made in the calculation of the gradient, in order to reduce the needed CPU-time and to avoid cumbersome calculations.

Section 6.1 gives a short literature review on the inverse modelling of transport. Section 6.2 presents the mathematical formulation for the extension of the self-calibrating method to the coupled inverse modelling of groundwater flow and mass transport. The focus is on calculating the gradient. Section 6.3 handles the computer implementation of the extended self-calibrating method. Finally, section 6.4 presents a synthetic study in which concentration data are used as conditioning information.

6.1 Literature review inverse modelling of transport

In this section some of the methods for the inverse modelling of mass transport, are discussed in detail.

6.1.1 Propagating and updating of conditional concentration ensemble moments

One of the first to condition flow and transport simulations on concentration measurements were Graham and McLaughlin (1989a, 1989b). They use ensemble concentration moments to characterise a solute plume. Conditioning to concentration measurements is achieved by conditioning the ensemble moments to the available field data. In the first article (Graham and McLaughlin, 1989a) the formulation for the temporal evolution of non-conditional concentration ensemble moments is determined (these are the moments which do not depend on concentration measurements) in combination with a numerical method to solve the moment propagation equations. In the second paper (Graham and McLaughlin, 1989b) the formulation is extended for conditional concentration ensemble moments. The concentration ensemble moments are updated by the Kalman filter approach at the times that new concentration measurements become available.

Derivation of non conditional concentration moments

Graham and McLaughlin consider steady-state flow and dispersive transport for their analysis. It is assumed that the initial conditions and boundary conditions of both the groundwater flow and mass transport equation are perfectly known, although they state that the boundary conditions could be considered random functions. Hydraulic conductivity is considered to be a random space function, which may be non-stationary, with both mean and covariance variable in space. Due to the fact that hydraulic conductivity is a random space function, velocity and concentration are also random space functions. The pore scale dispersion tensor is assumed to be a deterministic variable that is related to the mean velocity. Random velocity and random concentration are expanded around a spatially variable mean using a small perturbation approach. From this expansion, the linearized cross covariance between velocity and concentration and the covariance of concentration are determined. The approximation is valid if higher-order moments of the velocity and concentration perturbations become arbitrarily small, which is true in case of a small variance of hydraulic conductivity (the variance of log conductivity should be smaller than one). As a result, a system of coupled partial differential equations is built, which describes the propagation in time of the mean concentration, the velocity-concentration cross-covariance and the concentration covariance. From the random velocity field, the mean and covariance are known. The moment equations are solved numerically by Galerkin finite elements. The mean concentration, velocity-concentration cross-covariance and the concentration covariance can be calculated at any time or location. These moments yield information about the contaminant plume behaviour, like uncertainty on concentrations, or the spread of the mean plume in time and space. However, Graham and McLaughlin state that non-conditional concentration statistics are not useful in practice, as for example for remediation studies, because too much uncertainty is left.

Derivation of conditional concentration moments

In the second paper, Graham and McLaughlin (1989b) extend the methodology from the first paper to obtain conditional concentration moments. The same perturbation approach is used to develop the equations that describe the evolution of the mean concentration, the velocity-concentration cross-covariance and the concentration covariance between measurement times. However, the important difference is that these moments are conditioned now on available concentration, hydraulic conductivity and hydraulic head measurements. The moments are conditioned on all measurements that become available at a certain time step. When, at a later time, new measurements become available, the moments are updated. The equations that describe the temporal evolution of the moments are based on a linearization of the state equation about the current conditional means of velocity and concentration, instead of the unconditional means of velocity and concentration. The equations for the propagation of the velocity-concentration cross-covariance and the concentration covariance also change in the sense that conditional moments are propagated by these equations. The updating of the moments when new measurements become available is a key element of the approach. The updating is done by a Kalman filtering. The updated moments are found from a linear combination of the propagated moments (the model prediction) and measurement residuals (differences between simulated and measured values, for example concentrations). If the measurements are considered perfect (no measurement error) at the measurement locations the values for the measured variables are reset to the measured values. Since the residuals measure the error in the estimated propagation of the moments they are used to update the estimate not only at the measurement locations, but everywhere in the domain. The specification of the effect of each measurement residual (the distribution over space) is made by solving a matrix equation from the Kalman filter approach. Another equation is used to update the velocity and concentration (cross) covariances. However, the moment propagation equations do not consider the update of the velocity covariance. It was found that the calculations were extremely CPU-intensive. Therefore, a simplification was made by dividing the Kalman filter in two coupled components (the so-called partitioned filtering algorithm). In that case, the concentration moments are conditioned only on concentration measurements and the velocity moments on conductivity and head measurements. This is justified by the weak correlation between concentration and head or conductivity.

A synthetic study is made with continuous contaminant injection from a line source (the release history is perfectly known) in a 2D confined aquifer, with a mildly fluctuating heterogeneous conductivity field, through which steady-state flow and non-reactive mass transport are simulated. Analytical non-conditional moments are used to make an initial guess of different characteristics of the flow parameters. Concentration measurements at different

times are incorporated by the method described in order to update the characterisation of the spatially distributed concentration field. It is illustrated that the plume is characterised better at later times, when it has been conditioned to measurement data at more time steps. The prediction variance is a good tool to use for the decision on the location of new monitoring wells.

Application of the method in a case study

Graham and McLaughlin (1991) apply the method proposed in their earlier papers (Graham and McLaughlin, 1989a, 1989b) to the chloride concentration data from the Borden tracer test. It is one of the first case studies in which concentration data are used together with hydraulic conductivity and hydraulic head data to calibrate the results of contaminant transport simulations.

The Borden site is located in the federal state of Ontario in Canada. The site consists of relatively homogeneous sands and is characterised by a relatively small spatial variability in hydraulic conductivity. Experimental hydraulic conductivity data can be fitted well by a lognormal distribution. Furthermore, hydraulic conductivity is assumed to have a constant expected spatial mean and an isotropic spatial covariance function. The release of chloride is from a rectangular prism with extensions of 4 m by 4 m by 6 m. The average input concentration of chloride is 337 mg/l. The measured chloride concentrations during the period of the tracer test at various locations are averaged over the vertical since the authors apply a 2D transport model. If the uppermost or lowermost vertical sampling point measured a concentration above the background, the concentration was assumed to reach background within the distance of one vertical sampling interval. Similarly, in the horizontal dimension if the outermost sampling wells measured greater than background concentration, the concentration was assumed to reach background at the next (unsampled) row of monitoring wells. Concentration measurement errors are assumed to be uncorrelated in space and time so that the measurement error covariance is a diagonal matrix with uniform non-zero values. Half of the concentration measurements are used in the calibration process and the other half of the measurements is used to compare the predicted and measured concentrations. The values selected for local dispersivity are 0.5 m for the longitudinal direction and 0.05 m for the transversal direction. These values are chosen somewhat high for numerical convenience.

The simulated chloride concentrations 85 and 260 days after the release are compared with the measured concentrations. Advection and diffusion are included in the transport model. The unconditional estimates of the concentration ensemble statistics, according to the method described in the article of Graham and McLaughlin (1989a), show that the peak concentrations and average spreading of the tracer plume are predicted reasonably. However, there is significant uncertainty associated with these predictions. The computed residual concentrations show that the magnitude of this uncertainty was

estimated accurately. It is shown that the standard deviation in the residuals is less after 260 days (8.84 mg/l) than after 85 days (14.29 mg/l). The average residual value is close to zero. Conditioning to chloride concentration measurements results in the simulation of a more irregular chloride plume. The simulated concentration values fit better the measured concentrations after conditioning. The standard deviation in the residuals is 10.89 mg/l after 85 days and 7.57 mg/l after 260 days. The average residuals are closer to zero than in the case that the chloride concentration data are not used in the conditioning.

Comments

This method has the following limitations:

- The method is used to characterise the concentration field by means of hydraulic head, conductivity and concentration measurements. However, the hydraulic conductivity field, which is the source of uncertainty, is not updated.
- The method is limited to formations that are moderately heterogeneous in hydraulic conductivity, because a first-order perturbation approach is used. Moreover, it is also assumed that the hydraulic conductivity is multi-lognormally distributed.
- The Kalman filter is very CPU-intensive, and the authors point out that this is a severe limitation for the application of the algorithm. At each time step the different moments have to be updated for all the aquifer.
- The linear estimation technique employed in the Kalman filter approach is appropriate for normally distributed variables. However, concentrations are in general not normally distributed. This problem is not addressed in the work.
- The authors state that it is possible to address the uncertainty on the boundary conditions. However, it is not clear how this uncertainty and the uncertainty on the initial conditions are treated.

6.1.2 A semi-analytical Lagrangian approach

Rubin formulated the conditioning of transport results on concentration measurements in a Lagrangian framework (Rubin, 1991b). In a first of two papers Rubin considers the conditioning of the concentration ensemble moments on hydraulic head, conductivity and velocity measurements (Rubin, 1991a). In a second paper, he indicates how this approach can be extended to condition also on concentration measurements (Rubin, 1991b). However, the focus in the second paper is merely on describing the characteristics of the spatial and temporal concentration moments.

Conditioning of concentration moments on hydraulic head, hydraulic conductivity and velocity measurements

Like Graham and McLaughlin (1989a, 1989b) Rubin assumes that transmissivity is a random space function, with a small variance (the variance of log transmissivity should be smaller than one) and a multilognormal probability density function. However, as opposed to Graham and McLaughlin, he makes the assumption that transmissivity is stationairy in both mean and variance. The analysis is limited to 2D steady flow in an infinite domain, without recharge. Like Graham and McLaughlin (1989a, 1989b), Rubin also linearizes the groundwater flow equation using a first-order perturbation expansion. As a result, the local random fluctuation of the point velocity and the spatial covariance of the velocity field can be obtained. These two moments characterise completely the multivariate velocity probability density function, because the velocity is also multinormal distributed. From the assumption that log transmissivity is multinormally distributed, and the linearization of the state equations, it follows that the velocity is also multinormal distributed. The expressions derived relate the random space function of velocity to the random space functions of transmissivity and hydraulic head. Since these random space functions are linearly related and log transmissivity is multinormally distributed, it follows that they constitute a multivariate joint random field which is exhaustively characterised by the (cross) covariances between the different variables and the expected values of the random space functions. Rubin derives the cross covariances between transmissivity, hydraulic head and velocity and the spatial covariances of hydraulic head residuals, transmissivity and velocity.

In addition, the analysis is extended to the transport of particles by advection from a continuous source. The transport is expressed by a Lagrangian description for the translation of small elements of solute mass. The probability density function of a particle following a certain trajectory, being in a certain area at a certain time, is multivariate normal, due to the multinormality of the velocity random space function. Rubin derives the displacement mean and the displacement covariance tensor. From the displacement covariance tensor the expected value of the displacement variance over the ensemble of displacements can be obtained. The next step in the approach is to show how these relations can be easily extended to the conditional case, with measurements of transmissivity, hydraulic head and velocity. The equations derived for the conditional trajectory random function and the conditional displacement covariance tensor are solved numerically, by a standard particle tracking method that moves particles through a conditional velocity field. However, how to obtain this conditional velocity field is fundamental for solving the problem. The conditional mean velocity at each location in the aquifer is obtained from a sum of the unconditional mean velocity and a linear combination of the transmissivity residuals, velocity residuals and hydraulic head residuals. The coefficients that weight the different residuals are obtained by solving a cokriging system.

Conditioning of concentration moments to concentration measurements

Rubin (1991b) extended the approach to incorporate concentration measurements. Concentration measurements are incorporated by obtaining first the deviations from the measured concentrations with respect to the expected concentrations (for a specified time and a specified location). From these deviations a weighted linear combination is taken to obtain the deviations at any other time and any other location. The weights are obtained by solving a cokriging system, which yields an unbiased estimation with minimum variance. In order to solve the cokriging system, it is necessary to infer the covariances of the time-space concentration field. Since from a practical point of view it is impossible to infer these covariances, Rubin derives them from the state equations. The probability density function of the displacement of one particle can be obtained by tracking a sufficiently large number of small elements of solute mass through a conditional velocity field. The two-particle displacement probability density function can be inferred similarly. Given a certain spatial discretization, the number of particles in each cell can be counted, so that the concentrations can be calculated. As a result, the covariances of concentrations can be obtained. In addition, the spatio-temporal covariances of concentration can be used together with concentration measurements to interpolate the concentration residuals.

The paper also illustrates the structure of the concentration moments.

1) It is shown that the correlation function is anisotropic, nonstationary and nonsymmetrical, with a larger correlation between concentrations along the axis parallel to the flow direction than perpendicular to it. Graham and McLaughlin (1989b) obtained similar results.
2) The correlation between the concentrations at any two points with fixed coordinates on a Lagrangian coordinate system increases with travel time.
3) The correlation as function of the distance reaches negative values (for distances a bit bigger than the range value) before in the limit (very large distances) a zero correlation is approached.
4) The concentration variance is finite.

Furthermore, Rubin finds in studies that conditioning on concentration measurements may be very effective to reduce the prediction uncertainty. Concentration data obtained at early time steps near the centre of the plume are the most valuable. The spatial configuration of the sampling locations has an important impact on the uncertainty reduction. In general it is better to take samples normal to the streamline than taking them parallel to the streamline.

Comments

- Like in the method of Graham and McLaughlin, the different data (hydraulic head, conductivity, velocity and concentration measurements) are used to characterise better the concentration field. However, the

hydraulic conductivity field, which is the only source of uncertainty, is not updated in the methodology.

- The method is limited to formations that are moderately heterogeneous in hydraulic conductivity, because of the first-order perturbation approach used. Moreover, hydraulic conductivity has to follow a multi-lognormal distribution. The influence of the boundaries should be negligible. Rubin assumes 2D flow in an infinite domain so that in case of a multinormally distributed log transmissivity, and applying the first-order perturbation approach, the velocity is also multinormally distributed. In the case of presence of boundaries, this assumption would not hold, even if log transmissivity is distributed multinormal, the velocity distribution will deviate from multinormally, and thus, the velocity random function will not be completely characterised by its first two moments. Rubin states that the boundaries have an influence only within 2 integral scales from them (Rubin and Dagan, 1988; Rubin and Dagan, 1989).
- Although Graham and McLaughlin use a Kalman filter approach, and Rubin uses cokriging, these approaches are very similar and rely on linear estimation, resulting in an unbiased estimate with minimum variance.
- The method of Rubin seems to be less CPU-intensive than the method of Graham and McLaughlin. The method of Graham and McLaughlin requires the derivation of the spatio-temporal covariances, so that the moment propagation equations have to be solved over the entire domain and for each time step. In the method of Rubin it is sufficient to generate enough two-particle realizations over any period of time desired, to determine the concentrations.
- The linear estimation technique employed in the cokriging approach is appropriate for normally distributed variables. However, concentration is in general not normally distributed. This problem is not addressed in the work.
- It is not clear how uncertainty on boundary conditions and initial conditions could be handled.

6.1.3 A general framework for coupled inverse problems

Sun and Yeh (1990a, 1990b) discuss coupled inverse models in groundwater in general, and the coupled inverse modelling of groundwater flow and mass transport in particular. Sun and Yeh, on the contrary to Graham and McLaughlin and Rubin, consider the groundwater flow and the mass transport equation as a coupled set of partial differential equations, so that concentration data can improve the characterisation of groundwater flow. Sun and Yeh (1990a, 1990b) do not present a specific approach in these papers, but focus on some important issues in any kind of approach. These issues are highlighted below.

The objective function: multiple objectives

Sun and Yeh (1990a) state that the coupled inverse modelling of groundwater flow and mass transport can be considered a vector optimisation problem. It is a vector optimisation problem because different parameters, i.e. hydraulic heads and concentrations, are involved. These parameters are measured in different units and therefore it is necessary to introduce weights for the contribution of each variable. Sun and Yeh (1990a) propose two approaches to obtain the weights:

- The weights can be selected according to the preference of the modeller. The modeller decides which data type to reproduce better. This procedure is normally interactive.
- A non-interactive procedure could be based on the maximum likelihood criterion. The weights can be estimated together with the other parameters. In this approach, the mismatches of the head and concentration data are weighted by their covariance matrices. If measurement or estimated errors are independent these covariance matrices reduce to diagonal matrices. The weights are in that case inverse proportional to the variances and can be determined in an iterative procedure, together with the other parameters.

Optimisation approach

Sun and Yeh (1990a) also discuss the gradient calculation for a coupled inverse problem. They state that three methods exist to calculate the derivatives of the objective function with respect to the independent parameters: the influence coefficient method, the sensitivity equation method and the adjoint state method. Since the number of unknown parameters is generally larger than the number of observations, the adjoint state method is generally the most efficient procedure. If the number of unknown parameters is less than the number of observations, the sensitivity equation method is more efficient.

Sun and Yeh (1990a) extend the adjoint state approach to coupled inverse problems and present several rules of adjoint operators. They also show, using numerical experiments, that the contributions of a given observation in the identification of a parameter can be easily obtained. Finally, they state that the numerical solution of the adjoint equations may require higher-order basis functions as oscillation problems are likely to occur in the solution of the adjoint state equation. Higher-order basis functions are able to reduce the problems of overshoot and undershoot. In case oscillation (overshoot and undershoot) of the numerical solution of the adjoint equations occurs serious errors in the solution are expected.

6.1.4 The zonation procedure extended to the coupled inverse modelling of flow and transport

The zonation procedure to identify flow and transport parameters from concentration measurements (and possibly other kind of measurements), is

very different from the methods described in sections 6.1.1 and 6.1.2. Some important differences are the way of linearizing the problem and the fact that the data are used to improve the estimations of flow and transport parameters. The method is an extension of the method developed by Carrera and Neuman for the inverse modelling of steady and transient groundwater flow by the zonation procedure (Carrera and Neuman, 1986a, 1986b, 1986c). The extension was carried out by Medina and others (Medina *et al.*, 1990; Medina, 1993 and Medina and Carrera, 1996). The method was also applied in a synthetic study to contaminant source characterisation (Wagner, 1992) and the calibration of a regional groundwater flow model in an area with sea water intrusion (Iribar *et al.*, 1997).

The zonation procedure to condition flow and transport parameters on concentration measurements.

Medina and Carrera (1996) consider the coupled groundwater flow and mass transport equations. The equations are coupled by the groundwater flow velocity. The concentration measurements are used in this method to update not only transport parameters, but also the spatially distributed hydraulic conductivity field. This is a clear advantage as compared with the methods by Graham and McLaughlin and Rubin, in which concentration measurements are not used to update flow parameters. The groundwater flow equation may be transient. The transport equation included advection, dispersion, diffusion, decay, linear adsorption, sinks and sources and diffusion into the rock matrix. The calibration process consists of the same steps as described by Carrera and Neuman for the inverse modelling of groundwater flow and are given below (Medina, 1993; Medina and Carrera, 1996):

1) Initial estimates of the different flow and transport parameters are made. The parameter values, like hydraulic conductivity, may be constant for all the considered study area, or they may be different for different zones. However, in general the number of zones is limited. The parameters are estimated for a limited number of zones in order to reduce the number of parameters that has to be calibrated. This, in turn, is done in order to achieve a stable solution. It was found that if the number of parameters that has to be estimated is too large, the problem becomes ill posed (Medina, 1993; Carrera and Neuman, 1986b).

2) The groundwater flow equation and mass transport equation are solved numerically by finite elements and the temporal domain is discretized by finite differences.

3) The objective function value is calculated. Three contributions to the objective function are considered:

- The squared differences between the measured and simulated hydraulic heads, weighted by the hydraulic head covariance matrix.
- The squared differences between initially estimated values for parameters and the updated parameter values, also weighted by the corresponding covariance matrix. All parameters subjected to calibration can be included

here, like conductivities, storativity coefficients, retardation coefficients etcetera.

- The squared differences between measured and simulated concentrations, weighted by the concentration covariance matrix. The covariance matrix of the initial parameter estimates is normally obtained by geostatistical methods. The three contributions can be weighted and their weighted sum gives the objective function. For concentration values both a normal and a lognormal distribution can be considered. In the last case the logarithms of concentration are used in the objective function.

4) The maximum likelihood method is used to update the values for the different parameters. An expression is found which has to be minimised, in order to maximise the likelihood of the parameters. The maximum likelihood estimator yields asymptotically an unbiased estimation with a normal distribution so that the probability density functions for the output variables are characterised completely by the expectation and the covariance matrix, that is to say, non linear effects are neglected.

5) The minimisation is carried out by the Marquardt method, which means that the Jacobian matrix containing the derivatives of the states with respect to the model parameters has to be calculated. Alternatives would be conjugate gradients or Quasi-Newton algorithms, which do not require the Jacobian. However, Medina and Carrera state that, in many cases, the Marquardt method yields a faster convergence compensating the extra time needed to calculate the Jacobian. The different parameters are updated by the optimisation algorithms.

6) The groundwater flow and mass transport equation are solved for the new parameter values. If the simulated values are now sufficiently close to the measured values, the calibration process is terminated. If the simulated values are not close enough to the measured values, steps 4 and 5 are repeated. The procedure continues until the reproduction of the experimental data is satisfactorily. However, this may not always be the case, and also other convergence criteria are used (Medina, 1993). The calibration may also stop in the following situations:

- The norm of the gradient of the objective function falls below a certain value.
- The relative reduction of the objective function value in consecutive iterations decreases below a defined value.
- The norm of the vector that contains differences in parameter values between two consecutive iterations falls below a certain value.
- The relative reduction in the norm of the gradient of the objective function decreases below a defined value.

The procedure described earlier requires a conceptual groundwater flow and mass transport model (Medina, 1993; Carrera and Neuman, 1986a). Different model criteria are considered that include the number of parameters describing the conceptual model. It is found that the Kashjap criteria is the most robust criteria for conceptual model identification (Medina, 1993).

Medina (1993) discusses a number of synthetic studies and two case studies. A case study deals with the transport of uranium in a crystalline rock sample (Medina, 1993; Medina and Carrera, 1996). The experiment consists of establishing a constant gradient through a granite sample and injecting a short rectangular pulse of uranium at one end. The water was sampled at the opposite end. The first 102 samples are used for the calibration and the last 96 samples, which are taken after increasing the flow threefold, are used for validation. After the test the granite sample was sliced perpendicular to the flow direction and activity was measured by alpha autoradiographies providing an idea of the mass distribution in the sample at the end of the test. The samples are used as indicative of sample scale heterogeneity and the uranium remaining in the sample at the end of the test was assumed proportional to total activity. Three conceptual models to represent this transport were tested:

Model 1. Water flows through discrete preferential paths (advection, dispersion, linear adsorption and matrix diffusion are considered).

Model 2. Water flows through discrete preferential paths, but the diffusion in the rock matrix can be neglected (advection, dispersion and linear adsorption are considered).

Model 3. Non Fickian dispersion occurs so that the different flow paths have to be simulated independently (for each flow path a different equation with advection, dispersion and linear adsorption is considered).

It is found that model 1 and model 3 give the best fit. However, model 2 is conceptually simpler. The model selection criterion of Kashyap is given the best score for model 1. A prediction with each conceptual model and its best parameters is made and the results obtained are compared with the 96 validation data. Model 1 gives the best fit. Model 1 also gives the best predictions of the distribution of uranium in the sample at the end of the test. These results show that the model selection criterion of Kashyap did a good job.

A second case study was related to an uranium contamination in the municipality of Andújar in Andalucia in Spain (Medina, 1993).

Comments

- The method can be used to estimate different flow and transport parameters. The concentration measurements can be used to update flow parameters and the uncertainty in all flow and transport parameters can be considered. As such, it has an enormous flexibility as compared to the methods of Graham and McLaughlin or Rubin.
- Moreover, the method is not restricted to moderately heterogeneous conductivity fields and the assumption of an infinite domain. The conductivity field may be strongly heterogeneous and any type of boundary conditions can be considered. Also, the groundwater flow equation may be transient.

- The accuracy of the estimates is modeled by a covariance matrix that is derived after a linearization of the flow equation. Because of this linearization, the covariance is only approximate and should be used with caution, for instance, to generate stochastic realisations.
- A disadvantage of the approach is that the degree of heterogeneity is limited by the number of zones in which the aquifer is partitioned. Increasing the number of zones so that hydraulic conductivity is spatially distributed on a fine grid results in unstable solutions.

Application of the method to contaminant source characterisation.

A synthetic study (Wagner, 1992) illustrates that the zonation procedure extended to the conditioning on concentration data has interesting properties for groundwater contamination studies, like the characterisation of the contaminant source. In this synthetic study the maximum likelihood method is used to estimate simultaneously some flow and transport parameters, and some characteristics (release time, location) of the contaminant source. The conservative contaminants are subjected to steady-state groundwater flow in a confined aquifer and are released from a line source on the eastern boundary of the simulated system. The model parameters are assumed deterministic, but unknown. It is assumed that the error covariance matrix for hydraulic heads and the error covariance matrix for contaminant concentrations are diagonal matrices. The diagonal elements of the hydraulic head error covariance matrix are all equal to a common variance; the diagonal elements of the concentration error covariance matrix, however, are equal to the square of the corresponding true concentration. Both matrices are multiplied by the hydraulic head error variance and the concentration error variance respectively. These error variances are additional unknowns that are jointly estimated with the model parameters. A normal distribution for the errors is assumed.

The simulation of flow and transport on the "true" aquifer using the "true" values for the different parameters gives the "true" hydraulic head values and concentrations. Some samples are taken from this true field and a realistic measurement error is simulated and added to these sampled values. The inverse method is used to estimate the hydraulic conductivity of two zones, the longitudinal and transversal dispersivity coefficients, the effective porosity, the prescribed flux at the eastern boundary, the geometry of the contamination source and the period of mass release. The following situations are considered:

1) Only flow and transport parameters are estimated. No error in the contaminant release function is considered. The resulting estimated parameter values are very close to the "true" values.
2) Flow and transport parameters, and also the contaminant flux from the source are estimated. The results are still very good, although the uncertainty in the estimates has grown somewhat and the errors are slightly larger.
3) Flow and transport parameters and the contaminant fluxes for more time periods are estimated. The program is asked to calibrate the mass release in a

period that includes the "real" period during which there was mass release and another period, of same duration, during which there was no mass release in reality. The program estimated the mass release very good for the period in which there was mass release, and estimated a mass release close to zero for the period in which there was no mass release. The errors did not increase as compared with the 2nd situation, but the uncertainty of the estimates increased.

4) Flow and transport parameters and the location of the contaminant source are estimated. As an initial guess the contaminant source is located within an area which is twice as big as the real spatial extend of the contaminant source. Also in this case the estimated parameter values are close to the real ones. The contaminant source is correctly located. However, the uncertainty associated with the prediction is more elevated than in the 2nd and 3rd case. In general, the inverse method seems to be more sensitive to the amount of contaminant introduced in the system than to the spatial or temporal location of the sources.
5) The estimation of the hydraulic head error variance and the concentration error variance together with flow and transport parameters and the contaminant flux from the sources yields also very good results.

The synthetic study illustrates that the zonation procedure that also conditions to concentration data has a potential for successful application to real-world groundwater contamination problems. However, the considered "real" situation is still simple as compared to a real-world groundwater contamination problem, especially because the spatial distributed hydraulic conductivity field is simple.

Application of the method in the calibration of a regional groundwater flow model with seawater intrusion.

Another application of the maximum likelihood method for inverse modelling of coupled groundwater flow and solute mass transport is given by Iribar *et al.* (1997). The application consists of the calibration of a regional groundwater flow model. The authors state that this is the first calibration of a regional groundwater flow model with help of both transient head and concentration data.

The study area is the Llobregat delta deep aquifer, a few kilometres Southwest of Barcelona, Spain. The deep delta aquifer is confined by clay, silt and fine sand wedge-shaped sediments. These sediments act as an aquitard that exhibits a very low vertical permeability. The aquitard is covered by sands, gravels and silt. This set constitutes the shallow delta aquifer, mostly a water-table one. The shallow delta aquifer and deep delta aquifer have some hydraulic continuity on the fringes of the delta. Intensive aquifer exploitation during the last decades caused a decrease in hydraulic head values in the central part of the aquifer, which in turn resulted in sea-water intrusion.

A 2D transient groundwater flow model with extraction by pumping and injection by leakage is used. Spatial variability in groundwater density is not included in the code; equivalent fresh water heads are used. Leakage coefficients have been defined according to the aquitard thickness and the leakage water concentration was assumed to be 300 mg/l chloride. Four areas of varying aquitard thickness have been considered. All the boundaries are assumed impermeable, except where the aquifer contacts the sea and where it contacts another aquifer. At the permeable boundaries, constant head and constant concentration boundary conditions are imposed. Groundwater pumping was simulated as a prescribed sink term. For the areas with a very thin aquitard, direct recharge from the surface has been considered. The imposed recharge for these zones is 360 mm per year and the chloride concentration is 300 mg/l. Different transmissivity zone patterns were used in the inverse modelling. The 2D version of the advection-dispersion equation is used for the simulation of chloride transport. Simulations are carried out for a period of 20 years, with time steps of 1 month. Historical data were used to estimate the initial spatial distribution of head and concentration by interpolation/extrapolation from the measured data.

From the initial modelling, it was found that the transmissivity zoning had to be changed. Many runs were made in order to select the transmissivity. The concentration data made the discrimination between the different conceptual models possible. Zones of higher transmissivity were generated which are consistent with the geological paleochannels of the site. With the best zonation model, the heads could be fitted well by calibrating flow and transport parameters. However, it was more complicated to reproduce the concentration data. A central salinity plume and a freshwater pocket were reproduced adequately, but in other areas the progress of the sea water intrusion front was poorly reproduced. Error analysis suggests that the reliability is higher in the central part of the aquifer and lower near the edges. In general, it is stated that by means of inverse modelling and the use of concentration data the model of the aquifer is improved:

1) A better fit of the measured heads to the computed heads than in any of the previous models is obtained.
2) Some features of the saline water intrusion could be explained, which was not possible by previous models.
3) The model explicitly accounts for paleochannels, which are consistent with the geology of the site.

This study gives an interesting application of inverse modelling. It is shown how concentration data are used to make a better conceptualisation of an aquifer. The study illustrates also that a real-world case study results in more sources of uncertainty, with an effect on the calibration of the parameters, than a synthetic study like the one carried out by Wagner (1992).

6.1.5 Other approaches

Harvey and Gorelick (1995) also linearize the groundwater flow equation, like Graham and McLaughlin (section 6.1.1) and Rubin (section 6.1.2), but as opposed to these approaches, an iterative procedure is used to update the conductivity field. Harvey and Gorelick use hydraulic conductivity measurements, hydraulic head measurements and solute arrival time in an inverse modelling procedure. The method consists of the following steps:

1. All measurements are used to estimate the mean conductivity, conductivity variance and correlation length of the conductivity field. The values are estimated by the maximum likelihood method that includes the linearization of the flow and transport equation.
2. The measurement data (conductivities, heads and arrival times) are used to determine improved estimates of the hydraulic conductivities at each grid cell and the covariances between the residuals. The matrices with the hydraulic conductivity-hydraulic head and hydraulic conductivity-arrival time covariances are approximated through the flow and transport equations. The procedure is similar to the one by Hoeksema and Kitanidis (1984) (see also section 3.1.1), but extended for the conditioning to solute arrival times.
3. The estimate of the conductivity field and the covariance matrix of the residuals are again updated with additional data. The covariances between the new data and the conductivity field are calculated from the flow and transport equation and the improved estimate of the covariance matrix obtained in step 2.
4. The final estimates of the conductivity and the matrix of residuals are used to generate conditional realisations of the conductivity field. Solute transport can be generated through each of these realisations to build a probability density function of an output variable.

In short, the procedure can be considered an extension of the method by Kitanidis and others to incorporate travel time data. Furthermore, a sequential conditioning procedure allows to obtain improved estimates of the covariance matrices.

Harvey and Gorelick (1995) present a synthetic study from which the most important conclusions are:

- Solute arrival times improve the accuracy of the conductivity field estimate. The solute arrival times include information about the conductivity field not provided by the head or conductivity estimates.
- Sequential conditioning provides better estimates of the conductivity field than using the conditioning information all at once. It is found that a first data set is able to improve the estimation of the mean and covariances of the conductivity field. In a next conditioning stage, using other experimental information, the new first-order approximation is improved due to the previous conditioning stage.
- Using arrival times instead of concentrations has the following advantages:

1. Arrival times are independent of the amount of dilute solute introduced in the aquifer.
2. Quantiles of arrival times are relatively insensitive to measurement errors.
3. It may not be important to know the local dispersivity if the median arrival time is used as conditioning information.
4. Because arrival time is proportional to conductivity, the spatial statistical parameters of conductivity can be estimated from arrival time measurements without repeating numerical flow and transport simulations.
5. The tails of the breakthrough curve did not provide much extra information on the conductivity field as compared with the median arrival time. This suggests that using many concentration measurements at each well may not provide much better estimates of the conductivity field than considering a single quantile of the breakthrough curve from many wells.
6. The relationship of arrival times-conductivities is probably closer to linear than the relationship concentrations-conductivities.

It should be stressed that although Harvey and Gorelick (1995) relax the problems associated with a linearization of the groundwater flow and mass transport equation, the sequential approach is expected to be inferior to an approach in which the equations are not linearized. Some of the advantages they give for using travel times instead of concentrations are related with the linearization approach.

A number of articles is found in the literature in which a (slightly) modified variant of the zonation procedure was applied. Especial attention should be given to the study of Sonnenborg *et al.* (1996) as it is the first real-world case study in which flow and transport parameters are estimated together with parameters on the mass release from the contamination source. Sonnenborg *et al.* apply the zonation method of Medina and Carrera, with the difference that the method of characteristics is used to simulate flow and transport. The method of characteristics involves a particle-tracking procedure to represent advective transport. The results of the particle tracking procedure are transformed, at each time step, in concentrations. Sonnenborg *et al.* optimise the measurement weights (including the trade-off between concentration and head data) in the maximum-likelihood expression of Medina and Carrera.

Sonnenborg *et al.* (1996) apply the methodology to a shallow unconfined aquifer in which contaminant was released during four years. Since 1980 the site has been intensively monitored. Flow parameters, non-reactive transport parameters and the source concentration were estimated. All three identification criteria used found that dividing the aquifer in four zones was optimal. The use of transient head data together with transmissivities and concentration data yielded the best results. Using only steady-state head

observations, without transmissivities, did not yield satisfactory results. The estimates of the parameters were physically reasonable. It was also found that, in some cases, the particle-tracking method might not be suited to solve the inverse problem. This is basically due to the limited number of particles used to calculate the concentrations. A small perturbation of, for instance, transmissivity, might yield a sensitivity coefficient equal to zero because the perturbation is too small to move a particle to a neighbouring grid cell. On the contrary, the change of a particle that carries a high concentration from one grid cell to another may result in a very high sensitivity coefficient. In both cases, computed sensitivity coefficients may not be realistic.

Mayer and Huang (1999) extended the zonation procedure of Carrera and Neuman (1986abc) to the coupled groundwater flow and mass transport problem. Strangely, no reference is given to others who extended already the method years before. However, a main difference is that the method uses a smooth conductivity field as input, with the aim to calibrate the variogram parameters instead of the zonal hydraulic conductivity values. Another difference with the proposed method by Medina and Carrera is that genetic algorithms are used in the optimisation, instead of classical gradient-based algorithms. Mayer and Huang (1999) applied the methodology on the MADE tracer experiment, a large-scale, natural-gradient, field tracer study conducted in an alluvial aquifer near Columbus (Mississippi, United States). At the site, a dense grid of samplers is installed; the concentration and head data from the first 132 days were used for inverse modelling and concentration and head data from the next 92 days were used for predictive modelling. They use full 3-D groundwater flow and mass transport models. Different parametrization schemes are compared. It is found that dividing the aquifer in three zones with different hydraulic conductivity reduces the objective function value much more than using one constant hydraulic conductivity. However, the best results are obtained for a geostatistical parametrization; the kriged hydraulic conductivity field is used as input and the variogram parameters are calibrated. The geostatistical parametrization yields a good prediction of the hydraulic head values and also quite good predictions of the later concentration distributions. The geostatistical parametrization yielded a lower dispersivity value than the zonation procedure, possibly due to the fact that the geostatistical parametrization accounts for part of the macro-dispersion. It was found that genetical algorithms hardly improved the convergence as compared to gradient-based methods. Furthermore, they were found to be much more CPU-intensive.

Xiang *et al.* (1992) propose a somewhat different methodology to solve the coupled inverse groundwater flow and mass transport problem. The objective function is not the typical sum of squared differences between measured and simulated heads and measured and simulated concentrations, but the sum of absolute differences between these values. This optimisation approach gives not as much weight to the largest outliers as the sum of squared differences does.

Xiang *et al* derive the sensivities of the flow and transport equations with respect to the hydraulic conductivities, the dispersivities, the porosities and the solute source concentrations. They consider maximum likelihood estimates of these parameters, which are spatially constants or constants within a limited number of zones. Xiang *et al* present two numerical examples, one for a homogeneous aquifer and one for an aquifer divided in two zones. It is found that the parameter estimates are quite robust for measurement errors.

Wen *et al.* (1998) condition conductivity fields to conductivity data, hydraulic head data and fractional flow rate data. This conditioning is carried out in the context of multiphase flow modelling, but the expressions could be used for travel time data. Like Harvey and Gorelick (1995) travel times instead of concentration data are used in the conditioning in that case. However, a main advantage of the method by Wen *et al.* (1998) is that the state equations are not linearized. Wen *et al.* (1998) extended the sequential-self calibrating method further to include the fractional flow rate data. The derivatives of the objective function with respect to the hydraulic conductivities include now the match to the fractional flow rate data. The conditioning is carried out in an iterative fashion until all the data are matched sufficiently close. A main advantage of the approach by Wen and others, as compared with other approaches that also do not linearize the groundwater flow and mass transport equation, is that multiple equally likely solutions of the problem are obtained. A synthetic example shows the additional value of fractional flow rate data for the improved characterisation of the hydraulic conductivity spatial distribution.

Anderman and Hill (1999) use information on mass transport to estimate groundwater flow and mass transport parameters. However, they decouple the groundwater flow and mass transport equation in order to reduce computational costs and to get fast results. Nevertheless, the method is fully iterative until convergence is obtained. The method consists of the following steps:

1. The concentration data are plotted and the concentration distribution along the plume centreline is identified. It is assumed that the advective front is located at the 50-percent concentration contour. The flow parameters are estimated using the trial advective-front location.
2. Next, also the transport parameters (dispersivities) are estimated.
3. The updated trial advective-front location is calculated with the groundwater flow and mass transport model.
4. In case the updated location is close to the previous location convergence is achieved. If this is not the case the flow and transport parameters are modified (back to step 1).

A synthetic numerical experiment (Anderman and Hill, 1999) shows that the decoupled multistage iterative method is less accurate than a simultaneous method. Nevertheless, the method was able to estimate flow and transport parameters that improved the fit to the concentration data. The required CPU-

time was greatly reduced. The method was demonstrated on a very simple example and one may have serious doubts on the method performance for a heterogeneous aquifer.

An inverse methodology that is quite different from the ones presented before is published in the context of the recovery of a contaminant release history (Skaggs and Kabala, 1995; Skaggs and Kabala, 1998). The concentration measurements are the basis for estimating the concentration distributions at earlier times. The objective is in general to estimate the release function. The release function (or concentration distributions at earlier times) is estimated by Tikhonov regularisation. Tikhonov regularisation makes the solution less sensitive to errors by requiring that the solution satisfies a smoothness criterion besides reproducing the data. The concentration measurements may contain errors. In a synthetic example (Skaggs and Kabala, 1998) multiple equally likely contaminant release functions were generated; the basis for the uncertainty were the corrupted concentration data. The aquifer properties were assumed to be known perfectly. It was found that it was more difficult to recover the mass release for larger measurement errors and for sharp releases. The authors state that the methodology could be extended to aquifer parameter uncertainty. Skaggs and Kabala (1995) use the method of quasi-reversibility (solving the transport equation backwards in time) to obtain the contaminant release functions. The solutions found were less accurate as compared to the ones obtained by Tikhonov regularisation. Skaggs and Kabala (1995) did not consider parameter uncertainty; only measurement errors.

6.2 Mathematical formulation of the coupled inversion

The objective is to generate multiple equally likely realisations of the parameters controlling groundwater flow and mass transport so that each realisation reproduces the experimental hydraulic conductivity data, hydraulic head data and concentration data. This objective will be achieved through an inverse procedure, in which hydraulic head data will serve to update flow parameters and the concentration data will serve to update both flow and transport parameters.

6.2.1 Steps in the extended self-calibrating method

The extended self-calibrating method consists of the following steps:
1) A seed log-conductivity (Y=log$K$) is generated conditional to Y data, using, for instance, sequential simulation (Gómez-Hernández and Journel, 1993). This step is the same as for the sequential self-calibrating method that only considers groundwater flow. In case transient groundwater flow is simulated also a seed field of storativity coefficients (Z=$\log_{10}S$) may be generated. Furthermore, in case reactive transport is simulated also a seed field with retardation factors (R) is generated. This latter seed field is conditioned to data on retardation factors. An alternative is to consider a spatially constant retardation factor. The iteration counter is set to zero.
2) The steady-state or transient 2-D or 3-D groundwater flow equation is solved for the current log-conductivity field and log-storativity field, with given external stresses, boundary and initial conditions. In addition, the 2-D or 3-D mass transport equation is solved. Dispersion, linear adsorption, radioactive decay and mass sinks and sources can be considered. As compared with the sequential-self calibrating method applied to groundwater flow, now the mass transport equation has to be solved, too. Initial concentrations must be supplied. The initial concentrations may be known, at most, at a few locations from which an estimate of the initial concentration over the entire aquifer has to be inferred. Therefore, the initial concentrations are in general subject to an important uncertainty.
3) An objective function is defined that includes the mismatches between simulated and observed heads and concentrations:

$$J = \sum_{t=1}^{N_t}\sum_{i=1}^{N_h}\xi_{it}(h_{i,t}^{SIM} - h_{i,t}^{MEAS})^2 + \psi_3\sum_{t=1}^{N_{tc}}\sum_{i=1}^{N_c}\zeta_{it}(c_{i,t}^{SIM} - c_{i,t}^{MEAS})^2 \qquad (6.1)$$

where the first term corresponds to the head discrepancies at the different time steps (if only steady-state flow is simulated this corresponds to the first and only time step) and the second term to the discrepancies between measured and simulated concentrations. The contributions from the discrepancies between initial estimates of conductivities or storativities and updated conductivity or storativity values are omitted here (their trade-offs are supposed to be equal to zero). N_h is the number of head measurement locations, N_t the number of time

steps with head measurements, $h_{i,t}$ the heads, N_C is the number of concentration measurement locations, N_{TC} the number of time steps with concentration measurements, $c_{i,t}$ the concentrations and the superscripts *SIM* and *MEAS* refer to "simulated" and "measured" respectively. The weights ξ_{it} and ζ_{it} are chosen inverse-proportional to the estimated measurement errors. The value of the trade-off coefficient ψ_3 should be chosen in accordance with the desired reproduction of the head and concentration data, with the head and concentration differences along the domain and with the estimated variances of head and concentration. The trade-off value should be such that the reproduction of the hydraulic head and concentration measurements is balanced. In case the simulated concentration values do not correspond exactly with the locations of the measurement data the simulated values can be interpolated in a similar way (by inverse squared distance weighting) as the hydraulic head data as explained in section 3.3.

The parameter values are conditional to the h and c data when J is smaller than a predefined tolerance value. The parameter values are accepted when this condition is met.

If J is not small enough, a perturbation of the input parameters is calculated and added to their current values. The parameters that are subjected to calibration are log conductivity, and possibly also prescribed heads on the boundaries, storativity coefficients, retardation coefficients (in case of reactive transport) and mass sources. The perturbation of the Y field, Z field, R field and prescribed boundary heads are parameterized as function of the individual perturbations at a number of master blocks, in the same way as seen in section 3.2. Also the comments related to the master blocks (see sections 3.2 and 3.3) hold here. The objective function is again minimized by non-linear optimisation.
4) The gradient vector g contains the derivatives of J with respect to the perturbations of Y at the master locations and possibly also the perturbations of the prescribed heads at the master locations, the perturbations of Z at the master locations, the perturbations of R at the master locations and the perturbation of the mass sources. The gradient is determined using the adjoint-state formulation. The formulation is presented in detail later.
5) The updating direction is calculated from the gradient found and computed in a similar way as for the inverse modelling of only groundwater flow. The following algorithms are alternated: steepest descent, Fletcher-Reeves conjugate gradient, Hestenes-Stiefel conjugate gradient and quasi-Newton. Once the updating direction is determined, a linear search in that direction is carried out to determine the scalar parameter that yields the perturbation vector minimising the objective function in the updating direction. The magnitude of the perturbations at the master locations are again constrained so that the final logconductivity field and the final logstorativity field are within plus/minus three ordinary kriging standard deviations of the ordinary kriging estimates at the master locations obtained by ordinary kriging of the data. The perturbations of the prescribed heads along the boundaries are also constrained by user-

defined maximum allowed changes. The perturbation of the spatially variable retardation coefficients is also constrained by expert knowledge. In general, too few experimental data will be available to constrain the perturbation of the retardation coefficients by kriging standard deviations. Finally, the perturbation of the amount of injected mass is also constrained by expert knowledge.
6) The resulting perturbations at the master locations are interpolated by ordinary kriging to the rest of the blocks. The perturbation ΔY field is added to the last iteration Y field, the perturbation ΔZ field is added to the last iteration Z field, the perturbation ΔR field is added to the last iteration R field, the interpolated perturbation of the prescribed heads is added to the prescribed heads from the last iteration and the perturbation of the mass sources is added to the mass sources from the last iteration. The iteration counter I is increased by one and the algorithm returns to step 2.

In section 6.2.2 details are presented on the methodology, mainly on step 4. With respect to the other steps:

- Step 1. The methodology to generate the log-conductivity, log-storativity and the retardation coefficient seed was presented in section 2.1. The only difference with the inverse modelling of groundwater flow is that in case of reactive transport a retardation coefficient seed is also generated.
- Step 2. Since the conditioning to concentration data is considered, the forward solution of the mass transport equation is needed. Section 2.2.2 presented the methodology to solve numerically the mass transport equation.
- Step 3. Equation 6.1 gives the objective function for the case that both head and concentration data are used as conditioning data.
- Step 5. The non-linear optimisation algorithms and the linear search are similar to the inverse modelling of groundwater flow only. The only difference is that the gradient may contain partial derivatives with respect to retardation coefficients at the master blocks and the mass sources. The perturbations of retardation coefficients and mass sources are also constrained.
- Step 6. The perturbations are interpolated by kriging, the only difference is that this interpolation may also be applied on the retardation coefficients.

In the next section, step 4, the calculation of the gradient of the objective function, is detailed. The gradient includes the perturbation of hydraulic conductivity, prescribed heads on the boundaries, storativity coefficient, retardation coefficient and mass sources.

The perturbation of the dispersivity coefficients is not considered in the method for the following reasons:

- It is considered that the perturbation of the dispersivity coefficients is irrelevant because the spatial variability of conductivity accounts for most of the dispersive part of the mass transport.

- We believe that it is hard to distinguish in the inverse condition between the dispersion caused by the spatially variable conductivity and the dispersion related with the intra-cell dispersivity coefficient.

6.2.2 Calculating the gradient of the objective function

The procedure for calculating the gradient is related to the work by Carrera and Medina (1990) with some modifications. The conditioning to concentration measurements is very CPU intensive and the step consuming most CPU is the calculation of the gradient of the objective function with respect to the perturbation parameters (conductivities and possibly prescribed heads, storativity coefficients, retardation coefficients and mass sources). The adjoint state formulation is used in the gradient calculation in order to reduce CPU time. However, we will see that for the calibration of concentrations, the Jacobian containing the derivatives of heads with respect to the perturbation parameters also has to be computed. Therefore, it may be advantageous to use the adjoint state formulation only to the transport equation, and the sensitivity equations for the flow equation.

The matricial notation of the transport equation (equation 2.10) was:

$$\left(\left(\left[\frac{E}{R}\right]\right)-\left[\frac{1}{\Delta t}\right]-[\lambda_D]+\left[\frac{q_s^{out}}{\phi}\right]\right)\{C^{t+1}\}+\{F\}=-\frac{1}{\Delta t}\{C^t\}$$

where E/R is the matrix that contains the terms E_{lm} (the convection and dispersion terms) divided by R_{lm}, (the interblock retardation factors), $[1/\Delta t]$ is a diagonal matrix with one divided by the time step on the diagonal terms, $[\lambda_D]$ is a matrix with the decay constants on the diagonal, $[q_s^{out}/\phi]$ is a matrix with the mass extractions divided by the porosity on the diagonal terms, C the vector with the concentration values at time step t or time step t+1 and F the vector with mass injection and boundary conditions.

The state of the transport equation for two subsequent time steps is as follows (the state of the flow equation was introduced in section 3.2):

$$\{\Theta_t\}=\left(\left(\left[\frac{E}{R}\right]\right)-\left[\frac{1}{\Delta t^t}\right]-[\lambda_D]+\left[\frac{q_s^{out}}{\phi}\right]\right)\{C^t\}+\{F\}+\frac{1}{\Delta t^t}\{C^{t-1}\}=0$$

$$\{\Theta_{t+1}\}=\left(\left(\left[\frac{E}{R}\right]\right)-\left[\frac{1}{\Delta t^{t+1}}\right]-[\lambda_D]+\left[\frac{q_s^{out}}{\phi}\right]\right)\{C^{t+1}\}+\{F\}+\frac{1}{\Delta t^{t+1}}\{C^t\}=0$$

where Δt^t is the time step between t-1 and t, Δt^{t+1} the time step between t and t+1 and C^t is an N-dimensional vector of concentrations for the time step t. The

state $\{\Theta\}$ contains the states of the transport equation at all N_{ts} steps that the mass transport equation is solved.

The Lagrangian including the transport is now:

$$\Im = J + \{\lambda\}^T \{\Psi\} + \{\mu\}^T \{\Theta\}$$

where μ is the N x N_{ts} dimensional vector of Lagrange multipliers for the transport part, N being the number of grid cells and N_{ts} the number of transport time steps. For each time that the adjoint transport equation is solved an N dimensional vector of Lagrange multipliers is estimated. The obtained Lagrange multipliers for the state $\{\theta_t\}$ are $\{\mu^t\}$, the ones for the state $\{\theta_{t+1}\}$ are $\{\mu^{t+1}\}$ etcetera.

The derivatives of the Lagrangian with respect to the perturbation parameters are given now by the following equation:

$$\frac{d\Im}{d\{p\}} = \frac{dJ}{d\{p\}} = \frac{\partial J}{\partial\{p\}} + \frac{\partial J}{\partial\{h\}}\frac{\partial\{h\}}{\partial\{p\}} + \{\lambda\}^T\left(\frac{\partial\{\Psi\}}{\partial\{p\}} + \frac{\partial\{\Psi\}}{\partial\{h\}}\frac{\partial\{h\}}{\partial\{p\}}\right) + \frac{\partial J}{\partial\{C\}}\frac{\partial\{C\}}{\partial\{p\}} + \{\mu\}^T\left(\frac{\partial\{\Theta\}}{\partial\{p\}} + \frac{\partial\{\Theta\}}{\partial\{h\}}\frac{\partial\{h\}}{\partial\{p\}} + \frac{\partial\{\Theta\}}{\partial\{C\}}\frac{\partial\{C\}}{\partial\{p\}}\right)$$

This equation can be rearranged to:

$$\frac{dJ}{d\{p\}} = \frac{\partial J}{\partial\{p\}} + \left(\frac{\partial J}{\partial\{h\}} + \{\lambda\}^T\frac{\partial\{\Psi\}}{\partial\{h\}} + \{\mu\}^T\frac{\partial\{\Theta\}}{\partial\{h\}}\right)\frac{\partial\{h\}}{\partial\{p\}} + \{\lambda\}^T\frac{\partial\{\Psi\}}{\partial\{p\}} + \left(\frac{\partial J}{\partial\{C\}} + \{\mu\}^T\frac{\partial\{\Theta\}}{\partial\{C\}}\right)\frac{\partial\{C\}}{\partial\{p\}} + \{\mu\}^T\frac{\partial\{\Theta\}}{\partial\{p\}} \tag{6.2}$$

The derivatives $\partial J/\partial p$, $\partial J/\partial h$, $\partial\Psi/\partial h$, $\partial h/\partial p$ and $\partial\Psi/\partial p$ were given in section 3.2. The derivatives $\partial\Theta/\partial h$ are omitted as their evaluation is very cumbersome and the gradient was found to be just slightly worse estimated in case that these contributions were omitted. The other derivatives are given here. The Lagrange multipliers for the adjoint transport equation are obtained by solving the following equation:

$$\frac{\partial J}{\partial\{C\}} + \{\mu\}^T\frac{\partial\{\Theta\}}{\partial\{C\}} = 0 \tag{6.3}$$

Equation 6.2 can be simplified by using the equations 3.6 and 6.3:

$$\frac{dJ}{d\{p\}} = \frac{\partial J}{\partial\{p\}} + \{\lambda\}^T\frac{\partial\{\Psi\}}{\partial\{p\}} + \{\mu\}^T\frac{\partial\{\Theta\}}{\partial\{p\}} \tag{6.4}$$

First we will see how the Lagrange multipliers for the adjoint transport equation are calculated. The derivatives of equation 6.3 are given by:

$$\frac{\partial J}{\partial \{C^t\}} = 2\psi_3 \sum_{i=1}^{N_C} \zeta_{it} (c_i^{t,SIM} - c_i^{t,MEAS}) \tag{6.5}$$

Only the derivatives of the state equations for times t (equation 6.6) and t+1 (equation 6.7) are non-zero.

$$\frac{\partial \{\Theta_t\}}{\partial \{C^t\}} = \left(\left[\frac{E}{R}\right] - \left[\frac{1}{\Delta t^t}\right] - [\lambda_D] + \left[\frac{q_s^{out}}{\phi}\right] \right) \tag{6.6}$$

$$\frac{\partial \{\Theta_{t+1}\}}{\partial \{C^t\}} = \frac{1}{\Delta t^{t+1}} \tag{6.7}$$

where some introduced superscripts and subscripts t refer to the transport time step; $c_i^{t,SIM}$ and $c_i^{t,MEAS}$ are simulated and measured concentrations at the transport time step t.

Substituting equations 6.5 until 6.7 in equation 6.3 gives the following expression:

$$\{\mu^t\}^T \left(\left[\frac{E}{R}\right] - \left[\frac{1}{\Delta t^t}\right] - [\lambda_D] + \left[\frac{q_s^{out}}{\phi}\right] \right) = -2\psi_3 \sum_{i=1}^{N_C} \zeta_{it} \left(c_i^{t,SIM} - c_i^{t,MEAS}\right) - \frac{1}{\Delta t^{t+1}} \{\mu^{t+1}\}^T \tag{6.8}$$

The adjoint state transport equation is very similar to the transport equation, the main difference being the right-hand side term that contains the mismatches between the measured and simulated concentration values. Another important difference is that the adjoint transport equation has to be solved backwards in time, like the adjoint flow equation. The backwards solution of the adjoint transport equation starts from $\{\mu^{Nts+1}\}=0$ as equation 6.7 is equal to zero for the time step N_{ts}+1.

The adjoint state equations can also be formulated continuous in time. In some cases, this formulation may have important advantages. Appendix II presents the adjoint state formulation for the case that the temporal domain is not discretized.

The next step is to obtain the derivatives of equation 6.4. The derivatives of Ψ with respect to p were given already in section 3.2.

$$\frac{\partial\{\Theta_t\}}{\partial\{p\}}=\left(\frac{\partial([E/R])}{\partial\{p\}}\right)\{C^t\}+\frac{\partial\left[q_x^{out}/\phi\right]}{\partial\{p\}}\{C^t\}+\frac{\partial\{F\}}{\partial\{p\}} \tag{6.9}$$

where p are the perturbations of log conductivity, prescribed boundary heads, storativity coefficient, retardation coefficient and mass sources.

The most time consuming partial derivatives to calculate in equation 6.9 are $\partial[E/R]/\partial p$. The derivatives of pore groundwater velocities with respect to the perturbation parameters have to be calculated. Only the derivatives $\partial[E/R]/\partial p$ related to convective transport are considered, in order to avoid cumbersome calculations. This simplification should have a minor impact on the results in case advective transport dominates over dispersive transport.

The derivatives given below are for a geometric interblock conductivity mean and for the case that the neighbour grid cell m is not a cell with a prescribed head value. The expressions for a harmonic interblock conductivity mean and a neighbour grid cell m with prescribed heads are similar. The expressions are approximate, as the contributions of the dispersion to the derivatives are neglected. This approximation is supposed to be good in case convective transport dominates over dispersive transport.

The used notation is explained in section 2.2.2.1 below equation 2.10.

$$\frac{\partial(E/R)_{lm}}{\partial\Delta Y_k}=0 \qquad m\notin\{N,S,W,E,U,D\}\vee m\in\{\Gamma^c\} \tag{6.10}$$

$$\begin{aligned}\frac{\partial(E/R)_{lm}}{\partial\Delta Y_k}&\approx\frac{\partial\left(\alpha K_{lm}\dfrac{h_l-h_m}{(\Delta x_{lm})^2\phi R_{lm}}\right)}{\partial\Delta Y_k}=\\&=\alpha\frac{h_l-h_m}{(\Delta x_{lm})^2\phi R_{lm}}A_{lm}\frac{\lambda_l^k+\lambda_m^k}{2}+\frac{\alpha K_{lm}}{(\Delta x_{lm})^2\phi R_{lm}}\frac{\partial(h_l-h_m)}{\partial\Delta Y_k} \qquad m\in\{W\}\wedge m\notin\{\Gamma^c\}\end{aligned} \tag{6.11}$$

$$\begin{aligned}\frac{\partial(E/R)_{lm}}{\partial\Delta Y_k}&\approx\frac{\partial\left(\alpha K_{lm}\dfrac{h_m-h_l}{(\Delta x_{lm})^2\phi R_{lm}}\right)}{\partial\Delta Y_k}=\\&=\alpha\frac{h_m-h_l}{(\Delta x_{lm})^2\phi R_{lm}}A_{lm}\frac{\lambda_l^k+\lambda_m^k}{2}+\frac{\alpha K_{lm}}{(\Delta x_{lm})^2\phi R_{lm}}\frac{\partial(h_m-h_l)}{\partial\Delta Y_k} \qquad m\in\{E\}\wedge m\notin\{\Gamma^c\}\end{aligned} \tag{6.12}$$

$$
\begin{aligned}
\frac{\partial (E/R)_{ll}}{\partial \Delta Y_k} \approx & -\sum_{m\in\{W\}}\left(\alpha\frac{h_l-h_m}{(\Delta x_{lm})^2\phi R_{lm}}A_{lm}\frac{\lambda_l^k+\lambda_m^k}{2}+\frac{\alpha K_{lm}}{(\Delta x_{lm})^2\phi R_{lm}}\frac{\partial(h_l-h_m)}{\partial\Delta Y_k}\right)+\\
& -\sum_{m\in\{E\}}\left(\alpha\frac{h_m-h_l}{(\Delta x_{lm})^2\phi R_{lm}}A_{lm}\frac{\lambda_l^k+\lambda_m^k}{2}+\frac{\alpha K_{lm}}{(\Delta x_{lm})^2\phi R_{lm}}\frac{\partial(h_m-h_l)}{\partial\Delta Y_k}\right)+\\
& -\sum_{m\in\{S\}}\left(\alpha\frac{h_l-h_m}{(\Delta y_{lm})^2\phi R_{lm}}A_{lm}\frac{\lambda_l^k+\lambda_m^k}{2}+\frac{\alpha K_{lm}}{(\Delta y_{lm})^2\phi R_{lm}}\frac{\partial(h_l-h_m)}{\partial\Delta Y_k}\right)+\\
& -\sum_{m\in\{N\}}\left(\alpha\frac{h_m-h_l}{(\Delta y_{lm})^2\phi R_{lm}}A_{lm}\frac{\lambda_l^k+\lambda_m^k}{2}+\frac{\alpha K_{lm}}{(\Delta y_{lm})^2\phi R_{lm}}\frac{\partial(h_m-h_l)}{\partial\Delta Y_k}\right)+\\
& -\sum_{m\in\{D\}}\left(\alpha\frac{h_l-h_m}{(\Delta z_{lm})^2\phi R_{lm}}A_{lm}\frac{\lambda_l^k+\lambda_m^k}{2}+\frac{\alpha K_{lm}}{(\Delta z_{lm})^2\phi R_{lm}}\frac{\partial(h_l-h_m)}{\partial\Delta Y_k}\right)+\\
& -\sum_{m\in\{U\}}\left(\alpha\frac{h_m-h_l}{(\Delta z_{lm})^2\phi R_{lm}}A_{lm}\frac{\lambda_l^k+\lambda_m^k}{2}+\frac{\alpha K_{lm}}{(\Delta z_{lm})^2\phi R_{lm}}\frac{\partial(h_m-h_l)}{\partial\Delta Y_k}\right)
\end{aligned}
\tag{6.13}
$$

In the expressions above k refers to a master block. N (North), S (South), E (East), W (West), U (Up) and D (Down) refer to the position of the neighbour cell with respect to the cell indexed with l. Γ^c refers to the contour at which concentrations are prescribed. Remember that α is a weight equal to 0.5 in case of central weighting and equal to zero or one in case of upstream weighting. R_{lm} and R_{ll} are elements of the matrix E/R, R being the retardation coefficients evaluated at the interfaces of two neighbouring grid cells, calculated by the arithmetic average of the retardation coefficients for the grid cells l and m.

In the above expressions partial derivatives of hydraulic head with respect to perturbations of log decimal hydraulic conductivity appear. The values for these derivatives can be obtained by solving the flow sensitivity equations. Remember that the matricial expression for the transient groundwater flow equation was:

$$
\left([A]-\frac{[D]}{\Delta t}\right)\{h^{t+1}\}+\{q\}=-\frac{[D]}{\Delta t}\{h^t\}
$$

The sensitivity equation is then given by:

$$
\left([A]-\frac{[D]}{\Delta t}\right)\left\{\frac{\partial h^{t+1}}{\partial\Delta Y_k}\right\}+\left(\frac{\partial[A]}{\partial\Delta Y_k}-\frac{\partial[D]}{\Delta t\partial\Delta Y_k}\right)\{h^{t+1}\}+\frac{\partial\{q\}}{\partial\Delta Y_k}=-\frac{\partial[D]}{\Delta t\partial\Delta Y_k}\{h^t\}-\frac{[D]}{\Delta t}\left\{\frac{\partial h^t}{\partial\Delta Y_k}\right\}
\tag{6.14}
$$

This expression simplifies in the case of steady-state groundwater flow to:

$$
[A]\left\{\frac{\partial h}{\partial\Delta Y_k}\right\}+\frac{\partial[A]}{\partial\Delta Y_k}\{h\}+\frac{\partial\{q\}}{\partial\Delta Y_k}=0
$$

The sensitivity equation has the same format as the groundwater flow equation, the head derivatives with respect to the hydraulic conductivity perturbations being the unknown vector. The other derivatives in the sensitivity equation are the ones that were already calculated when the flow contribution to the gradient was obtained (section 3.2)

The derivatives of the vector F with respect to the hydraulic conductivity perturbations also give non-zero derivatives due to the contribution of the prescribed concentration boundary conditions. Below the expression is given for a geometric intrablock conductivity mean and the case that the neighbour grid cell has not an imposed prescribed head value. Similar expressions are obtained for a harmonic intrablock conductivity mean and prescribed heads at the neighbour grid cell m.

$$
\begin{aligned}
\frac{\partial F_l}{\partial \Delta Y_k} \approx & -\sum_{\substack{m\in\{W\}\\ m\in\Gamma^c}}\left(\alpha\frac{h_l-h_m}{(\Delta x_{lm})^2\phi R_{lm}}A_{lm}\frac{\lambda_l^k+\lambda_m^k}{2}+\frac{\alpha K_{lm}}{(\Delta x_{lm})^2\phi R_{lm}}\frac{\partial(h_l-h_m)}{\partial\Delta Y_k}\right)c_m^\Gamma + \\
& -\sum_{\substack{m\in\{E\}\\ m\in\Gamma^c}}\left(\alpha\frac{h_m-h_l}{(\Delta x_{lm})^2\phi R_{lm}}A_{lm}\frac{\lambda_l^k+\lambda_m^k}{2}+\frac{\alpha K_{lm}}{(\Delta x_{lm})^2\phi R_{lm}}\frac{\partial(h_m-h_l)}{\partial\Delta Y_k}\right)c_m^\Gamma + \\
& -\sum_{\substack{m\in\{S\}\\ m\in\Gamma^c}}\left(\alpha\frac{h_l-h_m}{(\Delta y_{lm})^2\phi R_{lm}}A_{lm}\frac{\lambda_l^k+\lambda_m^k}{2}+\frac{\alpha K_{lm}}{(\Delta y_{lm})^2\phi R_{lm}}\frac{\partial(h_l-h_m)}{\partial\Delta Y_k}\right)c_m^\Gamma + \\
& -\sum_{\substack{m\in\{N\}\\ m\in\Gamma^c}}\left(\alpha\frac{h_m-h_l}{(\Delta y_{lm})^2\phi R_{lm}}A_{lm}\frac{\lambda_l^k+\lambda_m^k}{2}+\frac{\alpha K_{lm}}{(\Delta y_{lm})^2\phi R_{lm}}\frac{\partial(h_m-h_l)}{\partial\Delta Y_k}\right)c_m^\Gamma + \\
& -\sum_{\substack{m\in\{D\}\\ m\in\Gamma^c}}\left(\alpha\frac{h_l-h_m}{(\Delta z_{lm})^2\phi R_{lm}}A_{lm}\frac{\lambda_l^k+\lambda_m^k}{2}+\frac{\alpha K_{lm}}{(\Delta z_{lm})^2\phi R_{lm}}\frac{\partial(h_l-h_m)}{\partial\Delta Y_k}\right)c_m^\Gamma + \\
& -\sum_{\substack{m\in\{U\}\\ m\in\Gamma^c}}\left(\alpha\frac{h_m-h_l}{(\Delta z_{lm})^2\phi R_{lm}}A_{lm}\frac{\lambda_l^k+\lambda_m^k}{2}+\frac{\alpha K_{lm}}{(\Delta z_{lm})^2\phi R_{lm}}\frac{\partial(h_m-h_l)}{\partial\Delta Y_k}\right)c_m^\Gamma
\end{aligned}
\tag{6.15}
$$

Next the derivatives with respect to the perturbation of prescribed boundary heads are given.

$$
\frac{\partial(E/R)_{lm}}{\partial\Delta h_k^\Gamma}=0 \qquad m\notin\{\Gamma^h\}\vee m\in\{\Gamma^c\}
$$

$$\frac{\partial(E/R)_{lm}}{\partial\Delta h_k^{\Gamma}} \approx \sum_{\substack{m\in W\\ m\in\Gamma^h\\ m\in\Gamma^c}} \frac{\alpha K_{lm}}{(\Delta x_{lm})^2\phi R_{lm}}\frac{\partial(h_l-h_m)}{\partial\Delta h_k^{\Gamma}} + \sum_{\substack{m\in E\\ m\in\Gamma\\ m\in\Gamma^c}} \frac{\alpha K_{lm}}{(\Delta x_{lm})^2\phi R_{lm}}\frac{\partial(h_m-h_l)}{\partial\Delta h_k^{\Gamma}} +$$

$$\sum_{\substack{m\in S\\ m\in\Gamma^h\\ m\in\Gamma^c}} \frac{\alpha K_{lm}}{(\Delta y_{lm})^2\phi R_{lm}}\frac{\partial(h_l-h_m)}{\partial\Delta h_k^{\Gamma}} + \sum_{\substack{m\in N\\ m\in\Gamma\\ m\in\Gamma^c}} \frac{\alpha K_{lm}}{(\Delta y_{lm})^2\phi R_{lm}}\frac{\partial(h_m-h_l)}{\partial\Delta h_k^{\Gamma}} +$$

$$\sum_{\substack{m\in D\\ m\in\Gamma^h\\ m\in\Gamma^c}} \frac{\alpha K_{lm}}{(\Delta z_{lm})^2\phi R_{lm}}\frac{\partial(h_l-h_m)}{\partial\Delta h_k^{\Gamma}} + \sum_{\substack{m\in U\\ m\in\Gamma\\ m\in\Gamma^c}} \frac{\alpha K_{lm}}{(\Delta z_{lm})^2\phi R_{lm}}\frac{\partial(h_m-h_l)}{\partial\Delta h_k^{\Gamma}}$$

The derivatives of hydraulic head with respect to the perturbation of the prescribed head boundary conditions are again obtained by solving sensitivity equations. For the steady-state groundwater flow equation the sensitivity equation is:

$$[A]\left\{\frac{\partial h}{\partial\Delta h_k^{\Gamma}}\right\} + \frac{\partial[A]}{\partial\Delta h_k^{\Gamma}}\{h\} + \left\{\frac{\partial q}{\partial\Delta h_k^{\Gamma}}\right\} = 0 \qquad (6.16)$$

In this expression, the derivatives of q with respect to prescribed heads were already obtained for the groundwater flow equation. The derivatives of A with respect to the prescribed boundary heads are zero. Therefore, the vector with the derivatives of head with respect to prescribed boundary heads is the only unknown.

Some of the derivatives of the elements of F with respect to the perturbation of prescribed boundary heads are also different from zero.

$$\frac{\partial F_l}{\partial\Delta h_k^{\Gamma}} \approx -\sum_{\substack{m\in\{W\}\\ m\in\Gamma^h\\ m\in\Gamma^c}}\left(\frac{\alpha K_{lm}}{(\Delta x_{lm})^2\phi R_{lm}}\frac{\partial(h_l-h_m)}{\partial\Delta h_k^{\Gamma}}\right)c_m^{\Gamma} - \sum_{\substack{m\in\{E\}\\ m\in\Gamma^h\\ m\in\Gamma^c}}\left(\frac{\alpha K_{lm}}{(\Delta x_{lm})^2\phi R_{lm}}\frac{\partial(h_m-h_l)}{\partial\Delta h_k^{\Gamma}}\right)c_m^{\Gamma} -$$

$$-\sum_{\substack{m\in\{S\}\\ m\in\Gamma^h\\ m\in\Gamma^c}}\left(\frac{\alpha K_{lm}}{(\Delta y_{lm})^2\phi R_{lm}}\frac{\partial(h_l-h_m)}{\partial\Delta h_k^{\Gamma}}\right)c_m^{\Gamma} - \sum_{\substack{m\in\{N\}\\ m\in\Gamma^h\\ m\in\Gamma^c}}\left(\frac{\alpha K_{lm}}{(\Delta y_{lm})^2\phi R_{lm}}\frac{\partial(h_m-h_l)}{\partial\Delta h_k^{\Gamma}}\right)c_m^{\Gamma} -$$

$$-\sum_{\substack{m\in\{D\}\\ m\in\Gamma^h\\ m\in\Gamma^c}}\left(\frac{\alpha K_{lm}}{(\Delta z_{lm})^2\phi R_{lm}}\frac{\partial(h_l-h_m)}{\partial\Delta h_k^{\Gamma}}\right)c_m^{\Gamma} - \sum_{\substack{m\in\{U\}\\ m\in\Gamma^h\\ m\in\Gamma^c}}\left(\frac{\alpha K_{lm}}{(\Delta z_{lm})^2\phi R_{lm}}\frac{\partial(h_m-h_l)}{\partial\Delta h_k^{\Gamma}}\right)c_m^{\Gamma}$$

The derivatives of hydraulic heads with respect to the perturbation of prescribed boundary heads are obtained applying equation 6.16.

Some of the matrix elements of E/R have non-zero derivatives with respect to the calibration of log-storativity and the same holds for some of the vector elements of F. Below an example is given for some of the matrix elements of E/R. The expressions are similar for other elements of E/R and F.

$$\frac{\partial(E/R)_{lm}}{\partial \Delta Z_k} \approx \frac{\partial\left(\alpha K_{lm} \dfrac{h_l - h_m}{(\Delta x_{lm})^2 \phi R_{lm}}\right)}{\partial \Delta Z_k} = \frac{\alpha K_{lm}}{(\Delta x_{lm})^2 \phi R_{lm}} \frac{\partial(h_l - h_m)}{\partial \Delta Z_k} \qquad m \in \{W\} \wedge m \notin \{\Gamma^c\}$$

The derivatives of hydraulic head with respect to log-storativity are obtained by solving the following sensitivity equation:

$$\left([A] - \frac{[D]}{\Delta t}\right)\left\{\frac{\partial h^{t+1}}{\partial \Delta Z_k}\right\} + \left(\frac{\partial [A]}{\partial \Delta Z_k} - \frac{\partial [D]}{\Delta t \partial \Delta Z_k}\right)\{h^{t+1}\} + \left\{\frac{\partial q}{\partial \Delta Z_k}\right\} = -\frac{\partial [D]}{\Delta t \partial \Delta Z_k}\{h^t\} - \frac{[D]}{\Delta t}\left\{\frac{\partial h^t}{\partial \Delta Z_k}\right\} \qquad (6.17)$$

This sensitivity equation has to be solved for all the time steps that the transient groundwater flow equation is solved and for each master block at which the log-storativity is perturbed.

In case that the retardation factor is spatially constant, the calibration of the spatially constant retardation factor is simple and just the derivatives of the matrices in which the retardation coefficient appear are non-zero:

$$\frac{\partial(E/R)_{lm}}{\partial \Delta R} \approx -\alpha K_{lm} \frac{h_l - h_m}{(\Delta x_{lm})^2 \phi(R)^2}$$

In case for the retardation factor a spatial random function model is adopted, the spatially variable retardation factor can be calibrated in a similar way as the storativity coefficient. It is assumed that the retardation factor is calibrated at a limited amount of master blocks. The perturbations at the master blocks are interpolated by ordinary kriging to the rest of the grid cells. The result is a smooth perturbation that is added to the spatially variable retardation field. An example of the sensitivity of a matrix element $[E/R]_{lm}$ with respect to a change in the master block value is:

$$\frac{\partial(E/R)_{lm}}{\partial \Delta R_k} \approx -\alpha K_{lm} \frac{h_l - h_m\left(0.5\chi_l^k + 0.5\chi_m^k\right)}{(\Delta x_{lm})^2 \phi R_{lm}^2} \qquad m \in \{W\} \wedge m \notin \{\Gamma^c\}$$

where χ_l^k is the ordinary kriging weight for the interpolation of a retardation coefficient perturbation for master block k to the grid cell l. Similar expressions are obtained for the other matrix elements. Remember that the retardation coefficient evaluated at the interface between grid cells is the arithmetic average of the retardation coefficients at the two grid cells. The ordinary kriging weights are obtained from solving an ordinary kriging system:

$$\begin{bmatrix} C_{\Delta R_1 \Delta R_1} & \cdots & C_{\Delta R_{N_R} \Delta R_1} & 1 \\ \vdots & C_{\Delta R_k \Delta R_k} & \vdots & 1 \\ C_{\Delta R_1 \Delta R_{N_R}} & \cdots & C_{\Delta R_{N_R} \Delta R_{N_R}} & 1 \\ 1 & 1 & 1 & 0 \end{bmatrix} \begin{Bmatrix} \chi_l^1 \\ \chi_l^k \\ \chi_l^{N_R} \\ m \end{Bmatrix} = \begin{Bmatrix} C_{\Delta R_1 \Delta R_l} \\ \vdots \\ C_{\Delta R_{N_R} \Delta R_l} \\ 0 \end{Bmatrix}$$

The left-hand side matrix of the above ordinary kriging system contains the modelled spatial covariances between the master block locations. The right hand side vector contains the modelled spatial covariances between a grid cell l and the different master blocks. The unknowns are the kriging coefficients χ and the Lagrange multiplier m. The total number of master blocks at which the retardation coefficient is perturbed is N_R. The perturbations of the retardation coefficient at a grid cell are given then by:

$$\Delta R_l = \sum_{k=1}^{N_R} \chi_l^k \Delta R_k$$

There is physical evidence for spatial cross-correlation between hydraulic conductivity and retardation coefficients. In case that a spatial cross correlation is considered, the perturbation of retardation coefficients should affect the hydraulic conductivity values so that some of the derivatives of the elements of the E/R matrix and the F vector with respect to the perturbation of R will be non-zero. Moreover, hydraulic conductivity perturbations would also affect the values of the retardation coefficients so that also some of the derivatives of the E/R matrix with respect to hydraulic conductivity would be non-zero. The expressions for these partial derivatives are very similar to the ones presented in the equations 6.10 until 6.13 and 6.15. Finally, cokriging should be used to interpolate the conductivity and retardation perturbations to the rest of the grid cells.

Since for linear adsorption, porosity and retardation factor cannot be distinguished, we can conclude that porosity could be calibrated in a similar way for non-reactive transport, whereas for reactive transport it would be impossible to distinguish between porosity and retardation factor.

Another transport parameter that can be subjected to conditioning are mass sinks and sources. Frequently there is considerable uncertainty on the spatial and temporal distribution of mass injection so that it is interesting to consider the calibration of this parameter. Only the derivatives of the F vector are different from zero in case the amount of mass injected is calibrated. The non-zero derivatives of the F vector for the cells with mass sources are:

$$\frac{\partial \left(\dfrac{q_s^{in}(x_i, y_i, z_i, t_i) c_s(x_i, y_i, z_i, t_i)}{\phi} \right)}{\partial \Delta \left(q_s^{in}(x_j, y_j, z_j, t_j) c_s(x_j, y_j, z_j, t_j) \right)} = \frac{1}{\phi} \qquad i = j$$

We consider as calibrating parameter the mass flux into the aquifer given by the product $q_s\ c_s$. In case the pollution does not enter from a small spot, but from a larger area, master blocks could be used to calibrate the mass flux into the aquifer.

As stated before, the next steps to be taken to determine the parameter perturbations at all grid cells (non-linear optimisation algorithms, linear search, ordinary kriging) are similar to the ones taken for the inverse modelling of groundwater flow only.

6.3 Numerical aspects of the conditioning to concentration data

This section details some of the numerical aspects of the procedure presented in section 6.2. Many of the numerical aspects discussed in section 3.3 (the presence of multiple zones, the variogram definition, locating and rotating the master blocks, solving the linear system of equations, calculating the updating direction from the gradient, interpolating the perturbations) are similar for the inverse modelling of mass transport and are not repeated here. Only a limited amount of numerical aspects related to the computer implementation have to be presented in this section. Oscillations and numerical dispersion in the solution of the mass transport equation and the numerical procedure to obtain the gradient of the objective function receive special attention.

Oscillations and numerical dispersion

In section 2.2.2.1 these aspects were already addressed. The Peclet number should be, as a rule of thumb, below two in order to avoid oscillations in the solution of the mass transport equation. However, for this condition to be met the dispersion has to be, in general, large. If we consider that the spatially heterogeneous conductivity accounts for the macrodispersion, the user supplied dispersivity coefficients are related to the intra cell dispersion. A frequently applied "rule" in literature is that in those cases the longitudinal dispersivity coefficient is 0.1 times the grid cell size. However, this would give a Peclet number of 10. Therefore, in order to avoid oscillations dispersivity coefficients have to be supplied that are thought to be too high. Notice that reducing the grid cell sizes can not avoid this problem because we also have to reduce the longitudinal dispersivity coefficient as it is related to the grid cell dispersion.

INVERTO allows to set back the simulated concentrations at a certain time step to a user-defined maximum value and a user-defined minimum value (normally equal to zero) in case the calculated concentrations go beyond these limits. The occurrence of oscillations is reported in the debug file. Setting back the concentrations to a maximum or a minimum value has, especially in the context of inverse modelling some important advantages:

- In case the concentrations are not set back, the generated oscillations become more severe for the later time steps. Finally, very high or low concentrations are likely to be generated for mass transport. Setting back the concentrations to the maximum or minimum possible concentrations avoids this, but has of course the disadvantage that a problem that occurs in the numerical solution of the mass transport equation is "occulted". However, in practice it is frequently found that at a few grid cells and for a certain transport time step some oscillation occurred (with just small deviations) and that after setting back the concentrations the oscillations did not reappear at any of the locations and for any of the remaining time steps. In such a case it is thought that, in spite of the mistake made, it was acceptable to continue the

simulation. This hypothesis is checked by verifying that the mass balance is close to zero.

- It is also possible that oscillations occur for a certain, updated conductivity field, but that the oscillations disappear for later re-updated conductivity fields. In such a case it would have been a pity if the inverse conditioning could not have been terminated because for an intermediate solution very high or very low simulated concentrations would have been generated. The solution is therefore to set back the concentrations to the maximum or minimum allowed values and continuing the inverse modelling, although the intermediate solution is to some extent affected by the numerical problems. For later iterations and re-updated conductivity fields (that match the experimental information closer) the oscillations frequently disappear.

Upstream weighting should be applied in convection dominated transport. Upstream weighting is able to avoid numerical oscillations and allows for dispersivity coefficients that are lower than the ones that could be used without numerical problems in symmetric weighting. However, upstream weighting introduces another numerical problem: numerical dispersion. The Courant number (see section 2.2.2.1) should be, as a rule of thumb, below one in order to avoid numerical dispersion. Numerical dispersion can be easily avoided by reducing the time steps. The problem is, than, the increase in the CPU-time needed. Especially for the case of the simulation of mass transport in strongly heterogeneous formations this is a serious problem. Since then the largest groundwater velocities determine the maximum allowed transport time step size. Especially in case of important contrasts in groundwater flow velocities (as is the case in strongly heterogeneous formations) the time step sizes have to be very small in order to avoid numerical dispersion. In the context of inverse modelling the following additional problems with respect to numerical dispersion occur:

- The groundwater flow velocities are modified in the calibration. A time step size that is initially small enough to avoid numerical dispersion may later be too large because the maximum groundwater flow velocities in the simulation domain increased. However, this problem can be handled by checking the groundwater flow velocities as the calibration properties.
- As we saw in section 3.3, in the linear search procedure the gradient is multiplied with a value in order to obtain the perturbations of the parameters. This value is optimised and in the optimisation procedure the perturbations of the parameters increase in subsequent steps (see section 3.3) until a clearly worse result in terms of objective function value is obtained. It is expected that for those large perturbations numerical dispersion occurs. However, this is not a problem as the large perturbations are not used to update the conductivity field. It is even not a problem if for an intermediate, updated conductivity field significant numerical dispersion occurs. It is crucial whether for the final, conditioned velocity field numerical dispersion was introduced in the solution of the mass transport equation.

- The reduction of the time step size in order to avoid numerical dispersion is especially a problem in case of inverse modelling as the mass transport equation has to be solved numerous times.

The trade-off between the reproduction of concentration data and head data

Equation 6.1 contains a trade-off value that is able to balance the reproduction of the head and concentration data. In section 6.2 it is stated that the trade-off value has to be chosen considering the desired reproduction of the head and concentration data.

The desired reproduction of the data is in big part a subjective decision. For some reason, more importance may be given to the reproduction of head data or concentration data, depending on the objective of the study. However, the estimated error variance of the data should be taken into account. As shown in section 4.2, erroneous measurement data should not be reproduced too close.

The head and concentration differences along the simulation domain are normally also taken into consideration in determining the trade-off value. In case for example the maximum head difference along the domain is 10 m and the maximum concentration difference 1000 g/l a difference between simulated and measured concentration of 10 g/l could be acceptable, while such a difference (10 m) for hydraulic head off course would not be acceptable. In case a difference of 0.25 m between simulated and measured hydraulic head would be considered acceptable, the hydraulic head data (expressed in metres) have to be reproduced 25 times closer than the concentration data (expressed in g/l). The subjective determination of the trade–off value requires some interaction with the user.

Also more formal procedures can be used to determine the trade-off value. In general, the aim is to characterise the aquifer as well as possible. The question is then which data type carries more information on the formation. In synthetic studies the head, concentration, conductivity and velocity fields can be compared with reference fields for different trade-off values. In practical studies such a comparison can not be carried out, but an alternative would be to split the data set in two parts and use part of the data in the inverse modelling and other part of the data for comparing the simulated and measured values. The trade-off value could be determined by evaluating the performance for different trade-off values.

Another alternative is to use the variances of the head or concentration data. In this case the trade-off is equal to the variance of the concentration data divided by the variance of the hydraulic head data.

Solving the sensitivity equations

In equations 6.14 and 6.17 partial derivatives of parameters with respect to hydraulic head appear. These derivatives are found by solving linear systems of equations like 2.8 or 2.11. These linear systems of equations have to be solved for each master block. The equations are very similar to the groundwater flow equation and therefore the comments given in section 3.3 with respect to the accuracy of the solution found, convergence problems etc. also hold for solving a linear system of sensitivity equations.

Calculating the gradient of the objective function

The contributions to the gradient can be divided between contributions related to the groundwater flow part and contributions related to the transport part. However, in the derivatives of matrices and vectors of the discretized transport equation with respect to the hydraulic conductivity perturbations also expressions related to the groundwater flow equation appear. For example, the flow sensitivity equations have to be solved for each master block and each time step. In case all the derivatives of head with respect to hydraulic conductivity have to be stored temporarily a large amount of memory is occupied. The needed memory can be reduced by organising the gradient calculation in a more efficient way. Figure 6.1 presents the steps taken for calculating the gradient elements corresponding to the hydraulic conductivity perturbation. The program calculates first the gradient elements corresponding to the perturbation of the hydraulic conductivities, later the derivatives with respect to the perturbation of the prescribed boundary heads, and later possibly the derivatives with respect to other parameters that are perturbed. Figure 6.1 does not show the calculation of the derivatives with respect to the perturbation of the prescribed boundary heads and other parameters. However, these derivatives are obtained in a similar way as the derivatives with respect to the hydraulic conductivities, although less evaluations have to be made to obtain them.

The following strategies are applied in order to reduce the needed CPU-time to calculate the gradient:

- During the calculation of the derivatives of the flow equation with respect to the perturbation of hydraulic conductivity or prescribed boundary heads already the required left-hand side matrix and right-hand side vector needed to solve the flow sensitivity equations are built. The flow sensitivity equations, on their turn, have to be solved in order to obtain the derivatives of the transport equation with respect to the hydraulic conductivity perturbation (see also section 6.2).
- The derivatives of hydraulic head with respect to hydraulic conductivity perturbations and perturbations of prescribed boundary heads contribute to the derivatives of the transport equation with respect to

Figure 6.1 Flow diagram of the gradient calculation for the coupled inverse modelling of groundwater flow and mass transport (on this page and the next two pages). The formulation of the adjoint state equation according Appendix II is used.

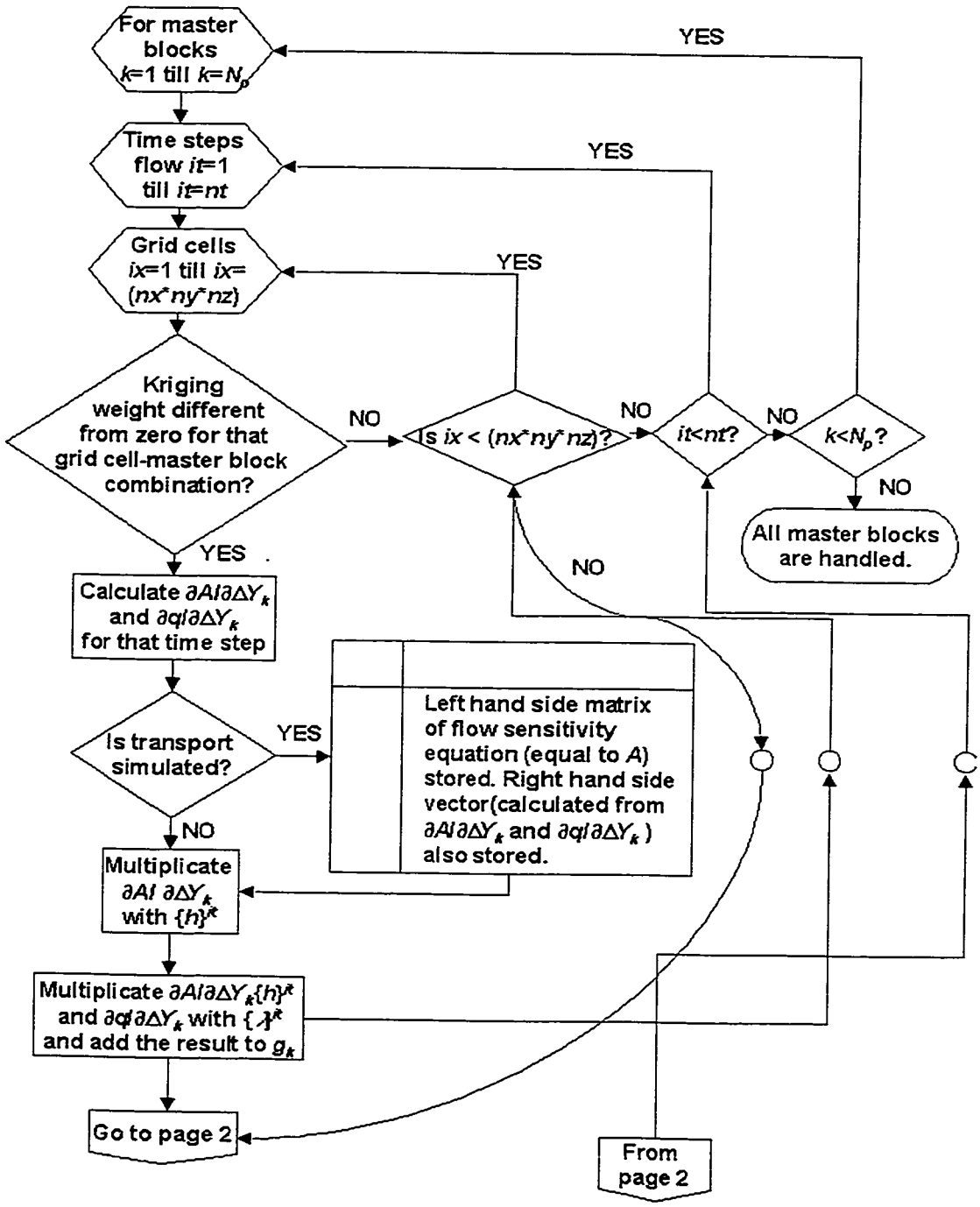

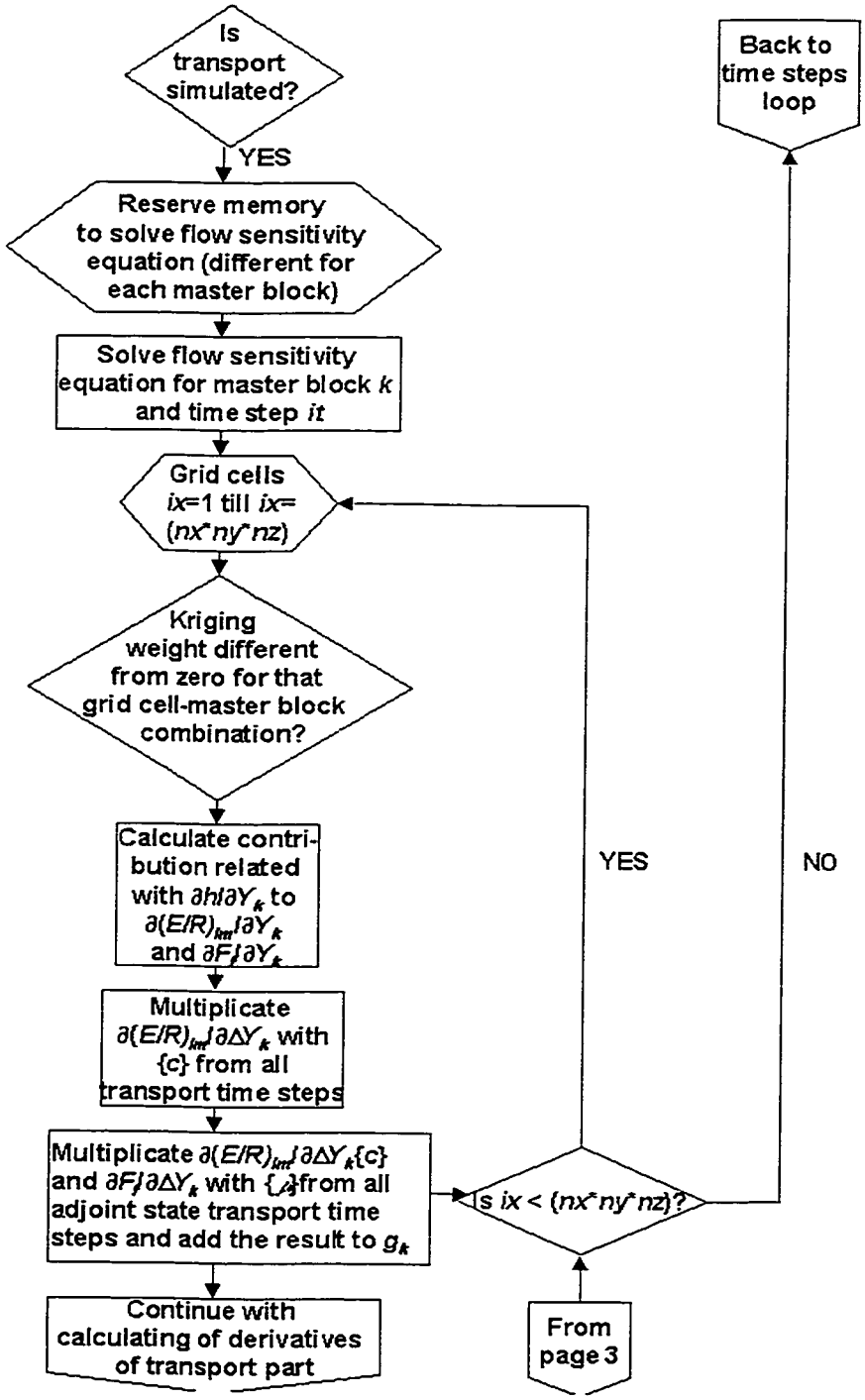
Is transport simulated?
YES
Reserve memory to solve flow sensitivity equation (different for each master block)
Solve flow sensitivity equation for master block k and time step it
Grid cells ix=1 till ix= (nx*ny*nz)
Kriging weight different from zero for that grid cell-master block combination?
Calculate contribution related with ∂h/∂Y_k to ∂(E/R)_km/∂Y_k and ∂F_i/∂Y_k
Multiplicate ∂(E/R)_km/∂ΔY_k with {c} from all transport time steps
Multiplicate ∂(E/R)_km/∂ΔY_k{c} and ∂F_i/∂ΔY_k with {λ} from all adjoint state transport time steps and add the result to g_k
Continue with calculating of derivatives of transport part
Is ix < (nx*ny*nz)?
YES
NO
From page 3
Back to time steps loop

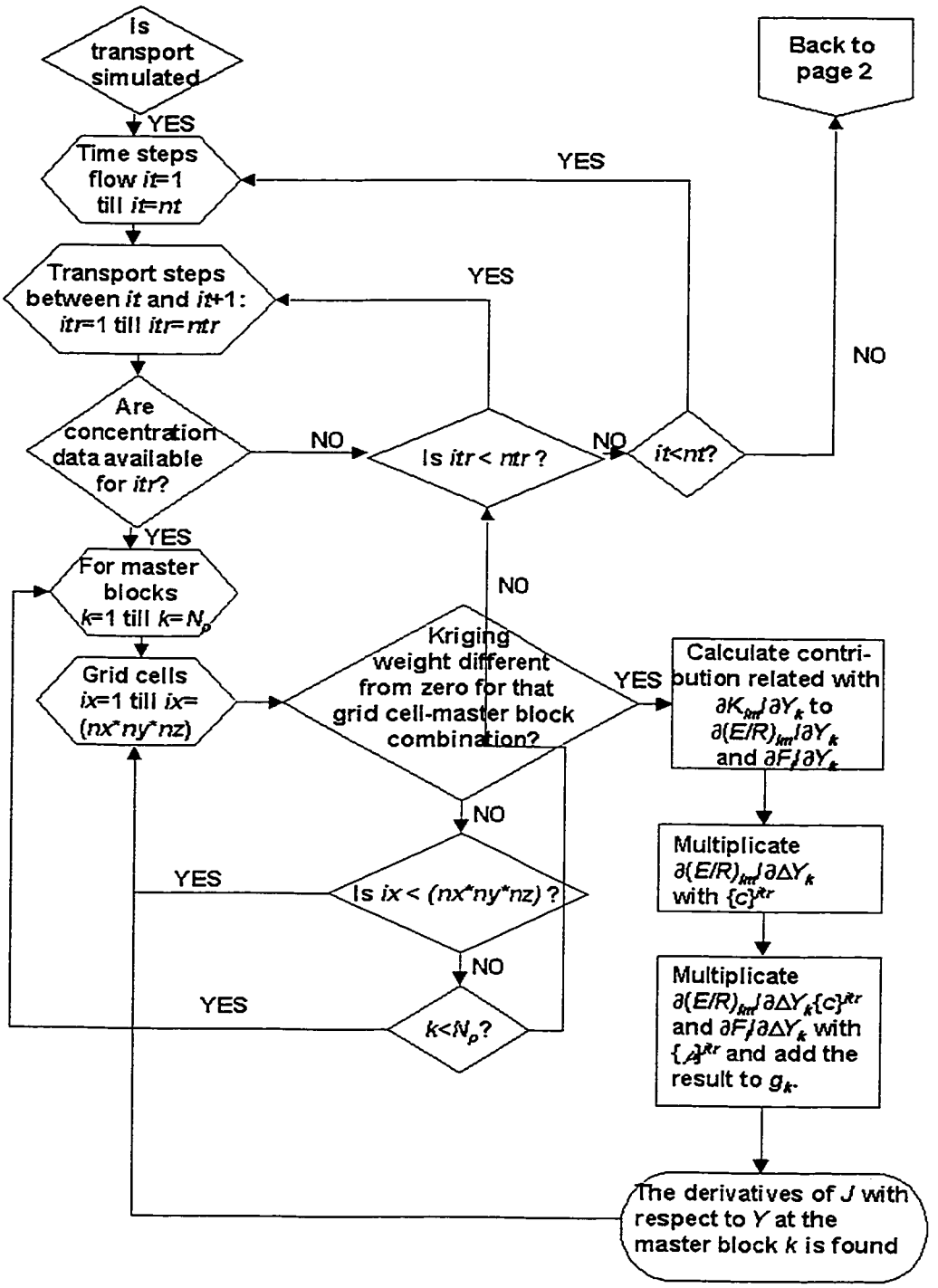
Is transport simulated
YES
Time steps flow it=1 till it=nt
Transport steps between it and it+1: itr=1 till itr=ntr
Are concentration data available for itr?
NO
YES
For master blocks k=1 till k=Np
Grid cells ix=1 till ix=(nx*ny*nz)
Kriging weight different from zero for that grid cell-master block combination?
YES
NO
Calculate contribution related with ∂Kkm/∂Yk to ∂(E/R)km/∂Yk and ∂Fj/∂Yk
Multiplicate ∂(E/R)km/∂ΔYk with {c}itr
Multiplicate ∂(E/R)km/∂ΔYk{c}itr and ∂Fj/∂ΔYk with {λ}itr and add the result to gk.
Is ix < (nx*ny*nz) ?
YES
NO
k<Np?
YES
NO
Is itr < ntr ?
NO
YES
it<nt?
YES
NO
Back to page 2
The derivatives of J with respect to Y at the master block k is found

these perturbation parameters. These contributions are calculated in the loop where the derivatives of the flow equation with respect to these parameters are calculated. However, the contributions have to be multiplied by the simulated concentration values and the simulated transport adjoint state values. This is not a problem because the solution of the transport equation and the adjoint transport equation were stored in 4-D arrays. The contributions are calculated in the flow loop in order to reduce the storage costs. The derivatives do not have to be stored and are used immediately to calculate the contributions to the gradient.

- Another contribution of the derivatives of the transport equation with respect to the hydraulic conductivity perturbations is related to the derivatives of hydraulic conductivity with respect to hydraulic conductivity perturbations. The derivatives can only be non-zero in case concentration measurement data were available for that (transport) simulation time step. (in case the adjoint state equations are formulated continuous in time, see Appendix II). Therefore in each transport time step loop first a check was made whether concentration data are available. In order to calculate the derivatives also the groundwater flow velocities are needed. The groundwater flow velocities in space and time are stored in a 4-D array.
- Like for the gradient calculation in case of flow only, a check is made whether for a grid cell-master block combination the kriging weight is different from zero. In case the kriging weight is zero, the next grid cell-master block combination is handled in order to avoid unnecessary calculations.

6.4 Synthetic study on the coupled inverse modelling of flow and transport and the worth of concentration data

The theory presented in section 6.2 was implemented in the software INVERTO and tested in a synthetic study. This study was a test case for the conditioning algorithm and an objective was to study whether the software was able to condition a sufficiently large number of realisations sufficiently close to the experimental data in a not too elevated CPU time. Another aim was to study the impact of the concentration data on the characterisation of the aquifer properties. In this synthetic study, only the transmissivity field is unknown and the boundary conditions, dispersivity coefficients and contaminant release information are perfectly known. An interesting future extension would be to consider multiple sources of uncertainty, like transmissivities and contaminant release information or both transmissivities and retardation coefficients.

In the literature the studies on the coupled inverse modelling of groundwater flow and mass transport are limited. Furthermore, we are not aware of studies on the worth of concentration data in the context of Monte Carlo simulation.

6.4.1 Reference fields

The study domain has extension of 500 m by 500 m and is divided in 50 by 50 squared grid cells of 10 m in the size.

A reference log transmissivity field is generated with an average transmissivity of -6.0 $\log_{10}(m^2/s)$ and a standard deviation of 0.5 $\log_{10}(m^2/s)$; it is moderately heterogeneous. The method can also be applied on strongly heterogeneous transmissivity fields, but the CPU-time needed would increase significantly, because the time step would have to be smaller in order to avoid numerical dispersion (see also section 2.2.2.1). The variogram of log transmissivity is spherical with a range of 125 m, zero nugget and sill of 0.25 $(\log_{10}(m^2/s))^2$.

Steady-state groundwater flow is simulated with prescribed head boundaries on the South and North and impermeable boundaries on the West and East. The prescribed head value is 5 m along the southern boundary and 0 m along the northern boundary. These prescribed head values force a flow from the south to the north.

On the southern boundary, a line contamination source is present. The contaminants are introduced in the system by a constant concentration of 1.0 unit (standardised concentration) along a 100 m long transect on the southern boundary. For the rest of the southern boundary the prescribed concentration values are equal to zero. On the northern boundary also prescribed concentrations equal to zero are imposed. These boundary conditions are justified because during the time of the transport simulation the northern boundary is far enough from the contaminant plume. The contaminants do not

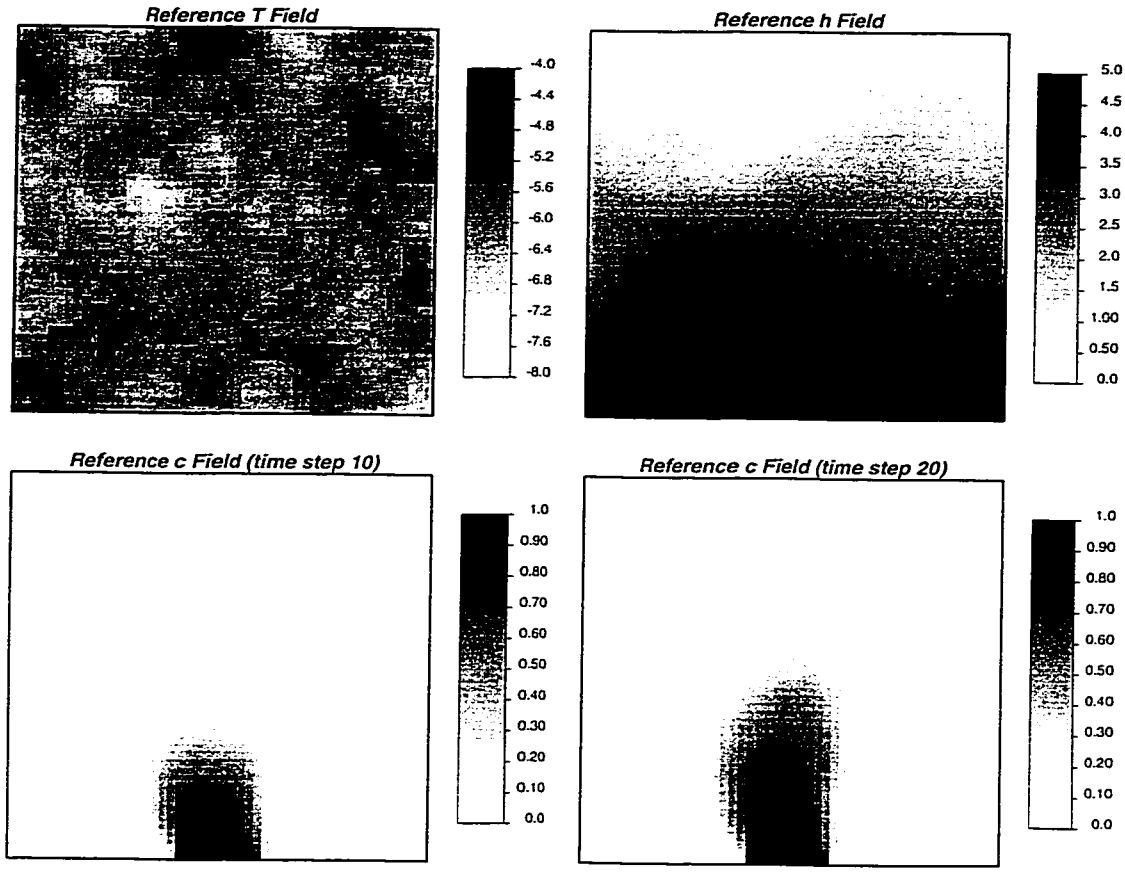

Figure 6.2. Reference transmissivity field, steady-state head field and concentration fields for time step 10 and time step 20.

show retardation or any chemical reaction and are subject to dispersion. The longitudinal dispersion coefficient is set equal to 10 m. This value is large for numerical convenience. The mass transport equation is solved for time steps of 10^9 seconds (31.69 years) until $2 * 10^{10}$ seconds (633.76 years).

Figure 6.2 shows the reference transmissivity, hydraulic head and concentration fields.

6.4.2 Scenarios studied

100 equally likely solutions to the inverse problem are calculated for eight different scenarios. The scenarios differ in the kind of conditioning data. Table 6.1 illustrates the kind of data used in each of the eight scenarios. In four of the eight scenarios (scenarios 2, 4, 6 and 8) 20 transmissivity data are used in the conditioning procedure. The transmissivity data are obtained from random sampling of the reference transmissivity field. Also in four of the eight scenarios (scenarios 3, 4, 7 and 8) 20 steady-state head data are used as conditioning information. The steady-state head data are sampled at the same locations as

	20 Y data?	20 h data?	13 c data?
Scenario 1	NO	NO	NO
Scenario 2	YES	NO	NO
Scenario 3	NO	YES	NO
Scenario 4	YES	YES	NO
Scenario 5	NO	NO	YES
Scenario 6	YES	NO	YES
Scenario 7	NO	YES	YES
Scenario 8	YES	YES	YES

Table 6.1. Studied scenarios in the synthetic study.

the transmissivity data. Finally, in four of the studied scenarios (scenarios 5, 6, 7 and 8) concentration data are used in the conditioning procedure. For those scenarios a coupled inversion procedure was done. The concentration data are sampled from the reference concentration field for the last time step ($2 * 10^{10}$ seconds) and the 13 data are taken from a monitoring line perpendicular to the mean flow direction. No concentration data from earlier time steps are available. Figure 6.3 shows the location of the measurement data.

For the eight different scenarios the aim was to reproduce the hydraulic head and concentration data as close as possible since the data were taken error-free. The transmissivity data are reproduced exactly. In case that both hydraulic head and concentration data are used as conditioning information it is necessary to define a trade-off value (the parameter ψ_3 in equation 6.1) in order to weight the two pieces of information. It was found that a value equal to 1.0 yields optimal results in this study. Larger trade-off values did not result in a sufficiently close reproduction of the hydraulic head data.

100 master blocks are located in the simulation domain with the same density in the x- and the y-direction. Figure 6.4 shows as an example, one realisation not conditioned to any information and one realisation conditioned to transmissivity, steady-state head and concentration data. The figure illustrates that the realisation conditioned to all the information is closer to the reference fields than the unconditional realisation. In the unconditional realisation the contaminant plume extends much further than in the reference field.

6.4.3 Evaluation of results

For each of the eight scenarios 100 equally likely realisations are generated. Each of the realisations is compared with the reference fields. The following performance measures are defined:

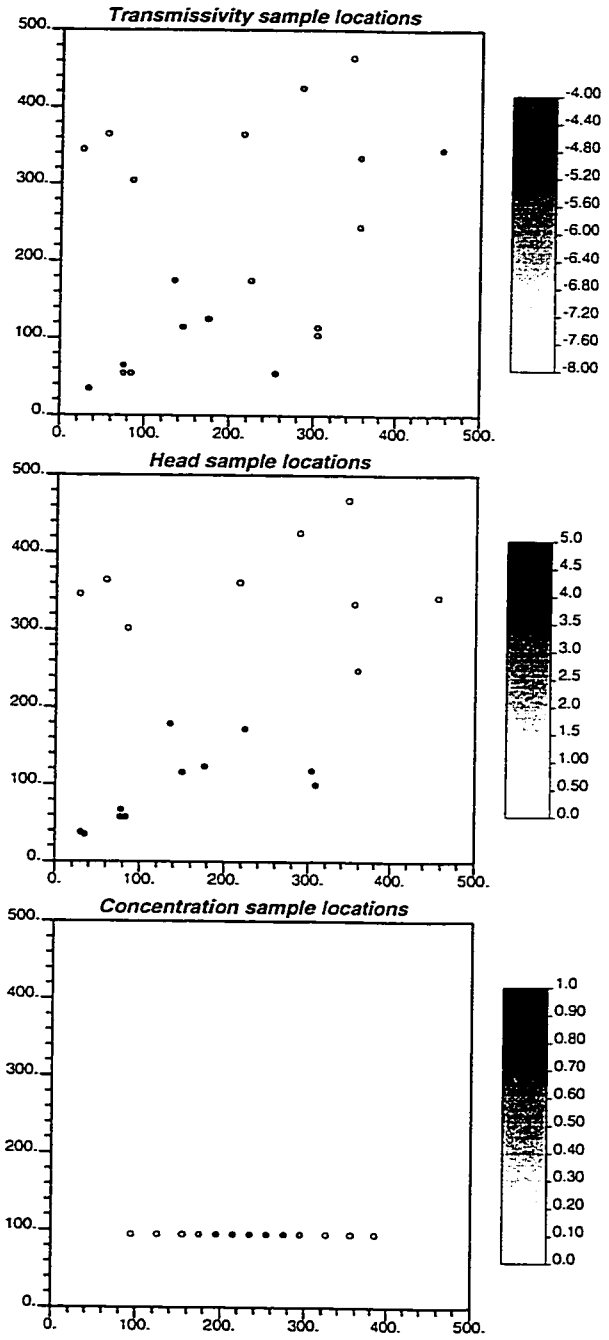

Figure 6.3. Sample locations of transmissivity, steady-state piezometric head and concentration at time step 20.

Figure 6.4. (above) One realisation, not conditioned to any data (scenario 1). (below) One realisation, conditioned to all the information (scenario 8).

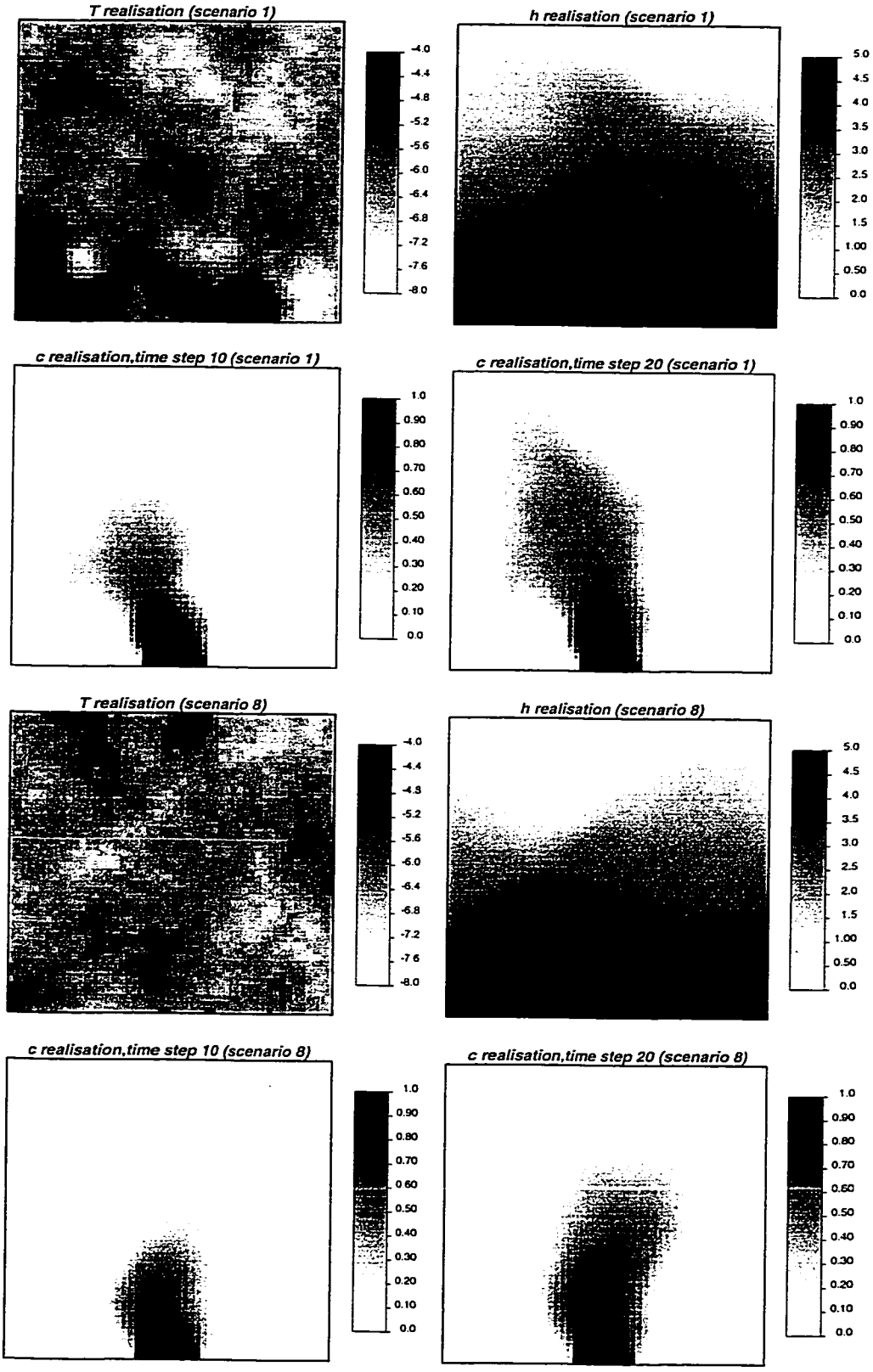

$$AAE(X) = \frac{1}{NNODES} \sum_{i=1}^{NNODES} \left| \overline{X}_{SIM,i} - X_{REF,i} \right|$$

$$AESD(X) = \frac{1}{NNODES} \sum_{i=1}^{NNODES} \sigma_{X,}$$

where *AAE* is the average absolute error, *AESD* the average ensemble standard deviation, *NNODES* the number of discretization grid cells, and *i* is a grid cell index, *X* represents either decimal log transmissivity, steady-state hydraulic head or mass concentration at a certain time step, the overbar indicates ensemble average, the subscript *SIM* refers to the realisations, and the subscript *REF* to the reference values; finally, σ_{Xi} is the ensemble standard deviation of *X* at a given node. In addition, *AAE(h)* is the average absolute error for hydraulic head, *AAE(c)* the average absolute error for concentration and *AAE(Y)* the average absolute error for log transmissivity. *AESD(h)*, *AESD(c)* and *AESD(Y)* are the average ensemble standard deviation for hydraulic head, concentration and log transmissivity respectively.

6.4.4 Results

Table 6.2 shows the calculated *AAE* for transmissivity, hydraulic head and concentration for the eight scenarios. The results are standardised so that *AAE* is equal to 100 for the scenario with no conditioning data. Figure 6.5 shows the ensemble averaged transmissivity, hydraulic head and concentration fields for some of the scenarios.

The *AAE* for transmissivity, hydraulic head and concentration are below 100 for all the scenarios with conditioning data. It means that the presence of conditioning data resulted in all cases in an improved characterisation of the transmissivity, hydraulic head and concentration field.

	AAE(Y)	*AAE(h)*	*AAE(c)*
Scenario 1	100	100	100
Scenario 2	92	93	68
Scenario 3	91	49	97
Scenario 4	81	34	70
Scenario 5	96	92	54
Scenario 6	91	90	58
Scenario 7	88	52	43
Scenario 8	79	35	37

Table 6.2. The standardised average absolute error (scenario 1=100) for the characterisation of the transmissivity, steady-state head and concentration (averaged over 20 time steps) field.

Figure 6.5. (From the left to the right and from above to below, continuing on the next page): Ensemble averages of transmissivity for scenario 1, scenario 2 and scenario 8; ensemble averages of steady-state head for scenario 1, scenario 3 and scenario 8; ensemble averages of concentration at time step 20 for scenario 1, scenario 4 and scenario 8.

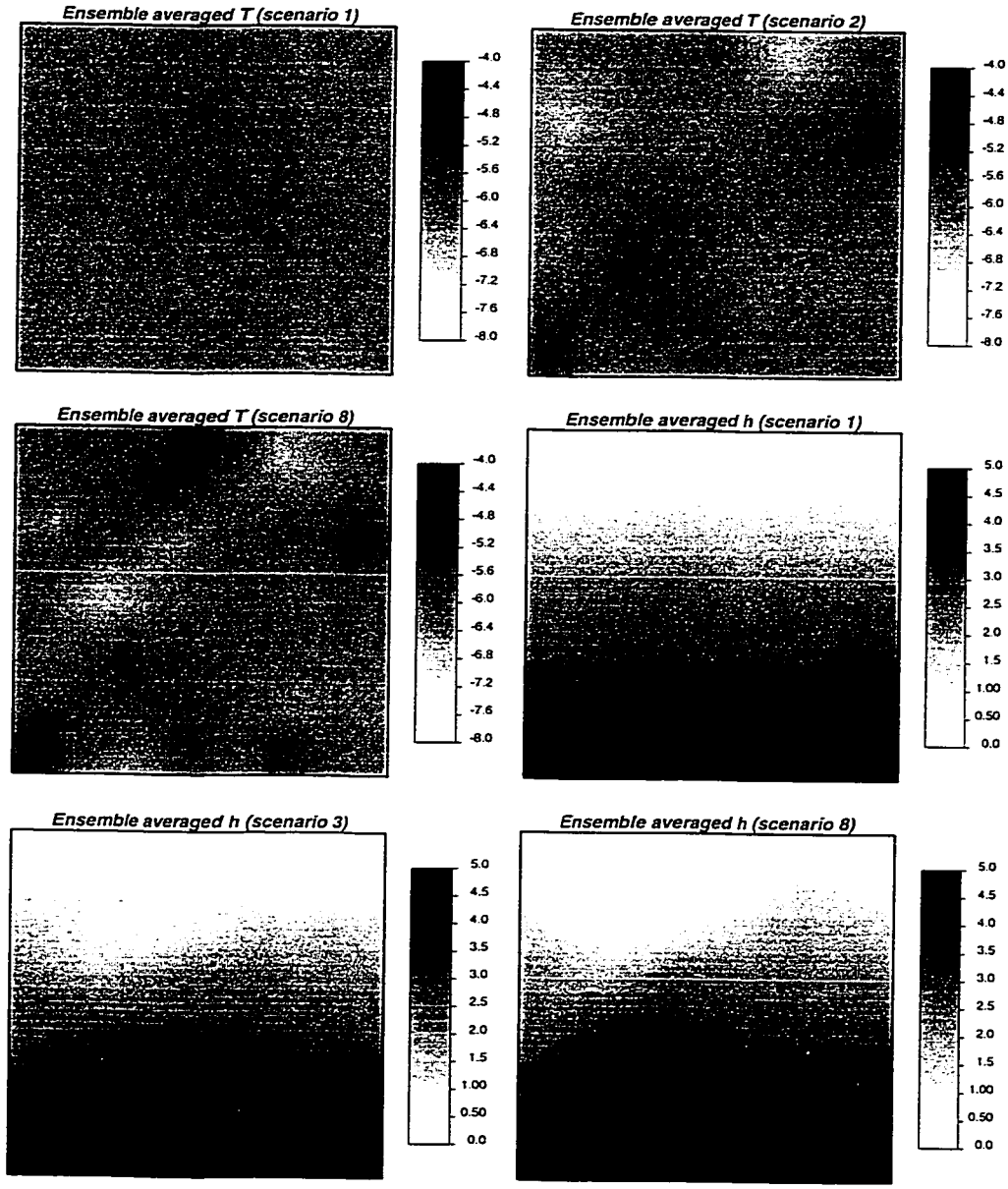

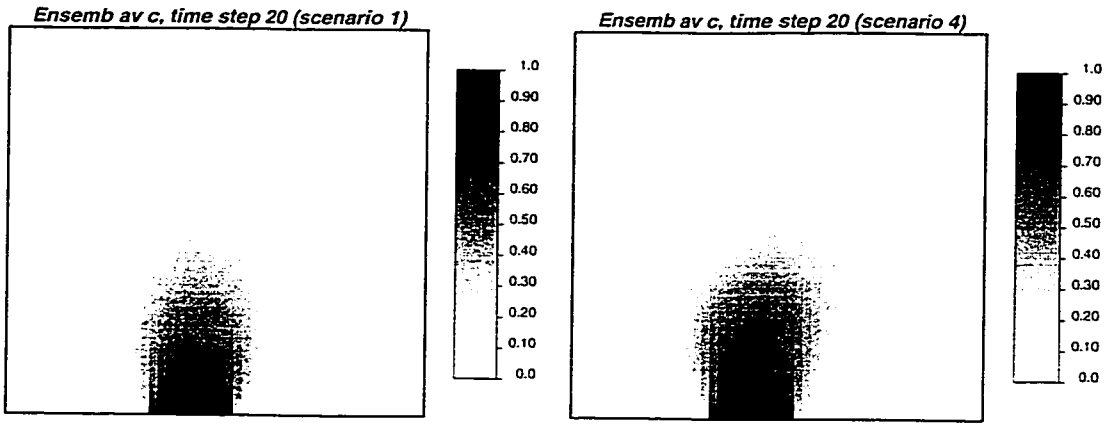

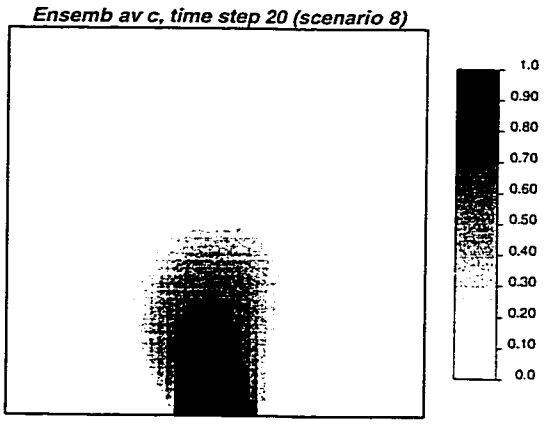

6.4.4.1 Results for just one piece of conditioning information

In case just one type of conditioning information is available, either only transmissivity data (scenario 2), steady-state head data (scenario 3) or concentration data (scenario 5), the characterisations of transmissivity, steady-state head and concentration improve. In case just transmissivity data are available, the characterisation of the transmissivity improves (*AAE*(*Y*)-reduction 8%), but also the characterisation of the steady-state head field (*AAE*(*h*)-reduction 7%) and especially the characterisation of the concentration field (*AAE*(*c*)-reduction on average 32% over the 20 time steps). It shows that transmissivity, through the groundwater flow equation, improves the characterisation of the hydraulic head field and through the groundwater flow velocities also the characterisation of the concentration field. The conditioning to just hydraulic head data yields a similar *AAE*(*Y*) reduction (9%), a much more pronounced *AAE*(*h*) reduction (51%) and just a small *AAE*(*c*) reduction (on average 3% over the 20 time steps). It is not straightforward to explain why head and transmissivity data had such a different impact on the characterisation of the concentration field in this case. Finally, the use of concentration data only yields also an *AAE*(*Y*) reduction (4%), *AAE*(*h*) reduction (8%) and especially *AAE*(*c*) reduction (46%). In case that the *AAE* are calculated just over the upstream part of the aquifer (the concentration monitoring

locations divide the aquifer in an upstream and a downstream part) the reductions are much more important: 20% when using transmissivity, 46% when using hydraulic head and 71% when using concentrations. This illustrates that the *AAE*(*Y*) and *AAE*(*h*) reductions are close to zero for the downstream part of the aquifer, but very important for the upstream part of the aquifer. This is logical as the concentrations give information on groundwater flow velocities (and thus the transmissivities and hydraulic heads) of the upstream part of the aquifer but not on the downstream part. The characterisation of the concentration field improves both for the upstream part of the aquifer and the downstream part, but also in this case the improvement is more significant for the upstream part.

Now we will have a look at the temporal evolution of the *AAE*(c). Figure 6.6 shows the temporal evolution of the *AAE*(*c*) for scenario 1 (no conditioning data) and the temporal evolution of the *AAE*(*c*) for scenario 5 (13 concentration data). Figure 6.6 gives also the reduction on *AAE*(*c*) introduced by the conditioning.

For the whole aquifer, the *AAE*(*c*) increases throughout the simulation time and reaches its maximum at the last simulation time step (time step 20). This is both the case for scenario 1 (no conditioning information) and scenario 5 (conditioning to concentration data). The concentration data at time step 20 reduce the *AAE*(*c*) for all time steps, but do not stop the *AAE*(*c*) increase in time. The *AAE*(*c*) reduction (the *AAE*(*c*) for scenario 5 (13 concentration data) divided by the *AAE*(*c*) for scenario 1 (no conditioning data)) reaches its maximum at time step 6 (52%) and its minimum at time step 20 (39%). At first sight it is surprising that the maximum *AAE*(*c*) reduction is not achieved at time step 20. However, this can probably be explained by the fact that the conditioning data improve the characterisation of the upstream aquifer parameters and therefore the larger *AAE*(*c*) reductions are obtained when the plume still did not enter into the downstream part of the aquifer.

If the *AAE*(*c*) is calculated just over the upstream part of the aquifer the largest *AAE*(*c*) in scenario 1 (no conditioning data) is found for time step 9 and the *AAE*(*c*) decreases slowly for later time steps. See again Figure 6.6. This posterior decrease is associated with the position of the main concentration gradient. At later time steps the transition zone between low concentrations (close to zero) and high concentrations moves into the downstream part of the aquifer and due to the fact that the maximum *AAE*(*c*) is associated with this transition zone, the *AAE*(*c*) for the upstream part decreases slightly for later time steps. In case the concentration data are used in the inverse modelling (scenario 5) the lowest *AAE*(*c*) are found for time step 20. It is clear that this difference is due to the conditioning information at time step 20. The conditioning information at time step 20 makes that the maximum *AAE*(*c*) moves away from time step 20: from time step 9 in scenario 1 to time step 2 in case concentration data are available.

Figure 6.6. Plots of the *AAE(c)* evolution and the *AAE(c)* reduction as function of the simulation time step. Compared are the scenarios 1 and 5 and the results are calculated both for the whole aquifer and the upstream part of the aquifer only.

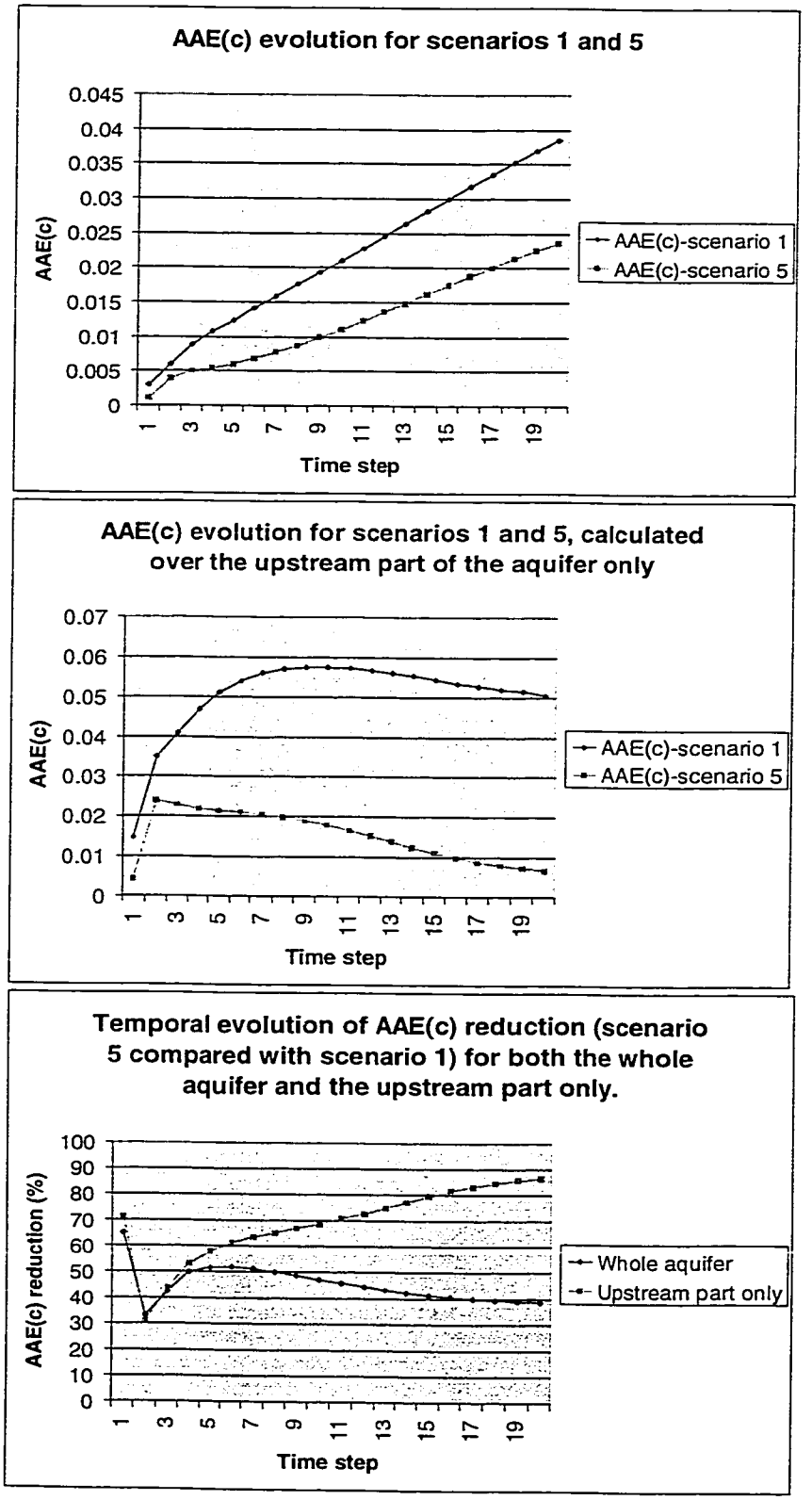

The maximum $AAE(c)$ reduction (87%) is also obtained at time step 20, and for earlier time steps the $AAE(c)$ reduction is less.

6.4.4.2 Results for different kinds of conditioning information

In case both transmissivity and hydraulic head data are available (scenario 4) the AAE reductions are larger and close to the sum of the AAE-reductions for the scenarios 2 (just transmissivity data) and 3 (just hydraulic head data). The $AAE(Y)$ reduction is 19%, the $AAE(h)$ reduction 66% and the $AAE(c)$ reduction on average 30% over the 20 time steps.

The combination of concentration and transmissivity data (scenario 6) results in a stronger AAE-reduction than just concentration data or just transmissivity data. However, in this case the AAE-reduction is by no means the sum of the AAE-reductions of scenario 2 (just transmissivity data) and scenario 5 (just concentration data). The $AAE(Y)$ reduction is 9% (the sum would have been 12%), the $AAE(h)$ reduction 10% (the sum would have been 15%) and the $AAE(c)$ reduction 42%. It should be noticed that the use of just concentration data yielded a stronger $AAE(c)$ reduction.

The combination of concentration and hydraulic head data (scenario 7) yields important $AAE(c)$ reductions: the $AAE(Y)$ and $AAE(h)$ reductions are close to the sum of the $AAE(Y)$ and $AAE(h)$ reductions for scenario 3 (just hydraulic head data) and scenario 5 (just concentration data). The $AAE(c)$ reduction (57%) is even larger than the sum of the $AAE(c)$ reductions for scenario 3 (just hydraulic head data; reduction 3%) and scenario 5 (just concentration data; reduction 46%).

Finally, in case all conditioning information is used (scenario 8) the best results are obtained. The $AAE(Y)$ reduction is 21%, the largest reduction from the scenarios studied. As found in other synthetic studies, the AAE-reduction for hydraulic head is usually much bigger than the $AAE(Y)$ reduction, but it is the improved characterisation of the transmissivity field that guarantees that in other flow regimes also an improved characterisation of the groundwater flow will be obtained. The $AAE(Y)$ reduction for scenario 8 is nearly equal to the sum of the $AAE(Y)$ reductions for just transmissivity data (8%), just hydraulic head data (9%) and just concentration data (4%). Figure 6.5 shows that the conditioning data depicted the principal zones of enhanced and reduced transmissivity. The $AAE(h)$ reduction is 65%, and a slightly larger reduction (66%) was obtained for scenario 3, with just hydraulic head and transmissivity data. The concentration data did not help to reduce further the $AAE(h)$ which may be due to a less accurate reproduction of the hydraulic head data. In case both hydraulic head and concentration data are used as conditioning information the reproduction of the hydraulic head data tends to be slightly worse, but with the compensation that the concentration data are closely reproduced. Nevertheless, the final $AAE(h)$ reduction for scenario 8 is again

very close to the sum of the *AAE*(*h*) reductions for just transmissivity data (7%), just hydraulic head data (51%) and just concentration data (8%). Finally, the *AAE*(*c*) reduction (again averaged over the 20 time steps) reaches also its maximum in case all the conditioning information is used (63%). The reduction is around 66% for the time steps 9 until 20, but for the first time steps the reduction is smaller. Figure 6.5 shows that the conditioning data are able to characterise approximately the contaminant plume, while in the unconditional case the contaminant plume covers a smaller part of the aquifer than in the reference. The *AAE*(*c*) reduction is smaller than the sum of the *AAE*(*c*) reductions for just transmissivity data, just hydraulic head data and just concentration data. It is found that hydraulic head data have an important additional value to concentration data, on the contrary, transmissivity data have little additional value to concentration data. However, these findings may differ for other boundary conditions.

For scenario 5 (conditioning to only concentration data) it was found that the *AAE*-reductions are much larger for the upstream part of the aquifer. Is this still the case if besides concentration data also hydraulic head and/or transmissivity data are used in the inverse modelling? The *AAE*(*Y*) reductions are larger in the upstream part of the aquifer for all cases that concentration measurement data are available. We saw that for scenario 5 the overall *AAE*(*Y*) reduction was 4%, while in the upstream part it was 20%. For scenario 6 (concentration and transmissivity data) the overall reduction is 9%, and the reduction for the upstream part is 28%. For scenario 7 (concentration and head data) the contrast in *AAE*(*Y*) reduction between the upstream and downstream part is reduced: the overall reduction is 12% and the reduction for the upstream part is 26%. For scenario 8 (concentration, head and transmissivity data) the overall reduction is 21% while it is 35% for the upstream part. It can be concluded that the head and transmissivity data give an additional *AAE*(*Y*) reduction, but the additional value of the concentration data is evident, especially from the ensemble statistics of the upstream part of the aquifer. This is not the case for the *AAE*(*h*) reduction. While for scenario 5 (concentration data only) there was a strong contrast with an overall *AAE*(*h*) reduction of 8% and a reduction in the upstream part of 46%, for all other scenarios with concentration data the contrast is less or even inexistent. For scenario 6 (concentration and transmissivity data) the overall *AAE*(*h*) reduction was 10% and for the upstream part 28%. In case also hydraulic head data are available (scenarios 7 and 8) the *AAE*(*h*) reduction is not stronger for the upstream part than for the rest of the aquifer. Finally, the *AAE*(*c*) reduction is in all cases larger in the upstream part of the aquifer than in the rest of the aquifer. For scenario 5 (just concentration data) we saw already that the overall *AAE*(*c*) reduction was 46% and the reduction for the upstream part was 71%. For scenario 6 (concentration and transmissivity data) the contrast is even bigger: 42% *AAE*(c) reduction for all the aquifer and 83% for the upstream part only. The head data reduce the contrast in *AAE*(*c*) reduction as they were more capable to improve the characterisation of the concentration field downstream of the monitoring locations. For scenario

7 (concentration and head data) the overall *AAE*(*c*) reduction was 57% and for the upstream part it was 69%. In case head, concentration and transmissivity data are available (scenario 8) the overall *AAE*(*c*) reduction was 63% and for the upstream part it was 72%.

The behaviour of the *AAE*(*c*) as function of the simulation time step is the same for the scenarios 6, 7 and 8 as for the scenario that just concentration data were available (scenario 5). The *AAE*(*c*), when calculated over the whole aquifer, increased continuously in time. On the contrary, the *AAE*(*c*) calculated over the upstream part of the aquifer reached its maximum very fast after the start of the transport simulations (time step 1 or 2) and decreased afterwards.

6.4.4.3 Average Ensemble Standard Deviations

Table 6.3 shows the calculated *AESD* for each of the scenarios. The general conclusion is that the conditioning data result in a reduction of the *AESD*. It means that the updated, ensemble averaged, transmissivity, hydraulic head and concentration fields are not only closer to the reference fields (*AAE*-reduction), but also that the uncertainty on these estimates is smaller (*AESD*-reduction). Figure 6.7 shows the ensemble averaged standard deviations of the transmissivity, steady-state head and concentration fields for some of the scenarios.

Looking into more detail we see that the *AESD*-reductions are smaller than the *AAE*-reductions. Nevertheless, the *AESD*-reductions are also considerable. The *AESD*(*Y*) reduction is 19% for the scenarios 4 and 8. This is quite close to the maximum *AAE*(*Y*) reduction (for scenario 8) of 21%. It is found that transmissivity and head data help to reduce the uncertainty on the transmissivity field. Figure 6.7 clearly illustrates the impact of the conditioning transmissivity data. However, when conditioning to concentration data, the

	AESD(*Y*)	*AESD*(*h*)	*AESD*(*c*)
Scenario 1	100	100	100
Scenario 2	85	79	95
Scenario 3	96	59	97
Scenario 4	81	51	82
Scenario 5	107	105	108
Scenario 6	88	82	90
Scenario 7	98	61	84
Scenario 8	81	50	69

Table 6.3. The standardised average ensemble standard deviation (scenario 1=100) for the characterisation of the transmissivity, steady-state head and concentration (averaged over 20 time steps) field.

Figure 6.7. The following ensemble standard deviations are displayed (From the left to the right and from above to below, continuing on the next page): transmissivity for scenario 1, scenario 2 and scenario 8; steady-state head for scenario 1, scenario 3 and scenario 8; concentration for scenario 1, scenario 4 and scenario 8.

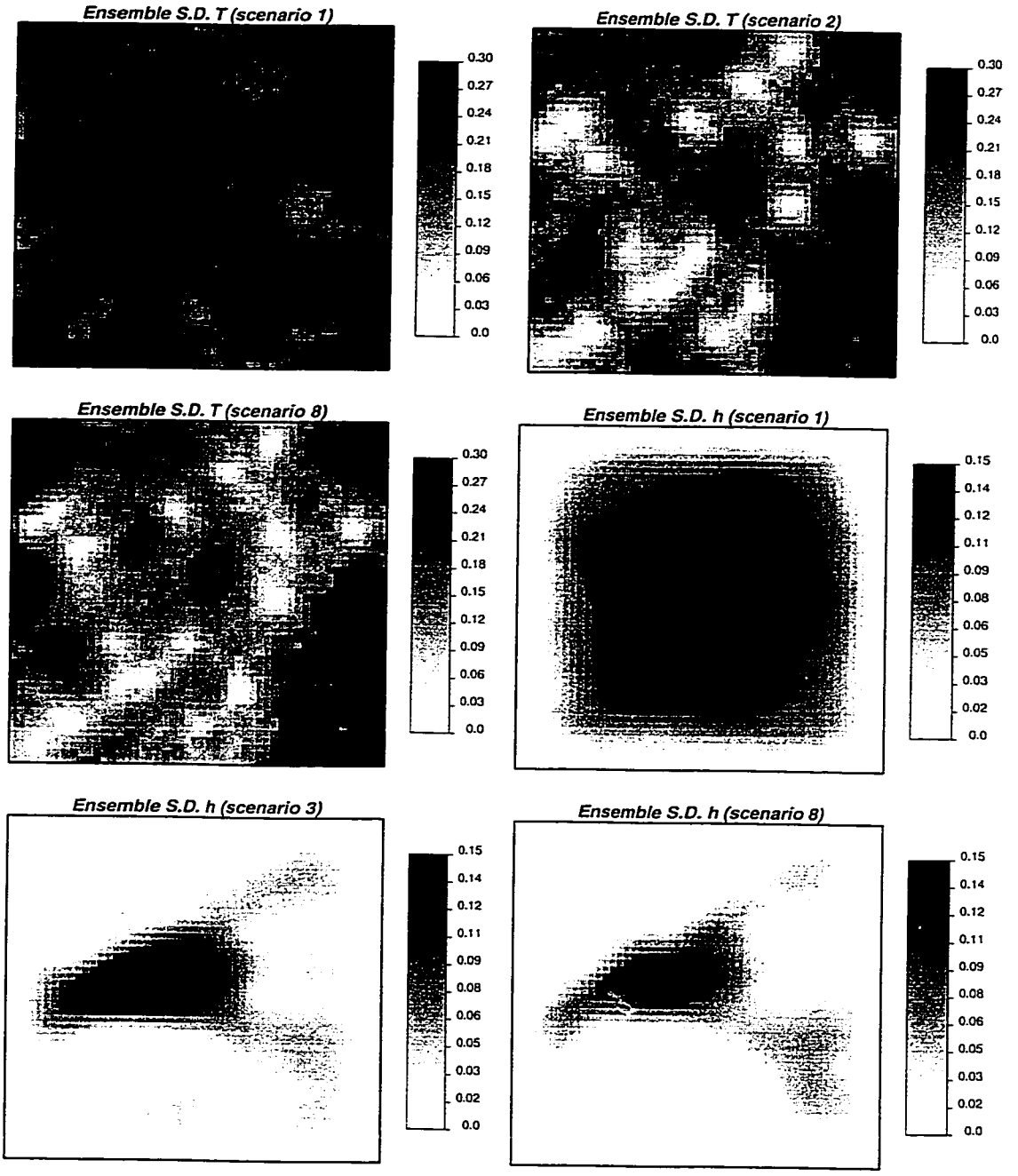

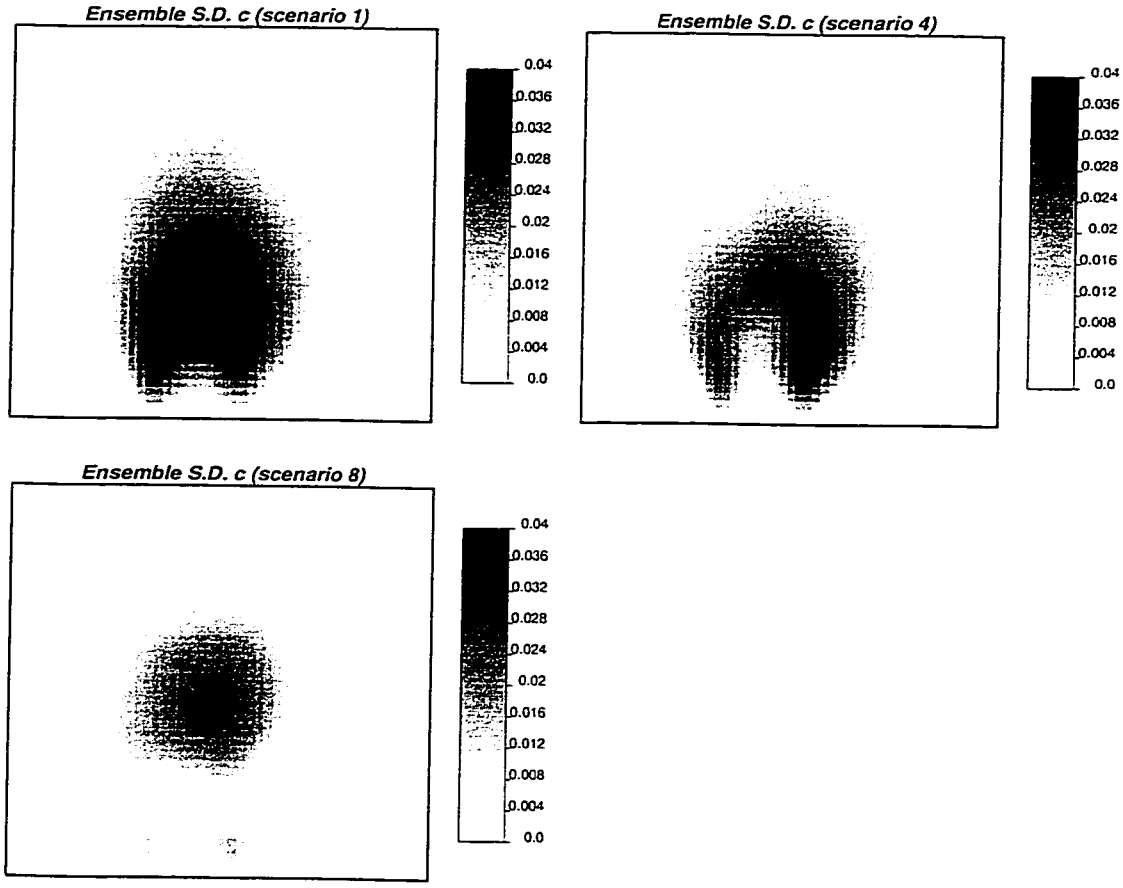

surprising result is that the uncertainty on the transmissivity field increases. In case that just concentration data are used in the conditioning (scenario 5) the *AESD*(*Y*) increase is 7% as compared with the scenario with no conditioning data. In case that also transmissivity data are used (scenario 6) an *AESD*(*Y*) decrease of 12% is observed, this decrease is smaller than the decrease of 15% observed when only transmissivity data were used in the conditioning. For the case that head data are also used in the conditioning, the concentration data do not reduce the *AESD*(*Y*).

For the uncertainty on the head field, conditioning to concentration data also results in an *AESD*(*h*) increase with respect to the unconditional case. However, the increases are smaller than for *AESD*(*Y*). For scenario 5 the *AESD*(*h*) is 5% larger than for the case with no conditioning data. In case that both head and transmissivity are available, the additional presence of concentration data (scenario 8) yields a small *AESD*-decrease, from 49% to 50%. It means that the maximum *AESD*(*h*) reduction is achieved in case all conditioning data are used.

The steady-state head data contribute the most to the *AESD*(h) reduction: in case that only steady-state head data are available, an *AESD*(h) reduction of 41% is already achieved. Figure 6.7 shows how the zone with local *AESD*(h) above 0.15 reduces in case conditioning data are used. If the maps are compared with the head sample locations (Figure 6.3) it is clear that the larger *AESD*(h) correspond to zones with few experimental head data.

The uncertainty on the concentration field, characterised by means of the *AESD*(c) also shows an increase in case that only concentration data are used in the conditioning. *AESD*(c) for the scenario in which only concentration data are used is 8% larger than the scenario with no conditioning data. In this case, it is easier to explain this increase. In the ensemble averaged field for the unconditional case the contaminant plume covers a smaller part of the aquifer than in the reference field. The part that is not covered by the contaminant plume has a low ensemble standard deviation. For the scenario that also concentration data are used in the conditioning, the position of the contaminant plume is better characterised and its location is closer to the reference plume. However, this also means that the uncertainty on the contaminant concentration increases in those parts of the aquifer in which for the case of no conditioning data the contaminant concentration was close to zero. In case more conditioning data are available the *AESD*(c) finally decreases and the lowest *AESD*(c) is found for the scenario where transmissivity, head and concentration data are available; the found *AESD*(c) reduction is 31%. The *AESD*(c) reduction is clearly smaller than the *AAE*(c) reduction. It is thought that this is also –in part– due to the initial mismatch on the position of the contaminant plume. Finally, it can be concluded that the concentration data contribute the most to the *AESD*(c) reduction (in case all the conditioning data are available), but head and transmissivity data also have an important contribution to reduce the uncertainty. Figure 6.7 illustrates that the local *AESD*(c) reduces for more conditioning data and shows also that the largest local *AESD*(c) correspond to the zones with an elevated concentration gradient.

6.4.5 Discussion and conclusions

The synthetic study illustrates that when concentration data are also used for conditioning, the characterisation of the transmissivity, steady-state head and concentration field are improved. The value of the concentration data is clearly demonstrated by the synthetic study. The impact of the concentration data on the characterisation of the upstream part of the aquifer is especially noticeable. The synthetic study also illustrates that the best results are obtained in case transmissivity, head and concentration data are used together. The uncertainty also reduces in the conditioning process; the lowest variances are found for the cases that transmissivity, steady-state head and concentration data are used as conditioning information. However, in this specific case the presence of just concentration data yielded an average ensemble standard deviation larger than in case no conditioning data are available. For the characterisation of the

concentration field this is due to a mismatch between the average plume in the unconditional case and the reference plume.

This study shows the importance of the conditioning to concentration data. However, in this synthetic study just one source of uncertainty - the transmissivities - was considered. In reality many more sources of uncertainty should be considered, like boundary conditions, porosity, local dispersivities and, in some cases, the information on the mass sources. In controlled conservative tracer experiments the amount of injected mass is nearly exactly known and the additional uncertainty may be limited. However, the application of this methodology on contaminated sites with an uncertain mass release history is more complicated. In those studies, the spatio-temporal characterisation of the contamination source is of especial interest. A main question is to what extent it is possible to characterise the aquifer transmissivities and the contaminant source together, given a limited amount of conductivity data, a strongly spatially variable hydraulic conductivity and limited information on the contaminant release history. To what extent is it possible to get an improved aquifer characterisation and a reduced uncertainty in case of multiple sources of uncertainty? As the methodology allows calibrating mass release information and porosity, this issue could be addressed in a synthetic study. In short, the developed methodology should be applied in more complicated synthetic cases with multiple sources of uncertainty and in a real-world case study in order to find out what is the worth of concentration data in those cases. Nevertheless, this synthetic study gives promising results with respect to the worth of concentration data. Together with uncertainty on the porosity also uncertainty on the retardation coefficient can be considered. However, the methodology at present just allows considering linear retardation by adsorption.

Another urgent issue is the implementation of more accurate numerical schemes to solve the mass transport equation. Higher-order interpolation could avoid overshoot and undershoot in strongly advection-dominated problems.

7 Conclusions and future research

7.1 Conclusions

The principal conclusions related with the research on the stochastic inverse modelling of groundwater flow and mass transport are:

- A literature research showed that it is very common to linearize the groundwater flow equation in the solution of the inverse problem. However, the disadvantage of this linearization approach is that it is not valid for large transmissivity variances. Furthermore, some of these approaches can not be extended easily for complex boundary conditions, complex aquifer geometries, etcetera. The majority of the approaches aims at estimating a single-best solution to the inverse groundwater flow problem. Few methods have been developed that consider the coupled inverse modelling of groundwater flow and mass transport. These methods linearize, in general, the mass transport equation and they all aim at estimating a single-best solution to the coupled inverse problem.

- The software INVERTO (written in the C-language) has been developed and implements the extended self-calibrating approach. The self-calibrating approach does not linearize the groundwater flow or the mass transport equation and calculates many equally likely solutions to the (coupled) inverse problem, instead of just one single-best solution.

- The sequential self-calibrating method was successfully extended to handle transient groundwater flow and the joint calibration of transmissivities and storativities. The adjoint state approach reduces the CPU-time needed and, although the inverse modelling of transient groundwater flow is more CPU-intensive, a sufficiently large number of realisations can be generated for cases with less than 10,000 grid cells in a reasonable amount of time. The transient head data yield, in general, only local modifications of the transmissivity field and their impact on the characterisation of the transmissivity field is more limited than a similar number of steady-state head data. The transient head data also allow to generate storativity fields. The results on the joint conditioning of transmissivities and storativities have been satisfying. Both the ensemble variances of transmissivity and the storativity decrease.

- It is important to have good estimates of the transmissivity and hydraulic head measurement errors. In case that the estimated measurement errors are smaller than the real measurement errors, the experimental data may be reproduced too close and artefacts will appear on ensemble averaged maps. It is also found that in that case the characterisation of the transmissivity and

head fields is worse while the estimate of the transmissivity ensemble variance becomes unrealistic low.

- The concept of multiple statistical populations has been successfully applied on the modelling of groundwater flow in fractured rock. In two extensive 3-D case studies it was possible to reproduce a large amount of experimental information reasonably well. In the Sellafield case study, an important increase in the background conductivity was observed during the calibration process. In the Aspö case study the average background conductivity did not increase, but locally important increases were observed, indicating the presence of minor fractures. In spite of the fact that the realisations in the two case studies were conditioned to a large amount of experimental information, a large ensemble variance still remained in the results of the prediction of the outcome of independent tracer test(s).

- The approach was extended to the coupled inverse modelling of groundwater flow and mass transport. The gradient can be calculated in an efficient way by not considering the contributions of the dispersive flux to the gradient.

- In a synthetic study it was found that concentration data help greatly to improve the characterisation of transmissivity, hydraulic head and concentration. Moreover, the ensemble standard deviation was reduced with the help of the concentration data. The concentration data mainly improve the characterisation of the upstream part of the aquifer.

7.2 Suggestions for future research

- The study of the impact of the quality of the measurement data on the simulation results showed that it is necessary to make an estimate of the transmissivity measurement error and the hydraulic head measurement error. The impact on the quality of the simulation results was demonstrated. Nevertheless, it would be interesting to extend the study to biased measurement data, non Gaussian distribution of measurement errors, and the impact of measurement errors on the estimate of the transmissivity variogram. Furthermore, it would be interesting to extend the study to measurement errors in the concentration data.

- With respect to the modelling of groundwater flow in fractured media it will be important to improve the representation of the fractures in the model. Currently the fracture planes are too coarse. An improvement could be achieved by refining the discretization and/or improving the linear system solver. However, it is not expected that this will yield a significant improvement in the nearby future. An alternative is to represent the fracture grid cells in a different way in the model. They could be modelled as 2-D embedded features in a 3-D matrix. The fracture planes could still be

discretized by squared grid cells and some connections between the fracture plane grid cells and the neighbouring matrix grid cells will have to be introduced.

- It will also be important to consider the implementation of a different linear system solver in INVERTO. Especially for the simulation of groundwater flow in fractured media the large conductivity contrasts may make it difficult to find an accurate solution to the linear system of equations. Probably a more potent linear system solver can be found that reduces the mentioned problems.

- In this dissertation the methodology for the coupled inverse modelling of groundwater flow and mass transport was presented. A synthetic study illustrated the worth of concentration data. However, the only source of uncertainty was the spatially variable transmissivity field. Another synthetic study should show the worth of concentration data in case we consider more sources of uncertainty. Besides the spatially variable transmissivity field it would be realistic to consider the spatially variable porosity/retardation field (porosity and retardation cannot be distinguished in the inverse modelling procedure for linear adsorption) and the uncertainty on the mass release. Furthermore, it is also important to test the methodology in a real-world case study. Controlled tracer experiments offer an interesting data base to be used in the coupled inverse modelling. The advantage of the controlled tracer experiments is that although the sources of uncertainty (transmissivity, porosity) increase as compared with the synthetic study, the mass release information is still perfectly known. Moreover, in general other types of experimental data are available from these kind of experiments.

- In the section on coupled inverse modelling, the numerical problems were also mentioned. Ideally, we would like to use a longitudinal grid cell dispersivity equal to one tenth of the grid cell size. Currently, in order to avoid overshoot and undershoot a larger dispersivity coefficient has to be supplied. The implementation of higher order interpolation algorithms in INVERTO could reduce the problems of overshoot and undershoot.

- The extension of the methodology to unconfined aquifers and the joint conditioning of spatially variable recharge and transmissivity fields is also an important research area. The estimation of spatially distributed recharge fields has various problems: no experimental information, different units, a correlation with transmissivity of unknown magnitude and the need to consider cyclic variations. Nevertheless, for many applications this extension, including the non-linear behaviour of unconfined aquifers, is very important.

Appendix I. INVERTO manual.

Below detailed instructions are given on the format of the input files for the computer programme INVERTO (Version invert2d).

I.1 The main input parameter file

The program calls the input parameter file named invert2d.par. We describe the contents of this parameter file.

Line 1: INTERBLOCK_AVERAGE. Type of interblock *K* average. If a harmonic interblock average is desired HARMONIC should be specified; if a geometric interblock average has to be used GEOMETRIC should be specified. See section 2.2.1 for details.

Line 2: LOG_TYPE. This flag indicates whether the user expresses the *K* and *S* variogram parameters (line 30 until line 52 of the main input parameter file) in decimal or natural logarithm. DECIMAL is specified for decimal logarithm, NATURAL for natural logarithm. It should be stressed that the unity of the variogram parameters is independent of the *K* unity used in TFILE (see later). In TFILE *K* always has to be expressed in decimal logarithm.

Line 3: KRIGING_TYPE. The kriging type should always be set to ORDINARY. It means that the perturbations are interpolated by ordinary kriging (see also sections 2.1.2.2 and 3.2.2).

Line 4: DBG_LEVEL. The output debugging level. Options are: NONE, MINIMUM, MEDIUM and MAXIMUM. It is strongly recommended to set the debugging type to MINIMUM in order to avoid extremely big output files. In case an aquifer is discretized in more than thousand grid cells a debugging type equal to MEDIUM or MAXIMUM will result very fast in gigabytes of output.

Line 5: OPTIMIZATION_TYPE. This parameter specifies the optimisation type that will be used in the first iteration for calculating the updating direction from the gradient vector (see also section 3.2.4). The options are: STEEPEST DESCENT, CONJUGATE_GRADIENTS and FR_CJG. FR_CJG is recommended. After a maximum of five iterations (see also section 3.3) the optimisation type is changed in order to accelerate the convergence.

Line 6: NX, NY, NZ. The number of grid cells in the *x* direction, the number of grid cells in the *y* direction and the number of grid cells in the *z* direction. In case 2-D flow is simulated NZ=1. For an irregular aquifer NX, NY and NZ should be big enough to include all aquifer grid cells. Consequentially, many inactive cells are also included. Increasing the total number of grid cells means

increasing the CPU time needed. Case studies have been carried out for 55,000 and 75,000 grid cells, but even the inverse modelling of steady-state groundwater flow on a very fast work station may cost more than 12 hours of CPU time.

Line 7: CELLSIZE_FLAG, DX, DY, DZ. If CELLSIZE_FLAG is set to 1 not all the grid cells have equal sizes. If the flag is set to 0 all the cells have equal dimensions. The width of the grid cell is expressed in metres. In case CELLSIZE_FLAG=0 the dimensions of the grid cells are defined by DX, DY and DZ; DX, DY and DZ being the lengths of the grid cells in respectively the x-direction, y-direction and z-direction. For the special case that DX=DY=DZ the aquifer is divided in squared (2-D) or cubic cells (3-D). In case CELLSIZE_FLAG=1 a file will be opened that contains information on the geometric definition of the grid.

Line 8: DISTR_STORFLAG, S. The first parameter indicates whether a spatial distributed storativity coefficient will be supplied to a program or a constant value. If the flag is set equal to 0 a constant value is expected, if the flag is set equal to 1 or 2 spatially distributed values are read from a file. In case DISTR_STORFLAG=1 the distributed storativities are not calibrated and in case DISTR_STORFLAG=2 the distributed storativities are calibrated. The second parameter is the value for the (constant) storativity coefficient, which only will be taken into account if DISTR_STORFLAG=0. However, in case DISTR_STORFLAG=1 or DISTR_STORFLAG=2 also a value has to be supplied, although this value will not be used for calculations in the program. In case of 2-D flow the storativity coefficient is dimensionless and in case of 3-D flow the storativity is expressed in [L^{-1}]. See also section 2.2.1.

Line 9: TIMES_FLAG, NSTEPS, DT0, DTCOEF. The first parameter (TIMES_FLAG) defines whether the time increments at which the groundwater flow equation is solved are determined by DTCOEF, or given in a file. In case they are defined in a file, TIMES_FLAG=1, otherwise TIMES_FLAG=0. Defining the time increments in a file gives the user more flexibility in selecting the times at which the groundwater flow equation has to be solved. This may be especially of use in case of multiple pumping tests, starting at different times. In case of steady state flow the time increments should not be read from a file. The other three parameters (NSTEPS, DT0 and DTCOEF) define the time steps at which the groundwater flow equation is solved. The following cases can be distinguished:

- Steady state flow. The following values have to be put: NSTEPS=0, DT0=0 and DTCOEF=1. The groundwater flow equation is solved for one time step (at time zero).
- Different steady state flow situations: NSTEPS = number of different steady state flow situations minus one (e.g. in case of three different steady state flow situations NSTEPS=2), DT0>1.0E20 and DTCOEF=1. The groundwater flow equation is solved for the different steady state flow situations and DT0

is assigned an arbitrary very big value in order to indicate that multiple steady state solutions are handled (this very big DT0 value does not correspond with a real time value).

- Transient flow: NSTEPS = number of times that the groundwater flow equation has to be solved, DT0= the time (in seconds) for the first solution of the groundwater flow equation (important: 1.0E-20<DT0<1.0E20), DTCOEF= the multiplication factor which is used to determine the time increments. An example: if DT0=10 seconds and DTCOEF=1.5 the time increments will be: 10*1.5=15 seconds, 15*1.5=22.5 seconds etc. which results in solutions at 10 seconds, 10+15=25 seconds and 25+22.5=47.5 seconds. In case the time increments are read from a file (TIMEFLAG=1) DTCOEF is not used to determine the increments.

In general the same holds for the number of time steps as for the number of grid cells. Reducing the number of time steps saves CPU time. In the synthetic studies and case studies carried out for this dissertation the number of time steps was in all cases less than 70. Especially in case of a big number of grid cells (ten thousands) and an elevated number of time steps the needed CPU time on a fast work station will be of several days.

Line 10: OVER_RELAXATION. This is an optimisation parameter. It is the minimum scalar value used to multiply the updating vector at the first step in the linear search. See also section 3.3. A value of 1.0E-10 gives in general good results, but the debugging information should be given a look in order to see whether the value should be increased or decreased. The value should be changed if during the linear search, with the subsequent increasing of the scalar value (starting from the user-defined minimum scalar value), the objective function value for the first iteration(s) is not close to the old objective function value or if at the latest iterations still a significant decrease in the objective function value is found. In the first case the OVER_RELAXATION should decrease and in the second case it should increase.

Line 11: GAUSS_ERROR, MAXGAUSSITER. These are two other optimisation parameters. If the objective function value decreases below the value of GAUSS_ERROR the optimisation process terminates. The user should decide what he/she considers to be an acceptable error, taking into account the accuracy of the hydraulic head measurements. If the number of inner iterations exceeds MAXGAUSSITER the program also stops. One outer iteration has a maximum of 19 inner iterations. In practice it is found that 1500 inner iterations, which equal normally about 75-100 outer iterations, are sufficient to terminate the calibration process (MAXGAUSSITER=1500).

First optional line: CELLSIZEFILE. This line is only included in this input file in case CELLSIZE_FLAG=1. The line has to contain the name of the file that contains the information on the cell sizes. The program will open the file to read

the information. More information on the data to be included in the file is given in the section I.2.

Second optional line: SOLUTIONTIMESFILE. This line is only included in case TIMES_FLAG=1. The name of the file with the time increments from which the solution times of the groundwater flow equation are obtained. The program will open the file to read the information. More information on the content and format of SOLUTIONTIMESFILE is given in a separate section. See section I.3.

Line 12: TFILE. The name of the file with the spatially distributed $\log_{10} K$, maximum and minimum $\log_{10} K$ and information on the eventual division of the aquifer in zones. The program will open this file to read the information. More information on the content and format of TFILE is given in the separate section I.4.

Third optional line: STORFILE. This line is only read in case DISTR_ STORFLAG= 1 or DISTR_ STORFLAG= 2. It includes the name of the file with the spatially distributed storativity coefficients. See section I.5 for more information.

Line 13: BCSFILE. The name of the file in which the status of the grid cells is specified. More information on the content and format of BCSFILE is given in section I.6.

Line 14: H0_FLAG. This flag indicates whether steady or transient flow is simulated. If the value is set to 0 steady state flow is assumed (possibly a number of steady state flow situations for different moments), if the value is set to 1 transient groundwater flow is assumed.

Line 15: INITIAL_FLAG. This flag indicates whether, in case of transient groundwater flow, initial hydraulic heads are supplied by the user (in that case the flag is set equal to 1), or estimated by solving the steady state groundwater flow equation, using the given conductivities, boundary conditions and recharges/discharges (the flag is set to 0).

Line 16: HTFLAG. This parameter indicates whether there are prescribed hydraulic head values which change in time. If HTFLAG=0 there are not, if HTFLAG=1 there are and in that case the corresponding information will be read later from a file.

Line 17: S_FLAG. This flag indicates whether the (uniform) storativity coefficient is calibrated. If the flag is set equal to 1 the storativity coefficient will be calibrated; if the flag is set to 0 the storativity coefficient will not be calibrated. In case of steady state flow this flag should logically always be set to zero, in order to avoid unnecessary calculations. The flag should also be set to

zero in case distributed storativities are specified (DISTR_STORFLAG=1 or DISTR_STORFLAG=2).

Line 18: S_FACTOR. A factor that determines how much the uniform storativity coefficient is allowed to change in one outer iteration. This factor has not any significance in case distributed storativities are calibrated. See below:

$$\frac{S^{(l)}}{S\_FACTOR} \leq S^{(l+1)} \leq S^{(l)} S\_FACTOR$$

$S^{(l+1)}$ is equal to the updated storativity coefficient (at iteration l+1) and $S^{(l)}$ is equal to the old storativity coefficient (at iteration l). However, the storativity coefficient is allowed to change more than S_FACTOR over a number of iterations; S_FACTOR just determines the maximum change in one iteration. S_FACTOR should be defined in accordance with the uncertainty on the value of the storativity coefficient. If the uncertainty is relatively small, S_FACTOR should for example be set to 10. If the uncertainty is (very) big a value of 100 may be more adequate.

Line 19: H0FILE. The name of the file with the initial heads. The program will open this file to read the information. More information on the content and format of H0FILE is given in the section I.7.

Fourth optional line: HTFILE. This line is only read if HTFLAG=1. The user should supply the name of the file with the prescribed time variant hydraulic head values. The program will open this file to read the information. More information on the content and format of HTFILE is given in the section I.8.

Line 20: NWELLS. The number of recharge and discharge locations. Included are not only wells or water injection locations, but also prescribed flux boundaries. All the grid cells at which an extraction or injection of water is assigned, including prescribed flux boundaries, should be included in counting NWELLS. If for example an aquifer is simulated with pumping at grid cell (27,27,1), injection of water at grid cell (22,7,1) and prescribed flux boundary conditions along the Southern boundary from (1,1,1) until (40,1,1) NWELLS is equal to 42.

A number of optional lines equal to NWELLS follows with: Ordinal, WELLX, WELLY, WELLZ, RATECHANGE. Thus, if NWELLS=0 no lines are read and if NWELLS>0 information should be supplied on the discharge and recharge locations. One line should be included for each location with the following information: (1) an ordinal, (2) the grid cell x-index of the location, (3) the y-index of the location, (4) the z-index of the location and (5) the number of different discharge or recharge rates at the locations. For the ordinal any integer number can be taken, but for the user the most convenient will be to use the ordinal 1 for the first line, the ordinal 2 for the second line, etc. The number of

discharge or recharge rates at each grid cell should include the starting discharge or recharge rate. The "starting" discharge or recharge rate (for the first time step) is also used to calculate the steady state head solution. See also section I.9.

Another optional line: WELLSFILE. The name of the file with the information on discharges and recharges should be given here. This line only has to be included in case the number of discharge and recharge locations is at least one. More information on this file is given in section I.9.

Line 21: NPRIOR. The number of grid cells with hydraulic conductivity measurements. At these locations the hydraulic conductivity perturbation is fixed to zero in case the estimated measurement error variance is equal to zero. In case the estimated measurement variance is not equal to zero, the perturbation at these grid cells is proportional to the measurement error variance.

A number of optional lines equal to NPRIOR follows with: Ordinal, PRIORX, PRIORY, PRIORZ. Thus, if NPRIOR=0 no lines are read and if NPRIOR>0 information on grid cells with hydraulic conductivity measurements is read. One line should be included for each grid cell where one or more hydraulic conductivity measurements have been taken. The lines should contain the following information: (1) an ordinal, (2) the grid cell x-index of the location, (3) the y-index of the location and (4) the z-index of the location. The NPRIOR data locations are supplied because those are also included in the master blocks. The K perturbations at the measurement locations depend on the user supplied hydraulic conductivity measurement error (see later). In any case, TFILE contains maximum and minimum allowed hydraulic conductivities for each grid cell (see also section I.4), which should be equal to the kriged hydraulic conductivity plus or minus three times the kriging standard deviation. This means that at K measurement locations, in case of a nugget equal to zero, the maximum and minimum hydraulic conductivity value will be equal to the simulated hydraulic conductivity value. In other words, also by means of the imposed constraints on the perturbation of the hydraulic conductivity field the hydraulic conductivity value will be maintained at the measurement locations.

Line 22: NPARAM, NPARAMZONE2, NKRIGZONES, NKRIGDAT. These parameters are respectively the number of master blocks (not including NPRIOR) in zone 1, the total number of master blocks in the rest of the zones, the number of zones and the number of master blocks used to krige a perturbation at a location. In many cases the user will just define one zone and in that case NPARAM master blocks are distributed over all the area. If just one zone is defined NPARAMZONE2=0 and NKRIGZONES=1. Dividing the aquifer in more than one zone means assigning different variograms to the different zones. The aquifer should not be divided in more than one zone just because of the fact that the expected average hydraulic conductivity differs

between zones or because of a probable difference in variogram. There should be a clear evidence that the variogram differs significantly between different parts of the aquifer. An example is the presence of fractures at a 3-D site. The non fractured zone may have an isotropic or slightly anisotropic variogram, while the fractures may have a strongly anisotropic variogram with the direction of major continuity in the fracture plane. The number of master blocks for the rest of the zones, NPARAMZONE2, is not specified per zone and these master blocks will be distributed by the program over the rest of the zones. However, in each zone at least a minimum of NKRIGDAT master blocks will be located. The advice is to use between 8 and 12 master bocks to krige a perturbation at a grid cell, so that NKRIGDAT should have a value between 8 and 12.

In case that the aquifer is divided into multiple zones, care should be taken on the distribution of the master blocks between the different zones. The master blocks are located on a regular grid with random starting point for zone one, but located randomly for the other zones. It is therefore convenient to take as zone number one the most extended zone.

The algorithm that locates the master blocks on the aquifer grid cells takes into account these requirements:

- In the first zone a number of master blocks $N_{p,Y1}$ has to be located. These master blocks are located on a regular grid with random starting point. The density of the master blocks in the three coordinate directions, as specified by the user, is taken into account.
- In the rest of the zones a total amount of master blocks equal to $N_{p,Y}$-$N_{p,Y1}$ is located.
- A minimum of master blocks equal to the number of master blocks to be used in the kriging system is located in each of the other zones.
- The total set of master blocks is checked on doubles; two master blocks located at the same grid cell. Doubles result in a singular left-hand side kriging matrix. In case doubles are detected a new master block location is generated. The location of the master block is accepted in case it is located in the correct zone and at an active cell. The algorithm does not locate master blocks on the boundaries, but also the location of master blocks at internal prescribed head boundaries or internal inactive cells is avoided. Finally, in case the location of the master block is accepted the new set is re-checked on doubles.

Furthermore, we advice to place two master blocks per correlation range. If we have for example an aquifer of extensions 2000 m x 2000 m with a variogram range of 400 m 100 master blocks (10 x 10) should be placed according to this rule of thumb. However, the user should also take into account that NPARAM+NPARAMZONE2 should be less than 1000 in order to avoid very high CPU costs. Although according to the rule of thumb thousands of master

blocks should be located, the best is to reduce the total amount of master blocks below 1000.

Line 23:NO_PAR_BLOCKS_X, NO_PAR_BLOCKS_Y, NO_PAR_BLOCKS_Z. These parameters are used to lay out the master blocks on a regular grid with a random starting point. However, they correspond only to zone 1, and not to the rest of the zones. This means that in the other zones master blocks are placed randomly. The three parameters correspond to the number of master blocks in the x-direction, the number of master blocks in the y-direction and the number of master blocks in the z-direction. The three parameters multiplied give the total number of master blocks placed on a regular grid in zone 1. Therefore, the product of these three values should give an amount of master blocks equal to or less than NPARAM. The difference in master blocks between NPARAM and the product of the three parameters is distributed randomly over zone 1. By assigning the three parameter values the aquifer geometry and the anisotropy of the K variogram should be taken into account. For example, if the spatial continuity in the horizontal plane is two times bigger than the spatial continuity in the vertical plane (and NX=NY=NZ) NO_PAR_BLOCKS_Z should be approximately two times bigger than NO_PAR_BLOCKS_X and NO_PAR_BLOCKS_Y. A more complicate example: if NX=30, NY=30 and NZ=15 and the spatial continuity (range) in the x-direction is two times bigger than in the y-direction and four times bigger than in the z-direction NO_PAR_BLOCKS_Z should be the same as NO_PAR_BLOCKS_Y (half of the cells, but also half of spatial continuity) and two times bigger than NO_PAR_BLOCKS_X (half of the cells, but a range four times shorter). It is important to take into account aquifer geometry and spatial correlation in determining the values for the three parameters; adjusting the spatial configuration of the master blocks to the conductivity anisotropy results in a faster convergence.

Line 24: PARBOX_MINX, PARBOX_MAXX, PARBOX_MINY, PARBOX_MAXY, PARBOX_MINZ, PARBOX_MAXZ. These six parameters can be used to limit the part of the aquifer where master blocks are active. The first parameter is the lower x index of the block where master blocks are active, PARBOX_MAXX gives the upper x index of the zone where master blocks are active, and in addition the lower y index, the upper y index, the lower z index and the upper z index are given. Master blocks which are laid out outside the box defined by these six parameters have a perturbation equal to zero. An example: if an aquifer is discretized into 40 cells in the x-direction, 50 cells in the y-direction and 10 cells in the z-direction (NX=40, NY=50 and NZ=10) and the six parameters have values of, respectively, 7, 33, 20, 50, 3 and 7, an inner block is defined reaching from x=7 to x=33, y=20 until y=50 and z=3 until z=7. Master blocks outside the defined inner block have perturbations zero.

In few cases it is useful to define an inner block that sets perturbations to zero in the rest of the aquifer. An example for which the limitation could be useful is

the calibration of a pumping test in a very CPU-intensive problem. However, premises for limiting the perturbations are that the transient simulations start from uniform heads and that the pumping test just influences a small part of the aquifer. In that case an inner block could be defined around the pumping location: the needed CPU time is reduced significantly and the end result is not affected by the measure.

Line 25: BCSFLAG, NPARBCS, MAXDELTABCS. The parameter BCSFLAG indicates whether the hydraulic heads at the prescribed head boundaries will be calibrated. If BCSLAG=1 prescribed head values at the boundaries will be calibrated, if BCSFLAG=0 they will not be calibrated. The parameter NPARBCS is equal to the number of master blocks located on the prescribed head boundary cells. Finally, the parameter MAXDELTABCS gives the maximum allowed head change at a boundary grid cell with imposed head values. The value MAXDELTABCS is the same for all prescribed head boundary grid cells and should be determined using expert knowledge.

Line 26: NPAR_S, NPAR_SX, NPAR_SY, NPAR_SZ. These parameters are respectively the number of master blocks for the storativity calibration, the number of these master blocks in the x-direction, the number of master blocks in the y-direction and the number of master blocks in the z-direction. The amount of master blocks NPAR_S to be used for the conditioning of the storativity field can also be determined by the rule of thumbs detailed before. The master blocks are also laid out on a regular grid with random starting point. The grid is composed of a number of master blocks in the x-direction (NPAR_SX), y-direction (NPAR_SY) and z-direction (NPAR_SZ). The number of master blocks in the three coordinate directions should be determined using the same rules as detailed for line 23. NPAR_S should be equal to or bigger than the product of NPAR_SX, NPAR_SY and NPAR_SZ. The difference in master blocks between NPAR_S and the product of three parameters is distributed randomly over the simulation domain. The storativity perturbations are interpolated using NKRIGDAT master blocks.

Line 27: PAR_BLOCKS_FLAG. This flag indicates whether master blocks are changed during the optimisation. If PAR_BLOCKS_FLAG=1 the positions of the master blocks are changed during the optimisation, if PAR_BLOCKS_FLAG=0 not. It is strongly advised to change the master blocks during the optimisation: it increases the convergence and avoids the appearance of artefacts on the maps. The defined number of master blocks NPARAM, NPARAMZONE2 and NPARBCS and also the spatial configuration of the master blocks in zone 1 as defined by NO_PAR_BLOCKS_X, NO_PAR_BLOCKS_Y and NO_PAR_BLOCKS_Z are not affected by changing the master blocks during the optimisation.

Line 28: REALIZATIONBLOCKS_FLAG. This flag indicates whether the position of the master blocks is user defined. If

REALIZATIONBLOCKS_FLAG=1 the master blocks will be located by the program; the blocks in zone 1 will be located systematically with a random starting point and the blocks in the rest of the zones randomly. However, if REALIZATIONBLOCKS_FLAG=0 the user will define the positions of all the master blocks. In that case the information read on line 23 will not be taken into account. It is strongly recommended to let the computer assign the positions of the master blocks.

Line 29: SEED. This is an integer number used to replace the master blocks randomly after a series of iterations. (The master blocks are only replaced during the calibration if PAR_BLOCKS_FLAG=1.) In principle any integer number can be used here.

A number of optional lines equal to NPARAM+NPARAMZONE2+NPARBCS. This number of lines is only read in case REALIZATIONBLOCKS_FLAG=0. Each line should contain the following information for the localisation of one master block: (1) an ordinal, (2) the grid cell x-index of the grid cell, (3) the y-index of the grid cell and (4) the z-index of the grid cell. The advice is to give first the master block locations for zone 1, later the master block locations for zone 2 (if any) etc. and finally the master block locations at prescribed head boundary cells. Like before, it is recommended to chose the ordinals in a logical manner, like for example restarting the counting with 1 for the master block locations of each new zone. Remember that each zone should contain at least NKRIGDAT master blocks and that not two master blocks can be located on the same grid cell. The user defined localisation of the master blocks should be carried out only in very specific cases, in which the user can specify clearly which are the expected advantages of localising the master blocks in that way.

Line 30: OBSHFILE. The name of the file with the observed hydraulic heads. The program will open this file to read the information. More information on the content and format of OBSHFILE is given in the section I.10.

Line 31: DBGFILE. The name of the output file with detailed output information. The program will open this file to write information. See section I.11 for more information.

Line 32: FINALTFILE. The name of the output file with the updated hydraulic conductivities. The program will open this file in order to print the updated hydraulic conductivities after each macro-iteration. More information on the context and format of FINALTFILE are given in section I.12.

Line 33: FINALHFILE. The name of the output file with the updated hydraulic heads for the different steps. The program will open this file in order to print the updated hydraulic heads after each macro-iteration. More information on the context and format of FINALHFILE are given in section I.13.

Line 34: FINALBCSFILE. The name of the output file that contains the hydraulic head perturbations at grid cells with prescribed head boundary values. The program will open this file for printing the hydraulic head perturbations at the grid cells with prescribed head values. More information on the context and format of FINALBCSFILE are given in section I.14.

Line 35: NUGGET. The nugget of the hydraulic conductivity variogram for zone 1, expressed either in decimal or natural logarithm (depending on the specification made at line 2 of the main input file).

Line 36: MEAS_ERROR. The measurement error variance of hydraulic conductivity for zone 1, expressed either in decimal or natural logarithm. The user should provide an estimate of the measurement error variance. The estimated nugget of the hydraulic conductivity variogram for zone 1 should be divided in a measurement error variance and a rest (corresponding to small scale spatial variability). The measurement error variance can be estimated taken into account the uncertainty of the measurement techniques and the like.

Line 37: VARIOGRAM_TYPE. The variogram type of the hydraulic conductivity for zone 1 is specified. The user should choose between nine different variogram models, which should be specified as follows:

- 1 for a spherical variogram
- 2 for an exponential variogram
- 3 for a Gaussian variogram
- 11 for a double spherical model
- 12 for a spherical model for the first structure and an exponential model for the second structure
- 13 for a spherical model for the first structure and a Gaussian model for the second structure
- 21 for an exponential model for the first structure and a spherical model for the second structure
- 22 for a double exponential model
- 23 for an exponential model for the first structure and a Gaussian model for the second structure
- 31 for a Gaussian model for the first structure and a spherical model for the second structure
- 32 for a Gaussian model for the first structure and an exponential model for the second structure
- 33 for a double Gaussian model

Line 38: SILL1. The sill for the first structure of the *K* variogram for zone 1, expressed in either the decimal or natural logarithm. Sill is defined here as the sill of structure 1 minus the nugget effect (In fact it is a contribution to the total sill.).

Line 39: SILL2. The sill for the second structure of the K variogram, expressed in either the decimal or natural logarithm. The sill is also in this case defined as the sill of structure 2 minus the nugget effect.

Line 40: ANIS_ANGLE1, VERT_ANISANGLE1. The two angles which are used to define the 3-D anisotropy of the first structure used to model the spatial variability of hydraulic conductivity. The first angle rotates the axis of principal spatial continuity in the horizontal plane, with the x-axis as reference. A positive rotation angle is used for counter-clockwise rotation and a negative rotation angle for clockwise rotation. The second angle rotates the horizontal plane counter clockwise around the axis of principal spatial continuity found after the first rotation. See also section 2.1.2.1 for more details.

Line 41: ANIS_ANGLE2, VERT_ANISANGLE2. The same parameters as given on line 40, but now for an eventual second structure.

Line 42: RANGEMAX1, RANGEMIN1, RANGEVERT1. These parameters correspond to the three ranges of the three principal axes of the anisotropy ellipse. The first range corresponds to the spatial continuity in the direction obtained after the first rotation. The second range corresponds to the range in the direction perpendicular to it; the direction of minor spatial continuity in the horizontal plane. The third range corresponds to the range in the third dimension, perpendicular to the horizontal plane that contains the two directions with corresponding ranges defined before. In case of an exponential or Gaussian structure these parameters do not correspond to the effective range. The effective range is three times larger than the given range parameter in case of an exponential model and $\sqrt{3}$ times larger in case of a Gaussian model. See also section 2.1.2.1

Line 43: RANGEMAX2, RANGEMIN2, RANGEVERT2. These parameters correspond to the three ranges of the three principal axes of the anisotropy ellipse of the second defined structure. The parameters are defined in the same way as described before for line 42.

Line 44: NUGGET_S. The nugget of the log storativity variogram for zone 1, expressed either in decimal or natural logarithm (also in case of storativity depending on the specification made at line 2 of the main input file).

Line 45: MEAS_ERROR_S. The measurement error variance of the storativity coefficient for zone 1, expressed either in decimal or natural logarithm. The user should provide an estimate of the measurement error variance. The estimated nugget of the storativity coefficient variogram for zone 1 should be divided in a measurement error variance and a rest (corresponding to small scale spatial variability). The measurement error variance can be estimated taken into account the uncertainty of the measurement techniques etc.

Line 46: VARIOGRAM_TYPE_STORATIVITY. The variogram type of the storativity coefficient for zone 1 is specified. The user should choose between nine different variogram models, which should be specified as follows:

- 1 for a spherical variogram
- 2 for an exponential variogram
- 3 for a Gaussian variogram
- 11 for a double spherical model
- 12 for a spherical model for the first structure and an exponential model for the second structure
- 13 for a spherical model for the first structure and a Gaussian model for the second structure
- 21 for an exponential model for the first structure and a spherical model for the second structure
- 22 for a double exponential model
- 23 for an exponential model for the first structure and a Gaussian model for the second structure
- 31 for a Gaussian model for the first structure and a spherical model for the second structure
- 32 for a Gaussian model for the first structure and an exponential model for the second structure
- 33 for a double Gaussian model

Line 47: SILL1_S. The sill for the first structure of the storativity coefficient variogram for zone 1, expressed in either the decimal or natural logarithm. Sill is defined here as the sill of structure 1 minus the nugget effect (In fact it is a contribution to the total sill.).

Line 48: SILL2_S. The sill for the second structure of the storativity coefficient variogram, expressed in either the decimal or natural logarithm. The sill is defined as the sill of structure 2 minus the nugget effect.

Line 49: ANIS_ANGLE1_S, VERT_ANISANGLE1_S. The two angles that are used to define the 3-D anisotropy of the first structure used to model the spatial variability of the storativity coefficient. The first angle rotates the axis of principal spatial continuity in the horizontal plane, with the x-axis as reference. A positive rotation angle is used for counter-clockwise rotation and a negative rotation angle for clockwise rotation. The second angle rotates the horizontal plane counter clockwise around the axis of principal spatial continuity found after the first rotation. See also section 2.1.2.1 for more details.

Line 50: ANIS_ANGLE2_S, VERT_ANISANGLE2_S. The same parameters as given on line 49, but now for an eventual second structure.

Line 51: RANGEMAX1_S, RANGEMIN1_S, RANGEVERT1_S. These parameters correspond to the three ranges of the three principal axes of the anisotropy ellipse. The first range corresponds to the spatial continuity in the

direction obtained after the first rotation. The second range corresponds to the range in the direction perpendicular to it; the direction of minor spatial continuity in the horizontal plane. The third range corresponds to the range in the third dimension, perpendicular to the horizontal plane that contains the two directions with corresponding ranges defined before. In case of an exponential or Gaussian structure these parameters do not correspond to the effective range. The effective range is three times larger than the given range parameter in case of an exponential model and $\sqrt{3}$ times larger in case of a Gaussian model. See also section 2.1.2.1

Line 52: RANGEMAX2_S, RANGEMIN2_S, RANGEVERT2_S. These parameters correspond to the three ranges of the three principal axes of the anisotropy ellipse of the second defined structure. The parameters are defined in the same way as described at line 51.

Optional lines: Line 36 until Line 52 are repeated for all defined zones. In case just one zone is defined no more variogram information is given by the user. If more zones are defined, the lines 36 until 52 are repeated for zone 2, later zone 3 etc. Nevertheless, only for hydraulic conductivity the variogram parameters can differ between the zones. For the storativity coefficient the same variograms should be defined for the zones.

Optional line: FINALSFILE. The name of the output file with the updated storativity coefficients. The program will open this file in order to print the updated storativity coefficients after each macro-iteration. More information on the format of FINALSFILE is given in section I.15.

Line 53: TRADEOFF. This parameters penalise the perturbation of the hydraulic conductivity field. See also section 3.2. The parameter corresponds to ψ_1 in equation 3.1. Normally these trade-off coefficients are set to zero, unless the user has special motives to penalise the perturbation of the conductivity field. The effect of setting the parameter to a positive value is that especially large perturbations are penalised; the hydraulic conductivity field is forced not to change too much and especially local big perturbations are avoided.

Line 54: This line should always contain the following file name: "iaja75000.out". This file is opened, filled and read by the iterative solver of the linear system of equations.

Line 55: This line should always contain the following file name: "acol75000.out". Also this file is used by the iterative solver of the linear system of equations.

Line 56: This line should always contain the following file name: "b75000.out". This is a third file that is needed by the iterative solver of the linear system of equations.

Line 57: This line should always contain the following file name: "h75000.out". This is the fourth and last file that is used by the iterative solver of the linear system of equations.

I.2 CELLSIZEFILE (optional). The file with the information on the the grid cell sizes.

This file contains the sizes of all the grid cells. The grid cell sizes in one column, one row and one layer are constant. In the file are first specified the grid cell sizes in the x-direction, then the grid cell sizes in the y-direction and finally the grid cell sizes in the z-direction. On the first line of the file Δx_{1jk} is specified, which is the size of the first grid cell in the x-direction. In addition, the grid cell sizes for the other columns (Δx_{2jk}, Δx_{3jk}, ..., $\Delta x_{nx,jk}$) are specified. On each line one value is supplied. In addition the grid cell sizes for the rows, Δx_{i1k}, Δx_{i2k}, ..., $\Delta x_{i,ny,k}$, are given. Finally, Δz_{ij1}, Δz_{ij2}, ..., $\Delta z_{ij,nz}$ are specified. In case 2-D groundwater flow in a horizontal layer is simulated just Δz_{ij1} is specified. Any non-zero value can be specified. This value has not any importance for the simulation of 2-D groundwater flow. The CELLSIZEFILE has a number of lines equal to $nx+ny+nz$.

I.3 SOLUTIONTIMESFILE (optional). The file with the time increments at which the groundwater flow equation has to be solved.

The program will open this file (if TIMES_FLAG=1) and the time increments are read. The time increments are ordered in a column, the first number being the first time increment, the second number the second time increment etc. The time increments define the times at which the groundwater flow equation will be solved. The first time at which the groundwater flow equation is solved is in any case equal to DT0, defined at line 9 of the main parameter input file inverto.par. The second time at which the groundwater flow equation is solved is then given by DT0 plus the first time increment, defined in SOLUTIONTIMESFILE. This file has a number of lines equal to NSTEPS-1.

I.4 TFILE. The file with the hydraulic conductivities.

TFILE, specified at line 12 of the main parameter file inverto.par, should contain one line of information for each grid cell (the total number of grid cells is equal to NX x NY x NZ) and each line should contain the following information: (1) the $\log_{10} K$; (2) the maximum hydraulic conductivity $\log_{10} K_{max}$, (3) the minimum hydraulic conductivity $\log_{10} K_{min}$ and (4) the hydraulic conductivity zone. The

hydraulic conductivity K is the grid cell conductivity, expressed in $\log_{10}(m^2/s)$ (transmissivity) or $\log_{10}(m/s)$ (conductivity) and is usually obtained by geostatistical simulation (see also section 2.1.2.3). $\text{Log}_{10}\ K_{max}$ is the user defined maximum conductivity for the grid cell and $\log_{10}\ K_{min}$ the user defined minimum value. The conductivity is not allowed to go beyond these extremes in the calibration process. Normally $\log_{10}\ K_{max}$ is set equal to the kriged $\log_{10}\ K$ value plus two or three times the kriging standard deviation and $\log_{10}\ K_{min}$ the kriged value minus two or three times the kriging standard deviation. If the $\log_{10}\ K$ variogram is the same for all the grid cells just one zone is specified so that for all the grid cells the hydraulic conductivity zone is set equal to one. If the $\log_{10}\ K$ variogram differs between grid cells the zone (numbered 1, 2, 3 etc.) is indicated for each of the grid cells. This results in the following format of TFILE: first for the lower left bottom grid cell (indices x=1, y=1 and z=1) the four mentioned values are given, afterwards for the grid cell right of it (x=2, y=1 and z=1) and then for the next grid cell right of it until all the grid cells in the row are handled ($x=nx$, y=1, z=1). Next another row is handled (x=1, y=2, z=1) and when all the rows are cycled through ($x=nx$, $y=ny$, z=1), the next plane is handled (z=2). The last grid cell for which the four values are given corresponds to the upper right top grid cell ($x=nx$, $y=ny$, $z=nz$).

In case transient groundwater flow is simulated, starting with steady state groundwater flow (in the first time step) the first column of TFILE should correspond to the $\log_{10}\ K$ obtained after conditioning to steady state head data. In practice it is found that first conditioning to steady state head data, and later to transient state head data, avoids convergence problems in the conditioning process.

I.5 STORFILE (optional). The file with the storativity coefficients.

STORFILE should contain one line of information for each grid cell, in a similar way as for TFILE. The grid cells are also cycled through as described in the section of TFILE. Each line contains three data: the decimal logarithm of the storativity coefficient ($Z= \log_{10}\ S$), a maximum allowed storativity coefficient (Z_{max}) and a minimum allowed storativity coefficient (Z_{min}) In case DISTR_STORFLAG=1 the maximum and minimum Z so not interfere in the calculations. However, the maximum allowed Z should be above Z and the minimum allowed Z should be below Z. In case DISTR_STORFLAG=2 the maximum and minimum allowed Z have an importance in the calibration of the storativity coefficients. The storativity Z at a grid cell is not allowed to go beyond the imposed limits Z_{max} and Z_{min}. Normally Z_{max} is set equal to the kriged Z value plus two or three times the kriging standard deviation and Z_{min} the kriged value minus two or three times the kriging standard deviation. The storativity coefficient was dimensionless in case of 2-D flow and expressed in $[L^{-1}]$ in case of 3-D flow. Notice that the storativity coefficient is specified in

decimal logarithm, while the uniform storativity coefficient (specified at line 8 of the input file inverto.par) should be specified without transformation.

I.6 BCSFILE. The file with information on the cell status.

The program will open this file and the status of the different grid cells is read in the same sequence as described in the section of TFILE. The following status are possible: 1 ACTIVE GRID CELL, 0 INACTIVE GRID CELL, -1 GRID CELL WITH PRESCRIBED HEAD VALUE and -2 GRID CELL WITH PRESCRIBED FLUX VALUE. An inactive grid cell is for example used to define no flow boundaries. In case of an irregular aquifer the grid cells which do not belong to the aquifer are also indicated as non active grid cells. The prescribed head values at grid cells are defined in the file H0FILE and the prescribed flux values at grid cells in the file WELLSFILE.

I.7 H0FILE. The file with the initial heads.

The file H0FILE contains the user supplied initial hydraulic head values at the grid cells. The initial head values are given in a column with one hydraulic head value at each line, corresponding to one grid cell. The format in which the grid cells are cycled through is the same as for TFILE and BCSFILE. In all cases, supplying initial heads which are close to the head solution of the steady state groundwater flow equation or the solution of the transient groundwater flow equation at the first time step favours a fast convergence. The supplied initial heads are used as the first guess solution of the groundwater flow equation. H0FILE is also used to give the hydraulic head values for the grid cells with prescribed head boundary conditions. The grid cells that in BCSFILE are indicated to have prescribed head values should therefore have in H0FILE the correct prescribed head value. Furthermore, in case transient groundwater flow is simulated and the initial heads are indicated to be user supplied (by setting INITIAL_FLAG=1), the hydraulic heads read from H0FILE correspond to the head solution at the first time step. In that case all the supplied hydraulic head values are used so that care should be taken to define for each of the grid cells the hydraulic head value. In case INITIAL_FLAG=0 it is not necessary to supply in case of transient groundwater flow the exact initial head values. The program assumes that the steady state solution is used as the initial solution of the groundwater flow equation and calculates internally the steady state solution as starting point of the calibration. In case of transient groundwater flow it is important to supply a hydraulic conductivity field which has been conditioned already to steady state head values.

I.8 HTFILE (optional). The file with the time variant prescribed head values.

The file HTFILE contains the time variant prescribed hydraulic head values. For each time step the grid cells are indicated which have a prescribed hydraulic head value. The grid cells which in BCSFILE were already indicated to have (permanently) a prescribed hydraulic head value do not have to be included in this file, unless the prescribed head value changes in time. The number of time variant prescribed head values at the different time steps at which the groundwater flow equation is solved is equal to NO_HTLOC. The first line of HTFILE gives the value NO_HTLOC and in addition NO_HTLOC lines with information about the hydraulic head values follow. Such a line contains the cell indices *ix, iy, iz,* the time step *it* and the prescribed head value. An example: 1 1 1 4 –40.70 means that the lower left bottom cell (indices (1,1,1)) at the 4th time step of the simulation has a fixed hydraulic head value of –40.70 m. If this grid cell has a prescribed head value at more time steps of the simulation for each such a time step the information is repeated and all these time steps should be included in determining NO_HTLOC.

I.9 WELLSFILE (optional). The file with information on discharges and recharges.

This file contains information on discharges and recharges. In the main parameter input file inverto.par the number of discharge and recharge locations has been specified and the number of different recharge or discharge rates at each of these locations. The file WELLSFILE contains a number of lines equal to the number of different recharge/discharge rates at each discharge/recharge location, summed over all recharge/discharge locations. The information in WELLSFILE should be ordered such that first for a discharge/recharge grid cell the different recharge and discharge rates are given. Next, a different discharge/recharge location is handled. One line contains information for one discharge/recharge location and one injection/extraction rate. One line contains the following information: (1) x-index of discharge/recharge location, (2) y-index of discharge/recharge location, (3) z-index of discharge/recharge location, (4) starting time (in seconds) of applied recharge/discharge rate and (5) the discharge/recharge rate in m^3/s. INVERTO converts these values internally to m/s (2-D) or s^{-1} (3-D), taking into account the grid cell dimensions. In this respect, the following considerations are of importance:

- For all the recharge/discharge locations the starting time of the first applied discharge/recharge rate should be less than DT0 (the first time for which the groundwater flow equation is solved). This recharge/discharge is supposed to be the steady state recharge/discharge rate.
- The groundwater flow equation should be solved at times just before the discharge/recharge rate changes, because the program applies a constant discharge/recharge rate during a time step.

I.10 OBSHFILE. The file with the observed hydraulic heads.

This file contains the observed hydraulic head values. The format of the file is the following:

First line: The number of locations with hydraulic head measurements should be given (independent of the number of times that the hydraulic head is measured at that location). In addition a number of blocks of information follows equal to the number of observation locations. Each block has a header line with general information and in addition observed values are given. The header line contains the following information for the observation location: (1) the x-index of the grid cell, (2) the y-index of the grid cell, (3) the z-index of the grid cell, (4) the number of time steps for which there are observations, (5) a weight for that observation location, (6) the exact location of the grid cell along the x-axis, also expressed in cell indices, (7) the same for the exact location along the y-axis and (8) the same for the exact location along the z-axis. In addition, a number of lines equal to the number of given time steps follows with at each line (1) the time in seconds and (2) the observed hydraulic head value for that time.

The maximum number of time steps for which observed hydraulic head values can be given is equal to the number of time steps for which the transient groundwater flow equation is solved multiplied by two, plus two. This is in any case enough to compare the measured and the simulated hydraulic head values at all the times at which the groundwater flow equation is solved. More observed head values are of no use as they can not be compared with the simulated hydraulic head values of the groundwater flow model. The observed head values are interpolated in time to the time steps at which the groundwater flow equation is solved. The following rules should be taken into account for defining the times with measured hydraulic heads in the OBSHFILE:

- In order to compare the measured and simulated hydraulic head for a time step at which the groundwater flow equation is solved, it is enough to supply an experimental hydraulic head value for that time step.
- If such an experimental head value is not available two head measurements as close as possible to the simulation time step, one just before the simulation time and one just after the simulation time, should be given. The given data should be, in any case, after the last simulation time step and before the next simulation time step. This procedure should also be applied for the first and last time step; if for example no measurement is available for the last time step a measured value just before that last time step and just after that last time step should be given.
- In case these two head data are also not available the user should supply the value "-999.95" which indicates that no observations are available. This value should be given for the exact time at which the groundwater flow

equation is solved, in order to avoid that this value is used in any interpolation.

- In case steady state flow is simulated, observed hydraulic head values should be given for the steady state flow situation with a specified time equal to DT0=0.

The weight specified for a observation should be set to 1.0 in the actual version of the program. The program does not take into account yet differing weights for different observations.

The exact locations of the head observation locations should be specified so that the simulated head values can be compared with the measured head values at the measurement locations; the simulated head values are interpolated to obtain the numerical solution of the groundwater flow equation at the exact position of the head measurement locations. The exact locations of the head observation locations are also expressed in cell indices, and not in co-ordinates. For example: (1.00; 1.00; 1.00) corresponds exactly to the centre of the lower left bottom grid cell and (1.50; 1.00; 1.00) corresponds to the edge between this lower left bottom grid cell and the grid cell right of it.

I.11 DBGFILE. The output file with debug information.

This file contains debug information on the inverse modelling. We suppose that a minimum DBG_LEVEL has been specified. All read parameters are echoed to this file and the user should check this file in order to make himself/herself sure that the information is read correctly. In addition, information on the calibration process is given. After each macro iteration the experimental and simulated head values are compared, the objective function value is given and the updated conductivity field is printed. The user should search for the string "objective function" in order to get the objective function values after each iteration. Above the specified objective function value in the debug file the simulated and experimental head values are compared and below it intermediate objective function values, during the linear search, are given.

I.12 FINALTFILE. The output file with the final conductivities.

This file is printed after each macro-iteration and contains the updated hydraulic conductivities. Each line gives the conductivity value for one grid cell. The grid cells are cycled through in the traditional order. In case the inverse conditioning is interrupted due to, for instance, an electricity cut-down, the stored conductivities allow to continue the modelling from intermediate modelling results.

I.13 FINALHFILE. The output file with the final head values.

This file is printed after each macro-iteration and contains the hydraulic head values related to the updated parameter values. Each line gives the hydraulic head value for one grid cell. First the hydraulic head values are given for the first time step at which the groundwater flow equation is solved. The grid cells are cycled through in the traditional order. In addition, the hydraulic head values for subsequent time steps are given. The hydraulic head solutions for different time steps are separated by some blank lines and each new block of hydraulic head values is introduced by "Solution for time step ..".

I.14 FINALBCSFILE. The output file with the final prescribed head boundary values.

This file is printed after each macro-iteration and contains the hydraulic head perturbation at the boundary grid cells. Information for one grid cell is plotted on one line. The line contains the grid cell indices (x-index, y-index and z-index) together with the total applied head perturbation (updated hydraulic head value minus initial hydraulic head value). Only in case the prescribed head values along the boundaries are allowed to change values different from zero are expected. In case the prescribed head values are allowed to change it is important to use the updated boundary head values together with the updated conductivities in an eventual re-start of the simulation.

I.15 FINALSFILE. The output file with the final storativity coefficients.

This file is only printed in case distributed values for the storativity coefficients are calibrated. The file is printed after each macro-iteration and contains the updated values for the storativity coefficients. Each line gives the storativity coefficient for one grid cell. Again the grid cells are cycled through in the traditional order. In case the inverse conditioning is interrupted due to, for instance, an electricity cut-down, the stored storativities allow to continue the transient groundwater flow modelling from intermediate modelling results.

I.16 The main input transport parameter file

The program calls the input parameter file named transp4.par in case TRANSPORT_FLAG=1 in the main parameter input file inverto4.par. We describe the contents of transp4.par.

Line 1: POROSITY. The spatially constant aquifer porosity value is given. This value is used to calculate seepage groundwater flow velocities from Darcian groundwater flow velocities.

Line 2: AQDEPTH. The average vertical aquifer depth. This value is needed to calculate groundwater flow velocities in the 2-D case.

Line 3: NO_TR_INCR, TR_STEP. These parameters indicate at which times the mass transport equation has to be solved. The first parameter is equal to the number of times that the mass transport equation has to be solved. The initial conditions are not included in NO_TR_INCR so that the number of times at which the mass transport equation has to be solved is in fact equal to the number of time increments. The second parameter is equal to a (constant) time step. If for example NO_TR_INCR=10 and TR_STEP=1 the mass transport equation is solved at t=1, 2, 3, 4, 5, 6, 7, 8, 9 and 10 seconds. Apart from this, initial conditions are specified for t=0.

Line 4: UPWWEIGHT1, UPWWEIGHT2, UPWWEIGHT3, UPWWEIGHT4, UPWWEIGHT5, UPWWEIGHT6. These parameters are related to the weighting procedure in the numerical solution of the mass transport equation. The first two parameters are related to the weighting of two neighbour grid cells along the x-direction, the next two parameters are related to the weighting along the y-direction and the last two parameters are related to the weighting along the z-direction. In case upstream weighting is applied UPWWEIGHT1=1, UPWWEIGHT2=0, UPWWEIGHT3=1, UPWWEIGHT4=0, UPWWEIGHT5=1 and UPWWEIGHT6=0. Upstream weighting avoids oscillations in the solution but gives more numerical dispersion. In case symmetric weighting is applies all values are equal to 0.5. If no oscillations occur for symmetric weighting, there is no need to use upstream weighting.

Line 5: CMAX, CMIN. The maximum and minimum allowed concentration values, in kg/m^3 or g/l in the simulation domain. CMIN should be equal to zero, while CMAX may be a very high value unless it is unknown that the concentration value can not go beyond a certain value.

Line 6: CMAXPRINT, CMINPRINT. In order to check whether oscillations occur the user may want that messages are printed to the debugfile. In case the simulated concentration values go above CMAXPRINT or below CMINPRINT a message is printed to the debugfile.

Line 7: DISPFLAG, ALPHAL, ALPHAT, APLPHAV. The first parameter takes into account whether dispersion is considered in the solution of the mass transport equation. If DISPFLAG=1 dispersion is considered. In case DISPFLAG=0, dispersion is not considered. The next three parameters are the three dispersion coefficients α_L, α_T and α_V. ALPHAL is the longitudinal dispersion coefficient, expressed in metres. ALPHAT is the transversal coefficient, also expressed in metres. At the moment, the program uses ALPHAT as the dispersion coefficient for the two directions perpendicular to the longitudinal one. Therefore, ALPHAV is not used in the calculations. Some authors introduced a third dispersion coefficient. In the future the program could be adapted to use the third dispersion coefficient.

Line 8: CONC_TRADEOFF. The objective function for the coupled inversion of groundwater flow and mass transport (equation 6.1) consists of at least two parts, a part related to the mismatch of the head data and a part related to the mismatch of the concentration data. In the optimisation procedure weights have to be given to the two parts of the objective function. CONC_TRADEOFF is the weight for the concentration part, relative to the weight for the hydraulic head part (parameter ψ_3 of equation 6.1). In case CONC_TRADEOFF=100 the sum of the squared differences between measured and simulated concentrations is multiplied by a factor 100 (the squared differences between measured and simulated heads are not multiplied). The value for CONC_TRADEOFF has to be chosen taken into consideration the estimated accuracy of the measurement data, the desired reproduction of both the head and concentration data, the head and concentration variances in the simulation domain and the maximum head and concentration differences along the domain.

Line 9: CONC0FILE. The name of the file that contains the initial concentrations. The program will open this file to read the information. More information on the content and format of C0FILE is given in section I.17.

Line 10: BCONCFILE. The name of the file that contains the transport boundary conditions. The program will open this file to read the information. More information on the content and format of BCONCFILE is given in section I.18.

Line 11: EXPCONCFILE. The name of the file that contains the experimental concentration values. The program will open this file to read the information. More information on the content and format of EXPCONCFILE is given in section I.19.

Line 12: VELOCFILE. The name of the outputfile with the calculated pore groundwater velocities. The program will open this file to print the calculated groundwater flow velocities. More information on the content and format of VELOCFILE is given in section I.20.

Line 13: FINALCFILE. The name of the outputfile with the updated concentrations for the different steps. The program will open this file in order to print the updated concentrations after each macro-iteration. More information on the content and format of FINALCFILE is given in section I.21.

Line 14: TPDBGFILE. The name of the output file with detailed output information on the inverse modelling of mass transport. The program will open this file to write information. More information on the content and format of TPDBGFILE is given in section I.22.

I.17 CONC0FILE. The file with the initial concentrations.

The file C0FILE contains the user supplied initial concentration values at the grid cells. The initial concentration values are given in a column with one concentration value at each line, corresponding to one grid cell. The format in which the grid cells are cycled through is the same as for the input and output files for the groundwater flow part. The initial concentrations are the solution of the mass transport equation for t=0. C0FILE is also used to give the concentration values for the grid cells with prescribed concentration values.

I.18 BCONCFILE. The file with information on the transport boundary conditions.

The program will open this file and the transport boundary conditions are read. The sequence in which the grid cells are read is the same as for CONC0FILE. The following status are possible: 1 ACTIVE GRID CELL, 0 IMPERMEABLE GRID CELL and -1 GRID CELL WITH PRESCRIBED CONCENTRATION VALUE. The condition of impermeable grid cell can also be used for grid cells with just a dispersive mass flux, in case the advective transport is dominant. In case of an irregular aquifer the grid cells which do not belong to the aquifer are also indicated as non active grid cells. The prescribed concentration values at grid cells are defined in the file CONC0FILE.

I.19 EXPCONCFILE. The file with the experimental concentration values.

This file contains the experimental concentration values. The format of the file is the following:

First line: NCONCMEAS, MAXTIMESCONCMEAS. The first parameter indicates the number of observation locations with at least one concentration measurement. The second parameter gives the number of observation times for

the observation point(s) with the maximum number of observations. In case of, for example, four observation points and 7 observation times for observation point 1, 5 observation times for observation point 2 and 3 and 11 observation times for observation point 4 MAXTIMESCONCMEAS=11.

In addition a number of blocks of information follows equal to the number of observation locations. Each block has a header line with general information and in addition observed values are given. The header line consists the following information for the observation location: (1) the x-index of the grid cell, (2) the y-index of the grid cell, (3) the z-index of the grid cell and (4) the number of time steps for which there are observations. In addition, a number of lines equal to the number of given time steps follows with at each line (1) the transport simulation time step (1, 2, 3, etcetera; not the real time in seconds is given) and (2) the observed concentration value for that time step.

In the present version of INVERTO the concentration measurements are assigned to the grid cell centres. The spatial interpolation of simulated concentration values to the concentration observation locations is not contemplated yet. More over, the concentration measurements have to coincide with the exact solution times of the transport equation. No temporal interpolation of observed concentration values is contemplated.

I.20 VELOCFILE. The file with the pore groundwater velocities.

This file contains the pore groundwater velocities. These groundwater velocities are calculated by means of the hydraulic conductivities, the hydraulic head values, the porosity and the aquifer depth (2-D case). The groundwater flow velocities are calculated at the cell interfaces. Therefore, the pore groundwater velocities in the x-direction (v_x), y-direction (v_y) and z-direction (v_z) are evaluated at different locations. The groundwater velocities are printed in columns, the first column contains the groundwater velocities in the x-direction (v_x), the second column contains the groundwater velocities in the y-direction (v_y) and the third column contains the groundwater velocities in the z-direction (v_z). The format in which the velocities are printed is similar to the usual format. The counter cycles fastest on x, then on y and finally on z. The result is that for v_x the groundwater flow between cells (1,1,1) and (2,1,1) is given, next the groundwater flow between (2,1,1) and (3,1,1), continuing along the first row until the groundwater flow between (nx-1,1,1) and (nx,1,1). Later the second row is handled, and so on, until row ny. In case of 3-D flow the second layer is handled afterwards, continuing until layer nz. For vy first the groundwater flow between (1,1,1) and (1,2,1) is given, next the groundwater flow between (2,1,1) and (2,2,1), continuing until the groundwater flow between (nx,1,1) and (nx,2,1). In addition, the groundwater flow velocities for the second row are printed and the first layer is terminated with the groundwater flows between (nx,ny-1,1) and (nx,ny,1). In case of 3-D flow the second layer is handled afterwards, continuing

until layer *nz*. Finally, for *vz* first the pore groundwater flow velocity between (1,1,1) and (1,1,2) is given, next the groundwater flow velocity between (2,1,1) and (2,1,2), continuing along the first row until the velocity between (*nx*,1,1) and (*nx*,1,2) and terminating the first layer with the groundwater flow between (*nx*,*ny*,1) and (*nx*,ny,2). In addition, the next layer is handled and the last specified v_z is for the interface of the grid cells (*nx*,*ny*,*nz*-1) and (*nx*,*ny*,*nz*).

I.21 FINALCFILE. The file with the final concentration values.

This file is printed after each macro-iteration and contains the concentration values related to the updated parameter values. Each line gives the concentration value for one grid cell. First the concentration values are given for the first time step at which the mass transport equation is solved. The grid cells are cycled through in the traditional order. In addition, the concentration values for subsequent time steps are given. The concentration solutions for different time steps are separated by some blank lines and each new block of concentration values is introduced by "Concentrations for Timestep ..".

I.22 TPDBGFILE. The output file with debug information on the transport simulations.

This file contains debug information on the (inverse) modelling of mass transport. The amount of output to this file is determined by the DBG_LEVEL defined in the main parameter input file inverto4.par. We suppose that a minimum DBG_LEVEL has been specified. All read parameters are echoed to this file and this allows the user to check whether the correct values for the parameters are read. Also the solutions of the adjoint state transport equation are printed. In addition, information on the calibration process is given. After each macro iteration the experimental and simulated concentration values are compared and the objective function value is given. The user should search for the string "Total objective function" in order to get the objective function values after each iteration. Also the contribution of the mismatch of the concentration data to the total objective function value is given. Below the "Total objective function" the measured and simulated concentration values are printed. In case oscillations in the solution of the mass transport equation occur these are also printed to the debug file. The user can search for the string "shoot" to find whether oscillations occurred.

Appendix II. Adjoint state equations continuous in time.

It may be advantageous not to discretize the temporal domain for the solution of the adjoint state equations. In that case the objective function is formulated continuous in time:

$$J = \sum_{i=1}^{N_h} \int_0^t [\xi_{it}] \{h_{i,t}^{SIM} - h_{i,t}^{MEAS}\}^2 dt + \psi_3 \sum_{i=1}^{N_C} \int_0^t [\zeta_{it}] \{c_{i,t}^{SIM} - c_{i,t}^{MEAS}\}^2 dt$$

The notation is the same as in equation 6.1 (section 6.2).

The groundwater flow equation and the mass transport equation for which the temporal domain is not discretized are given by:

$$[A]\{h(t)\} + \{q\} = [D]\frac{\partial\{h(t)\}}{\partial t}$$

$$\left(\left(\left[\frac{E}{R}\right]\right) - [\lambda_D] + \left[\frac{q_s^{out}}{\phi}\right]\right)\{C(t)\} + \{F\} = \frac{\partial\{C(t)\}}{\partial t}$$

The symbols were introduced in section 2.2 (equations 2.7 and 2.10). The difference is that hydraulic head and concentration are continuous in time, which is denoted by (t).

The states of the groundwater flow equation and the mass transport equation are:

$$\Psi(t) = [A]\{h(t)\} + \{q\} - [D]\frac{\partial\{h(t)\}}{\partial t} = 0$$

$$\Theta(t) = \left(\left(\left[\frac{E}{R}\right]\right) - [\lambda_D] + \left[\frac{q_s^{out}}{\phi}\right]\right)\{C(t)\} + \{F\} - \frac{\partial\{C(t)\}}{\partial t} = 0$$

Notice that in this case the states are also continuous in time.

The Lagrangian for this formulation is:

$$\Im = J + \int_0^t \{\lambda(t)\}^T \{\Psi(t)\} dt + \int_0^t \{\mu(t)\}^T \{\Theta(t)\} dt$$

The derivatives of the Lagrangian with respect to the perturbation parameters are:

$$\frac{d\Im}{d\{p\}}=\frac{dJ}{d\{p\}}=\frac{\partial J}{\partial\{p\}}+\int_0^t\frac{\partial J}{\partial\{h(t)\}}\frac{\partial\{h(t)\}}{\partial\{p\}}dt+\int_0^t\{\lambda(t)\}^T\left(\frac{\partial\{\Psi(t)\}}{\partial\{p\}}+\frac{\partial\{\Psi(t)\}}{\partial\{h(t)\}}\frac{\partial\{h(t)\}}{\partial\{p\}}\right)dt+$$
$$\int_0^t\frac{\partial J}{\partial\{C(t)\}}\frac{\partial\{C(t)\}}{\partial\{p\}}dt+\int_0^t\{\mu(t)\}^T\left(\frac{\partial\{\Theta(t)\}}{\partial\{p\}}+\frac{\partial\{\Theta(t)\}}{\partial\{h(t)\}}\frac{\partial\{h(t)\}}{\partial\{p\}}+\frac{\partial\{\Theta(t)\}}{\partial\{C(t)\}}\frac{\partial\{C(t)\}}{\partial\{p\}}\right)dt$$

Rearranging gives:

$$\frac{dJ}{d\{p\}}=\frac{\partial J}{\partial\{p\}}+\int_0^t\left(\left(\frac{\partial J}{\partial\{h(t)\}}+\{\lambda(t)\}^T\frac{\partial\{\Psi(t)\}}{\partial\{h(t)\}}+\{\mu(t)\}^T\frac{\partial\{\Theta(t)\}}{\partial\{h(t)\}}\right)\frac{\partial\{h(t)\}}{\partial\{p\}}\right)dt+ \qquad (II.1)$$
$$\int_0^t\{\lambda(t)\}^T\frac{\partial\{\Psi(t)\}}{\partial\{p\}}dt+\int_0^t\left(\left(\frac{\partial J}{\partial\{C(t)\}}+\{\mu(t)\}^T\frac{\partial\{\Theta(t)\}}{\partial\{C(t)\}}\right)\frac{\partial\{C(t)\}}{\partial\{p\}}\right)dt+\int_0^t\{\mu(t)\}^T\frac{\partial\{\Theta(t)\}}{\partial\{p\}}dt$$

As for the discrete adjoint state equations, the derivatives $\partial\Theta/\partial h$ are omitted as their evaluation is very cumbersome and the gradient was found to be just slightly worse estimated in case that these contributions were omitted.

The adjoint states related with the groundwater flow and the mass transport equation can be obtained from:

$$\frac{\partial J}{\partial\{h(t)\}}+\{\lambda(t)\}^T\frac{\partial\{\Psi(t)\}}{\partial\{h(t)\}}=0 \qquad (II.2)$$

$$\frac{\partial J}{\partial\{C(t)\}}+\{\mu(t)\}^T\frac{\partial\{\Theta(t)\}}{\partial\{C(t)\}}=0 \qquad (II.3)$$

The derivatives that appear in the equations *II*.2 and *II*.3 are given by the following equations:

$$\frac{\partial J}{\partial\{h(t)\}}=2\sum_{i=1}^{N_h}\int_0^t[\xi_{it}]\{h_{i,t}^{SIM}-h_{i,t}^{MEAS}\}dt \qquad (II.4)$$

$$\frac{\partial\{\Psi(t)\}}{\partial\{h(t)\}}=[A] \qquad (II.5)$$

$$\frac{\partial J}{\partial\{C(t)\}}=2\psi_3\sum_{i=1}^{N_C}\int_0^t[\zeta_{it}]\{c_{i,t}^{SIM}-c_{i,t}^{MEAS}\}dt \qquad (II.6)$$

$$\frac{\partial\{\Theta(t)\}}{\partial\{C(t)\}}=\left(\left(\left[\frac{E}{R}\right]\right)-[\lambda_D]+\left[\frac{q_s^{out}}{\phi}\right]\right) \qquad (II.7)$$

The equations differ from the versions where the temporal domain is discretized (compare with the equations 3.8 until 3.10 and 6.5 until 6.7).

Combining the equations *II*.4, *II*.5 and *II*.2 results in the following linear system of equations to find the adjoint states related with the flow part:

$$[A]\{\lambda(t)\}^T=-2\sum_{i=1}^{N_h}\int_0^t[\xi_{it}]\{h_{i,t}^{SIM}-h_{i,t}^{MEAS}\}dt$$

This equation only has to be solved for the time steps that head measurements are available. In case just at a few times measurements are available, the number of times that the equation has to be solved may be reduced greatly as compared with the case that the adjoint equation is discretized in time.

The linear system to solve the adjoint states for the transport part are obtained from the combination of equations *II*.6, *II*.7 and *II*.3:

$$\left(\left(\left[\frac{E}{R}\right]\right)-[\lambda_D]+\left[\frac{q_s^{out}}{\phi}\right]\right)\{\mu(t)\}^T=-2\sum_{i=1}^{N_C}\int_0^t[\zeta_{it}]\{c_{i,t}^{SIM}-c_{i,t}^{MEAS}\}dt$$

Also this equation has to be solved only for the time steps that concentration measurements are available.

The application of equations *II*.2 and *II*.3 reduce equation *II*.1 to the following expression:

$$\frac{dJ}{d\{p\}}=\frac{\partial J}{\partial\{p\}}+\int_0^t\{\lambda\}^T\frac{\partial\{\Psi(t)\}}{\partial\{p\}}dt+\int_0^t\{\mu\}^T\frac{\partial\{\Theta(t)\}}{\partial\{p\}}dt$$

The derivative $\partial J/\partial\{p\}$ is equal to zero. The derivatives of the states with respect to the perturbation parameters are given by:

$$\left\{\frac{\partial\Psi(t)}{\partial p}\right\}=\left[\frac{\partial A}{\partial p}\right]\{h(t)\}+\left\{\frac{\partial q}{\partial p}\right\}-\left[\frac{\partial D}{\partial p}\right]\frac{\partial\{h(t)\}}{\partial t} \qquad (II.8)$$

$$\left\{\frac{\partial\Theta(t)}{\partial p}\right\}=\left[\frac{\partial[E/R]}{\partial p}\right]\{C(t)\}+\left\{\frac{\partial(q_s^{out}/\phi)}{\partial p}\right\}\{C(t)\}+\left\{\frac{\partial F}{\partial p}\right\} \qquad (II.9)$$

The difference between equations *II*.8 and *II*.9 and the equations 3.12 and 6.9 is that head and concentration are not discretized in time. The derivatives only have to be evaluated for the time steps that head or concentration measurements are available. For the other time steps the Lagrange multipliers are equal to zero so that it is not necessary to calculate the contribution from the derivatives. In some specific cases this may reduce the computer burden significantly and in those cases this formulation of the adjoint state equations is preferred as compared to the formulation presented in section 6.2.

References

Adams J (1998). *Preliminary results of selective pressure build-up tests in borehole KI0023B.* Technical note TN-98-27b. TRUE Block Scale Experiment. SKB Publication.

Adams J, Andersson P, Meier P (1999). *Preliminary results of selective pressure build-up tests in borehole KI0025F02.* International Technical Document ITD-99-27. TRUE Block Scale Experiment. SKB Publication.

Anderman ER, Hill MC (1999). A new multistage groundwater transport inverse method: Presentation, evaluation and implications. *Water Resources Research,* 35(4), 1053-1063.

Andersson C, Laaksoharju M (1999). *Mixing calculation of March 1998 groundwater chemical data.* International Technical Document ITD-00-09. SKB Publication.

Andersson C, Säfvestad A (2000). *Compilation of groundwater chemistry data from the Prototype repository.* International Technical Document ITD-00-04. SKB Publication.

Andersson P, Ludvigson JE, Wass E (1998). *Combined interference tests and tracer tests. Performance and preliminary evaluation.* Technical note TN-98-28b. TRUE Block Scale project. Preliminary characterization stage. SKB Publication.

Andersson P, Ludvigson JE, Wass E, Holmqvist M (1999). *Interference tests and tracer tests PT-1 - PT-4.* International Technical Document ITD-99-19. TRUE Block Scale. Detailed characterization stage. SKB Publication.

Andersson P, Ludvigson JE, Wass E, Holmqvist M (2000a). *Interference tests, dilution tests and tracer tests, Phase A.* TRUE Block Scale. Tracer test stage. Final draft.

Andersson P, Wass E, Holmqvist M (2000b). *Tracer tests, Phase B. TRUE Block Scale. Tracer test stage.* Incomplete first draft.

Bakr AA, Gelhar LW, Gutjahr AL (1978). Stochastic analisis of spatial variability in subsurface flows, 1. Comparison of one- and two-dimensional flows. *Water Resources Research,* 14(2), 263-271.

Beauheim RL (1987a). *Interpretation of the WIPP-13 Multipad Pumping Test of the Culebra Dolomite at the Waste Isolation Pilot Plant (WIPP) Site.* Sandia National Laboratories.

Beauheim RL (1987b). *Analysis of Pumping Tests of the Culebra Dolomite Conducted at the H-3 Hydropad at the Waste Isolation Pilot Plant (WIPP) Site.* Sandia National Laboratories.

Byegård J, Winberg A (2000). *Proposal for injection schedule for TRUE Block Scale Phase C tests.* Internal inform.

Capilla JE, Gómez-Hernández JJ, Sahuquillo A (1997). Stochastic simulation of transmissivity fields conditional to both transmissivity and piezometric data. 2. Demonstration on a synthetic aquifer. *Journal of Hydrology,* 1-4(203), 175-188.

Capilla JE, Gómez-Hernández JJ, Sahuquillo A (1998). Stochastic simulation of transmissivity fields conditional to both transmissivity and piezometric data. 3. Application to the Culebra Formation at the Waste Isolation Pilot Plan (WIPP), New Mexico, USA. *Journal of Hydrology,* 207, 254-269.

Carlsten S (1998a). *Results from borehole radar measurements in KI0023B.* Technical note TN-98-14b. TRUE Block Scale experiment. SKB Publication.

Carlsten S (1998b). *Results from borehole radar measurements in KI0025F02.* International Technical Document ITD-99-02. TRUE Block Scale experiment. SKB Publication.

Carrera J, Glorioso L (1991). On geostatistical formulations of the groundwater flow inverse problem. *Advances Water Resources Research,* 14(5), 272-283.

Carrera J, Medina A (1990). An improved form of adjoint-state equations for transient problems. In: Peters A et al. (Eds.). *Computational methods in Water Resources X,* 199-206. Kluwer Academic Publishers.

Carrera J, Navarrina F, Vives L, Heredia J, Medina A (1990). Computational aspects of the inverse problem. In: G. Gambolati et al. (Eds.) *Computational methods in surface hydrology.* Computational Mechanics Publications.

Carrera J, Neuman SP (1986a). Estimation of aquifer parameters under transient and steady state conditions: 1. Maximum likelihood method incorporating prior information. *Water Resources Research,* 22(2), 199-210.

Carrera J, Neuman SP (1986b). Estimation of aquifer parameters under transient and steady state conditions: 2. Uniqueness, stability, and solution algorithms. *Water Resources Research,* 22(2), 211-227.

Carrera J, Neuman SP (1986c). Estimation of aquifer parameters under transient and steady state conditions: 3. Application to synthetic and field data. *Water Resources Research,* 22(2), 228-242.

Cauffman TL, LaVenue AM, McCord JP (1990). *Groundwater flow modeling of the Culebra dolomite, vol. 2, Data base,* Contractor Rep. SAND89-7068/2. Sandia National Laboratory.

Chu L, Reynolds AC, Oliver DS (1995). Computation of sensitivity coefficients for conditioning the permeability field to well-test pressure data. *In Situ,* 19(2), 179-223.

Cosma C, Enescu N, Heikkinen P, Keskinen J (1998). *Seismic VSP and HSP investigations in KI0023B and integrated evaluation using old crosshole data from KA2511A-KA2563A and VSP data from KA2511A.* Technical note TN-98-26b. TRUE Block Scale project. SKB Publication.

Dagan G (1982a). Stochastic modelling of groundwater flow by unconditional and conditional probabilities, 1. Conditional simulation and the direct problem. *Water Resources Research,* 18(4), 813-833.

Dagan G (1982b). Analysis of flow through heterogeneous random aquifers, 2. Unsteady flow in confined formations. *Water Resources Research,* 18, 1571-1585.

Dagan G (1985). Stochastic modelling of groundwater flow by unconditional and conditional probabilities: the inverse problem. *Water Resources Research,* 21(1), 65-72.

Dagan G, Rubin Y (1988). Stochastic identification of recharge, transmissivity, and storativity in aquifer transient flow: a quasi-steady approach. *Water Resources Research,* 24(10), 1698-1710.

De Marsily G (1986). *Quantitative hydrogeology.* Academic press.

De Marsily G, Lavedau G, Boucher M, Fasanino G (1984). Interpretation of interference test in a well field using geostatistical techniques to fit the permeability distribution in a reservoir model. In: Verly GW, David M, Journel AG, Marechal A (Eds.) *Geostatistics for Natural Resources Characterization. Proceedings of the NATO Advanced Study Institute, South Lake Tahoe, California, September 6-17,* p. 831-849. D. Reidel.

Dershowitz B (2000). *Conductive background fractures in the area investigated in the tracer test stage (TTS).* International Technical Document ITD-00-03. TRUE Block Scale Project. SKB Publication.

Deutsch CV, Journel AG (1992). *GSLIB Geostatistical Software Library and Users Guide.* Oxford University Press.

Deutsch CV, Journel AG (1998). *GSLIB, Geostatistical Software Library and Users Guide. Second edition.* Oxford University Press.

Doe T (1999). *Reconciliation of the March '99 structural model and hydraulic data.* International Technical Document ITD-99-20. TRUE Block Scale Project. SKB Publication.

Finisterle S, Najita J (1998). Robust estimation of hydrogeologic model parameters. *Water Resources Research,* 34(11), 2939-2947.

Freeze RA, Cherry JA (1979). *Groundwater.* Prentice-Hall, Inc.

Gelhar LW (1986). Stochastic subsurface hydrology from theory to applications. *Water Resources Research,* 22(9), 135S-145S.

Gelhar LW, Axness CL (1983). Three-dimensional stochastic analysis of macrodispersion in aquifers. *Water Resources Research,* 19(1), 161-180.

Gentzschein B (1996). *Pressure build-up tests performed prior to cement grouting carried out during drilling of borehole KA2563A.* Technical note TN-97-10b. TRUE Block Scale Project. SKB Publication.

Gentzschein B (1997a). *Detailed flow logging of core borehole KA2563A.* Technical note TN-97-07b. TRUE Block Scale Project. SKB Publication.

Gentzschein B (1997b). *Detailed flow logging of core boreholes KA2511A, KI0025F and KA3510A using a double packer system.* Technical note TN-97-23b. TRUE Block Scale Project. SKB Publication.

Gentzschein B (1998). *Detailed flow logging in core borehole KI0023B using a double packer system.* Technical note TN-98-05b. TRUE Block Scale Project. SKB Publication.

Gentzschein B, Ludvigson JE (2000). *Single-hole hydraulic tests and short-term interference tests in KI0025F03.* International Technical Document ITD-00-05. TRUE Block Scale Project. SKB Publication.

Gentzschein B, Morosini M (1998). *Selective pressure build-up tests in borehole KI0025F.* Technical note TN-98-29b. TRUE Block Scale Project. SKB Publication.

Goovaerts P (1997). *Geostatistics for natural resources evaluation.* Oxford University Press.

Gómez-Hernández JJ, Cassiraga EF (1994). Theory and practice of sequential simulation. In: Armstrong, M and Dowd, PA (Eds.), *Geostatistical Simulations,* p. 111-124. Kluwer Academic Publishers.

Gómez-Hernández JJ, Journel AG (1993). Joint simulation of MultiGaussian random variables. In: Soares, A (Ed.) *Geostatistics Tróia '92,* volume 1, p. 85-94. Kluwer Academic Publishers.

Gómez-Hernández JJ, Sahuquillo A, Capilla JE (1997). Stochastic simulation of transmissivity fields conditional to both transmissivity and piezometric data. 1. Theory. *Journal of Hydrology*, 1-4(203), 162-174.

Gómez-Hernández JJ, Srivastava RM (1990). ISIM3D: An ANSI-C three dimensional multiple indicator conditional simulation program. *Computer and Geosciences*, 16(4), 395-400.

Gómez-Hernández JJ, Wen XH (1998). To be or not to be multi-Gaussian? A reflection on stochastic hydrogeology. *Advances in Water Resources Research*, 21(1), 47-61.

Graham WD, McLaughlin D (1989a). Stochastic analysis of nonstationary subsurface solute transport. 1. Unconditional moments. *Water Resources Research*, 25(2), 215-232.

Graham WD, McLaughlin D (1989b). Stochastic analysis of nonstationary subsurface solute transport. 2. Conditional moments. *Water Resources Research*, 25(11), 2331-2355.

Graham WD, McLaughlin D (1991). A stochastic model of solute transport in groundwater: Application to the Borden, Ontario, Tracer Test. *Water Resources Research*, 27(6), 1345-1359.

Graham WD, Neff CR (1994). Optimal estimation of spatially variable recharge and transmissivity fields under steady-state groundwater flow. Part 2. Case study. *Journal of Hydrology*, 157, 267-285.

Graham WD, Tankersley CD (1994). Optimal estimation of spatially variable recharge and transmissivity fields under steady-state groundwater flow. Part 1. Theory. *Journal of Hydrology*, 157, 247-266.

Grenier C, Mouche E, Dewiere L (1996). Stochastic modelling of groundwater flow by the method of conditional probabilities: theoretical study and numerical evaluation. In: *Calibration and reliability in groundwater modelling. Proceedings of the ModelCARE'96 Conference.* IAHS Pulication no. 237, p. 95-104. Kluwer Academic Publishers.

Guadagnini A, Franzetti S (1999). Contamination of pumping wells and time-related capture zones in heterogeneous formations. *Groundwater*, 37(2), 253-260.

Gutjahr AL, Gelhar LW, Bakr AA, MacMillan JR (1978). Stochastic analysis of spatial variability in subsurface flows, 2. Evaluation and application. *Water Resources Research*, 14(5), 953-959.

Gutjahr A, Wilson J (1989). Co-kriging for stochastic flow models. *Transport in Porous Media,* 4, 585-598.

Gutjahr A, Bullard B, Hatch C, Hughson L (1994). Joint conditional simulations and the spectral approach for flow modelling. *Stochastic Hydrology and Hydraulics,* 8(1), 79-108.

Hanna S, Yeh TCJ (1998). Estimation of co-conditional moments of transmissivity, hydraulic head and velocity fields. *Advances in Water Resources Research,* 22(1), 87-95.

Harvey and Gorelick (1995). Mapping hydraulic conductivity: Sequential conditioning with measurements of solute arrival time, hydraulic head, and local conductivity. *Water Resources Research,* 31(7), 1615-1626.

Hendricks Franssen HJWM, Gómez-Hernández JJ (1997). Impact of random function model choice on groundwater travel time estimates. In: Soares A, Gómez-Hernández JJ, Froidevaux R (Eds.) *GeoENV I - Geostatistics for environmental applications,* p. 101-110. Kluwer Academic Publishers.

Hendricks Franssen HJWM, Gómez-Hernández JJ, Sahuquillo A, Capilla JE (1999). Joint simulation of transmissivity and storativity fields conditional to hydraulic head data. *Advances in Water Resources Research,* 23, 1-13.

Hermansson J (1998a). *October 1997 structural model; update using characterisation data from KA2511A and KI0025F.* Technical note TN-97-35B. TRUE block scale project. SKB Publication.

Hermansson J (1998b). *September 1998 structural model; update using characterisation data from KI0023B.* Technical note TN-98-18B. TRUE block scale project. SKB Publication.

Hermansson J, Follin S (1997). *Update of the structural model using characterization data from KA2563A, KA3510A and KA2511A. Scoping stage.* Technical note TN-97-19b. TRUE block scale project. SKB Publication.

Hoeksema RJ, Kitanidis PK (1984). An application of the geostatistical approach to the inverse problem in two-dimensional modeling. *Water Resources Research,* 20(7), 1003-1020.

Hughson DL (1997). *A geostatistical inverse method for conditioning randomly heterogeneous transmissivity fields on transient hydraulic head data.* PhD thesis. New Mexico Institute of Mining and Technology.

Hughson DL, Gutjahr A (1998). Effect of conditioning randomly hetereogeneous transmissivity on temporal hydraulic head measurements in transient two-dimensional aquifer flow. *Stochastic hydrology and hydraulics,* 12, 155-170.

Iribar V, Carrera J, Custodio E, Medina A (1997). Inverse modelling of seawater intrusion in the Llobregat delta deep aquifer. *Journal of Hydrology,* 198, 226-244.

Journel AG (1983). Non-parametric distributions of spatial distributions. *Mathematical Geology,* 15(3), 445-468.

Journel AG, Huijbregts C (1978). *Mining geostatistics.* Academic Press.

Journel AG, Rossi ME (1989). When do we need a trend model? *Mathematical Geology,* 21(7), 715-739.

Kinzelbach W (1986). *Groundwater modelling: An introduction with sample programs in BASIC.* Elsevier.

Kitanidis PK (1986). Comment on "Stochastic modelling of groundwater flow by unconditional and conditional probabilities: The inverse problem" by Gedeon Dagan. *Water Resources Research,* 22(6), 984-986.

Kitanidis PK (1996). On the geostatistical approach to the inverse problem. *Advances Water Resources Research,* 19(6), 333-342.

Kitanidis PK, Vomvoris EG (1983). A geostatistical approach to the inverse problem in groundwater modelling (steady state) and one-dimensional simulations. *Water Resources Research,* 19(3), 677-690.

LaVenue AM, Cauffman TL, Pickens JF (1990). *Groundwater Flow Modelling of the Culebra Dolomite: Volume I - Model Calibration,* Contractor Rep. SAND89-7068/1. Sandia National Laboratory.

LaVenue AM, RamaRao BS, de Marsily G, Marietta MG (1995). Pilot point methodology for automated calibration of an ensemble of conditionally simulated transmissivity fields. 2. Application. *Water Resources Research,* 31(3), 495-516.

Mayer AS, Huang C (1999). Development and application of a coupled-process parameter inversion model based on the maximum likelihood estimation method. *Advances in Water Resources Research,* 22(8), 841-853.

Medina A (1993). *Joint estimation of the parameters of the flow and transport equation (in Spanish).* Ph.D thesis. Technical university of Catalonia.

Medina A, Carrera J (1996). Coupled estimation of flow and solute transport parameters. *Water Resources Research,* 32(10), 3063-3076.

Medina A, Carrera J, Galarza G (1990). Inverse modeling of coupled flow and solute transport problems. *ModelCARE 90: Calibration and reliability in groundwater modelling.* IAHS Publications, 195, 185-194.

NIREX (1995a). *The 3D geological structure of PRZ.* Tech. Report S/95/005. NIREX.

NIREX (1995b). *The 3D geology and hydrogeology of the RCF South Shaft Location.* Tech. Report S/95/007. NIREX.

NIREX (1995c). *Sellafield geological and hydrogeological investigations, factual report – compilation of maps and drawing.* Tech. Report S/95/002. NIREX.

Oliver DS (1994). The incorporation of transient pressure data into reservoir characterization. *In Situ,* 18(3), 243-275.

Oliver DS (1996). Multiple realizations of the permeability field from well test data. *Society of Petroleum Engineers Journal,* 1(2), 145-154.

Oliver DS, Cunha LB, Reynolds AC (1997). Markov Chain Monte Carlo methods for conditioning a permeability field to pressure data. *Mathematical Geology,* 29(1), 61-91.

Oliver DS, He N, Reynolds AC (1996). Conditioning permeability fields to pressure data. *Proceedings from the Fifth European conference on the mathematics of oil recovery;* Leoben, Austria; September 3-6, 1996.

RamaRao BS, LaVenue AM, de Marsily G, Marietta MG (1995). Pilot point methodology for automated calibration of an ensemble of conditionally simulated transmissivity fields. 1. Theory and computational experiments. *Water Resources Research,* 31(3), 475-493.

Rouhianen P, Heikkinen P (1998a). *Difference flow measurements in borehole KI0025F02 at the Äspö hard rock laboratory.* Technical note TN-98-35B. TRUE Block Scale Project. SKB Publication.

Rouhianen P, Heikkinen P (1998b). *Flow measurements in boreholes KA3510A and KA2598A at the Äspö hard rock laboratory.* Technical Document TD-99-14. TRUE Block Scale Project. SKB Publication.

Rouhianen P, Heikkinen P (1999a). *Difference flow measurements in boreholes KA2563A and KA2511A at the Äspö HRL.* International Technical Document ITD-99-11. TRUE Block Scale Project. SKB Publication.

Rouhianen P, Heikkinen P (1999b). *Difference flow measurements in borehole KI0025F03 at the Äspö HRL.* International Technical Document ITD-99-26. TRUE Block Scale Project. SKB Publication.

Rubin Y (1991a). Prediction of tracer plume migration in disordered porous media by the method of conditional probabilities. *Water Resources Research,* 27(6), 1291-1308.

Rubin Y (1991b). The spatial and temporal moments of tracer concentration in disordered porous media. *Water Resources Research,* 27(11), 2845-2854.

Rubin Y, Dagan G (1987a). Stochastic identification of transmissivity and effective recharge in steady groundwater flow. 1. Theory. *Water Resources Research,* 23(7), 1185-1192.

Rubin Y, Dagan G (1987b). Stochastic identification of transmissivity and effective recharge in steady groundwater flow. 2. Case study. *Water Resources Research,* 23(7), 1193-1200.

Rubin Y, Dagan G (1988). Stochastic analysis of boundaries effects on head spatial variability in heterogeneous aquifers, 1, Constant head boundaries. *Water Resources Research;* 24, 1689-1697.

Rubin Y, Dagan G (1989). Stochastic analysis of boundaries effects on head spatial variability in heterogeneous aquifers, 2, Impervious boundary. *Water Resources Research,* 25(4), 707-712.

Sahuquillo A, Capilla JE, Gómez-Hernández JJ, Andreu J (1992). Conditional simulation of transmissivity fields honouring piezometric data. In: Blain WR, Cabrera E (Eds.) *Hydraulic Engineering Software IV, Fluid Flow Modeling,* p. 201-214. Kluwer.

Säfvestad A, Andersson C (1999a). *Compilation of groundwater chemistry data collected during drilling of the Select-2 boreholes.* Technical document TD-99-61. SKB Publication.

Säfvestad A, Andersson C (1999b). *Detailed characterisation stage water sampling campaign, class 2, WBS 3.3.1.2.* International Technical Document ITD-99-28. TRUE Block Scale project. SKB Publication.

Scales LE (1985). *Introduction to non-linear optimisation.* Macmillan Publishers Ltd.

Skaggs and Kabala (1995). Recovering the history of a groundwater contaminant plume: Method of quasi-reversibility. *Water Resources Research,* 31(11), 269-2673.

Skaggs and Kabala (1998). Limitations in recovering the history of a groundwater contaminant plume. *Journal of Contaminant Hydrology,* 33, 347-359.

Smith L, Schwartz FM (1981a). Mass transport, 2. Analysis of uncertainty in prediction. *Water Resources Research,* 17(2), 351-369.

Smith L, Schwartz FM (1981b). Mass transport, 3. Role of hydraulic conductivity in prediction. *Water Resources Research,* 17(5), 1463-1479.

Sonnenborg TO, Engesgaard P, Rosbjerg D (1996). Contaminant transport at a waste residual deposit. 1. Inverse flow and nonreactive transport modeling. *Water Resources Research,* 32(4), 925-938.

Sun NZ, Yang S, Yeh WG (1998). A proposed stepwise regression method for model structure identification. *Water Resources Research,* 34(10), 2561-2572.

Sun NZ, Yeh WWG (1990a). Coupled inverse problems in groundwater modeling, 1, Sensitivity analysis and parameter identification. *Water Resources Research,* 26(10), 2507-2525.

Sun NZ, Yeh WWG (1990b). Coupled inverse problems in groundwater modeling, 2, Identifiability and experimental design. *Water Resources Research,* 26(10), 2527-2540.

Sun NZ, Yeh WWG (1992). A stochastic inverse solution for transient groundwater flow: parameter identification and reliability analysis. *Water Resources Research,* 28(12), 3269-3280.

Svensson U (1997). *A site scale analysis of groundwater flow and salinity distribution in the Äspö area.* Technical note TN-98-17B. SKB Publication.

Tullborg EL (1998). *Mineralogical and geochemical characterization of samples taken from borehole KI0025F (zone Z), KA2563A, and KA3573A (Structure 5).* Technical note TN-98-21b. TRUE Block Scale Experiment. SKB Publication.

Vassolo S, Kinzelbach W, Schaefer W (1998). Determination of a well head protection zone by stochastic inverse modelling. *Journal of Hydrology,* 206, 268-280.

van Leeuwen M, te Stroet CBM, Butler AP, Tompkins JA (1999). Stochastic determination of the Wierden capture zones. *Groundwater,* 37(1), 8-17.

Wagner BJ (1992). Simultaneous parameter estimation and contaminant source characterization for coupled groundwater flow and contaminant transport modelling. *Journal of Hydrology,* 135, 275-303.

Wang HF, Anderson MP (1982). *Introduction to groundwater modelling. Finite difference and finite element methods.* WH Freeman and Company.

Webster R, Burgess TM (1980). Optimal interpolation and isarithmic mapping of soil properties III Changing drift and universal kriging, *Journal of Soil Science* 31, 505-524.

Wen XH (1995). *Geostatistical methods for prediction of mass transport in groundwater.* PhD thesis. Stockholm University Press.

Wen XH, Deutsch CV, Cullick AS (1998). Integrating pressure and fractional flow data in reservoir modeling with fast streamline based inverse method. *Society of Petroleum Engineers* 48971, 1-15.

Wen XH, Cvetkovic V (1995). *Models of groundwater flow and mass transport in fractured media.*

Wen XH, Gómez-Hernández JJ (1996). The constant displacement scheme for tracking particles in heterogeneous aquifers. *Ground Water,* 34(1), 135-142.

Wen XH, Gómez-Hernández JJ, Sahuquillo A, Capilla JE (1996). The significance of conditioning on piezometric head data for predictions of mass transport in groundwater modelling. *Mathematical Geology,* 28(7), 951-968.

Wen XH, Kung CS (1995). A Q-BASIC program for modelling advective mass transport with retardation and radioactive decay by particle tracking. *Computers & Geosciences,* 21(4), 463-480.

Wen XH, Kung CS (1996). Implementation of the constant displacement scheme in random walk. *Computers & Geosciences,* 22(4), 369-377.

Xiang Y, Sykes JF, Thomson NR (1992). A composite L_1 parameter estimator for model fitting in groundwater flow and solute transport simulation. *Water Resources Research,* 29(6), 1661-1673.

Yeh TCJ, Gutjahr AL, Jin M (1995). An iterative cokriging-like technique for ground-water flow modeling. *Groundwater,* 33(19), 33-41.

Yeh TCJ, Jin M, Hanna S (1996). An iterative stochastic inverse method: Conditional effective transmissivity and hydraulic head fields. *Water Resources Research,* 32(1), 85-92.

Zheng C, Bennett GD (1995). *Applied contaminant transport modelling.* Theory and practice. John Wiley and Sons, Inc.